# Respiratory circulation in the abalone *Haliotis iris*

---

A thesis submitted in
fulfillment of the requirements for the Degree of
Doctor of Philosphy
in the
School of Biological Sciences
University of Canterbury

by

**Norman Lawrence Charles Ragg**

---

University of Canterbury

2003

# Contents

## Chapter 3: Vascular morphology



## Chapter 4: Respirometry and ventilation

## Chapter 8: General discussion

# Abstract

An integrated description of the respiratory system of the abalone *Haliotis iris* is presented. These animals are believed to be inherently primitive and still bear the ancestral gastropod gill arrangement, thus allowing physiological examination of a 'living fossil'. Ventilation, gaseous diffusion, blood transport and the anatomical arrangement of the vascular system are examined under a range of conditions. Resting *H. iris* consume an average of 0.47μmol $O_2$.g live weight$^{-1}$.h$^{-1}$, 87% of which is taken up across the gills, the remainder diffuses directly into the foot and epipodium. A 300g abalone ventilates its gills at a rate of 28mL.min$^{-1}$, a rate which, due to low resistance to diffusion (diffusion limitation index = 0.47) and a well matched ventilation/perfusion conductance ratio, is adequate to support the quiescent animal. Increased oxygen demand is accommodated by an increase in cardiac stroke volume, elevating output from 9.1 to 24.4 μL.g$^{-1}$.min$^{-1}$. At rest the right gill is the predominant gas exchanger, receiving 95.7% of the branchial blood flow, when cardiac output is elevated the left gill becomes equally perfused, effectively doubling the diffusing surface. Ventilation does not increase, and an increased reliance on assistance from external water currents is seen. Previously undescribed components of the vascular system, notably an extensive sinus of mixed venous and arterial blood surrounding the gut and a large vessel that offers a bypass to the right kidney, provide a low resistance circuit between the heart and gills, bypassing the major organs and muscles. The low resistance circuit allows haemolymph to pass from the aorta to the base of the gills with minimal loss of pressure and no phase shift in the pulse, allowing blood to cross the gills with maximal inertia and instantaneous pressure gradient. *Haliotis iris* therefore appears to have exploited its limited physiological resources to the maximum in the routine operation of its gas exchange system. It is concluded that further improvement could not occur without substantial remodeling of the body plan, which may account for the abandonment of the system by higher gastropods.

*Para Mamá... por supueso*

Maria Lucila Bianchi de Ragg

1940 - 2000

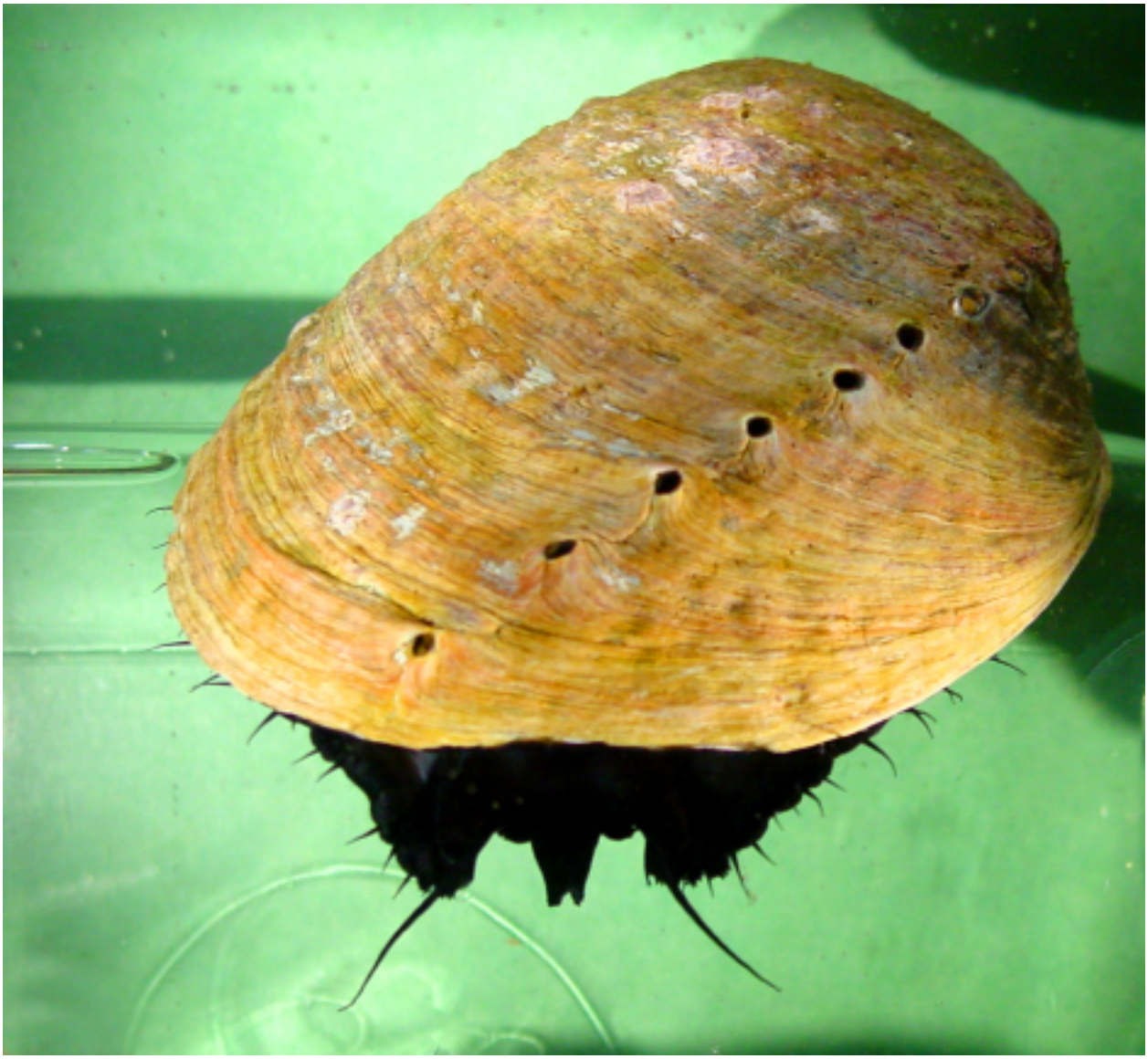

# Chapter 1

# General Introduction

## 1.1. What is an abalone?

Abalone are a distinctive group of marine snails, readily identified by a row of holes extending from the left anterior margin of the shell. A number of the larger, temperate species inhabit rocky intertidal and shallow subtidal areas. The flesh of these abalone is regarded as a gastronomic delicacy, a fact which, combined with their relative ease of capture, has resulted in a long, if somewhat one-sided relationship between abalone and man. The abalone have therefore acquired a wealth of colloquial names, including paua (New Zealand), ormer/ormeau (Europe), awabi (Japan), perlemon (South Africa), sea ear and muttonfish.

*Taxonomy*

The phylogeny of the Mollusca remains unclear. In fact it is not even clear whether the Conchifera (the taxon encompassing Mollusca and its immediate precursors) are in fact monophyletic (Lindberg and Ponder 1996). Molluscs appear to share a common ancestry with annelids, evident from the characteristic spiral cleavage and trochophore larvae found in both phyla (Barnes 1986). The theory may be corroborated by the discovery of repeated pairs of organs (gills, nephridia, shell muscles) in the primitive molluscan class Monoplacophora, reminiscent of a metameric organisation (Barnes 1986). Lindberg and Ponder (1996), however, suggest the arrangement may be adaptive, with ontogenic addition of organs dictated by the requirements of increasing size.

While acknowledging the uncertainties surrounding the current nomenclature of molluscs, the generally accepted classification of abalone is as follows:

Phylum: Mollusca
Class: Gastropoda
Subclass: Prosobranchia
Order: Archaeogastropoda
Superfamily: Pleurotomariacea
Family: Haliotidae

Genus: *Haliotis*
Subgenus: *Paua*
Species: *iris*

The order Archaeogastropoda is still defined according to morphological characteristics, using a system established by Bouvier in 1887 (Voltzow 1994). The continued use of the Archaeogastropoda

as a monophyletic taxon remains highly controversial (see Hickman 1988 for details) but is used here in the absence of a more satisfactory classification. It should be noted that many contemporary texts refer to the order Vetigastropoda, recognising the the patellogastropods as a separate order. Vetigastropoda and Archaeogastropoda are otherwise synonymous (e.g. Turgeon et al. 1998). Archaeogastropods possess a rhipidoglossan radula, aspidibranch (bipectinate) gills and a diotocardian (2 auricle) heart (Voltzow 1994). Remaining extant prosobranchs are classified within the superorder Caenogastropoda, containing both the meso- and neogastropods. The caenogastropods typically have a taenioglossan, or more specialised radula and a single pectinibranch gill (Voltzow 1994).

Polyplacophora are often regarded as extant examples of the ancestral mollusc condition; the basal gastropods (Pleurotomariacea, Fissurellacea, Trochacea) share the polyplacophoran's pedal nerve chord arrangement (Lindberg and Ponder 1996), supporting the suggestion that these 3 superfamilies represent the ancestral gastropods. Of the 4 archaeogastropod superfamilies, Pleurotomariacea and Fissurellacea retain 2 bipectinate gills, and therefore more closely resemble the ancestral gas exchanger arrangement, while Trochacea and Neritacea have lost the right gill (Voltzow 1994).

Abalone is the common name give to all members of the family Haliotidae. The Haliotidae are presumed to have originated from an evolutionary burst in the early Paleozoic that caused the initial radiation of the Archaeogastropoda (Wagner 1996). Taxonomically, the abalone are therefore considered basal to the subsequent evolutionary radiation of the Prosobranchia, a position that is also reflected in the abalone's anatomical arrangement (discussed below).

The species examined in this thesis is blackfoot abalone, *Haliotis iris*, the largest and most common abalone species found in coastal New Zealand waters. A major incentive for undertaking the investigations described in the current project has been the primitive status of abalone. *Haliotis iris* is therefore particularly suitable as it represents the only extant member of the subgenus *Paua* (Lee and Vacquier 1995), this subgenus also contains the oldest known fossil abalone species, *H. lomaensis*, dated at 66Ma (Lindberg 1992). It is therefore possible that *Paua* represent the least differentiated of living abalone.

Contemporary authors tend to alternately attribute the species *Haliotis iris* to either Martyn or Gmelin. According to Powell (1979), the description by Martyn predates that of Gmelin by 7 years. The species is therefore regarded as *Haliotis iris* Martyn (1784) in the current study.

## 1.2. Biology of Abalone

*Ecology*

The shell of *H. iris* consists largely of a single expanded whorl, with a low profile and enlarged aperture (Purchon 1977, Barnes 1986). The shell bears the thick nacreous layer characteristic of many archaeogastropods (Voltzow 1994); in the case of *H. iris* the pyramidal aragonite of the shell

lining creates intense and distinctive blue-green to pink refraction colours. The original slit seen in early prosobranchs is partially occluded in abalone, forming a series of shell holes (tremata), augmenting the strength of the shell (Purchon 1977). The inclusion of exhalant apertures or a slit in the shell is regarded as the early gastropod solution to the sanitation problem caused when the anus was brought towards the anterior by torsion (Barnes 1986).

When compared to most other abalone species, *H. iris* has a relatively smooth shell, low and narrow tremata (shell holes) and simple epipodium, adaptations indicative of a hydrodynamically exposed habitat (frequently >0.7 $m.s^{-1}$ water current) (Tissot 1992). As with most archaeogastropods, the ripidoglossan radula limits *H. iris* to a grazing feeding habit (Purchon 1977). However, *H. iris* exploits the rapid water currents of its environment by adopting a sedentary habit, waiting for macroalgal fragments dislodged by wave action (e.g. Wells et al. 1998). When drifting food particles are perceived by the cephalic and epipodal tentacles *H. iris* raise the shell and often the anterior foot, which are then used to trap moving algal material (Poore 1972, Allen et al. 2001).

Internally the abalone retain a high degree of bilateral symmetry, reminiscent of the ancestral gastropod condition (Russell and Evans 1989). A general displacement of visceral organs to the left side of the animal is attributed to hypertrophy of the right shell muscle rather than the evolutionary reduction of the right-side organs (Yonge 1947). The abalone have retained paired gills (ctenidia), heart auricles and kidneys. The paired arrangement has been lost in higher prosobranchs (the caenogastropods, e.g. Fretter and Graham 1994), implying that fundamental limitations are associated with this arrangement.

A number of potentially limiting features of the archaeogastropod body plan have been implicated in its subsequent abandonment by higher prosobranchs. Abalone, like most archaeogastropods, are broadcast spawners, synchronously releasing eggs or sperm (Voltzow 1994). Gametes from the single gonad pass into a duct, which opens directly into the right kidney (Purchon 1977). The gonadal arrangement of gamete delivery directly into the right kidney for subsequent broadcast dispersion has apparently prevented the archaeogastropods from developing internal fertilization strategies. Yonge (1947) suggests it is this reproductive limitation that has restricted the distribution of archaeogastropods and prevented their invasion of freshwater or terrestrial habitats.

The paired organ arrangement is not readily accommodated within the increasingly anisotropic spiraled shell used by living gastropods (Linsley 1978), perhaps favouring the loss of left-side organs. Conspicuously, however, some archaeogastropods retain the original paired organ arrangement and are still ecologically successful, notably the abalone and keyhole limpets (fissurelids). These animals are usually restricted to exposed rocky coastal areas. It could therefore be suggested that the ancestral anatomical arrangement is not specifically disadvantageous provided the animal inhabits a region of rapidly moving, highly oxygenated seawater. Attention is therefore directed towards the respiratory systems of the abalone: the gas exchange surfaces and the mechanisms of seawater ventilation and blood perfusion.

*Respiration and the cardiovascular system*

The abalone have an open vascular system, lacking defined endothelium-lined capillaries linking the venous and arterial systems, hence the tissues are bathed directly by haemolymph (e.g. Jorgensen et al. 1984, Bourne et al. 1990). The vascular system is largely composed of lacunae and capacious sinuses, as a result the haemolymph is often considered to be poorly partitioned amongst the tissues (Jorgensen et al. 1984). However, Jorgensen et al. (1984) have observed a high degree of directability in the haemolymph of *Haliotis cracherodii*, which hints at a previously undescribed level of organisation in the abalone blood system. The blood volume is believed to be large, as this is a generic feature of open circulatory systems and haemolymph is, in part, associated with hydrostatic muscle antagonist function, assisting with movement, as well as circulation (Wells and Smith 1987).

The fact that the gas exchange system is at times unable to meet the abalone's oxygen demands is reflected by the well-studied anaerobic capacity of the muscle tissues. Vertebrate muscle produces L-lactate as an end product of anaerobic glycolysis, while molluscs produce D-lactate, often in conjunction with one or more opines (usually octopamine, strombine or alanopine; Baldwin et al. 1992). In abalone D-lactate is produced along with the unusual opine tauropine, the product of a condensation reaction with taurine, catalysed by tauropine dehydrogenase (Gäde 1988, Baldwin et al. 1992). During functional anaerobiosis (i.e. exertion) tauropine production appears to predominate in the working adductor and foot muscles (Baldwin et al. 1992) while more D-lactate is accumulated during environmentally induced hypoxia (Wells and Baldwin 1995). Gäde (1988) suggests the evolution of the tauropine pathway simply reflects an exploitation of the most abundant free amino acid, this being taurine in abalone. Abalone are described as facultative anaerobes, readily switching to anaerobic metabolism when $O_2$ becomes compromised (e.g. Wasson 1984), overall anaerobic and pH buffering capacity however, is not particularly high compared to more active prosobranchs such as whelks (Wells and Baldwin 1995). Abalone lack the anaerobic pathways producing propionate and acetate from glycogen, a feature that Gäde (1988) suggests indicates relatively poor adaptation to anaerobiosis compared to many molluscs (notably mussels and oysters).

## 1.3. The Project

In the words of Depledge and Phillips (1986) "there is little information available regarding the relationships between cardiac activity, circulatory dynamics, and oxygen uptake in intact gastropods". A significant problem encountered when considering how best to address this information deficit is the rapid evolutionary radiation seen amongst gastropods, resulting in a wide range of gas exchange strategies. It is therefore difficult to select a representative model for the class. The strategy adopted by the current project has therefore been to focus attention on the ancestral trunk of the prosobranch tree. The closest extant prosobranch family to the undifferentiated ancestral Bellerophantacea are the Haliotidae. A large and accessible member of the haliotidae, the blackfoot abalone, *Haliotis iris*, was therefore selected to provide an integrated description of gas exchange and circulatory function in an evolutionary precursor to modern gastropods.

While the overt objective of the project was to describe the integrated functioning of gas exchange surfaces and haemolymph (blood) to the delivery of oxygen, the determination of the effect of the animal's state, i.e. stress and activity, was considered equally important. As an examination of the respiratory role of the haemolymph was central to the project, the adopted approach began with a determination of the quantity of circulating haemolymph. With a haemolymph volume baseline established, the effects of routine disturbance on volume were described. The gross structure of the vascular system was then examined, paying particular attention to previously undescribed features and to the supply of haemolymph to potential respiratory surfaces. Regional respirometry and haemolymph sampling were used to evaluate the contribution made by the ctenidial (gill) uptake to whole animal oxygen requirements and to locate secondary sites of gas exchange. The abalone's capacity to ventilate its respiratory surfaces and the role of external water currents were also examined. Focus was then placed on the principal organs of gas exchange, the ctenidia. Efficiency and flexibility in the ctenidial gas exchange were quantified by examining limitation and matching in the ventilation, perfusion and diffusion processes.

Studies were initially performed on the more accessible right ctenidium, with the expectation that a simple extrapolation would allow the integrated functioning of both ctenidia to be described. However, preliminary investigations revealed a radically different perfusion pattern in the left ctenidium that was dependent upon the stress level of the animal. A study of the specific perfusion of either ctenidium was therefore undertaken, with an examination of the effects of extreme stress and recovery. Lastly, cardiac function was described in conjunction with the previously acquired morphological information to establish the mechanisms used to optimise haemolymph supply to respiratory surfaces. Once again the effects of varying levels of stress and activity were considered. The project concludes with a discussion of the role played by the haemolymph in supporting gas exchange and convection and considers the reasons for the abandonment of the 'primitive' archaeogastropod features by higher gastropods.

In most animal taxa the functioning of the ancestral gas exchange systems can only be inferred from evolutionary trends, due to the extinction or rarity of living examples. The abalone therefore provide a rare opportunity to examine respiratory function in an evolutionary precursor and consider the role of limitations in the gas exchange system in driving the exceptional radiation that has resulted in the wide range of structures and strategies seen in the modern gastropods.

# Chapter 2

# Section 2.1

# Haemolymph volume, filtration rates and mixing in the abalone, *Haliotis iris* Martyn: a comparison of $^{51}$Cr-EDTA and $^{14}$C-inulin as extracellular markers

## 2.1.1. Introduction

Information on the volume of blood contained within the vascular system is essential for a full understanding of the respiratory functions of the circulation, and its haemodynamics. With the exception of cephalopods (e.g. Martin et al. 1958, O'Dor and Wells 1984), molluscs possess open vascular systems (e.g. Voltzow 1994) in which the blood (or, strictly, haemolymph) bathes the cells directly. The blood thus comprises the whole of the extracellular fluid volume (ECFV), except for stored urine and pericardial fluid. The ECFV is typically measured as the volume of distribution of an intra-vascular marker (e.g. Hickman 1972, Martin et al. 1958). The method assumes that that the marker is not metabolized and does not enter cells and, after reaching homogeneity within the vascular space, its concentration declines exponentially due to clearance via the excretory system. Thus, clearance of such a marker from the blood may also be used for simultaneous estimation of primary urine formation via ultrafiltration. A number of compounds have been employed for such measurements although the assumptions have not always been critically evaluated.

Numerous studies have examined the suitability of vertebrate glomerular filtration (GFR) markers for use in lower animals and indicate that their handling is highly variable among different taxa. For example, inulin was reabsorbed from the urine of teleost fish (Beyenbach and Kirschner 1976, Babiker et al. 1979) and crabs (Greenaway 1981). Greenway (1981) concluded that $^{51}$Cr-EDTA was preferable to $^{3}$H-inulin and $^{14}$C-PEG (polyethylene glycol) as a volume and clearance marker for the crab *Holthuisana transversa*, as it showed the least evidence of reabsorption. Babiker and Rankin (1975) also recommended $^{51}$Cr-EDTA for clearance studies in fish, due to ease of handling and counting of the isotope, despite noting that it was reabsorbed more readily than inulin.

Inulin has been used to determine ECFV and filtration rates in a number of molluscan studies (Potts 1954, Berger et al. 1978, Hodgson 1981, Jones and Kamel 1984, O'Dor and Wells 1984). In a survey of molluscan haemolymph volumes, Martin et al. (1958) compared inulin with silver proteinate, colloidal HgS, T-1824 dye and rabbit haemoglobin, concluding that inulin provided the most appropriate tool for determining ECFV as the others tended to complex with haemocytes or blood proteins. However, Taylor and Andrews (1988) estimated an inulin space somewhat larger than the $^{51}$Cr-EDTA space in the mesogastropod *Littorina littorea*, implying that the latter may be more realistic.

We have previously reported rather large changes in body mass associated with handling stress in abalone (Ragg et al. 2000). To further quantify this response, and to investigate possible involvement of the excretory system, it is therefore important to better understand the fate and kinetics of ECFV and filtration markers in this animal. The present study was devised as part of a more comprehensive investigation of the functioning of the cardio-respiratory system of the New Zealand abalone (paua) and of the consequences of clamping down to the substratum and handling disturbance in experimental and commercial operations. The objective of the current paper is to assess the suitability of two most commonly used markers, $^{51}$Cr-EDTA and $^{14}$C-inulin, and subsequently to determine a reliable protocol for the application of the preferred marker for measurement of haemolymph volume and filtration rate in *Haliotis iris*.

Primitive molluscs typically possess large, poorly mixed vascular spaces (Martin et al. 1958) and a number of authors have proposed that that the large right shell adductor muscle and foot may be functionally isolated from the main blood circuit by valves (Crofts 1929, Bourne and Redmond 1977a, Russell and Evans 1989). Hence, in addition to a sampling site in the main circulation, the present study includes a haemolymph sampling site in the adductor muscle haemocoel to examine mixing between these circuits to provide an indication of the time required for complete homogenization of the marker throughout the extracellular space.

## 2.1.2. Materials and Methods

Adult Blackfoot abalone, *Haliotis iris* Martyn 1784, of 130 – 280g live weight were collected from Banks Peninsula, South Island, New Zealand. The abalone were transported in damp air at 5ºC to a recirculating seawater facility at the University of Canterbury (salinity ~34‰, 1000 mOsm kg$^{-1}$) where they were held for at least 5 weeks prior to experimentation. The holding system and experimental chambers were maintained at 15ºC. The animals were offered a diet of artificial pellets (Adam and Amos™ AAFD) and dried seaweed (*Gracilaria* sp.) *ad libitum*. One day prior to experimentation a randomly selected animal was removed from the system, weighed following 2 minutes inversion on blotting paper, cannulated as described below, and placed in a laboratory holding system. At the end of each trial the animal was shucked and its shell weighed, flesh weight was subsequently determined by subtraction.

*Blood sampling sites*

Two blood sampling sites were selected: the right efferent ctenidial vein and the intra-muscular lacunar space of the right adductor muscle. The right efferent ctenidial vein is a large surface vessel providing access to haemolymph of the main circulation as it enters the heart. The poorly perfused lacunae of the adductor muscle were assumed to be representative of the peripheral circulation.

A diamond cutting wheel attached to a Dremel™ drill was used to cut a shell window measuring 30 x 10mm, approximately 10mm posterior to the oldest patent shell hole, revealing the right efferent ctenidial vein. The vein was cannulated using a 25gauge needle inserted into a few cm of 0.4mm i.d. nylon tubing secured to the shell. The cannula was filled with saline (0.2µm filtered seawater) to minimize occlusion by haemocyte aggregation. A large, empty *H. iris* shell with a perforation corresponding to the centre of the adductor scar was placed on top of the experimental animal to locate a standardised position in the centre of the dorsal adductor muscle. The dorsal shell surface was ground clean of epibionts and swabbed with ethanol, a sterile 2mm bit was used to penetrate the shell and create a well approximately 10mm deep in the muscle. Loose tissue was rinsed from the wound using sterile seawater and briefly dried in a filtered air stream. A Pyrex tube fitted with a removable stopper was inserted through the shell and sealed with cyanoacrylate adhesive to form a sampling well.

The animals generally appeared unperturbed by the manipulations, although a few individuals were excluded from the trial due to grazing of the mantle epithelium during window cutting. Each abalone was allowed 24h to recover and acclimate to the laboratory seawater system, following which one of 2 ECFV marker treatments was administered.

*Treatment 1: $^{51}$Cr-EDTA marker*

The experimental apparatus consisted of a circular 500 mL chamber housing the animal on a removable platform. Peristaltic pumps supplied fresh seawater at approximately 0.5 volume exchanges per hour and re-circulated water through a heat exchanger to maintain 15°C.

After 24 h acclimation $^{51}$Cr-EDTA was introduced into the vascular system. Initially a Hamilton Gastight™ syringe with a fixed 25gauge needle was inserted directly into the efferent ctenidial cannula tube and 50µl of saline and haemolymph were removed to clear the deadspace. A second syringe was used to inject 100.0 µL of $^{51}$Cr-EDTA solution (Amersham UK Ltd., 100µCi.ml$^{-1}$) over a 5-minute period, followed by the 50µl of haemolymph/saline previously removed. A Gastight syringe equipped with a fine, round-tipped needle was used to remove blood that had passively collected in the adductor well, this initial sample was discarded. Duplicate 10 µL samples of the isotope injectate were taken to determine specific radioactivity. Haemolymph samples were subsequently removed to determine radioactivity from both sites at 1h intervals for 12h; approximately 25µl were removed on each occasion from the cannula, having cleared the deadspace, and all of the pooled haemolymph from the adductor well was taken (typically 10 – 40 µL). Volumetrically accurate sub-samples, taken using calibrated Gilson™ positive displacement pipettes, were then transferred to 20ml glass liquid scintillation vials containing 6ml of filtered seawater.

The marker radioactivity in the blood samples (typically 25 µL) was determined by liquid scintillation counting (Beckman LS2800) in a medium of 6ml filtered seawater and 14ml Beckman Ready-Solv™ MP liquid scintillation cocktail. All count data were corrected for background, counter efficiency and decay.

*EDTA clearance methods*

Appearance of the radioactive marker in the chamber water was monitored by determination of mean counts per minute (CPM) of water passing through the gamma counter, over 10min intervals. Gamma counter efficiency had previously been determined by comparing the measured activity of a $^{51}$Cr-EDTA standard against that measured by a liquid scintillation counter using a known volume of the same standard. Total radioactivity within the seawater system could therefore be determined by equation 2.1.1.

$$A = \frac{A_{\gamma}.V}{V_{\gamma}.E_{LSC}} \qquad \text{Equation 2.1.1.}$$

Where $A$ is the total radioactivity (dpm) within the system water and $A_{\gamma}$ is the activity measured by the gamma counter (CPM) corrected for decay, $V$ is the total volume of water within the system, $V_{\gamma}$ is the effective counting volume of the gamma well (equivalent to 1.05ml sample in LSC) and $E_{LSC}$ is the efficiency with which the liquid scintillation counter measured the $^{51}$Cr-EDTA standard activity (14.38%).

The activity increase due to isotope lost from the animal was subsequently calculated using equation 2.1.2.

$$\Delta A = V.(x_2 - x_1) + x.F.t \qquad \text{Equation 2.1.2.}$$

Where total activity entering the water, $\Delta A$ (dpm), is calculated from the difference in total activity between adjacent sample periods, $V.(x_2 - x_1)$, $x_1$ and $x_2$ being the corresponding specific activity of the water (dpm.mL$^{-1}$); activity lost in effluent water is accommodated by the product of the mean specific activity between $x_1$ and $x_2$ (x, dpm.mL$^{-1}$), the water outflow rate, $F$ (mL.h$^{-1}$) and sample interval, $t$ (h).

Seawater samples were also assayed for radioactivity at intervals throughout these trials. It was apparent that $^{51}$Cr-EDTA was cleared from the blood at a considerably faster rate than it appeared in the medium. To determine whether substantial amounts of isotope were being sequestered, some trials were extended (up to 320 h) and the specific radioactivity of isolated tissues was also determined.

Animals selected for tissue activity analysis were shucked and rapidly dissected to provide duplicate tissue samples from the left and right kidneys, right ctenidium, right adductor muscle (dorsal region), digestive gland (central region), left hypobranchial mucous gland and foot muscle (ventro-lateral). Samples of tissue (approximately 50mg) were isolated, briefly blotted, weighed, placed in a LSC vial and digested in 2 mL of tissue solubilizer (Beckman 450) at 50°C for 24 h. About 5 drops of glacial acetic acid were added to neutralize the solution and reduce

chemoluminescence. Samples were diluted with 4 mL filtered seawater and 14 mL of scintillation cocktail. Prior to dissection, triplicate blood samples were also taken from the efferent ctenidial cannula and treated in the same way as the tissue, allowing calculation of the apparent haemolymph space.

*Treatment 2: $^{14}$C-inulin marker*

The marker $^{14}$C-inulin carboxylic acid (Amersham, UK; 1.0 µCi.mg$^{-1}$) was also used. Each animal was injected with 2mg (2 µCi) dissolved in 100µL sterile seawater. Animal manipulations and sampling methods were essentially the same as for those receiving EDTA treatment. In this series, appearance of radioactivity in the medium was monitored using a slow peristaltic pump (10 mL.h$^{-1}$) and an auto-sampler (Gilson) to advance the sampling tubes. Sub-samples (6 mL) of medium collected during each hour of the trial were then transferred to LSC vials.

Tissues were dissected to measure radioactivity. In pilot studies, animals were held for 130 – 320 h before dissection to investigate the possibility of sequestration within specific tissues. As this seemed to be minor, tissue sampling was standardised to 12h post-injection to provide an indication of haemolymph volume (ECFV) of the selected tissue. The tissue samples were solubilized as described above and the radioactivity of all samples was determined by liquid scintillation counting.

*Calculations:*
*Blood Volume, Clearance and Appearance Rates*

Haemolymph volume was estimated from the volume of distribution of the marker (after Hickman 1972). As described above, the marker (EDTA or inulin) was allowed to mix throughout the vascular system and its concentration (radioactivity) monitored by serial blood sampling. Once mixed, the method assumes that subsequent decline in haemolymph radioactivity (clearance) is due to a simple first order exponential due primarily to urine filtration. This exponential decline was used to calculate the theoretical radioactivity in the blood at the time of injection, by correcting for loss of marker during the mixing time. Thus the natural logarithm of marker concentration (dpm.µL blood$^{-1}$) was plotted against elapsed time (h) and least squares linear regressions fitted to predict the haemolymph radioactivity at time zero. The total activity of marker injected (dpm) divided by the zero-time marker concentration (dpm µL$^{-1}$) gave instantaneous volume of distribution (µL) and converted to mL.100g wet flesh mass$^{-1}$.

The slope of ln(marker activity) against time is the clearance rate constant (the fraction cleared per unit time) and is expressed here as %.d$^{-1}$. Where marker was measured in the medium, a corresponding appearance rate constant was calculated. The cumulative total radioactivity which had appeared in the seawater was calculated at each sample time, correcting for losses due to the slow seawater renewal and for sample removal. This yielded the percentage of the injectate still remaining in the animal (A`, equation 2.1.3).

$A` = 100-\{(\Sigma\Delta A/A_{Total}).100\}$ Equation 2.1.3.

Where $A_{Total}$ is the total marker activity initially injected and $\Sigma\Delta$A the cumulative total activity in the medium. The appearance rate constant was estimated as the slope obtained by linear regression of ln($A$`) against time.

*Blood composition*

After 12 h had elapsed an additional 110µl of haemolymph was taken from both the efferent ctenidial cannula and adductor well (or as much as possible). Blood osmolality was determined in10µL sub-sample and in the chamber seawater (Wescor 5200 vapour pressure osmometer). The remaining haemolymph was 10-fold diluted in concentrated nitric acid and assayed for copper by electrothermal AAS (GBC Avanta).

*Statistical analyses*

Most of the analyses performed required a simple comparison of 2 data sets to be made. Simple t-tests (paired and unpaired) proved to be adequate for this purpose.

# 2.1.3. Results

The haemolymph specific activity of both $^{14}$C-inulin and $^{51}$Cr-EDTA, following injection into the right efferent ctenidial vein and sampling from the same site, decreased steeply during the first two

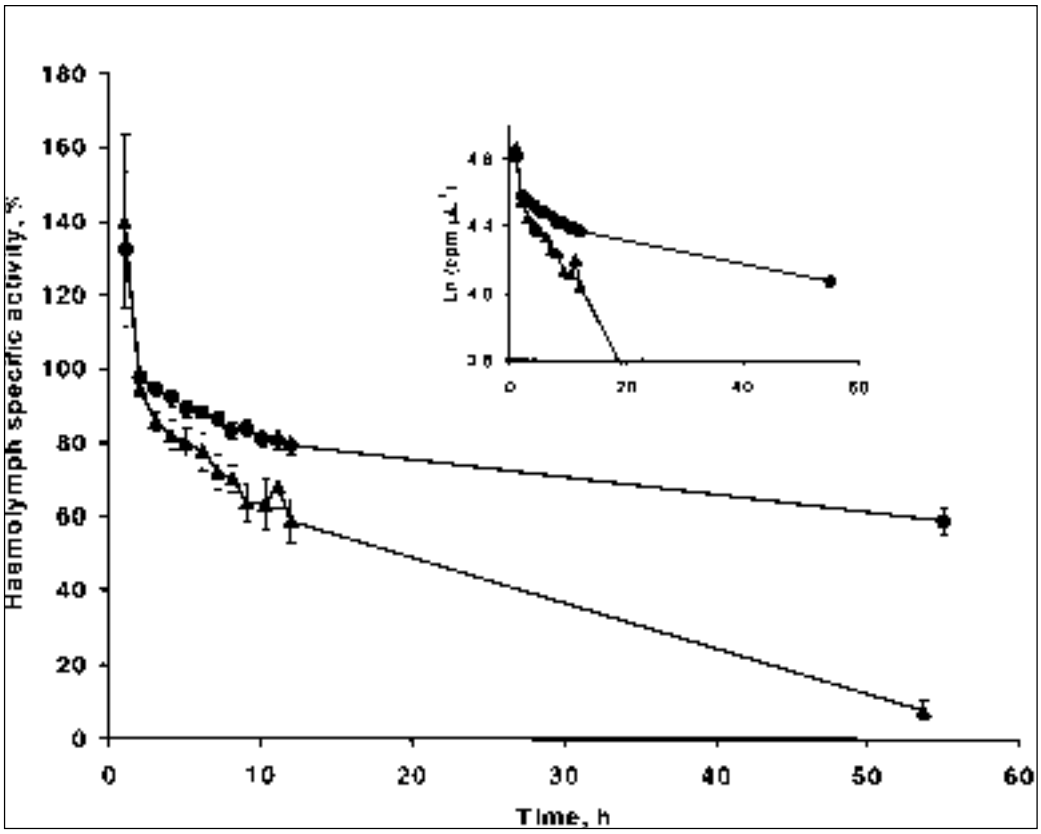


**Figure 2.1.1:** Clearance of $^{14}$C-inulin (circles) and $^{51}$Cr-EDTA (triangles) from the haemolymph. The specific radioactivity of the marker is expressed as a percentage of the radioactivity (dpm.µL$^{-1}$) at 2h (estimated individually from log-linear regression of 2 – 12h data). Values are means ± SEM; n = 9 (inulin) and 8 (EDTA) up to 12h, n = 3 and 4, respectively, thereafter.

| time interval | 1 – 2 h | 2 – 6 h | 2 – 12 h | 6 – 12 h | 12 – 120 h |
|---|---|---|---|---|---|
| Inulin clearance (%.d$^{-1}$) | 601.5 (9) | 63.3 (9) | 49.7 (9) | 46.9 (9) | 22.5 ± 1.0 (3) |
| Inulin appearance (%.d$^{-1}$) | | | 26.9 (10) | | 20.1 (4) |
| EDTA clearance (%.d$^{-1}$) | 762.8 (7) | 117.2 (7) | 107.3 (7) | 97.1 (7) | |
| EDTA appearance (%.d$^{-1}$) | | | 13.7 (7) | | |
| Inulin space (mL.100g tissue$^{-1}$) | | 55.4±3.1(9) | 57.0±3.6(9) | 57.9±4.2(9) | 72.3±8.8 (3) |
| EDTA space (mL.100g tissue$^{-1}$) | | 57.0±5.9(6) | 57.7±5.0(6) | 59.4±5.6(6) | |
| Filtration rate (mL.100g tissue$^{-1}$.d$^{-1}$) | | | 28.3 (9) | | 16.1 ± 1.2 (3) |

**Table 2.1.1:** The rate constants for clearance from the haemolymph (%.d$^{-1}$), and appearance in the sea water (%.d$^{-1}$), of $^{14}$C-inulin and $^{51}$Cr-EDTA injected into, and sampled from, the right efferent ctenidial vein, calculated for different time intervals. The volumes of distribution (mL.100g tissue$^{-1}$) of these markers (inulin and EDTA spaces) are shown for different sample periods. Filtration rates (mL.100g tissue$^{-1}$.d$^{-1}$) calculated from inulin clearance and the inulin space are shown for different intervals.

Note: The rate constants were calculated from mean values of haemolymph or seawater activity for the number of animals indicated in parenthesis (see Figures 2.1.1, 2.1.3 and 2.1.4 for SEM). Inulin and EDTA spaces and filtration rates were individually calculated and are the means ± SEM (n = number of animals).

hours (Figure 2.1.1). A slower rate of decline was recorded between 2 and 12 hours and, in the case of inulin, the clearance rate constant decreased further between 12 and 120 hours post-injection (Table 2.1.1). The behaviour of the two markers clearly differed. After 55 h, about 60% of the injected inulin remained in the circulation whereas only about 8% of the EDTA was present in the haemolymph (Figure 2.1.1).

The volumes of distribution of the two markers were estimated from the specific activities in the haemolymph at the time of injection, extrapolated from semi-log plots of blood radioactivity in the periods 2 – 12 h, 2 – 6 h, and 6 – 12 h (Table 2.1.1). These values are all quite similar and not significantly different, either between time intervals, or between markers. Although the value for the inulin space is higher in the period 12 – 120h (72.3 ± 8.8 mL.100g tissue$^{-1}$), it is similar to that for the same three animals in the 6 – 12h period (69.6 ± 6.2 mL.100g tissue$^{-1}$). The 2 – 6 h values were considered to represent the best estimates of blood volume (see Discussion) and were 55.4 ± 3.1 mL.100g tissue$^{-1}$ (n = 9) (37.7 ± 1.9 mL .100g total mass$^{-1}$) for inulin and 57.0 ± 5.9 mL.100g tissue$^{-1}$ (n = 9) (36.7 ± 4.8 mL.100g total mass$^{-1}$) for EDTA. Shell mass was 32.1 ± 1.1% of total live weight (n = 16; range 27 – 40%).

The markers appeared in the seawater at an increasing rate during the first two hours and then at a constant rate thereafter (Figure 2.1.2). The appearance rate constants for the period 2 – 12h (26.9%.d$^{-1}$ for inulin, 13.7%.d$^{-1}$ for EDTA) were lower than the corresponding clearance rate constants (substantially so in the case of EDTA) for the same animals in this interval (49.7%.d$^{-1}$ for inulin, 107.3%.d$^{-1}$ for EDTA). The difference was more pronounced for EDTA, where clearance and appearance rates differed by a factor of 8. In four animals, the appearance of inulin in the medium was monitored for 120 hours. The appearance rate constant for these animals was similar during the 2 – 12h (19.2 ± 0.6%.d$^{-1}$) and 12 – 120 periods (20.1%.d$^{-1}$) and also similar to the clearance constant in this period (Table 2.1.1).

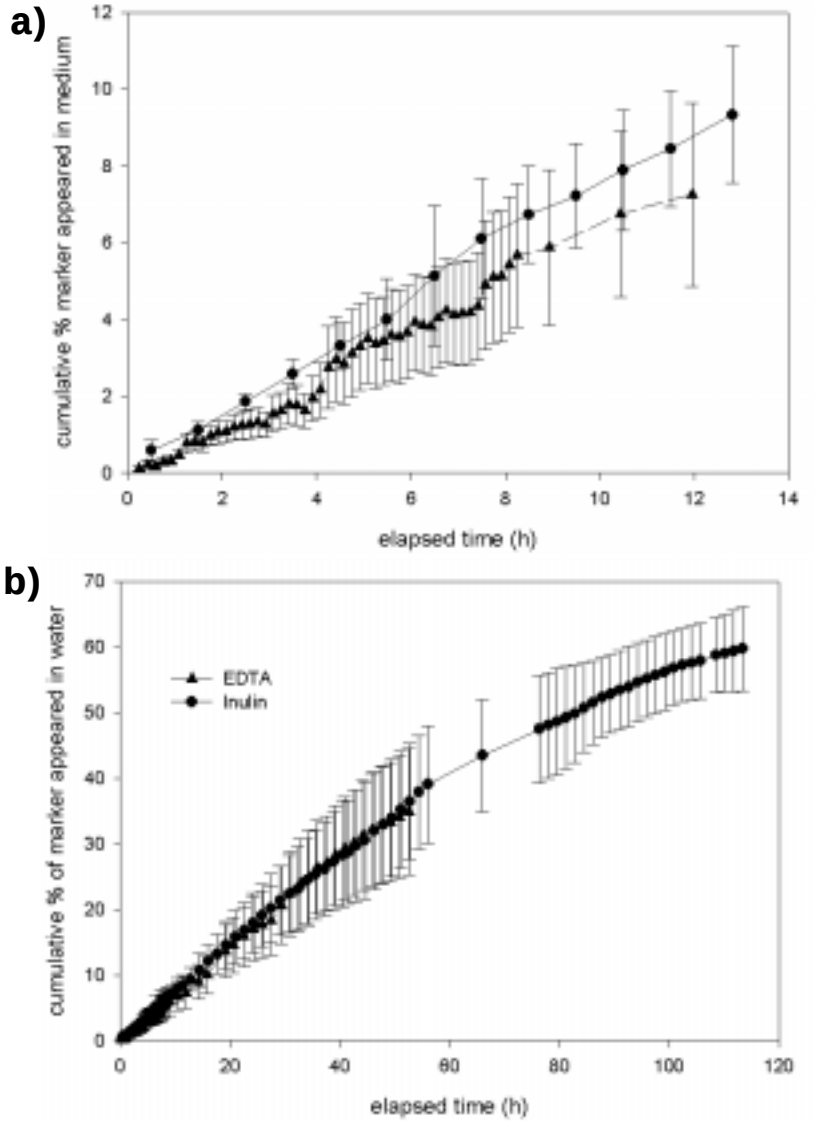


**Figure 2.1.2:** Cumulative appearance of $^{14}$C-inulin (circles) and $^{51}$Cr-EDTA (triangles) in the seawater following injection into the right efferent ctenidial vein. **a)** 0 – 12h after injection and **b)** 0 – 120h after injection. Values are percentages of the total quantity of marker injected (means ± SEM, n = 10 to 12 h, n = 4 therafter).

While the activities of the two markers in the efferent ctenidial samples decreased, their activities in adductor haemolymph samples increased, and sometimes slightly exceeded levels in the efferent ctenidial vein (Figure 2.1.4). There was no obvious difference in the time course of mixing of inulin and EDTA (figure 2.1.4). Because of marker clearance from the main circulation, the kinetics of adductor activity were complex but clearly equilibration between the two sample sites was quite slow. Over the first 6h, the fractional equilibration (1 – adductor/efferent ctenidial) approximated a first order exponential with rate constant of 32.6%.h$^{-1}$ for inulin and 38.3%.h$^{-1}$ for EDTA, corresponding to half mixing times of 2.13 h and 1.81 h, respectively.

Five of the abalones injected with inulin were sacrificed after 12h and the radioactivity of selected tissues was measured. Expressed as the inulin space relative to the haemolymph radioactivity at this time (Figure 2.1.5), this is a measure of the ECFV (haemolymph) within the tissue, but would overestimate this volume if radioisotope is taken up by the cells. The values ranged from 12 – 17 mL.100g tissue$^{-1}$ in the digestive gland, foot and adductor muscle to 60 – 70 mL.100g tissue$^{-1}$ in the two kidneys, right ctenidium and epipodium.

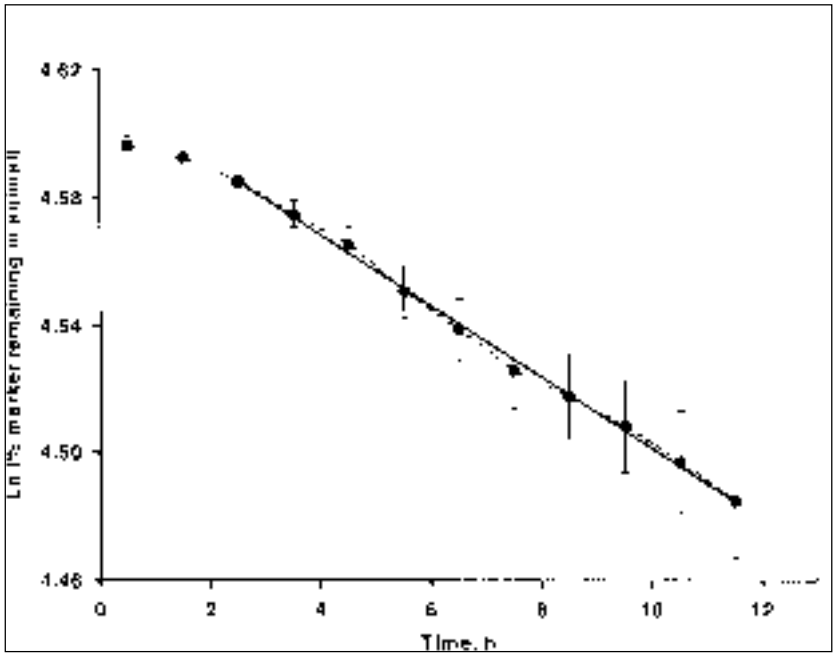


**Figure 2.1.3:** Appearance of $^{14}$C-inulin in the seawater, following injection into the efferent ctenidial vein, expressed as the percentage remaining in the animal. The regression line fitted has a slope of -0.0112 $h^{-1}$, $r^2$ = 0.997 (26.9 ± 0.5 % $d^{-1}$) (means ± SEM, n = 10).

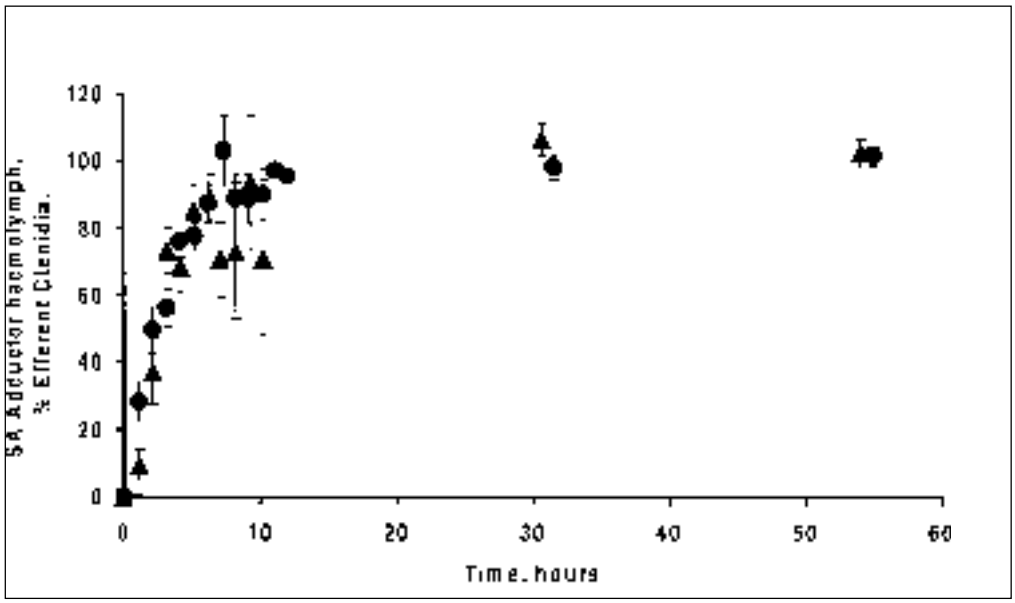


**Figure 2.1.4:** Equilibration of glomerular filtration markers ($^{14}$C-inulin = circles, $^{51}$Cr-EDTA = triangles) into lacunar haemolymph sampled from the shell adductor muscle, following injection of the marker into the right efferent ctenidial vein. The specific radioactivity in the adductor haemolymph is expressed as a percentage of the (falling) radioactivity in the efferent ctenidial haemolymph. See Figure 2.1.1 for the time course of efferent ctenidial blood activity changes and n values.

In three of the animals injected with inulin, and two injected with EDTA, tissue samples were assayed for radioactivity after much longer periods of time (80 – 320 h; Table 2.1.2). Very high values of inulin and EDTA spaces relative to the 12h-inulin values indicate that each of these tissues sequestered both markers to some degree. The highest retention was seen in the kidneys and digestive and mucous glands, particularly for EDTA. In fact, individual tissue specific activities (not shown) generally decreased between 12 and 320 h. The high values for the inulin and EDTA spaces after these times reflect the fact that haemolymph radioactivity decreased at a much higher rate than tissue radioactivity. However, EDTA radioactivity in the left kidney at 320h was double that at 80h despite a 30-fold decrease in blood levels.

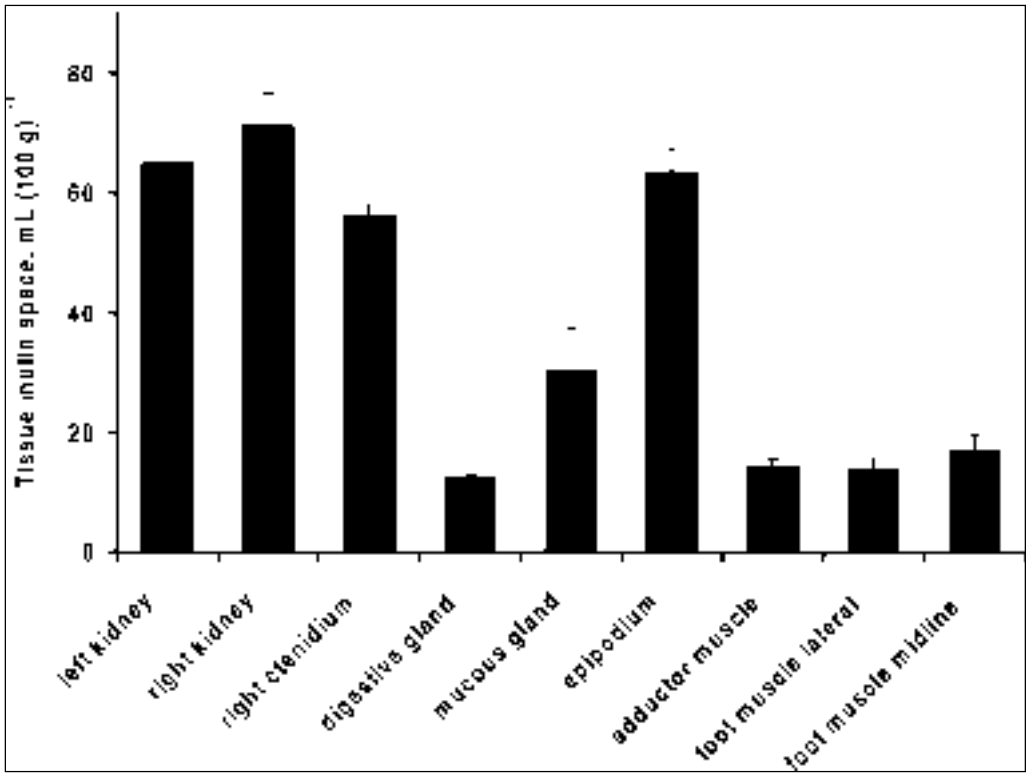


**Figure 2.1.5:** Inulin space, (mL.100g tissue$^{-1}$), estimating ECFV, of selected abalone tissues, calculated from the specific radioactivity of the tissues relative to that of the blood 12h after efferent ctenidial injection of $^{14}$C-inulin (means ± SEM, n = 5).

The osmolality and concentration of copper (indicating haemocyanin) were measured in paired samples of efferent ctenidial and adductor haemolymph, obtained more than 12h after isotope injection. The efferent ctenidial haemolymph (976 ± 7 mmol kg$^{-1}$) was slightly, but significantly, hyposmotic to adductor blood (1015 ± 5 mmol.kg$^{-1}$; $t_{0.05,\ 13df} = -4.94$, $p < 0.001$) although, as shown above, marker concentrations fully equilibrated between these sites. Efferent ctenidial haemolymph was also significantly hyposmotic to the surrounding sea water (1024 ± 4 mmol.kg$^{-1}$; $t_{0.05,\ 15df} = 7.89$, $p < 0.001$), whereas the adductor haemolymph was isosmotic to seawater ($t_{0.05,\ 13df} = 1.56$, $p = 0.07$). Conversely, the copper concentration in haemolymph from the efferent ctenidial site (32.1 ±3.3mg.l$^{-1}$) was only about two thirds that of the adductor haemolymph (22.0 ±3.9 mg l$^{-1}$; $t_{0.05,\ 17df} = 2.86$, $p = 0.005$).

# 2.1.4. Discussion

*Suitability of the markers*

A principal aim of the current study was the assessment of the suitability of $^{51}$Cr-EDTA and $^{14}$C-inulin as volume and clearance markers in the large, slow-mixing vascular system of *Haliotis iris*. Both radioactive markers were developed as glomerular filtration rate (GFR) markers for use in the study of human renal pathology, but have also frequently been utilized for similar purposes in animals. As the requirements of a good GFR and blood volume marker are essentially the same (non-toxic, stable, not sequestered by tissues, removed from the blood by filtration only), it is not surprising that proven GFR markers are frequently used to assess blood volume. Numerous studies

| Marker | Time post-injection, h | Volume of distribution of marker in tissue relative to haemolymph, mL.100g tissue$^{-1}$ | | | | | | |
|---|---|---|---|---|---|---|---|---|
| | | left kidney | right kidney | digestive gland | mucus gland | right ctenidium | adductor muscle | foot muscle |
| **$^{51}$Cr-EDTA** | 80 | 602 | 6873 | 10 | 74 | 82 | 16 | 1 |
| | 320 | 41082 | 136225 | 949 | 1191 | 182 | 583 | 405 |
| **$^{14}$C-Inulin** | 130 | 142 | 174 | 162 | 50 | 60 | 25 | 25 |
| | 145 | 93 | 116 | 35 | 51 | 79 | 32 | 25 |
| | 320 | 524 | 656 | 615 | 747 | 356 | 48 | 78 |

**Table 2.1.2:** The volumes of distribution of $^{51}$Cr-EDTA and $^{14}$C-inulin in selected tissues of *Haliotis iris* 80 – 320 hours after injection into the right efferent ctenidial vein. Each row represents values from a single animal relative to the haemolymph activity at the same time, standardised by wet tissue mass.

have compared the suitability of GFR markers for use in lower animals, the conclusions are, however, highly variable between taxa. Inulin has been shown to be re-absorbed from the urine of teleost fish (Beyenbach and Kirschner 1976, Babiker et al. 1979) and crabs (Greenaway 1981), suggesting that it may be an unsuitable GFR, and possibly ECFV marker in these groups. The use of $^{51}$Cr-EDTA as an alternative to inulin has been recommended in the crab *Holthuisana transversa*, as it showed no evidence of re-absorption (Greenaway 1981), and also for measuring renal clearance in fish (Babiker and Rankin 1975).

In molluscs, inulin has long been used to determine ECFV and haemolymph clearance rate (e.g. Potts 1954). In their base-line survey of molluscan haemolymph volumes, Martin et al. (1958) compared inulin space to silver proteinate, colloidal HgS, T-1824 dye and rabbit haemoglobin, ultimately suggesting that inulin provided the most appropriate tool for determining ECFV as the remainder tended to complex in some way with haemocytes or blood proteins. Inulin space, usually measured using a $^{3}$H- or $^{14}$C- radiolabel, has subsequently represented the standard measure of molluscan ECFV (e.g. Berger et al. 1978, Hodgson 1981, Jones and Kamel 1984, O'Dor and Wells 1984).

More recently, Taylor and Andrews (1988) utilized $^{51}$Cr-EDTA to estimate ECFV and clearance in the mesogastropod *Littorina littorea*. Taylor and Andrews also compared their ECFV estimates to inulin space in a subset of animals, finding inulin space to be approximately 23% larger than EDTA. The difference was not significant due to large variability in the inulin data. In contrast, the results of the present study give a calculated $^{14}$C-inulin space of 55.4 ±3.1% of wet tissue, slightly lower than the 57.0 ±5.9% for $^{51}$Cr-EDTA. $^{51}$Cr-EDTA was also cleared from the abalone haemolymph at a significantly faster rate than $^{14}$C-inulin (107.3%.d$^{-1}$ and 49.7%.d$^{-1}$, respectively). For both markers, however, the rate of appearance in the medium was significantly lower than the corresponding clearance from the haemolymph. It seems likely that some of the marker enters another pool, in addition to the extracellular fluid and chamber water, rather than appearance simply lagging behind clearance from the blood.

The possibility that the marker could be entering an intracellular pool was investigated by examining tissue activity 3 – 13d after injection. In the 3 inulin-treated animals examined all blood and tissue activity approached background. The 2 EDTA-treated animals, however, showed evidence of accumulation within the left and, particularly, right kidney (Table 2.1.2). If wet tissue weight fractions of 0.4% * for the right kidney and 0.3% for the left (D. Just, personal communication) are assumed, approximately 6% of injected $^{51}$Cr-EDTA remained in the right kidney of an animal dissected after 80h and 4.3% after 320h, while 0.4% was found in the left kidney at 80h and 1% at 320h. There is also evidence for tissue sequestration of $^{51}$Cr-EDTA in Tilapia, notably in the head kidney (Babiker et al. 1979).

As $^{14}$C-inulin clearance rate is constant between measurements taken 2 – 6h after injection and there is little apparent sequestration of the marker by tissues, it is suggested that the haemolymph volume estimate of 55.4% of wet tissue is a reliable value. Large haemolymph volumes are characteristic of molluscs with open circulation, and an inulin space of 55% is in fact fairly modest compared to those determined for other prosobranchs. Jones and Trueman (1970) record a mean inulin space of 65.7% for the archaeogastropod *Patella vulgata*, Little (1967) 64.6% for *Strombus gigas*, Jones and Kamel (1984) 61.7% for *Littorina littorea*. The inulin space of *H. iris* corresponds more closely to an approximate volume of 44% calculated from the data of Taylor and Andrews (1988) for *L. littorea*. Similar ECFV are typically recorded in bivalves (Harrison et al. 1958, Hodgson 1981, see Jones 1983 for review). It has been suggested that inulin space also includes the coelomic spaces of the pericardial fluid and urocoel of the kidneys (Potts 1954; Taylor and Andrews 1988), which Martin et al. (1958) suggest constitutes about 8.5% of the inulin space, determined by comparing inulin and silver proteinate spaces in *Aplysia*. However, unless reflux of inulin to the haemolymph occurs, the coelom is technically a pool external to the blood and will not affect blood volume determined by marker dilution corrected for clearance.

It is clear from the inulin space data presented in figure 2.1.5 and the microsphere distribution data of Jorgensen et al. (1984) that the highly vascularised tissues (the kidneys, gills and epipodium) represent a fairly small proportion of the abalone's soft tissues. Conversely, the massive muscle blocks that account for approximately 66% of the tissue mass have a low resident haemolymph volume (Jorgensen et al. 1984). Where, then, is the large haemolymph volume distributed? Numerous authors (e.g. Crofts 1929, Bourne and Redmond 1977a, Jorgensen et al. 1984) have described the large haemal spaces of the arterial and venous cephalic sinuses. In *H. iris* the cephalopedal venous sinus has been shown to extend posteriorly into a capacious sinus system that envelopes the entire alimentary tract (chapter 3 of this thesis). It is suggested that these extensive sinuses account for much of the haemolymph volume and the slow rate of mixing in the system. The gut sinuses are apparently absent in other abalone species that have received detailed morphological studies (e.g.

*Note that the right kidney is effectively impossible to isolate from its intimate association with the digestive system (Crofts, 1929) and organ weights are therefore approximate. If the value of 0.9 ±0.1% of tissue weight, proposed by Jorgensen et al. (1984) were used, the amount of marker retained by the whole organ would be more than double the values proposed above.

*H. tuberculata*: Crofts 1929, *H. corrugata*: Bourne and Redmond 1977a, *H. ruber*: Russell and Evans 1989). It may be that other Haliotids therefore have smaller haemolymph volumes and/or faster rates of mixing. This suggestion could form the basis of an interesting comparative study that would help to elucidate physiological radiation in the Haliotidae.

A large haemolymph volume may provide the abalone with a number of advantages. Martin et al. (1958) suggest that large blood volume may be an energetically inexpensive means to increase bulk on a low value diet, reducing vulnerability to predators; the suggestion is corroborated by the even larger blood volumes found in the shell-less, inherently more vulnerable opisthobranchs. Noting the reverse Bohr shift and negative Root effect displayed by abalone haemocyanin, allowing oxygen saturation to be maintained at lower pH, Wells et al. (1998) suggest that the haemolymph may be better described as an oxygen storage rather than delivery system, protecting more metabolically sensitive tissues from anoxia. A large volume would complement such a storage function. The haemocoel of molluscs has also been associated with structural support and movement (e.g. Hodgson 1981, Trueman and Brown 1985), additional volume reserves may therefore allow these functions to continue during times of activity while maintaining normal circulatory function. Taylor and Andrews (1988) discuss the large haemolymph volume in osmoconforming marine gastropods acts as a buffer against excessive solute flux during acute osmotic stress. Their results also indicate that the intra-, rather than extra-cellular fluid volume increases during hypo-osmotic shock, leading to the suggestion that large vascular spaces reduce the risk of circulatory blockage due to tissue swelling. Molluscs also lack blood clotting factors (Armstrong et al. 1971, Hodgson 1981, Taylor et al. 1994), relying on local muscular action and haemocytes to plug wounds, the amount of blood lost before such mechanisms can take affect may be considerable, hence a large blood volume would be advantageous.

*Clearance and Urine Production*

As discussed above, neither $^{14}$C-inulin nor $^{51}$Cr-EDTA behaves as an ideal filtration marker, as both appear in the medium at a slower rate than they are cleared from the haemolymph. The rates of appearance of inulin and EDTA in the medium, however, are not significantly different, despite the difference in molecule size (MW $^{14}$C-inulin = 5175Da, $^{51}$Cr-EDTA = 362Da), suggesting that appearance of either marker may approximate urine production. Extreme caution should be exercised when using marker clearance or appearance to estimate urine flow. Although most filtration is assumed to occur in the auricles of archaeogastropods, resulting in primary urine that is ultimately voided from the kidneys (Andrews 1985), Simkiss and Wilbur (1977) have shown that large molecules, including $^{14}$C-inulin, can readily pass from the haemolymph directly across the molluscan epidermis. Thus 8.7% of injected inulin appearing in the mucus trail of *Helix* within 1.5h; fluorescein, with a similar molecular weight to EDTA, behaved similarly. Reciprocally, the same authors also found *uptake* of inulin across the foot epidermis. Without direct sampling of the urine it is also not possible to determine whether re-absorption or secretion of a marker occurred (Harrison 1962; Beyenbach and Kirschner 1976). Although it therefore seems inappropriate to estimate urine

production, it should be noted that the haemolymph clearance of 49.7 ml.100g$^{-1}$.d$^{-1}$, calculated from $^{14}$C-inulin clearance (2 – 12h) and volume of distribution, corresponds well to the urine production rate of 14 – 50ml.100g$^{-1}$.d$^{-1}$ measured directly in *Haliotis rufescens* (Harrison 1962).

*Blood Mixing and Heterogeneity*

Most published work dealing with blood volume markers mentions the need to ensure the marker is fully mixed throughout the vascular space before volume of distribution can be used as an estimate of blood volume. Typically a marker is injected and an arbitrary mixing time allowed before a single blood sample is taken or, alternatively, sequential blood samples are taken, as here, to determine when clearance rate becomes constant, implying dilution has ceased. No study was found that included blood samples from the peripheral vasculature to determine absolute mixing time within the blood. The right adductor muscle was selected as a peripheral site as several authors have suggested the adductor of abalone contains no haemolymph, with all interstitial space occupied by collagen connective tissue (Trueman and Brown 1985, Frescura and Hodgson 1992, Olaechea et al. 1993). However, Crofts (1929) describes a 'shell muscle artery' arising from the anterior aorta to supply the muscle. Sparsely distributed arterioles have also been found in adductor muscle transverse sections (personal observation), leading to the attempt at blood collection by passive pooling. The marker mixing rates determined in this way showed that, although fairly constant clearance from the efferent ctenidial blood is achieved in <2h, implying a fully mixed pool, it actually takes approximately 2h for the adductor haemolymph to reach half the marker concentration of the main circulation. While the haemolymph sampled from the adductor well was collected over a 1h period, resulting in a slight over-estimate of mixing time, it is clear that at least 7 – 9h should be allowed for complete marker homogenization (figure 2.1.4). In contrast, Harrison (1962) has found that the additional extracellular pools of the pericardial fluid and urine reach equilibrium with inulin in the main circulation within 1h. The error in clearance and blood volume estimates as a result of incomplete mixing with the adductor haemolymph is presumably small, as the adductor haemolymph volume is small. More substantial errors may arise if adductor mixing is representative of all the peripheral lacunar beds of *H. iris*, which may contain a far larger fraction of the circulating haemolymph. Bourne and Redmond document peripheral resistance 'an order of magnitude higher than those found in mammals' in *H. corrugata* (1977b) and systolic aortic pressures <8cm $H_2O$ (1977a). Jones (1983) attributes the long circulation time, and hence slow mixing, of mollusc haemolymph to this combined influence of low vascular pressure and high resistance of the lacunar beds.

Homogenous distribution of the marker between the main circulation and the adductor lacunae was eventually achieved and subsequently sustained (figure 2.1.4). This was considered to be a suitable demonstration that the same pool was being sampled at both sites. However, consistent compositional changes were noted between the adductor and efferent ctenidial haemolymph. Post-branchial haemolymph was hyposmotic while adductor muscle haemolymph was isosmotic with the surrounding seawater. The latter observation is unremarkable in an osmoconforming marine

organism, however the maintenance of lowered osmotic pressure in the post-branchial haemolymph warrants investigation. As no osmolyte concentrations were measured in the current study, reasons for the reduced osmolality are highly speculative. Haemolymph in the right efferent ctenidial vein will have recently passed through both the right kidney and the right gill (Crofts, 1929), either organ may be associated with the active removal of osmolytes for excretion against a concentration gradient (Little 1981), resulting in the observed 5% drop in haemolymph osmolality.

Haemocyanin concentration differed markedly between the sample sites, adductor haemolymph containing an average of 20% less pigment than the post-branchial blood. The possibility that the adductor well sampled fluid from a different pool or resulted in contamination was rejected as no corresponding difference in marker concentration was observed. It is possible that the observations are an artifact of different sampling procedures used at either site. Some tissue damage was inherent to the creation of an adductor well, hence the initial wound healing process of amoebocyte plugging (Armstrong et al. 1971, Taylor et al. 1994) could serve as a partial filtration barrier to the large haemocyanin molecules. However, no time dependency in adductor haemocyanin levels was observed, surprising if a filtering cell plug was developing. Mangum (1979) measured the haemocyanin concentration of haemolymph from the pedal vein, kidney and afferent ctenidial vein of the conch *Busycon*. She observed a stable 10-fold dilution of haemocyanin in the foot of the resting animal. The dilution is attributed to the uptake of seawater into the haemocoel of the foot, allowing it to attain a larger volume than that permitted by the shell during retraction; a haemolymph concentration site is implicit to this hypothesis, possibly occurring in the kidney (Mangum, 1979). Although less dramatic heterogeneity in haemocyanin concentration was observed in the current investigation, the possibility that the haemolymph could be regionally diluted and concentrated remains an intriguing possibility.

*Haemolymph Content of Tissues*

As tissues of *H. iris* showed minimal sequestration of inulin after 130 – 320h (Table 2.1.2), it is suggested that the inulin space of tissues excised after 12h (figure 2.1.5) is representative of haemolymph content. The right and left kidneys have the largest specific haemolymph content (71.2 and 65ml.100g tissue$^{-1}$ respectively), in *H. cracherodii* these tissues are also the most metabolically active and receive the highest haemolymph flow (Jorgensen et al. 1984). When compared to corresponding tissue haemolymph flows measured by Jorgensen et al., the kidneys and foot would receive approximately one volume exchange per minute, while the digestive gland, despite having a low resident volume (12.5ml.100g$^{-1}$) possesses a well-defined network of capillary-like vessels (Crofts, 1929) supplying approximately 4 volume exchanges per minute. The haemolymph-rich epipodium (63.6ml.100g$^{-1}$, present study) however only receives 18ml.100g$^{-1}$.min$^{-1}$ in *H. cracherodii*.

*Application of the Kinetic Method for Blood Volume Determination*

As discussed above, the kinetic method for determining haemolymph volume from sequential samples after inulin injection appears to reliably determine ECFV in *H. iris*. Three distinct phases were seen in marker dilution in the haemolymph. The first occurred within the first 2h after injection, and relates to initial mixing in the main circulation. The second phase, typically occurring between 2 and 6h represents the combined effects of mixing into the peripheral vasculature and clearance. The third stage (>6h) represents clearance alone and, perhaps, tissue sequestration. Although the marker kinetics during the intermediate (2 – 6h) phase are complex, the net effect is to produce a simple exponential dilution of the isotope. This period was chosen to extrapolate to determine instantaneous volume of distribution as clearance was constant and a relatively short period had elapsed since injection, minimising errors due to fluctuations in clearance rate and tissue sequestration.

A more important cause of variability between haemolymph volume estimates relates to the standardization by flesh weight. Flesh weight, independent of absolute haemolymph volume, will vary due to gonad condition, gut content and water trapped in the pallial cavity, possibly explaining some of the variability in $^{14}$C-inulin space. The reciprocal is also possible, that blood volume under constant environmental conditions may vary; the hypothesis that activity state and manipulation may affect blood volume are the subject of a subsequent study (see chapter 2, part 2).

# Section 2.2

# Haemolymph volume, clearance and mixing in the abalone, *Haliotis iris* Martyn – Effects of shell clamping and handling

## 2.2.1. Introduction

Due to their abundance and size, members of the archaeogastropod family Haliotidae, the abalone, represent an unusually accessible group in which to study the vascular arrangement and function of primitive gastropods. Before interpreting the results of such investigations however, it is essential to obtain an understanding of the effects of the animals' own responses to disturbance and manipulation.

In the past, studies dealing with the effects of handling upon shellfish species have tended to consider the implications of the temporary environmental changes associated with handling rather than the effects of the manipulation itself. The exceptions have been situations where obvious physical damage is incurred by the exoskeleton (Spencer et al., 1992; Jakob and Wang, 1994; Zhou and Shirley, 1995). In aquatic organisms the most obvious environmental change associated with handling is emersion, the direct effects upon the organism may be investigated, for example Ryder et al. (1994) and Wells and Baldwin (1995) specifically examine the metabolic responses of *Haliotis iris*. Alternatively, the indirect effects of emersion, resulting from behavioural responses to air exposure, such as valve closure in bivalves (e.g. Spencer et al., 1992; Jones et al., 1993; Waller et al., 1995) may be considered.

Repeated handling (removal from tank surface and 30s emersion to drain the branchial chamber) of an abalone has been shown to induce weight loss, which is slowly recovered over a period of hours/days (Ragg et al. 2000). An increase in haemocyanin concentration also associated with handling (Behrens 1999), combined with a calculated haemolymph content of >50% of wet tissue mass (section 2.1 of this thesis) implies that at least some of the weight reduction may be due to fluid loss from the haemolymph. As some degree of manipulation is inherently associated with laboratory investigations concerning abalone, an understanding of the effects of handling upon the animal seems essential.

The primary escape response of most prosobranch molluscs is to retreat within their shell. There is evidence that haemolymph may be lost in the process of this retraction in several prosobranchs, notably the large marine species *Busycon carica* and *Polinices duplicatus* (Mangum 1979) and pulmonate snails, which possess a specialized haemal pore for the purpose (Lever and Bekius 1965, Martin 1983). In *Littorina* sp. a circulatory bypass is opened through the nephridial gland when retraction commences, allowing haemolymph to flow directly to the rectal sinus, avoiding the main circulation (Andrews and Taylor 1988). The sinus terminates in a muscular papilla which possesses an opening, allowing haemolymph venting in some littorinids (Fretter 1982 cited in Andrews and Taylor 1988), or a weak zone that is easily ruptured in *L. littorea* (Andrews and Taylor 1988). If pressure surges are insufficient to cause venting, haemolymph is retained in the compliant rectal sinus until the snail re-emerges (Andrews and Taylor 1988). Whilst the above examples are associated with the retraction of a large, everted foot into a limited cavity within a helical shell, there has been no examination of the corresponding action in abalone. Abalone (auriform shell) and limpets (patelliform shell) possess a low profile, wide aperture shell in which most or all helical coiling has disappeared. The primary escape mechanism in these molluscs is therefore a clamp rather than a retraction, whereby the shell is pulled onto a hard substrate by contraction of the right adductor muscle. As with helical snails, all soft body parts must be accommodated within the shell, complicated by the need to maintain a very high tenacity adhesion to the substrate (e.g. Smith 1991). The acute effects of clamping upon abalone blood pressure have been described (Trueman and Brown 1985) and possible shunting of blood to by-pass the pedal system in this state has been the subject of speculation (Crofts 1929, Russell and Evans 1989, Wells et al. 1998).

Using the techniques established in section 2.1, the present study aims to further examine the effects of a clamped state upon vascular function by determining whether circulating haemolymph volume and concentration is effected and whether perfusion of the contracted adductor muscle is compromised. The large right adductor muscle of *Haliotis* has been considered to contain no vascular space whatsoever (Trueman and Brown 1985, Frescura and Hodgson 1992, Olaechea et al. 1993); however, Ragg et al. (2000) and Jorgensen et al. (1984) show that a small, slowly exchanging haemolymph pool does exist in this muscle, and an afferent artery is identified by Crofts (1929). The abalone adductor tissue is known to have limited scope for aerobic metabolism, rapidly employing anaerobic pathways during acute exercise (Wells et al. 1998, Donovan et al. 1999). The extent to which aerobic metabolism and the supply of anaerobic substrates are supported by the haemolymph is not known; the first step in establishing the involvement of the haemolymph is the determination of the extent to which activity affects haemolymph exchange in the working muscle. Hence mixing rates between the main circulation and the lacunar tissue of the right adductor muscle are also quantified in animals in a ‘resting’, ‘clamped’ or ‘handled’ state.

The glomerular filtration rate (GFR) marker $^{14}$C-inulin is used here to determine haemolymph volume in *Haliotis iris* (Martyn). Volume and mixing rate in animals under *steady* clamp or handled conditions are compared to corresponding values from the resting animal. The extent to which haemolymph volume changes might be associated with dilution and concentration of the haemolymph is also examined, by monitoring haemocyanin as well as inulin concentration.

## 2.2.2. Methods

Adult *H. iris* (300 - 430g live weight) were collected from Banks Peninsula, South Island New Zealand in June 1999 and transported in air at 5°C to the Pendarves Abalone Farm, Rakaia, New Zealand. Animals were acclimated to a tank environment of fast-flowing seawater 15 ±1°C, 1000mOsm.kg$^{-1}$ and fed Adam & Amos AAFD artificial abalone diet for a minimum of 5 months prior to experimental manipulation. All experiments were performed at the University of Canterbury.

Haemolymph volume, clearance and mixing were determined by monitoring changes in the concentration of an intra-vascular marker. Following baseline studies carried out to establish a suitable protocol for determining these parameters in *H. iris* (section 2.1 of this thesis), $^{14}$C-carboxylic acid inulin (Amersham UK, 1.0µCi.mg$^{-1}$) was selected as the marker. Co-identity between $^{14}$C-inulin space and extra-cellular fluid volume (ECFV) was assumed. Baseline haemolymph parameters were established following isotope injection into the resting animal and subsequently re-assessed using a second marker injection when the animal was deemed to be in a new steady state resulting from handling or clamping.

*Handling Treatment*

Previous results (Behrens 1999, Ragg et al. 2000) have suggested that *H. iris* repeatedly handled at 10min intervals lost weight and that a stable, lower weight was maintained if the handling increment was then increased to 30min. As reliable interpretation of volume of distribution results requires a stable ECFV, a handling protocol was designed to attain the steady-state weight.

The animal was removed from its chamber, attachment to the removable platform was gently broken using a thin plastic spatula and external water drained by holding the abalone head-down. When no further fluid was seen to drip from the animal, it was weighed and returned to the chamber; emersion time was usually <45s. The animal was handled in this way at 10min intervals for 1h; the interval was then increased to 30min. After 2h the animal was assumed to have reached a stable weight and the second $^{14}$C-inulin injection was administered, as described below. Continued handling at 30min intervals was used to maintain the reduced weight level.

*Clamping Treatment*

As no data were available linking weight change and clamping activity in abalone, an initial weight trial preceded the haemolymph volume/clearance experiments. Ten randomly selected animals were placed in individual 1.0L containers receiving fresh seawater. Five of the animals were induced to clamp to the container floor by applying gentle manual torsion to the shell. The stimulus to clamp was reinforced at 10min intervals for 60min and then and 30min intervals for a further 11h. All animals (5 treatment, 5 control) were weighed within their drained containers at 2h intervals, in each case the chamber was tilted for 45s allowing water to drain anteriorly from the branchial chamber.

The simple weight trial revealed that a reduced, stable flesh weight was attained after 2h of induced clamping (figure 2.2.1.). A similar protocol was therefore applied to *H. iris* receiving marker injections. To standardize the rather arbitrary application of torque, a modified electrical screwdriver was used. The screwdriver fitted an improvised bayonet mounting adhered to the central, dorsal shell surface (slightly posterior to the adductor well site) and was used to apply a constant, gentle torque. By reversing polarity of the DC power supply, stimulus to clamp was re-enforced by reversing the direction of torque. As with the initial weight trial, the stimulus was applied at 10min intervals for the first hour, then maintained at 30min intervals. Animals were weighed before and after 12h of treatment.

At the end of each trial the animal was shucked, re-weighed and the shell weighed, allowing flesh weight to be calculated. The undisturbed flesh weight was used to standardize all measured haemolymph parameters.

The techniques used in the present study are essentially those established in section 2.1 for use with quiescent abalone. However, certain modifications were necessary to allow a re-estimation of haemolymph parameters following a second isotope injection and the cannulation arrangement was modified to accommodate movement of the mantle with respect to the shell around the cannulation site. Briefly:

Each animal was prepared by cutting a small, triangular window of approximately 10mm side length 30mm posterior to the last patent shell hole, exposing the right efferent ctenidial vein. The vein was cannulated by using a 23gauge needle to create a puncture into which 0.4mm i.d. nylon tubing was fed; after approximately 10mm had entered the vein lumen, the cannula tube was glued to the shell and filled with sterile saline. A second haemolymph sampling site was created by drilling through the dorsal shell into the right adductor muscle to a depth of 10mm using a sterilized 2mm bit. A glass tube fitted with a removable stopper was glued to the shell using cyanoacrylate adhesive to seal the adductor sampling well.

Following cannulation, animals were acclimated to an experimental system for 48h; the system consisted of a round, 15ºC water-jacketed, 500ml chamber housing the animal on a removable platform, supplied with fresh seawater at 250mL.h$^{-1}$. Twenty five microlitres of haemolymph were drawn to clear deadspace in the cannula (typically <10ml) and 100ml (~2mCi) of $^{14}$C-carboxylic acid inulin dissolved in sterile seawater containing 0.3% amaranth dye were injected over 7min, followed by the 25ml of deadspace haemolymph and 25ml of clearing “saline” (= 0.2mm-filtered seawater; this technique was used to ensure the cannula remained patent after every haemolymph removal). Animals that showed evidence of amaranth leakage were discarded from the data set. Two 10ml sub-samples of the injectate were mixed with 2ml of saline and 1ml of Beckman biodegradable counting scintillant and specific radioactivity measured in a Beckman LS2800 liquid scintillation counter (LSC). Efferent ctenidial haemolymph samples (25ml) were subsequently removed at 2h intervals for 12h. During each interval 5-50ml of haemolymph typically drained passively into the adductor well, this was also collected. Volumetric accuracy was ensured by sub-sampling haemolymph samples using calibrated Gilson™ positive-displacement micropipettes.

The results presented in section 2.1 showed an initial period of rapid marker dilution in the haemolymph, lasting for 1 – 2h. After 2h the dilution settled into a simple exponential that represented clearance to the urine and slow mixing into the small haemolymph pool represented by the adductor lacunae. The ECFV was therefore estimated as the instantaneous volume of distribution of $^{14}$C-inulin, calculated by linear extrapolation to zero (= injection) time of the partial logarithmic relationship between specific efferent ctenidial haemolymph activity and time from samples taken 2 – 12h after injection. Total activity injected was divided by instantaneous specific activity to give volume of distribution. The log-linear gradient of the exponential decline in marker activity was taken to be the clearance rate constant. As doubts have been raised concerning incomplete mixing of the marker within the main vasculature within 2h of injection (Martin et al. 1958; section 2.1 of this thesis), only the 4 – 12h samples were used for volume of distribution and clearance determination.

Rate of mixing between the main vasculature and the peripheral lacunae of the adductor muscle was quantified using the half-time of mixing constant, described in section 2.1. Adductor haemolymph activity was expressed as a percentage of the corresponding efferent ctenidial haemolymph activity in what was assumed to be an asymptotic convergence. The half-time of mixing constant is the calculated time taken for adductor activity to reach 50% of efferent ctenidial activity.

*Haemolymph Volume, Mixing and Clearance during Clamping or Handling*

One day after the initial marker injection the animal was weighed in its drained container (to minimize disturbance). A blood sample was taken from the efferent ctenidial cannula and the animal subsequently subjected to 2h of clamping or handling treatment. A further efferent ctenidial haemolymph sample was taken to determine residual activity due to the first injection, $A_F$ (dpm.µl$^{-1}$), and a second $^{14}$C-inulin dose injected in the same way as the first. Clamping or handling was sustained, as described below, during a 12h period. Two-hourly haemolymph samples were again used to determine clearance and mixing time; instantaneous volume of distribution was determined after correction for marker present from the first injection (equation 2.2.1.).

$$V_{Clamp} \text{ or } V_{Handled} = \frac{A`_{Inst} - A_F}{A`_{Total}} \qquad \text{Equation 2.2.1}$$

Where $V_{Clamp}$ or $V_{Handled}$ is the instantaneous volume of distribution of $^{14}$C-inulin in a clamped or handled animal (µl) and $A`_{Inst}$ is the calculated instantaneous specific activity in the efferent ctenidial haemolymph sample at the time of second marker injection and $A`_{Total}$ is the total activity of the second injectate (dpm µl$^{-1}$).

*Haemoconcentration*

The possibility that haemocyanin or $^{14}$C-inulin might be concentrated as a result of handling or clamping was investigated by comparing haemolymph samples taken immediately before and after

the initial 2h of treatment. Haemocyanin concentration was estimated from copper, all of which was assumed to be bound to haemocyanin (Ellerton and Lankovsky 1983). Copper concentration was measured by taking duplicate 10µl sub-sample of efferent ctenidial haemolymph. Haemolymph copper was determined by an electrothermal atomic absorption spectrophotmetric copper assay (GBC Avanta) using samples 10-fold diluted in concentrated nitric acid, as described in section 2.1.2.

In the absence of other effects, $^{14}$C-inulin marker concentration would be expected to decline according to the clearance rate constant (specific to each treatment). Residual activity due to the first marker injection ($A_F$) was therefore estimated during the course of the clamping or handling treatment by correcting for clearance during the treatment. An exponential decline function of $e^{-kt}$ was assumed, where k is the clearance rate constant ($h^{-1}$) subsequently calculated during clamping or handling, t the elapsed time (h). Predicted and observed marker concentrations were compared statistically for evidence of concentration.

## 2.2.3. Results

*Weight Changes:*

*1. Due to Clamping*

The results of the preliminary assessment of the effects of clamping on flesh weight are summarized in figure 2.2.1. Following 2h continuous clamping, initially reinforced at 10min intervals, flesh weight had fallen significantly to 89.6 ± 2.0% ($SE_{mean}$) of the undisturbed weight ($t_{0.05,\ 4df}$ =5.17, p=0.003). Subsequent 2-hourly measurements, whilst clamping was reinforced every 30min, showed the weight to remain stable (90.1 ±0.6% of undisturbed weight) over a further 10h clamping period. A small, but significant weight loss ($t_{0.05,\ 4df}$ =5.30, p=0.003) was also observed in the control animals, which fell to a stable 96.7 ±0.3% of initial weight.

*2. Due to Handling*

The animal weights recorded as part of the handling treatment are summarized in figure 2.2.2. A steady weight loss was observed in all animals during the initial 2h handling period, resulting in a 2 – 11% reduction in flesh weight. Increasing the interval between handling treatments to 30min resulted in a relative stabilization of weight. However most animals experienced some continued weight loss during the final 10h (figure 2.2.2); final flesh weights were 85.4 – 99.1% of their undisturbed value. Weight loss between 0 and 2h and between 2 and 12h was significant (F = 14.04, p <0.001, repeated measures ANOVA followed by Fisher's least significant difference pairwise comparison). A characteristic pattern was noted in most of the animals, following weight loss during the first 2h a subsequent stable period of 2 – 3h was proceeded by renewed weight loss, apparently accompanied by venting of mucus from the mantle cavity.

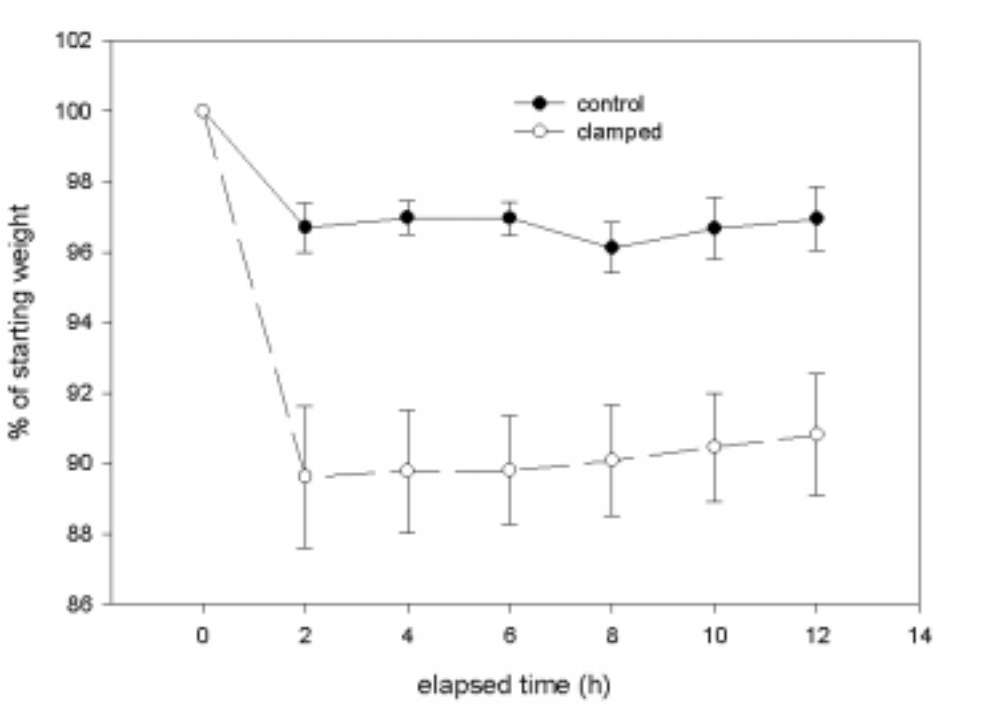


**Figure 2.2.1.**: Relative flesh weights of adult *Haliotis iris* induced to clamp by gentle torque applied to the shell, reversed in direction every 10min for 1h then every 30min for a further 11h, compared to the weight of otherwise undisturbed animals (Mean $\pm SE_{mean}$, treatment n = 5, control n = 5).

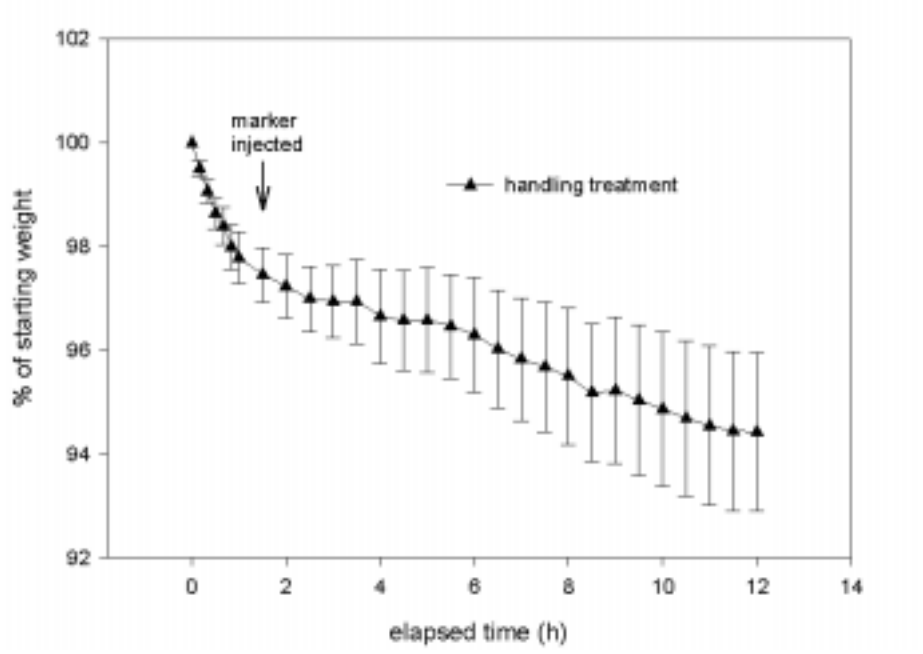


**Figure 2.2.2.**: Relative flesh weights of abalone, measured as part of periodic handling every 10min for 1h, then every 30min for a further 11h (Mean $\pm SE_{mean}$, n = 11).

*Haemolymph Volume Changes*

Absolute haemolymph volume, as determined by instantaneous volume of distribution of $^{14}$C-inulin, fell significantly from 54.1 ±3.3 mL.100g$^{-1}$ to 44.0 ±3.1 mL.100g$^{-1}$ as a result of handling, and to 41.1 ±1.2 mL.100g$^{-1}$ due to clamping treatment (Handling: paired-$t_{0.05, 11df}$ = 2.41, p = 0.034; Clamping: $t_{0.05, 7df}$ = 2.40, p = 0.047). When standardised by resting flesh weight, relative haemolymph volume also fell significantly due to either treatment (see table 2.2.1. Handling $t_{0.05, 11df}$ = 3.02, p = 0.011; Clamping: $t_{0.05, 7df}$ = 2.39, p = 0.048). Considerable variability was associated with haemolymph

volume in the resting animals (30.3 – 75.0% of flesh weight) and during handling (30.4 – 62.2%); however, variability was far more constrained in clamped animals (36.0 – 48.4%).

*Marker Clearance Rate*

The clearance rate constant, the fraction of injected marker cleared per hour, approximately doubled due to either treatment, rising from mean undisturbed values of 0.88 – 1.17%.$h^{-1}$ to 2.28 ±0.27%.$h^{-1}$ during handling or 1.62 ±0.14%.$h^{-1}$ due to clamping (table 2.2.1). For both treatments the increase above the resting rate was highly significant (Handling:paired-$t_{0.05,\ 11df}$ = 3.05, p = 0.011; Clamping: $t_{0.05,\ 8df}$ = 6.68, p < 0.001). When standardised with corresponding calculated haemolymph volume, generating a value for the amount of haemolymph cleared per 100g tissue per day, the increase above resting rate was less marked but remained significant (Handling: t = -2.32, p = 0.040; Clamping: t = -4.53, p = 0.002), as shown in table 2.2.1.

*Marker Mixing Rate*

Calculated half-time mixing values for marker homogenization between the efferent ctenidial and adductor haemolymph were highly variable in resting animals (-0.1 – 9.5h), this variability increased during both handling (-2.1 – 16.0h) and clamping treatments (0.9 – 28.7h). An indication of mixing rate in undisturbed animals and during subsequent clamping is shown in figure 2.2.3, where haemolymph activity has been standardised by the predicted zero-time activity following the first isotope injection (the same pattern is seen during handling). No consistent or significant differences were detected between half-mixing times (table 2.2.1).

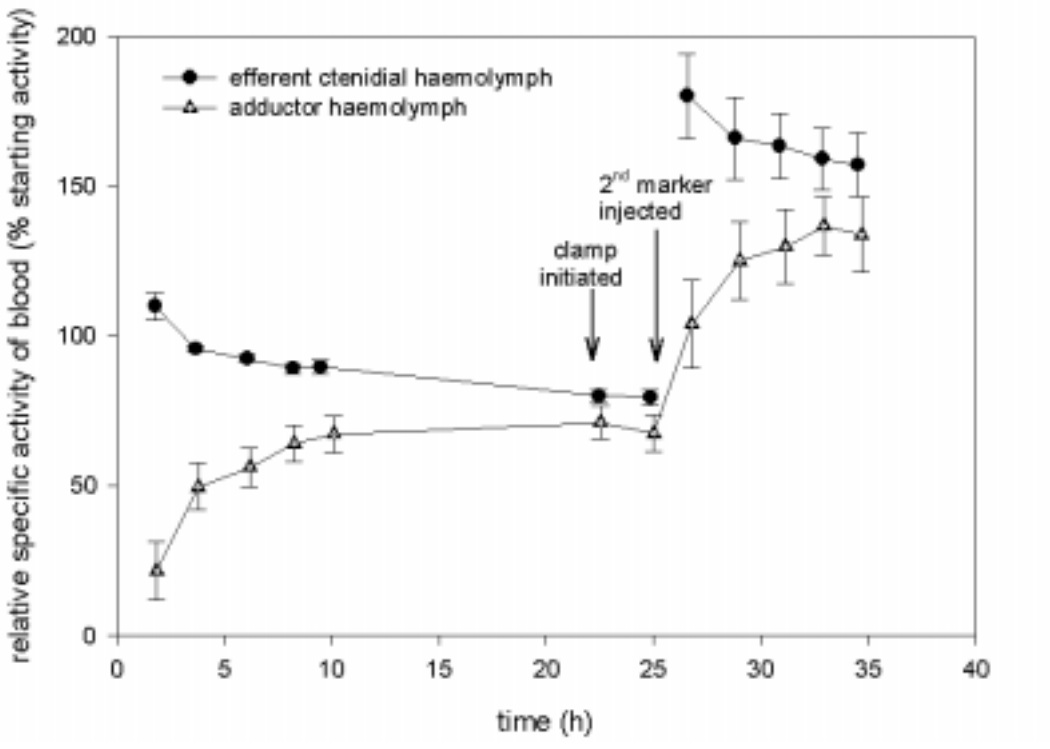


**Figure 2.2.3.**: Mixing of $^{14}C$ inulin to the right adductor muscle haemolymph following injection into the main vascular system in undisturbed abalone and subsequently during induced clamping. Haemolymph radioactivity is expressed as a % of instantaneous haemolymph at the time of the first isotope injection (predicted by extrapolated).

*Haemolymph Copper and Haemoconcentration*

Mean copper concentration in efferent ctenidial haemolymph was observed to increase from 34.9 ±2.8 mg.$L^{-1}$ (n = 9) to 39.1 ±4.3 mg.$L^{-1}$ as a result of 2h handling treatment, rising to 41.5 ±4.3 mg.$L^{-1}$ after 12h of treatment (figure 2.2.4). Over 2h of clamping, copper concentration increased by approximately 7%, from 41.4 ±3.2 mg.$L^{-1}$ to 44.4 ±4.0 mg.$L^{-1}$, rising slightly to 45.7 ±3.3 mg.$L^{-1}$ after 12h (figure 2.2.4). Approximately half of the abalone subjected to either treatment showed a substantial increase in copper concentration, the remainder displayed only a minor increase or decrease (see discussion below). Consequently, the observed increases in copper concentration were not significant (handling: nested one-way ANOVA, $F_{2, 16} = 2.96$, p = 0.08; clamping: $F_{2, 20} = 3.39$, p = 0.054). By making the assumption that copper (haemocyanin) was homogenously distributed throughout the vascular system, it was possible to estimate total haemolymph copper (efferent ctenidial haemolymph copper concentration multiplied by estimated absolute haemolymph volume). Resting animal values of 3.2 ±0.3mg Cu were found to be conserved during handling or clamping treatments (see table 2.2.1).

$^{14}$C-inulin concentration following 2h of either treatment displayed a similar pattern to copper, approximately half of the animals showing a distinct concentrating effect whilst the remainder declined as predicted by clearance rate estimates. Consequently the resulting marker concentrations, shown on figure 2.2.4, were not significantly different higher than expected (handling: t = -2.20, p = 0.054; clamping: t = 1.30, p = 0.22).

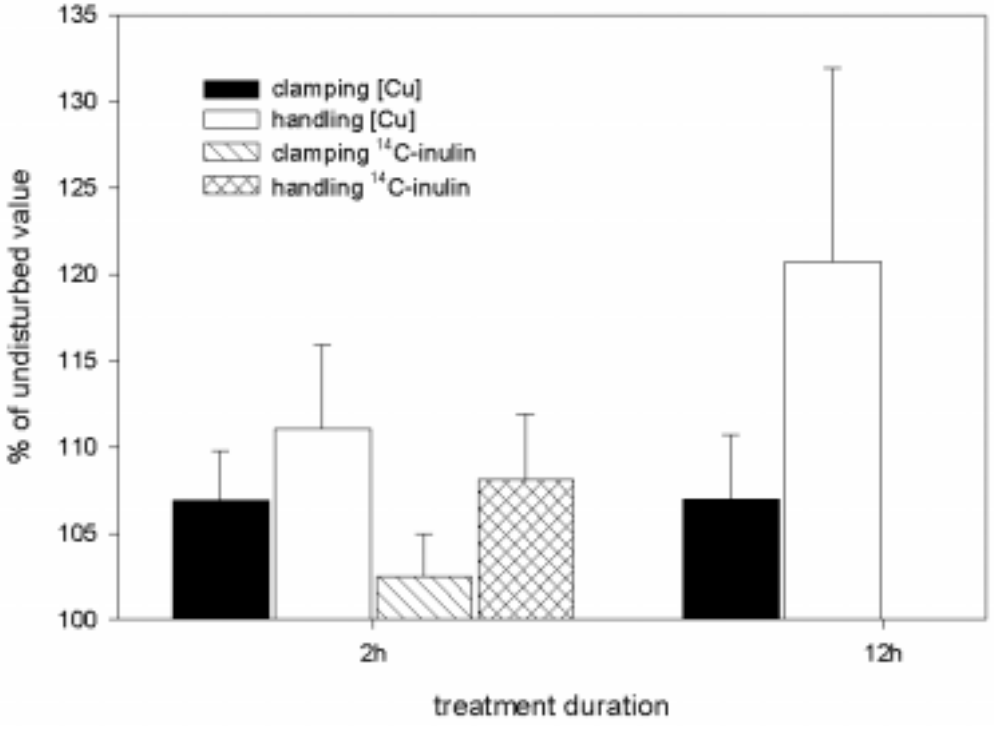


**Figure 2.2.4.**: Haemolymph copper and marker concentrations after 2 and 12h of handling or clamping treatment, expressed as % of concentration predicted from resting animal data (Mean ±$SE_{mean}$).

| Parameter measured | Pre-treatment value | Treatment Value |
|---|---|---|
| **1. Treatment = Handling** | | |
| Haemolymph volume (mL.100g tissue$^{-1}$) | 54.1 (3.3)* | 44.0 (3.1)* |
| Clearance: | | |
| Rate Constant (%.h$^{-1}$) | 1.17 (0.20)* | 2.28 (0.27)* |
| ml haemolymph/100g/d | 15.3 (2.6)* | 23.4 (2.6)* |
| Adductor half-mixing time, $t_{½mix}$ (h) | 3.7 (0.8) | 4.8 (1.7) |
| [Cu] (mg.L$^{-1}$) | 34.8 (3.5) | 43.6 (5.4) |
| Total copper in haemolymph (mg) | 3.4 (0.4) | 3.2 (0.5) |
| **2. Treatment = Clamping** | | |
| Haemolymph volume (mL.100g tissue$^{-1}$) | 52.2 (3.5)* | 41.1 (1.2)* |
| Clearance: | | |
| Rate Constant (%.h$^{-1}$) | 0.88 (0.12)* | 1.62 (0.14)* |
| ml haemolymph/100g/d | 10.6 (1.5)* | 15.8 (1.5)* |
| Adductor half-mixing time, $t_{½mix}$ (h) | 3.7 (0.9) | 5.5 (2.4) |
| [Cu] (mg.L$^{-1}$) | 41.4 (1.1) | 45.7 (3.3) |
| Total copper in haemolymph (mg) | 3.3 (0.3) | 3.2 (0.3) |

**Table 2.2.1.**: Critical *Haliotis iris* haemolymph parameters determined using $^{14}$C-inulin marker in animals at rest and subsequently subjected to repeated handling or induced to clamp. Mean values are given with $SE_{mean}$ in parentheses, n=12 for clamping treatment, n=9 for handling. The asterisk * denotes parameters that differ significantly between the resting and treatment state.

# 2.2.4. Discussion

*Relationship between haemolymph volume and weight*

The initial impetus for the investigations carried out here was the observation of weight loss and apparent haemoconcentration in the abalone as a result of disturbance. The hypothesis tentatively developed therefore proposed that a substantial fraction of the observed weight loss could be explained by direct loss of fluid from the haemolymph to the environment. However, when instantaneous volume of distribution of $^{14}$C-inulin is used to estimate haemolymph volume during a period of sustained disturbance, a more complex relationship becomes apparent. During sustained clamping or repeated handling haemolymph volume frequently falls by a greater amount than can be accounted for by weight loss. After 2h of handling, abalone had lost 2.9 ±0.6g.(100g of undisturbed flesh weight)$^{-1}$ and a calculated 10.1 ±2.0 mL haemolymph.(100g flesh)$^{-1}$. To avoid handling effects, animals induced to clamp could not be weighed during the haemolymph volume measurement period; mean volume loss (10.3 ±4.3mL.(100g tissue)$^{-1}$) was, however, numerically consistent with weight loss observed in the preliminary clamping trial (10.4 ±2.0g.(100g)$^{-1}$). Individual abalone

were weighed immediately before and after the 12h clamping trial, no correlation between individual weight loss and haemolymph volume loss was observed (r»0); a similar absence of correlation was noted in the handling trial (r=0.15). Harris and Andrews (1982) suggest that water may be readily exchanged between the gut lumen and haemolymph in crabs, providing some buffer to osmotic shock or dehydration. Similarly, during investigations of haemolymph volume recovery in terrestrial slugs, Martin and Deyrup-Olsen (1982) note that fluid was initially taken up from an unidentified internal pool. Extensive haemolymph sinuses are closely associated with the gut of *H. iris*, indicating that a similar exchange mechanism could occur. Haemolymph water lost to the gut would have no associated change in animal weight and may subsequently permit a more rapid recovery of haemolymph volume.

The reliability of the techniques employed to determine haemolymph volume should be discussed in light of the surprising discrepancy between weight loss and haemolymph volume reduction, described above. The merits of the kinetic marker technique, calculating instantaneous volume of distribution by extrapolation have been discussed by Hickman (1972) and in section 2.1 of this thesis. As the technique requires that marker concentration in serial haemolymph samples decline at a constant exponential rate, it is reasonably robust insofar as spurious values are identified by non-linearity in the semi-logarithmic relationship, Ln(marker concentration): time. Strong linear relationships were consistently found for the logarithmic decline in haemolymph marker concentration (in resting animals mean $r^2 = 0.75 \pm 0.06$, during clamping $r^2 = 0.80 \pm 0.06$, during handling $r^2 = 0.82 \pm 0.05$). There therefore seems little reason to doubt the predicted instantaneous volume of $^{14}C$ inulin distribution values.

*Why is haemolymph volume lost?*

At the simplest level it could be said that volume is lost from a clamping abalone due to a need for accommodation. The soft body parts of an undisturbed, healthy adult *Haliotis iris* simply occupy too large a volume to allow the shell to be pulled tightly onto the substrate. Rather than protecting vulnerable tissues, a rapid clamp in response to an acute stimulus can, and occasionally does, cause damage by trapping regions of the epipodium or shell margin (personal observation). In such animals the response to isolated, acute stimuli usually takes the form of a partial clamp or 'flinch', involving the retraction of the epipodal tentacles and foot margin, the shell is pulled down slightly presenting only the cornified epithelium of the epipodium to the environment (Crofts 1929). When the stimulus is frequent or sustained, as in populations exposed to high levels of incident light, wave exposure, predator disturbance or the artificial mechanical disturbance employed in the current experiments, the epipodium is also withdrawn. The shell is thereby allowed contact the substrate covering all tissues and permitting the generation of suction to augment attachment tenacity (Trueman and Brown 1985, Smith 1991). Direct observation suggests that at least 30min is required for the shell to first contact the substrate and all associated weight loss occurs within 2h of first stimulus (figure 2.2.1).

Handling, although an unnatural perturbation, is unavoidable in the course of experimental and commercial manipulations of the abalone. In the experiments described here, 'handling' involved the removal of the abalone from the water, separation from its platform using a plastic spatula followed by a brief period of emersion whilst the animal was drained and weighed. Individual responses were variable; initial emersion and contact with the spatula caused most animals to flinch and subsequently clamp firmly after several manipulations. Firmly clamped individuals required forceful separation from the substrate, briefly increasing the compression force acting on the soft tissue and perhaps exacerbating the affects of clamping. Animals that did not react to emersion and removal from the platform tended to twist violently when inverted for weighing. It is therefore unsurprising that the physiological parameters measured showed most variability in handled animals (see table 2.2.1).

Bourne and Redmond (1977a) document approximately 5-fold increases in pressure within both the venous and arterial haemolymph of *Haliotis corrugata* during an acute clamp (few seconds), causing vascular pressure spikes of up to 10cm $H_2O$. Similar pressure spikes have also been measured during clamping in the main circulation and adductor muscle of *H. midae* (Trueman and Brown 1985) and in the pedal musculature of *H. kamtschatkana* (Voltzow 1986). An increase in haemolymph pressure at the ultrafiltration sites (believed to be the auricles) will cause a concurrent increase in urine formation (Martin 1983); the elevated clearance volumes reported in table 2.2.1 are certainly still well within the urine production capabilities recorded for *H. rufescens* (Harrison 1962). It is significant, however, that Bourne and Redmond's (1977a) pressure surge would be sufficient to drive ultrafiltration across other surfaces, even in high colloid osmotic pressure cephalopod haemolymph (2.5 – 4.0cm $H_2O$, Schipp and Hevert 1981). Simkiss and Wilbur (1977) show the molluscan epidermis to be highly permeable with little apparent selective retention of even relatively large molecules, including $^{14}C$ inulin (5,175Da). As numerous regions of the abalone vasculature allow the haemolymph to pass directly beneath the epidermal layer, notably in the gills, left kidney, mantle and hypobranchial glands (e.g. Crofts 1929) an increase in net vascular pressure might cause a transcutaneous efflux of both plasma water and inulin.

Other authors have noted Haemolymph clearance rates that increase with frequency of disturbance. The clearance of $^{14}C$ inulin by shore crabs, *Carcinus maenas*, increases 5-fold if the crabs are handled and haemolymph withdrawn at hourly, compared to 12-hourly intervals (Harris and Andrews 1982). Extra-renal sites are frequently implicated in disturbance-related clearance. For example, in a study of the effects of handling upon terrestrial slugs, Deyrup-Olsen and Martin (1982) describe copious skin secretions originating from the haemolymph, the quantity of which increases rapidly in proportion to frequency of disturbance if handled more than once every 4h. In teleost fish, handling stress indirectly results in an increase in gill permeability (Fletcher 1992). The fact that the primitive bipectinate gill arrangement of abalone represents a diffusion surface that is unusually large for a gastropod and accounts for approximately 40% of the total haemolymph pressure attenuation (Bourne and Redmond, 1977a) suggests that, as in marine fish (e.g. Kischner 1980), the gills may be an important site of water and inulin clearance.

Haemolymph loss in response to disturbance has been described in several prosobranchs, as with abalone this loss appears to be associated with a need to reduce tissue volume when retraction into a shell is the principal defense response (Lever and Bekius 1965, Mangum 1979). However, Martin and Deyrup-Olsen (1982) describe dramatic venting of haemolymph into the mantle cavity of terrestrial slugs, mediated by neurotropic chemicals *not* pressure; in the absence of a confining shell the authors suggest the mechanism is principally associated with the need to vent hypotonic fluids to prevent swelling. Deyrup-Olsen and Martin (1982) also document the exudation of large volumes of fluid, apparently plasma, across the epidermis of slugs in response to even very gentle handling. Rapid release of haemolymph by pulmonates is also believed to play a role as a predator deterrent (see reviews by Martin and Deyrup-Olsen 1982 and Martin 1983). In abalone however, large volumes of mucus released by the hypobranchial glands are believed to fulfill this role, as well as assisting in the removal of waste from the mantle cavity (Crofts 1929). Hypobranchial mucus release was not observed in clamping animals but was frequently associated with animals that had been repeatedly handled for 4 – 5h. As mucus is considered, in part, to be a filtrate of the haemolymph (Simkiss and Wilbur 1977) and additional weight loss is associated with mucus venting in *H. iris* (figure 2.2.1), it must be assumed that haemolymph volume is further reduced during this stress reaction. Simkiss and Wilbur (1977) also show that $^{14}C$ inulin is rapidly cleared from the haemolymph into the mucus trail of *Helix*, it seems likely therefore that the production of mucus is *H. iris* is partially accountable for the elevated clearance rate measured during handling.

In marine teleosts handling stress results in a suppression of drinking (Fletcher 1992). Part of the abalone's response to disturbance involves the retraction of the head, preventing the feeding movements associated with the ingestion of food and most imbibed water (De With 1996). Clamping and handling are therefore likely to restrict oral water uptake. As transcutaneous water uptake in a marine osmoconformer is likely to be minimal and haemolymph clearance is shown to increase (table 2.2.1), loss of haemolymph volume seems an inevitable consequence.

*Haemolymph Mixing*

Mixing of marker throughout the vascular system was formally quantified by calculation of the time required for marker activity in the adductor muscle to reach half that of the efferent ctenidial haemolymph. Whilst the pool represented by the adductor haemolymph is not sufficiently large that incomplete mixing has a discernible effect upon total ECFV calculation (see section 2.1), marker mixing time to this tissue provides valuable information on the role of haemolymph in supporting metabolic function. Neither handling nor clamping had a consistent affect upon mixing to the adductor, other than an increased variability between individuals (table 2.2.1). The implication is that perfusion of the muscle is unaffected by the treatments and, surprisingly, that pressure differentials caused by manipulation or muscular contraction do not consistently assist haemolymph mixing between these pools. Similar observations have been made in the hagfish, where induced swimming failed to increase apparent blood exchange between the main circulation and the slowly exchanging subcutaneous sinus (Forster et al. 1989). The results presented suggest that activities such as clamping

reduce haemolymph volume, hence if mixing rate to the adductor tissues remains constant the muscle will receive a smaller absolute flux volume of haemolymph. The apparent lack of vascular response to support the working muscle must increase dependence upon the well-documented anaerobic capacity of this tissue (e.g. Gäde 1988, Ryder et al. 1994).

Russell and Evans (1989) have suggested that previously described valves between the pedal and cephalopedal venous sinuses and between the pedal arteries and cephalic arterial sinus, or perhaps simple muscular compression, could serve to isolate the pedal vasculature during clamping. Although not directly examined in the present study, 3 of the animals subjected to 12h of clamping treatment were subsequently removed from their containers and a single haemolymph sample taken from the posterior pedal sinus. Specific marker activity in the pedal haemolymph was essentially identical to that removed 5min previously from the efferent ctenidial cannula ($t_{0.05,\ 2df} = -1.32$, $p = 0.16$). Whilst this observation reveals little about the nature of haemolymph exchange between the main and pedal circulation during a sustained clamp, the presence of well mixed marker in the pedal haemolymph implies that this pool is included in the ECFV calculation.

*Conservation of haemolymph protein*

Slugs appear to lose whole blood, including haemocyanin, haemocytes and dextran marker (MW 70,000Da) during emergency venting into the mantle cavity (Martin and Deyrup-Olsen 1982). However a partial filtrate of the haemolymph, cell-free and with reduced haemocyanin content, may also may also be lost as a surface exudation (Deyrup-Olsen and Martin 1982 and reviewed by Martin 1983). The apparent conservation of haemocyanin content by *H. iris* implies that if extra-renal haemolymph volume reduction occurs, it is likely to resemble the latter exudation process rather than the well-documented venting of whole haemolymph seen in pulmonates (Lever and Bekius 1965, Martin and Deyrup-Olsen 1982, Martin 1983). The conclusion that haemocyanin is conserved during haemolymph volume loss in *H. iris* may be overly presumptuous as the protein is normally concentrated within the left kidney, providing a possible reservoir (Andrews 1981). Martin (1983) suggests that haemoconcentration/dilution during retraction and expansion might explain the large variability in haemocyanin concentration documented in abalone. Individual *H. iris* showed up to 35% increase in haemocyanin concentration during 12h of clamping and up to 62% increase during handling in the present trials. It therefore seems reasonable to suggest that repeated disturbance in the wild may have a major impact upon circulating haemocyanin concentration, but that disturbance alone is unlikely to cause the 4 to 10-fold variation in concentration described in Australian (Ainslie 1980) or 10 to 900-fold variation in Californian species (Pilson 1965). Further study into the site and nature of fluid lost from the abalone would provide valuable information in the determination of overall physiological impact of clamping or handling upon the animal.

The results presented here provide an indication of the severe impact retraction into the shell has upon the circulatory status of *H. iris*. An important complementary study would be an investigation of the mechanics of extrusion and the mechanisms of volume recovery. Eversion from a helical shell is achieved with assistance from air pressure in the lung of terrestrial pulmonates

whilst water pumped into the mantle cavity may assist the process in marine prosobranchs (Dale 1974); for example, Brown (1964) notes that retracted *Bullia* will not emerge if its shell is pierced. The presence of shell holes above the mantle cavity prevent abalone from generating hydrostatic pressure (Trueman and Brown 1985); protraction is therefore dependent upon the slow recovery of haemolymph volume and filling of the pedal vasculature (Mangum 1979, Trueman and Brown 1985). Some 15 – 20h are required for the full inflation of the foot of the conch *Busycon* (Mangum 1979), this time-course is consistent with the time taken for *H. iris* to recover weight lost after removal of 11-13% of the circulating haemolymph (H.H. Taylor, N. L. C. Ragg and S. Condliffe – unpublished data). It is therefore recommended that 24h post-handling recovery are allowed if experimental abalone are required to be in an 'undisturbed' state, and that the implications of subsequent disturbance should be appreciated in the form of carefully designed controls.

# Chapter 3

# Morphology of the vascular system and gas exchange organs of *Haliotis iris*

## 3.1. Introduction

Interest in the anatomy of the circulatory system of abalone began with Milne-Edwards (1846 – cited in Crofts 1929). Detailed descriptions of the vasculature of *Haliotis tuberculata* were subsequently made by Perrier (1889), Cuénot (1899 - cited in Crofts 1929), Fleure (1902 – cited in Crofts 1929) and Crofts (1929). Contemporary studies have combined anatomical descriptions with physiological measurements of haemolymph pressure (Bourne and Redmond 1977a, Russell and Evans 1989) and flow (Bourne 1975, Bourne and Redmond 1977b, Jorgensen et al. 1984). The most comprehensive anatomical study is that of *Haliotis tuberculata* carried out by Doris Crofts (1929). As a preparatory stage in the design of the experiments reported in this thesis, preliminary morphological examinations were carried out to confirm that the vascular arrangement of *H. iris* generally conformed to the arrangement as understood from studies of other haliotids. However it was apparent that a number of previously undescribed vascular features were present in *H. iris*, justifying a more systematic description.

The overall objective of this thesis is to provide an integrated physiological description of gas exchange and oxygen transport in the abalone. The present morphological investigations were designed to compliment this objective. The descriptions of Crofts (1929) have been used as a foundation from which the vascular features of *H. iris* of particular relevance to gas exchange and transport are described:

- haemolymph supply to the left and right gills, the principal gas exchange organs
- supply to other possible sites of gas exchange: the epipodium and mantle
- supply to the main $O_2$ target regions (e.g. main muscle blocks and organs)
- general sequential arrangement of resistance elements (i.e. vascular beds) and possible shunts.

The pair of large bipectinate gills clearly represents the principal site of gas exchange (chapter 4) and has accordingly formed the focus of many of the experiments described in this thesis. To

compliment these studies the detailed structure of the gills is also examined here, with particular consideration of the features that facilitate oxygen diffusion from the surrounding seawater into the haemolymph.

*Current Knowledge*

The detailed description of vascular anatomy, and the direction of haemolymph flow inferred by Crofts (1929) for *Haliotis tuberculata* has been generally accepted by her contemporaries as representative of the genus. The following description briefly summarises the currently accepted vascular arrangement, based on Crofts' work, unless stated otherwise. The vascular connections are depicted schematically in figure 3.1.

The small median pallial artery emerges directly from the dorsal region of the ventricle and supplies the hypobranchial (mucous) glands and left mantle region. With this one exception, all haemolymph is pumped from the ventricle into the common aortic trunk. It should be noted that an aortic bulb has been described in *H. rubra* (Russell and Evans 1989) and *H. corrugata* (Bourne and Redmond 1977a), but not in *H. tuberculata* (Crofts 1929). The aortic trunk bifurcates almost immediately, forming the anterior aorta and the first visceral artery. The latter supplies the posterior region of the digestive gland and gonad. The anterior aorta runs towards the head, giving rise to a number of arteries in the process, mainly associated with the digestive system. The largest side branch is the second visceral artery, which supplies the anterior digestive gland, gonad and alimentary canal. More anteriorly 4 – 8 intestinal arteries also leave the aorta (Russell and Evans 1989), as does a single artery supplying the right shell adductor muscle. As the aorta enters the head region, it widens to form the cephalic arterial sinus (CAS), which gives rise to the pedal and epipodal arteries dorsally and the buccal, tentacular and optic arteries anteriorly.

In open vascular systems arterial haemolymph typically reaches the respiring tissues via a system of lacunae that bathes the cells directly. However, Voltzow (1994) noted that areas of higher $O_2$ demand tend to have a capillary style vasculature whereas regions requiring haemolymph for hydraulic support have a more open, lacunar structure. As haemolymph is collected, an increasingly organised venous system is described. The cephalopedal venous sinus (CVS) collects haemolymph from the foot, adductor muscle, epipodium and cephalic regions. Haemolymph is conducted from the CVS to the anterior region of the right kidney via the abdominal venous system, spongy tissue that also received haemolymph from the circum-pallial vessel (see figure 3.1 caption for alternative system described in *H. rubra*). Haemolymph from the posterior region also passes into the right kidney, mainly via the hepato-genital vein, draining the digestive gland, and the median visceral vein, which also takes haemolymph from the stomach region.

Most circulating haemolymph therefore passes through the right kidney. Haemolymph drains, via four efferent veins into the renal sinus, which leads directly into the basibranchial sinus. The Basibranchial sinus receives additional haemolymph from the small rectal vein and also connects to the left kidney via a small vessel. From the basibranchial sinus haemolymph passes into the left

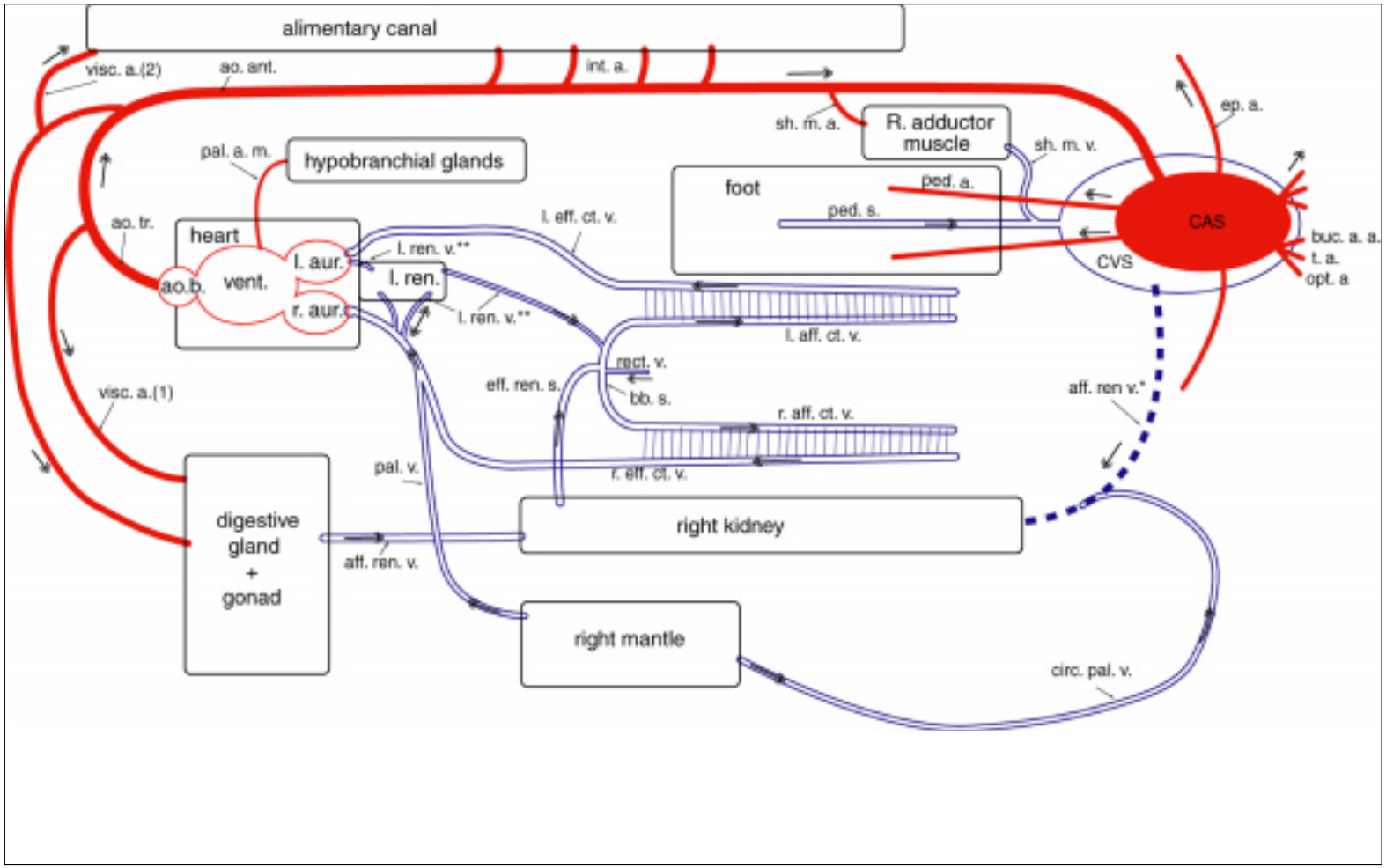


**Figure 3.1:** Overview of generally accepted vascular connections in abalone, based on descriptions by Crofts (1929) and Russell and Evans (1989). Arterial components are drawn in red, the venous system in blue; feathered arrows indicate the proposed direction of flow.

* Russell and Evans (1989) describe a distinct vessel conveying haemolymph from the CVS to the right kidney in *H. ruber*, whereas Crofts (1929) states that spongy lacunar tissue performs this function in *H. tuberculata*.

** The vascular connections of the left kidney appear to vary considerably between abalone species. Crofts (1929) describes vessels connecting the kidney to the right efferent ctenidial vein and the left auricle, through which she believed the flow to be tidal; Crofts also describes an efferent route draining into the basibranchial sinus of *H. tuberculata*. This is the description depicted here. In *H. ruber*, Russell and Evans (1989) state that afferent vessels drain from the abdomenal visceral sinus system into the left kidney and that all efferent haemolymph passes to the basibranchial sinus via a series of vessels.

and right afferent ctenidial veins and crosses the gills. The left efferent ctenidial vein passes directly into the left auricle, while the right efferent ctenidial vein also receives haemolymph from the right pallial vein, draining the right mantle, as well as connecting to the left kidney via 2 vessels, before entering the right auricle. The left kidney also connects to the left auricle, and may have tidal haemolymph flow, as described below (section 3.3.5).

# 3.2. Methods

*Corrosion casting*

The principal technique used to elucidate the vascular layout of *Haliotis iris* was corrosion casting. Corrosion casting involved a low pressure injection of a low viscosity resin which subsequently polymerised, allowing flesh to be dissected away or digested, revealing casts of the haemolymph space. Trial and error showed the following techniques to be effective:

Injection sites were usually cannulated using the techniques described in chapters 2, 5, 6 and 7. If the pedal sinus was chosen as an injection site, a 23gauge needle was inserted directly into the vessel, on the midline of the pedal sole, approximately 20mm from the anterior foot margin.

The animal was anaesthetised in a solution of 40ppm Aqui-S™ in circulating 15°C, aerated seawater. Complete narcosis* was usually achieved within 15 – 20min, indicated by a failure to retract cephalic and epipodal tentacles in response to touch. The abalone was then cooled to approximately 4°C in a tray of ice while the casting compound was prepared following the technique described in table 3.1.

| | |
|---|---|
| compound A | dissolve 0.225g Benzoyl peroxide in 9mL Methyl-methacrylate |
| | (optional) colour with few mg of Batson's #17 dye (red or blue) |
| compound B | combine 0.225mL N,N-Dimethyl alanine with 6mL Hydroxypropyl methyl-methacryalate |
| | (optional) colour with 200µL carbolfucsin pink |

**Table 3.1**: Recipe to produce 15mL of methyl-methacrylate casting resin.

Compounds A and B were also cooled on ice, to slow subsequent polymerisation, and then combined. A 5mL disposable syringe was used to inject the resin directly into the prepared cannula line or needle until resistance was felt, halting injection. Practically, this ensured that perfusion pressures did not exceed approximately 10 – 15cm$H_2O$, the highest vascular pressures that are likely to be experienced *in vivo* (see chapter 7). The abalone was subsequently immersed in seawater and warmed to room temperature to allow the resin to polymerise. If an *in situ* examination of the cast was required, with the tissues intact, a dissection was performed within 12h of casting. Alternatively the tissue was digested using 20% NaOH at room temperature**.

* There was minimal use of anaesthetics during the current project as the attendant loss of muscle tone tended to result in excessive haemorrhage from cannula insertion points. The anaesthetic technique described here, however, was highly effective and recommended for non-invasive procedures or occasions where haemorrhage is not a concern. Abalone can be recovered in moving, aerated seawater within 10min.

** The digestive gland/gonad region of mature males may accumulate excessive lipid, which is not removed by NaOH. Lipid can be digested by 1 – 2d immersion in pancreatin solution: 2.2g Pancreatin and 17.5g KOH dissolved in 1 L distilled water.

A number of injection protocols were used, depending on the target region to be cast:

CC1 – Venous cast was made by direct injection of resin into the pedal sinus. Displaced haemolymph was drained from an incision into the ventricle.

CC2 – Arterial and gill cast was made by injection of resin into a cannula inserted into the right efferent ctenidial vein, immediately anterior to the heart. Haemolymph was vented by cutting the pedal sinus.

CC3 – Combined venous/arterial cast. Up to 15mL of resin were injected into the right efferent ctenidial vein, followed by 15mL of resin stained a contrasting colour in the pedal sinus. Haemolymph was drained from the epipodium. No consistent colour was used. Casts were designated 'shell on' or 'shell off', depending whether the shell was removed prior to tissue digestion.

CC4 – Right mantle region cast. Up to 15mL blue resin were injected into a cannula in the (right) pallial vein followed by a similar amount of pink resin into the circum-pallial vessel, cannulated slightly anterior to the heart region (see chapter 7 for cannulation details). Haemolymph was drained from the pedal sinus, however some inevitably remained within the mantle/circum-pallial vessel region, causing some subsequent fragmentation of the cast.

CC5 – As CC1 but pedal sinus is perfused sequentially with blue then red resin.

CC6 – Single colour is injected into the circum-pallial vessel.

Casts were stored in a 0.01% Benzalkonium chloride solution to prevent microbial overgrowth.

*Scanning Electron Microscopy (SEM)*

The target organ was dissected from the animal and pre-fixed in 4% glutaraldehyde* solution for 2.5h at room temperature. Unwanted material was then trimmed away and the sample immersed in 3% buffered glutaraldehyde for a further 6d at 4°C. The fixative was exchanged once during this period. Samples were cut from the fixed tissue and post-fixed in 2% osmium tetroxide solution (in distilled water) for 24h at 4°C. After rinsing in distilled water for 3.5h, the samples were dehydrated in a graded ethanol series (50% - 100%, minimum 2h at each concentration). They were then passed through an amyl acetate series (25% amyl acetate: 75% absolute ethanol, 50:50, 75:25, 100% amyl acetate, minimum 2h in each) before being dried in a liquid $CO_2$ critical point drier (Department of Zoology, University of Canterbury custom-built apparatus).

Corrosion cast samples were prepared for examination with the SEM by simple air-drying (55°C for 24h). All samples were then mounted on 1cm-diameter aluminium SEM stubs with conductive carbon paint (ProSciTech I003), and subsequently sputter coated with ca. 40 nm of gold/palladium in a Polaron E5000 SEM Coating Unit. Stubs were viewed in a Leica S440 Scanning Electron Microscope at accelerating voltages of 10-18 kV. LEO™ software (version 2.4) was used for view manipulation and image capture.

*Light Microscopy*

Juvenile *H. iris* <20mm maximum length (i.e. short enough to fit across a microscope slide) were obtained from the Pendarves Abalone Farm, Rakaia, New Zealand. Abalone were anaesthetised as

* The primary fixative was buffered with 0.1M sodium cacodylate made up in a solution of 50% seawater, 50% distilled water, pH 7.3.

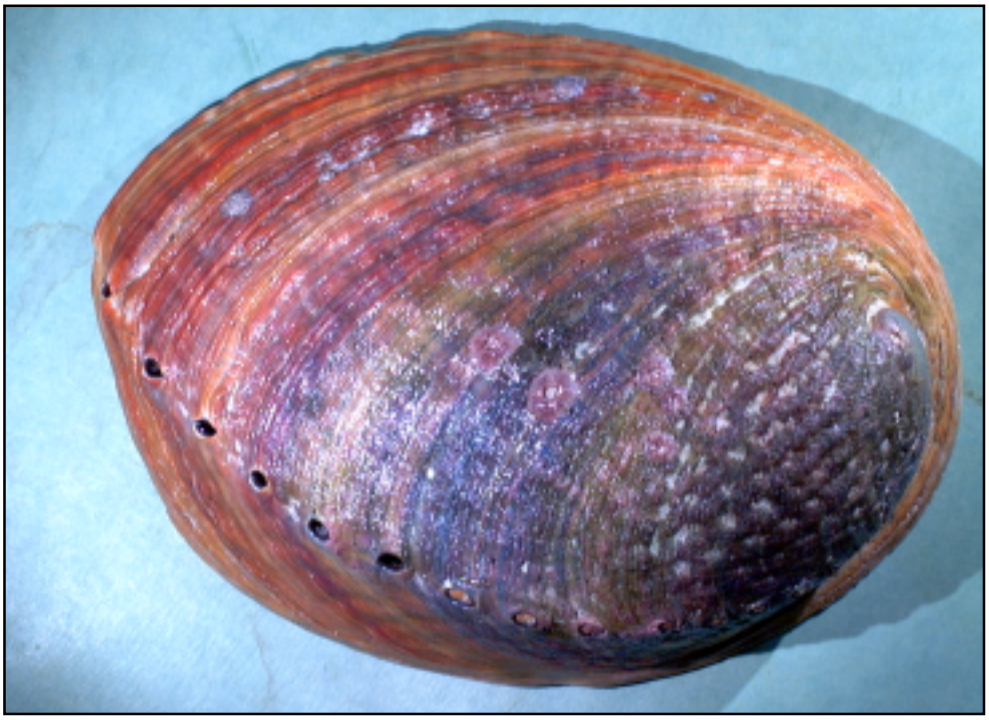

**Figure 3.2**: Dorsal view of adult *Haliotis iris* shell showing normal tremata formation and, unusually, no encrusting epibionts.

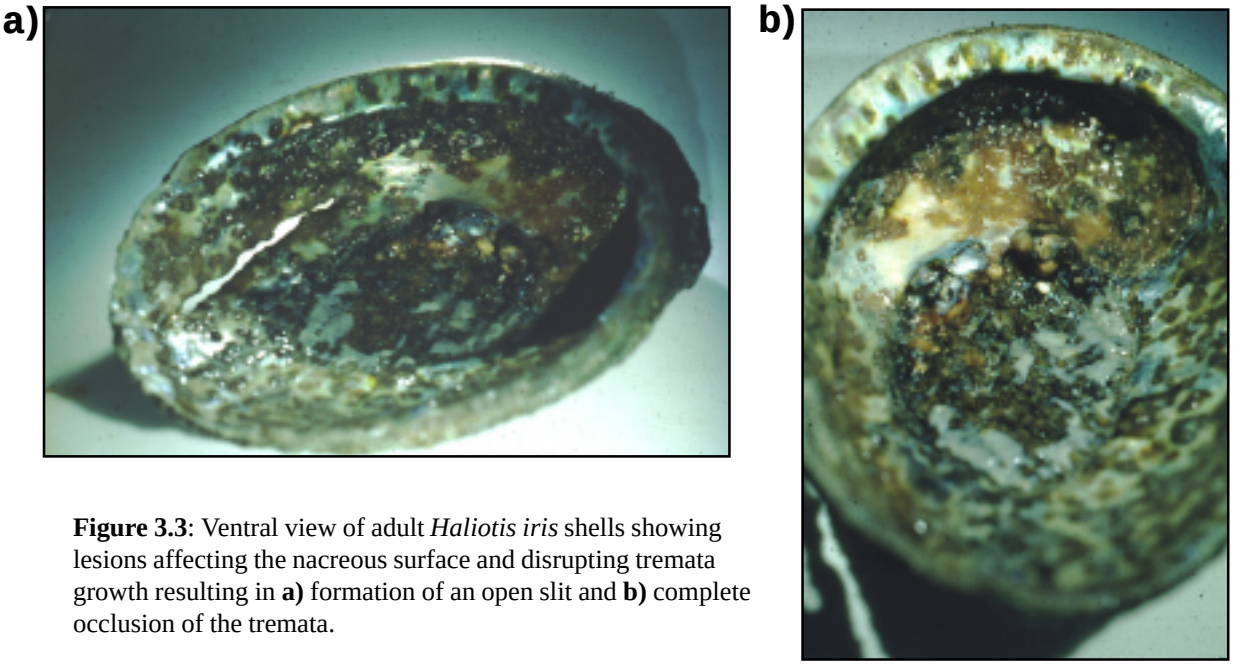


**Figure 3.3**: Ventral view of adult *Haliotis iris* shells showing lesions affecting the nacreous surface and disrupting tremata growth resulting in **a)** formation of an open slit and **b)** complete occlusion of the tremata.

described above and then fixed by immersing the entire juvenile, or target region of adult in Bouin's solution for a minimum of 48h.The tissue was dehydrate using an ethanol series.

Specimens were embedded in celloidin wax, having established that the more commonly used Paraplast wax was too soft, resulting in subsequent tearing on the microtome. A steel blade microtome (Leica) was used to cut continuous series of 10µm sections in the transverse plane. Sections were mounted slides using Haupt's adhesive before staining using Mallorie's triple stain. Photographs were taken using a Zeiss AxioCam HRC CCD camera (1300 x 1030 pixels) mounted on a Zeiss Axioskop 2 MOT epifluorescent compound microscope. Images were acquired using AxioVision 3.1 software (Carl Zeiss Vision).

*Dissection*

Fresh dissections proved more instructive if complimented by examination of fixed abalone perfused with stained gelatin. Isotonic gelatin was prepared by dissolving gelatin powder in 80°C seawater (15:1, g water: g gelatin) and stained with amaranth. The abalone was anaesthetised and warm gelatin injected in the same way as the casting resin described above. The animal was chilled to harden the gelatin and then fixed in 70% ethanol in seawater. Dissection of fixed specimens usually involved thick (1 – 5mm) serial sectioning to trace the path of haemolymph vessels.

*Digital imaging*

Digital images were taken with a Sony Cybershot™ mounted on a dissecting microscope (Zeiss Stemi 2000-C) or a Nikon Fujix™ HC-300Zi fitted with a macro lens. Light, contrast and colour saturation were adjusted using Adobe Photoshop® 5.0, labels and stenciled outlines were added using Adobe Illustrator® 8.0.

Nomenclature and abbreviations have, as far as possible, followed those used by Crofts (1929) (see Abbreviations section).

# 3.3. Results and Discussion

### 3.3.1. *External morphology*

The most conspicuous external feature of the abalone is its shell. As with other members of the genus, the shell of *Haliotis iris* is an auriform, planar spiral bearing a line of secondary apertures, known as tremata, originating from the left side of the anterior growing margin. *Haliotis iris* usually has 5 – 7 open tremata (figure 3.2). However, this species is prone to epibiont fouling (Dunphy and Wells 2001), with overgrowth of the tremata often leading to premature occlusion or growth deformities (figure 3.3). Healthy *H. iris* may respond to overgrowth by periodic grinding of the tremata region (personal observation), a behavioural trait resulting in the removal of sculpturing associated with the holes, and the appearance of nacre through the external conchiolin. The tremata are considered to be the normal exhalant route for abalone (Voltzow 1983), their occlusion therefore has serious implications for gas exchange; this topic is considered in greater detail in chapter 4.

Infestation by boring polychaetes, leading to secondary lesions may also affect shell morphology (figure 3.3), retarding shell growth and causing a separation of nacreous layers.

In wild populations, shorter, higher adult shells are often associated with sheltered areas, while longer, flatter shells are found in exposed areas (personal observation). The morphological dichotomy is indirectly adaptive, resulting from faster somatic growth associated with more exposed populations. The phenomenon is readily observed in juvenile *H. iris* grown under standardised conditions in captivity, where inter-individual growth variation is reflected in the shell profile (personal observation).

Figure 3.4 shows the major morphological features of *H. iris* visible after shucking. The large paired bipectinate gills are concealed anteriorly by the lobes of the left mantle and posteriorly by the mantle cavity, considered to be unusually deep compared to other prosobranchs (Purchon 1977).

### 3.3.2. *Gross structure of the vascular system*

The first impression conveyed by most of the vascular corrosion casts made of *Haliotis iris* is that the left side of the animal is represented by a near-solid mass of resin (e.g. figure 3.5). Clearly *H. iris* possesses a more extensive vascular system than that described by Crofts (1929) for *H. tuberculata*. This observation in *H. iris* is also consistent with the large haemolymph volume determined for this animal (55.4 mL.100g flesh weight$^{-1}$, section 2.1 of this thesis).

*Gut sinus system*

The most conspicuous, previously undescribed, vascular feature apparent in the corrosion casts is an extensive sinus that, with the exception of the rectum, follows the entire alimentary tract. This gut sinus is described here, referring to each section of the sinus according to its corresponding gut region.

The gut sinus system ‘begins’ in the head, with the cephalopedal venous sinus (CVS, figure 3.6 and 3.14), that has been described by numerous authors (e.g. Crofts 1929, Bourne and Redmond 1977a, Russell and Evans 1989). The CVS surrounds the cephalic arterial sinus (CAS) and the odotophore, opening anteriorly to allow passage of the retractable mouthparts (Z, figure 3.6) and ventrally where the pedal and epipodal arteries emerge (see below). Within the lumen of the digestive tract, a valve identifies the entrance to the oesophagus (Crofts 1929), hence as the haemolymph sinus extends posteriorly it is referred to as the oesaphageal sinus* (figures 3.6). The oesophageal sinus is a direct continuation of the CVS, remaining initially wide as it surrounds the oesophageal pouches and the aorta, as well as the oesophagus itself. The oesophageal pouches terminate at the level of the oldest patent shell hole (Crofts 1929), posterior to this the oesophageal sinus narrows markedly and descends to the ventral surface of the left mantle region. Once level with the heart, the sinus widens rapidly to surround the crop, which occupies most of the posterior, left, ventral quadrant of the abalone.

* The sinus should not be confused with the oesophageal sinus described by Crofts (1929), which refers to a small vessel draining the oesophageal pouch region.

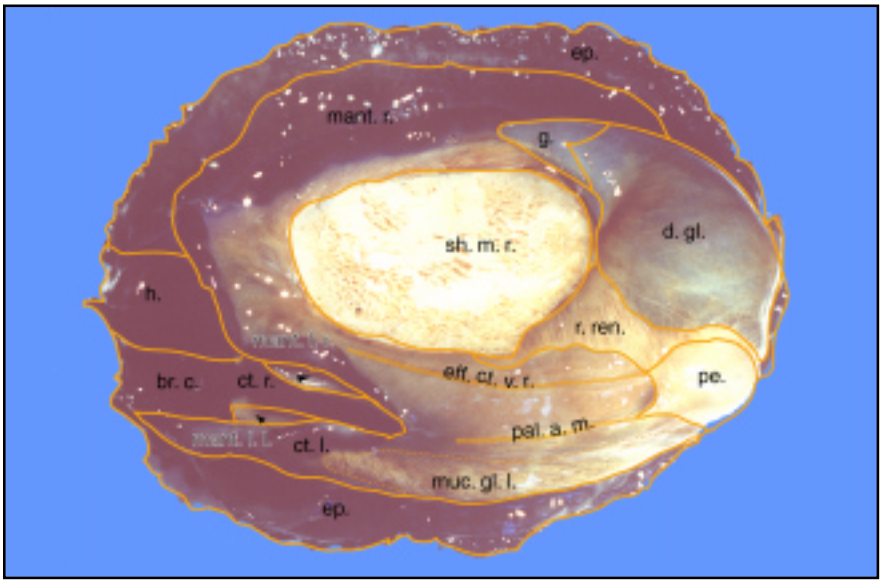


**Figure 3.4**: Major body regions visible from the dorsal surface of *Haliotis iris*, following removal of the shell.

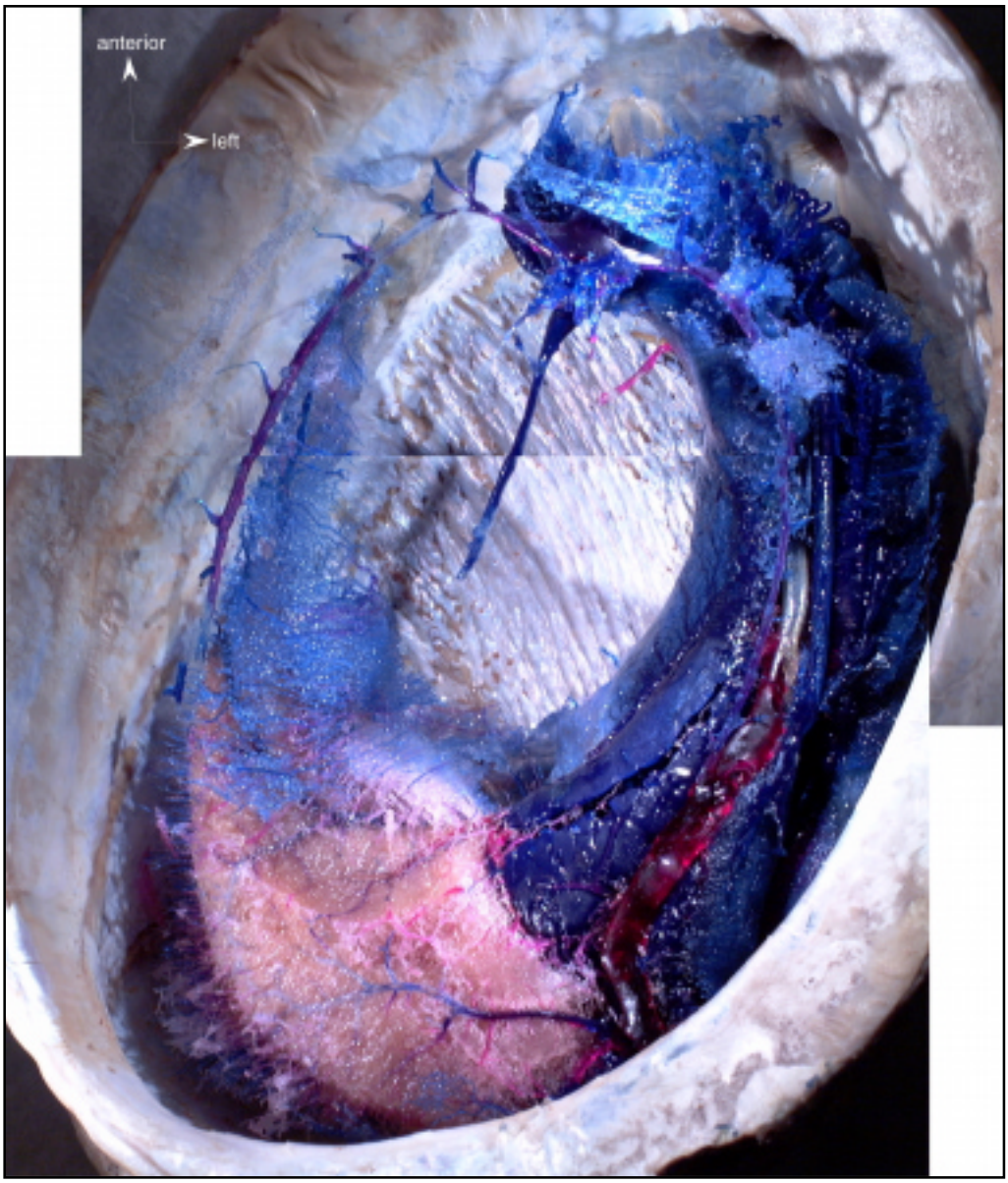


**Figure 3.5**: Two-colour vascular corrosion cast of *Haliotis iris* (blue = venous, pink = arterial). As with most casts, the left-side vasculature has preferentially filled; the anterior pedal sinus, epipodal arteries and the superficial capillaries of the gonad have also filled. (Casting protocol CC3 – shell on, blue into pedal sinus, pink into right efferent ctenidial vein).

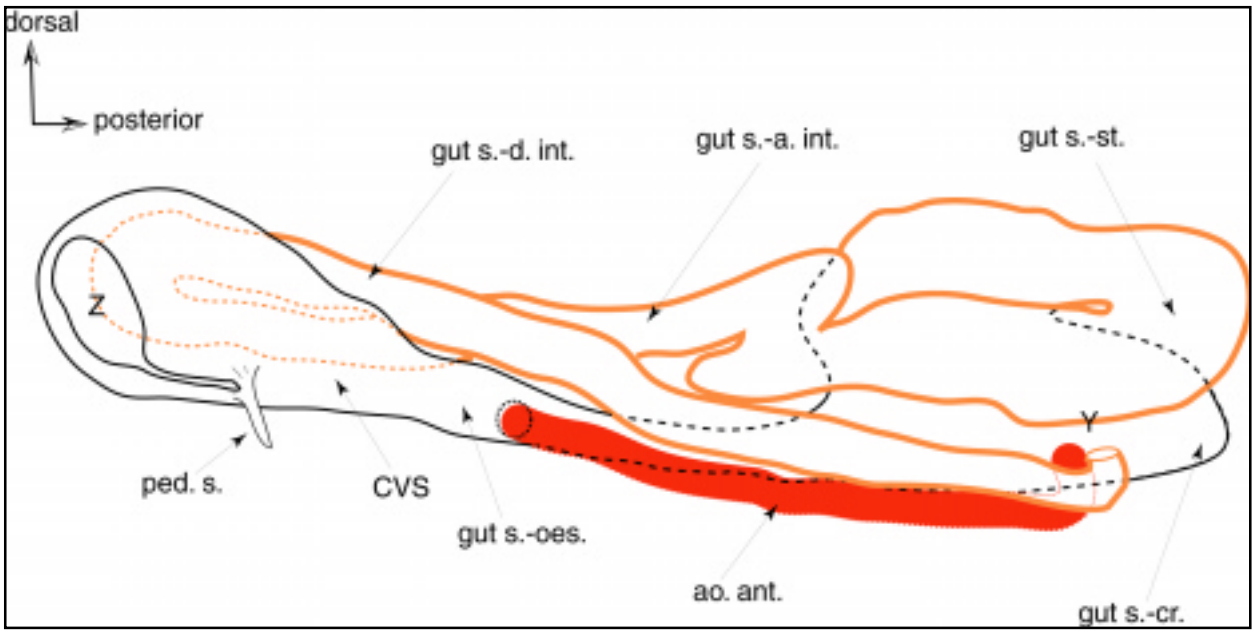


**Figure 3.6**: Schema showing arrangement of the gut sinuses of *Haliotis iris* viewed from the left. The position of the regions of the gut sinus associated with the intestinal loop (gut s.-a. int. and gut s.-d. int.) to the right of the head are shown by a dotted orange line. The anterior aorta (ao. ant.) is included for reference, descending from the heart (position Y) and running anteriorly to enter the region surrounded by the oesophageal sinus (gut s.-oes.) and cephalopedal venous sinus (CVS). The CVS junction with pedal sinus (ped. s.) and internal cavity (Z), accommodating the feeding apparatus and cephalic arterial sinus, are also shown.

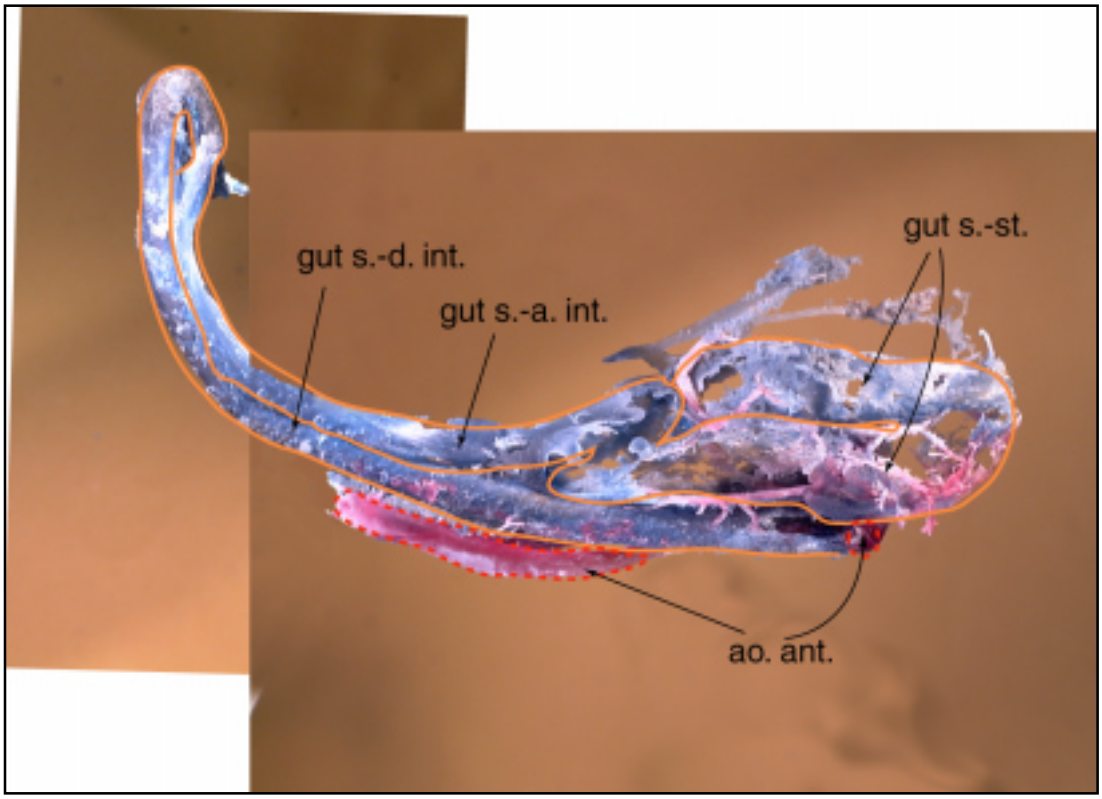


**Figure 3.7**: Vascular corrosion cast viewed from left/dorsal. Pink resin represents the aortic/arterial space, blue resin has filled the venous system. All superficial casting has been removed, along with the cephalopedal venous sinus, leaving only the gut sinuses (highlighted by orange border). Perspective and labels correspond approximately to those of figure 3.6. (Casting protocol CC3 – shell on, blue into pedal sinus, pink into right efferent ctenidial vein).

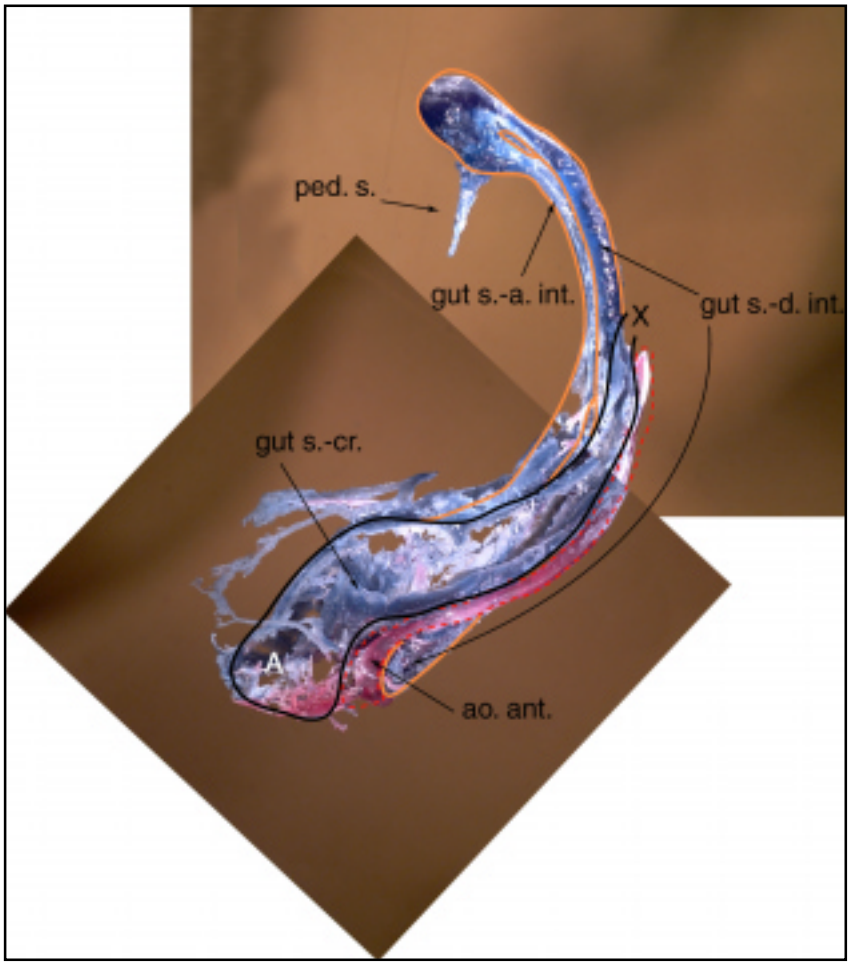


**Figure 3.9**: Montage showing the ventral side of the vascular corrosion cast described in figure 3.7. The spiral caecum region where the crop sinus rises to form the stomach sinus is marked A; the fracture line where the cephalopedal venous sinus and anterior oesophageal sinus have been removed is marked X. (Casting protocol CC3 – shell on, blue into pedal sinus, pink into right efferent ctenidial vein).

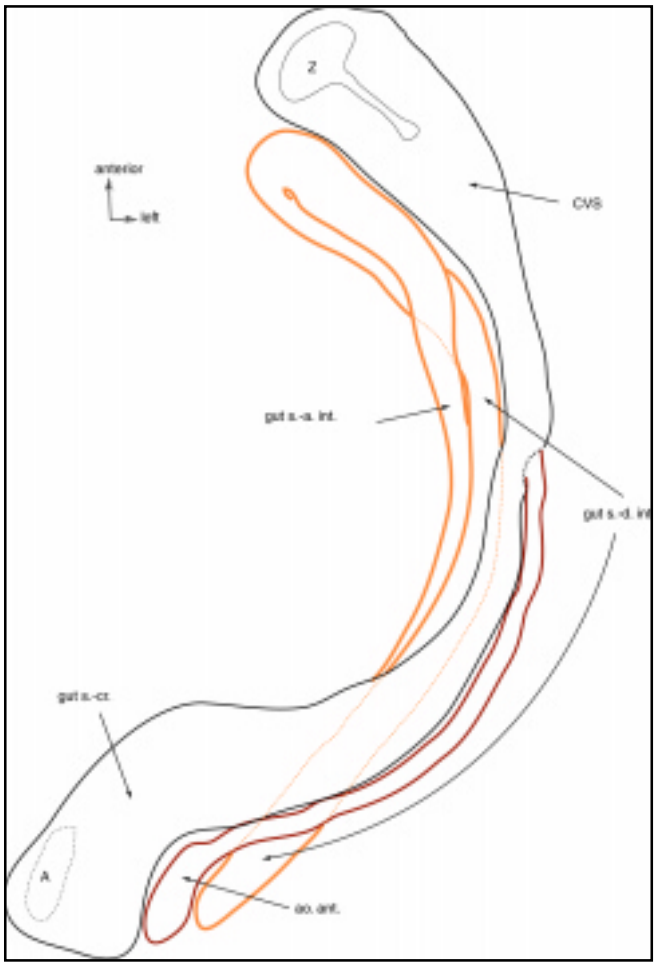


**Figure 3.8**: Arrangement of gut sinuses viewed ventrally. As in figure 3.6, the aorta (ao. ant.) is included for reference. The position of the stomach sinus, which joins the crop sinus (gut s.-cr.) at A to the ascending intestinal sinus (gut s.-a. int.) has not been marked to preserve clarity.

At its posterior extreme, within the digestive gland, the crop abruptly ends, opening dorsally (A on figures 3.8 and 3.9), via a semicircular valve, into the spiral caecum region of the stomach (Crofts 1929). The stomach sinus overlies the crop sinus, surrounding the stomach and spiral caecum (figure 3.6). The stomach runs anteriorly before narrowing to form the intestine to the right of the heart. In this region the sinus also narrows and is referred to as the ascending intestinal sinus. The ascending limb of the intestine and its sinus move through a 'dog-leg' near the posterior end of the branchial chamber to run dorsally. The sinus then passes to the right of the descending limb and enters the cephalic region ventrally (figure 3.6). Crofts (1929) reports that the ascending intestine of *H. tuberculata* runs dorsally over the right kidney. This is not the case in *H. iris*, where both limbs of the intestinal loop remain ventral to the kidney. On the right side of the head the intestine turns through 180°, the sinus volume increases considerably and a projection descends into the pedal sinus (figure 3.9). As the intestine completes its turn the sinus narrows again, descending ventrally and posteriorly towards the heart. The descending intestinal sinus passes immediately to the right of the aortic trunk before ending abruptly at the ventral surface of the pericardium (Y on figure 3.6). The intestine, now defined as the rectum, passes through the ventricle, emerging anteriorly through the pericardium, where it receives a venous branch from the basibranchial sinus (rectal vein – see below), but does not possess a sinus. The rectum terminates at the anus, beneath the oldest patent shell hole.

The 3-dimensional arrangement of the gut sinus is complex (e.g. figures 3.6 and 3.8) as, embryologically, ano-pedal flexure has allowed the development of a folded alimentary canal (Lindberg and Ponder 1996) and coiling and torsion have then twisted the gut (Purchon 1977).

The gut sinus is noticeably thin or absent in the muscular regions of the alimentary canal, the oesophageal narrowing before the crop, and most of the stomach (figure 3.7), implying an incompatibility between peristalsis and the presence of a sinus. Throughout the remainder of the alimentary tract the gut wall is thin and the lumenal contents are moved by ciliary action (Crofts 1929). The gut sinus may therefore offer a degree of mechanical support, as well as metabolic support for the metabolically active cells of the gut (mucocytes, secretory, phagocytic and ciliated cells). The large venous reserve surrounding the gut is also likely to offer environmental stability, buffering against acute changes in oxygen levels and temperature fluctuation. The haemolymph jacket should also facilitate the transfer of digestive products into the circulatory system. Phagocytes, presumably originating from the haemolymph, have been found in the gut lumen (Crofts 1929) where they potentially assist in digestion. Obviously the proximity of a large haemolymph reserve could provide a source of such cells.

The gut sinuses of *H. iris* readily filled with casting resin and were clearly apparent on any venous cast. Other studies have used corrosion casting techniques on other abalone species, notably Bourne and Redmond (1977a) working on *H. corrugata* and Russell and Evans (1989) with *H. rubra*. No trace of a gut sinus was identified in these abalone species. It would therefore be of considerable interest to establish the function of this sinus, to allow the reasons for its presence or absence in an abalone species to be further elucidated.

In corrosion casts the gut sinuses not only represent the largest vascular feature of *H. iris* but also physically hold the casts together. Hence for practical reasons associated with the progressive dissection of the casts, all subsequent vascular systems are described according the their relationship to these sinuses.

### 3.3.3. *Vascular systems afferent to the gut sinuses*

*Arterial supply to the gut sinuses*

The ventricle pumps haemolymph into the aortic trunk. An aortic bulb described within the pericardial cavity of *H. corrugata* (Bourne and Redmond 1977a) and *H. cracherodii* (Jorgensen et al. 1984) is apparently absent in *H. iris*. The aortic trunk bifurcates ventral to the heart. The posterior branch of the bifurcation has previously been described as the first visceral artery (Crofts 1929, Bourne and Redmond 1977a); for consistency in the nomenclature however, the vessel is referred to here as the posterior aorta (ao. pos., figures 3.10 and 3.11). Corrosion casts of the posterior aorta reveal a number of small, parallel vessels leaving to the right, these vessels unite in a common artery, referred to here as the crop sinus artery, which supplies the ventral side of the crop sinus (figures 3.10 and 3.11). In the cast shown in figure 3.10 the arterial system was filled with pink resin from the right efferent ctenidial vein, the venous system with blue resin injected into the pedal sinus. The crop sinus correspondingly shows a mixture of ‘venous’ and ‘arterial’ haemolymph.

Posterior to the crop sinus artery, the posterior aorta gives rise to an artery supplying the cardiac lobe of the right kidney, before continuing to the posterior, where it is now referred to as the first visceral artery (visc. a.(1), after Crofts 1929).

*Vasculature of the foot and adductor muscles*

Using corrosion casting techniques, the small shell muscle artery, supplying the right adductor muscle, was located (figure 3.12). As described by Crofts (1929), the artery originates from the anterior aorta as it approaches the head region. The artery is seen to emerge through the right side of the oesophageal sinus and curve dorsally (figure 3.12). The arrangement of the sinus draining the right adductor muscle (sh. m. s., figure 3.13) also closely resembles that described by Crofts (1929). In contrast Bourne et al. (1990) describe arterial supply to the adductor muscle of *H. kamtschatkana* via the pedal arteries. Corrosion casting shows the sinus to originate at the anterior-dorsal extremity of the muscle, identified by the muscle scar on the nacreous surface of the shell (sh. m., figure 3.13). The shell muscle sinus passes vertically through the adductor tissue, draining into the pedal sinus as it ascends to meet the CVS (figure 3.13 and Crofts 1929). As noted by other authors (e.g. Trueman and Brown 1985; Frescura and Hodgson 1992), the adductor muscle tissue is extremely dense, with little associated vascular space. It therefore proved impossible to trace any vascular path, other than the principal artery and venous sinus serving the tissue.

Anteriorly the aorta widens to form the cephalic arterial sinus (CAS), which lies ventrally within the cavity of the CVS and bathes the odontophore (Crofts 1929). In a whole animal corrosion cast the CAS is only visible through a ventral groove in the CVS, through which it emerges posteriorly,

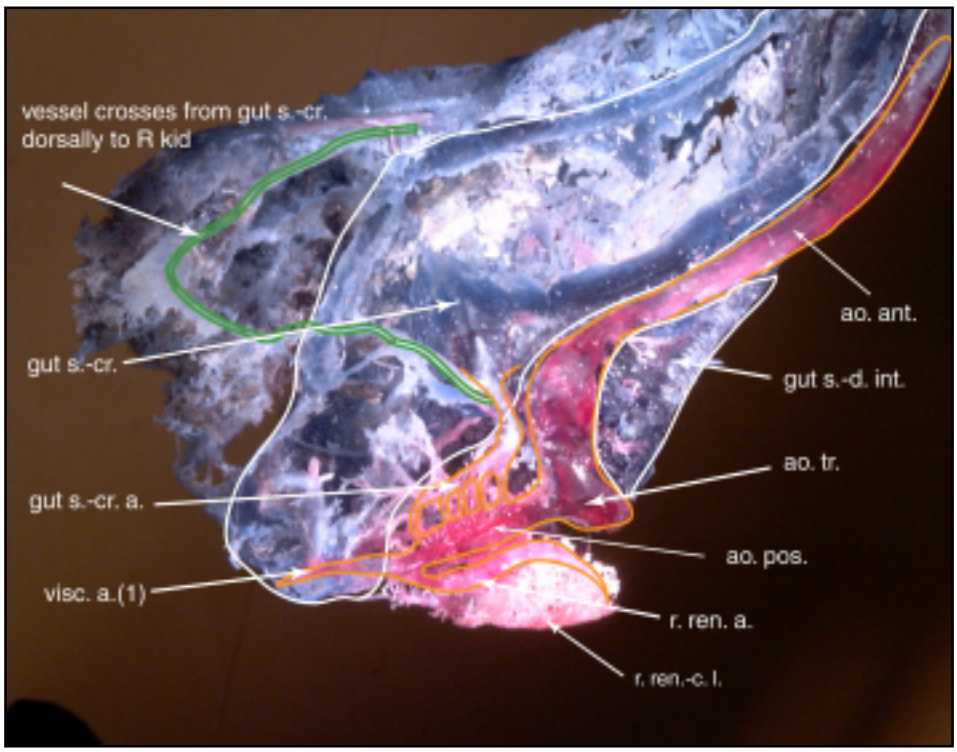


**Figure 3.10**: Vascular corrosion cast of posterior, ventral region. The posterior aorta (ao. pos.) is shown to supply arterial haemolymph to the crop sinus (gut s.-cr.) via parallel elements that drain into the crop sinus artery (gut s.-cr. a.). The posterior aorta also supplies arterial haemolymph to the cardiac lobe of the right kidney (r. ren.-c. l.). (Casting protocol CC3 – shell on, blue into pedal sinus, pink into right efferent ctenidial vein).

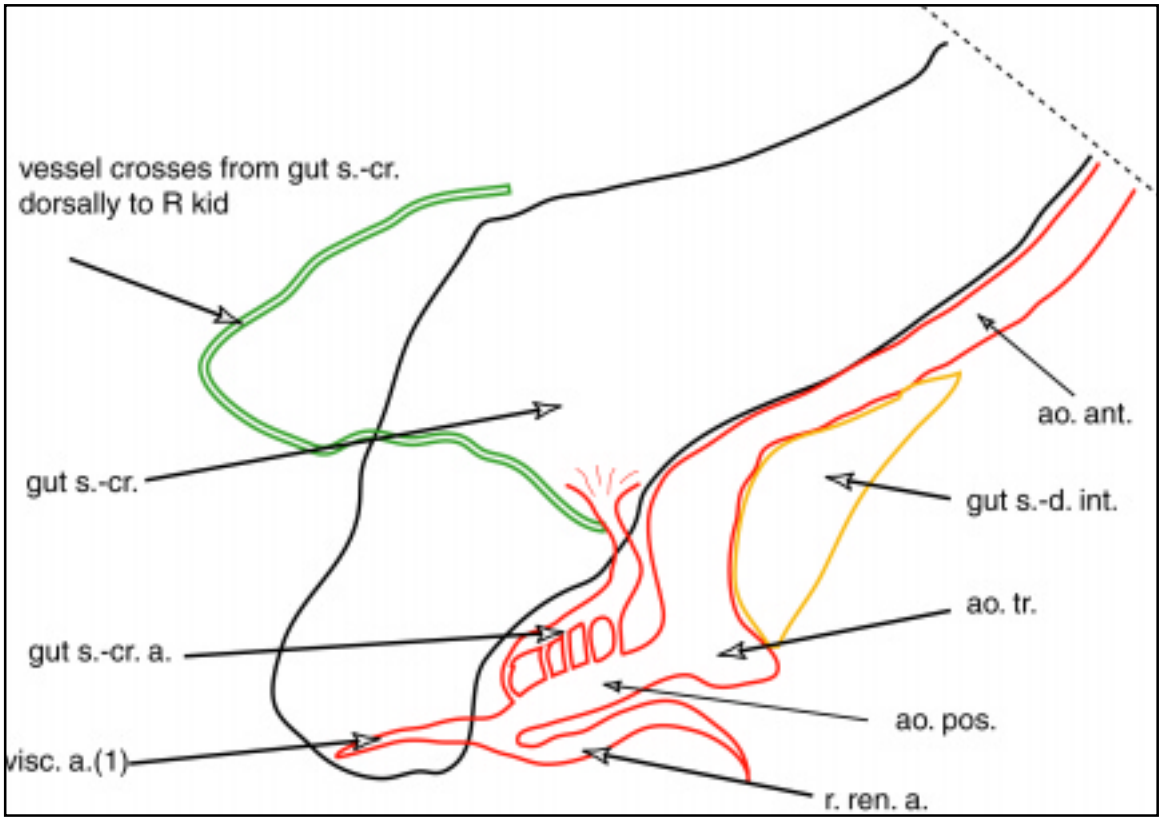


**Figure 3.11**: Diagrammatic representation of the vascular arrangement shown in figure 3.10.

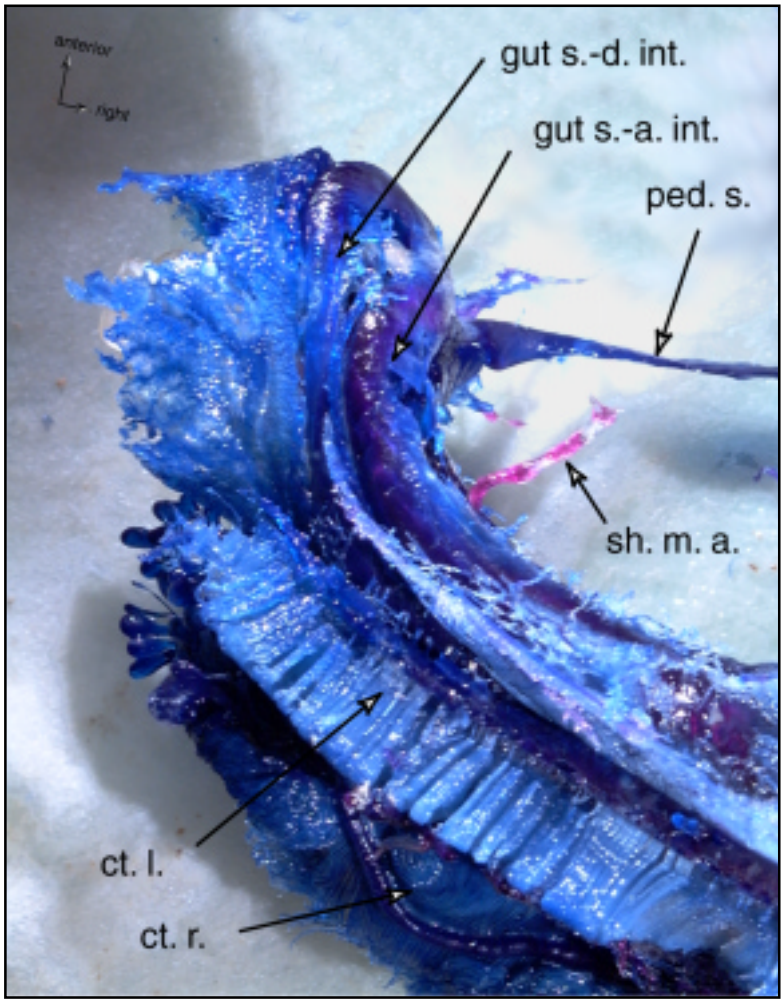


**Figure 3.12**: Corrosion cast showing the anterior, dorsal region, viewed slightly to the right. The shell muscle artery (sh. m. a.), supplying the right adductor muscle, is seen emerging through the oesophageal sinus. (Casting protocol CC3 – shell on, blue into pedal sinus, pink into right efferent ctenidial vein).

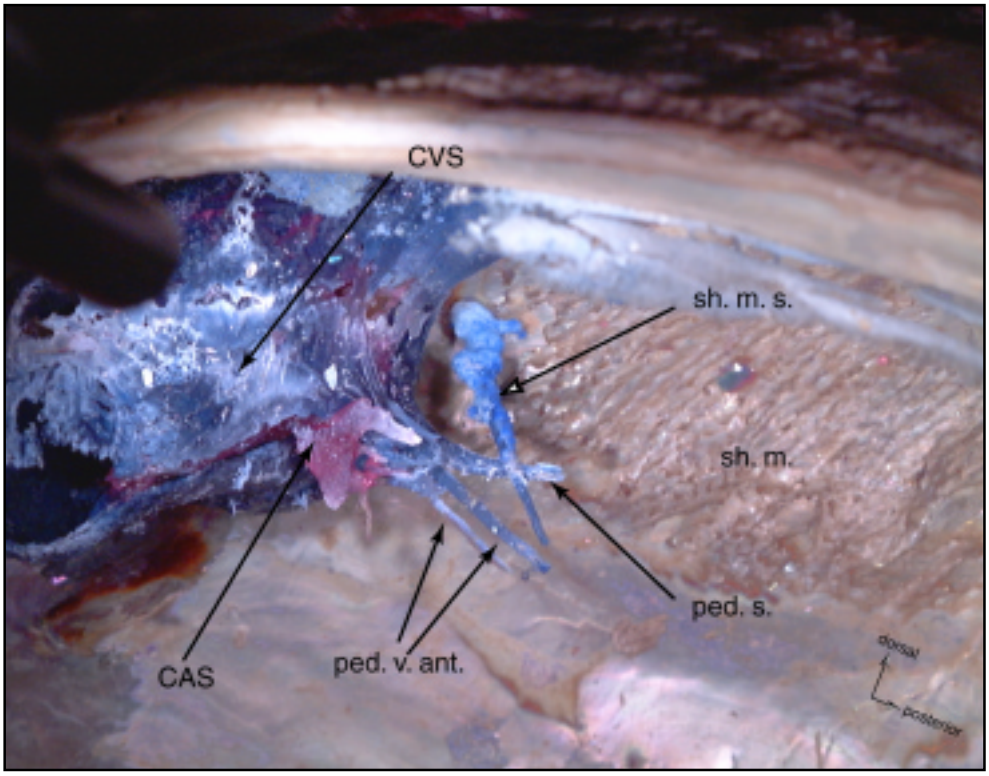


**Figure 3.13**: Left/ventral view of vascular corrosion cast (blue = venous, pink = arterial) showing the venous sinus draining the right adductor muscle (sh. m. s.) into the pedal sinus (ped. s.). Note that the anterior lobes of the foot were folded ventrally, resulting in the apparent posterior projection of the anterior pedal veins (ped. v. ant.).

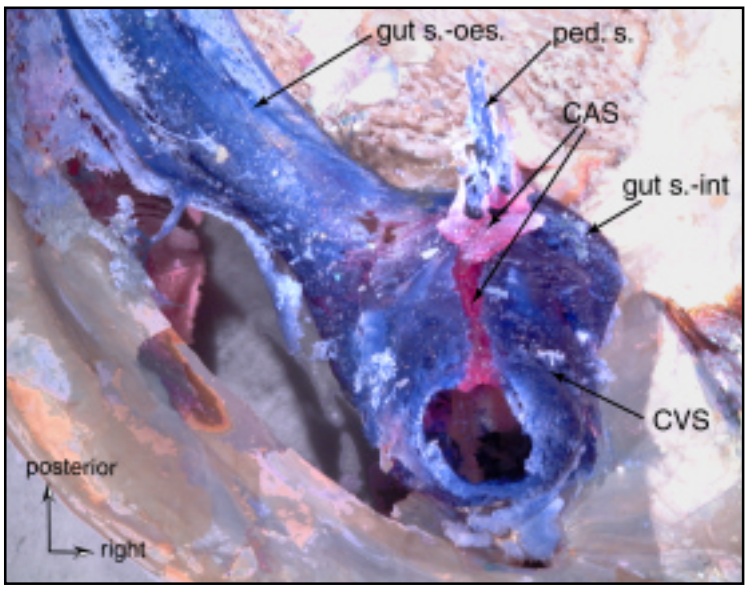


**Figure 3.14**: Ventral/anterior view of vascular corrosion cast of the cephalic region. Pink resin represents arterial space, blue venous space. Continuity between the oesophageal sinus (gut s.-oes.) and CVS is seen; deceptively, the anterior extreme of the intestinal sinus (gut s.-int) also appears continuous with the right side of the CVS. The CAS is visible through a ventral slit in the CVS, through with it emerges posteriorly to form the epipodal and pedal arteries. (Casting protocol CC3 – shell on, blue into pedal sinus, pink into right efferent ctenidial vein).

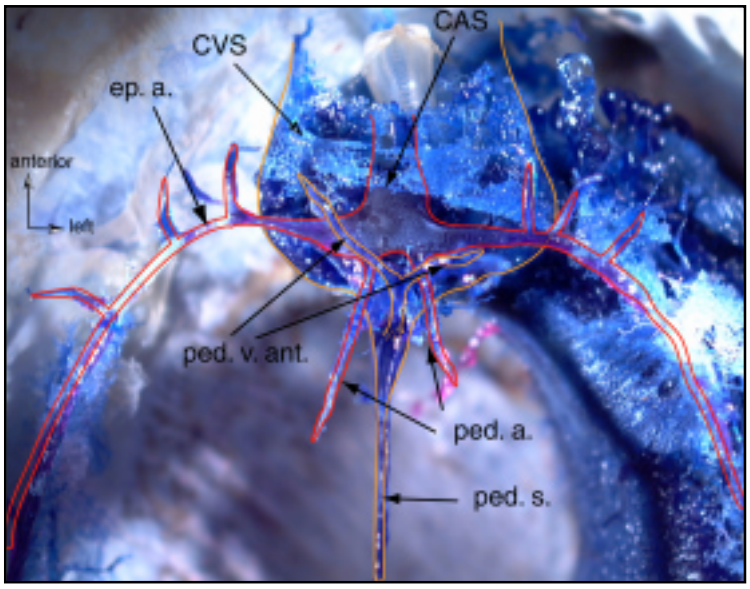


**Figure 3.15**: Ventral view of vascular corrosion cast of the head region. The CAS is seen to emerge from the posterior end of the ventral slit in the CVS. The ventral CAS divides to form 4 vessels, the left and right epipodal arteries (ep. a.) and pedal arteries (ped. a.). Immediately posterior to the emergence of the CAS, the pedal sinus receives the recently united anterior pedal veins and joins the CVS. (Casting protocol CC3 – shell on, blue into pedal sinus, pink into right efferent ctenidial vein).

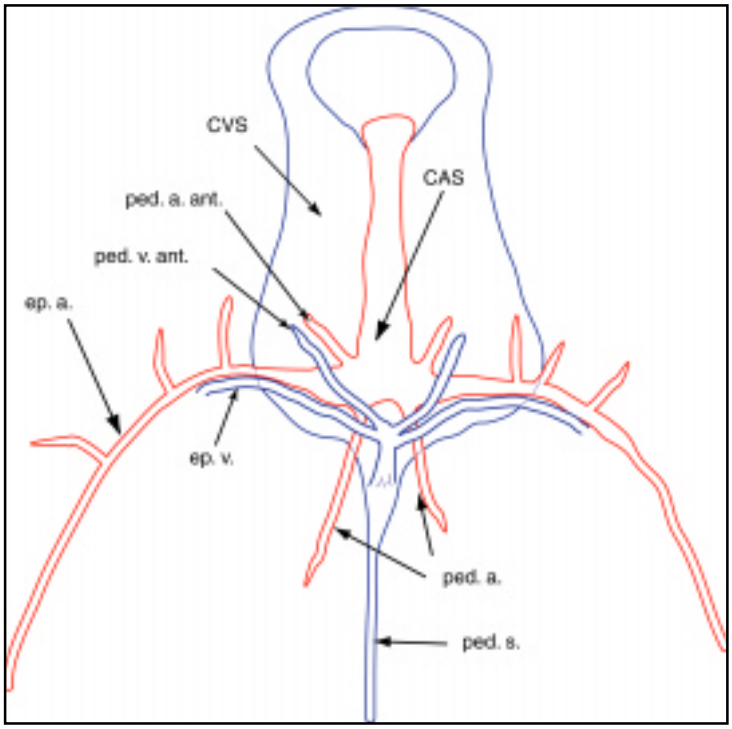


**Figure 3.16**: Diagrammatic representation of the junctions between epipodal, pedal and cephalic haemolymph spaces shown in figure 3.15.

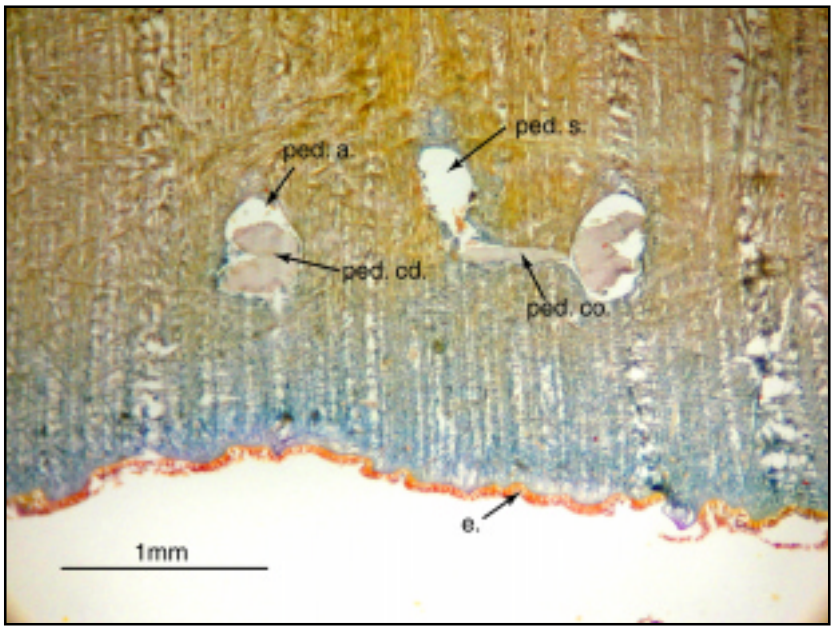


**Figure 3.17**: Transverse wax section through pedal mid-region of juvenile *Haliotis iris* showing central pedal sinus (ped. s.) and restricted haemolymph space of pedal arteries (ped. a.), due to presence of nervous tissue, the pedal ganglionated cords (ped. cd.), in the lumen. Part of a lateral commissure connecting the ganglia is also shown. Note the tendency towards increased collagen (blue-stained by Mallorie's triple stain) and reduced muscle fibre density (orange) within the vicinity of the pedal sole epithelium (e.).

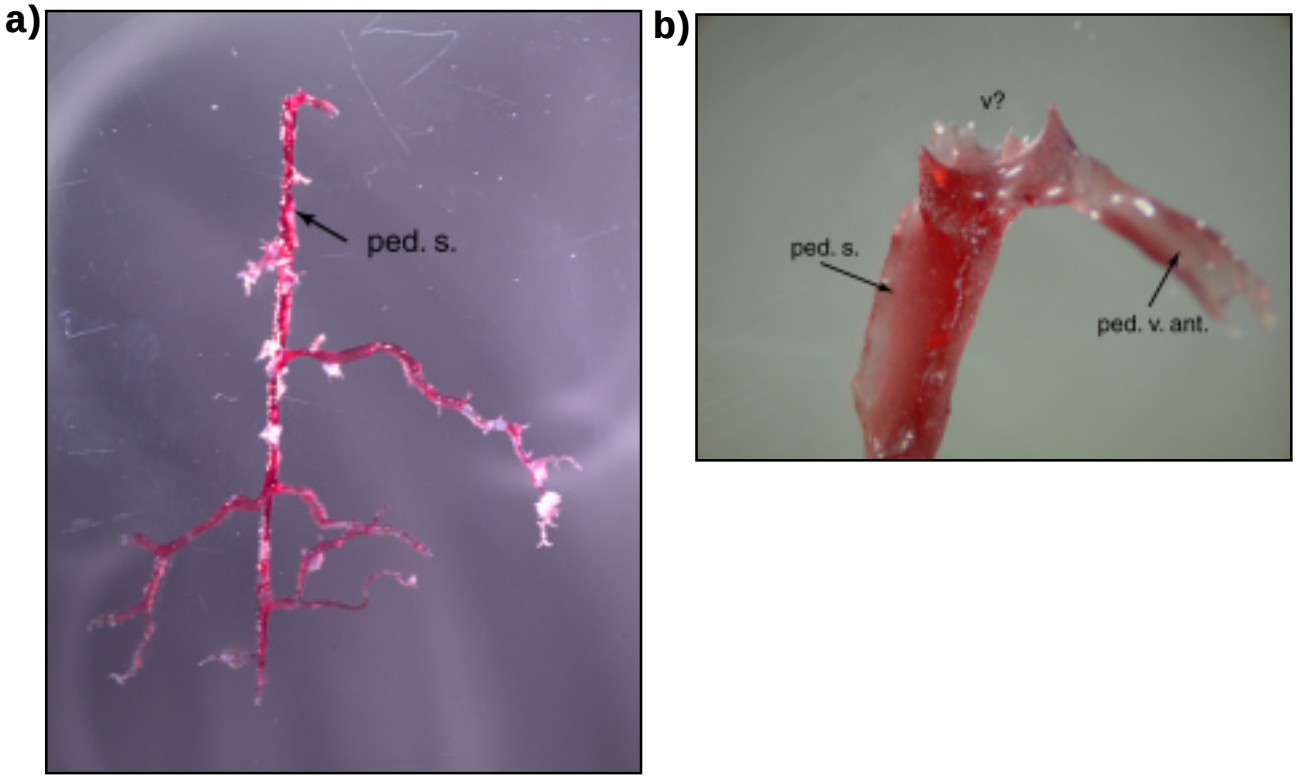


**Figure 3.18**: Corrosion cast of pedal sinus of *Haliotis iris* showing **a)** major vessels draining foot, **b)** junction with the common trunk of the anterior pedal veins showing an abrupt termination characteristic of a valve (v?), as the sinus enters the CVS. (Casting protocol CC1, pink).

giving rise to the epipodal and pedal arteries (figures 3.14, 3.15 and 3.16), as previously described for *H. corrugata* (Bourne and Redmond 1977a) and *H. cracherodii* (Jorgensen et al. 1984). The pedal arteries descend towards the sole of the foot and run posteriorly either side of the midline (figure 3.17). The haemolymph capacity of these vessels is limited due to the presence of nervous tissue in the lumen, as shown in figure 3.17. Haemolymph is collected from the foot in a number of large lateral vessels draining to the pedal sinus (figure 3.18a). The anterior pedal veins drain the anterior lobes of the foot into a common trunk, which ascends to join the pedal sinus as it enters the CVS (figure 3.15). On a number of occasions casts of the pedal sinus showed an abrupt termination at the entrance to the CVS (e.g. figure 3.18b), suggestive of the impression left by an occluded valve. Crofts (1929) describes such a valve in *H. tuberculata* and Bourne and Redmond (1977a) go on to describe valves between the CAS and pedal arteries in *H. corrugata*. As Russell and Evans (1989) point out, the presence of valves on the pedal arteries and sinus is of considerable functional importance, as they could allow the foot haemocoel to be isolated during a pressure surge. Direct evidence for the presence of a valve, i.e. through dissection or thin sectioning, was equivocal due to the great complexity of tissue in the cephalopedal region. On one occasion horizontal sectioning revealed a muscular aperture that appeared to be a valve at the anterior extreme of the pedal sinus, as shown in figure 3.19. Physiological evidence for the presence of a valve is presented in chapter 7.

The epipodium, like the foot, also receives its haemolymph supply directly from the CAS. The left and right epipodal arteries project laterally from the ventral surface of the CAS and run posteriorly along the inner circumference of the epipodium (figures 3.15, 3.16 and 3.20a). The epipodal veins are intimately associated with these arteries, forming a concentric horseshoe sinus around each artery (figure 3.20b), ultimately draining into the common trunk of the anterior pedal veins (figure 3.16). The epipodal venous system would therefore also be affected by the presence of a valve between the pedal sinus and CVS. Crofts (1929) and Bourne and Redmond (1977a) also describe numerous minor arteries serving the cephalic region (figure 3.1). This description has not been further elaborated here. All cephalic venous return is assumed to drain into the CVS.

Crofts (1929) and Russell and Evans (1989) describe arteries leaving the anterior aorta to supply the intestinal loop, oesophagus and oesophageal pouches. As these arteries pass through the gut sinuses it proved impractical to trace their path using the casting techniques employed here. Croft's description of these arteries is therefore accepted. No corresponding veins were seen to traverse the gut sinus, it is therefore suggested that all venous return from the alimentary canal is initially collected by the gut sinus system.

### 3.3.4. *Vascular short-circuits between the gut sinuses*

The CVS-gut sinus system follows the alimentary canal but, unlike the gut lumen, does not represent a truly linear cavity. At a number of locations, reflected sections of the sinus abut each other and haemolymph can readily cross from one sinus region to another. Two examples are conspicuous in corrosion casts:

In *H. tuberculata* (Crofts 1929), *H. corrugata* (Bourne and Redmond 1977a) and *H. rubra* (Russell and Evans 1989) the pedal sinus drains exclusively into the CVS. In *H. iris*, however, the pedal sinus crosses the valve region described above and then bifurcates, draining into both the CVS (figure 3.14) and the intestinal sinus (figure 3.9). In addition to dividing venous flow from the foot/epipodium, this bifurcation may also provide a means for haemolymph to flow directly between the CVS and intestinal sinus.

The descending limb of the intestine crosses the dorsal surface of the crop, within this region the respective gut sinuses share a common haemal space. Haemolymph therefore presumably mixes freely between the descending intestinal sinus and the crop sinus.

### 3.3.5. *Vascular systems efferent to the gut sinuses*

*Digestive gland*

The digestive gland is a tubule complex that provides sites for absorption of partially digested food and nutrients, secretion of digestive enzymes, nutrient storage and elimination of undigestible matter (Voltzow 1994). If the foot and epipodium are displaced in a live *H. iris*, a network of superficial vessels can be seen traversing the ventral digestive gland. If casting resin is then injected into the venous system, these vessels can clearly be traced to their origin at the crop sinus (figure 3.21). As the gut sinus system apparently operates at near-arterial pressures (see chapter 7), it is suggested that haemolymph flows from the crop sinus into the digestive gland, these previously undescribed vessels are therefore termed ‘digestive gland portal veins’ (d. gl. p. v.). When the superficial lacunae and vessels are removed, the portal veins are seen to extend along the adductor muscle side of the digestive gland to the distal tip of the conical appendage (figure 3.23). If the arterial system is also filled with resin and the tissue digested, a system of arteries emerging through the crop sinus and overlying the portal veins is revealed (figure 3.22a and b). According to Crofts (1929), these are the hepato-genital arteries, originating from the second visceral artery, the first and largest branch of the anterior aorta. Jorgensen et al. (1984) describe the finest branches of these arteries, and their lacunae, as closely resembling capillaries. The degree of lacunar organisation and the presence of an endothelium could not be readily established with the techniques used here. The tissue was certainly highly vascularised and the permanent lacunae were seen to give rise to transient arborizations into the gonadal tissue as seasonal sexual development progressed (figures 3.22a and 3.24).

*Right kidney afferents*

Crofts (1929) describes a single superficial venous network draining the digestive gland into the anterior lobe of the right kidney of *H. tuberculata*. In *H. iris* there are two, the nomenclature proposed by Crofts, the median visceral vein, is therefore used with the distinction of inferior or superior, as described below. The inferior median visceral vein can be traced from near the tip of the conical appendage, running along the ventral side of the anterior surface of the digestive gland (facing the adductor muscle). The vein ascends to the dorsal surface, where it is joined by at least 2 other major

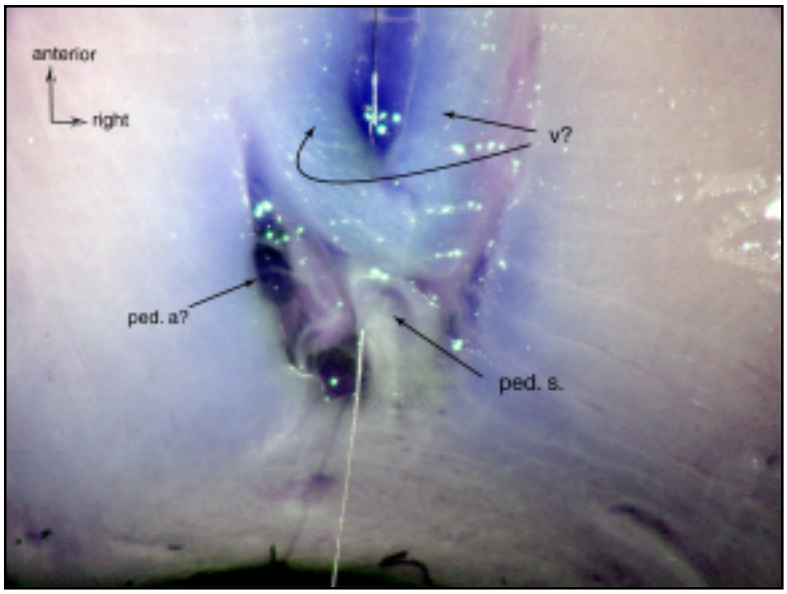


**Figure 3.19**: Thick horizontal section through the cephalopedal region (dorsal and ventral to the head sinuses) of an ethanol-fixed, adult *Haliotis iris* perfused with coloured gelatin. Wire shows continuity between pedal sinus lumen (ped. s.) and a region that appears to contain a muscular valve (v?).

a)

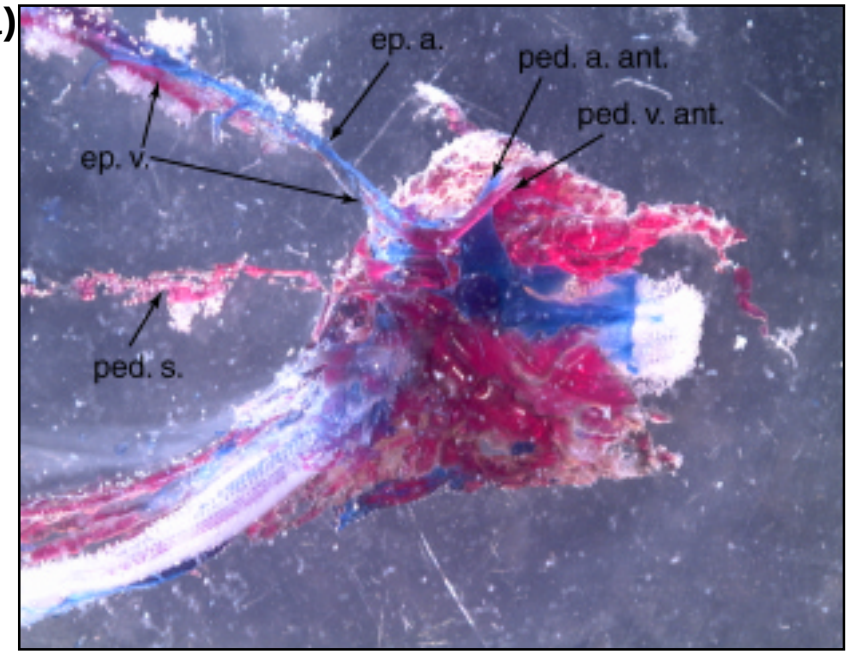


**Figure 3.20**: Partially-filled vascular corrosion cast of cephalic/anterior epipodal region, viewed ventrally. **a)** Arrangement of epipodal and anterior pedal vessels serving the right side of *Haliotis iris*; **b)** intimate association between the right epipodal artery (ep. a.) and vein (ep. v.). (Casting protocol CC3 – shell off, pink into pedal sinus, blue into right efferent ctenidial vein).

b)

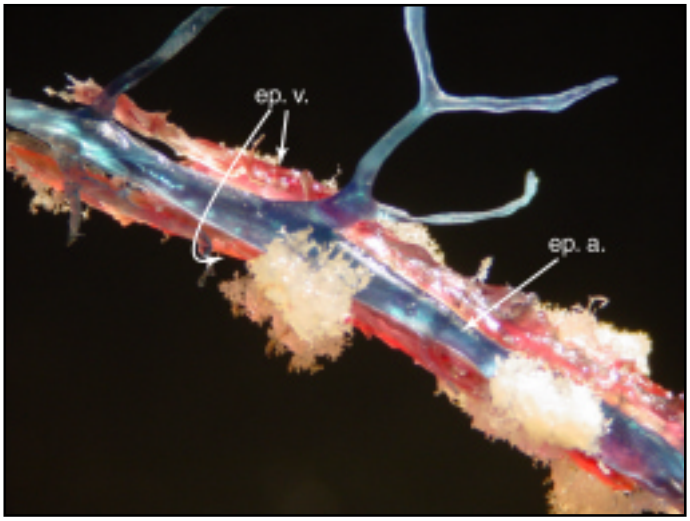

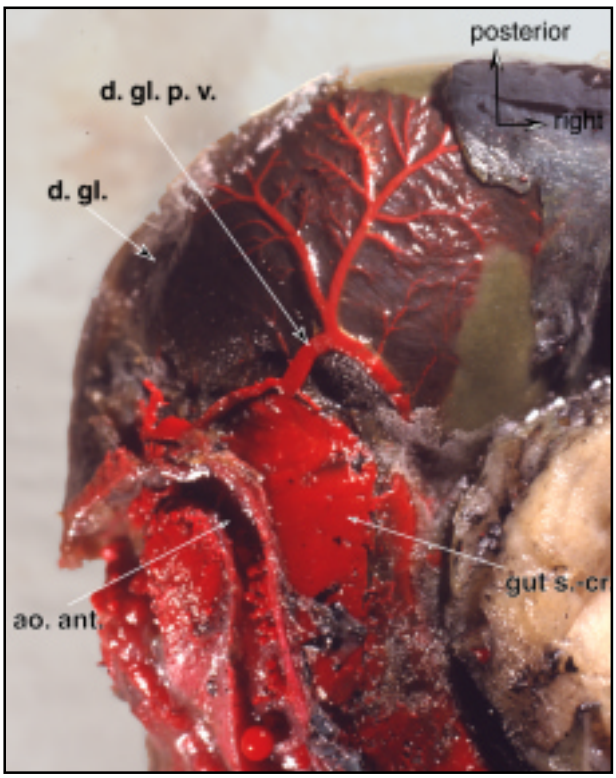


**Figure 3.21**: Venous corrosion cast photographed *in situ*, before tissue digestion. Ventral view of posterior region showing the crop sinus draining into the digestive gland via digestive gland portal veins (direction of haemolymph flow is inferred). (Casting protocol CC1 – red).

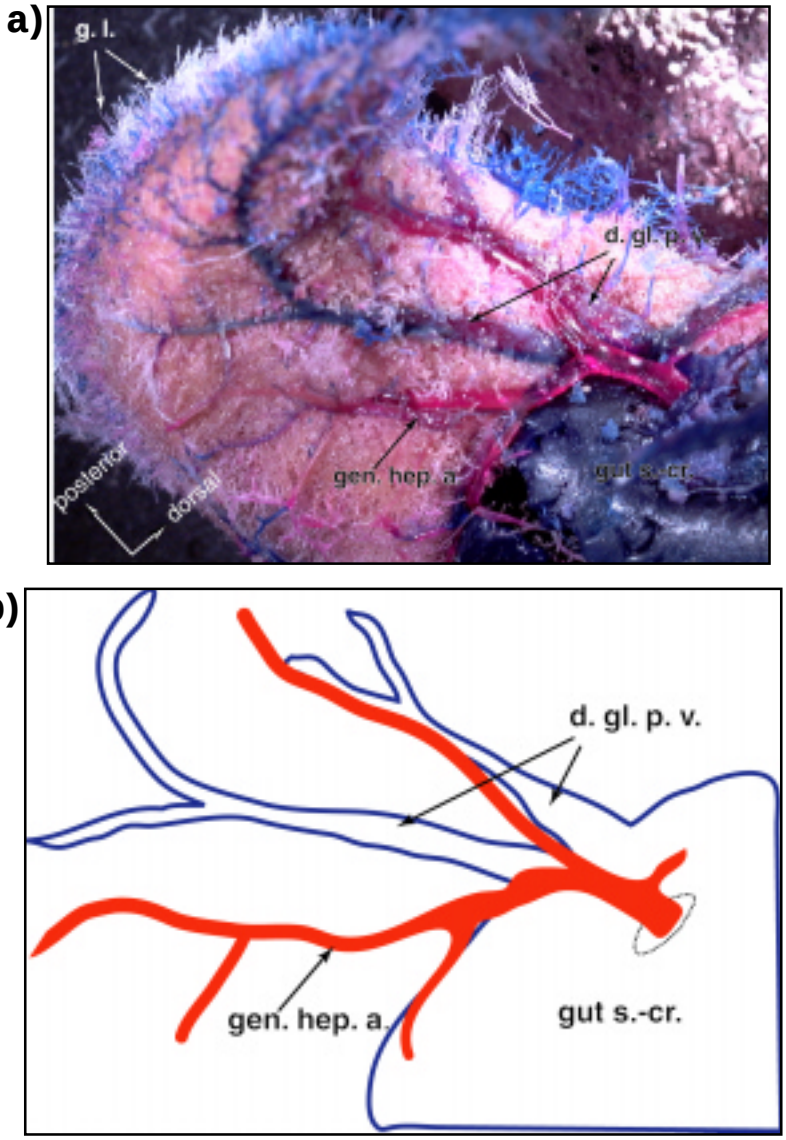


**Figure 3.22**: Two-colour vascular corrosion cast of *Haliotis iris*, blue represents venous space, pink arterial space. (Casting protocol CC3 – shell on, blue into pedal sinus, pink into right efferent ctenidial vein). **a)** Cast shows crop sinus (gut s.-cr.) draining mixed venous/arterial haemolymph into the digestive gland (defined by pink lacunae) via the digestive gland portal veins (d. gl. p. v.). The hepato-genital arteries (gen. hep. a.) emerge through the crop sinus to overlie the portal veins. Note the fine, arborising lacunae that extend through the overlying gonad tissue (g. l.). **b)** Schematic representation of the major vessel organisation shown in a).

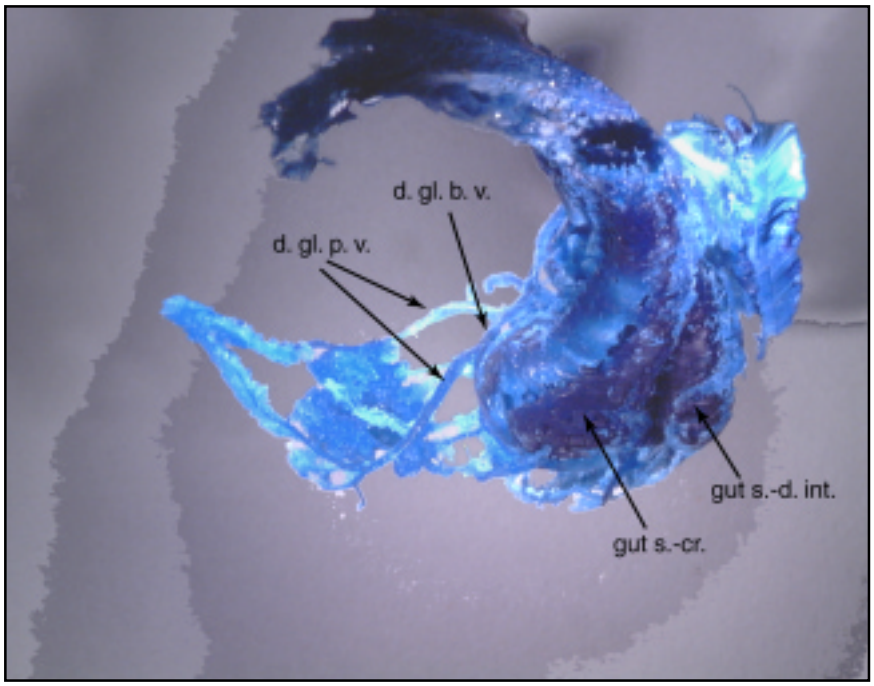


**Figure 3.23**: Venous corrosion cast, ventral view of posterior region. Superficial vessels and lacunae have been removed, showing the digestive gland portal veins (d. gl. p. v.) extending to the distal end of the conical appendage (digestive gland/gonad). (Casting protocol CC1 – blue).

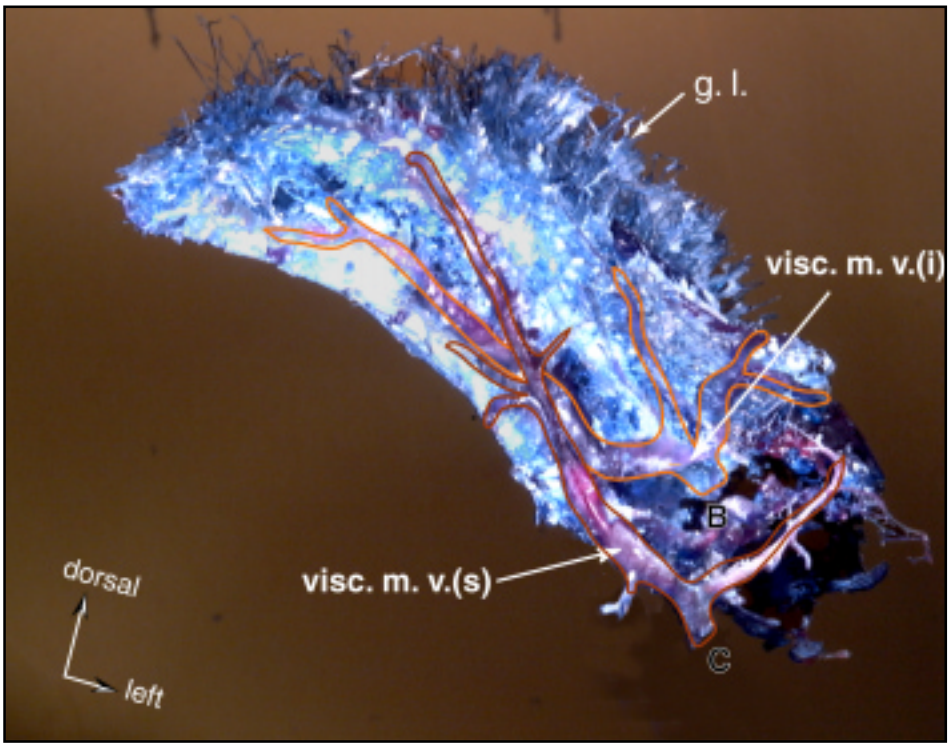


**Figure 3.24**: Corrosion cast showing the median visceral veins (visc. m. v. (i) and (s)) draining from the anterior and dorsal surfaces of the digestive gland (dense blue lacunae) into the afferent veins of the right kidney at B and C. (Casting protocol CC3 – shell on, blue into pedal sinus, pink into right efferent ctenidial vein).

vessels (figure 3.24), before draining into the anterior and posterior lobes of the right kidney (figure 3.25). The superior median visceral vein originates from a dorsal position on the conical appendage, initially descending ventrally, the vein returns to the dorsal surface, crossing over the inferior vein in the process (hence 'superior'). The superior vein is joined by a small vessel that originates from the ventral surface of the crop sinus, apparently providing a shunt between the crop sinus and right kidney ('digestive gland bypass vessel', d. gl. b. v. – figures 3.10, 3.11 and 3.23). The superior vein then joins a large vein from the left/ventral digestive gland, before dividing into numerous afferent vessels and draining into the anterior lobe of the right kidney, slightly anterior to the inferior vein (figure 3.25).

*Lobes of the right kidney*

The extensive right kidney (more correctly: renal organ) is technically a coelomoduct (Voltzow 1994). In abalone it is divided into four lobes (Crofts 1929). For ease of reference these have been named. The posterior lobe lies dorsal to the heart and extends posteriorly into the digestive gland. The cardiac lobe forms a crescent around the posterior side of the pericardium. The anterior lobe occupies the interstitial space between, and dorsal to, the limbs of the intestinal loop. The ventral lobe is smaller, lying to the right of the left kidney, anterior to the heart.

The major afferent vessels to the right kidney have been described above. The median visceral veins convey haemolymph to the anterior region of the posterior lobe and the entire anterior lobe of the right kidney, regions not directly contacting the digestive gland. It appears that numerous short afferents carry haemolymph directly from the digestive gland into the remaining right kidney regions. There are two clear exceptions to the apparently simple sequential arrangement of all haemolymph flow from the gut sinuses to the digestive gland and then to the right kidney. The first, as described above (figures 3.11 and 3.23), is the digestive gland bypass vessel which conducts haemolymph directly from the crop sinus into the afferent vein supplying the anterior right kidney lobe. The second is a very large vessel originating from the cephalic region, the renal bypass vein. The latter is described in detail below.

*Right renal bypass vein*

Examination of corrosion casts of the anterior right kidney vasculature reveals a large vessel running from the right side of the cephalic region; the vessel runs posteriorly between the limbs of the intestinal sinus, within the left mantle, pressed against the adductor muscle (figures 3.26 and 3.28a). The vessel enters the anterior lobe of the right kidney and hence, without further preparation, appears to represent a simple renal afferent. Crofts (1929) noted "Perrier stated that the large anterior efferent renal vein conveys blood in a direct stream, from the abdominal perivisceral lacunae to the ctenidia, without breaking up in the renal tissues. All my evidence points against Perrier's view". Both Crofts (1929) and Perrier (1889) worked with the European abalone, *H. tuberculata*; the former proposed an open lacunar system draining haemolymph from the anterior region into the right kidney (see figure 3.1), the latter a distinct vessel running directly to the efferent renal sinus. The present study suggests that Perrier's interpretation is correct, at least for *H. iris*.

If the lacunae of the anterior lobe of the right kidney are carefully cleared away from a vascular cast, the bypass vessel is clearly seen to traverse the kidney lobe and join directly to the efferent renal sinus (figures 3.27a and b). Tracing the bypass vein towards the anterior is problematic using corrosion casting techniques as the vessel becomes enveloped by the intestinal sinuses (figure 3.26). The most effective technique for tracing the vein's path proved to be the injection of amaranth-stained gelatin into the venous system, followed by serial sectioning of 2 – 3mm thick transverse sections. Using this technique the bypass vein, inflated with pink gelatin, could be readily identified, juxtaposed to the intestine (e.g. figure 3.28a). Serial sectioning allowed the vessel to be followed anteriorly and was found to join the sinus surrounding the ascending intestine as it enters the cephalic region (figure 3.28b).

In addition to serving as a low resistance shunt past the right kidney, the bypass vein also receives the efferent haemolymph from the entire anterior lobe and part of the posterior lobe (eff. ren. v., figure 3.27a and b).

*Right kidney efferents*

The right kidney bypass vein and the vessels draining the cardiac, ventral and posterior lobes meet in the efferent renal sinus (figure 3.29). The sinus then narrows slightly towards the left, en route to the basibranchial sinus, at which point a large valve is encountered. The valve is readily located in dissection by opening the basibranchial and efferent renal sinuses lengthways, the valve is seen as 2 collagen-like bundles occluding the junction between the sinuses (figure 3.30a). The valve can be forced open (figure 3.30b), but retains its elasticity and returns to a natural occluding state when the pressure is released. The apparently collagenous nature of the valve tissue is clearer in wax sections, where the valve is seen to be fibrous, staining blue with Mallorie's triple-stain (figures 3.31a and b). No such valve has been reported in other abalone species. Most of the abalone's venous return passes through the efferent renal sinus; the valve therefore occupies a critical position of influence upon the systemic circulation. It may, for example, facilitate gill perfusion by rectifying flow or prevent pressure surges from damaging the lamellae. Possible roles for this valve are considered in greater detail in chapter 7.

*Right kidney urocoel*

A description of the excretory system per se was not an objective of the current study. However, during the examination of right kidney vascular arrangement, an important feature of the urocoel was observed. Crofts (1929) plainly states that *H. tuberculata* lacks a true ureter; instead the urocoel narrows to a simple pouch, which conveys excretory products to an opening to the right of the rectum. A different arrangement was observed in *H. iris*. The right kidney urocoel drains into a collecting duct slightly anterior to the heart (figure 3.32), the duct runs anteriorly, juxtapose to the right side of the rectum, draining into the branchial chamber at the level of the basibranchial sinus. A microvilli brush border is seen along much of the duct's length (figure 3.31b), implying a reabsorptive function, the duct is therefore considered to be a dynamic ureter in *H. iris*. Amongst the prosobranchs described to date, only a few freshwater species, notably *Viviparus* spp., are believed to have a ureter (Voltzow 1994).

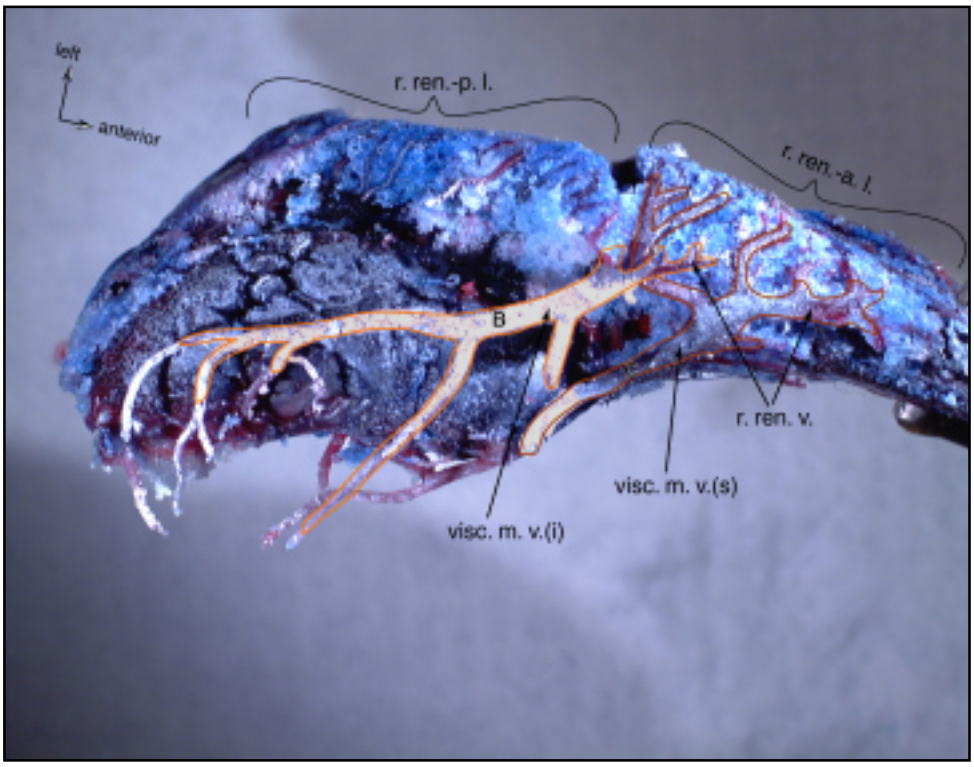


**Figure 3.25**: Dorsal view of corrosion cast showing the main venous drainage from the digestive gland into the anterior and posterior lobes of the right kidney (r. ren.-a. l. and r. ren.-p. l., respectively). Positions corresponding to severance points B and C in figure 3.24 are marked accordingly. (Casting protocol CC5).

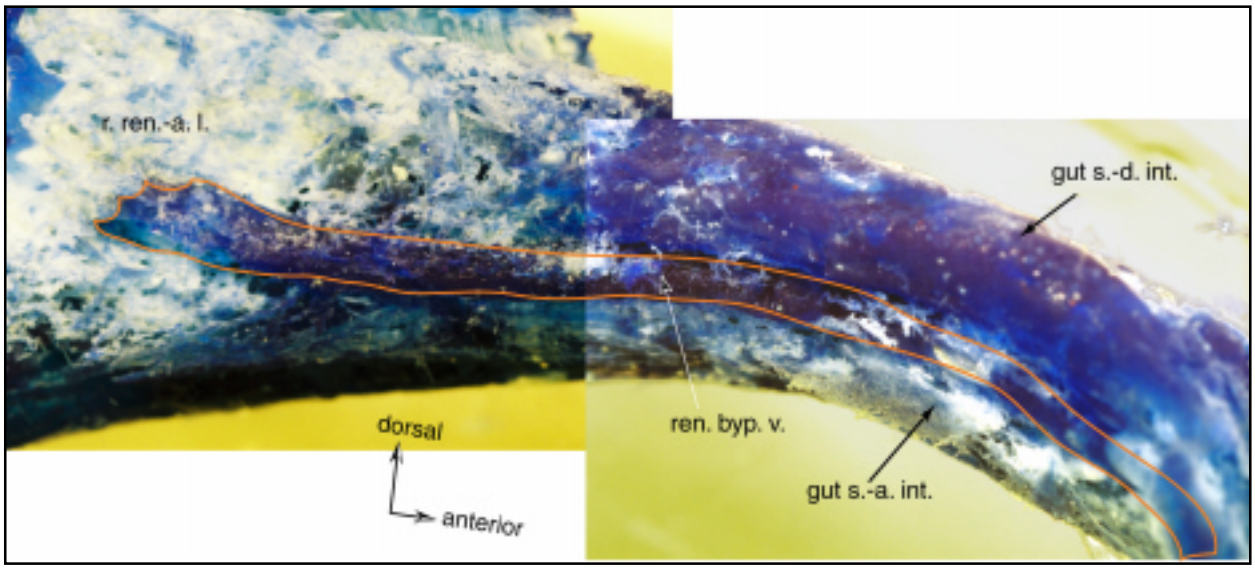


**Figure 3.26**: Right-side view of venous corrosion cast showing right kidney bypass vein (ren. byp. v.) running between the ascending (gut s.-a. int.) and descending (gut s.-d. int.) limbs of the intestinal sinus, disappearing beneath the lacunae of the anterior lobe of the right kidney (r. ren.-a. l.). (Casting protocol CC1 – blue).

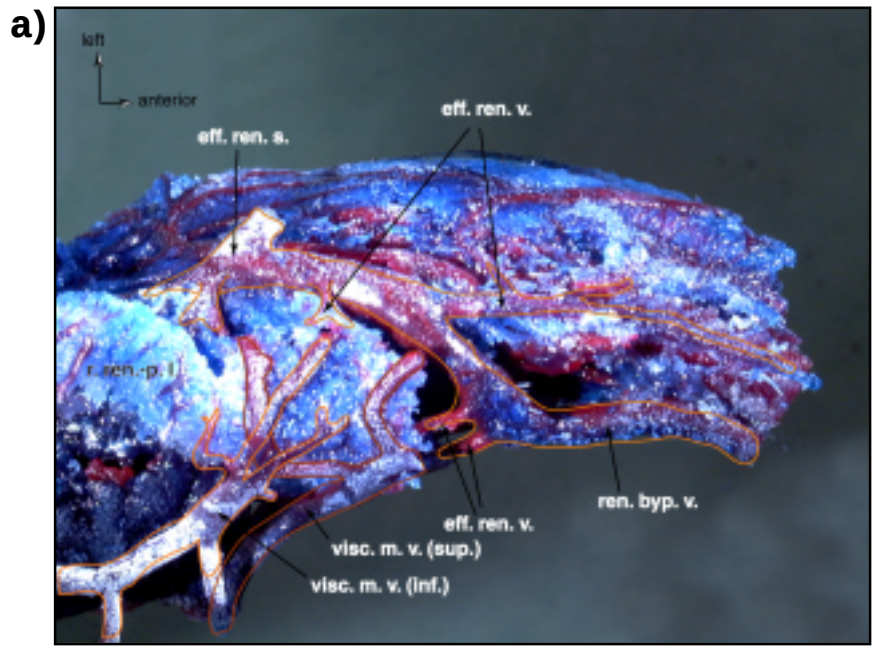


**Figure 3.27**: Vascular corrosion cast, using a sequential injection of blue, followed by red resin to maximise contrast (blue remains in lacunar beds, red in main vessels. **a)** Dorsal view of cast with anterior right kidney lobe removed, showing the right kidney bypass vein (ren. byp. v.) crossing dorsally from the right side of the viscera, before descending to join the efferent renal sinus (eff. ren. s.). (Casting protocol CC5). **b)** Schema showing the arrangement of major vessels photographed in a). Serrated lines indicate a major vessel that has been cut or disappears from the field of view.

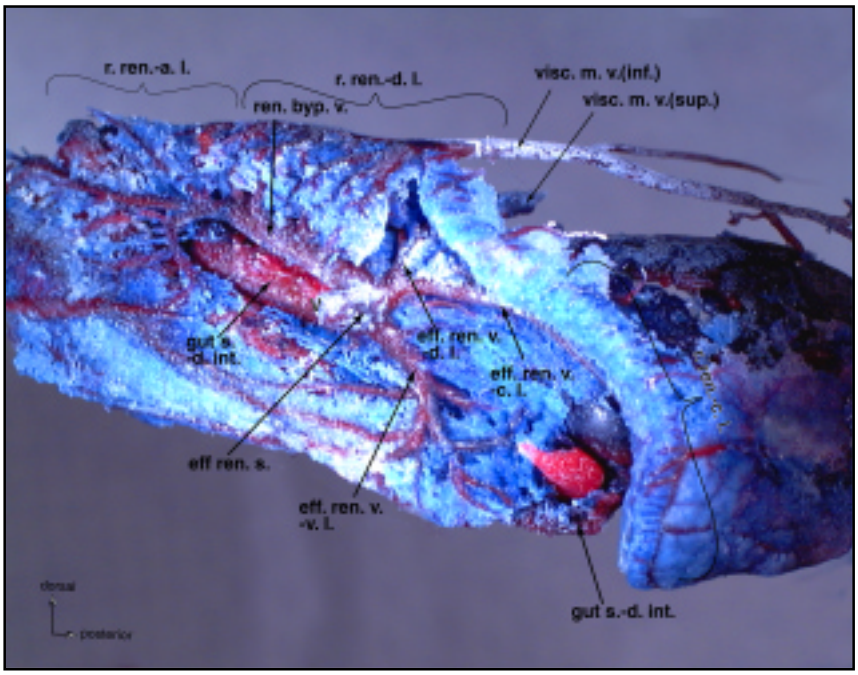


**Figure 3.29**: Left side view of cast shown in figure 3.27, overlying cast of gills and heart has been removed to expose the efferent vessels draining the four lobes of the right kidney (eff. ren. v.-p. l. = posterior lobe, -c. l. = cardiac lobe, v. l. = ventral lobe, ren. byp. v. = renal bypass vein which also acts as efferent vessel to the anterior lobe). The sinus surrounding the descending intestinal limb (gut s.-d. int.) is also seen as it crosses the ascending limb and again at its terminus against the pericardium. (Casting protocol CC5).

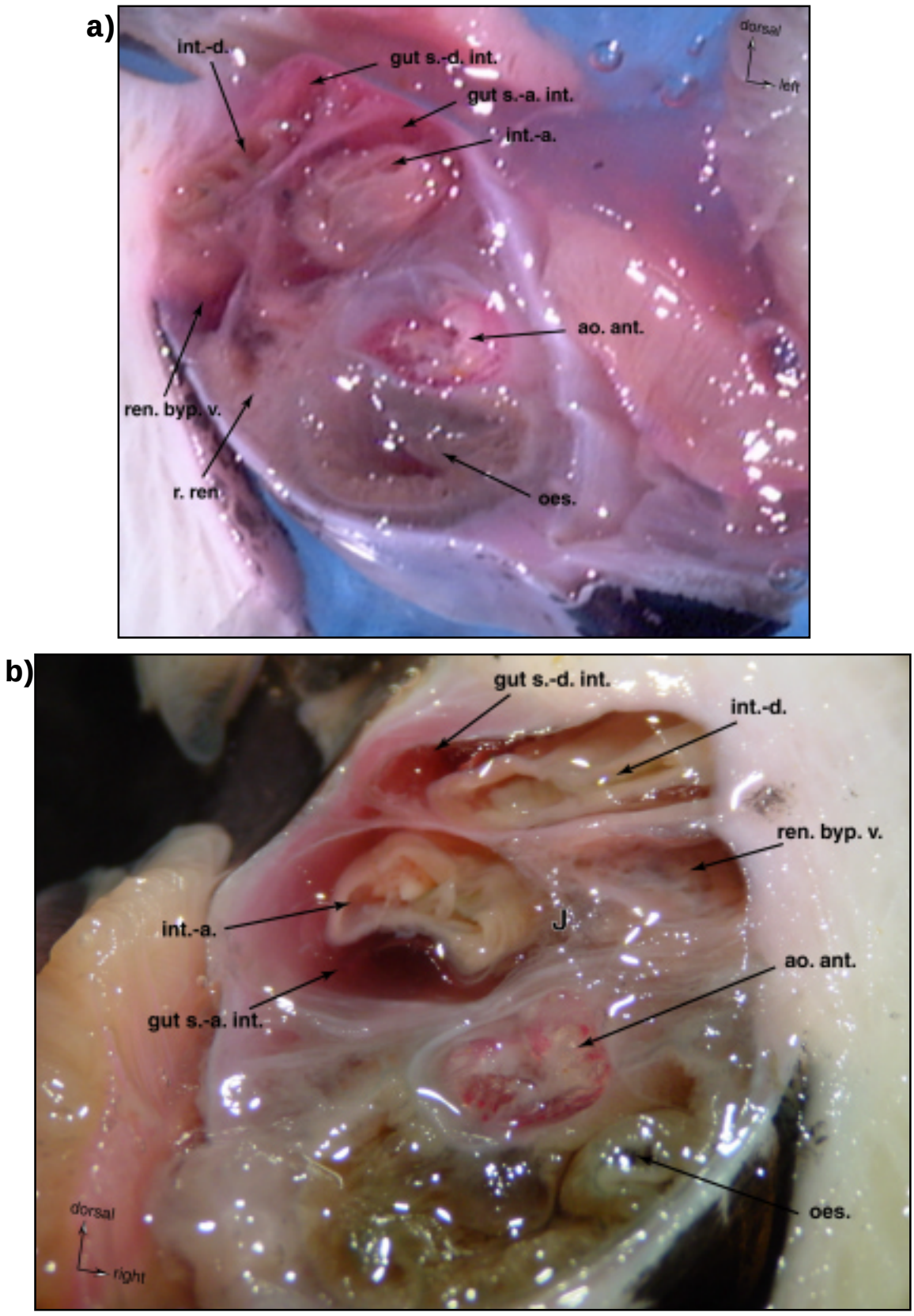


**Figure 3.28**: Amaranth+gelatin injected *Haliotis iris*, followed by fixation in 70% ethanol. **a)** TS viewed towards posterior, through intestinal region at the level of the second oldest shell hole. The right kidney bypass vessel (ren. byp. v.) deforms to fill the interstitial space to the right of the circular-profile limbs of the intestinal loop. **b)** TS viewed towards anterior, slightly posterior to odontophore. The right kidney bypass vessel has remained to the right of the intestine and is shown joining the ascending intestinal sinus (gut s.-a. int.) at J, slightly posterior to the intestinal U-bend, to the right of the head.

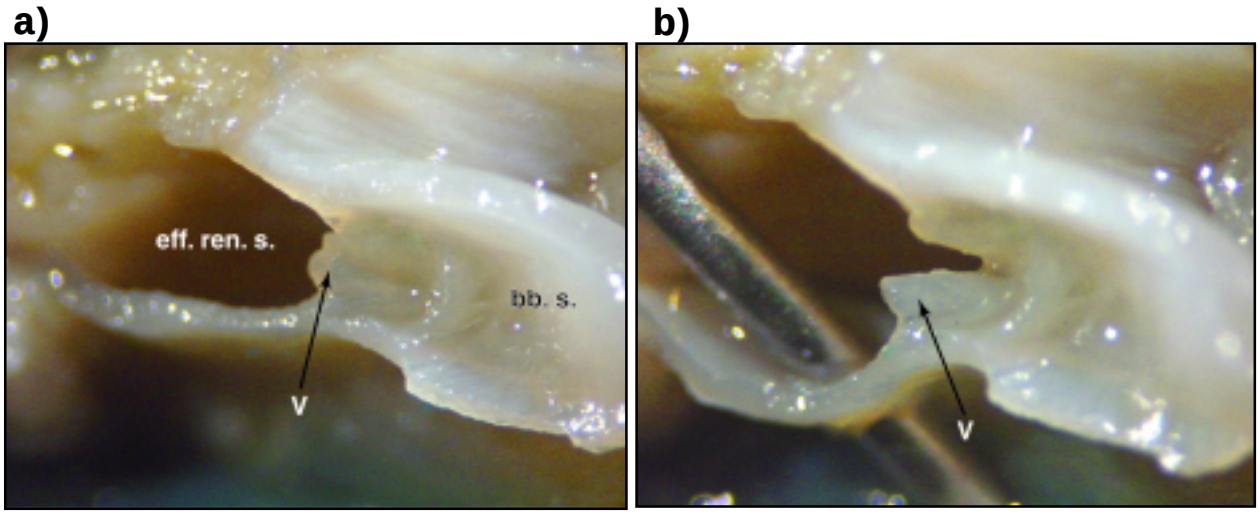


**Figure 3.30**: Fresh dissection showing bisection of efferent renal sinus (eff. ren. s.) and associated valve **a)** relaxed (closed position) and **b)** pinned open.

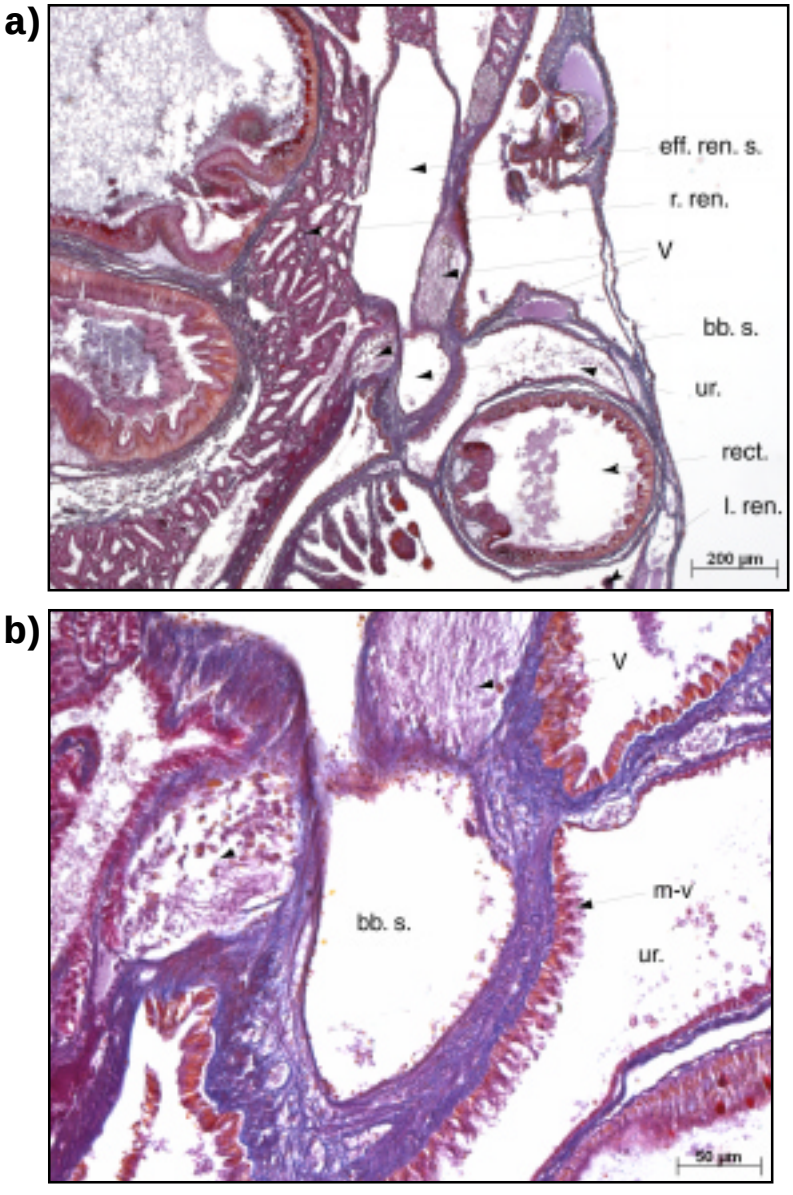


**Figure 3.31**: 7µm wax TS from an adult *Haliotis iris* showing **a)** an overview of the efferent renal sinus (eff. ren. s.) / basibranchial sinus (bb. s.) region and **b)** close-up of the valve separating these sinuses.

The location of the valve in the efferent renal sinus is readily identified as a break point in corrosion casts (e.g. figure 3.33a). The overlying vascular cast, including the gills and heart, can therefore be lifted away from the efferent renal cast. This action reveals an intimate association between the vascular spaces of the heart and those of the efferent renal sinus and veins draining the cardiac and ventral lobes. Figure 3.33a shows a cast of the efferent renal area, figure 3.33b shows the same region with the heart cast in position, showing the close geographical association between these vascular spaces. The pericardium is in fact continuous with the walls of these efferent renal vessels, a phenomenon that Crofts (1929) has also described in *H. tuberculata*. A hypothesis was therefore formulated, suggesting that pericardial movements during the normal cardiac cycle would influence the volume of the renal sinuses; if resistance is lower in the downstream direction, compression of the sinuses would facilitate flow into the basibranchial sinus. If the valve serves a no-return function, it could then act to rectify this increased flow, resulting in an auxiliary pumping effect due to external heart movement. The hypothesis is examined in chapter 7.

Immediately downstream of the efferent renal sinus valve the vascular cavity widens into the basibranchial sinus, which delivers haemolymph to the gill lamellae via the left and right afferent ctenidial veins (figure 3.34). The rectal vein also joins the basibranchial sinus between the anterior afferent ctenidial veins (figure 3.34). This vein is described by Crofts (1929) as being efferent to the rectum, draining rectal haemolymph into the basibranchial sinus. Crofts also described a small vessel connecting the haemocoel of the left kidney of *H. tuberculata* to the basibranchial sinus which, in contradiction of Wegmann (1884, cited in Crofts 1929), she believed to be efferent to the left kidney. Russell and Evans (1989) describe a fundamentally different arrangement in *H. rubra*, where multiple afferent vessels drain from the abdominal visceral sinus into the left kidney and multiple efferents drain into the basibranchial sinus (see text of figure 3.1). Despite a geographical association that is so close it forces the basibranchial sinus to contour around the anterior tip of the left kidney (figure 3.34), specific thin section and corrosion cast investigations have failed to locate a corresponding connection in *H. iris*.

Given their importance as the principal gas exchange organs of the abalone, a specific section has been devoted to the vascular and anatomical detail of the gills (see section 3.3.6 below).

*Hypobranchial (mucous) glands*

The left and right efferent ctenidial veins receive haemolymph from the corresponding gills and connect to the corresponding auricle of the heart. The pallial vein (see below) also drains into the right efferent ctenidial vein slightly upstream of the heart (figure 3.36). Each gill is associated with a hypobranchial mucous gland which, together with the corresponding osphradium, form a functional unit (Yonge 1947, Voltzow 1994). Yonge (1947) suggests the hypobranchial glands are principally associated with branchial hygiene, as particulate matter contacting the hypobranchial glands is consolidated in mucus and transported to the dorsal shell holes via ciliated grooves. The right mucous gland is greatly reduced (Yonge 1947, Purchon 1977), overlying the rectum, between the posterior sections of the efferent ctenidial veins. Venous casts show the right mucous gland to drain

into the left afferent ctenidial vein via large numbers of fine, parallel lacunae (figure 3.35a and b). The larger left mucous gland lies dorsal to, and in confined by, the left efferent ctenidial vein. It is therefore suggested that the left mucous gland also drains into the left efferent ctenidial vein.

*Left kidney*

The function and vascular position of the left kidney are fundamentally different from those of the right. The left kidney receives haemolymph that has been cleared of metabolites, notably ammonia, by the right kidney (or perhaps the gills) and oxygenated at the gills, factors which greatly facilitate its role as a site of re-absorption (Fretter and Graham 1994). The left kidney urocoel is connected to the pericardial chamber via a low resistance renopericardial canal which, combined with the small volume and high surface area of the organ imply a rapid turnover of primary urine (Fretter and Graham 1994). The left kidney of *H. iris* has vascular connections with the right efferent ctenidial vein and the left auricle, a fact that has profound influence upon the filling of both auricles. When corrosion casting resin was injected into the right efferent ctenidial vein, rather than following the more direct route into the right auricle, the resin back-filled the right gill as far as the gas exchange surfaces of the lamellae and then flowed forward across the left kidney to fill the left auricle and left efferent ctenidial vein (figure 3.36). This perfusion pattern was highly repeatable and was also observed by Crofts (1929), when injecting dye into *H. tuberculata*. The possible importance of the low resistance route across the left kidney in controlling or accommodating changes in gill perfusion is discussed in chapter 6. In contrast to the present study, a tidal haemolymph flow has been described in the left kidney of *H. tuberculata* (Crofts 1929) as well as other archaeogastropods, and in the corresponding organ, the nephridial gland, in meso- and neogastropods, including a very detailed description in *Littorina littorea* (Andrews and Taylor 1988).

As noted by Crofts, two left renal veins join the right efferent ctenidial vein immediately anterior to the heart (figure 3.37a and 3.38a). For the reasons discussed below, these veins are tentatively assumed to be afferent and have been named accordingly. The larger of the 2 runs immediately beneath the mantle epithelium, crossing the rectum to join the superficial vasculature of the left kidney, this is referred to as the external afferent left renal vein (figure 3.38b). The smaller, slightly posterior vessel runs beneath (i.e. to the right of) the right kidney ureter and rectum, joining the internal surface of the left kidney (figure 3.37b), this is referred to as the internal afferent left renal vein. Crofts identified valves at the entrance to both vessels in *H. tuberculata*. Discontinuities in the vascular cast (figures 3.37a and 3.38a) suggest that these valves are also present in *H. iris*. The valves apparently prevent back-flow into the efferent ctenidial vein (Crofts 1929), defining the 2 vessels as afferent to the left kidney.

Thus the superficial vessels of the left kidney form a venous plexus with afferent connections to the right efferent ctenidial vein. These vessels diverge across the surface of the kidney, re-converging towards the ventral, posterior surface of the organ (figure 3.39a). Haemolymph then drains directly into the left auricle (figure 3.39b) as observed by Bourne and Redmond (1977a) in *H. corrugata*. The junction with the left auricle also appears to be protected by a valve, its position revealed by a discontinuity in the vascular cast (figure 3.39a, v?).

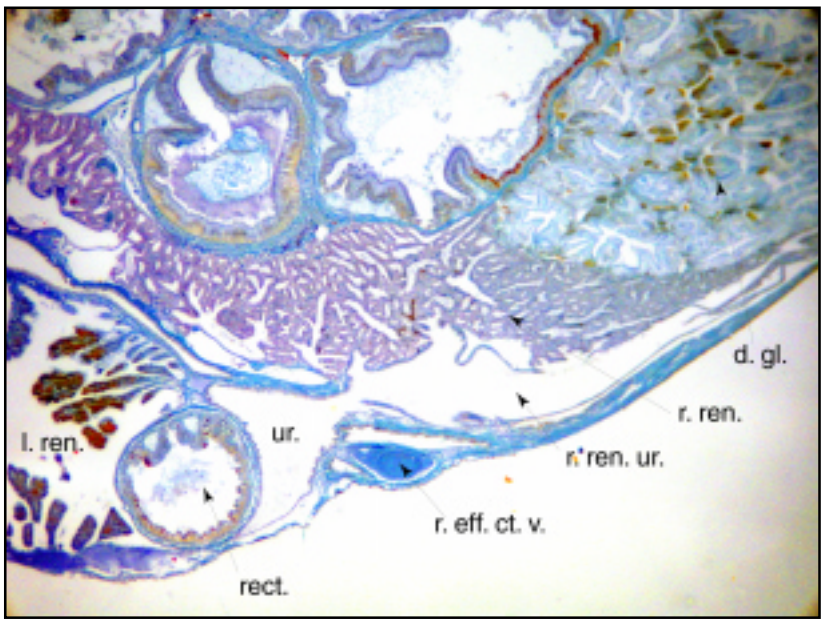


**Figure 3.32**: Micrograph of TS slightly anterior to heart showing the right kidney urocoel (r. ren. ur.) draining into a ureter which runs anteriorly along the right side of the rectum (rect.).

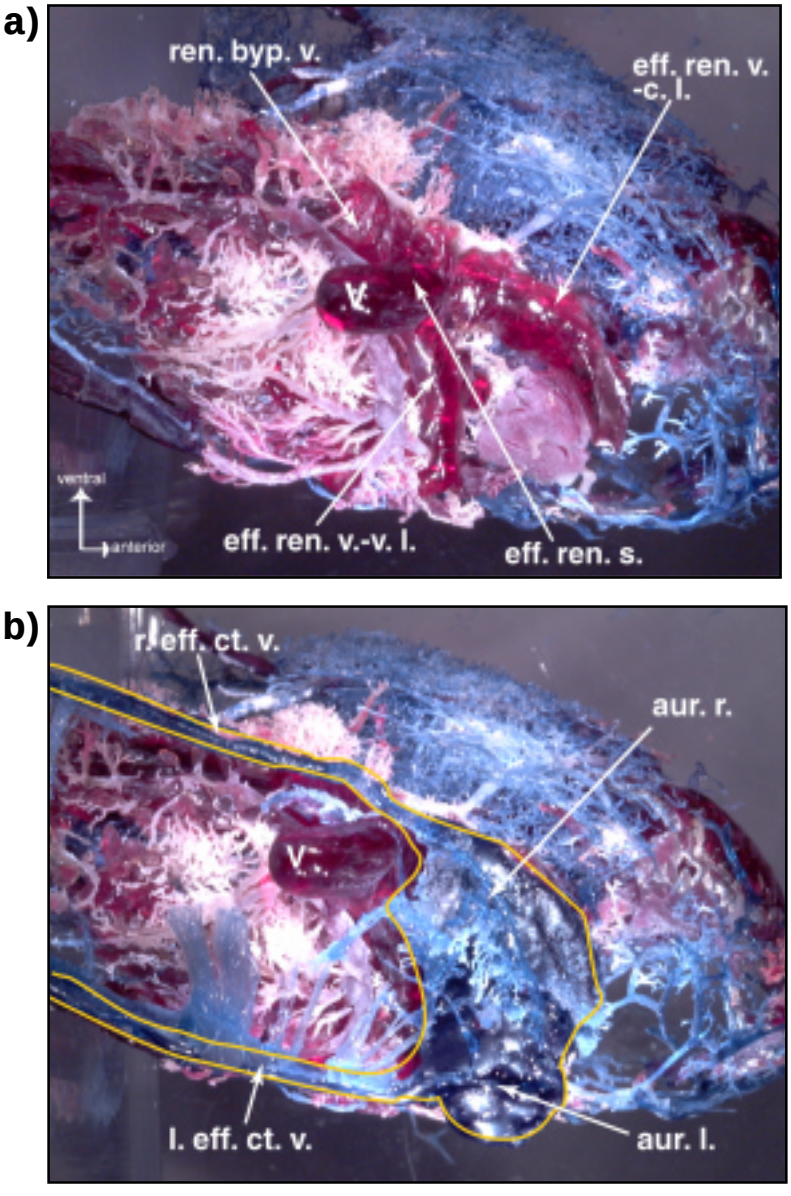


**Figure 3.33**: Left-side view of vascular corrosion cast, right kidney vasculature has been filled with pink resin, remaining spaces are blue. **a)** Efferent veins and sinus of the right kidney; all material downstream of the efferent sinus valve (V) has been removed, notably the gills and heart. **b)** Blue cast of the heart returned to its original position, overlying the efferent renal vasculature, to show the close association between the cardiac and efferent renal haemolymph spaces. (Casting protocol CC4).

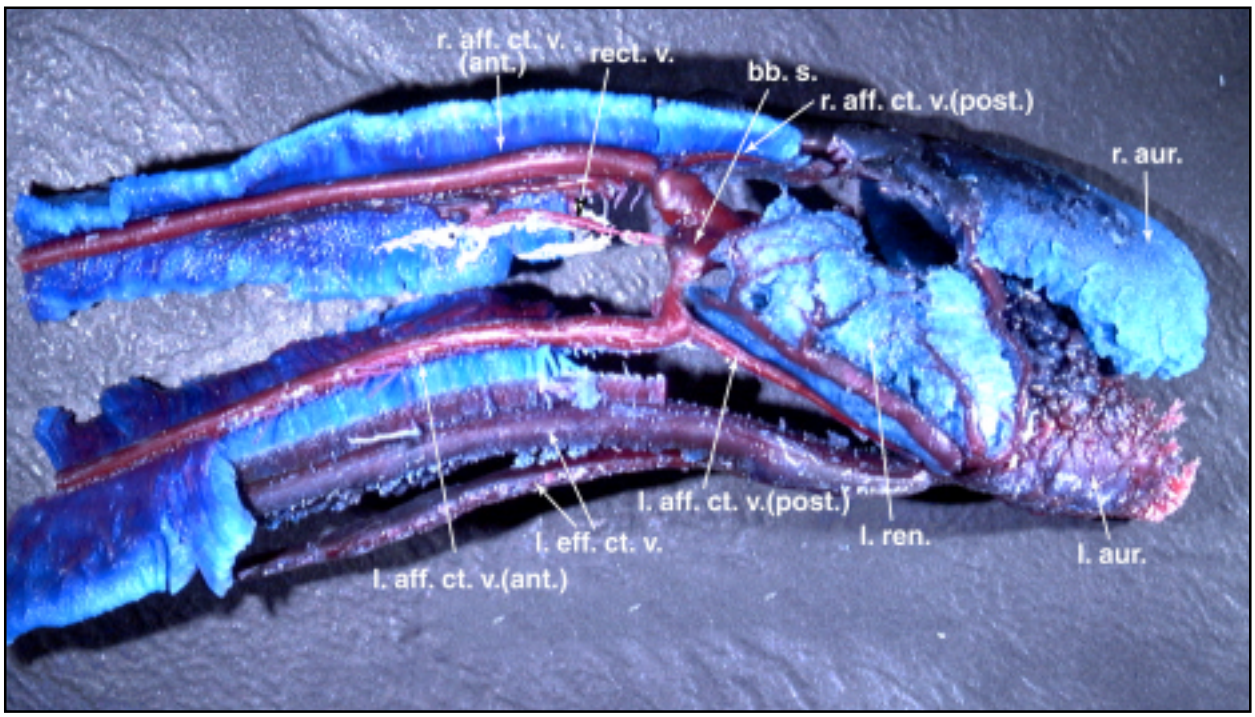


**Figure 3.34**: Corrosion cast showing the main vasculature downstream of the renal sinus. The basibranchial sinus (bb. s.) supplies haemolymph to the left and right gills and the rectal vein (rect. v.). The gills drain into the left and right efferent ctenidial veins (l. and r. eff. ct. v.) which conduct haemolymph to the left kidney (l. ren.) and the heart. (Casting protocol CC5).

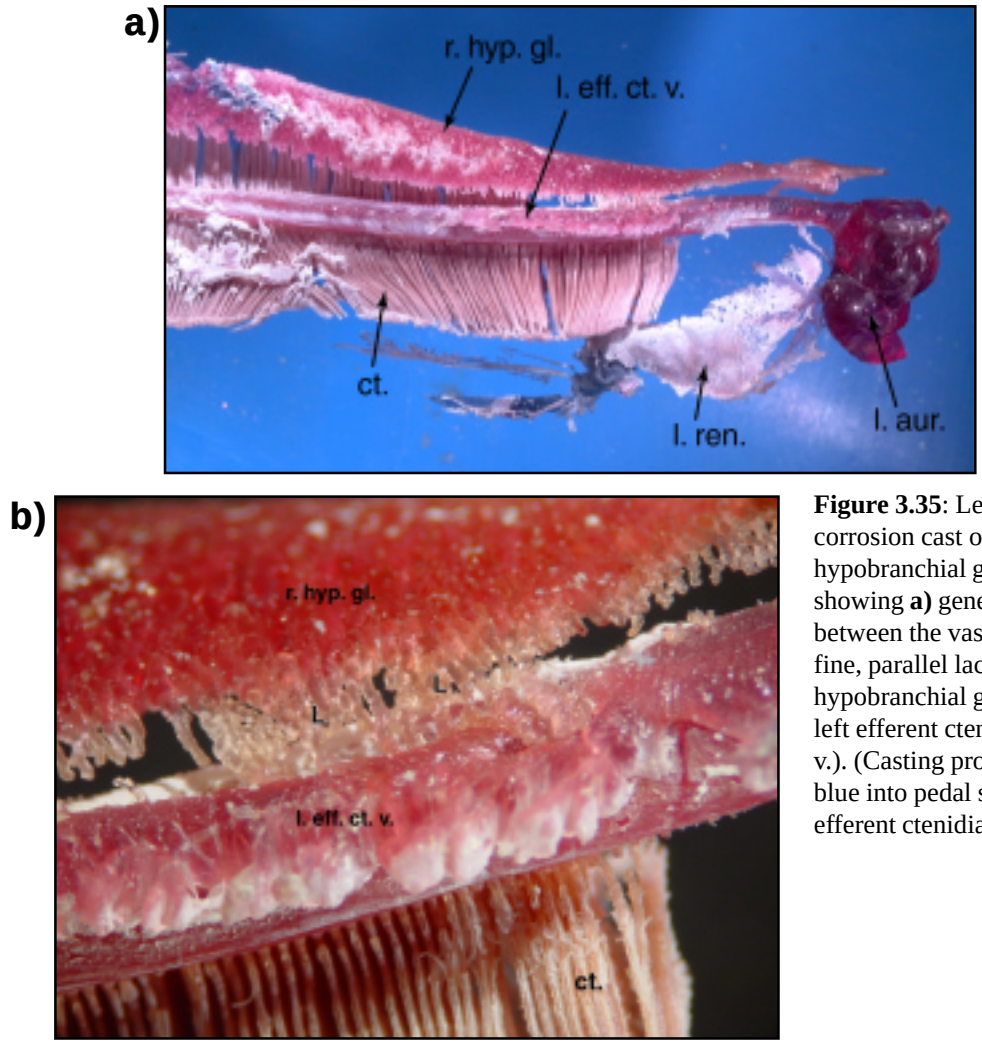


**Figure 3.35**: Left-side view of corrosion cast of left gill and right hypobranchial gland (=mucous gland) showing **a)** general association between the vascular spaces and **b)** fine, parallel lacunae (L) draining hypobranchial gland (r. hyp. gl.) into left efferent ctenidial vein (l. eff. ct. v.). (Casting protocol CC3 – shell off, blue into pedal sinus, pink into right efferent ctenidial vein).

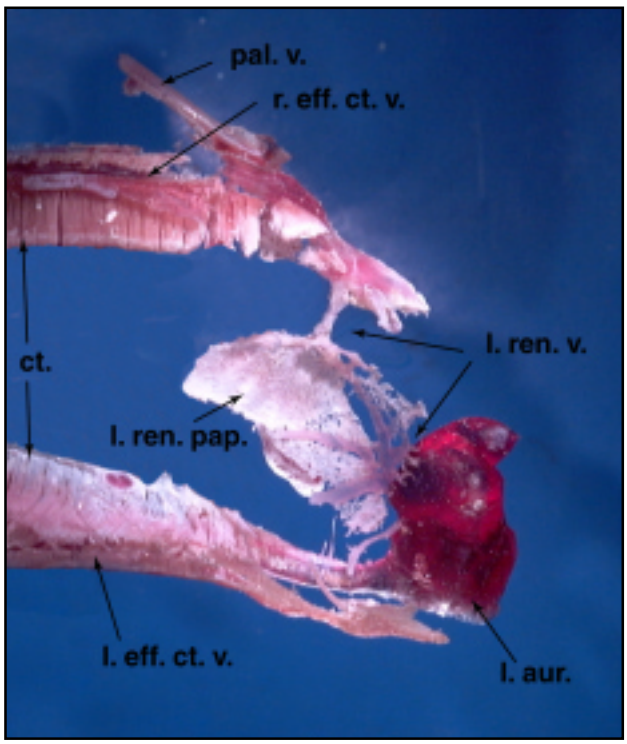


**Figure 3.36**: Partially filled vascular cast viewed from left, showing low resistance path taken by resin injected into right efferent ctenidial vein (r. eff. ct. v.), back-filling efferent side of right gill and flowing through left kidney to fill left auricle (l. aur.) and left efferent ctenidial vein. (Casting protocol CC3 – shell off, blue into pedal sinus, pink into right efferent ctenidial vein).

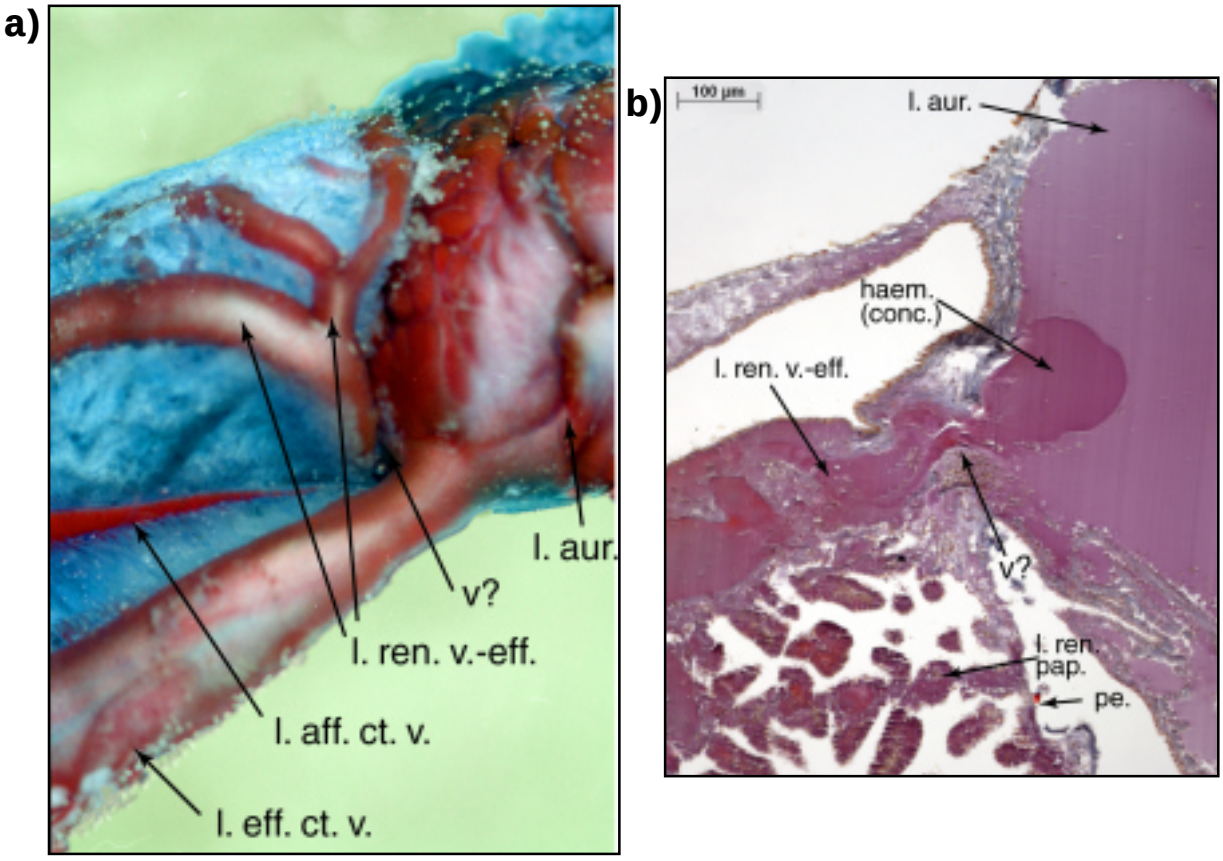


**Figure 3.39**: **a)** Left/ventral view of vascular cast of left kidney showing superficial vessels converging ventrally to drain, via an apparent valve constriction, into the left auricle. **b)** TS showing concentrated haemolymph draining from the efferent veins of the left kidney into the left auricle. (Casting protocol CC5).

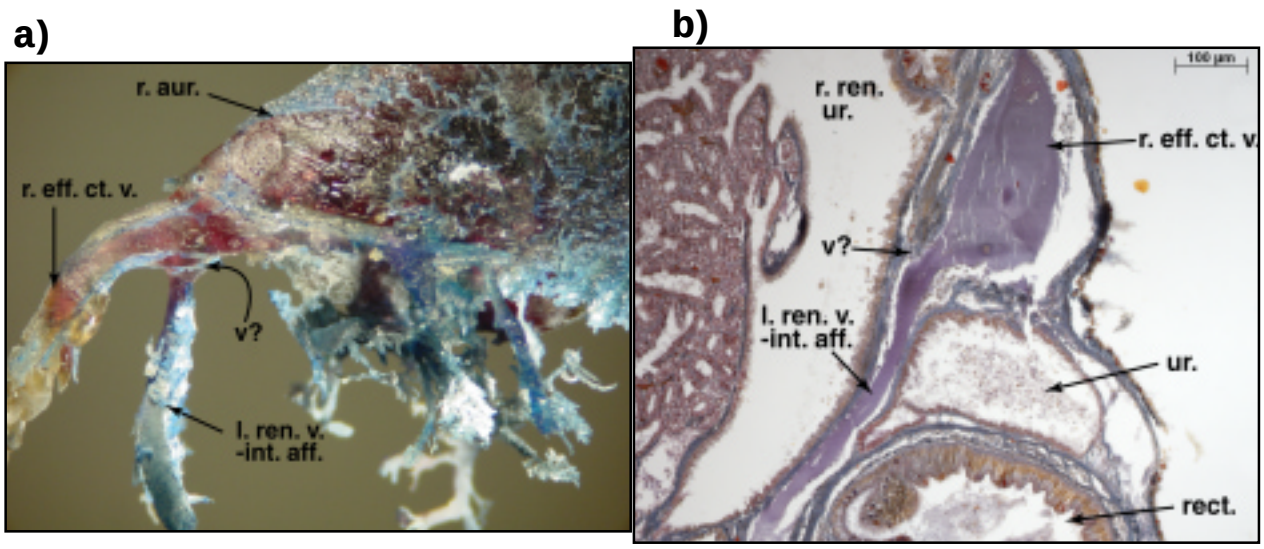


**Figure 3.37**: Connection between the right efferent ctenidial vein and the internal (i.e. right-side) afferent vein of the left kidney (l. ren. v.-int. aff.). **a)** Left-side view of corrosion cast with overlying material, notably the external afferent vein, removed revealing likely position of valve (v?) in internal afferent vein. (Casting protocol CC5). **b)** TS showing internal afferent vein leaving the efferent ctenidial vein, passing to the right of the rectum and right kidney ureter before joining the left kidney.

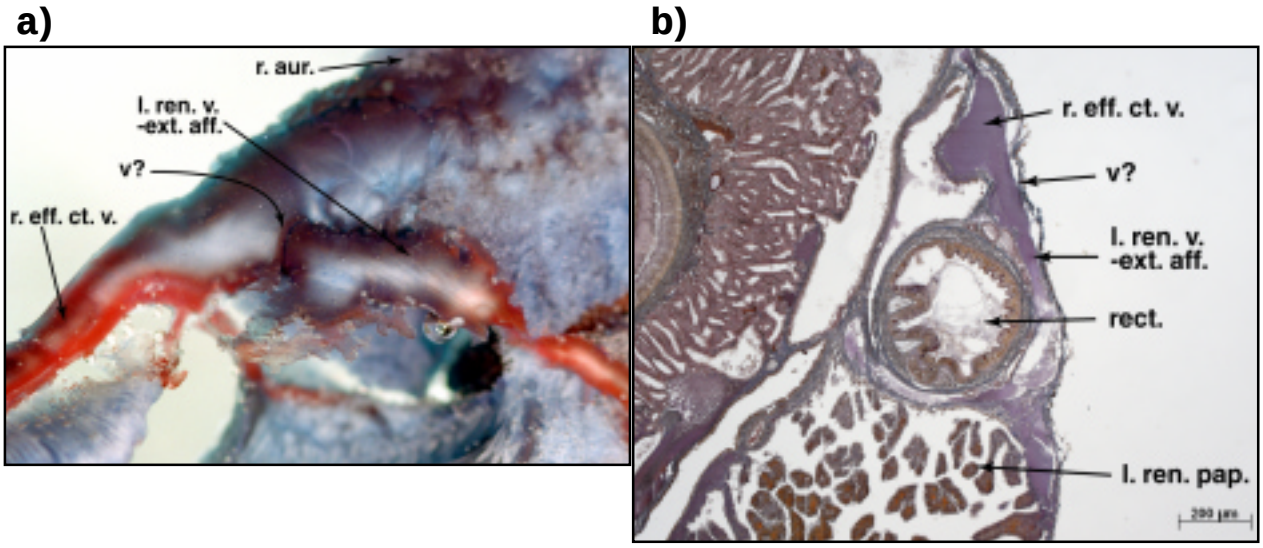


**Figure 3.38**: Connection between the right efferent ctenidial vein and the external (left-side) afferent vein of the left kidney (l. ren. v.-ext. aff.). **a)** Left-side view of intact cast showing probable valve position (v?) at entrance of external afferent vein. (Casting protocol CC5). **b)** TS showing superficial route of external afferent vein, passing over (left of) rectum before joining left kidney.

Small vessels descend from the superficial plexus into each of the renal papillae. It has been suggested that the left kidney papillae may serve to concentrate and store haemocyanin, by removal of haemolymph water at the papillae (Andrews 1981, Voltzow 1994), a function that may be retained as the left kidney evolved into the nephridial gland in higher prosobranchs, e.g. *Busycon* (Mangum 1979). The observation of concentrated haemolymph* draining from the left kidney into the more dilute systemic haemolymph of the left auricle lends weight to the haemoconcentration hypothesis (figure 3.39b). The haemocoel of the left kidney is relatively small, offering limited space for haemocyanin storage, once concentrated. It was noted, however, that a substantial haemolymph space within the left mantle extending from the anterior edge of the left kidney, follows the entire length of the left mantle, ultimately widening into the richly vascularised region of the anterior lobe of the left mantle (figure 3.40). In wax sections stained with Mallorie's triple stain the haemolymph proteins within this space appeared concentrated. The haemolymph was not readily displaced by casting resin, and therefore did not appear on any corrosion casts, implying a high resistance and slow haemolymph exchange. It is suggested that this region serves as a haemocyanin reservoir, and is tentatively termed the haemolymph gland. The mechanisms of storage and release warrant further investigation.

*Pallial circulation*

The pallial vasculature supplies the extensive mantle region to the right and posterior of the large adductor muscle. This vasculature is of interest, in the context of the current study, for a number of reasons. The pallial system is the only major vascular route to bypass the gills and has been considered a site of supplementary gas exchange in abalone (e.g. Crofts 1929) as well as other prosobranchs (Voltzow 1994). Croft's study (1929) represents the only detailed description of the pallial system currently available; her report, however, describes an apparent paradox. The 2 major vessels serving the right mantle, the (right) pallial vein and the circum-pallial vessel are both described as efferent routes, draining the mantle to the right and left, respectively. No afferent route was reported.

The mantle surrounds the entire circumference of the large adductor muscle and is responsible for secreting the characteristic iridescent blue nacreous layer that lines the shell of *H. iris*. To the right, the mantle is a simple sheet, in contact with the ventral shell surface; posteriorly it provides a pouch to accommodate the extension of the conical appendage during gonad development. The mantle passes over the head and forms the anterior right mantle lobe, separated from its left counterpart by a slit allowing ventilation through the shell holes (figure 3.4). In addition to the nacre-secreting dorsal mantle, a mantle roll also exists on the left, surrounding the viscera. To the posterior the mantle is greatly reduced, passing ventrally to the digestive gland before re-emerging as the right-side mantle. It is the haemolymph supply to the extensive right mantle that is examined here.

---

* Fixed haemolymph proteins, mainly consisting of haemocyanin, stain violet with Mallorie's triple stain. Haemolymph protein concentration is therefore considered to be a function of violet intensity in figure 3.39b.

The (right) pallial vein is readily traced with the naked eye, in a shucked, fresh adult *H. iris*. The vein originates towards the posterior of the right-side mantle, close to the adductor muscle. The vein runs anti-clockwise around the circumference of the adductor muscle, ultimately draining into the right efferent ctenidial vein, immediately before the heart. As drainage must be towards the auricular side of the heart, both the position and assumed direction of flow in the pallial vein agree with the interpretation made by Crofts (1929). The path of the circum-pallial vessel can also be traced with the naked eye in fresh specimens. Corrosion casting, however, was necessary to determine its origin. Once polymerised, the casting resin tended to fragment within the circum-pallial vessel, it therefore proved more instructive to dissect the cast *in situ*, rather than digest the flesh. These dissections clearly showed the attachment of the circum-pallial vessel to the left wall of the oesophageal sinus, shortly before it enters the head (figure 3.41a). In contrast, the circum-pallial vein of *H. tuberculata* has been described joining the abdominal lacunae, from which haemolymph percolates to the right kidney (Crofts 1929). In *H. iris* the circum-pallial vessel immediately descends from the oesophageal sinus to the ventral surface of the mantle, emerging at the point of separation of the anterior left mantle lobes (figure 3.41b). As described by Crofts, the vein follows the ventral side of the mantle, remaining near the margin, terminating in a bifurcation towards the anterior of the right mantle (figure 3.41b). No other vessels were found associated with the right mantle. The specific pressure relationships between the circum-pallial vessel and pallial vein are examined in chapter 7. Anatomically however, it seems clear that haemolymph must flow from the oesophageal sinus, through the circum-pallial vessel and into the lacunae of the right mantle, to be collected by the pallial vein. It was also noted that coloured corrosion resin injected into the CPV rapidly appeared in the region of the cardiac lobe of the right kidney, indicating the existence of a connection between these vascular spaces; the nature of this connection has still to be elucidated.

To help elucidate a possible gas exchange function for the right mantle, a cast of the lacunae between the circum-pallial and pallial veins was examined under the scanning electron microscope. The dorsal surface, in contact with the shell, had a much larger vascular volume, which consisted of a mass of fine, densely packed lacunae (figure 3.42a). The ventral surface, contacting the water possessed a coarser, more open lacunar system (figure 3.42b). The implication, therefore, is that the right mantle vasculature is arranged to supply the metabolically active nacre-secreting cells of the dorsal surface rather than to support gas exchange with the water across the ventral surface. This conclusion is a marked contrast to descriptions of the patellid archaeogastropods, that have specifically developed the ventral surface of the mantle into a gas exchange organ (Kingston 1968).

### 3.3.6. *The Gills*

*The afferent ctenidial veins*

The basibranchial sinus extends laterally to supply both afferent ctenidial veins. A simple ‘T’ junction is formed with the anterior and posterior branches of the slightly wider left afferent ctenidial vein. The posterior left afferent ctenidial vein supplies the small lamellae that lie in the direction of the heart (figure 3.34). To the right the basibranchial sinus drains into the anterior right afferent ctenidial

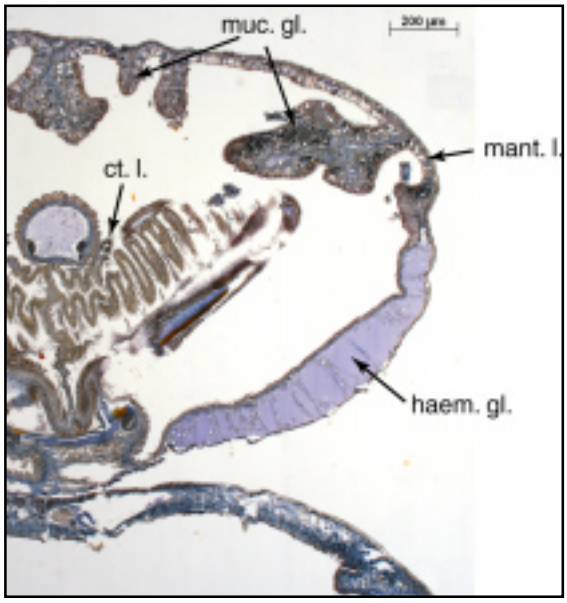


**Figure 3.40**: Wax TS of juvenile *Haliotis iris* at level of anus, viewed towards the posterior, showing an apparent gland in the left mantle containing concentrated haemolymph (haem. gl.). The gland continues from the anterior limit of the left kidney to the distal end of the anterior lobe of the left mantle.

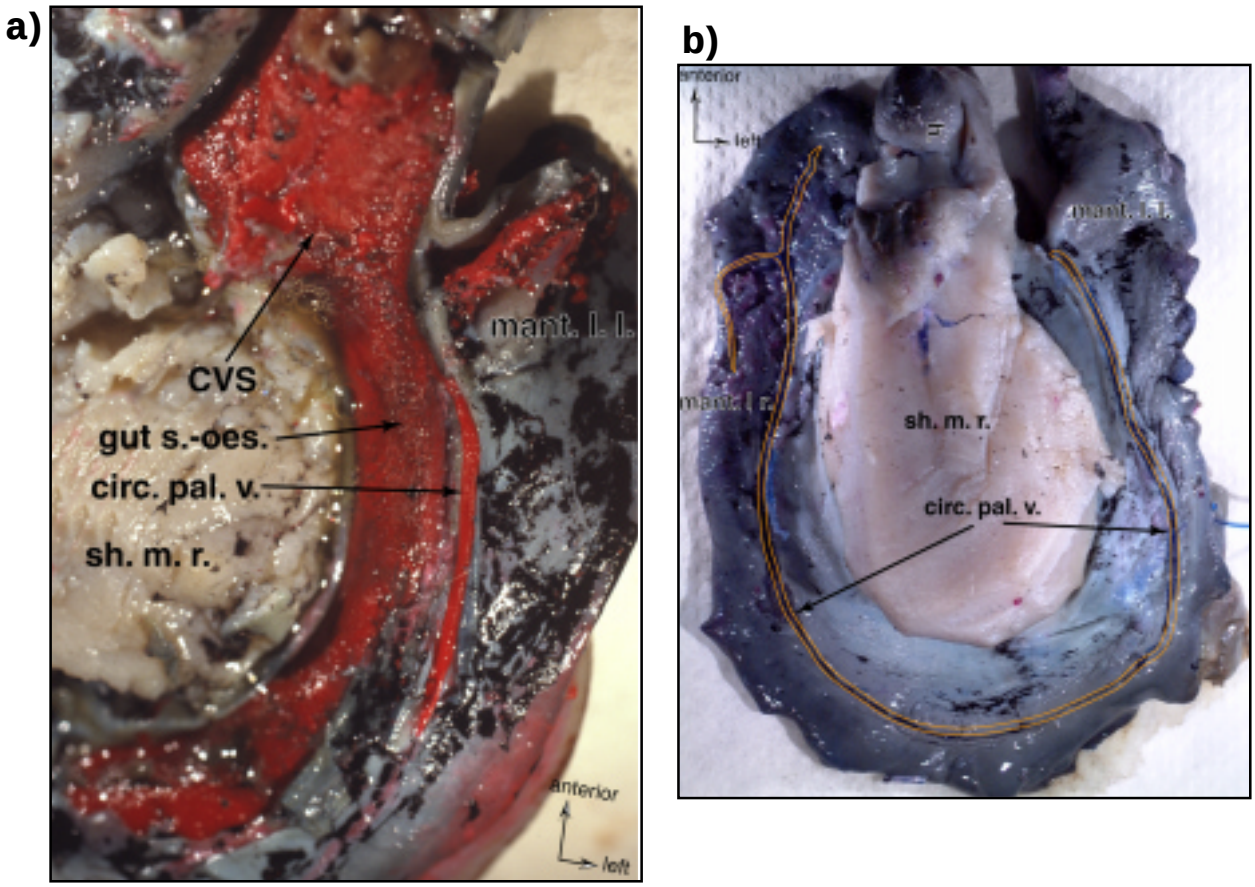


**Figure 3.41**: *In situ* dissection of *H. iris* with resin injected into the venous system (via the pedal sinus), to elucidate the path and connections of the circum-pallial vessel (circ. pal. v.). **a)** Ventral view with all ventral tissue removed from the anterior, left mantle region, revealing the junction between the circum-pallial vessel and the left wall of the oesophageal sinus (gut s.-oes.) immediately posterior to the head. (Casting protocol CC1 – red). **b)** Ventral view of blue resin (highlighted) showing the path of the circum-pallial vessel. The foot and epipodium have been removed and the circum-pallial vessel opened to show the resin. The connection to the oesophageal sinus is obscured by the anterior left mantle. (Casting protocol CC6 – blue).

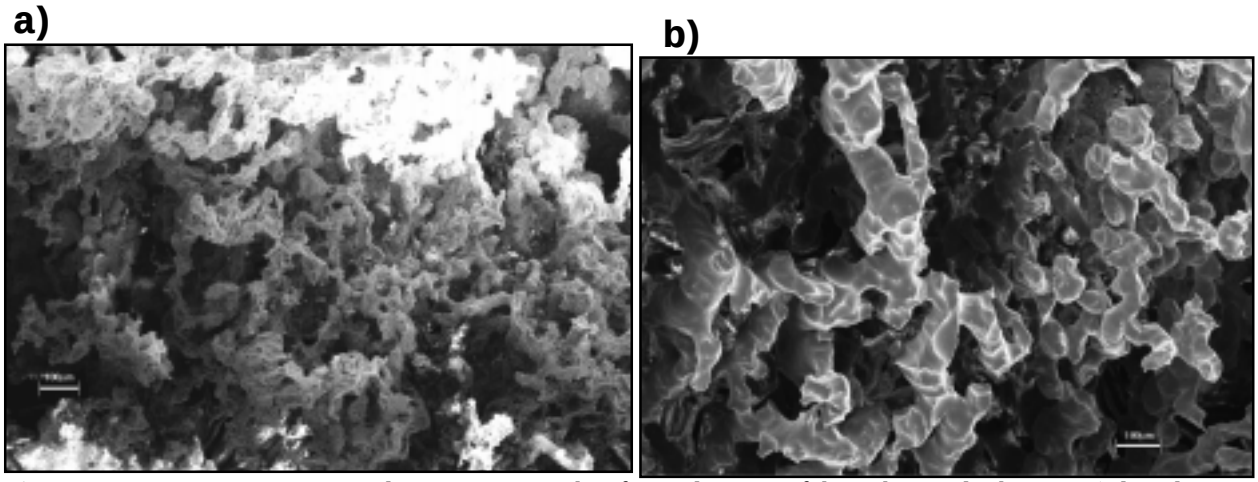


**Figure 3.42**: Low power scanning electron micrographs of vascular casts of the right mantle showing **a)** densely packed lacunae associated with dorsal surface, responsible for secreting shell nacre; and **b)** open lacunae of ventral surface contacting water. (Casting protocol CC4).

vein. The short, tapering posterior afferent ctenidial vein arises from a small aperture in the lumen of the anterior vein. Both anterior afferent ctenidial veins carry a pair of inclusions that appear to be nerves (figures 3.43a and b). Crofts (1929) identifies these as lateral branches of the rectal nerve.

*The lamellae*

The gills of *H. iris* are bipectinate, a term that describes the arrangement of lamellae on both sides of a midline running between the afferent and efferent veins. Each lamella generally mirrored its counter-part across the midline, although some heterogeneity in size was seem towards the extremities of both gills. No obvious external tissue differences were found between the anterior and posterior-facing surfaces of the lamellae. While the left gill is slightly longer, and bears more lamellae than the right, the morphology and size of the lamellae were similar for both gills. Hence the following description is generalised, applying to either surface of a lamella from either gill.

The lateral surface of a gill lamella can be divided into 3 distinct regions, arbitrarily classified here according to the nature of their physical support; these regions are labelled C, P and R on the diagrammatic representation of 2 lamellae shown in figure 3.44. These regions and their corresponding vascular spaces are described from the afferent to the efferent sides.

The internal walls of the afferent ctenidial veins are composed of a lattice of large muscle/ collagen bundles, as well as longitudinal muscles. On the lamellar side of the vein the lattice opens forming apertures for haemolymph drainage into the lamellae (figure 3.46). It is possible that the apertures can be occluded or enlarged by muscular action. Certainly extended lengths of the afferent ctenidial vein can actively constrict in response to extreme localised disturbance or tissue damage, effectively occluding the vessel (personal observation). The haemolymph is then distributed out along the afferent edge of each lamella by the afferent lamellar sinus, which supplies the putative gas-exchange surface, 'R' (figures 3.47a and b). The gas exchange surface is extensively folded, forming corrugations that run parallel to the lamellar mid-line (figures 3.47a and b). These corrugations also run parallel to the proposed direction of water and haemolymph flow (figure 3.44

– this study, Yonge 1947) and are presumed to facilitate the directing of water to achieve a counter-current flow with the haemolymph, as well as increasing the surface area available for diffusion. Similar corrugations have also been described in *H. rubra* (Russell and Evans 1989). The gas exchange surface has a uniform appearance in the SEM, apparently consisting of a single cell type, without mucocytes or ciliated cells (figure 3.48a). The external surface of these cells is deeply wrinkled (figure 3.48b), further augmenting the surface area available for gas exchange with the water.

At the efferent edge of the gas exchange surface, the haemocoel widens into the efferent lamellar sinus (figure 3.49). The efferent sinus is composed of the 'pillared' and 'cartilagenous' regions ('P' and 'C', respectively on figures 3.44 and 3.45), separated by a broad band of cilia. Under the SEM the external structure of the pillared and cartilaginous regions appears similar, composed of cuboidal epithelial cells interspersed with numerous mucocytes and ciliated cells that aggregate to form tufts (figure 3.50). Internally the tissue of the pillared region is supported by cross-bridging between the epithelial surfaces (figure 3.49), that closely resemble the pillar cells that perform a similar function in crustacean gills (Taylor and Taylor 1992). The cartilaginous region and ciliary band overly a sheet of cartilage-like material on each side of the haemocoel, extending from the efferent ctenidial vein (figure 3.51). The supporting cartilage forms an underlying sheet extending from the ciliary band to the efferent margin, where it widens and meets a separate sheet from the other face of the lamella; both sheets taper towards the distal tip (figure 3.52c). An articulating joint is clearly apparent in the efferent lamellar margin a short distance (~0.2mm) beyond the junction with the efferent ctenidial vein (figures 3.45 and 3.52a). The articulation appears to allow flexion of the distal half of

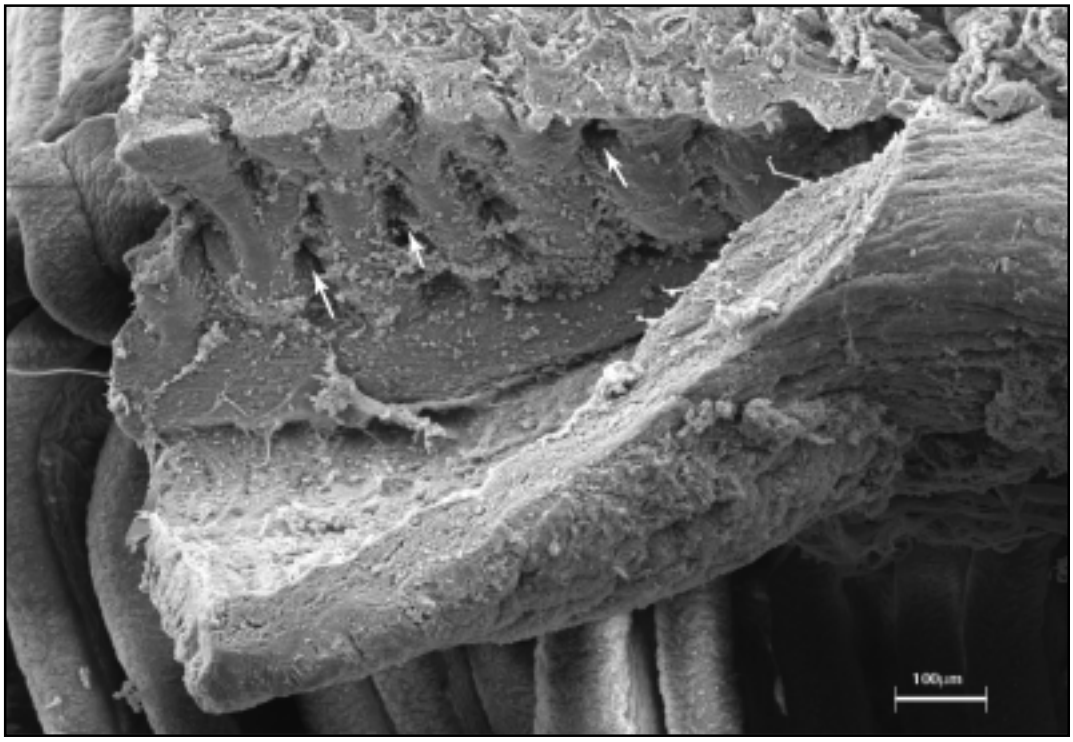


**Figure 3.46**: Scanning electron micrograph showing an afferent ctenidial vein that has been opened, revealing the pores (marked with white arrows) delivering haemolymph into the lamellae, in between the lattice-work of muscle and collagen bundles that forms the vessel wall.

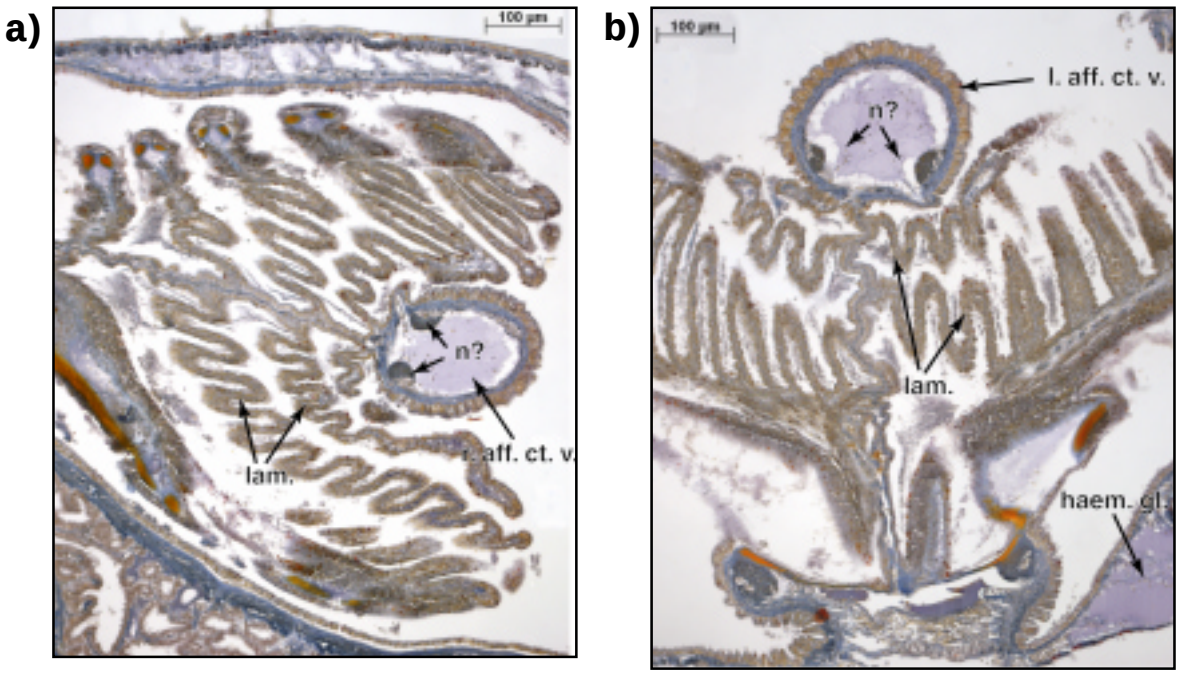


**Figure 3.43**: Wax TS of the afferent ctenidial veins of adult *Haliotis iris*, viewed towards the posterior, showing apparent nervous tissue (n?) running the length of the anterior veins. **a)** Right gill and **b)** left gill.

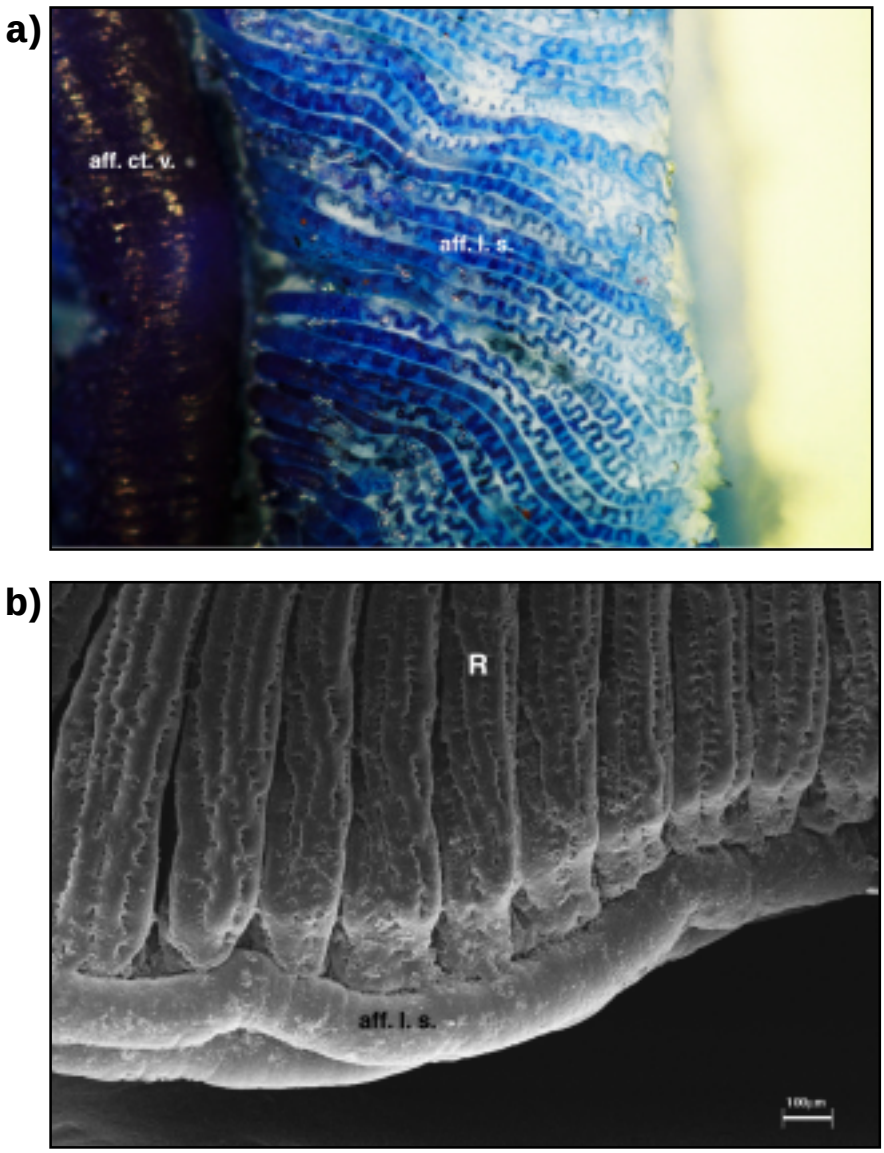


**Figure 3.47**: Corrosion cast of afferent region of gill lamellae. **a)** Extent of corrugations in gas exchange surface (R) visible through translucent cast of afferent lamella sinus (aff. l. s.). **b)** Scanning electron micrograph showing association between afferent lamella sinus and gas exchange surface when viewing the lateral face of the lamella.

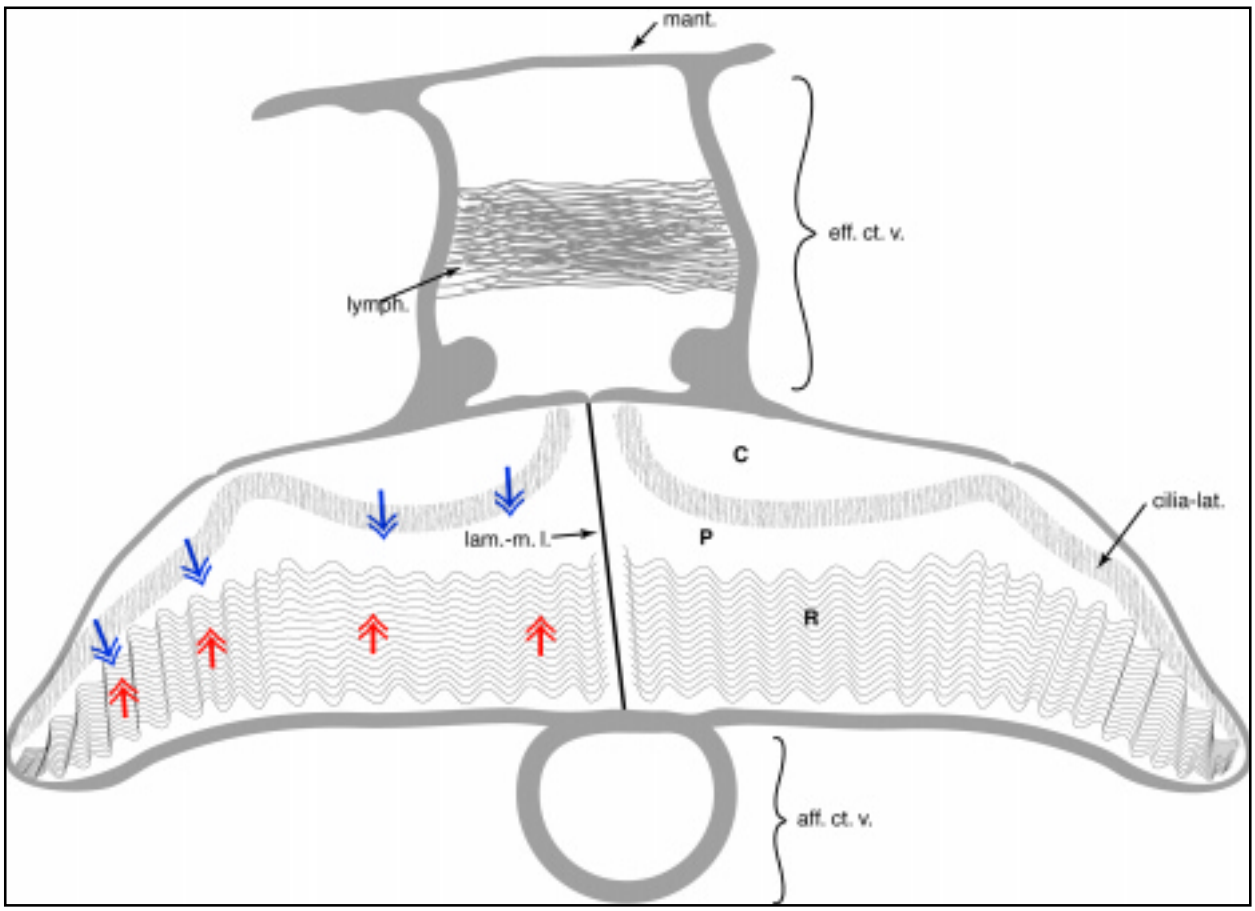


**Figure 3.44**: Diagrammatic representation of a section through a gill of *Haliotis iris* showing the external surface of a lamella pair. Three morphologically distinct regions of the lamella have been labeled: C, the cartilaginous efferent region, which ends in a dense band of lateral cilia (cilia-lat.). P is the pillared efferent region, supported by pillar cells across the lumen, rather than cartilage. R is the corrugated gas-exchange surface. The theoretical direction of water and haemolymph flow is indicated by blue and red arrows, respectively (after Yonge 1947).

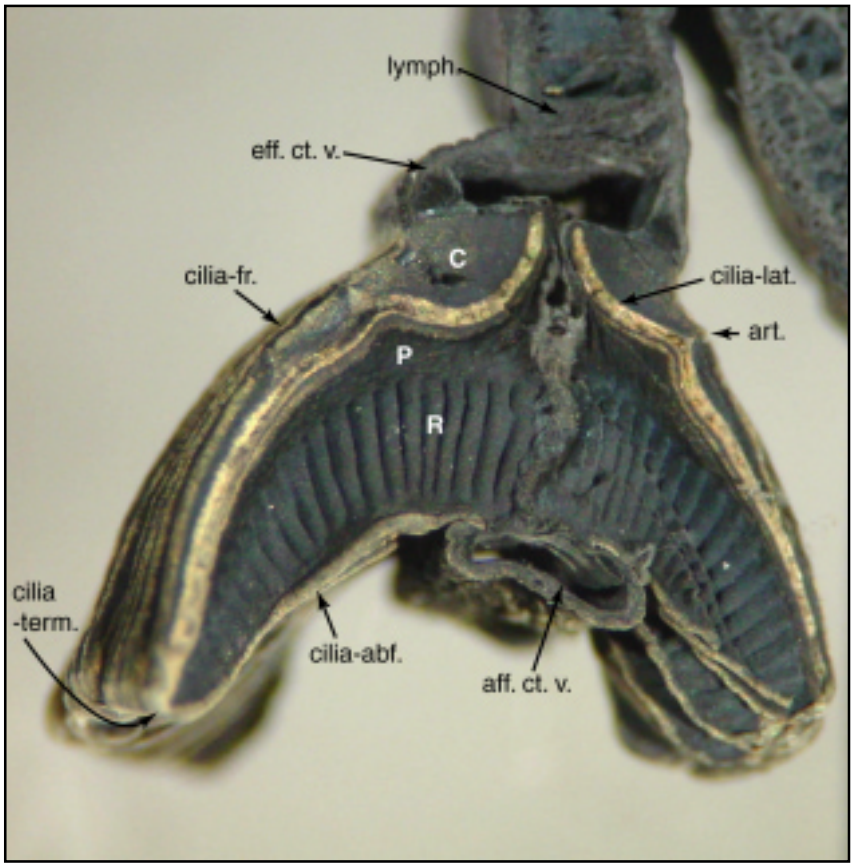


**Figure 3.45**: Section of *H. iris* right gill lamellae fixed with osmium tetroxide, high-lighting cilia as iridescent gold colour. Cilia have been classified according to their position on the lamella, after Yonge (1947): cilia-abf., the abfrontal cilia cover the afferent sinus of the lamella and the outer epidermis of the afferent ctenidial vein. The frontal cilia (cilia-fr.), cover the periphery of the efferent side of the lamellae, towards the distal tips of the lamellae they are referred to as terminal cilia (cilia-term.). The broad band of elongate lateral cilia (cilia-lat.) is clearly seen in the efferent sinus region of the lamella.

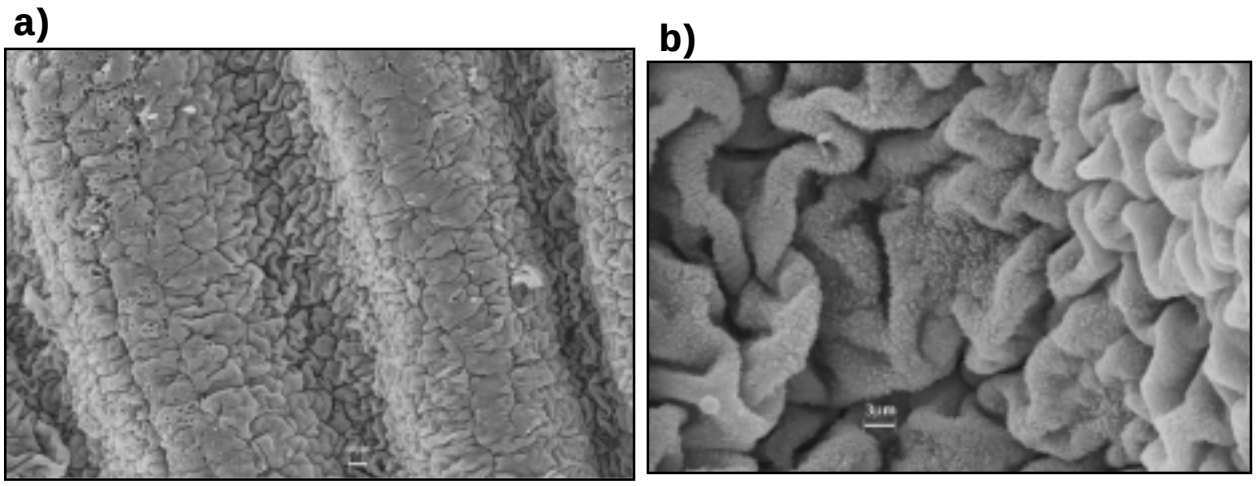


**Figure 3.48**: Scanning electron micrographs of the gas exchange surface of the gill lamellae of *Haliotis iris*. **a)** 1130x magnification showing a single cell type associated with this region, mucocytes and cilia are absent. **b)** 6400x mag. showing extensive folding of the individual cell membranes, further increasing the diffusion surface for gas exchange.

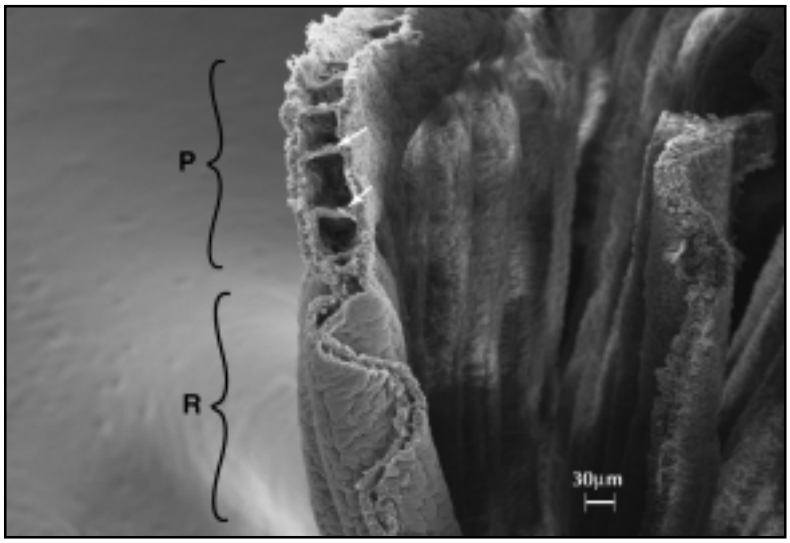


**Figure 3.49**: Scanning electron micrograph showing the efferent side of the gas exchange surface (R) joining the pillared region (P) of the efferent lamellar sinus, which has been opened to show the pillar cells.

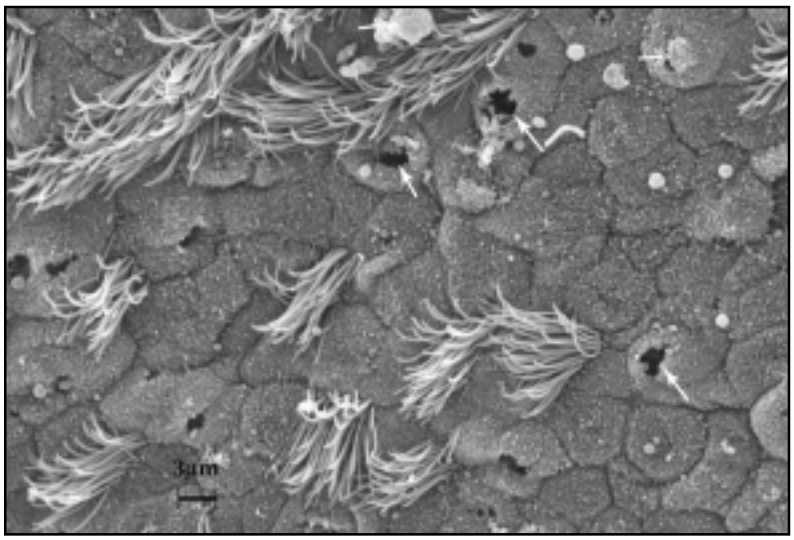


**Figure 3.50**: Scanning electron micrograph showing surface detail of the efferent lamellar sinus region of the gills of *H. iris*. Numerous void mucocytes are apparent, these are marked by plain arrows, the mucus goblets released are marked with a feathered arrow.

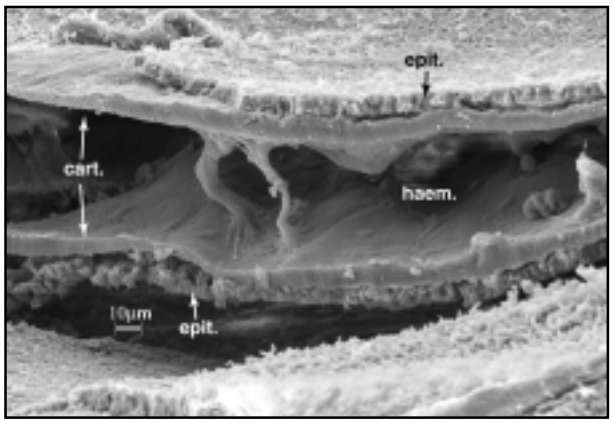


**Figure 3.51**: Scanning electron micrograph of section through 'cartilaginous' region ('C') of efferent lamellar sinus showing epithelial cells (epit.) overlying skeletal sheets that appear to be composed of extracellular cartilage (cart.) with pillar cells to support the haemal cavity.

**a)**

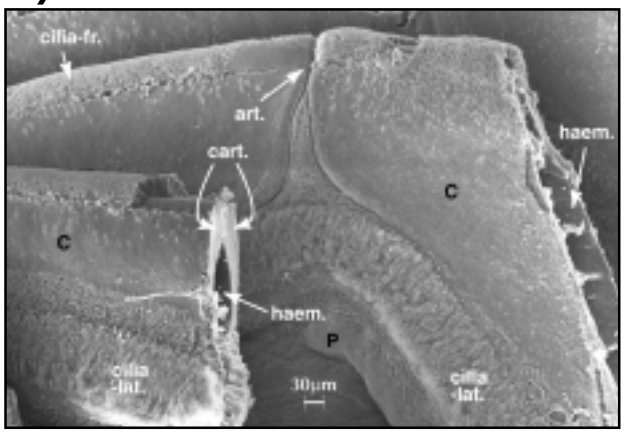


**b)**

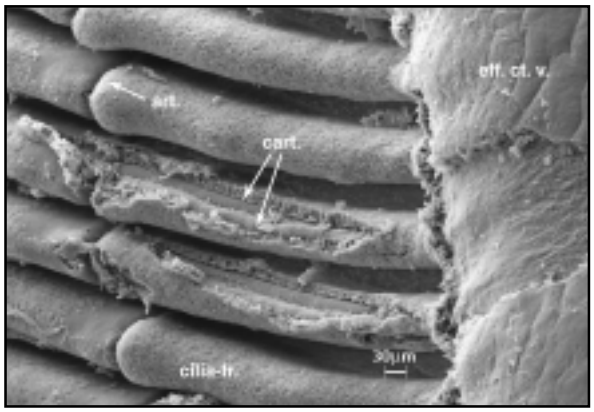


**Figure 3.52**: Scanning electron micrographs showing articulation of gill lamellae. **a)** Lateral view of lamellae cut away from the midline, showing an articulation point (art.) in the 'cartilaginous' region (C) of the efferent sinus. **b)** Lamellae attached to efferent ctenidial vein, viewed from efferent surface, showing tissue widening at the articulation points, assisting in spacing. The epidermis has been scraped from 2 lamellae, revealing the double rows of extracellular cartilage-like material supporting the efferent margin. **c)** Tear on lateral surface of lamella, showing the extent of cartilage support beyond the articulation point. **d)** Lateral view of lamella immediately efferent to the gas exchange region, showing a pleated gusset in the non-cartilaginous tissue to accommodate flexion at the articulation point.

**d)**

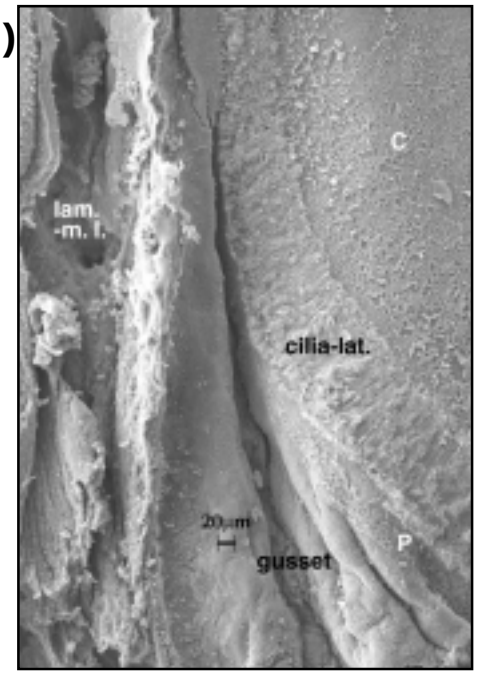


**c)**

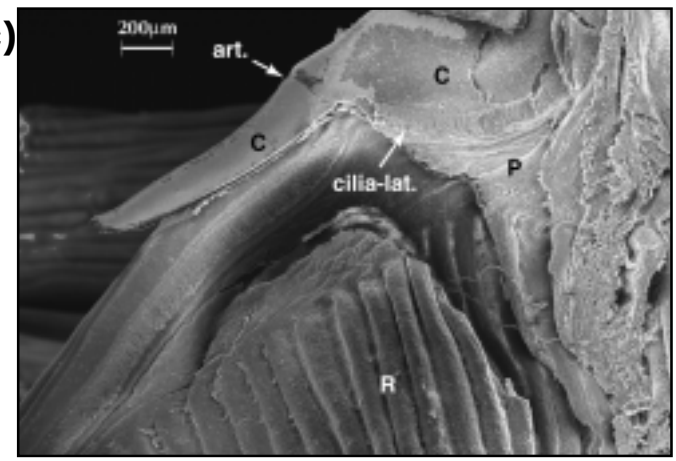

the lamella, reminiscent of the elbow of a bat's wing. Flexion is accommodated by a discontinuity in the cartilaginous region, filled with unsupported tissue resembling that of the pillared region (figure 3.52a). The articulating joint represents the widest point of the efferent margin (figure 3.52b) and may therefore assist in maintaining the spacing of channels for inhalant water currents, analogous to spacing structures used to maintain separation in the chitinous phyllobranchiate gills of amphibious and terrestrial crabs (Taylor and Taylor 1992). The entire lamella can also be displaced with respect to adjacent lamellae, within its own plane, by rotation about its attachment 'shoulder' on the efferent ctenidial vein (see figure 3.45). This motion is facilitated by an in-curving of the cartilage as it approaches the lamella midline, and by a distinct pleated gusset in the pillared region (figure 3.52d). Flexing of the lamella must also be accommodated by the gas exchange region, it is assumed that the flexible nature of its corrugated structure allows this region to deform without the need for specialised structures.

*Cilia*

Crofts (1929) describes the lateral cilia band of the lamella face as a spacer, serving to maintain separation between the lamellae. As shown in figure 3.53a, the cells supporting these lateral cilia are extremely long, resulting in a substantial thickening of the lamella in this region. It is therefore possible to concur with Crofts' interpretation, with the additional observation (noted above) that the articulation point also assists in maintaining separation at the efferent margin. The principal

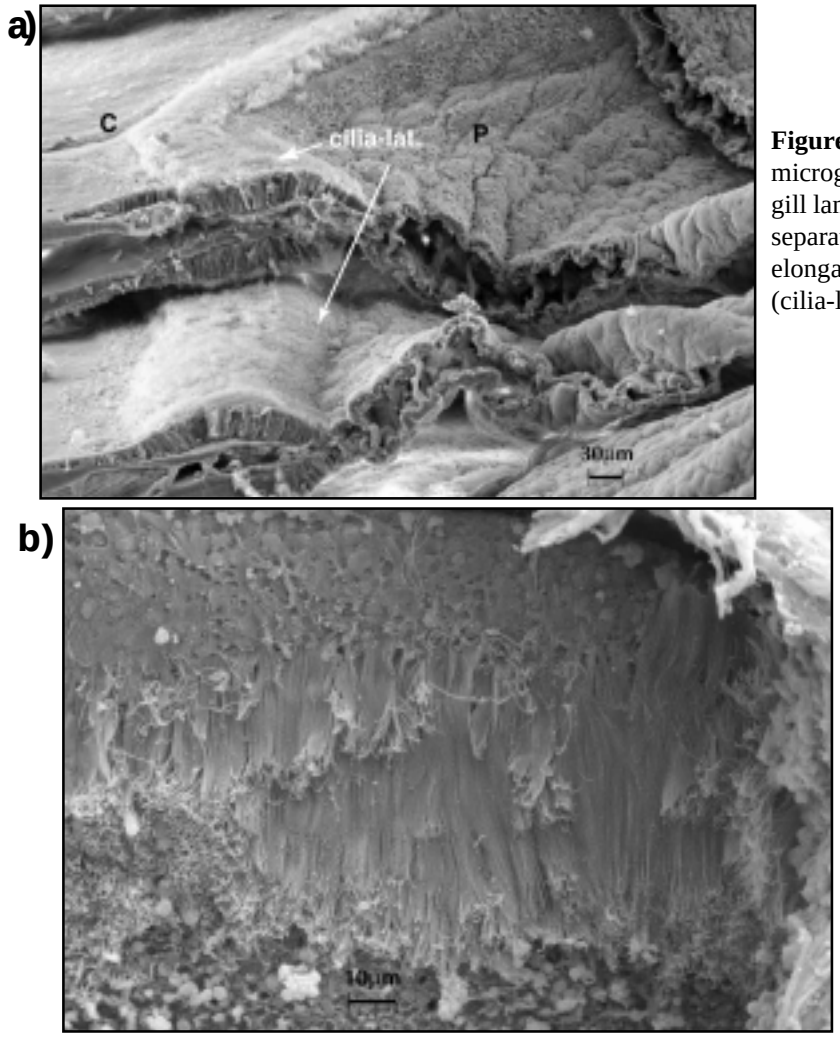


**Figure 3.53**: Scanning electron micrographs of the lateral cilia of *H. iris* gill lamellae. **a)** Oblique view of 2 lamellae separated from the midline, showing greatly elongated cells supporting the lateral cilia (cilia-lat.). **b)** Long, dense lateral cilia.

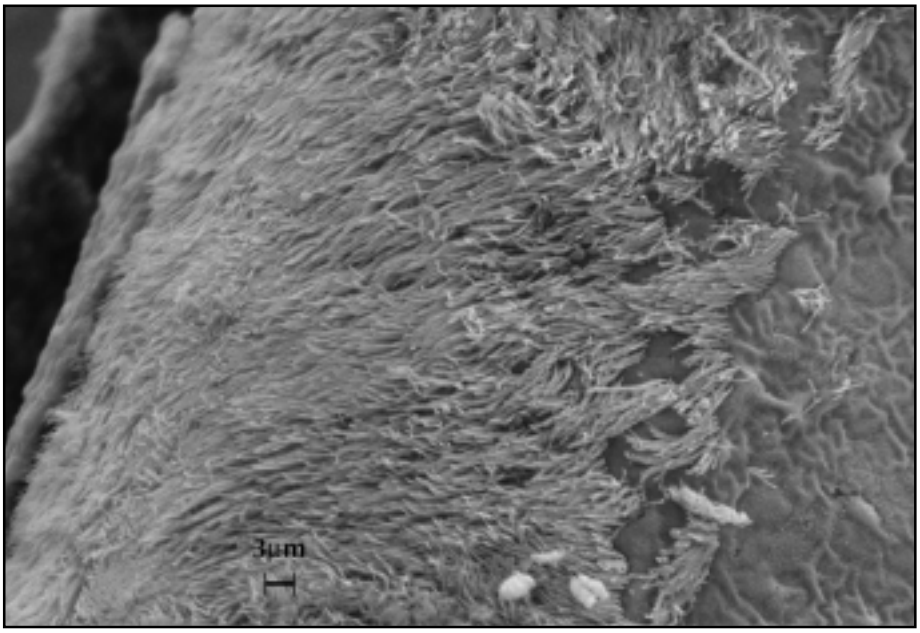


**Figure 3.54**: Scanning electron micrograph of the short, dense frontal cilia found along the efferent margin of each gill lamella.

function of the lateral cilia is presumably irrigation, rather than spacing. These cilia are extremely long (>50µm, figure 3.53b) and effectively ventilate the lamellae by creating a strong influent current between the efferent margins. The lateral cilia therefore create an irrigation stream that flows counter-current to the haemolymph flow, as described by Crofts (1929) and Yonge (1947). The merits of this arrangement are discussed in detail in chapter 5. Yonge (1947) also suggests that the elaborate skeletal support of the efferent lamella region is required to oppose the distorting effect of the powerful lateral cilia. In the absence of additional pumps, it also appears that the irrigation stream is sufficiently effective that it creates a net pressure gradient across the entire branchial chamber. In other words the lateral cilia function as the abalone's ventilatory pump, as well as locally irrigating the lamellae. This is considered to be the general ventilatory strategy in prosobranchs (Yonge 1947, Fretter and Graham 1994, Voltzow 1994). However Voltzow (1983) demonstrates the *H. kamtschatkana* uses a combination of cilia and external water movement to drive ventilation. Although energetically costly, the use of cilia rather than muscular contraction to drive ventilation confers the advantage that the fastest water velocities are encountered close to the tissue surface, facilitating gas exchange (Vogel 1994).

The remaining ciliated regions, associated with the lamella margin and external epithelium of the afferent ctenidial veins (figure 3.45), are apparently associated with hygiene. Particles are conveyed along the efferent margin to the distal tip by frontal cilia, around the tip to the afferent margin by terminal cilia and towards the afferent ctenidial vein by the abfrontal cilia (Yonge 1947). Cilia on the afferent ctenidial veins and mantle floor convey particles anteriorly to be shed to the right of the head (Yonge 1947). The terminal cilia of *H. tuberculata* are reported as being extremely long (up to 75µm, Crofts 1929, Yonge 1947), while in *H. iris* they appear no different to the short frontal and abfrontal cilia (<10µm, e.g. figure 3.54). The difference may reflect the higher turbidity of European coastlines inhabited by *H. tuberculata*, as these cilia have been implicated in the shedding

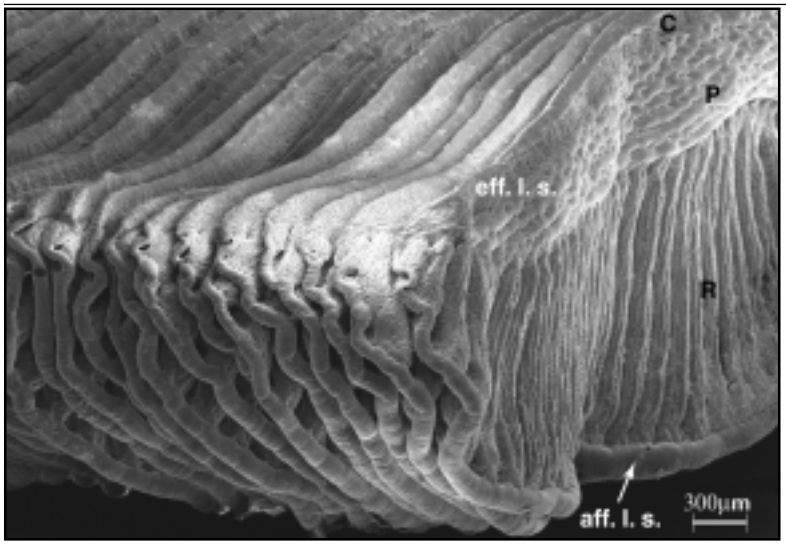


**Figure 3.55**: Scanning electron micrograph of vascular corrosion cast of *H. iris* gill lamellae, viewed from distal tips, showing no connection between the afferent and efferent sinuses other than via the gas-exchange surface (R). (casting protocol CC1).

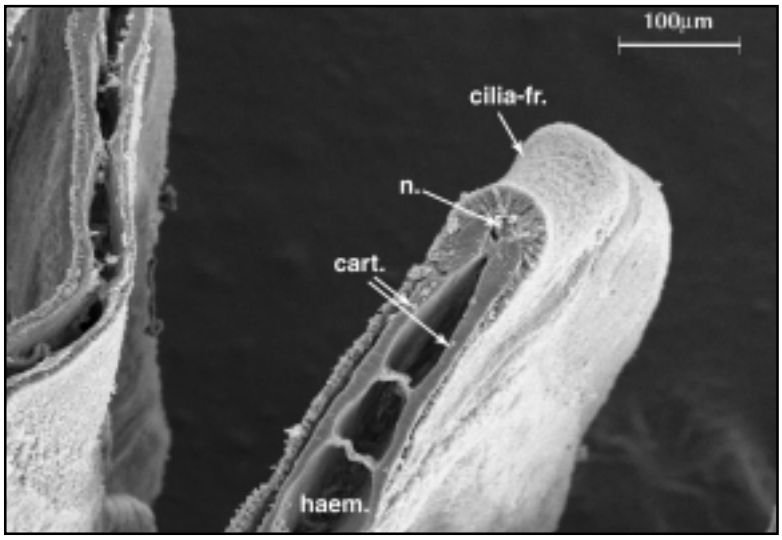


**Figure 3.56**: Scanning electron micrograph showing nerve running along the efferent margin of the gill lamella.

of fine particles into the exhalant flow (Yonge 1947). Yonge (1947) notes that the lateral face of *H. tuberculata* lamellae has no cilia other than the lateral band. This is not the case in *H. iris*, which shows ciliated tufts throughout the efferent region of the lamellae (figure 3.50), perhaps responsible for the distribution of mucus from the numerous goblet cells.

Crofts (1929) states that no channel exists between the afferent and efferent sinuses of the lamella, other than across the gas exchange surface. SEM examination of vascular casts of the lamellae confirms that this is, indeed, the case (figure 3.55). A potential bypass around the margin of the lamella is occluded by a nerve in the efferent margin (Crofts 1929 and figure 3.56).

*Efferent drainage*

The efferent region of the lamella is supported by 2 sheets of cartilage-like material that are prevented from excessive distension or collapse by pillar cells (e.g. figure 3.51). The pillar cells may offer more than passive support as seen in crab gills, which can directly influence transmural pressure and, consequently, perfusion of the lamella (Taylor 1990). Towards the midline each cartilage sheet curves away from the plane of the lamella to form the support for the opposing face of the next lamella (figure 3.58). The gill midline, separating the left and right side lamellae, is therefore

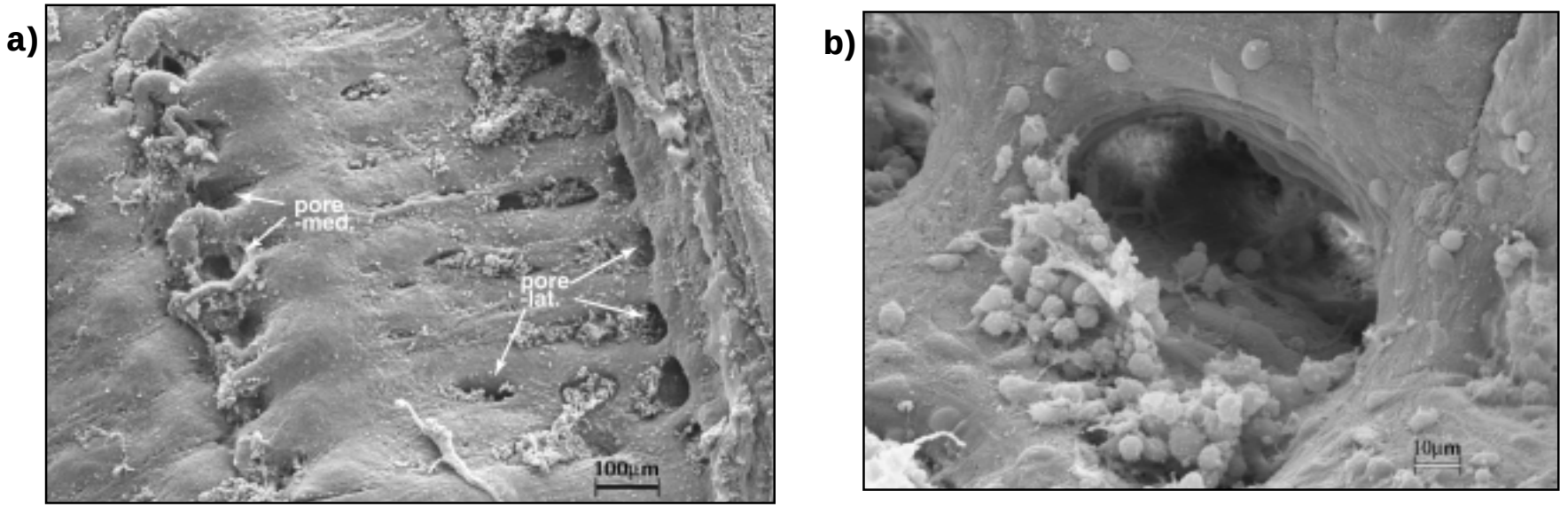


**Figure 3.57**: Scanning electron micrographs showing drainage arrangement from the lamellae into the efferent ctenidial vein. **a)** Drainage surface of efferent ctenidial vein showing median (pore-med.) and lateral pores (pore-lat.) draining from lamellae. **b)** Individual lateral pore and accumulated haemocytes. **c)** Perpendicular section through lamellar midline (lam.-m. l.) showing drainage from the midline haemocoel without supporting cartilage. **d)** Vascular corrosion cast of lamellae showing individual drainage via lateral pores and shared drainage path between 2 adjacent lamellae into the midline. (Casting protocol CC1).

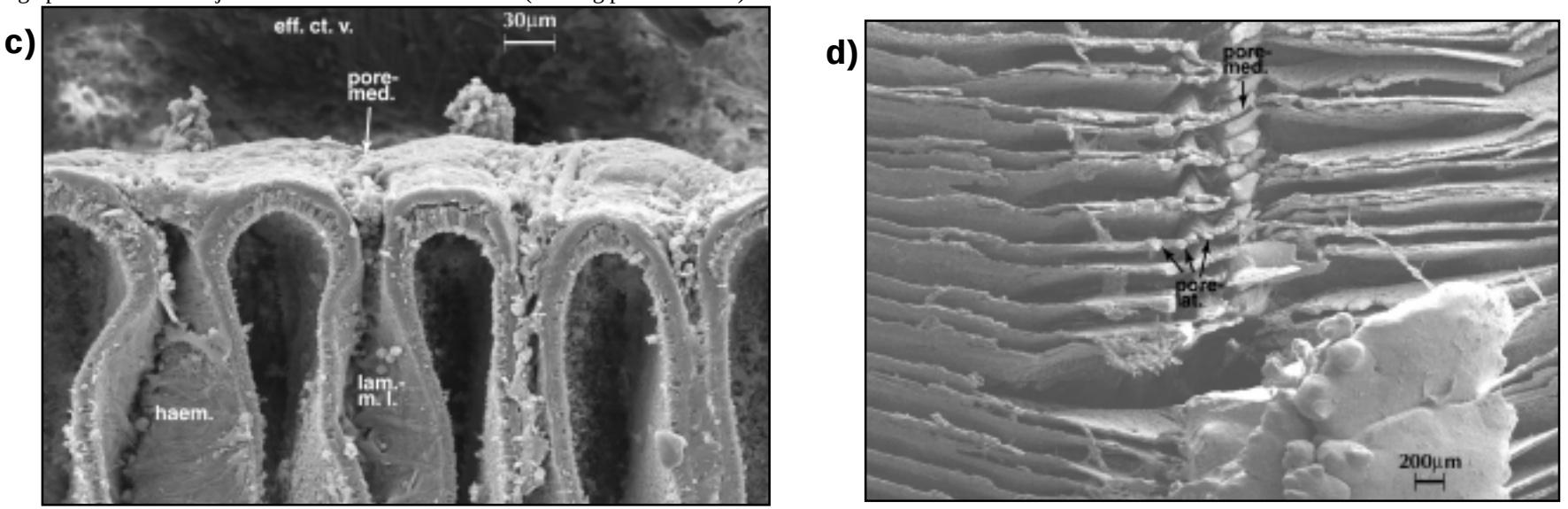

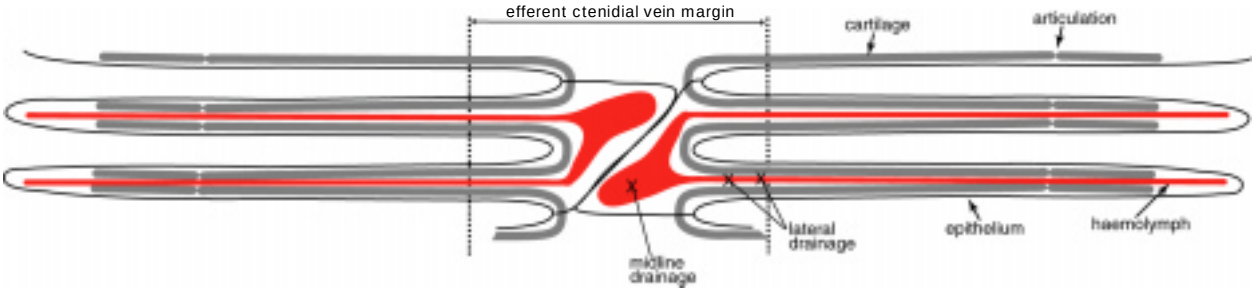


**Figure 3.58**: Plan of lamellar haemolymph drainage and cartilage organisation, viewed from the efferent surface. Each cartilage sheet supports opposing faces of adjacent lamellae while haemolymph from each adjacent pair mixes in the midline before draining into the efferent ctenidial vein.

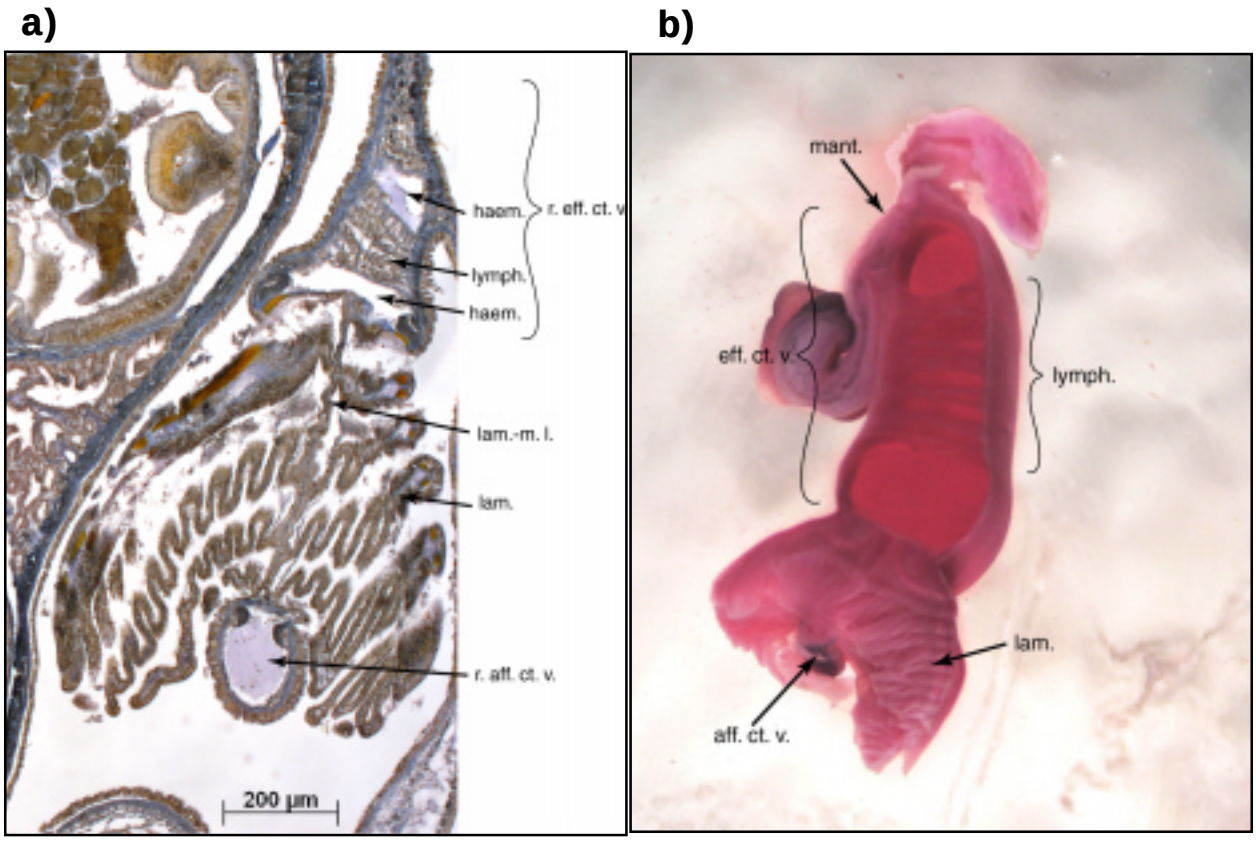


**Figure 3.60**: Broad band of 'lymphoid' tissue found in the lumen of the efferent ctenidial veins. **a)** Wax TS towards proximal (posterior) end of right gill, showing apparent combination of muscle, collagen and haemocytes in 'lymphoid' band. **b)** Thick TS cut from distal region of right gill of an amaranth/gelatin-perfused, fixed abalone, showing relative increase in size of efferent ctenidial vein and 'lymphoid' contents as lamellae become reduced.

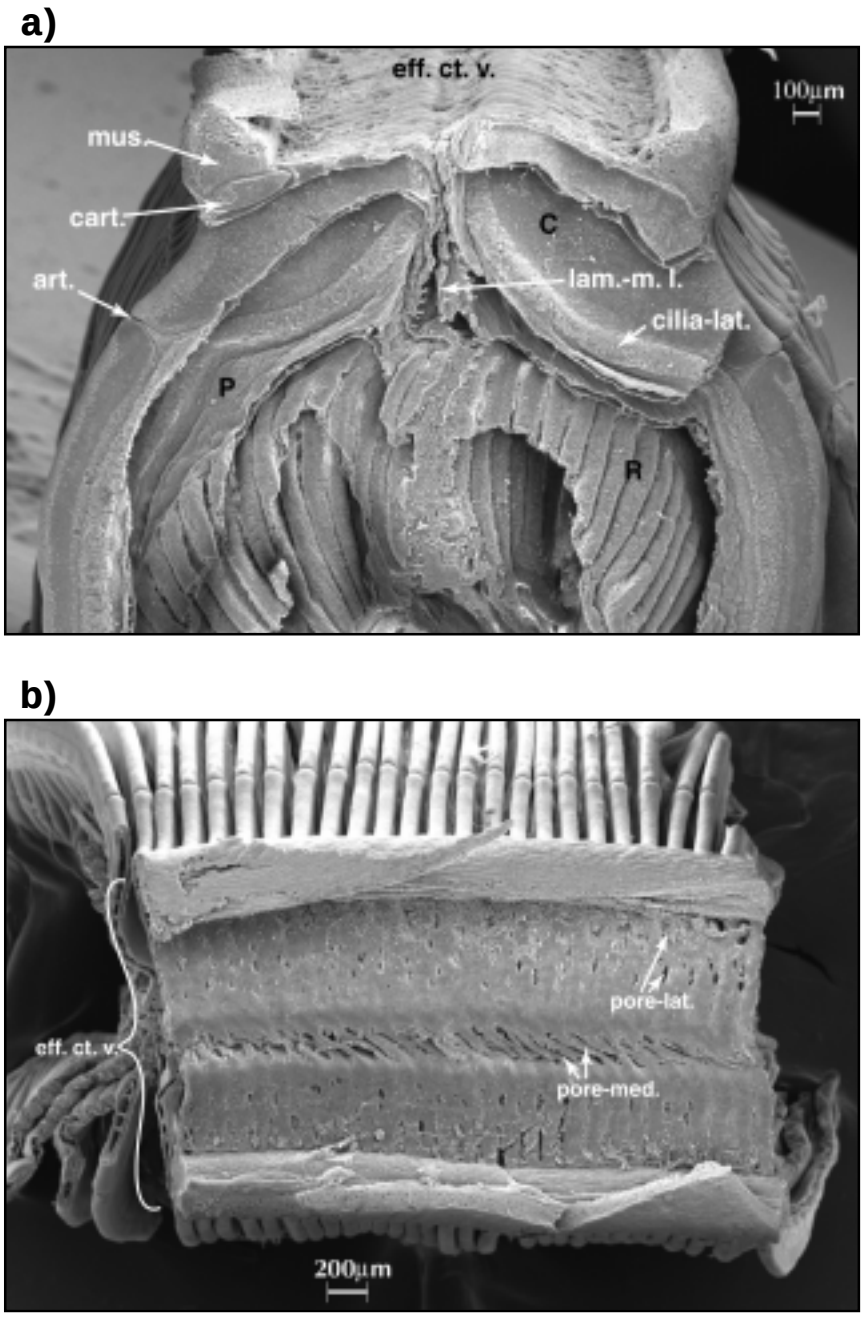


**Figure 3.59**: Scanning electron micrographs showing a potential mechanism for adjusting the vascular resistance of *Haliotis iris* gills. **a)** Lateral view of gill section showing the longitudinal muscle (mus.) and cartilage (cart.) running along either side of the efferent ctenidial vein. **b)** Opened efferent ctenidial vein showing effect of asymmetric movement of the muscle/ cartilage, slightly displacing one side of the vein and occluding the median pores. The smaller lateral pores remain open.

unsupported by cartilage. The haemal spaces of 2 adjacent lamellae meet in this midline region (figures 3.57d and 3.58) and drain into the efferent ctenidial vein via the median pores (figures 3.57a and d). Each adjacent pair of lamellae therefore represents a functional unit. The lateral walls of the efferent ctenidial vein possess longitudinal cartilage and muscle blocks that run the length of the gill (figure 3.59a). Asymmetric contraction of these muscles appears to cause a displacement of one side of the gill, effectively occluding the median pores in the process (figure 3.59b). Such an effect would be a highly effective means of increasing vascular resistance in one gill, favouring perfusion of the other; this concept is explored in detail in chapter 6. Haemolymph can also drain from the lamellae into the efferent ctenidial vein via median pores (2 – 4 per lamella, figure 3.57a and b). These pores appear to remain patent, even when the median pores are occluded (figure 3.59b).

A broad band of tissue traverses the lumen of the efferent ctenidial veins (figures 3.60a and b). Crofts (1929) referred to it as lymphoid tissue and hypothesised that it was involved in haemocyte production. Examination of Mallorie's triple-stained histological sections of *H. iris* gills certainly revealed cells that appeared to be anchored haemocytes. Conspicuously however, considerable amounts of muscle and collagen are also present (figure 3.60a). The lymphoid tissue therefore also appears to have a structural function, supporting the large, thin-walled vein along its entire length (figure 3.60b). While this tissue is able to prevent over-distension of the vein, it is suggested that its principal *in vivo* function is to prevent collapse during auricular suction (see chapter 7).

*Gill movements*

The integrated function of muscles of the lamellae and efferent and afferent veins, combined with a flexible cartilage framework, can be seen by removing the overlying region of shell and directly observing the gills. Each gill is highly distensible, retracting far into the branchial chamber in response to chronic disturbance or extending beyond the dorsal shell surface when left undisturbed. These movements have also been described in *H. tuberculata*. A characteristic 'Mexican wave' motion is seen following disruption of the lamellae, each lamella is lifted at its articulation point and repositioned in an apparent preening (realignment) process, commencing at the distal tip and travelling posteriorly. Individual lamellae may also withdraw from localised tactile stimulation.

# 3.4. Summary

The *in vivo* arrangement of all the vascular components described above is shown in figure 3.61 and represented in 'road-map' form in figure 3.62. The principal differences between the vascular organisation of *H. iris* and the generally accepted abalone arrangement described in section 3.1 become apparent if figures 3.62 and 3.1 are compared:

*H. iris* does not appear to have an aortic bulb. The first major branch of the aorta is referred to as the posterior aorta rather than first visceral artery as it subsequently gives rise to several arteries, serving separate body regions. Branches of the dorsal aorta supply the crop sinus, cardiac lobe of the right kidney and posterior digestive gland. The anterior aorta and its arteries appear to conform to Crofts' (1929) description of *H. tuberculata*, with the exception that the anterior region of the aorta runs within the region surrounded by the oesophageal sinus. Virtually all venous haemolymph is initially collected in the gut sinus/cephalopedal venous sinus (CVS) system. Most haemolymph is assumed to drain directly into the gut sinuses via adjacent lacunae, particularly from the alimentary canal. Haemolymph from the foot and right adductor muscles drains into the pedal sinus, which supplies both the CVS and anterior intestinal sinus (the 2 anterior regions of the gut sinus system). Posteriorly the gut sinuses drain into the portal veins supplying the digestive gland and gonad. The large median visceral veins subsequently collect haemolymph from the digestive gland and conduct it into the right kidney. Anteriorly the gut sinuses are drained by the circumpallial vessel, which serves as an *afferent* vessel to the right mantle region, and by the renal bypass vessel. The renal bypass vessel conveys haemolymph from the intestinal sinus directly to the efferent renal sinus,

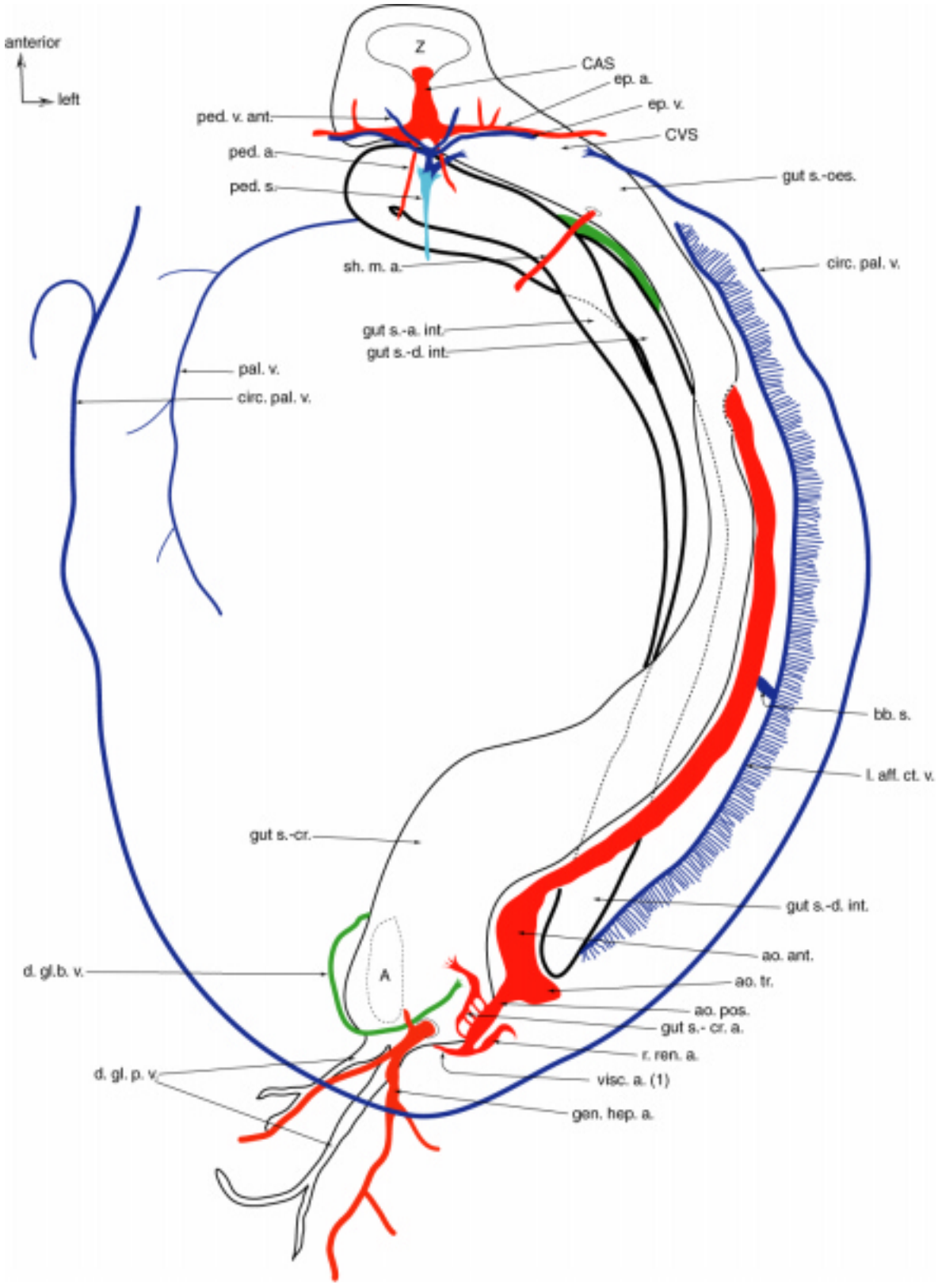


**Figure 3.61**: Overview of vascular arrangement of *Haliotis iris* viewed from ventral side. The crop sinus (gut s.-cr.) ascends to form the stomach sinus at position 'A' and 'Z' represents the internal cavity of the cephalopedal venous sinus (CVS) that accommodates the odontophore.

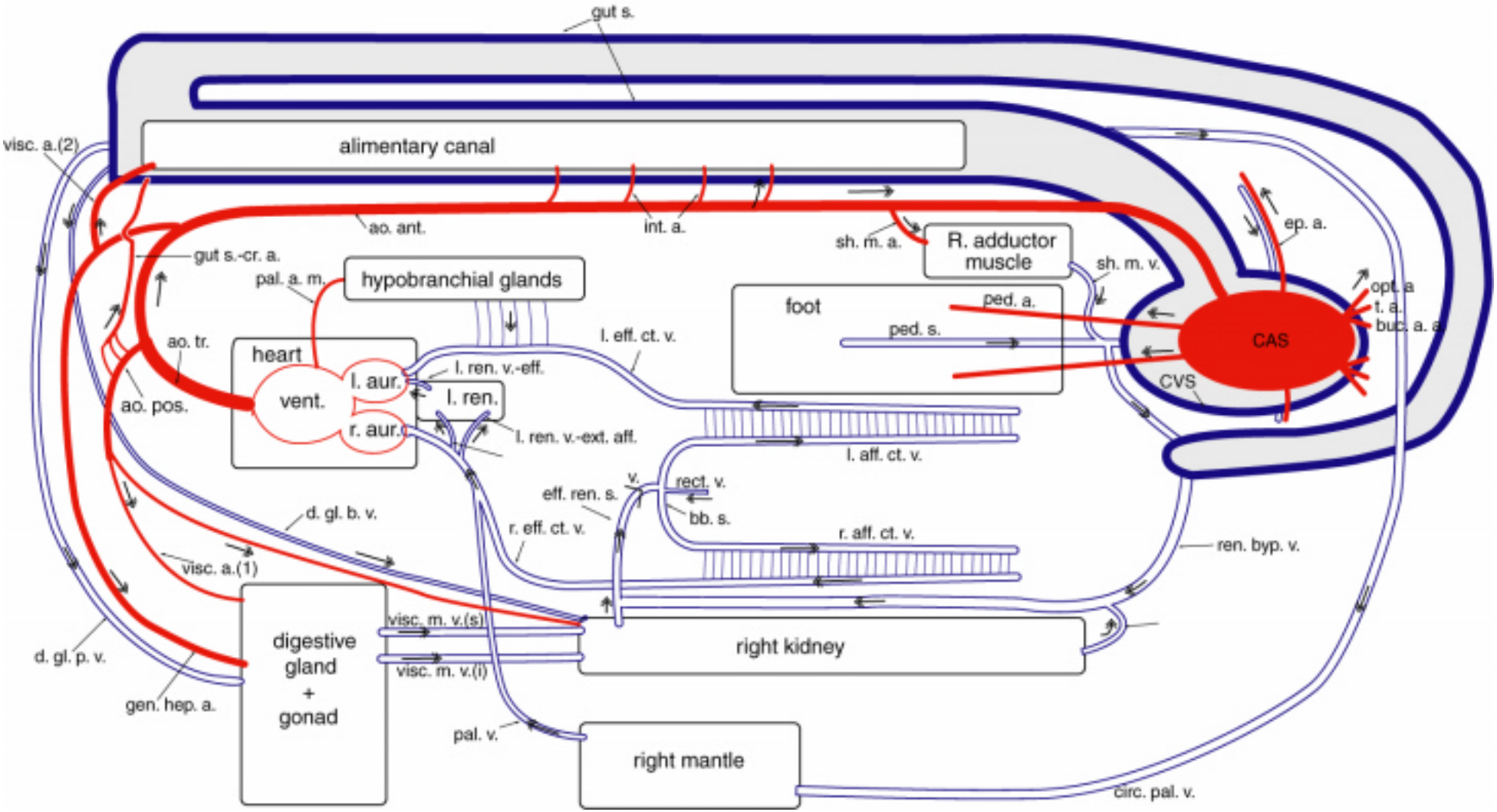


**Figure 3.62**: Overview of vascular connections in *H. iris*, based on morphological descriptions presented in the current study. Arterial components are drawn in red, venous sinuses in solid blue and veins in blue outline; feathered arrows indicate the inferred direction of flow.

where it mixes with efferent haemolymph leaving the right kidney. The renal sinus connects the basibranchial sinus via a valve (of unknown function). The basibranchial sinus connects with the rectal vein, as described by Crofts (1929), however the direction of flow still needs to be established. No connection was found between the basibranchial sinus and the left kidney. The basibranchial sinus supplies the afferent ctenidial veins and, subsequently the gill lamellae. The left efferent ctenidial vein collects haemolymph from the left gill and hypobranchial glands and drains into the left auricle. Haemolymph leaving the right gill enters the right efferent ctenidal vein, where it is joined by haemolymph leaving the right mantle via the pallial vein. Haemolymph from the right efferent ctenidial vein drains into both the right auricle and the left auricle, via the left kidney. Non-return valves in the left kidney veins are likely to prevent the tidal back-flow of haemolymph in this organ.

## 3.5. Conclusions

The above examination of the circulatory system of *Haliotis iris* is deliberately biased towards a consideration of the respiratory role of the haemolymph. The actual arrangement of the circulatory system appears to share this bias: vascular bypasses are available to the haemolymph across every major organ or tissue region, with the notable exception of the gills. The vascular design therefore appears to maximise pressure and retain haemolymph within a low resistance circuit until the gill lamellae are encountered. This concept is developed further, in conjunction with specific pressure data, in chapter 7. Perfusion of the other organs must, inevitably, be compromised by this arrangement. In particular the lacunae of the right kidney must offer a reasonable resistance to flow and a major bypass vessel is available, presumably resulting in slow exchange through the organ. This interpretation throws light on the reasons for the apparent hypertropy of this large and extensive organ in archaeogastropods, which is entirely absent in higher prosobranchs. An investigation into the mechanisms that allow adequate haemolymph exchange to occur through an organ in the presence of a low resistance shunt could prove highly enlightening.

There appear to be fundamental differences between the vascular organisation of *H. iris* and that of other abalone. No aortic bulb has been described in *H. iris* of *H. tuberculata* (Crofts 1929) but has been identified in *H. rubra* (Russell and Evans 1989) and *H. corrugata* (Bourne and Redmond 1977a). The extensive gut sinus system of *H. iris* has not been described in other haliotids, even though similar investigative tools have been used. The bypass vessels described here, notably the renal bypass, are either considered to be absent (Crofts 1929) or functionally unimportant in other abalone. The vascular connections of the left kidney also show fundamental differences between *H. iris, H. tuberculata* (Crofts 1929) and *H. rubra* (Russell and Evans 1989). Hence while haliotids present a conservative external morphology, the vascular layout hints at extensive radiation in this ancient genus.

# 3.6. Abbreviations

| Abbreviation | Full name |
|---|---|
| aff. l. s. | afferent sinus of lamella |
| aff. ct. v. | afferent ctenidial vein |
| aff. ren. v. | afferent vein to right kidney |
| ao. ant. | anterior aorta |
| ao. b. | aortic bulb (absent in *H. iris*) |
| ao. pos. | posterior aorta |
| ao. tr. | aortic trunk |
| art. | articulation point of lamellar cartilage |
| bb. s. | basibranchial sinus |
| br. c. | branchial chamber |
| buc. a. a. | anterior buccal arteries |
| CAS | cephalic arterial sinus |
| cart. | cartilage |
| cilia-abf. | abfrontal lamellar cilia |
| cilia-fr. | frontal lamellar cilia |
| cilia-lat. | lateral lamellar cilia |
| cilia-term. | terminal lamellar cilia |
| circ. pal. v. | circum-pallial vessel |
| ct. | ctenidia ('gill filaments') |
| ct. l. | left ctenidium ('gill') |
| ct. r. | right ctenidium ('gill') |
| CVS | cephalopedal venous sinus |
| d. gl. | digestive gland |
| d. gl. b. v. | digestive gland bypass vessel |
| d. gl. p. v. | digestive gland portal vein |
| eff. ct. v. r. | right efferent ctenidial vein |
| eff. ren. s. | efferent sinus of right kidney |
| eff. ren. v. | efferent vein draining right kidney |
| eff. ren. v.-c. l. | efferent vein draining the cardiac lobe of the right kidney |
| eff. ren. v.-d. l. | efferent vein draining the dorsal lobe of the right kidney |
| eff. ren. v.-v. l. | efferent vein draining the ventral lobe of the right kidney |
| ep. | epipidium |
| ep. a. | epipodal arteries |
| ep. v. | epipodal veins |
| epit. | epithelium |
| g. | gonad |
| g. l. | lacunae extending into gonad tissue |
| gen. hep. a. | hepato-genital artery |
| gut s.-a. int. | gut sinus – ascending intestine region |
| gut s.-d. int | gut sinus – descending intestine region |
| gut s.-cr. | gut sinus – crop region |
| gut s.-cr. a. | artery supplying crop sinus |
| gut s.-oes. | gut sinus – oesophageal region |
| gut s.-st. | gut sinus – stomach region |
| h. | head |
| haem. | haemolymph/haemocoel |
| haem. gl. | haemolymph gland |
| int. a. | intestinal arteries |
| int.(asc.) | ascending limb of intestinal loop |
| int.(des.) | descending limb of intestinal loop |
| l. aff. ct. v. | left afferent ctenidial vein |
| l. aff. ct. v.(ant.) | anterior branch of left afferent ctenidial vein |

| Abbreviation | Full name |
|---|---|
| l. aff. ct. v.(post.) | posterior branch of left afferent ctenidial vein |
| l. aur. | left auricle |
| l. eff. ct. v. | left efferent ctenidial vein |
| l. ren. | left kidney |
| l. ren. pap. | papillae of left kidney |
| l. ren. v.-eff. | efferent veins of left kidney |
| l. ren. v.-ext. aff. | external afferent left renal vein |
| l. ren. v.-int. aff. | internal afferent left renal vein |
| l. t. | lacunar tissue |
| lam. | gill lamellae |
| lam. m. l. | mid-line between gill lamellae |
| lymph. | lymphoid tissue |
| m-v | microvilli boarder of right ureter |
| mant. l. | left-side mantle |
| mant. l. l. | anterior left lobe of mantle |
| mant. l. r. | anterior right lobe of mantle |
| mant. r. | right-side mantle |
| muc. | mucocyte |
| muc. gl. l. | left mucous (hypobranchial) gland |
| mus. | muscle |
| oes. | oesophagus |
| opt. a. | optic artery |
| pal. a. m. | median pallial artery |
| pal. v. | (right) pallial vein |
| pe. | pericardium |
| ped. a. | pedal arteries |
| ped. s. | pedal sinus |
| ped. a. ant. | anterior pedal arteries |
| ped. v. ant. | anterior pedal veins |
| pore-lat. | lateral pore entering efferent ctenidial vein |
| pore-med. | median pore entering efferent ctenidial vein |
| r. aur. | right auricle |
| r. eff. ct. v. | right efferent ctenidial vein |
| r. hyp. gl. | right hypobranchial (mucous) gland |
| r. ren. | right renal organ (‘kidney’) |
| r. ren.-a. l. | anterior lobe of right renal organ |
| r. ren.-c. l. | cardiac lobe of right renal organ |
| r. ren.-p. l. | posterior lobe of right renal organ |
| r. ren. ur. | urocoel of right kidney |
| rect. v. | rectal vein |
| ren. byp. v. | right kidney bypass vein |
| sh. m. a. | shell muscle artery, supplies R adductor muscle |
| sh. m. r. | Right shell adductor muscle |
| sh. m. v. | shell muscle vein, drains R adductor muscle |
| t. a. | tentacular artery |
| ur. | ureter from right kidney |
| v. | valve |
| vent. | ventricle |
| visc. a. (1) | first visceral artery |
| visc. a. (2) | second visceral artery |
| visc. m. v.(inf.) | inferior median visceral vein |
| visc. m. v.(sup.) | superior median visceral vein |

# Chapter 4

# The role of body surfaces and ventilation in gas exchange of the abalone, *Haliotis iris*

The experiments describing natural ventilation rates in *H. iris*, the effects of forced ventilation and the contribution of the gills to whole animal oxygen uptake where performed by Assoc. Prof. H. H. Taylor, assisted by J. Taylor. The collation and analysis of the data pertaining to these experiments was also undertaken by H. H. Taylor. The initial design concepts of these experiments and the final integration of the results into the context of this chapter were carried out by N. L. C. Ragg.

## 4.1. Introduction

Members of the archaeogastropod family Haliotidae, the abalone, retain a pair of large, bipectinate ctenidia (gills). The gills show some left-side bias associated with coiling (the branchial chamber is displaced to the left and the left gill is slightly larger than the right) but are otherwise symmetrical, both across their own midlines and mirrored across the branchial chamber. The branchial chamber is ventilated by a unidirectional water current entering above and to the left of the head and exiting through the dorsal shell holes (or 'tremata'; Yonge 1947, Voltzow 1983). These features reflect the ancestral gastropod arrangement, in which a symmetrical body plan supported symmetrical bipectinate gills in a branchial cavity posterior and dorsal to the head (Fretter and Graham 1994). Instead of a row of holes, a median shell slit provided an exhalant route for ventilatory water (Barnes 1986). This gas exchanger arrangement, where bipectinate gills are used in conjunction with exhalant shell apertures, has been abandoned by all extant gastropod families, with the exception of the Pleurotomarioidea (which includes the Haliotidae) and Fissurelloidea (Voltzow 1994).

Those species that still bear paired bipectinate ctenidia have adopted strategies that appear to supplement gas exchange. The first strategy is morphological, exploiting the fact that any region where haemolymph and water are in close proximity may function as a respiratory surface. In some species the shell has become greatly reduced and is often overgrown by the mantle, maximising epidermal contact with the surrounding seawater. Typical examples include *Haliotis asinina* and *Scutus breviculus*. Other prosobranchs have developed specific body surfaces, other than the gills, as sites of oxygen uptake. For example, limpets from the archaeogastropod superfamily Patellacea have developed cilia to irrigate the richly perfused ventral folds of the mantle/epipodium, using an approximately counter-current arrangement to facilitate gas exchange (Kingston 1968). *Acmaea*

sp. and *Lottia* sp. use this arrangement to supplement oxygen uptake by a single gill, allowing a bimodal gas exchange in water and air (Kingston 1968). Member of the genus *Patella* have developed the mantle folds into secondary gills, abandoning the bipectinate gills entirely (Barnes 1986). The thin, well perfused mantle is another obvious gas exchange site exploited by many prosobranchs, particularly those adapted to amphibious or terrestrial habitats, where gill function would be severely compromised during aerial exposure (Voltzow 1994).

The second strategy is ecological, a heavy shell capable of sealing to the substratum is retained but the population distribution is limited to high energy rocky sub-tidal environments rich in dissolved $Po_2$. This strategy is utilised by most abalone and keyhole limpets. Under the influence of external flow these archaeogastropods with secondary shell apertures experience a combination of dynamic pressure, or ram effect, the Bernoulli principle and viscous entrainment, drawing water from the dorsal openings (Murdock and Vogel 1978). Voltzow (1983) showed that the left side of the head and anterior-facing holes are the inhalant routes of *H. kamtschatkana* and the dorsal holes are exhalant. The ventilatory paths were the same in moving or static water and could be induced in a dead animal by head-on flow (Voltzow 1983). The shell form of the abalone is clearly conducive to exploiting currents in the surrounding water. However the rate of endogenously driven flow (e.g. muscular or ciliary) and the quantitative effects of water current assisted ventilation upon gas exchange have not been determined.

The basic aim of the present investigations was therefore to construct a composite picture describing the role of alternative body surfaces and external water movement in supplementing the oxygen uptake and ventilation of the gills of *H. iris*.

Initially, whole animal oxygen consumption rates were established by closed-box respirometry, as was the abalone's capacity to regulate uptake as environmental oxygen levels declined. The relative roles of the gills and other body surfaces in meeting the abalone's oxygen requirements were then examined by masking the exhalant shell holes and artificially ventilating the branchial chamber, while monitoring the oxygen gradient between inhalant and exhalant water. The specific contribution of the epipodium and foot to total oxygen requirement was examined in a 2-chamber respirometer. As described in section 3.3.5 ('Pallial circulation'), the mantle is continuous between the left and right sides of the abalone and intimately associated with other tissues, including the digestive gland and gonad, towards the posterior and right side of the animal. It was consequently impossible to isolated the right mantle from all other metabolically active tissue. Evidence for net $O_2$ uptake by the mantle was therefore investigated by monitoring *in vivo* oxygen gradients in the haemolymph.

The roles of endogenously- and exogenously-derived ventilation in supporting gas exchange were examined separately. Normoxic endogenous ventilation rates were established by using an electromagnetic flowmeter to quantify exhalant flow. The technique was then expanded to assess the abalone's capacity to regulate ventilatory rates when challenged with increasing environmental hypoxia. The influence of exogenous flow (i.e. water currents) upon whole animal oxygen uptake

was examined in a flume respirometer, where uptake could be monitored over a range of flow velocities. In a moving water current, the gills of *H. iris* are irrigated by a combination of endogenous ciliary action, using the lateral cilia of the gill lamellae (Yonge 1947), and exogenously-induced flow (Voltzow 1983). The importance of this interaction was examined by measuring gill $O_2$ uptake over a range of branchial chamber ventilation rates.

# 4.2. Methods

*Animal collection, storage and preparation*

Adult *Haliotis iris* were collected from 3 sites in the South Island, New Zealand. In August 2000 animals were obtained from a sheltered site on the sublittoral of Lyttleton Harbour and from a semi-exposed site, a submerged reef in the centre of Akaroa Harbour. In August 2002 animals were collected from an exposed site in South Bay, Kaikoura. The abalone were transported to the University of Canterbury and acclimated to a 15°C holding system for a minimum of 2 months (see chapters 5 and 6 for system details). All subsequent manipulations and experiments were also conducted at 15°C.

*Whole animal $Mo_2$ and the effect of hypoxia*

Abalone sampled from the Akaroa population ranged from 190 to 330g live weight and consistently displayed normal shell morphology. Animals from Lyttleton tended to be smaller (115 – 270g) and displayed characteristics of repressed growth: relatively high shells and often a disrupted tremata

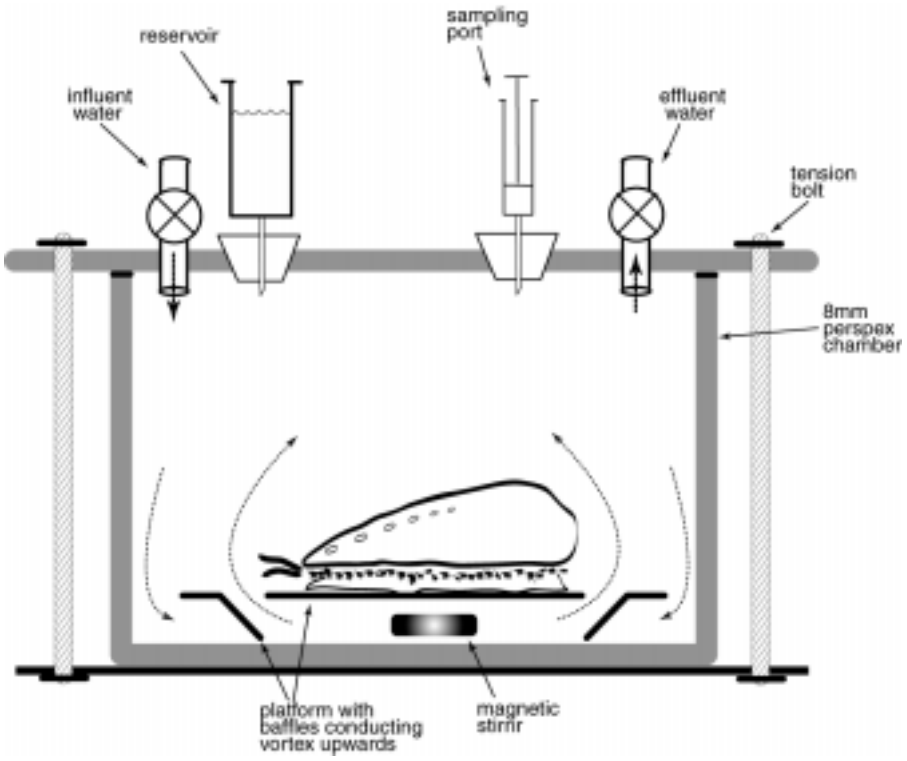


**Figure 4.1**: Lateral view illustration of a simple respirometer used to determine whole abalone oxygen consumption. Mixing is achieved by a vortex generated by a magnetic stirring flea, directed upwards by baffles in the abalone platform (dotted arrows).

(shell hole) formation (note that only animals with a normal tremata arrangement were used in the study). One week prior to use each abalone shell was cleaned of epifauna using a high speed grinding wheel (Dremel) and the animal then tagged.

Four respirometer chambers, described in figure 4.1, were connected in parallel to receive water from the holding system. The chambers were initially sterilized using hot fresh water and then conditioned with flowing seawater for 24h. A magnetic stirrer revolving at approximately 200 rpm beneath the loose-fitting animal platform, in combination with four 10mm holes and associated baffles was used to mix the chamber water. An arbitrary assessment of mixing efficiency required a bolus of trypan blue to mix homogenously within 1min of injection. Prior to use, each respirometer volume was determined by weight difference between the dry and distilled water-filled chamber.

The blank oxygen consumption of the respirometer water and chamber was measured in each chamber before (normoxia) and after (hypoxia) each animal trial. Blank values were determined by monitoring $Po_2$ change over a 3h period at normoxia, and a 24h period under hypoxic conditions. Following initial blank measurement each experimental abalone was weighed, following a 30s inversion on blotting paper. Individual volume was measured by seawater volume displacement and the value subtracted from chamber volume to determine the quantity of water present during each trial. The measurement of individual weight and volume allowed whole animal density to be calculated as 1.36 ±0.02 $kg.L^{-1}$(live flesh + shell).

One abalone was then placed in each respirometer chamber and allowed to acclimate for 12h overnight with a constant supply of normoxic seawater. Each chamber was subsequently isolated and $Po_2$ allowed to fall as a result of the abalone's metabolism. A small header reservoir maintained a pressure of approximately 10cm $H_2O$ and supplied makeup water (air saturated) via a 25gauge needle to replace water removed during sampling. At 10 – 15min intervals respirometer $Po_2$ was measured by withdrawing 1mL of seawater from a respirometer into a glass syringe and injecting it into an oxygen electrode chamber (Strathkelvin) in a 15°C water jacket, connected to an $O_2$ meter (Strathkelvin 781), calibrated against moist air. Normoxic readings were simply made after 2min contact with the electrode; however, as the $Po_2$ fell below 100 Torr it proved necessary to prime the electrode with 1mL of chamber water before inserting the sample to be measured.

As water $Po_2$ approached 10 Torr the animal was removed from the chamber. Makeup water was added to refill the respirometer, which was then re-sealed and hypoxic blank $O_2$ consumption determined.

The change in the blank rate of oxygen uptake between normoxic and hypoxic estimates was assumed to be linear with $Po_2$. A linear regression function was therefore used to fit an equation of the form shown in equation 4.1 to the simple interpolation between the 2 values. This allowed blank oxygen consumption ($B$, in $Torr.h^{-1}$) to be estimated for a specific $Po_2$ value, using the linear constants $m$ and $C$ generated from the regression (slope and y-intercept, respectively).

$$B = (m.Po_2) + C \qquad \text{equation 4.1}$$

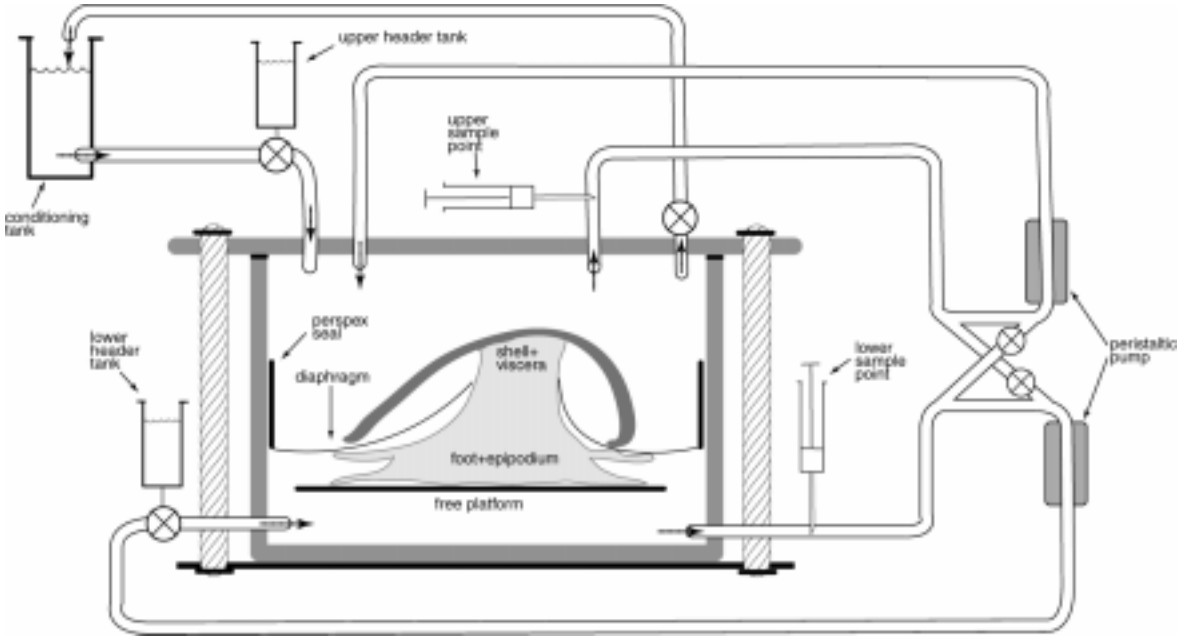


**Figure 4.2**: Plan of 2-chamber respirometer designed to isolated the foot + epipodium region from the remainder of the abalone. Upper and lower chambers are isolated by a perspex seal and latex diaphragm; the position of the abalone is shown in transverse section to demonstrate the seal achieved by the diaphragm around the adductor muscle. During acclimation (flow-though) water is exchanged between the respirometer and an aerated or nitrogenated reservoir, bypass taps are opened allowing free mixing between the upper and lower chambers. During $Mo_2$ measurement the respirometer is isolated and the bypass taps close, forcing circulating water to return to its original chamber.

Using equation 4.1 blank $O_2$ consumption was calculated for each sample interval, based on the mean water $Po_2$. Calculated oxygen consumption ($Mo_2$ in µmol.g$^{-1}$.h$^{-1}$) was accordingly corrected for non-abalone consumption using equation 4.2.

$$Mo_2 = \frac{((P_i - P_f) - (B.t)).S.V}{W.t} \qquad \text{equation 4.2}$$

Where $P_i$ and $P_f$ are the initial and final $Po_2$ readings (in Torr) for each sample interval of duration t (in hours). $V$ is the volume of water in the respirometer (in litres), $W$ is the wet weight of the abalone (in grams) and $S$ is the solubility of oxygen in seawater at 15°C (1.62 µmol.L$^{-1}$.Torr$^{-1}$).

The critical $Po_2$ level ($P_{crit}$), below which the abalone can no longer regulate its oxygen uptake rate to accommodate, was established statistically. Chamber $Po_2$ was seen to decline linearly with time until uptake became compromised, at which point the gradient changed rapidly. The discontinuity in the $Po_2$:time curve was taken to represent $P_{crit}$. Beginning with the highest $Po_2$ values, each point (paired $Po_2$ and time value) was individually added and the cumulative coefficient of determination ($r^2$) calculated. Addition of points in the linear region augmented the $r^2$ value, hence the $Po_2$ beyond which the $r^2$ declined for 3 or more consecutive points was considered to represent $P_{crit}$.

*Contribution of epipodium and foot to whole animal $Mo_2$*

The contribution of $O_2$ uptake by the foot and epipodium to total $Mo_2$ was determined by monitoring oxygen depletion in separate chambers of a closed respirometer. A modified version of the Perspex respirometer described in figure 4.1 was used. The chamber was equipped with a horizontal partition

and 2 closed external circuits (PVC tubing), one supplying the upper region of the respirometer the other supplying the lower (figure 4.2). Each circuit passed through a separate peristaltic pump that circulated the water at a rate of 1 $L.min^{-1}$, effectively providing mixing in each chamber.

The epipodium/foot region of the abalone was isolated from the rest of the animal by use of a latex dam. Trial and error (using dental dam, condoms etc.) revealed the natural contour and thickness of an examination glove was best suited to the task. A large circular section was cut from the palm to forefinger region of a large, unpowdered latex glove, the thumb was cut off, leaving a tapered 10mm orifice. The latex disc was stretched to fit onto a 180mm-diameter Perspex ring and glued in place (figure 4.3a); the ring was designed to fit tightly within the cylindrical respirometer. The diaphragm was conditioned in seawater until needed.

Adult *H. iris* weighing 230 – 400g collected from Kaikoura were used in this experiment. A previously cleaned, tagged and weighed individual was selected and transferred to an ice tray (4 - 6°C, damp air). To isolate the foot/epipodium the abalone was held perpendicular to the ice tray with one hand while the fingers of the other dilated the latex aperture. As the animal began to bend forward the aperture was fitted over the head and anterior foot, the posterior regions of the foot and epipodium were then gently pressed through the aperture using a finger or plastic spatula (figure 4.3b). The abalone was allowed to attach to a freely moving polycarbonate disc, preventing subsequent attachment to the floor of the respirometer and disruption of the latex seal. The abalone, with its latex assembly, was then placed into the respirometer filled with 15°C seawater. The respirometer was set to its 'open' configuration: water circulation was maintained between the respirometer and a reservoir of aerated seawater and bypass taps were opened allowing free exchange of water between the circuits of the upper and lower chambers. When all air bubbles had been removed and the animal was visibly settled, typically after 10 – 15min, the respirometer was set to

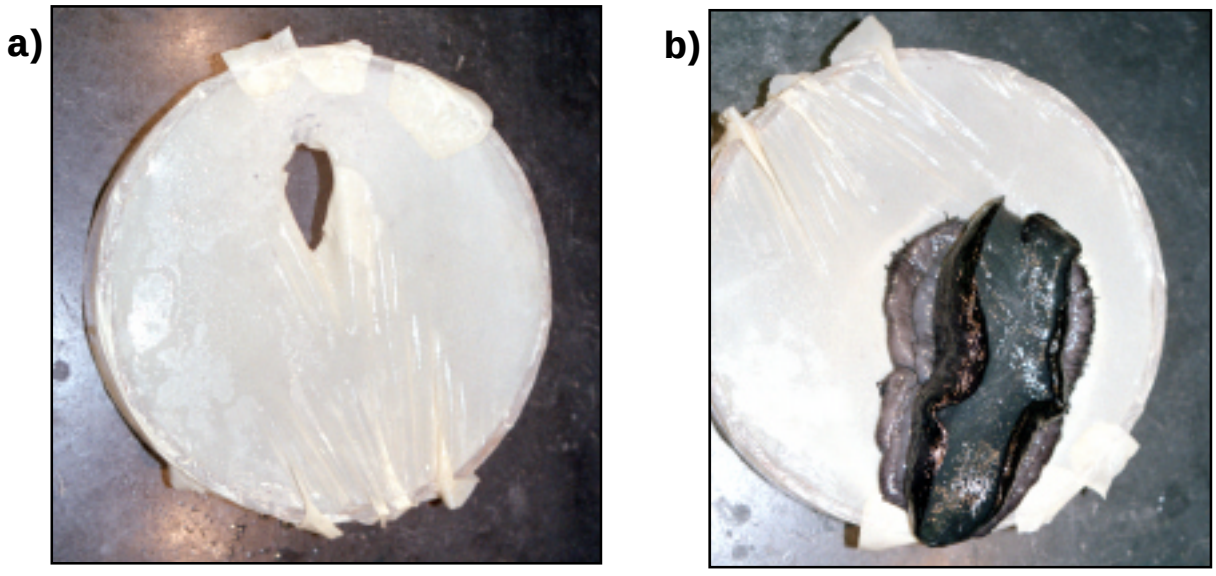


**Figure 4.3**: **a)** Latex diaphragm with a 10mm aperture stretched across a 180mm Perspex ring. **b)** Foot and epipodium of a 300g *Haliotis iris* projecting through the 10mm aperture, which seals around the right shell adductor muscle.

its 'closed' configuration: the respirometer was isolated from the reservoir and the bypass closed, the upper and lower circuits now served to homogenise the water of their corresponding chambers only.

Glass syringes (1mL) were used to sample water directly from the external circuits. Upper and lower chamber samples were taken simultaneously and held anaerobically until they could be analysed using an $O_2$ electrode (Microelectrodes Inc. MI-730, water jacketed at 15°C) connected to an $O_2$ meter (Strathkelvin Instruments 781.b) (maximum sample storage time was 2.5min). Four sequential paired samples were measured in this way over approximately 30min, allowing triplicate estimates of normoxic $Mo_2$ to be calculated for either chamber.

The respirometer was then returned to its 'open' position, this time exchanging water with a nitrogenated reservoir to lower $Po_2$. Exchange continued until respirometer $Po_2$ levels approached 30 Torr, the level associated with maximal evertion of the epipodium in the $P_{crit}$ experiment (typically required 10min exchange). The respirometer was 'closed' and a further set of 4 paired $Po_2$ measurements made to determine hypoxic $Mo_2$.

As in the $P_{crit}$ experiment, blank oxygen consumption was determined by monitoring $Po_2$ change in the empty, normoxic respirometer and in the hypoxic water remaining at the end of each trial. Equation 4.2 was used to determine $Mo_2$ in the upper and lower chambers. This required a specific value for chamber volume, $V$, in each case. As the relative volume of the upper and lower chambers varied between trials, depending on the exact position of the latex divider, volume determination was performed for each animal. As chamber volumes could not be measured directly, seawater volume was assumed to be equivalent to the volume of distribution of amaranth*. A 1mL bolus of amaranth standard was injected into the upper chamber and allowed to mix for 3min. The light absorbance of a sub-sample of chamber water was then measured at the amaranth absorption peak of 522.5nm (Anon. 1983), using a UniCam SP1800 UV spectrophotometer. Absorption was corrected using a seawater blank and fitted to a pre-prepared calibration curve to establish the amaranth volume of distribution. The process was repeated for the lower chamber (figure 4.4). This process also allowed a visual inspection of the integrity of the latex barrier and the efficiency of chamber mixing. The reliability of the amaranth technique was confirmed by comparing the sum of upper and lower chamber volumes, corrected for animal and seal volume, to the known total volume of the respirometer. Amaranth space was found to overestimate total respirometer volume by 17.9 ±4.7%, volume estimates ($V$) were adjusted accordingly.

*Whole body and branchial oxygen uptake in artificially ventilated animals*

The possible contribution of accessory gas exchange surfaces to oxygen uptake was also investigated using a second method. Each selected abalone (mean live weight 333 g) was masked, as described below, and placed in a stirred closed box respirometer (1.85 L) similar that shown in figure 4.1 but

* Amaranth proved consistently useful throughout this project as it represents one of the few visible compounds that does not seem to be perceived by the abalone. Amaranth is non-toxic, highly soluble in seawater and its intense maroon colour is visible at very low concentrations.

provided with two additional ports connected to an external peristaltic pump (Masterflex Tygon™ tubing). The mask was connected via a non-restraining loop of tubing to the inflow of the pump, which ventilated the animal at pre-determined flow rates and returned the water to the respirometer. Oxygen partial pressures ($Po_2$) of the inhalant and exhalent seawater were measured in 1mL samples taken anaerobically (using glass syringes) from the mask outflow, and from the base of the respirometer adjacent to the foot, respectively. Thus total oxygen consumption was calculated from the change in $Po_2$ of the water over time, while the branchial component of oxygen uptake was calculated from the inhalant-exhalant $Po_2$ difference and the ventilatory flow rate. Blank respirometer runs were used to correct for microbial respiration in the sea water (about 2% of abalone oxygen uptake).

Each abalone was allowed to settle in its respirometer overnight, receiving a constant exchange of normoxic seawater. Branchial $Mo_2$ was estimated under these conditions before isolating the chamber. Two series of measurements were made, both at 15°C. In the first, the abalone were ventilated at a constant rate (approximately 45 $mL.min^{-1}$) for about 5 hours, during which time the respirometer $Po_2$ decreased to below 20 Torr due to oxygen uptake by the animal. Water samples were taken at 0.25 h intervals, alternating inhalant and exhalent samples. Total oxygen consumption was thus calculated for 0.5 h periods while branchial oxygen consumption was estimated for the same interval by averaging branchial $Mo_2$ determined at the start and end of each period from simultaneous inhalant and exhalant $Po_2$ measurements.

The second series investigated the effect of varying the ventilatory flow rate on total and branchial oxygen uptake rates in normoxia. During settling in flowing seawater, the animals were ventilated at 45 $mL.min^{-1}$ and branchial $Mo_2$ was measured as before. The ventilatory flow was then increased to 85 $mL.min^{-1}$ for 40 min and this was followed by similar periods of ventilation at nominally 67, 48, 32, 15, 6.5 and 2.5 $mL.min^{-1}$. At the start of each ventilation treatment the animal was allowed to adjust to the new rate for 5 min with the respirometer open, and 5 min with it closed, before taking the first inhalant sample (0 min). This was followed by two exhalant samples at 4 min and 26 min, and a final inhalant sample 30 minutes. The chamber was then opened and flushed with fresh seawater before the next ventilation treatment. Total $Mo_2$ was calculated from the two inhalant samples as before. Inhalant $Po_2$ values corresponding to each exhalent sample were obtained by linear interpolation so that each ventilation rate produced two estimates of branchial oxygen uptake rate. These were averaged for comparison with the total rate. In pilot studies, randomised and increasing flow sequences were trialled but were considered unsatisfactory. Transiently very high oxygen uptake rates followed intervals of hypoventilation, presumably a consequence of internal hypoxia.

*Mantle as a site of $O_2$ uptake*

Oxygen uptake by the right mantle region of intact abalone could not feasibly be determined. Instead, net contribution to the haemolymph pool was examined, allowing the tissue region to be classified as a site of net $O_2$ uptake from the water or net consumption. The vessel supplying the right mantle

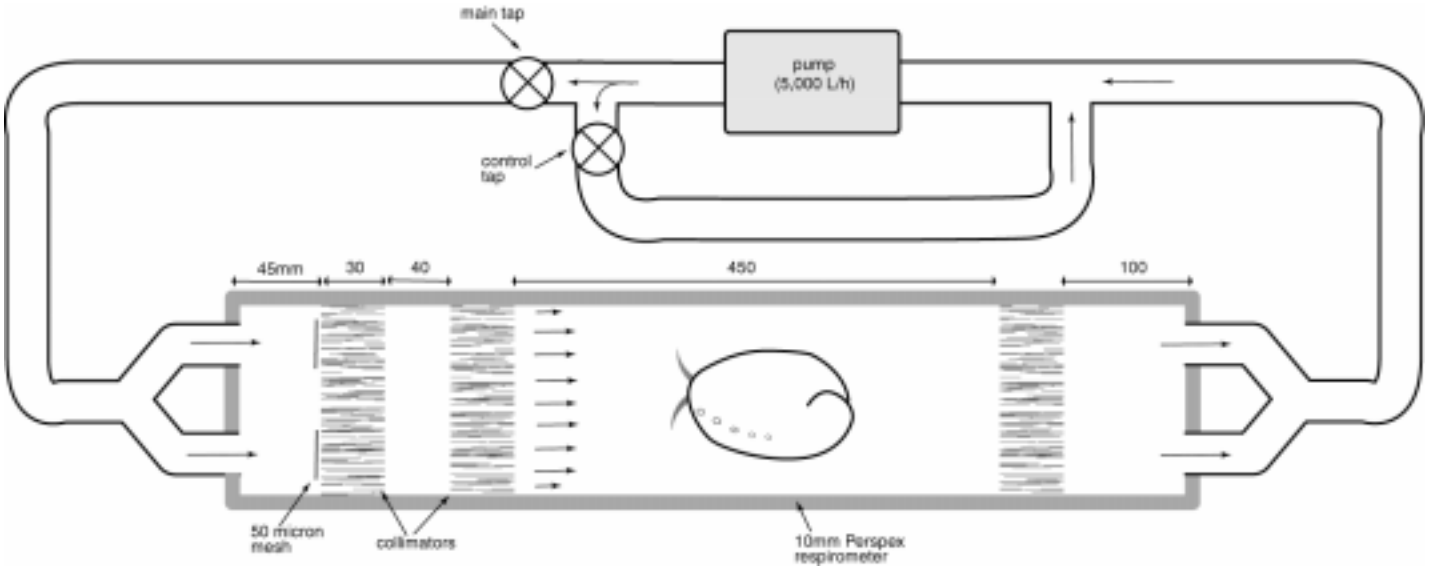


**Figure 4.5**: Plan of flume respirometer designed to monitor oxygen uptake under varying current velocities. Entire apparatus is immersed in a 10.7°C water bath to maintain an internal environment of 15.0°C.

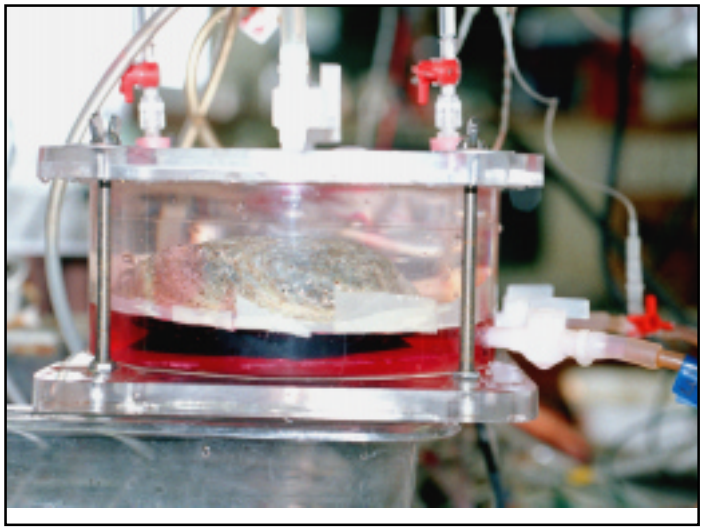

**Figure 4.4**: Two-chamber respirometer designed to measure $Mo_2$ of the foot and mantle, showing amaranth circulating in lower chamber.

**Figure 4.6**: Photograph showing flume respirometer in operation.

(the circum-pallial vein), the vessel draining the mantle (the pallial vein) and the aorta were cannulated as described in chapter 7-*preparation 2*. The abalone was then placed in a recirculating chamber similar to that described in chapters 5 and 6. Haemolymph sampling commenced immediately to take advantage of the animal's stressed condition, considered to be associated with maximal cardiac output (see chapter 6). Triplicate samples were taken for $Po_2$ determination from each vessel and also from the surrounding seawater, which provided a calibration reference. At each sample time two 100µL samples of haemolymph were slowly withdrawn (~1min) into a Hamilton Gastight™ syringe. The first sample was used to condition an oxygen electrode (MI-730) while the second sample was being withdrawn from the same vessel. The second sample was then injected into the electrode chamber and $Po_2$ recorded after 2min. As the 3 vessels could not be sampled simultaneously, the sequence of haemolymph sampling was randomised, with a lag of approximately 5min between the first and last withdrawal. Triplicate samples were repeated after 24h to provide $Po_2$ data on a contrasting recovery state.

*Ventilation and heart rate in static water and the effect of hypoxia*

The endogenous ventilatory water flow, generated by abalone, in the absence of significant external water currents, was measured using an electromagnetic flow meter (Carolina Instruments). A tunnel-shaped mask, closed at one end, was constructed from a 7 cm length of PVC tubing (~10 mm i.d., 2 mm wall) cut longitudinally to match the shell contour. The mask was attached to the cleaned and dried shell using cyanoacrylate gel adhesive and sealed with a hot glue gun so that it enclosed all of the patent tremata (shell holes). The output from the open end of the mask was directed through a cylindrical electromagnetic flow probe (IVM, 25mm long x 8 mm ID) calibrated by pumping seawater through the probe at known rates. Drift in the zero-flow signal was checked *in situ* at regular intervals during measurement periods by briefly occluding the probe; individual measurements were subsequently corrected by linear interpolation between these calibration checks.

The partial pressure of oxygen in the water was continuously monitored in an external circuit pumped at 1 $mL.min^{-1}$ through a 15°C thermostatted oxygen electrode cell (Strathkelvin). In some animals, the heart rate was measured simultaneously. Impedance electrodes (0.14 mm diameter insulated copper wire, with bared ends coiled to avoid piercing the animal) were inserted through 2 mm diameter holes drilled through the shell on either side of the heart. The electrodes were positioned to lightly contact the mantle epithelium and secured with cyanoacrylate glue and connected to an impedance coupler (Strathkelvin Instruments A100). Flow meter, oxygen and impedance signals were recorded to a computer data acquisition system (ADInstruments PowerLab M420, Chart software version 4.1.2) sampling at 100 Hz.

Measurements were made on abalone in a closed, covered 4 L chamber of seawater, which could be opened to permit a slow exchange of fresh seawater during recovery periods. An air stone, positioned as far from the animal as possible, bubbled air or nitrogen to modulate water $Po_2$. Recordings were made immediately after instrumentation ("disturbed"), after overnight recovery in aerated seawater ("settled") and during nitrogen bubbling ("hypoxic") and re-aeration ("recovery").

For normoxic animals, mean flow rate and cardiac frequencies were obtained from triplicate, 2 min sample records. During the hypoxic treatment, ~1 min records were centred on selected values of $Po_2$ (100, 70, 40, 25, 15, 10, 5, 2, <1, recovery 70 and recovery 100 Torr).

*Influence of external current velocity on whole animal $Mo_2$*

A flume respirometer was constructed to determine oxygen consumption under approximately laminar flow conditions (figure 4.6), based on a modification of the flow chamber design of Vogel and LaBarbera (1978). The flume was constructed of 10mm Perspex measuring 725 x 130 x 70mm (L x W x H), supplied by a 30mm diameter recirculation line. The system had an internal volume of 8.08L. A pump (Laguna, nominally 5,000 $L.h^{-1}$) provided a constant output that was regulated by use of a low resistance bypass loop and a main tap (figure 4.5a). Two influent pipes delivered water to the respirometer where collimators were used to rectify the flow to produce an approximately laminar profile. Each collimator was composed of several layers of Macrolux™ sheeting, a polycarbonate sandwich honeycombed with 3 x 3mm square channels 30mm in length. The influent side of the first collimator was guarded by 2 strips of 50µm mesh (figure 4.5a), preventing incoming water jets from disrupting the flow profile.

Three flow treatments were used in this experiment. 'Maximum flow' (16.4 $cm.s^{-1}$) was achieved by opening the main tap and closing the bypass tap, opening the bypass resulted in 'half flow' (4.6$cm.s^{-1}$) and a subsequent 45° occlusion of the main tap reduced chamber flow below detectable levels (<1$cm.s^{-1}$, 'zero flow'). Flow velocity was initially determined using a Schiltknecht Mini-air 2™ anemometer; the mean of 5 point readings across the central region of the flume was accepted as the mean flow velocity across the abalone. A Mylar vane was calibrated against a deflection scale to allow confirmation of flow when the respirometer was sealed and a small amount of amaranth solution was injected to determine that adequate mixing (complete homogenisation in <3min) continued during 'zero flow'.

An experiment was designed to address 2 hypotheses. The first suggested that external water currents are essential to ventilate the gills, and that $Mo_2$ will correspondingly increase as current velocity increases. The second hypothesis proposed that resting abalone in normoxic seawater are not reliant upon externally-derived ventilation, but endogenous ventilatory mechanisms are unable to accommodate increased oxygen demand, for example during recovery from hypoxic stress.

A cleaned abalone (South Bay, Kaikoura population) was selected and placed into the flume, facing into the current. The respirometer was operated with flow-through seawater, exchanged with a large, aerated reservoir, for 1h to allow air bubbles to be removed and the animal to settle. An $O_2$ electrode (Strathkelvin), connected to an $O_2$ meter (SI 781), was calibrated against damp air and connected to the respirometer using 1.0mm internal diameter polyethylene tubing (0.5mm wall thickness, 400mm total length). Respirometer water from the downstream end of the chamber was supplied to the electrode by a peristaltic pump at a rate of 8$mL.min^{-1}$. Each abalone was subjected to the three flow treatments, in random order, for 10min at a time. $Po_2$ was recorded at the start and

end of this period and used to calculate $Mo_2$ from equation 4.2. The process was repeated until triplicate $Mo_2$ values were obtained for each flow treatment. The orientation of the animal was also noted at the start of each measurement period. The abalone was then removed from the respirometer and placed in a damp, empty container at 15°C for 18h. As abalone are unable to irrigate their gills in air, emersion induces a state of environmental hypoxia (Wells and Baldwin 1995). The abalone was then returned to the respirometer and the $Mo_2$ monitoring protocol re-commenced immediately to obtain triplicate values for each flow during oxygen debt repayment. Blank oxygen consumption was determined by measuring $O_2$ depletion in the flume filled with normoxic seawater flowing at 4.6cm.s$^{-1}$.

*Statistics*

Changes in ventilation rate with progressive hypoxia were analysed using one-way analysis of variance and Dunnett's test for pair-wise comparison with a control (settled) value. All other comparisons utilised simple one- or two-way ANOVA and Tukey's test for post-hoc contrasts, unless stated otherwise. Statistical significance was accepted at $P < 0.05$.

# 4.3. Results

*Whole animal $Mo_2$ and $P_{crit}$*

Blank $O_2$ consumption (empty respirometer) increased from 0.26 ±0.35 µmol.L$^{-1}$.h$^{-1}$ in normoxia (~0.2% of abalone $Mo_2$ at 150.2 ±0.7 Torr) to 2.73 ±0.65µmol.L$^{-1}$.h$^{-1}$ under hypoxia (~3.5% of abalone $Mo_2$ at 35.3 ±2.8 Torr), presumably as a result of increased microbial substrate, in the form

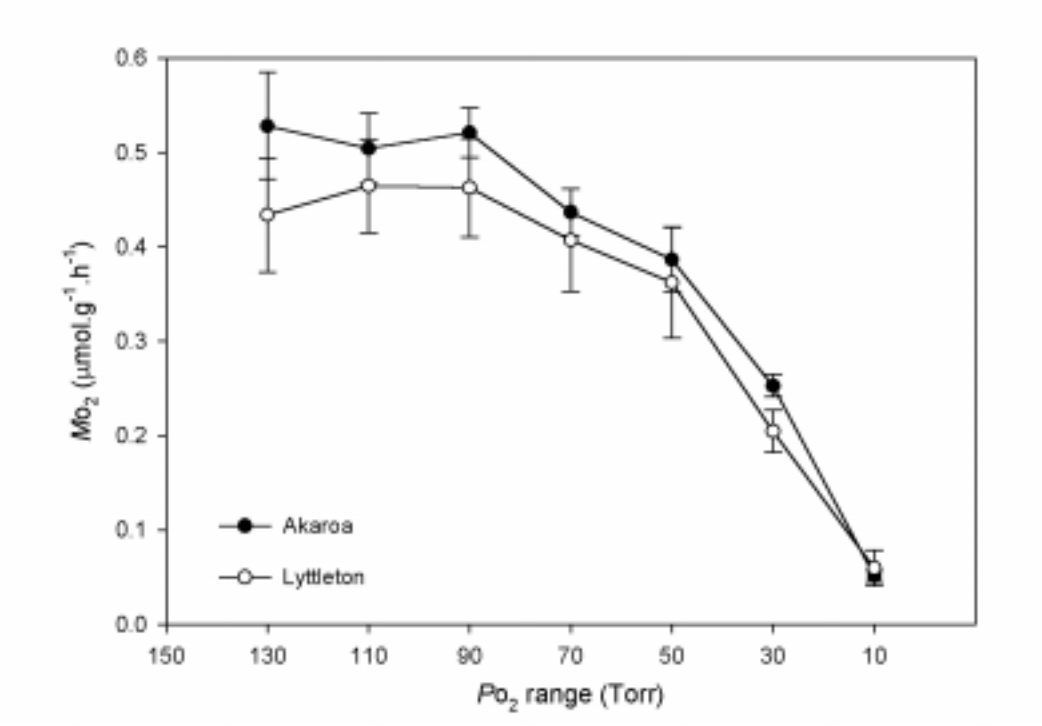


**Figure 4.7**: Mean oxygen uptake response of 2 populations of abalone (*H. iris*) to declining $Po_2$. Animals from Akaroa originate from a semi-exposed reef while Lyttleton abalone were collected from a sheltered sub-littoral.

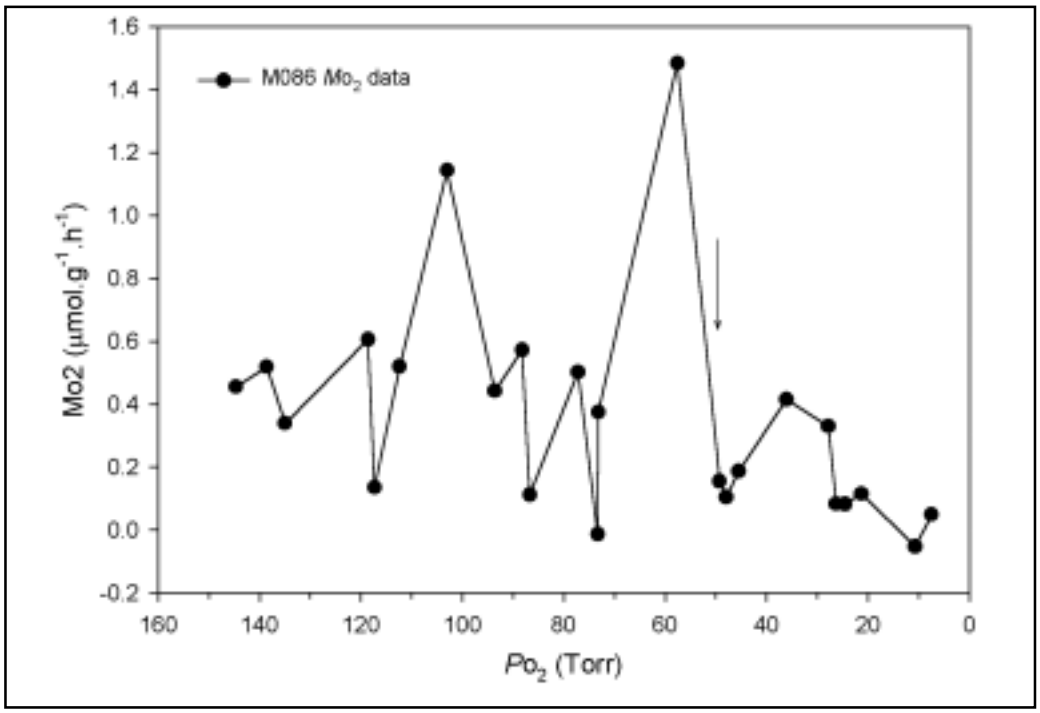


**Figure 4.8**: Oxygen uptake rate of a typical individual *H. iris* in response to declining $Po_2$. Normoxic $Mo_2$ is reasonably constant until $Po_2$ falls below 120 Torr, where periods of rapid uptake apparently compensate for sporadic failure to regulate $Mo_2$. Below $P_{crit}$ (marked by arrow) $Mo_2$ declines with $Po_2$.

of excreted ammonia and mucus. Normoxic $Mo_2$ ($Po_2$>120 Torr) of *H. iris* was 0.47 ±0.04 µmol.g$^{-1}$.h$^{-1}$. Mean $Mo_2$ rates were maintained until ambient $Po_2$ fell below the 80 – 100 Torr range (figure 4.7). If individual animal uptake is examined however, the $Po_2$ range between 40 and 120 Torr is characterised by a highly variable $Mo_2$ response (figure 4.8). In this range occasional peaks in uptake rate appear to compensate for sporadic failure to oxyregulate (figure 4.8), the effectiveness of this compensation is reflected in the mean $Mo_2$ rates shown in figure 4.7. The net effect of abalone respiration on seawater $Po_2$ in the closed respirometer was to cause a linear decline down to 45.2 ±4.7 Torr (n = 15; '$P_{crit}$'). Below this $Mo_2$ and, consequently, $Po_2$ depletion rate decreased rapidly, apparent as a deterioration in the coefficient of determination ($r^2$) of the $Po_2$:time relationship. Oxygen consumption was virtually undetectable below 20 Torr (mean $Mo_2$ at 0 – 20 Torr = 0.06 ±0.01µmol.g$^{-1}$.h$^{-1}$).

No significant difference was observed in the rate of oxygen consumption or in response to declining $Po_2$ for the abalone taken from a semi-exposed (Akaroa) compared with a sheltered site (Lyttleton. Figure 4.7; $F_{1,88}$ = 3.55, p = 0.06). Almost without exception the abalone were seen to fully extend their epipodium at low $Po_2$, this behaviour was first observed at 30.6 ±3.6 Torr (n = 13; figure 4.9b).

*Contribution of epipodium and foot to whole animal $Mo_2$*

Under normoxic conditions the whole abalone consumed 0.46 ±0.06µmol $O_2$.g$^{-1}$.h$^{-1}$ (n = 12) while the isolated foot-epipodium region consumed 0.06 ±0.01µmol $O_2$.g$^{-1}$.h$^{-1}$, representing 13.9 ±3.1% of whole animal uptake (figure 4.9a). When exposed to environmental $Po_2$ in the range of 45 – 30

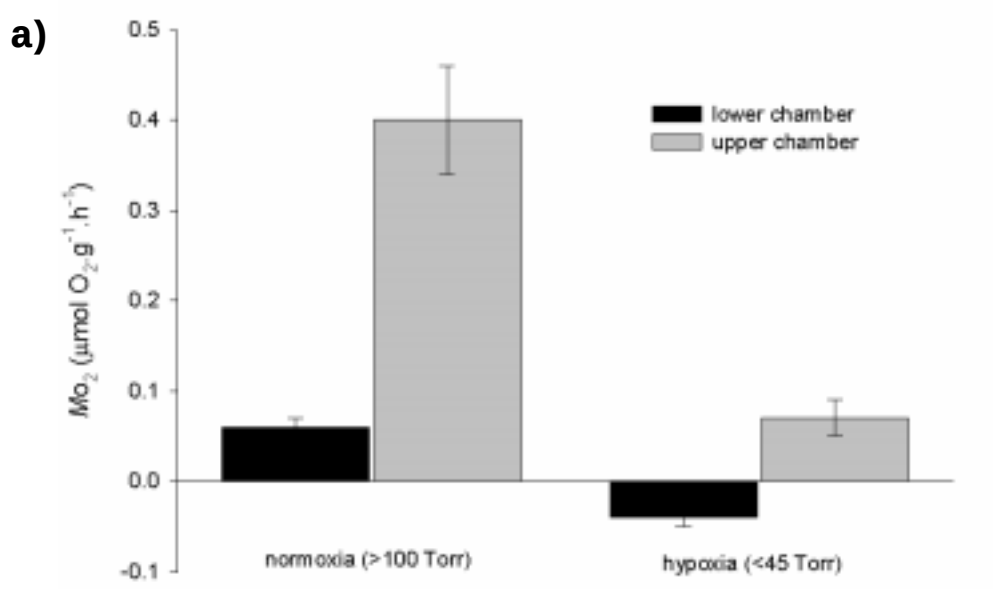


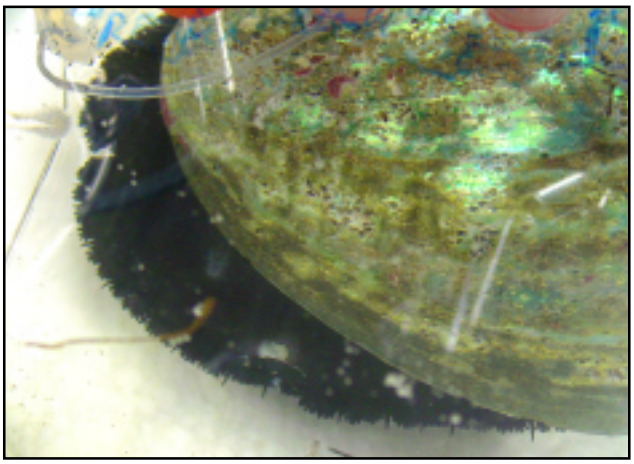


**Figure 4.9**: **a)** Oxygen consumption by the foot and epipodium ('lower chamber') compared to the gills and remaining body surfaces ('upper chamber') of *Haliotis iris* subjected to normoxic (>100 Torr) and hypoxic (<45 Torr) seawater. **b)** Photograph of posterior region of *H. iris* in hypoxic seawater showing fully extended epipodium.

Torr, upper chamber (i.e. gills and viscera) $Mo_2$ fell to 0.07 ±0.02µmol.$g^{-1}$.$h^{-1}$, while the foot-epipodium showed no detectable oxygen consumption (-0.03 ±0.02µmol.$g^{-1}$.$h^{-1}$).

*Whole animal and branchial oxygen uptake in artificially ventilated abalone*

Values of whole animal oxygen consumption by abalone, measured by closed box respirometry, and simultaneous estimates of oxygen uptake from the exhalant water were similar in normoxic water and declined at similar rates with self-generated hypoxia (Figure 4.10). The results therefore provide no support for the existence of accessory gas exchange surfaces. All animals extended the epipodium and tentacles at about 30 Torr, but this was not associated with any difference between total and branchial $Mo_2$. These animals were artificially ventilated at a mean rate of 44 mL.$min^{-1}$, about 1.6 times the endogenous ventilation rate of approximately 28 mL.$min^{-1}$ (see below) expected for *H. iris* of this size (mean weight = 333g). The rate of oxygen consumption declined uniformly with $Po_2$, showing neither the oxyregulatory plateau previously observed in naturally ventilating abalone between normoxia and 80 Torr (cf. Figures 4.7 and 4.10), nor the wide fluctuations in $Mo_2$ recorded in individuals (Figure 4.8). One animal (eliminated from the data set) clamped at about 35 Torr and maintained this state for 2 hours, during this period total and branchial oxygen uptake virtually ceased (0.02 - 0.03 µmol.$g^{-1}$.$h^{-1}$).

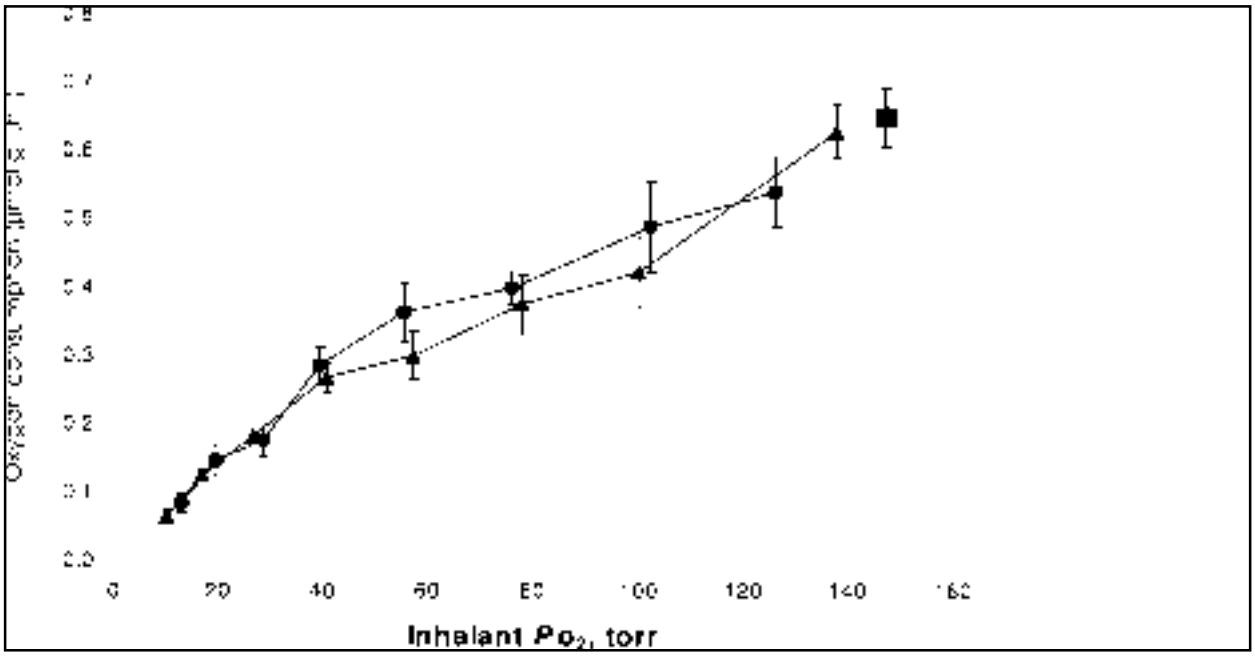


**Figure 4.10**: Dependence of total oxygen consumption (circles, µmol.g$^{-1}$.h$^{-1}$) and branchial oxygen uptake (triangles) by masked, artificially ventilated (mean 45 mL.min$^{-1}$) abalone on the inhalant $Po_2$ of the seawater during self-generated hypoxia in a closed system respirometer. The square symbol represents the mean branchial oxygen uptake before closure of the respirometer. Values are means ± SEM (n = 5 - 8).

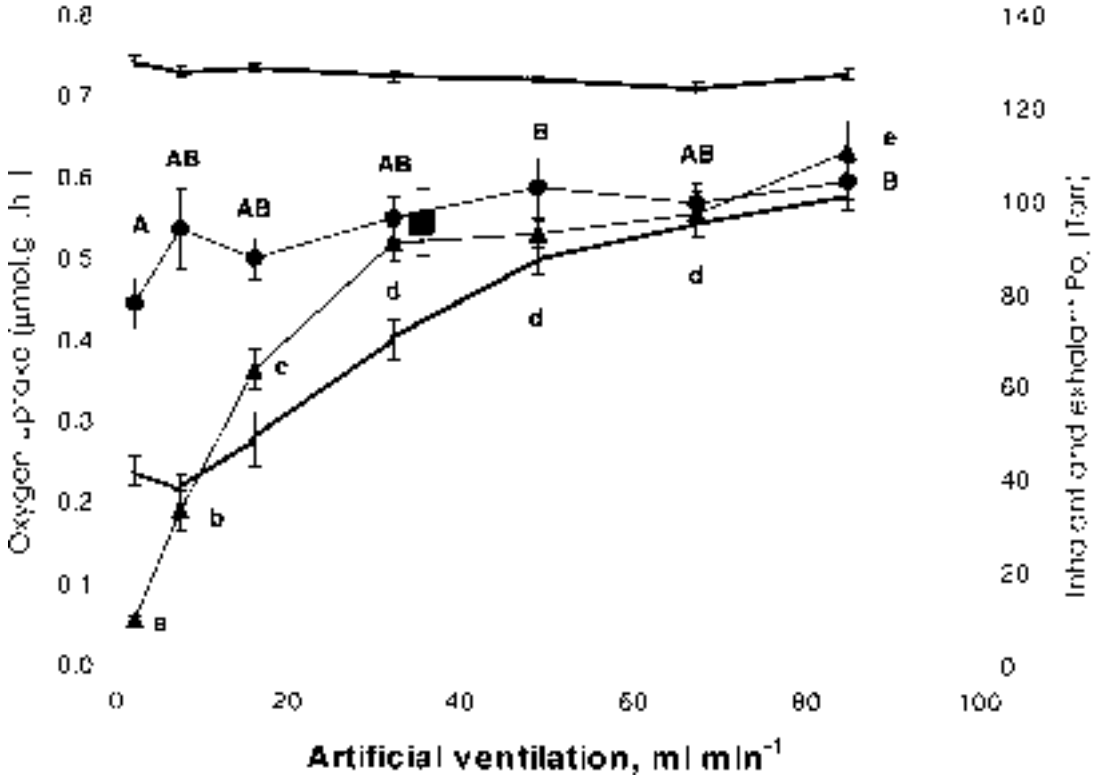


**Figure 4.11**: Dependence of total oxygen consumption (circles, µmol.g$^{-1}$.h$^{-1}$) and branchial oxygen uptake (triangles) on ventilation rate (mL.min$^{-1}$) in masked, artificially ventilated abalones. The square represents the mean branchial oxygen uptake before closure of the respirometer. The inhalant (upper line, no symbols) and exhalant (lower line, no symbols) $Po_2$ (torr) are also shown. Values are means ± SEM (n = 7). Significant differences among means of total and branchial oxygen uptake are indicated by different upper and lower case letters respectively (repeated measures ANOVA, $F_{6,36} = 3.26$, $p = 0.012$ and $F_{6,36} = 167.9$, $p < 0.001$, for total and branchial uptake, respectively; Tukey tests).

Whole animal oxygen consumption was significantly dependent on the rate of artificial ventilation (Figure 4.11; linear regression: y-intercept 0.487 ± 0.020 $\mu mol.g^{-1}.h^{-1}$, slope 0.00143 ± 0.00042 $\mu mol.g^{-1}.h^{-1}.ml^{-1}.min$, $p = 0.0012$, $r^2 = 0.20$, 48 df). When artificially ventilated at the mean endogenous rate of 28 $mL.min^{-1}$ the abalone consumed 0.528 $\mu mol.g^{-1}.h^{-1}$. Under artificial hyperventilation at 85 $mL.min^{-1}$ $Mo_2$ increased by 13% and decreased by only 15% in virtual apnoea at 2.2 $mL.min^{-1}$. At ventilation rates above the endogenous rate, branchial oxygen uptake was similar to the total consumption. In contrast, at ventilation rates below the endogenous rate, branchial oxygen consumption decreased steeply (figure 4.11). As discussed below, this may underestimate true branchial oxygen consumption at low artificial ventilation rates.

Maintenance of oxygen uptake with decreasing ventilation was associated with increased difference between inhalant and exhalent $Po_2$ (Figure 4.11). At artificial ventilation rates corresponding to the mean endogenous rate of 28 $mL.min^{-1}$, percentage $O_2$ extraction was estimated to be 49 %. At a ventilation rate of 85 $mL.min^{-1}$ this fell to 21%. As ventilation was reduced, extraction efficiency increased to a maximal value of 71% at 7.5 $mL.min^{-1}$, corresponding to a minimum exhalant $Po_2$ of 37.6 ± 3.0 Torr.

*Mantle as a site of $O_2$ uptake*

In stressed, recently cannulated abalone, haemolymph $Po_2$ in the aorta was 97.5 ±3.6 Torr (n = 7). Haemolymph $Po_2$ was 68.4 ±12.8 Torr within the circum-pallial vessel and 58.7 ±7.2 Torr in the

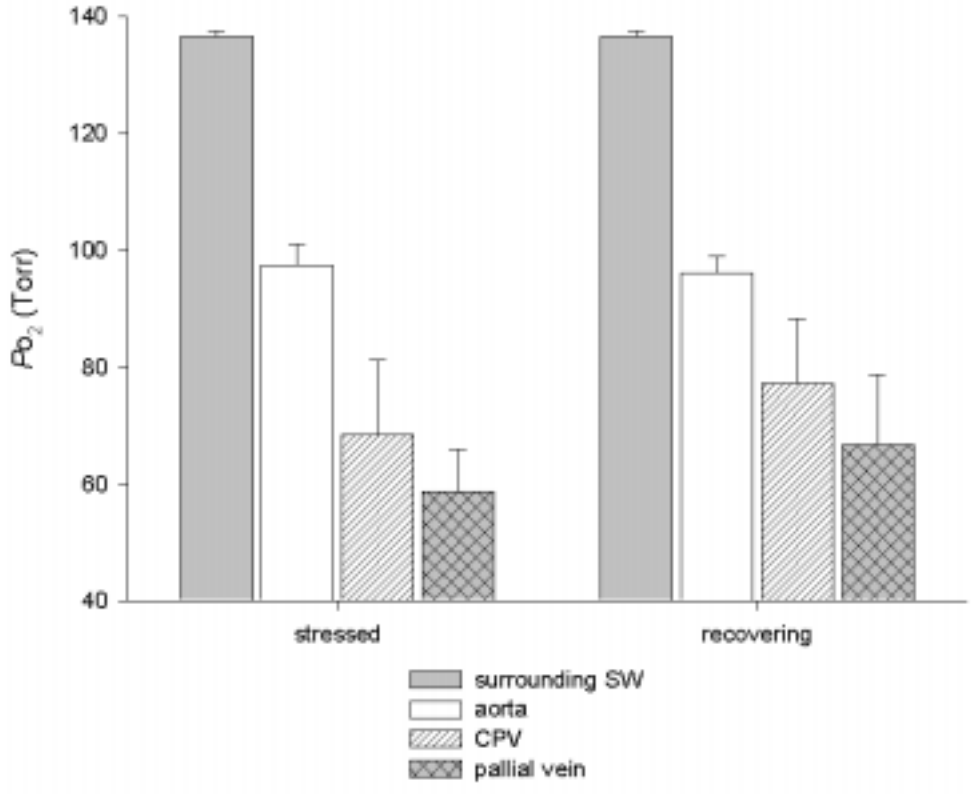


**Figure 4.12**: Oxygen partial pressures found in the haemolymph of the aorta, circum-pallial vein (CPV) and pallial vein of *H. iris* recently exposed to the stress of cannulation and following 24h recovery.

pallial vein (figure 4.12); the latter $Po_2$ difference, however, was non-significant ($F_{1,68} = 3.01$, $p = 0.09$). Allowing the abalone to recover for 24h had no significant effect on the $Po_2$ levels found in the pallial vessels ($F_{1,68} = 2.05$, $p = 0.16$).

*Ventilation and heart rate in static water and the effect of hypoxia*

Abalone, fitted with a mask and an electromagnetic flow probe, were returned to static normoxic sea water at 15°C. The mean endogenous ventilation rate of these air-exposed and disturbed animals, within the first half hour, was 94.3 ±14.2 $mL.min^{-1}.kg^{-1}$ (n = 6) and the heart rate was 23.6 ±0.9 $min^{-1}$ (n = 7). After overnight recovery in flowing, aerated seawater (16 – 20 h), ventilation was 84.0 ±12.2 (n = 7) $mL.min^{-1}.kg^{-1}$ and heart rate was 23.8 ±0.9 $min^{-1}$ (n = 7); neither parameter changed significantly from the disturbed state (paired *t*-test). On switching to nitrogen, the $Po_2$ of the water initially decreased rapidly, falling below 70 Torr in about 2 min, and subsequently declined more slowly. There was no significant change in ventilation rate down to a $Po_2$ of 15 Torr (Figure 4.13), which was achieved after 10 – 15 min nitrogen bubbling. Indeed, in 6 of 10 animals, ventilation rate was maximal at about 25 Torr. Below this $Po_2$, the mean ventilation rate decreased sharply to 25.4 ±9.4 $mL.min^{-1}.kg^{-1}$ at 0.5 Torr after about 30 minutes. Ventilation rate was dependent upon ambient $Po_2$ between 0.5 and 25 Torr (linear regression: y-intercept 31.2 $mL.min^{-1}.kg^{-1}$, slope 2.7 $mL.min^{-1}.kg^{-1}.Torr^{-1}$; $p < 0.001$, $r^2 = 0.34$, inclusion of higher $Po_2$ values did not improve the fit).

In contrast to ventilation rate, mean cardiac frequency decreased steadily with $Po_2$ down to 19.5 ±1.5 $min^{-1}$ at 25.6 Torr (linear regression $r^2 = 0.184$, $p = 0.002$), and then fell more sharply to 7.2 ±1.9 $min^{-1}$ at 0.5 Torr ($r^2 = 0.399$, $p < 0.001$).

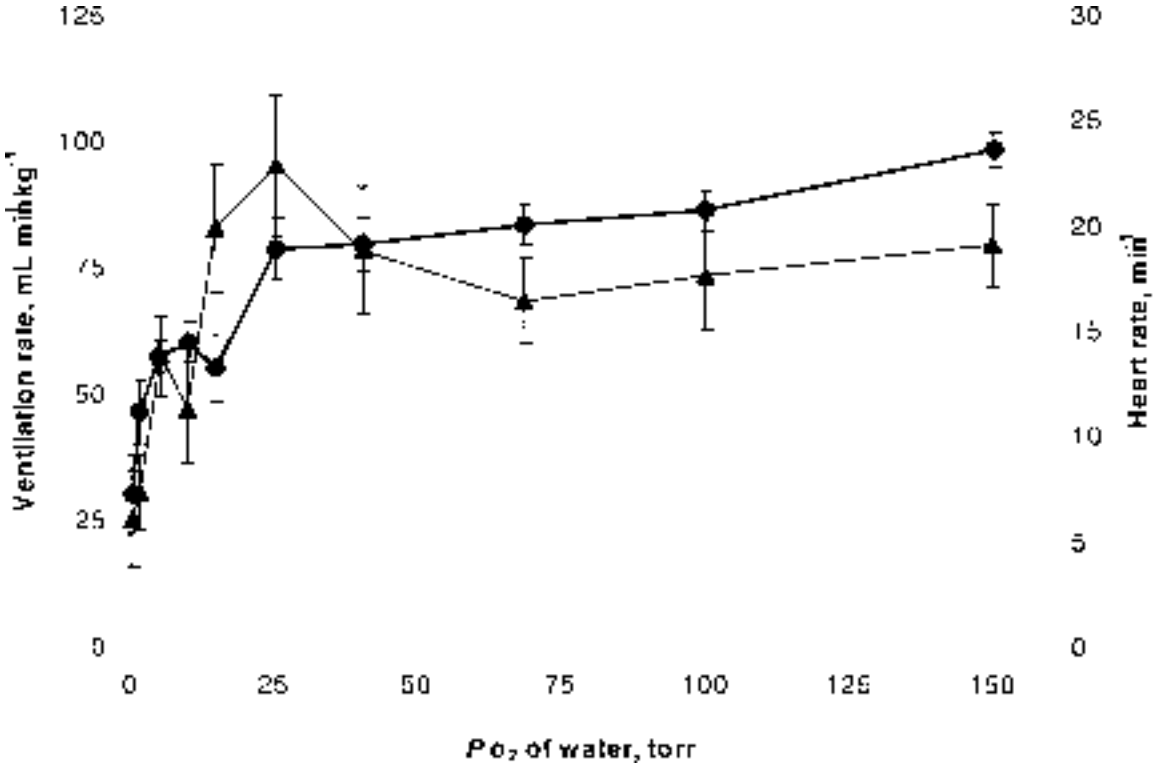


**Figure 4.13**: Dependence of ventilation rate (triangles, $mL.min^{-1}.kg^{-1}$) and heart rate (circles, $min^{-1}$) on $Po_2$ of the seawater (Torr) during nitrogen-induced hypoxia. Values are means ± SEM (n = 5-10).

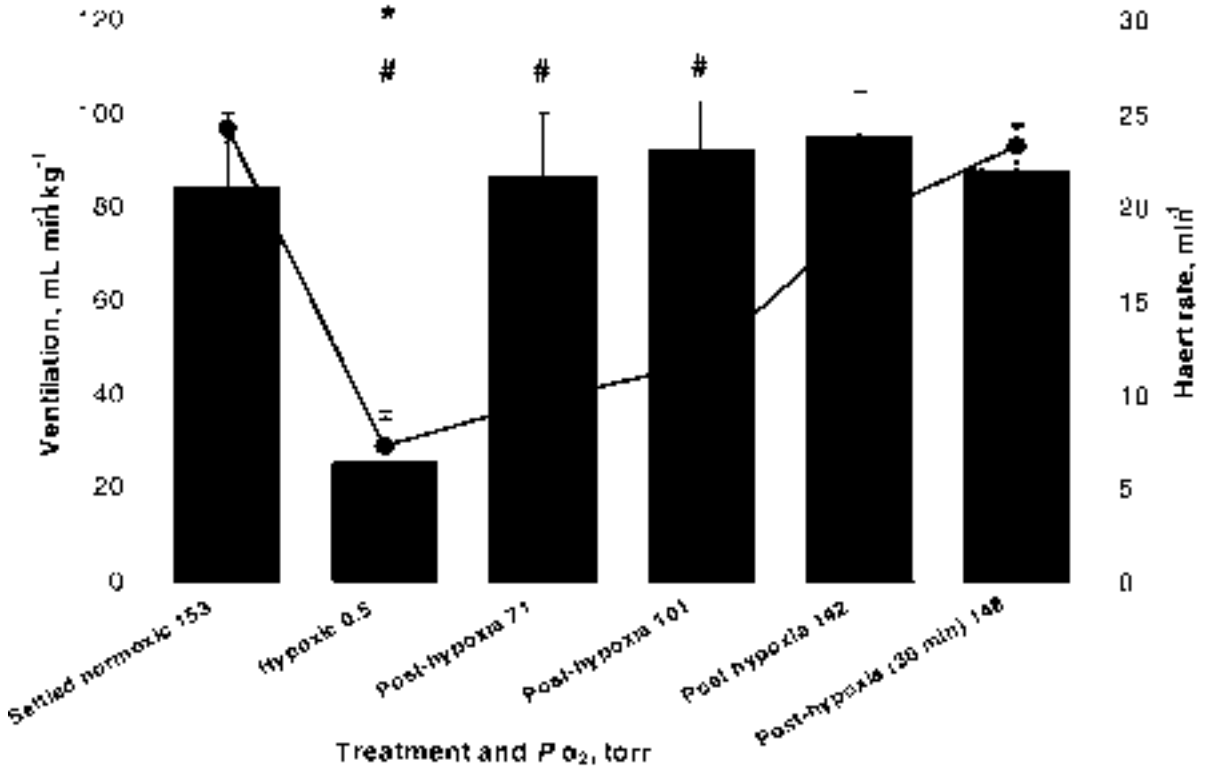


**Figure 4.14**: Endogenous (ciliary) ventilation rates (bars, mL.min$^{-1}$.kg$^{-1}$) and heart rate (circles, min$^{-1}$) in abalone settled for 16 – 20 h in normoxic seawater, at the end of a period (~30 min) of progressive nitrogen-induced hypoxia to mean 0.5 Torr, and during re-oxygenation to mean $Po_2$ levels of 71 Torr (~2 min), 101 Torr (~3 min), 142 Torr (~10 min) and 148 Torr (~30 min). Values are means ±SEM (n = 5-10). * and # indicate ventilation and heart rates significantly different from the settled value, respectively (one way ANOVA, $F_{5,49} = 3.71$, $p = 0.006$ and $F_{5,49} = 25.8$, $p < 0.001$, respectively. Specific differences located using Dunnett's test).

As the chamber was aerated again, the $Po_2$ of the water increased, reaching 70 Torr after about 2 min and 140 Torr in less than 10 min. Ventilation returned to the settled rate almost immediately but recovery from the hypoxic bradycardia was more gradual (Figure 4.14).

The ventilation trace was clearly oscillatory and in phase with the cardiac cycle (Figure 4.15). Irregular heartbeats were also present in the ventilation trace. In settled normoxic animals, the amplitude of the flow oscillation was high and the minima were often close to zero flow. However, as $Po_2$ declined, the amplitude of the ventilatory oscillation decreased and was eventually lost in noise, although mean flow rate and the amplitude of the cardiac impedance signal were relatively unaffected (Figures 4.15 and 4.16).

When the flow probe was briefly occluded and reopened to check for zero drift, it was noted that the mean flow was re-established over several seconds suggesting imperfect viscous or inertial coupling in the mechanism of flow generation (Figure 4.17).

Ventilation rates were highly variable due to a number of other behaviours evident in individual records. Some animals adjusted their position slightly or moved a short distance during the hypoxic treatment. This introduced changes in the flow baseline lasting many minutes. In switching from air to $N_2$, visual and mechanical disturbances were avoided. However, after a delay of a few minutes, when the $Po_2$ had decreased to about 70 Torr, all of the abalone responded by a series of bimodal

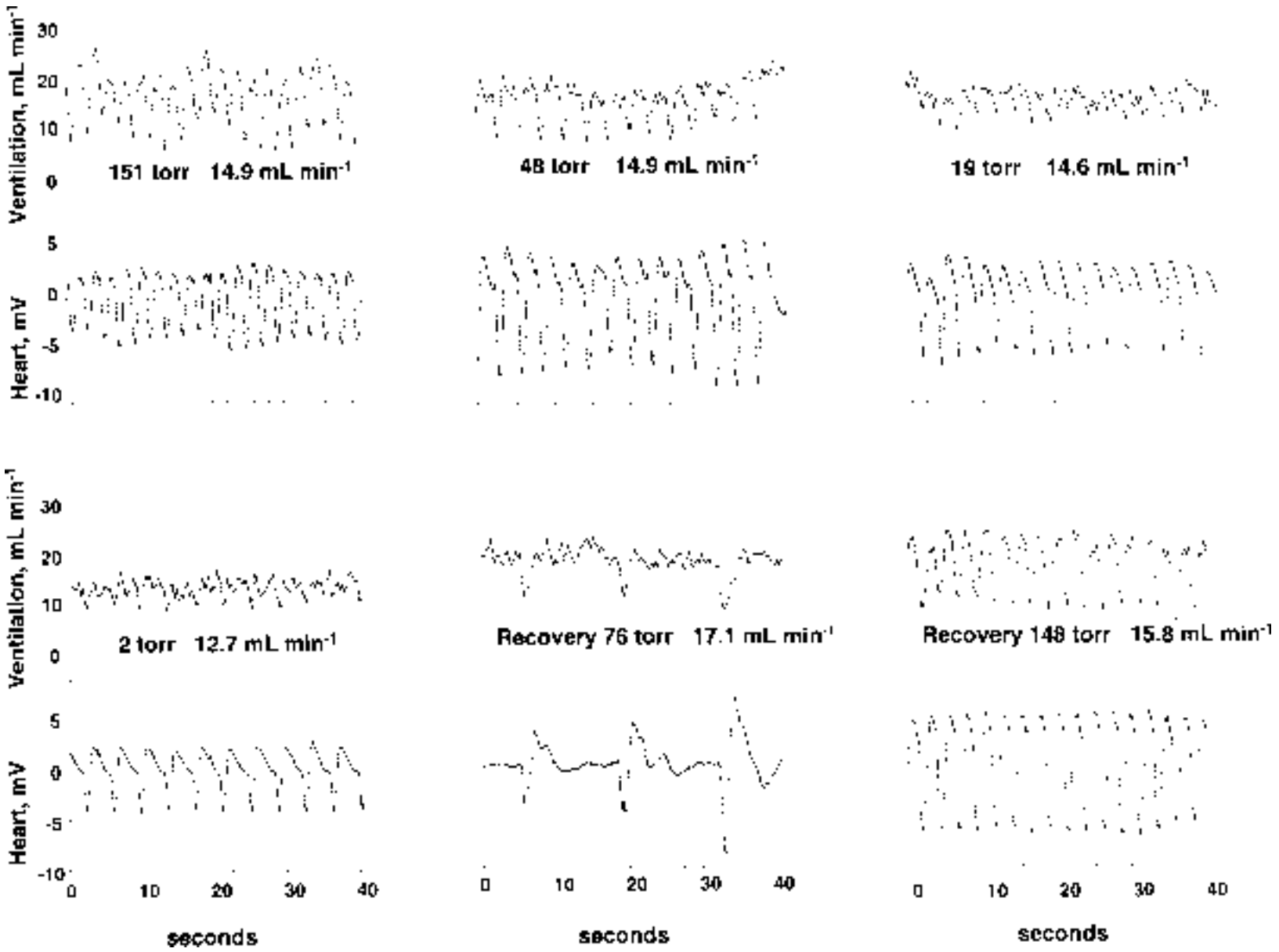


**Figure 4.15**: Simultaneous records of the ventilation waveform (mL.min$^{-1}$.kg$^{-1}$, electromagnetic flow meter, upper trace of each pair) and the heart impedance signal (mV, lower trace) in a single abalone during development of hypoxia and return to normoxia. Successive paired records are shown from left to right in the top row and then the lower row. Mean ventilatory flow and the $Po_2$ of the water (Torr) in each 40 s segment are also shown. Note the ventilatory oscillation in phase with the heart signal, the attenuation of the ventilatory oscillation, but not the heart signal, at low $Po_2$ (19 and 2 Torr), and the recovery of mean flow at 76 Torr during continued hypoxic bradycardia. Recording and display settings are the same throughout (100 Hz sampling, 51 point Bartlett smoothing).

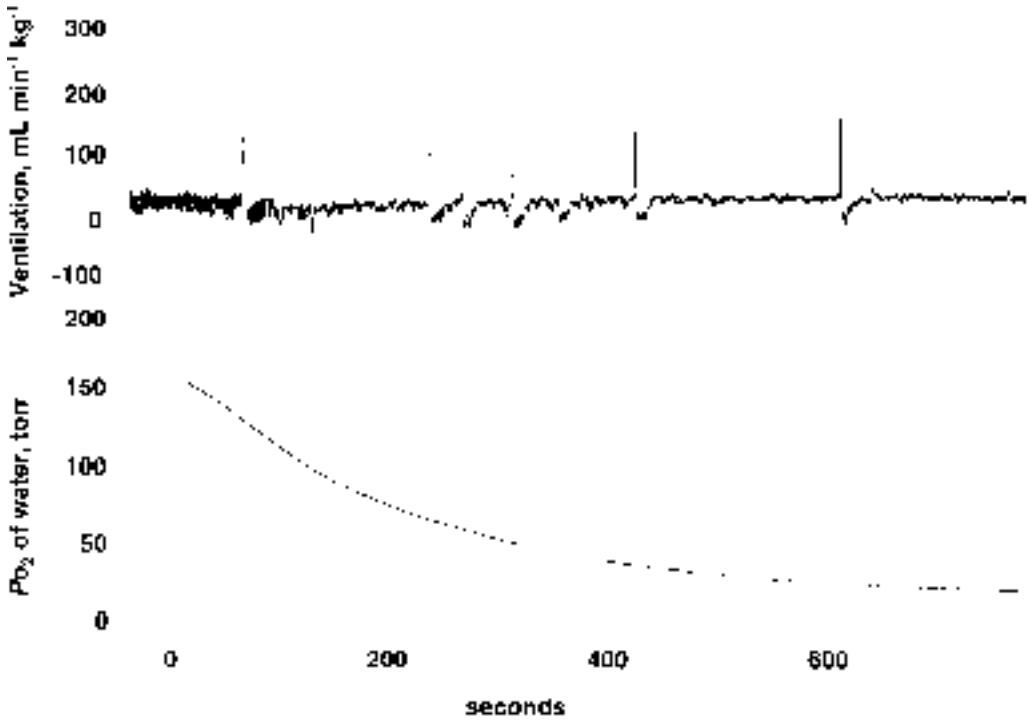


**Figure 4.16**: A representative record of ventilation (mL.min$^{-1}$.kg$^{-1}$, electromagnetic flow meter, upper trace) by a single abalone in relation to the $Po_2$ of the sea water (Torr, lower trace) during nitrogen-induced hypoxia. Note the attenuation of the flow oscillation at low $Po_2$ and the occurrence of a train of biphasic flow pulses, commencing at about 70 Torr. These 'flinches' correspond to sudden downward contractions and slower relaxation of the shell adductor muscle. (100 Hz sampling, 51 point Bartlett smoothing).

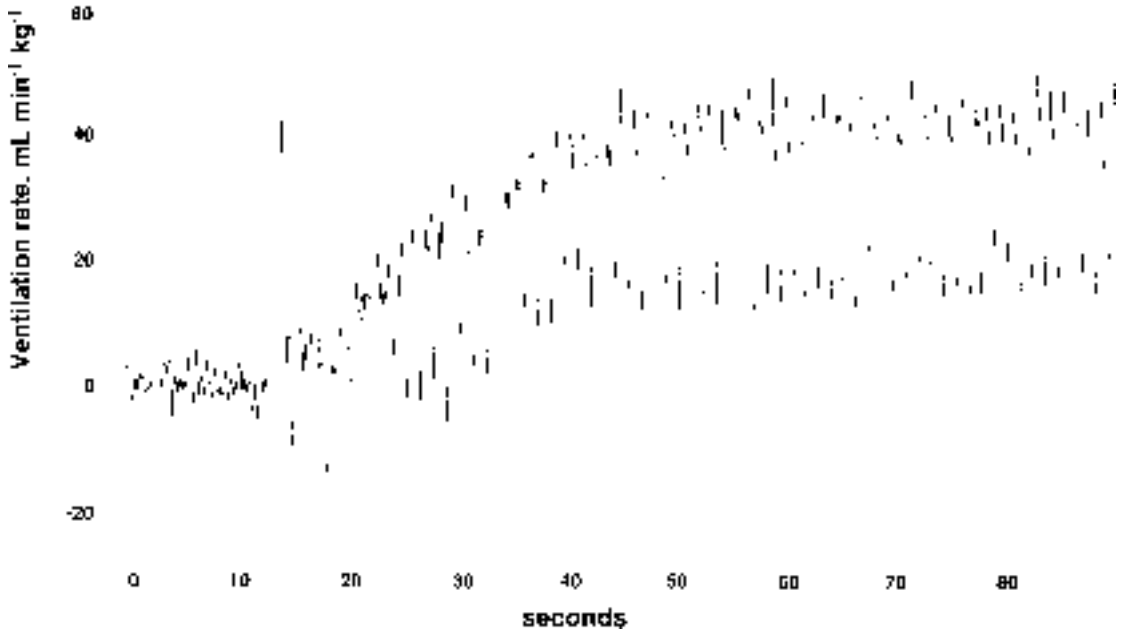


**Figure 4.17**: Electromagnetic flowmeter signal of ventilation during occlusion and opening (large artifact at 11s) of the flow probe for zero calibration. Mean ventilatory flow is re-established after the heart induced oscillation (100 Hz sampling, 51 point Bartlett smoothing).

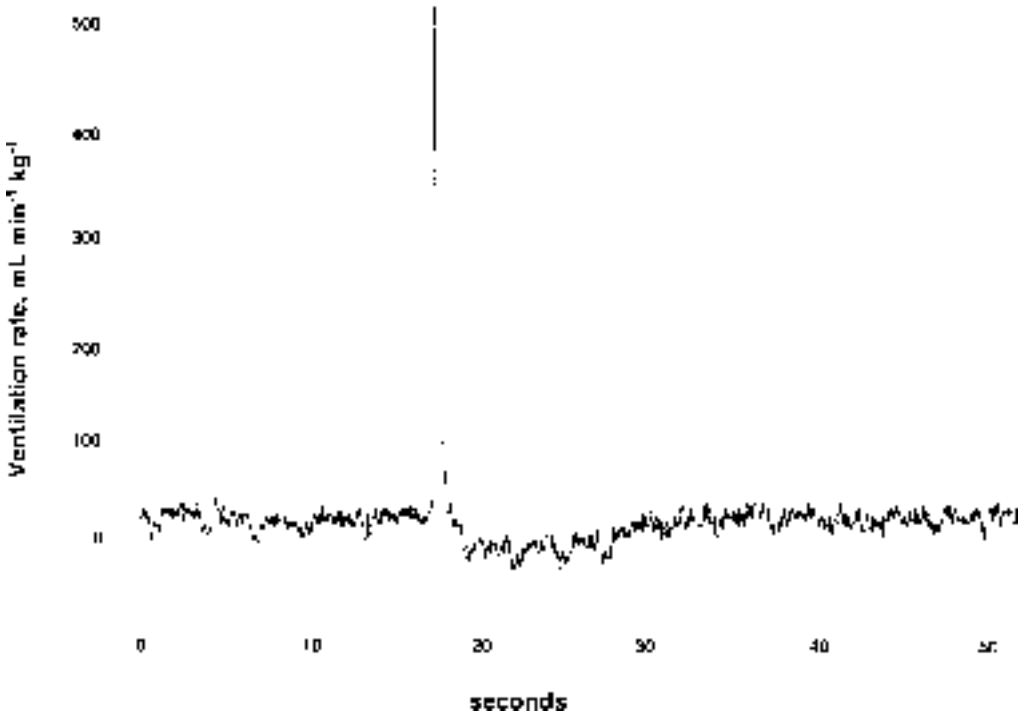


**Figure 4.18**: A single hypoxia-induced 'flinch' similar to those in Figure 4.16. The amplitude has been attenuated by smoothing (7-point Bartlett smoothing; 100 Hz sampling).

spikes in ventilation, 1 – 3 min apart, peaking at 300 to > 500 mL.min$^{-1}$ in about 200 ms (unsmoothed signal sampled at 100 Hz). This was followed by a slower decrease in flow below the mean ventilation rate (and sometimes reversal) lasting several seconds (Figures 4.16 and 4.18). These "flinches" were associated with a brief downward movement of the shell, presumably caused by transient contraction and subsequent relaxation of the right adductor muscle. The area under the forward phase was estimated as 2.23 ±1.13 mL (n = 6 animals, 4 – 11 spikes averaged). The area under the relaxation phase could not be estimated precisely but was similar suggesting the spike did not contribute to net unidirectional flow. Similar flinches were produced in settled animals in response to small vibrations or movements in the visual field. Less commonly, a series of bimodal ventilation peaks was associated with a twisting motion of the shell.

*Influence of external current velocity on whole animal $Mo_2$*

Blank oxygen uptake in the flume respirometer was 13.6 ±2.1 Torr.h$^{-1}$, and was similar after an experimental run. Resting animals consumed 0.35 ±0.13µmol.g$^{-1}$.h$^{-1}$ (n = 12) in the absence of directional flow ('zero' current). $Mo_2$ rose significantly to 0.98 ±0.15µmol.g$^{-1}$.h$^{-1}$ when the abalone were subjected to a current of 4.6cm.s$^{-1}$ (2-way nested ANOVA, using flow speed and pre- or post-emersion as treatments, individual was nested within flow speed; $F_{2,194}$ = 18.42, p < 0.001; figure 4.19). An additional 4-fold increase in current velocity caused $Mo_2$ to increase slightly to 1.11 ±0.16 µmol.g$^{-1}$.h$^{-1}$, which was not significantly different from oxygen consumption at 4.6 cm.s$^{-1}$ (p = 0.52, Fisher's Least Significant Difference pair-wise analysis). $Mo_2$ rates and the effect of current did not change significantly following 18h aerial exposure ($F_{1,194}$ = 1.59, p = 0.21; figure 4.19). It was noted, however, that the first $Mo_2$ value following re-immersion was conspicuously high (2.71

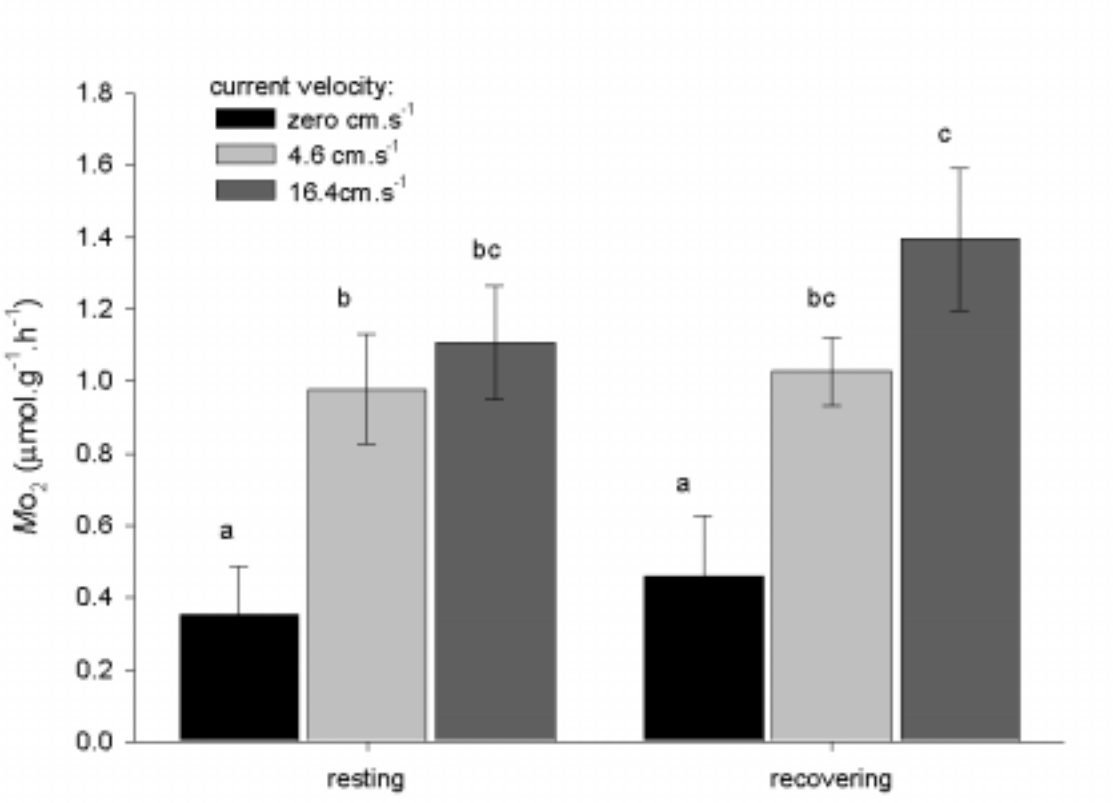


**Figure 4.19**: The effect of increasing current velocity on the $Mo_2$ of abalone at rest and following 18h of aerial exposure. In each group different letter codes represent specific significant differences ($p < 0.05$; Fisher's LSD).

±0.43µmol.g$^{-1}$.h$^{-1}$), irrespective of flow velocity. A re-analysis of the post-emersion $Mo_2$ data was therefore performed, including the replicate sequence as a variable. A nested 2-way ANOVA showed that the replicate number ($F_{2,76} = 10.7$, $p < 0.001$) and flow velocity ($F_{2,76} = 13.1$, $p < 0.001$) both had significant effects upon $Mo_2$. A Fisher LSD pair-wise comparison of sample order showed the first $Mo_2$ measurement of a flow treatment to be significantly higher than the subsequent 2 replicates ($p < 0.001$).

The abalone tended to be sedentary during this daytime experiment. Occasionally an animal rotated through 180° to face directly away from the current in the moving water treatments (4.6 and 16.4 cm.s$^{-1}$). A 5.15 ±0.56% weight loss was associated with 18h emersion.

# 4.4. Discussion

*Normoxic $Mo_2$*

The turbulent, closed-box respirometer appears to provide a reasonably standardised respiratory environment for adult *Haliotis iris*. In 3 separate experiments, different variation on the vortex-mixed respirometer were used to determine whole animal response to declining $Po_2$, isolate the relative contribution of the epipodium and foot to $Mo_2$ and measure $O_2$ uptake in the branchial chamber. These experiments generated consistent mean resting $Mo_2$ values of 0.47 ±0.04, 0.46 ±0.06 and 0.528 µmol $O_2$.g$^{-1}$.h$^{-1}$. Resting $Mo_2$ is generally lower than that measured in other abalone

| Species | $Mo_2$ (µmol.g$^{-1}$.h$^{-1}$) | conditions | Source |
|---|---|---|---|
| **adults:** | | | |
| *H. kamtschatkana* | 0.92 ±0.08 (SEM) | 10°C, resting, 40 – 99mm shell length | Donovan and Carefoot 1997 |
| *H. kamtschatkana* | ~0.4 | 10°C, recently disturbed, 100 – 150g live weight | Carefoot et al. 1993 |
| *H. iris* | 1.00 | 15°C, fitted 300g model to author's regression equations: log ($Mo_2$, mL.animal.h$^{-1}$) = 0.076 + 0.064(log dry flesh, g) | Bloomberg 1981 |
| *H. tuberculata* | 0.84 | 15°C, fitted 300g model to author's * regression equations: Ln($Mo_2$, µL.animal.h$^{-1}$) = 4.79 + 0.764(Ln dry flesh, g) | Peck et al. 1987 |
| *H. midae* | 0.15 | 14°C, fitted 300g model to author's regression equations: $Mo_2$ (µl.g$^{-1}$.h$^{-1}$)=0.03 (live weight, g)$^{0.83}$ | Barkai and Griffiths 1987 |
| **juveniles:** | | | |
| *H. laevigata* | 2.3 | 15.5°C, juveniles (mean weight = 4.48g) | Harris et al. 1998 |
| *H. tuberculata* | 2.8<br>13.6 | 20 - 22°C, juveniles (7-11g)<br>24 - 28°C, juveniles | McBride et al. 2001 |
| *H. fulgens* | 2.4<br>4.4 | 20 - 22°C, juveniles (7-11g)<br>24 - 28°C, juveniles | McBride et al. 2001 |
| *H. rubra* | 3.4 | 17°C, juveniles ~11g | Edwards et al. 2000 |
| **larvae:** | | | |
| *H. rufescens* | ~180 | 15°C, swimming veliger larvae | Shilling et al. 1996 |

* Used the log-linear relationship of Bloomberg (1981) relating dry flesh to live weight to standardise values to grams of total wet weight: log(dry flesh, g) = -1.08 + 1.11(log live weight, g)

**Table 4.1:** Oxygen consumption by different abalone species.

species (table 4.1), presumably due, at least in part, to the relatively large size of individuals used in the current experiments. Mass-specific oxygen uptake is expected to increase exponentially as size decreases (e.g. Barnes et al. 1988), hence smaller adult abalone have higher specific metabolic rates (reflected in $Mo_2$) than larger *H. iris* (typically 300 – 400g live weight) used here. This trend is increasingly apparent when the $Mo_2$ of juveniles and larvae are also examined (table 4.1). Scaling effects also tend to influence direct comparison of $Mo_2$ to those of other molluscs, which tend to be smaller than adult *H. iris*. Amongst the larger molluscs, $Mo_2$ values have been reported for resting *Nautilus* (0.59 – 1.23µmol $O_2.g^{-1}.h^{-1}$; Wells and Wells 1985) and for the conch *Busycon* (~0.7µmol $O_2.g^{-1}.h^{-1}$; Mangum and Polites 1980) that resemble those determined for *H. iris*.

*Oxyregulation*

$P_{crit}$ is defined as the threshold environmental $Po_2$ level below which an animal is forced to oxyconform, i.e. where uptake becomes entirely dependent upon environmental $Po_2$. The determination of $P_{crit}$ therefore requires some care, as demonstrated by the case of *Haliotis iris*. Figure 4.7 clearly shows that net $O_2$ uptake becomes compromised below 80 Torr, however individual animal data show that sporadic intervals of hyper-regulation are possible down to the 'true $P_{crit}$' of 45.2 ±4.7 Torr. A 3-phase $Mo_2$ response curve to environmental $Po_2$ was also seen in the prosobranchs *Busycon canaliculatum* and *Murex fulvescens* (Mangum and Polites 1980). In these gastropods $O_2$ uptake declined exponentially with environmental $Po_2$ down to 120 Torr and then showed strict oxyregulation down to $P_{crit}$ (40-50 Torr for *Busycon*, ~10 Torr for *Murex*), below which $Mo_2$ decline was linear with $Po_2$ (Mangum and Polites1980).

Many water breathing species are able to oxyregulate down to considerably lower $Po_2$ than *H. iris*. This is apparently achieved by strict maintenance of arterial $Po_2$ at low but constant levels. In animals with high affinity oxygen binding pigments, such as the crayfish *Astacus*, the teleost *Silurus glanis* and the haemoglobin carrying clam *Noetia ponderosa*, an arterial $Po_2$ of 7.5 Torr can be sufficient to saturate the protein and allow normal rates of gas exchange down to a $P_{crit}$ of 15 – 20 Torr (Massabuau et al. 1991). In the absence of binding pigment, such as in the large freshwater mussel *Anodonta cygnea*, arterial haemolymph can be maintained at stable, low $Po_2$ levels due to very low tissue $O_2$ demands, resulting in a $P_{crit}$ of 6.7 Torr (Massabuau et al. 1991). *Anodonta* seems unusual in this respect as molluscs lacking respiratory pigments tend to be pure oxyconformers (table 4.2), such as the lamellibranch *Modiolus* (Booth and Mangum 1978) or the prosobranch *Lunatia heros* (Mangum and Polites 1980), in both cases $Mo_2$ ceases below 10 – 15 Torr. In contrast *H. iris* possesses high affinity haemocyanin (Behrens et al. 2002), but keeps arterial $Po_2$ high in normoxic conditions (figure 4.12).

Table 4.2 compares experimentally-determined $P_{crit}$ in a range of molluscs. The general pattern seems to be one of considerable oxyregulatory capacity, reflected by a low $P_{crit}$. Exceptions are the bivalves without oxygen binding pigment in their haemolymph and the cephalopods, which typically cannot oxyregulate below about 70 Torr (Wells and Smith 1987), reflecting the high metabolic demands of their tissues and the invariably normoxic nature of their environment. Two other

| Species | $P_{crit}$ (Torr) | temp. (°C) | Source |
|---|---|---|---|
| **Prosobranchs:** | | | |
| *Lymnaea stagnalis (in air)* | ~7.5 | 15 | Massabuau et al. (1991) |
| *Austrolorbis glabratus* | <15 | 30 | Massabuau et al. (1991) |
| *Busycon canaliculatum* | 40-50 | 21-24 | Mangum and Polites (1980) |
| *Murex fulvescens* | ~10 | 22 | Mangum and Polites (1980) |
| *Lunatia heros* | N/A* | 22 | Mangum and Polites (1980) |
| **cephalopods:** | | | |
| *Nautilus pompilius* | 50 – 75 | 15-17 | Wells and Wells (1985) |
| **bivalves:** | | | |
| *Mytilus edulis* | 80–100 | 15 | Bayne (1971) |
| *Anodonta cygnea* | <7.5 | 13 | Massabuau et al. (1991) |
| *Pecten grandis* | ~15 | 20 | Massabuau et al. (1991) |
| *Modiolus demissus* | N/A* | 20-23 | Booth and Mangum (1978) |
| *Arctica islandica* | 40 - 50 | 10 | Taylor and Brand (1975a) |

*Pure oxyconformer

**Table 4.2**: Oxyregulatory capacity, quantified by $P_{crit}$, the lowest ambient $Po_2$ to which oxygen uptake regulation can occur, in a range of molluscs.

exceptions to the general rule of oxyregulation are the large prosobranchs *Busycon canaliculatum* (Mangum and Polites 1980) and *H. iris* (present study). The likely mechanisms of regulation and its limitations in the latter species are discussed below. When comparing performance amongst molluscs, it is important to consider two sources of intra-specific (even intra-individual) variability in oxyregulatory capacity have been identified in bivalves. The first shows that the degree of respiratory independence increases (i.e. $P_{crit}$ decreases) with increased size in *Arctica islandica* (Taylor and Brand 1975a). The second is a demonstration of the importance of nutritional stress in the mussel Mytilus edulis; unstressed *Mytilus* oxyregulate down to 80 – 100 Torr, whereas starved individuals show pure oxyconformity (Bayne 1971).

*Heart rate response to declining $Po_2$*

DeFur and Mangum (1979) showed that a range of invertebrate taxa (bivalve and gastropod molluscs, decapod crustaceans, xiphosurans and annelids) all tended to respond to increasing levels of hypoxia with progressive bradycardia. The conch *Busycon* showed imperfect heart rate regulation in response to declining $Po_2$, with no specific $P_{crit}$ (DeFur and Mangum 1979) while the abalone *H. ruber* maintained its heart frequency down to 80 - 100 Torr, below which it decreased steadily (Russell and Evans 1989). *H. iris* showed no such regulation, heart rate declining as $Po_2$ fell below the normoxic range. In contrast the cardiac frequency of the bivalves *Mytilus edulis* and *Arctica islandica* slowly increased as $Po_2$ fell, down to 40 – 60 Torr (Bayne 1971, Taylor and Brand 1975b), implicating increased haemolymph convection as a means of assisting oxyregulation. Differences in cardiac frequency response seem to disappear under severe hypoxia, as the heart rate of bivalves (Bayne 1971) and abalone (present study and Russell and Evans 1989) was seen to become erratic and sporadically arrest below 20 Torr. The invertebrate heart is not intolerant to hypoxia, however, as demonstrated here in *H. iris* and in the range of species examined by DeFur and Mangum (1979), where a heartbeat was maintained even after prolonged exposure to anoxia.

*Role of secondary gas exchange surfaces:*
*- The foot and epipodium*

The extensive, well-perfused epidermis of most molluscs seems well adapted to oxygen diffusion. It is therefore not entirely surprising that the molluscan gills often only contribute a fraction of the animal's $O_2$ requirements. In some gastropods and monoplacophorans the nephridium, rather than the gill, may be the main organ of gas exchange (Lindberg and Ponder 1996). Similarly the plicate canals of the bivalve excretory organs are also implicated in gas exchange in many species (Lindberg and Ponder 1996). Famme (1981) found the gills of *Mytilus edulis* had no specialised respiratory function, $O_2$ being taken up by all body surfaces. Similarly Depledge and Phillips (1986) estimated 30 – 50% of total $M_{O_2}$ of the large gastropods *Hemifusus* and *Busycon* was taken up directly into tissues rather than into the haemolymph. In contrast, Mangum and Polites (1980) estimate that only 15-20% of oxygen taken up by *Busycon* occurs outside of the ventilatory current, probably at the extremities of the foot. A similar value (13%) has been propose for direct cutaneous $O_2$ uptake by *Octopus vulgaris* (Wells 1992). Direct measurement in the present study has shown a similar situation to prevail in *H. iris*. Measurement of oxygen uptake from the ventilatory water, compared to whole animal $M_{O_2}$ showed that virtually all uptake occurred within the branchial chamber, regardless of $P_{O_2}$. In corroboration of these results and the observations of Mangum and Polites (1980), isolation of the foot and epipodium in resting *H. iris* showed these regions accounted for 13.9% of total $M_{O_2}$ in normoxia. Below 30 Torr the epipodium was extended maximally, but failed to take up any $O_2$ from the hypoxic environment (negative foot/epipodium $M_{O_2}$ are attributed to small errors incurred when using a mean blank $O_2$ uptake correction value). Analogous observations have been made in mussels, which tend to close their valves at low environmental $P_{O_2}$, but may subsequently gape and extend the mantle as if ventilating, however no oxygen uptake is associated with this extrusion (Booth and Mangum 1978). It has been suggested that the direct effects of hypoxia upon the central nervous system lead to a cessation of swimming in fish, rather than fatigue *per se* (Jones and Randall 1978). Similarly the extension of the epipodium in hypoxic conditions may be an indication of depressed motor neuron function and subsequent loss of muscle tone.

Thus, the function of hypoxic epipodal expansion remains unknown. Since the epipodal margin is a sensory structure, and hypoxic external seawater an unusual occurrence, an exploratory function may be hypothesised. It is also possible that the extension of the epipodium at low $P_{O_2}$ alters the geometry and hydrodynamics of ciliary ventilation of the branchial chamber, augmenting gas exchange at the cost of exposing soft tissues. Such a mechanism would be analogous to the geometric changes in the tracheal system of insects, especially the spiracles, in response to increasing hypoxia/ hypercapnia (e.g. Wells 1980).

The effects of ambient temperature were not considered in the present study, but may also represent an important determinant in the respiratory role of other body surfaces. This was observed by Mangum (1979) who noted the foot of *Busycon* changed from a target organ to a site of oxygen uptake as temperate declined from 22 - 10°C. Inter-specific differences should also be considered. Abalone species associated with more sheltered areas tend to possess thicker, more complex epipodia

(Tissot 1992), which may present an increased surface area for diffusion. A comparative study of the respiratory role of the epipodium amongst haliotids would therefore be of considerable interest, particularly if it included the reduced-shell *H. asinina*.

- *Haemolymph $Po_2$ gradients across the mantle*

The mantle is regarded as a major site of oxygen uptake in many molluscs, for example the lamellibranch *Modiolus demissus* (Booth and Mangum 1978) and the large prosobranch *Busycon* (Mangum and Polites 1980). Although total oxygen uptake by the mantle of *H. iris* could not be determined, the fact that $Po_2$ is higher in the haemolymph entering the region via the circum-pallial vessel than that leaving in the pallial vein (figure 4.12) conflicts with a proposed role as a gas exchange organ. Haemolymph $Po_2$ measurements corroborate morphological observations made in chapter 3, where the bulk of the mantle lacunae were shown to supply the nacre secreting dorsal surface, rather than the ventral surface contacting the water.

*Ventilation and $O_2$ extraction efficiency*

A water breather relying on its gills to meet its oxygen uptake requirements in declining $Po_2$ must either increase its ventilation rate and/or its $O_2$ extraction efficiency if it is to maintain a constant uptake rate. *H. iris* maintain a constant $Mo_2$ down to 80 – 100 Torr and then oxyregulate imperfectly down to 45 Torr. Ventilation in *H. iris* was unaffected by environmental hypoxia or subsequent oxygen debt in the abalone (figure 4.14), remaining between 85 and 95 $mL.kg^{-1}.min^{-1}$ unless compromised by virtual anoxia. When ventilation rate was artificially regulated the oxygen extraction efficiency was found to be highly labile, increasing from 49% extraction under typical resting ventilatory rates of 28 $mL.min^{-1}$ to 71% at 7.5 $mL.min^{-1}$. Although the impairment of exhalant flow creates an artificial situation (discussed below), the evidence points towards oxyregulation by increased uptake efficiency. If the physical nature of the diffusing barrier (the gill epithelium and associated mucus and boundary layer) is assumed to remain constant, increased extraction efficiency results from increased haemolymph perfusion rate of the lamellae or the recruitment of additional lamellae. During increased $O_2$ demand in normoxia both of these processes occur as a result of increased cardiac output due entirely to elevated stroke volume (see chapter 6). Although heart rate declines with $Po_2$ (figure 4.14), stroke volume may also be increased to account for the increased extraction efficiency.

The mussel *Mytilus edulis* shows a similar oxyregulatory response to *H. iris*, increasing extraction efficiency from 5 – 10% in normoxia to 30 – 40% at its $P_{crit}$ of 80 – 100 Torr (Bayne 1971). In contrast, another bivalve, *Arctica islandica*, maintains a constant extraction efficiency but increases its ventilatory rate considerably as $Po_2$ declines (Taylor and Brand 1975b). Most cephalopods have a similar strategy, typically oxyregulating down to about 70 Torr by increasing the depth and rate of mantle ventilation, rather than adjusting blood flow (Wells and Smith 1987).

*Endogenous ventilation and pulse*

In the absence of external water currents, *Haliotis iris* generates ventilatory flow adequate to support normal aerobic metabolism. A sizeable oscillation was detected in the endogenous ventilatory flow, synchronized with the cardiac pulse (figure 4.15). Apparent coupling between ventilation and heartbeat was also seen in *H. corrugata* and *H. kamtschatkana*, where ventilatory flow was pulsatile and 180° out of phase with the aortic pressure pulse, closely resembling the efferent ctenidial pressure pulse (Bourne et al. 1990). The mean ventilatory rate of a 400g *H. corrugata* was 42.5 $mL.min^{-1}$, the pulsatile component representing 51% of the flow (Bourne et al. 1990). It is tempting to suggest that cardiac interaction drives or assists unidirectional ventilation. However, differences in the rates of change of ventilation and heart rate during progressive environmental hypoxia and recovery in *H. iris* do not support this interpretation. Cardiac frequency fell steadily down to about $Po_2$ 25 Torr, and then more steeply. In contrast, ventilatory flow was maintained (and increased in most animals) down to 15 Torr. On re-aeration, endogenous ventilation was restored within seconds, whereas hypoxic bradycardia persisted for a further 10 -20 minutes into normoxia. This implies that ventilation changes in response to external oxygen levels, whereas heart rate reflects internal hypoxia. Further evidence for the lack of coupling between ventilation and the heart is that the amplitude of the ventilatory oscillation was attenuated below about 30 Torr while ventilatory flow and the amplitude of the impedance signal were still unaffected. The restoration of the ventilatory oscillation before net flow, following occlusion of the mask, also suggests that the two processes are independent.

Bourne et al. (1990) suggest that part of the pericardium or aorta might cyclically impinge upon the branchial water space, causing the observed ventilatory pulsatility. A plausible alternative interpretation is that the cardiac cycle is superimposed directly upon the unidirectional ventilatory flow driven by the lateral cilia of the gill lamellae. The gill lamellae of *H. iris* possess an articulating joint on the efferent margin (figure 3.52) that accommodates flexion in the wing-shaped lamellae (see section 3.3.6). In abalone preparations described in chapters 6 and 7 the shell region overlying the gills was removed. Direct observation of the gills revealed a rhythmic expansion, resulting in a transient raising of the lamella tips due to the action of the articulation point. The oscillations occurred with a periodicity resembling that of the cardiac cycle. It is therefore suggested that transient haemolymph pressure oscillations alter the lamella geometry as a direct result of ventricular movement. As the lateral cilia of the lamellae drive ventilation (Yonge 1947, Fretter and Graham 1994, Voltzow 1994), it seems likely that this localised movement of the ventilatory motor causes the observed pulsatility in water flow. Whether the flow oscillation has a respiratory function deserves further investigation. Oscillatory flow could reduce ventilatory dead spaces but the observation of oxygen extraction efficiencies exceeding 70%, at very low $Po_2$, where the flow pulse was attenuated, indicates that it is not a prerequisite. Furthermore, rapid fluctuations in the ctenidial flow might disadvantageously disrupt viscous coupling between cilia and water. Thus, it is possible that the oscillation occurs only downstream of, or parallel to, the ctenidial route.

The reduction of the cardiac pulse of ventilation at low $Po_2$ was repeatable but its basis is unknown. It seems that a change in the geometry of the branchial compartment made it less susceptible

to cardiac influence. This was possibly associated with the changes in the epipodium position observed at low $Po_2$. Under the increased metabolic load imposed by stress, *H. iris* can increase the rate of gill perfusion 3-fold (chapter 6 of this thesis). If similar haemodynamic responses occur in response to hypoxia it may be that increased turgor then keeps the lamellae in their fully extended position, preventing the 'flapping' apparently associated with pulsatile ventilation in normoxia.

*Artificial ventilation*

Both split-box and artificial ventilation respirometry have demonstrated that the epipodium and foot are unimportant as accessory gas exchangers. Branchial oxygen uptake completely accounted for whole body $Mo_2$ (figure 4.11). Paradoxically, when ventilation was reduced below the endogenous rate, branchial oxygen consumption decreased sharply below total $Mo_2$, apparently implicating another gas exchange site. This result, based on exhalant water sampled from the mask, can be reconciled if it is assumed that limiting flow through the tremata did not reduce ciliary ventilation of the ctenidia, which was redirected via an alternative exhalant route. It is important to further investigate this possibility. In some natural populations of *H. iris*, partially or completely occluded tremata are common (figure 3.2b). "Stacking" behaviour in the field and in commercial holding situations also results in extended periods of occlusion of the tremata (unpublished observation). The ability to maintain gas exchange in such situations clearly has survival value and would be pre-adaptive to loss of shell holes and slits in the higher gastropods.

*Influence of externally-assisted ventilation on oxygen uptake*

Artificially ventilated abalone were essentially oxyconformers whereas non-ventilated animals exhibited a plateau in oxygen consumption down to about 80 Torr (cf. figures 4.10 and 4.7). The reason for this difference is unclear. Partly this may relate to the wide variations in oxygen uptake observed in the latter group, which, in turn, may reflect spontaneous variations in ventilation associated with movements, or occasional clamping. Although decreases in artificial ventilation rate produced relatively small decreases in oxygen uptake, occasional observations on clamped animals indicated complete cessation of oxygen uptake. Such episodes would depress the average uptake as oxygen debts in abalone appear to be repaid extremely slowly over several days (Wells and Baldwin 1995). Thus the plateau should probably be considered a region of constraint on gas exchange rather than a regulation. In this respect, it is noteworthy that over the ranges of artificial ventilation (6.5 – 250 mL $kg^{-1}$ $min^{-1}$), and external water flow (4.6 – 16.4 cm $s^{-1}$), that were available in the laboratory, settled oxygen uptake did not appear to reach a plateau. Although, to some extent, these changes in oxygen uptake may be associated with adjustments to the size of the venous reserve, this is unlikely to be a complete explanation.

The flume respirometer used here to examine the effects of water current on $Mo_2$ did not permit measurement of $Mo_2$ at the fastest current velocities encountered by the abalone at an exposed site (>70cm.$s^{-1}$, Tissot 1992). Within the range of velocities that were available, increasing the current from zero to a modest 4.6cm.$s^{-1}$ caused $Mo_2$ to triple, while a subsequent 4-fold increase in

flow had no further significant effect (figure 4.19). These data are consistent with the findings of Tissot (1992) who describes approximately 2-fold increases in the velocity of ventilatory water in *H. kamtschatkana* and *H. rufescens* as a result of increased external flow from 0 to 10 $cm.s^{-1}$. Similarly, Murdock and Vogel (1978) found even a small $5cm.s^{-1}$ water current induced many times the still-water ventilation rate in a keyhole limpet. Even the gentle turbulence associated with water mixing in the cylindrical respirometers augmented mean $M_{O_2}$ from 0.35 $\mu mol.g^{-1}.h^{-1}$ (zero flow in flume) to 0.47 $\mu mol.g^{-1}.h^{-1}$ ($P_{crit}$ and 2-chamber respirometers). It therefore appears that some water movement greatly facilitates gas exchange, but the dynamic effects of faster flow impart only minimal further advantage. This observation would be expected from an endogenous ventilatory mechanism that is adequate to support normoxic $M_{O_2}$ but benefits from the removal of exhalant water from the vicinity of the branchial chamber.

Prolonged aerial exposure has been shown to induce environmental hypoxia in abalone (Baldwin et al. 1992, Wells and Baldwin 1995). $M_{O_2}$ would therefore be expected to increase on subsequent re-immersion until the oxygen debt is repaid. No such increase was detected using the mean $M_{O_2}$ data presented in figure 4.19. There are 3 possible explanations for the unchanged $M_{O_2}$:

1. Emersion failed to induce a state of hypoxia sufficiently severe to cause an oxygen debt.

2. $M_{O_2}$ increase was chronic but sufficiently small to avoid detection.

3. $O_2$ debt repayment occurred extremely quickly, information that was subsequently lost over the 1.5 – 2h sample averaging.

4. Ventilation and current flow limited $M_{O_2}$ in both the pre- and post-emersion treatments.

(To address suggestions 1 & 2): In previous experiments using air exposure to induce anaerobic stress *H. iris* were emersed for between 24h (at 20 - 22°C; Wells and Baldwin 1995) and 36h (Baldwin et al. 1992). The 18h emersion at 15°C use in the current study is therefore expected to induce a smaller oxygen debt. Wells and Baldwin (1995) note that adult *H. iris* repay their $O_2$ debt very slowly (many days) and also found strong negative correlations between animal size and the quantity of anaerobic end products (tauropine and D-lactate) accumulated. After 24h emersion at 20 - 22°C, *H. iris* of the size used in the present experiment showed low concentrations of either product (Wells and Baldwin 1995). Their results imply that larger *H. iris* have a greater tolerance to aerial exposure, only incurring a minor oxygen debt, that may avoid detection as increased $M_{O_2}$.

(To address suggestions 3 & 4): The fact that the mean of the first $M_{O_2}$ measurement following re-immersion was more than twice as high as any mean determined over the entire 1.5h monitoring period lends weight to the suggestion of rapid repayment. It is therefore suggested that most $M_{O_2}$ up-regulation occurs due to rapid reloading of haemocyanin, and perhaps tissue ATP and arginine phosphate, during the first 10 min of immersion. Mangum and Polites (1980) also noted that the haemocyanin-bearing gastropods *Busycon* and *Murex* exposed to repeated hypoxia showed no subsequent increase in $M_{O_2}$. It seems likely that these authors may also have overlooked an extremely acute $M_{O_2}$ response. The adaptive advantages of rapid re-establishment of a depleted venous $O_2$

reserve would be considerable. The initial rapid $Mo_2$ is independent of external current velocity, implying there is no intrinsic limitation of uptake due to flow. Furthermore, in chapter 6 the uptake of $O_2$ into the gill haemolymph in 'zero flow' is seen to increase nearly 3-fold in response to severe physical stress; the abalone therefore possesses a reasonable capacity to increase $Mo_2$ in the absence of externally-assisted ventilation.

Generalizations concerning the importance of external flow for *H. iris* can not easily be made. The extent to which external flow influences branchial chamber ventilation is largely governed by the sculpturing of the tremata (Tissot 1992). Healthy, relatively unfouled *H. iris* have naturally raised tremata (e.g. figure 3.2). However, calcarious build-up due to encrusting organisms or the characteristic grinding behaviour exhibited by *H. iris* to dislodge organisms overgrowing the shell holes (personal observation) commonly result in tremata openings that lie flush to the outer shell surface. Ventilation in abalone with raised tremata is greatly influenced by gentle water currents (5 – 15 $cm.s^{-1}$), but faster currents have little further affect (Tissot 1992). Conversely, ventilatory currents in abalone with smooth shells are not apparently influenced until external flow exceeds $20cm.s^{-1}$ (Tissot 1992). Sensitivity to flow in individual *H. iris* may therefore be determined by epibiont fouling rather than direct adaptation.

The hypothesis that the endogenous ventilatory mechanisms of the abalone gills are inadequate to sustain $Mo_2$ appears incorrect. Reasonable ventilatory rates are provided by the action of the lateral lamellar cilia which, coupled with a modest water movement to remove effluent seemingly supports maximal normoxic $Mo_2$. The ventilatory system may therefore be adapted to tolerate, rather than exploit the rapid water currents of the high energy environments inhabited by *H. iris*. Fish experiencing head-on currents above 50 – $80cm.s^{-1}$ cease active ventilatory pumping and ram ventilate, controlled by adjusting the gape (Jones and Randall 1978). Although the transition effectively transfers burden from the ventilatory muscles to the more efficient locomotory muscles, there is little obvious improvement in respiratory efficiency and it is suggested the transition primarily imparts a hydrodynamic advantage during fast swimming (Jones and Randall 1978, Vogel 1994). The energy saving associated with using externally derived rather than endogenous ventilation in the keyhole limpet *Diadora aspera* was also considered to be minimal (Murdock and Vogel 1978). Murdock and Vogel (1978) and Tissot (1992) therefore suggest the advantages of externally-induced water flow in keyhole limpets and abalone may be an indirect reduction in the cost of ventilation. For example, by lowering the amount of $O_2$ that must be extracted per unit ventilation volume and thereby reducing the perfusion required at the gas exchange surfaces. Ingestion rate in juvenile *H. laevigata* increased linearly with current velocity over an experimental range of 0 – $12cm.s^{-1}$ (Fleming et al. 1997), which may reflect increased olfactory awareness (Murdock and Vogel 1978), increasing phagostimulation by moving food particles (Allen et al. 2001) or increased exploratory activity permitted by higher $Mo_2$ (this study).

Abalone respiratory strategies could also impart a hydrodynamic advantage as unidirectional ventilation entering above the head and exiting through the dorsal shell holes could serve to reduce

drag and lift. Sessile benthic organisms in high energy areas are confronted by the risk of dislodgment, particularly if, as with many abalone populations, they are presented with rapidly accelerating water currents due to wave action (Vogel 1994). The major dislodgment risk is associated with lift (Vogel 1994) which can be effectively reduced by the presence of holes in the dorsal surface, a strategy that has been elegantly employed by the sand dollars (Telford 1983, Telford and Mooi 1987). Excessive flow may also be detrimental to the delicate gills. Both *H. kamtschatkana* (Voltzow 1983) and *Diadora* (Murdock and Vogel 1978) are able to control flow rates by hole occlusion using mantle tentacles or a siphon, respectively. *Haliotis iris* lacks such refinements, and may therefore risk gill damage if it adopts the typical limpet strategy (e.g. Warburton 1976) of facing into strong currents. *H. iris* must reduce flow induction by avoidance or orientation, facing away from a very rapid current and raising the posterior shell, creating a turbulent, generally higher pressure region above the shell holes (personal observation).

# 4.5. Conclusions

*Haliotis iris* are almost entirely dependent upon gas exchange at the gills, and subsequent haemolymph convenction to support all their respiring tissues. Lateral cilia on the gills provide adequate ventilation to support resting $M_{O_2}$ in still water, but seem unable to adjust the ventilation rate in response to increased demand or reduced $O_2$ availability. This suggests that abalone are adapted to a high $P_{O_2}$ environment and tolerate exposure to low $P_{O_2}$ by relying on a large venous $O_2$ reserve bound to haemocyanin (Wells et al. 1998) and their well-documented anaerobic capacity (e.g. Gäde 1988, Baldwin et al. 1992). Oxyregulation in large prosobranchs may involve metabolic compensation by the tissues, as well as a reliance upon the properties of the haemolymph. For example, while the presence of haemocyanin is implicated in oxyregulation of the conch *Busycon*, Mangum and Polites (1980) also found strong regulatory ability in isolated muscle tissue. The energy requirements of abalone muscle tissue are considered low compared to other molluscs (Gäde 1988), perhaps increasing tolerance to transient hypoxia. This suggestion warrants further investigation. It is concluded that, although, *H. iris* has physiological adaptations that readily cope with short term constraints on ventilation, optimal respiratory function and metabolic health probably benefit from the high water flows found in the sub-littoral surge zone.

# Chapter 5

# Oxygen uptake, diffusion limitation and capacitance of the bipectinate gills of the abalone, *Haliotis iris* (Prosobranchia: Archaeogastropoda)

## 5.1. Introduction

Abalone, that collectively comprise the genus *Haliotis* and the family Haliotidae (Gastropoda: Prosobranchia), are generally regarded as primitive gastropods. This categorisation is based upon the morphological arrangement of extant species, and upon the evolutionary stability of the family over geological time. For example, well preserved fossilized shells dated at 66Ma have been assigned to the extant subgenus *Paua* (Lindberg 1992), the only living member of this group being *Haliotis iris*. The Blackfoot abalone of New Zealand, *Haliotis iris* Martyn 1784, displays a body plan characteristic of the family, including paired organs and perforations (tremata) in the shell. Although the organs of Haliotids show a left-side bias associated with the development of a spiral shell, the arrangement is otherwise reminiscent of the bilateral symmetry and notched shell of the hypothetical ancestral gastropods (Russell and Evans 1989, Voltzow 1994).

A conspicuous feature of prosobranch evolution has been the tendency to abandon paired gills in favour of many other arrangements. Initially, the evolutionary trend appears to be a conservative tendency towards gill reduction (Purchon 1977, Fretter and Graham 1994). More specialised archaeogastropods (Trochoidea and Seguenzioidea) rely on a single bipectinate gill, while higher orders (Mesogastropoda, Neogastropoda) retain 'half', in the form of a monopectinate (pectinibranch) gill. The picture is confounded, however, by many ecologically successful gastropod groups that have either abandoned gills altogether, relying on cutaneous gas exchange, or have evolved secondary gills from other body surfaces (Voltzow 1994). In abalone the left gill is slightly larger than the right, however this asymmetry is attributed to hypertrophy of the right shell muscle rather than the evolutionary reduction of the right gill (Yonge 1947). The general morphology and current taxonomic status of abalone corroborates Yonge's statement that "the primitive molluscan ctenidium was probably essentially similar to that of a modern asymmetrical Zeugobranch, e.g. *Haliotis*".

The paired bipectinate gill arrangement is usually associated with secondary shell apertures. Ancestrally the aperture takes the form of a slot in extinct forms and some rare extant species, including *Scissurella* and *Pleurotomaria*, usually restricted to deep water (Barnes 1986). In the abalone and the keyhole limpets the slit has been partially occluded, forming one or more tremata. Distribution of these animals is usually restricted to rocky sub-littoral coastlines, where they experience strong water movements and high levels of dissolved oxygen (Barnes 1986). A convex object, such as a shell, that protrudes from the substratum into a moving water current will experience reduced pressure across its dorsal surface. If that surface is perforated, water will, in turn, be drawn through the aperture in accordance with Bernoulli's Principle (e.g. Vogel 1994). Dogma suggests that this externally induced water flow may therefore be required for the adequate ventilation of the bipectinate gills (Murdock and Vogel 1978, Voltzow 1983).

In the abalone a picture is therefore developed of an animal possessing an archaic gill design that requires external assistance to ventilate adequately, despite inhabiting a high $Po_2$ environment. The fact that abalone are inherently sluggish and have a well-documented facultative anaerobic capacity (e.g. Gäde 1988, Baldwin et al. 1992) seems to corroborate this view. The present study was designed to specifically examine the efficiency of the abalone gill as a gas exchanger and consider the broader implication that fundamental shortcomings in the bipectinate design may have been instrumental in the evolutionary radiation in modern prosobranch gas exchangers.

*Experimental approach*

After first confirming the inhalant and exhalant ventilatory routes, and the afferent and efferent haemolymph supplies to the ctenidia (gills), the quantities of water and haemolymph flowing past the gills, and the partial pressures and quantities of oxygen carried were measured. The quantity of oxygen extracted from ventilatory water, and the corresponding amount of oxygen added to the haemolymph were subsequently determined. The results allowed standard physiological indices to be applied to assess the overall efficiency of the gas exchange system, and the extent to which diffusion, perfusion and ventilation limit oxygen uptake across the lamellae. These indices also allowed comparisons to be made with those published for other gas exchangers. The models were originally developed to describe gas exchange in higher vertebrates and have subsequently been adapted for application to the counter-current gills of fish (Piiper 1982, Scheid 1982, Piiper and Scheid 1984, Randall and Daxboeck 1984). The validity of the application of these models to abalone is discussed.

# 5.2. Methods

*Source of animals*

Adult *Haliotis iris* (250 – 580g) were collected by SCUBA from South Bay, Kaikoura, New Zealand and transported in moist air at 6°C to holding facilities at the University of Canterbury, Christchurch. Animals were acclimated to a recirculating seawater system for at least 2 months prior to experimentation to minimise the variability attributable to exogenous environmental factors. A


**Figure 5.1**: Location of shell holes cut to expose the right efferent ctenidial vein (A) and the left afferent ctenidial vein (B), giving access to the basibranchial sinus. The impedance coupler leads are shown coiled around a cork for storage. The arrowhead indicates the position of the right efferent cannula.

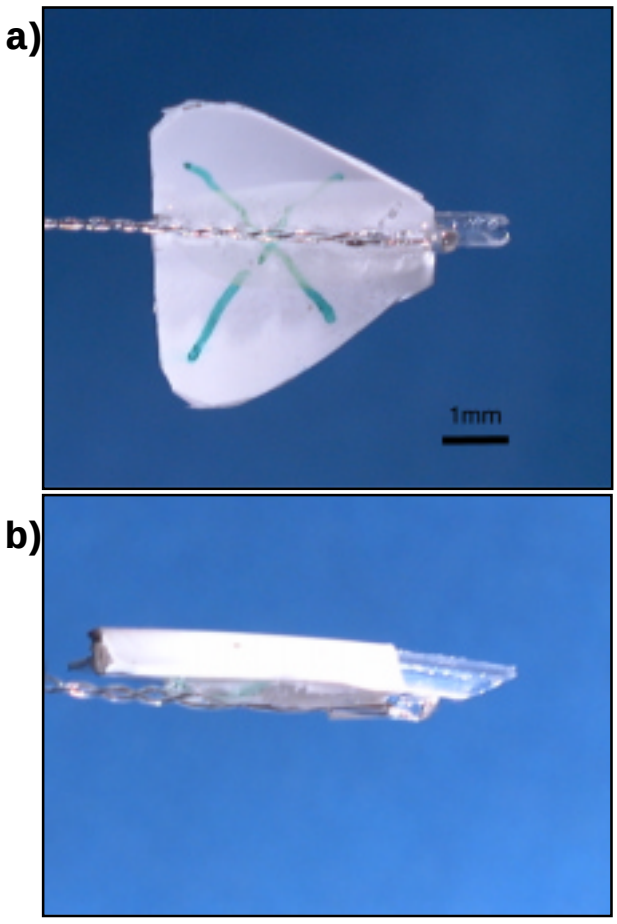


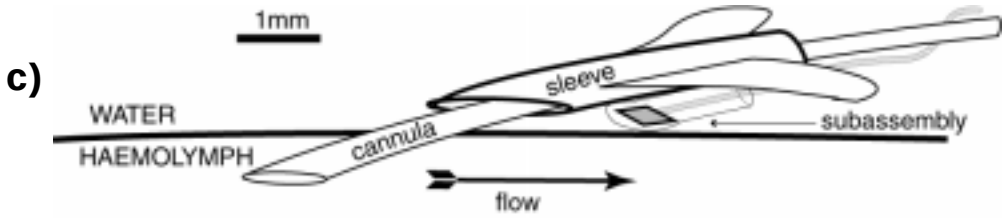


**Figure 5.2**: Retrograde cannula with customised pulsed-Doppler probe in position. The probe consists of a sub-assembly sealed in epoxy resin and mounted beneath a 0.86mmØ polyethylene sleeve. The 0.8mmOD cannula is threaded through the sleeve prior to insertion into the vessel; the assembly is subsequently held in position on the tissue surface by the cannula, PVC wings prevent rolling and tension in the Doppler leads keeps the sleeve at the cannula insertion point. **a)** Ventral view of sub-assembly attached to cannula sleeve, with wings to prevent roll. **b)** Lateral view of sub-assembly crystal beneath supporting sleeve. **c)** Schematic representation of Doppler probe located on venous cannula.

heat-exchanger maintained 15.0 ±0.5°C, tank covers and 10% water exchange per day kept salinity at 33 ±1‰ and, with biofiltration, ammonia at <0.1 mg $L^{-1}$ and pH8 – 8.2; water jets maintained currents of 5 – 15cm.$s^{-1}$ in the tanks. Abalone were weaned onto the Adam & Amos™ AAFD artificial diet using the techniques of Allen et al. (2001).

*Experimental Treatments*

Three ventilatory states were examined. To allow cannulation of the afferent ctenidial vein a section of shell overlying the gills had to be removed, as described above. To address the concern that this unnatural arrangement might influence the branchial environment, this shell section was replaced in an initial subset of animals and haemolymph-water $Po_2$ gradients compared between the 'window on' and 'window off' states. The presence of the shell section was found to have no significant effect upon the gill environment; the exposed gill preparation (as in figure 5.1) was therefore considered representative of the natural state. The third ventilatory state, using an exhalant mask to control water flow, was subsequently examined, as described below.

Animal Preparation

Abalone were starved for 24h prior to handling and all surgical manipulations took place in moist air at 4 - 6ºC. A diamond grinding wheel fitted to a Dremel™ flexible-shaft power drill was used to open two shell windows, exposing the central region of the gills and the right efferent ctenidial vein (figure 5.1). Two holes were also drilled either side of the heart using a 1.5mm dental burr and the stripped end of a 1m length of 0.202mm insulated copper wire was cemented into each hole with cyanoacrylate glue (these leads were later connected to the impedance coupler). The animal was allowed to recover for 24h in the holding system. The right efferent ctenidial vein was then cannulated, using a 23gauge needle to puncture the vessel 20mm anterior to the heart and 10mm of retrograde cannula (0.8mm external diameter) were inserted. Afferent haemolymph was sampled from the basibranchial sinus region, the common sinus supplying both gills (Crofts 1929). An anterior puncture was made in the left afferent ctenidial vein and a cannula (0.6mm external diameter) fed in until the tip approached the vessel's origin at the basibranchial sinus.

A pulsed-Doppler probe was used to quantify haemolymph flow through the right gill. A variety of probe arrangements and locations were examined; the most reliable is described here. Probes were constructed by attaching a Doppler crystal sub-assembly (Iowa Doppler Products) to a short length of 0.86mm internal diameter PE tubing (figure 5.2a and b). The assembly was threaded onto the right efferent ctenidial vein cannula, coming to rest at the point of emergence, with the Doppler crystal resting on the thin mantle tissue overlying the vein (figure 5.2c). All leads and cannulae were secured to the shell with cyanoacrylate glue; the animal was then placed in an experimental chamber (figure 5.3). The chambers were designed to allow ready access to the animal without causing disturbance; each consisted of a 150mm-diameter polycarbonate bowl containing 1 L of seawater in constant recirculation between an aerated 6 L reservoir and 15ºC heat exchanger. Makeup water was added from the holding system at a rate of 4 L.$h^{-1}$. In the abalone container, in-flowing water caused a gentle clockwise circulation (2 - 3cm $s^{-1}$) to prevent the formation of unstirred areas in the chamber.

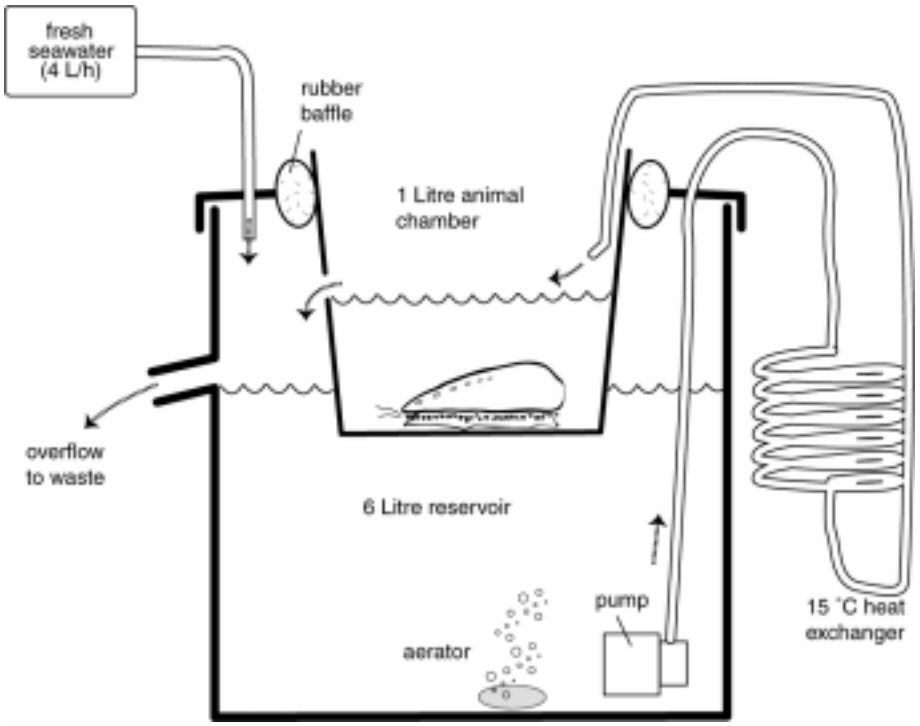


**Figure 5.3**: Laboratory holding system for abalone. Fresh seawater is supplied at a rate of 4 $L.h^{-1}$ to an aerated 6 L reservoir in constant circulation with a 15°C heat exchanger and the 1 L abalone chamber.

Following 24h recovery the cannulae were tested for patency and the impedance leads were connected to an impedance coupler (Strathkelvin Instruments A100) to record heart rate. The Doppler probe was connected to a directional pulsed-Doppler flowmeter (Bioengineering 545C-4) and the range systematically adjusted in 0.5mm (50mV) increments to locate the depth of fastest flow (largest signal). Careful orientation of the Doppler crystal in relation to the vessel proved critical. Course positioning was achieved during initial cannulation, while subsequent fine-tuning of the probe's horizontal position and perpendicular orientation could be performed by tweaking the probe leads. Data from the impedance coupler and pulsed-Doppler meter were acquired using a PowerLab 4/20 and Chart 4.1.2 software (ADInstruments).

*Sampling procedure*

Four fluids were sampled at each measuring time: the 'inhalant' and 'exhalant' seawater as well as the afferent and efferent haemolymph. While simultaneous samples would have been desirable, logistical limitations meant a delay of approximately 10min was incurred between the first and last sample of each cycle; sample order was therefore randomised. Glass 100µL syringes (Hamilton Gastight™) were used for all samples, and samples not used immediately were stored on ice for a maximum of 2min. The pH and $Po_2$ of all samples were determined using an $O_2$ electrode (Microelectrodes Inc. MI-730) connected to an $O_2$ meter (Strathkelvin Instruments 781.b) and a pH electrode (MI-710) connected to a pH meter (Radiometer PHM84) held in series in a 15°C microelectrode chamber (Cameron Instruments). Haemolymph was sampled by slow withdrawal (~50µL $min^{-1}$); 100µL were removed to clear dead-space, and condition the electrodes. A second

100µL withdrawal was used to determine $Po_2$ and pH; the sample was then centrifuged at 9,000*g* for 3min to remove cells and frozen at -18°C for later haemocyanin analysis. A final 100µL of haemolymph was used to determine total oxygen content, as described below.

The $Po_2$ and pH of seawater were determined in a similar way to the haemolymph. Mixed water in the holding chamber was assumed to be representative of inhalant seawater and water sampled just inside the dorsal shell holes assumed to be exhalant (after Voltzow 1983 and chapter 4 of this thesis).

To obtain values for oxygen uptake by the gills ($Mo_{2(gills)}$) it was necessary to control the rate of ventilation by the use of a mask. The mask consisted of a 10cm section of 12mm diameter PVC tubing cut obliquely to follow the shell contour, the mask was hot-glue sealed to the previously removed shell section of exhalant holes and the assembly re-attached to the shell. The open end of the exhalant mask was connected to a peristaltic pump drawing water at 48 mL.min$^{-1}$, a value representative of the maximum endogenous ventilatory rate measured in adult *H. iris* (see chapter 4), to ensure natural ventilation was not impeded. Water was sampled from the mask to establish true exhalant $Po_2$ and from the dorsal hole region, to test the assumption that this site represented the exhalant stream. Surrounding seawater $Po_2$ was measured and taken to represent inhalant water. The assumption was made that all oxygen uptake in the branchial chamber occurred at the gills, and $Mo_{2(gills)}$ calculated from equation 5.1.

$$Mo_{2(gills)} = \alpha.F_v.(P_i - P_e) \qquad \text{equation 5.1}$$

Where $P_i - P_e$ is the difference between inhalant and exhalant $Po_2$ (Torr) $\alpha$ the solubility of oxygen in seawater at 15ºC (1.6218 µmol.L$^{-1}$.Torr$^{-1}$) and $F_v$ the ventilatory flow (0.048 L min$^{-1}$).

Parameters that could only be calculated using a known ventilation rate were also estimated in naturally ventilating abalone by assuming a rate of 28mL.min$^{-1}$, the mean ventilatory rate of resting, adult *H. iris* measured in chapter 4.

Sampling continued until 5 replicate data sets were obtained for each animal under both natural and controlled ventilation conditions, or until logistical considerations precluded further sampling (usually failure to acquire a Doppler signal or cannula blockage). Where appropriate, data were standardised by animal weight, following the logic of Hughes (1982), referring to the use of total wet weight including all skeletal material: “this is the total mass that the animal must transport and for which respiration provides energy”. Wet weight was measured after allowing 30s for water to drain from the branchial chamber.

*Oxygen content determination*

Haemolymph oxygen content ($Co_2$) was determined using a galvanic cell oxygen content analyser (‘OxyCon’ manufactured by the Department of Physiology, University of Tasmania) calibrated against air and corrected for room temperature. Duplicate 50µL haemolymph samples were measured by sequential injection into the OxyCon cuvette, containing 1mL of scrubber*. Due to excessive

protein deposition, the scrubber solution was replaced, cuvette cleaned and the device re-calibrated between each pair of samples.

Abalone haemolymph is effectively isosmotic with surrounding seawater (Chapter 2, this thesis), it was therefore assumed that oxygen capacitance of the plasma was the same as seawater (1.6218 $\mu mol.L^{-1}.Torr^{-1}$ at 15°C; Dejours 1981). The proportion of haemolymph oxygen carried by haemocyanin was in turn determined by subtracting the dissolved oxygen component from the total content (mean of duplicate samples described above).

*Haemocyanin content*

Cell-free haemolymph samples were thawed and thoroughly mixed and aerated. Haemocyanin concentration was determined by diluting a 100µL sub-sample with 900µL of pH 8.8 buffered EDTA (10 $mmol.L^{-1}$ EDTA, 50 $mmol.L^{-1}$ glycine) in a 1cm path-length cuvette. The sample was oxygenated by shaking and light absorbence measured using a Unicam SP1800 UV spectrophotometer set to the oxyhaemocyanin peak of 346nm (Behrens et al. 2002). Absorbence data were converted to millimolar concentration using the haemocyanin-copper extinction co-efficient, $E_{mM\ Cu,\ 1cm} = 11.424 \pm 1.610$, reported by Behrens et al. (2002) for *H. iris* haemolymph. The co-efficient assumes that the haemolymph contains no apohaemocyanin or additional copper. Copper concentration data were converted to concentration of functional haemocyanin unit concentration by assuming a stochiometry of 2 Cu atoms per haemocyanin monomer, reversibly binding to one $O_2$ molecule.

Haemocyanin concentration and $Co_2$ data were combined to examine the role of this protein in oxygen delivery under normoxic conditions. The data were also used to assemble an *in vivo* oxygen-binding curve to allow comparison to be made with published *in vitro* curves.

*Blood flow and heart rate*

The continuous outputs of the impedance coupler and pulsed-Doppler meter were recorded during each haemolymph sampling period. The data acquisition software was subsequently used to calculate mean impedance pulse rate by a count of signal peaks. This method of determining heart rate proved extremely robust as the impedance coupler consistently providing clear signals. Mean Doppler output (in volts) was determined by cumulative integration of the signal (integral(V/dt)) divided by duration. The following calibration technique was subsequently employed. The animal was rapidly dispatched by decapitation, the ventricle was then punctured to create a low-resistance path and a suspension of Zeolite (commercial barbecue deodorizer, filtered through an 80µm mesh) in seawater pumped into the right efferent ctenidial vein cannula at a range of known flow rates. The Zeolite was initially observed to back-flow into the ctenidium until all efferent pores were blocked; it then flowed past the Doppler crystal and drained from the ventricle, the pulsed-Doppler signals generated in this way were used to plot an *in situ* calibration curve.

---

* Scrubber recipe: $6g.L^{-1}$ potassium fericyanide, $6g.L^{-1}$ potassium cyanide, $1mL.L^{-1}$ Triton-X, $1mL.L^{-1}$ Antifoam-A (Sigma), $15g.L^{-1}$ $Na_3PO_4.12H_2O$, $5g.L^{-1}$ $Na_2HPO_4$.

*Oxygen Diffusion and Capacitance*

The extent to which the gas exchange surfaces themselves limit oxygen uptake was examined by calculation of $L_{diff}$, the Diffusion Limitation Index. Formally, $L_{diff}$ represents the fractional equilibration between transfer without diffusion limitation and the actual transfer rate (Piiper 1982). The index (equation 5.2) returns a value between 0 and 1; a system that approaches 1 is considered entirely diffusion limited (zero transfer), an $L_{diff}$ close to zero indicates no diffusive resistance offered by a barrier.

$$L_{diff} = \frac{P_m - P_a}{P_m - P_v} \qquad \text{Equation 5.2}$$

Where oxygen partial pressure in the medium, $P_m$, is estimated from the mean of inhalant and exhalant seawater $Po_2$. Arterial and venous partial pressures, $P_a$ and $P_v$, are represented by efferent and afferent ctenidial haemolymph respectively.

The overall efficiency of the gills as a gas-exchange system was quantified by determination of $G_{diff}$, the diffusive conductance of the water-haemolymph barrier (Scheid 1982). $G_{diff}$ determines the amount of oxygen taken up per unit $Po_2$ difference across the respiratory surface (Wood & Randall 1981). Also referred to as *transfer factor* or *diffusing capacity* (D), $G_{diff}$ was calculated from equation 5.3.

$$G_{diff} = \frac{Mo_{2(gills)}}{(P_m - P_h)} \qquad \text{Equation 5.3}$$

Where $P_m$ is the mean medium $Po_2$ (mean of inhalant and exhalant seawater) and $P_h$ the mean haemolymph $Po_2$ (mean of afferent and efferent haemolymph). Total oxygen uptake by the gills, $Mo_{2(gills)}$, could only be determined when ventilation was artificially controlled.

All statistical analyses were performed using Statistica™ 6.0 software (StatSoft Inc., USA). All values are expressed as mean ± standard error of the mean.

# 5.3. Results

*Partial pressure gradients*

During unassisted ventilation the resting abalone lowered seawater $Po_2$ from 138.7 ±1.4 to 83.4 ±3.1 Torr (n=27) during a single pass through the branchial chamber. The presence or absence of the shell section bearing the dorsal holes had no significant effect upon the $Po_2$ of exhalant seawater ($F_{1,23} = 2.98$, $p = 0.10$). When a mask was applied and the animal ventilated artificially at 48 mL.min$^{-1}$ the mean exhalant seawater $Po_2$ was 91.3 ±3.3 Torr, which was not significantly different from the exhalant $Po_2$ measured in unventilated animals ($t_{.05, 8df} = -1.67$, $p = 0.07$).

In a passing through the right gill, haemolymph $Po_2$ was raised from 37.2 ±3.6 to 77.0 ±4.2 Torr, approaching equilibrium with the exhalant water (figure 5.4, table 5.1). Mean increase in $Po_2$ ($\Delta Po_2$) was 39.8 ±3.5 Torr. During forced ventilation, neither the afferent (41.8 ±4.8 Torr, n = 9) nor

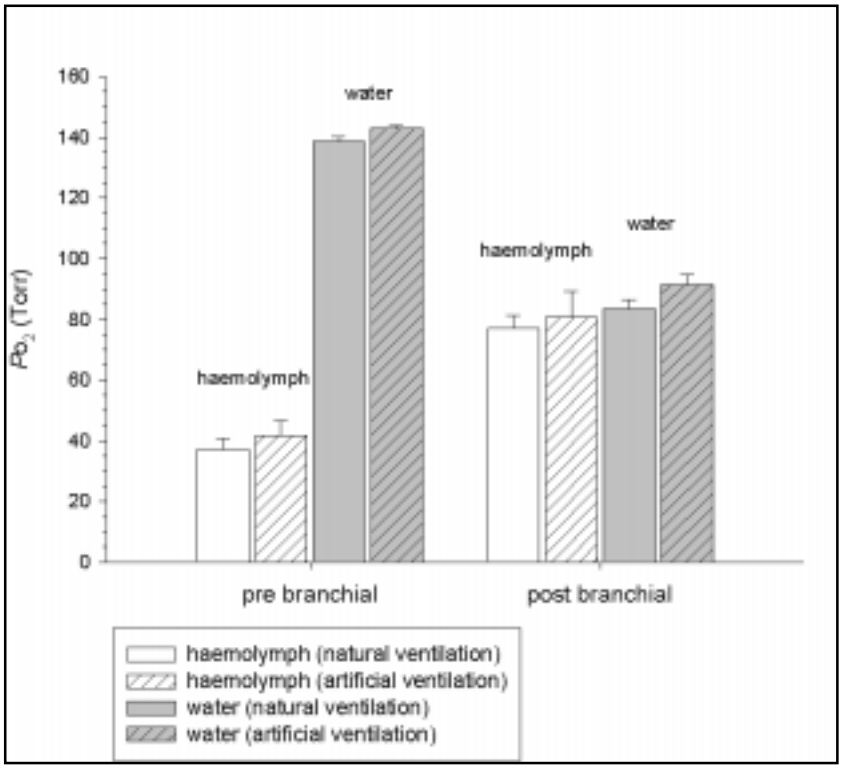


**Figure 5.4**: Pre- and post-branchial haemolymph and seawater $Po_2$ measured in adult *Haliotis iris* during natural ventilation and during forced ventilation at 48mL.min$^{-1}$.

the efferent ctenidial haemolymph $Po_2$ (80.8 ±8.5 Torr) differed significantly from the naturally ventilated state ($t_{.05,8}$ = 0.117, p = 0.455 and $t_{.05,8}$ = -0.374, p = 0.359 respectively).

*Diffusion Limitation*

In animals that were monitored during both natural and artificial ventilation, $L_{diff}$ for the right gill was 0.47 ±0.05 in static water and 0.52 ±0.13 with assisted ventilation (the difference was not significant, paired-$t_{.025,7}$ = -0.14, p = 0.89). Haemolymph and water $Po_2$ data for animals under forced and natural ventilation were therefore pooled to increase resolution when determining the between-individual variability of $L_{diff}$. Overall mean $L_{diff}$ for all resting individuals examined was 0.48 ±0.02 (n=21); significant variability was seen between abalone ($F_{20,60}$ = 5.26, p < 0.001), with individual $L_{diff}$ ranging from 0.25 ±0.08 to 0.75 ±0.04.

*Haemolymph Flow and Heart Rate*

Doppler-flow records were successfully obtained from 24 resting abalone. Haemolymph flow in the right efferent ctenidial vein was highly pulsatile, with calculated midstream flow velocity rising very rapidly to peak typically in excess of 40mm s$^{-1}$, velocity decrease was equally abrupt, falling to zero (or below the device detection limit). A Doppler record from a typical individual is shown in figure 5.5 a). Absolute flow calibration was successfully performed in 12 animals, each showing strong linear correlation between integrated Doppler signal and pre-determined flow ($R^2$ > 0.7). Absolute values of haemolymph flow could therefore only be determined in these 12 individuals.

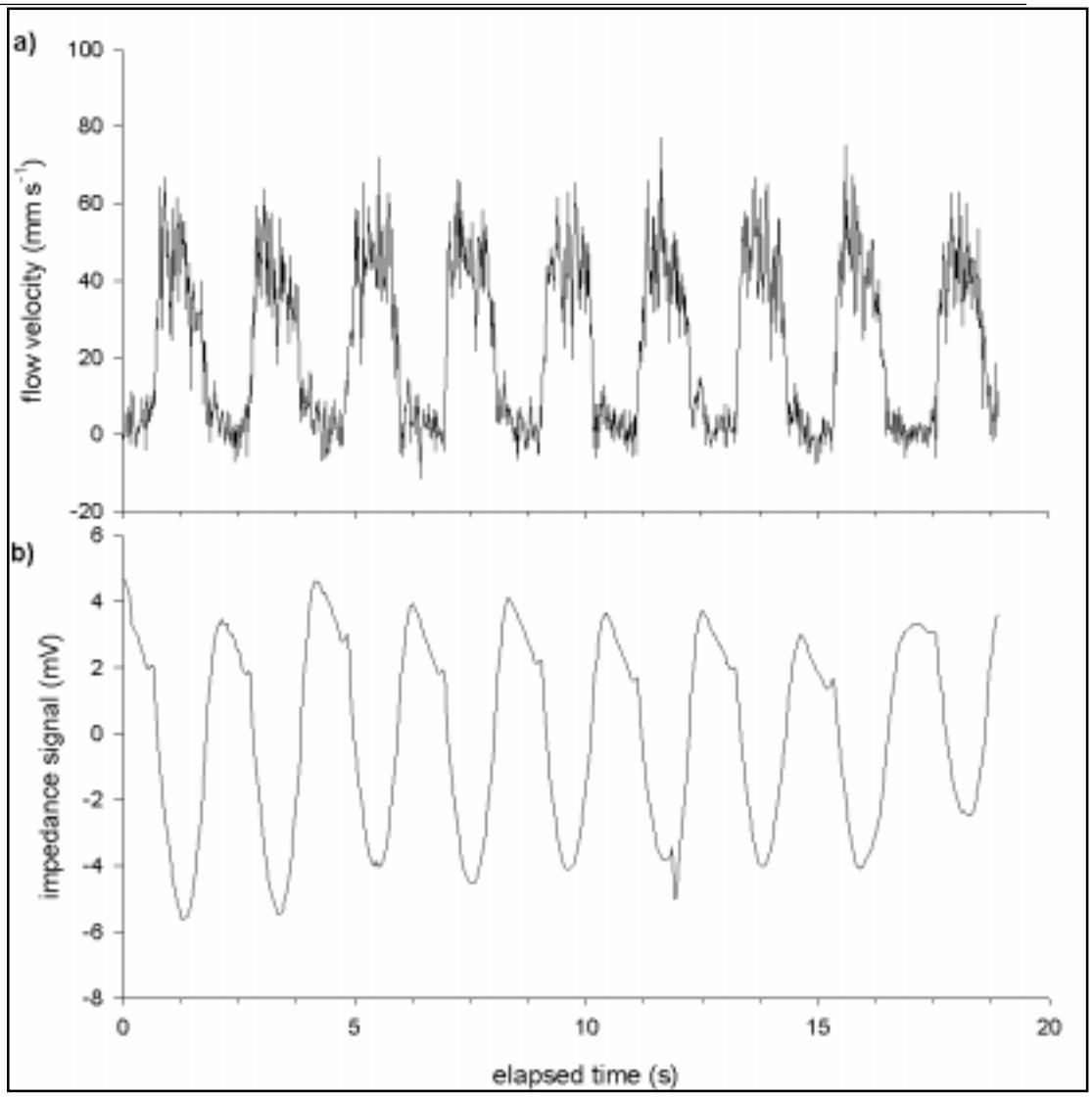


**Figure 5.5**: Example of the simultaneous output of a) the pulsed-Doppler meter measuring haemolymph velocity in the right efferent ctenidial vein and b) the impedance coupler used to determine heart rate. The major impedance oscillation is due to ventricular movement, the minor notches indicate auricular systole.

Mean haemolymph flow in naturally ventilating animals was 9.60 ±0.38 mL.min$^{-1}$ (n = 12). There were significant differences in flow between individuals ($F_{11,8}$ = 8.67, $p < 0.001$), but no significant correlation between haemolymph flow and animal size was detected (mean weight = 421.1g, range = 245 – 579g; $R^2 = 0.09$, n = 70). When subjected to forced ventilation, haemolymph flow through the right gill showed a small, but significant increase to 11.96 ±0.30 mL.min$^{-1}$ ($F_{1,72}$ = 6.98, p = 0.01).

An example of raw impedance signal is shown in figure 5.5b. Mean heart rate in naturally ventilating animals was 29.1 ±0.5 bpm. As with haemolymph flow, heart rate varied significantly among individuals ($F_{11,58}$ = 18.87, $p < 0.001$). Under forced ventilation heart rate showed a small, but significant increase, rising to 30.7 ±0.2 bpm ($F_{1,72}$ = 8.30, p = 0.005). Heart rate also showed a negative linear correlation to animal weight ($R^2 = 0.65$, y-intercept = 53.6 ±1.8, slope = -0.048 ±0.004 bpm.g$^{-1}$, n = 88).

| sample site: | Pre-branchial haemolymph L afferent ctenidial vein | Post-branchial haemolymph R efferent ctenidial vein |
|---|---|---|
| $Po_2$ (Torr) | 37.2 ±3.6 | 77.0 ±4.2 |
| $Co_2$ (mmol $O_2$.$L^{-1}$) | 0.226 ±0.006 | 0.346 ±0.006 |
| Hcy-bound $O_2$ (mmol.$L^{-1}$) | 0.160 ±0.005 | 0.218 ±0.005 |
| [Hcy] (mmol.$L^{-1}$) | 0.237 ±0.003 | 0.237 ±0.003 |
| mol $O_2$: mol Hcy | 0.63 ±0.02 | 0.91 ±0.02 |
| pH | 7.16 ±0.01 | 7.17 ±0.01 |

**Table 5.1**: Oxygen content and partial pressures in pre- and post-branchial haemolymph of the right gill of resting *Haliotis iris* at 15°C (values represent mean ±SEM; data are paired, n = 27).

*Oxygen Content of Haemolymph*

During its passage across the right gill, haemolymph oxygen content was raised from an average of 0.226 mmol.$L^{-1}$ to 0.346 mmol.$L^{-1}$ (table 5.1). The amount of Hcy-bound $O_2$ increased significantly from 0.160 to 0.218 mmol.$L^{-1}$ (table 5.1) in a pass across the gill ($F_{1,103}$ = 68.49, $p < 0.001$), as well as varying significantly between individuals ($F_{24,103}$ = 35.88, $p < 0.001$).

*Haemocyanin Concentration*

Haemocyanin concentration showed significant variability between individuals ($F_{24,101}$ = 43.66, $p<0.001$), ranging from 0.151 ±0.011 to 0.355 ±0.009 mmol.$L^{-1}$. As a measure of saturation, the molar ratio of $O_2$:haemocyanin was calculated for all samples, haemolymph entered the right gill with a mean ratio of 0.63, rising significantly to 0.91 in the efferent haemolymph (table 5.1; $F_{1,100}$ = 71.62, $p < 0.001$).

*pH and in vivo Binding Curve*

The seawater in the experimental chambers remained at pH 7.65 ±0.04 and pH 7.23 ±0.04 in the branchial chamber water bathing the gills. In this environment the haemolymph pH remained stable at 7.16 – 7.17 (table 5.1), small, but significant differences were detected between individuals ($F_{24,104}$ = 6.0, $p < 0.001$) but not between afferent and efferent ctenidial haemolymph ($F_{1,104}$ = 1.11, $p = 0.29$). An *in vivo* $O_2$ binding curve was constructed, plotting the molar ratio of $O_2$:haemocyanin against $Po_2$ (figure 5.6a and b). Figure 5.6a reveals considerable scatter associated with the functional $O_2$ binding curve data. However, a plot of mean data, grouped into 10 Torr bins, implied the pigment remained largely saturated over the haemolymph $Po_2$ range examined (10 – 130 Torr; figure 5.6b).

*$Mo_2$ and Total Contribution of Haemocyanin*

Total $O_2$ uptake rate from seawater passing through the branchial chamber, $Mo_{2(gills)}$, was determined during artificial ventilation, using equation 5.1. Mean $Mo_{2(gills)}$ was found to be 0.529 ±0.023 µmol.$g^{-1}$.$h^{-1}$. By substituting the corresponding haemolymph parameters into equation 5.3, total $O_2$ added to the blood at the right gill was found to be 0.174 ±0.017 µmol.$g^{-1}$.$h^{-1}$ (n = 12), accounting for an

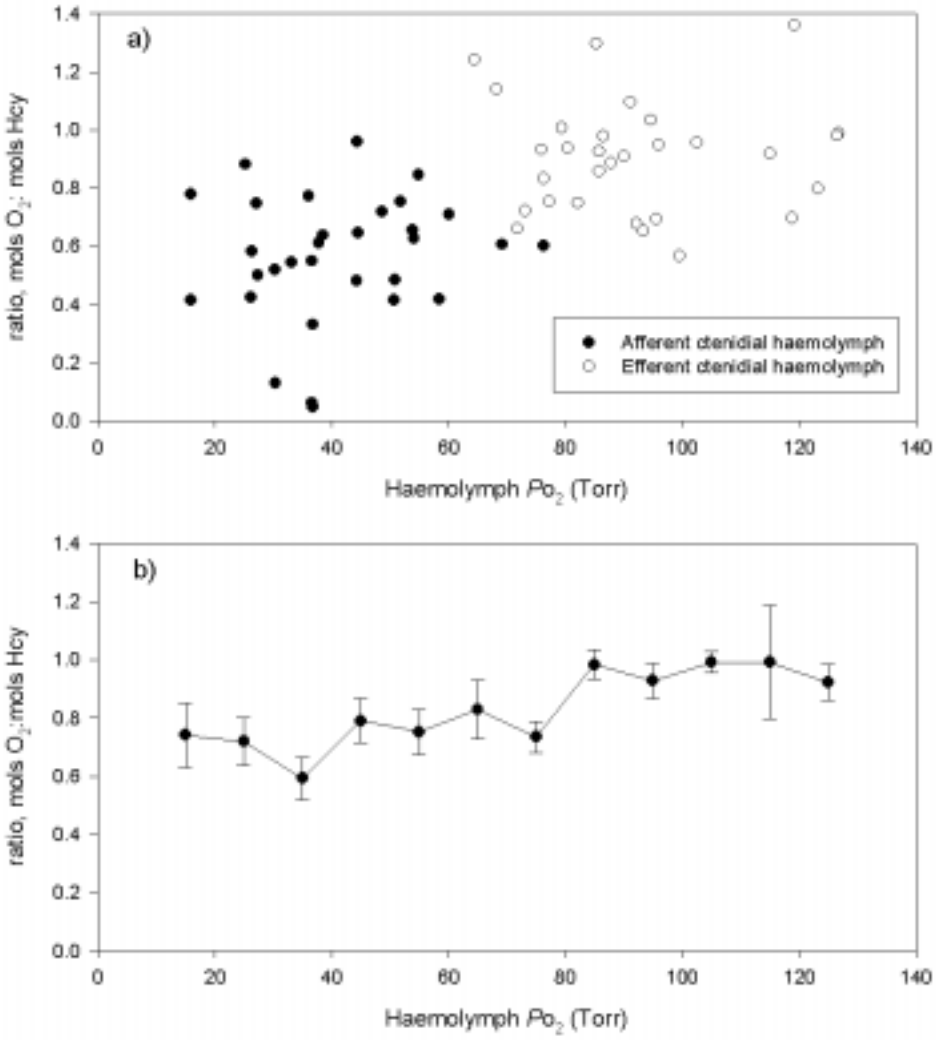


**Figure 5.6**: *In vivo* haemocyanin binding curve constructed using pre- and post-branchial haemolymph samples of known haemocyanin concentration, taken from adult *Haliotis iris*. **a)** Scatter plot using all data, **b)** curve plotted using data grouped into 10 Torr bins.

average of 39.8 ±7.5% of $Mo_{2(gills)}$. Hence if similar contributions are made by both gills, the tissues remove 0.3 – 0.4 µmol $O_2.g^{-1}.h^{-1}$ from the haemolymph. Standardised by oxygen content in the right efferent ctenidial vein, *H. iris* haemolymph releases 34.7 ±5.1% of its oxygen to the tissues, less than half of which (43.6 ±5.1%) was donated from haemocyanin.

*Diffusive Conductance*

Overall mean $G_{diff}$ was found to be 0.174 ±0.021 µmol $O_2.kg^{-1}.min^{-1}.Torr^{-1}$ (n = 8), individual animal $G_{diff}$ ranged from 0.123 ±0.011 to 0.296 ±0.027 µmol $O_2.kg^{-1}.min^{-1}.Torr^{-1}$.

# 5.4. Discussion

*The counter-current model*

The counter-current flow arrangement for the abalone gill has been inferred from morphological information. Haemolymph in the right afferent ctenidial vein has little alternative other than to cross the corrugated, sheet-like gas exchange regions of the lamellae to enter the efferent lamellar

| Parameter | formula | calculated value for artificially ventilated *H. iris* right gill **(estimates for natural ventilation state in parentheses)** |
|---|---|---|
| Ventilation extraction efficiency | $\frac{P_i - P_e}{P_i} . 100$ | 36.1 ±2.2% (39.8 ±2.2%) |
| Ventilation/ Perfusion ratio | $\frac{Q_w}{Q_h}$ | 1.21 ±0.09 (1.4 ±0.2) |
| $Po_2$ overlap | $u = \frac{P_a - P_e}{P_i - P_v}$ | -0.11 ±0.08 (-0.05 ±0.03) |
| Ventilatory/ Perfusive conductance ratio | $X = \frac{Q_w.\beta_w}{Q_h.\beta_h}$ | 1.41 ±0.18 (0.96 ±0.15) |
| Diffusive/ conductance ratio | $\frac{D}{Q_h.\beta_h}$ | 0.89 ±0.15 |

**Table 5.2**: Parameters used to describe the efficiency of a gas exchanger (after Piiper and Scheid 1984) applied to the right gill of *H. iris*. $P_i$ and $P_e$ represent the $Po_2$ of inhalant and exhalant water, respectively. $P_v$ and $P_a$ represent pre-branchial ('venous') and post-branchial ('arterial') haemolymph $Po_2$. $Q_w$ and $Q_h$ are the flow rates of ventilatory water and haemolymph, respectively. $\beta_h$ is the oxygen

sinuses and thereafter the right efferent ctenidial vein, following a pressure gradient derived from the right auricle (see chapters 6 and 7 for discussion of the constant volume heart model). The lateral cilia, which drive ventilation, are located in the interlamellar spaces (Yonge 1947). This arrangement would be expected to generate an efferent to afferent counter-current water flow, and this has been verified by the observation of dye or carmine particles being strongly drawn between the efferent interlamellar spaces and ejected from the afferent (Crofts 1929, Yonge 1947, personal observation). It is therefore considered appropriate to apply analytical models originally used to describe counter-current gas exchange systems in fish. It should be noted that the counter-current operation of the gills of higher decapods (during forward ventilation) has also been inferred from morphological observations McMahon and Wilkins (1983). When searching for corroborating physiological evidence McMahon and Wilkins (1983) note that arterial $Po_2$ is rarely, if ever, greater than exhalant $Po_2$, which they consider to be due to the effects of large ventilatory dead-space.

Table 5.2 lists a number of descriptive parameters calculated from the data presented above for the right gill of *H. iris*. The parameters are based on Piiper and Scheid's (1984) model for oxygen transfer in the fish gill.

*Oxygen carrying capacity*

*In vivo* post-branchial haemolymph oxygen content slightly exceeded maximum values predicted from haemocyanin content (figure 5.6a) and was therefore taken to represent maximum capacity of

*H. iris* haemolymph (mean = 0.346 mmol $O_2$.$L^{-1}$ at 15°C, table 5.1). The $O_2$ capacity of *H. iris* resembles values determined for the sedentary abalone *H. laevigata* and *H. ruber* (0.46 and 0.45 mmol.$L^{-1}$), but is somewhat lower than the more active *H. roei* (0.64 mmol.$L^{-1}$; Ainslie 1980b). Carrying capacity of abalone haemolymph in general is low compared to other water-breathers with binding pigment in their blood, e.g. *Busycon* (1.6 mmol.$L^{-1}$, Mangum and Polites 1980). The carrying capacity of crustacean haemolymph is also low (typically 0.5 – 1.5 mmol.$L^{-1}$) but this is offset by a high cardiac frequency, made possible by sarcoplasmic reticulum enrichment in the myofibres (Mangum 1983). The differences in capacity are presumably due to the relatively low concentrations of haemocyanin found in abalone, which in turn appears to correlate to the relatively low activity levels of these molluscs (Ainslie 1980a). However, oxygen carrying capacity doesn't follow simple phylogenetic trends, as pointed out by Mangum (1983) the capacity of sedentary lamellibranch haemolymph can, for example, often exceed that of highly developed and active cephalopods. Haemocyanin levels may be limited by their effect on colloid osmotic pressure, for example crustacean colloid osmotic pressures of 1.2 – 3.0 Torr have been measured, often exceeding hydrostatic pressure in the venous sinuses (Mangum 1983). Higher haemocyanin concentrations would therefore necessitate corresponding elevations of haemolymph pressure, if ultrafiltration is to occur and intra-/ extra-cellular water balance is to be maintained. Perhaps a more critical limitation to haemocyanin concentration in *H. iris*, however, is the cost of synthesis, considering the large volume of circulating haemolymph in this animal. In the most active animals to use haemocyanin, the cephalopod molluscs, Wells and Smith (1987) suggest the maximum blood $O_2$ capacity, approximately 2mmol.$L^{-1}$, is determined by viscosity increase due to the presence of high haemocyanin concentration. Taylor (1993) specifically examined this relationship in *H. iris* haemolymph and found a significant correlation between viscosity and haemocyanin concentration in 13 out of 20 animals examined.

*Ventilation/Perfusion ratio*

Given the relative paucity of diffusion and perfusion data relating to gastropod molluscs, more useful comparisons can be made to the gas exchangers of decapod crustacea. Decapods occur over a similar size range to abalone and share the challenges associated with a benthic habitat and rigid exoskeleton. Of particular relevance, however, is the observation that marine decapods maintain a low ventilation: perfusion ratio of about 1 – 4 (Taylor and Taylor 1992). If it is assumed that the right gill of *H. iris* receives half of the branchial ventilatory flow, a ventilation/perfusion ratio for this organ can be determined. Under forced ventilation conditions (48.1 ml seawater.$min^{-1}$) the ventilation/perfusion ratio of the right gill is estimated to be 1.2 (table 5.2), or 1.4 with unassisted ventilation, assuming endogenous ventilation proceeds at the mean rate of 28mL.$min^{-1}$ for resting *H. iris* of this size range (see chapter 4). Water breathers typically maintain a high ventilation rate to compensate for the low capacitance of oxygen in water, resulting in ventilation/perfusion ratios ranging from 10 to greater than 20 in fish gills (Jones and Randall 1978, Randall and Daxboeck 1984, Taylor and Taylor 1992). In decapods and abalone, however, the oxygen capacitance of haemolymph is also low (for the reasons discussed below); haemolymph flow must therefore also be kept correspondingly high.

*Oxygen Extraction from ventilatory water*

Resting *H. iris* remove approximately 36 - 39% of the oxygen from ventilatory water. This value is somewhat lower than the mean extraction efficiency of 49% measured in chapter 4 of this thesis. The latter value relates to a somewhat artificial situation where all the shell holes were masked and the abalone was artificially ventilated at 28mL.min$^{-1}$. As the forward projecting holes may be inhalant or tidal (Voltzow 1983), they were not masked in the current experiment. It is suggested that the full mask used in chapter 4 may have compromised one of the natural inhalant routes, resulting in increased residence time in the branchial chamber and hence increased $O_2$ extraction. The extraction efficiencies of 36 – 39% are regarded as more representative in the current context.

The extraction efficiency of *H. iris* is typical of marine invertebrates that do not rely on gills for filter feeding, e.g. 56% for *Haliotis* spp. and 38% for *Murex bandaris,* measured by Hazelhoff (1938 reported in Fretter and Graham 1994). Extraction efficiency is about 50% for *Busycon canaliculatum* and *Cryptochiton stelleri* (Mangum and Polites 1980), 42% for the giant clam *Tridacna squamosa* (in the dark), 30 – 60% for arenicolid polychaetes (Mangum 1982). Crabs and lobsters show similar extraction efficiencies at rest (34 – 44% during bilateral ventilation, rising slightly to ~50% during unilateral ventilation; McMahon and Wilkins 1983). Amongst other lamellibranchs and cephalopods interpretation of extraction efficiency is complicated by the additional functions of the ventilatory water, for filter feeding in the former, jet propulsion in the latter. As a result, wildly different efficiencies are seen within the 2 classes. For example, the mussel *Modiolus demissus* extracts 7-8% (Booth and Mangum 1978) and *Mytilus edulis* extracts 5 – 10% (Bayne 1971) of the ventilatory oxygen while the haemoglobin-bearing clam *Noetia ponderosa* extracts 60% (Booth and Mangum 1978). *Nautilus pompilius* uses only 7% of its ventilatory oxygen while the large *Octopus dofleini* extracts 80% (Mangum and Polites 1980). Paradoxically, extraction efficiency in Nautilus pompilius *falls* to about 4% during locomotion, despite increased demand, as the animal hyperventilates to allow jet propulsion (Wells and Wells 1985). Oxygen extraction also varies considerably amongst fish species, at rest a trout will extract 30 – 45% of inhalant oxygen, while tuna and carp remove 70 –80% (Randall and Daxboeck, 1984). It should be noted that the ventilation rate of archaeogastropods with secondary shell openings is almost inevitably increased by the action of currents in the surrounding water (Murdock and Vogel 1978, Voltzow 1983), presumably reducing extraction efficiency.

*Conductance ratios*

An alternative way of expressing ventilation/perfusion relationships, that takes into account differences in oxygen capacitance of the water and haemolymph, is the conductance ratio. The ratio of ventilatory water conductance/haemolymph conductance (the product of capacitance and flow) has considerable bearing on the efficiency of gas exchange. Counter-current gills where diffusion limitation is not prevalent are particularly sensitive to a mismatched conductance ratio, indicating a sub-optimal situation for exchange (Piiper and Scheid 1984). A mismatch, however, provides an indication of the steps an animal could take, i.e. by augmenting ventilation or perfusion, to restore unity and optimise transfer during increased demand.

Total haemolymph $O_2$ capacitance was determined for each individual abalone with at least 8 paired haemolymph $Co_2$ and $Po_2$ values spanning the arterial and venous range. Surprisingly, the data were adequately described by a straight line in all cases, rather than the expected sigmoidal curve; ultimately this proved convenient as a single capacitance could therefore be calculated for each animal from the slope of the graph. In this way the mean haemolymph capacitance co-efficient was found to be 2.64 ±0.17 μmol.$L^{-1}$.$Torr^{-1}$, compared to a seawater capacitance of 1.62 μmol.$L^{-1}$.$Torr^{-1}$ (Dejours 1981). Given the low $O_2$ capacitance of abalone haemolymph and near-unity in the ventilation: perfusion ratio, it is not surprising to find the conductance ratio (ventilatory water: haemolymph perfusion) for the right gill also approaches 1 (table 5.2). Ventilation and perfusion are therefore well matched in the resting abalone, implying that both must be increased if the gills are to sustain increased oxygen demands during exercise or stress. Such a condition may prevail in the pectinibranch gill of *Busycon*, where both ventilation rate and $O_2$ extraction efficiency from the water increase with increasing hypoxia below 100 Torr (Mangum and Polites 1980).

*Proportion of oxygen uptake entering haemolymph*

Of all oxygen consumed by fish, 6 – 27% is used directly by the tissues of the ventilatory system, notably the gill epithelia, and only 60 – 80% of oxygen taken from the water enters the blood at the gills (Randall and Daxboeck, 1984). Oxygen uptake into the unpigmented haemolymph of the bivalve *Placopecten magellanicus* and the echinoderm *Pteraster tesselatus* accounts for 42% and 29% of the animal's $Mo_2$, respectively (Thompson et al. 1980). In even more extreme examples, the haemolymph of the mussel *Modiolus* transports only 10-15% of all oxygen taken up from the medium (Booth and Mangum 1978) and the haemolymph of the mussel *Mytilus edulis* is thought to have no respiratory function whatsoever, despite ready equilibration with the external $Po_2$ (Famme 1981). Amongst the gastropods, Depledge and Phillips (1986) estimate that 30 – 50% of total $Mo_2$ of *Hemifusus* and *Busycon* diffuses directly into tissues.

In artificially ventilated abalone, 39.8 ±12.4% of $O_2$ taken up from the seawater entered the haemolymph of the right gill. If a similar uptake rate is present in the left gill, total uptake into the blood will resemble the 60-80% of branchial $Mo_2$ typically recorded in fish, with most of the balance required by the gill epithelia (Randall and Daxboeck, 1984). In molluscan gills ciliary ventilation facilitates gas exchange processes as fastest velocities are encountered close to the tissue surface. However the cilia are required to generate a steep velocity gradient, the process is therefore energetically costly (Vogel 1994), reflected in the high specific oxygen requirements of gill epithelia (e.g. *Crassostrea*, Willson and Burnett 2000). It therefore seems likely that the bulk of the deficit in abalone is also a result of direct uptake by the gill epithelia. For example, Mangum and Polites (1980) report specific $Mo_2$ values for gill tissue of *Busycon* an order of magnitude higher than whole animal $Mo_2$. Abalone ventilatory water also contacts the extensive hypobranchial mucus glands, which are also likely to have high metabolic activity and may also offer additional exchange surface for diffusion into the haemolymph.

*Oxygen delivery by the haemolymph*

Amongst other molluscs, the cephalopod *Nautilus pompilius* and the amphineuran *Cryptochiton stelleri* unload a relatively small percentage of their haemolymph oxygen (~40 and 48% respectively), retaining a large venous $O_2$ reserve (Mangum and Polites 1980). In contrast octopus, squid and the gastropod *Busycon canaliculatum* all unload over 80% of their haemolymph oxygen (Mangum and Polites 1980, Wells and Smith 1987, Wells 1992), while the bivalve *Placopecten magellanicus* unloads 60% of its haemolymph oxygen (Thompson et al. 1980). In the present study, *H. iris* haemolymph was found to release only 34.7% of its oxygen to the respiring tissues, less than half of which (43.6%) was donated by the haemocyanin. A venous reserve concentration of 0.226 mmol $O_2.L^{-1}$ remains in the haemolymph as it returns to the gills. As the capacitance of *H. iris* haemolymph is low, the volumetric contribution of haemolymph $O_2$ is also low at 0.11 ±0.02 mmol.$L^{-1}$, compared to an estimated 0.76 mmol $O_2.L^{-1}$ delivered by *Busycon* haemolymph (Florkin 1934 cited in Ainslie 1980b). In *H. ruber* 0.25 mmol $O_2.L^{-1}$ were delivered to the tissues, 86% of which was donated by haemocyanin, *H. laevigata* delivered 0.28 mmol.$L^{-1}$, 97% of which was bound to haemocyanin while *H. roei* delivered 0.40 mmol.$L^{-1}$, 91% on haemocyanin (Ainslie 1980b).

*The Role of Haemocyanin*

The *in vivo* relationship between haemolymph oxygen content and partial pressure was examined with the intention of producing a functional $O_2$ binding curve. The individual data, however, show considerable scatter (figure 5.6a). The scatter may be due in part to compound errors associated with combining $Co_2$, $Po_2$ and haemocyanin concentration data. As scatter was minimal within individual animal data sets, it seems likely that most of the variability is genuine, reflecting a variety of binding responses seen between individuals. Two haemocyanin isoforms have been found in *H. tuberculata* (Behrens et al. 2002). Each represents a functional haemocyanin monomer, which typically combine in clusters of 8, forming a sub-unit, which in turn form 2-ring didecamers (~8MDa) which can aggregate to form quaternary tube structures (Behrens et al. 2002). A six-layer cylinder of about 9MDa was previously recorded as the predominant polymer of *H. iris* haemocyanin, with 6 other molecular weight polymers detected by SDS-PAGE (Ellerton and Lankovsky 1982). The scope for a wide variety of haemocyanin states occurring *in vivo*, each displaying a characteristic suite of binding properties is therefore considerable. Similarly, Randall and Daxboeck (1984) note that numerous haemoglobin types, each with its own binding characteristics, may be present within the blood of an individual fish. Such heterogeneity, and effects of varying ratios of each pigment type might be expected to produce similar variability in whole blood binding to that seen here.

When mean haemocyanin parameters are examined, the general message is clear. Haemocyanin leaves the right gill 91% $O_2$ saturated and returns 63% saturated (table 5.1), reflecting the fact that the $Po_2$ range experienced between the pre- and post-branchial vessels lies towards the upper region of the binding curve (figure 5.6b). Native *H. iris* haemolymph at pH6.9 showed a very strong $O_2$ affinity, with $P_{50}$ of 3.9 – 4.0 Torr at 15°C (Behrens et al. 2002), ~3 Torr at pH 7 and 10°C and ~8 Torr at pH 7 and 20°C (Wells et al. 1998). The pronounced reverse Bohr effect seen in *Haliotis*

haemolymph caused mean $P_{50}$ to increase to 11.6 – 12.2 Torr when pH was raised to 7.7 (Behrens et al. 2002), or 10 – 20 Torr, depending on temperature (Wells et al. 1998). Pre-branchial haemolymph $Po_2$ recorded in the present study (mean 37.2 ±3.6 Torr) rarely fell to such low values. Resting *H. iris* therefore appear to make little use of their haemocyanin, the majority of $O_2$ is delivered to the tissues in solution (66.4%), allowing two-thirds of transported $O_2$ to remain in the haemolymph forming the venous reserve. These observations are consistent with the findings of Wells et al. (1998) who conclude the *in vivo* function of *H. iris* haemocyanin is poised towards storage to support aerobic tissues due periods of reduced $O_2$ availability.

The anatomical arrangement of the vascular system must be considered in conjunction with the above observations. As shown in chapter 4 the main vasculature provides alternative bypass routes to all organs and muscle blocks, with the exception of the gills. It is therefore incorrect to treat the system as a serial arrangement of target organs ending at the gills. It would be more appropriate to view the low resistance bypass routes through the main vasculature as a mixed pool that exchanges slowly with the higher resistance pools of the visceral organs and muscle blocks. Long haemolymph residence times would therefore be predicted in the lacunae serving most tissues, which is likely to cause localised $O_2$ depletion. It is suggested that the $Po_2$ environment surrounding most of the respiring cells is severely hypoxic, promoting unloading from haemocyanin. In the absence of a very high affinity pigment, oxygen delivery to the deep tissue might effectively cease.

Haemocyanin concentrations recorded here (0.237 ±0.003mmol.$L^{-1}$) correspond closely to those measured by Behrens et al. (2002) for resting *H. iris* (0.21 ±0.003 mmol.$L^{-1}$). By assuming a molecular weight of 53,000Da for the functional subunit of *H. iris* haemocyanin (Ellerton and Lankovsky 1983), mass-concentration was calculated to be 12.6 g.$L^{-1}$. This value lies towards the upper limits of the ranges reported for *H. roei* (3.6 – 15.1 g.$L^{-1}$), *H. laevigata* (2.4 – 14.2 g.$L^{-1}$) and *H. ruber* (1.0 – 9.9 g.$L^{-1}$) haemocyanin concentrations (Ainslie 1980a*). Oxygen binding affinities in the latter 3 species was lower than *H. iris* and the reverse Bohr effect was apparent in the physiological range, resulting in pre-branchial $P_{50}$ estimated to be 13 – 17 Torr, rising to 24 – 28 Torr in post-branchial haemolymph (Ainslie 1980b). The haemocyanin is therefore more effectively exploited, perhaps reflecting differences in the morphological arrangement of the vascular system.

The oxygen carrying characteristics of *H. iris* haemolymph appear to resemble those of decapod crustaceans more closely than those of other molluscs. In most molluscs, annelids and chelicerates the presence of haemocyanin increases the $O_2$ capacitance of the haemolymph by 5 – 10-fold, while in crustacea capacitance only increases 2 – 3-fold (Mangum 1983). If post-branchial *H. iris* haemolymph is assumed to be saturated, total $O_2$ capacitance is increased 2.7-fold due to haemocyanin. A similar lack of reliance upon haemocyanin may occur amongst crustacea. For example, at rest the venous $Po_2$ of the large crab *Cancer magister* remains within the saturated region of the haemocyanin binding curve; only during exercise is $Pvo_2$ pushed down into the steep region of the dissociation curve (McMahon and Wilkins 1983). However, in most crustaceans

* Haemocyanin concentration units are recorded in Ainslie 1980a as mg.$L^{-1}$, this is plainly a typographical error as source data of the same magnitude can be found in Ainslie (1977) recorded in mg.$mL^{-1}$.

haemocyanin donates in excess of 75% of the oxygen reaching the tissues, facilitated by a large normal Bohr shift that acts within the physiological pH range (Mangum 1983). In contrast tarantulas use only 50% of their haemolymph $O_2$ capacity at rest, this is increased after exercise by allowing arterial $Po_2$ to rise, saturating haemocyanin leaving the book lungs (Paul 1986).

*Diffusion Limitation*

Diffusion is the only means by which respiratory gases are exchanged between blood and external medium (Scheid 1982, McMahon and Wilkins 1983). Hence, while the convective delivery systems of ventilation and blood flow to a gas exchanger can be refined, the diffusion barrier presented by the exchanger is an inevitable consequence of the need to separate internal and external media. In gill systems this diffusion barrier often represents the rate limiting stage in oxygen transfer between the environment and the mitochondria.

- *Definition of* $L_{diff}$

The diffusion limitation index, or diffusive equilibration deficit, is defined as the fractional difference between gas transfer in the absence of diffusion limitation, and the actual transfer rate (Piiper 1982). Practically, $L_{diff}$ provides us with an indication of the extent to which either physical diffusion or convection in the form of blood flow limits gaseous exchange. It should be noted that $L_{diff}$ describes the net limitation across the diffusion surface, including boundary layers and mucus (discussed below; Scheid 1982). It should also be noted that calculated $L_{diff}$ based on mean water/haemolymph $Po_2$ differences probably overestimates the gradient across the exchange surface as ventilation/ perfusion inequalities, $Po_2$ gradients in the blood and consumption by the gill tissues are not considered (Randall and Daxboeck, 1984).

- *Assumptions of the* $L_{diff}$ *model*

The accurate determination of $L_{diff}$ is jeopardised by inconstancies in the parameters given in equations 5.2 and 5.5 (Piiper 1982). For example, medium $Po_2$ ($P_m$) may oscillate in a tidally ventilated system. Abalone, however, are ventilated by a unidirectional water flow, keeping $P_m$ fairly stable (pulsatility in the flow observed in chapter 4 does not change the direction of flow). Similarly the presence of haemocyanin suspended directly in the haemolymph eliminates the consideration of an additional diffusion barrier between plasma and erythrocyte. As *H. iris* haemocyanin remains largely saturated across the gills, the relationship between haemolymph *C*o2 and $Po_2$ in each individual animal tends to be linear, greatly facilitating the calculation of $\beta$, the co-efficient of haemolymph capacitance. Pulsatility in haemolymph also jeopardizes the validity of the model. This is particularly critical if the total volume of haemolymph at the exchange surfaces is less than the stroke volume, as in some fish (Jones and Randall 1978). Although not formally measured in the abalone, visual inspection of vascular corrosion casts suggests that it is highly unlikely the small ventricular volume could approach that of the extensive lamellar diffusion surfaces.

*- $L_{diff}$ in Haliotis iris*

An initial indication of the extent of diffusion limitation can be obtained by a cursory examination of $Po_2$, relatively large blood/medium and small artero-venous differences indicating diffusion limitation (Piiper 1982). Such an inspection of figure 2 reveals a reasonably large afferent-efferent haemolymph $Po_2$ gradient ($\Delta Po_2$ = 39.8 ±3.5 Torr; 'artero-venous difference' in a vertebrate model) and post-branchial haemolymph $Po_2$ that approaches equilibrium with the exhalant water. Hence the first impression is of a system where diffusion limitation is not prevalent.

Gas exchange systems where $L_{diff}$ is very small (< 0.05) are considered to be entirely convection (blood flow) limited, whereas $L_{diff}$ > 0.9 describes a transfer that is entirely diffusion limited (Piiper 1982). In vertebrates, such extremes are characterised by the lungs (human $L_{diff}$ < 0.01, Piiper 1982) and by cutaneous gas exchange in amphibians (salamander cutaneous $L_{diff}$ ~ 0.8; Piiper 1982, Feder 1995). Gill systems tend to show intermediate $L_{diff}$ values, with both diffusion and perfusion limitation influencing oxygen uptake. Taylor and Taylor (1992) summarise a range of $L_{diff}$ data for decapod crustacean gills ranging from 0.5 to 0.8. They argue that apparent diffusion limitation reflects the need to maintain a chitinous cuticle around the lamellae, which accounts for up to 80% of the total diffusion path (diffusion through chitin ~10x slower than through tissue; McMahon and Wilkins 1983). The apparent lack of predominance of diffusion limitation in the data presented in the present study is reflected in a calculated $L_{diff}$ of 0.48, implying diffusion and perfusion processes act equally to limit oxygen uptake. Molluscan gills lack a cuticle; in most, including *H. iris*, structural integrity is maintained by an elaborate framework of cartilage which supports, but does not interfere with the corrugated exchange surfaces of the lamellae (Yonge 1947, chapter 4 of this thesis), reducing the potential barrier to diffusion.

In a model proposed by Piiper (1982), 40 – 70% of all resistance to oxygen uptake in the counter-current fish gill could be attributed to inter-lamellar water. In a specific application of the model, the dogfish *Scyliorhinus stellaris* had an overall $L_{diff}$ of 0.6 and an $L_{diff}$ for the water barrier alone of 0.4. In abalone the ventilatory motor itself is located between the gill lamellae, taking the form of elongate bands of lateral cilia arranged across the efferent inter-lamellar region (Yonge 1947, chapter 4 of this thesis). Each inter-lamellar space is therefore irrigated by a constant, rapid flow of water, a process that presumably minimises the opportunity for the formation of unstirred layers in the inter-lamellar water.

Transmural pressure across the lamella surface also has a fundamental influence on diffusion limitation, a smaller gradient allowing thinner epithelium and blood sheet, reducing the physical diffusion barrier. The blood pressure within the secondary lamellae of fish gills is typically 20 – 40 Torr, requiring a relatively thick epithelium to withstand the associated transmural pressure gradient (Randall and Daxboeck, 1984). The problem is offset to some extent in tuna, where branchial water pressure may be raised, permitting a thinning of the gas exchange surface (Randall and Daxboeck, 1984); the obvious alternative is to operate with branchial vascular pressures that approach ambient. The latter arrangement is seen in abalone. In *H. iris* mean afferent ctenidial vein pressures of 3.30

±0.22 $cmH_2O$ fell to 1.16 ±0.11 $cmH_2O$ * in the right efferent ctenidial vein (chapter 7, this thesis). Similar values have been recorded in *H. corrugata*, where mean a afferent ctenidial pressure of approximately 4 $cmH_2O$ fell to a mean efferent ctenidial vein pressure of 1.9 $cmH_2O$ (Bourne and Redmond 1977a). In *H. kamtschatkana* (Krajniak and Bourne 1988) and *H. ruber* (Russell and Evans 1989) efferent ctenidial pressures of 1 – 2 $cmH_2O$ were also observed. Ciliary pumps generate very little pressure; for example the ventilatory/feeding currents of *Mya arenaria* and *Mytilus edulis* generate a maximum head of 0.28 $cmH_2O$ (Vogel 1994). Branchial chamber pressures recorded in *H. midae* correspondingly appeared to be about ambient (Trueman and Brown 1985). Similar pressures are likely to prevail in the branchial chamber of abalone, resulting in very small transmural pressure gradients, presumably permitting a thinner lamellar epithelium and reduced resistance to diffusion.

A variable of particular importance to gastropod molluscs is the transient diffusion barrier of mucus. Ultsch and Gros (1979) determined $O_2$ diffusivity through mucus (secreted by Carp, *Cyprinus carpio* skin) to be similar to that of water but estimated considerable increase in diffusive resistance in the presence of a mucus layer, which increased the functional thickness of the unstirred boundary layer. Randall and Daxboeck (1984) also note that excessive mucus retention between the secondary lamellae of fish gills will also increase resistance to water flow. In addition to mucus secreted by the abalone's specialised hypobranchial glands, the epithelium of the gill lamellae also contains abundant mucocytes (e.g. Harris et al. 1998, chapter 4 of this thesis). Mucus coating the exchange surfaces of *H. iris* lamellae is therefore likely to have an omnipresent effect on $O_2$ diffusion. Resistance to diffusion is expected to increase if mucus production is elevated in response to stress and ventilation may also become impaired if production is excessive or the hypobranchial glands release their dense mucus spindles (see Crofts 1929 for description).

- $G_{diff}$

As with $L_{diff}$, diffusive conductance ($G_{diff}$) examines the critical process of diffusion across the entire gas exchanger. Practical $G_{diff}$ can be used as a measure of overall efficiency of the gas exchange organ, as it assesses how effectively the exchanger exploits the medium/blood $Po_2$ gradient (equation 5.3). For this reason $G_{diff}$ has proven to be a valuable tool in the comparative study of gas exchangers. Amongst water breathers, physiological determinations of $G_{diff}$ tend to be restricted to fish. During routine oxygen uptake the active pelagic fish, represented by the dogfish, have $G_{diff}$ values of 0.4 – 0.67 µmol $O_2.kg^{-1}.min^{-1}.Torr^{-1}$ (Johansen 1982, Piiper 1982), while demersal fish (e.g. catfish and flounder) have $G_{diff}$ of approximately 0.3 µmol $O_2.kg^{-1}.min^{-1}.Torr^{-1}$ (Johansen 1982). The efficiency of $O_2$ transfer across the abalone gill, determined here by a $G_{diff}$ of 0.174 ±0.021 µmol $O_2.kg^{-1}.min^{-1}.Torr^{-1}$ is clearly somewhat lower. However the $G_{diff}$ in the haemoglobinless icefish, *Chaenocephalus aceratus*, is reported to be only 0.12 µmol $O_2.kg^{-1}.min^{-1}.Torr^{-1}$ (Johansen 1982), implying the $O_2$ binding pigment is accountable for the higher $G_{diff}$ rather than the design of the gas exchange organ. Direct comparison to invertebrate gill $G_{diff}$ is problematic as published values tend to be derived

* 1 $cmH_2O$ = 0.735 Torr = 98 Pa.

from morphometric data which, as noted by Maina (1998, p57) tend to substantially overestimate physiological $G_{diff}$. Hence very high $G_{diff}$ such as those calculated for nautilus (2.4 – 6.2 µmol $O_2$.kg$^{-1}$.min$^{-1}$.Torr$^{-1}$; Hughes 1982, Eno 1994) octopus (2.2 µmol $O_2$.kg$^{-1}$.min$^{-1}$.Torr$^{-1}$) and squid (23.3 µmol $O_2$.kg$^{-1}$.min$^{-1}$.Torr$^{-1}$; Eno 1994) are likely to be somewhat lower *in vivo*.

- *Relationship between $G_{diff}$ and $L_{diff}$*

A practical formula used to determine $L_{diff}$ is given in equation 5.2; it can also be shown theoretically that $L_{diff}$ can be expressed as the exponent of the diffusive/conductance ratio (equation 5.4 - assuming constant co-efficient of capacitance).

$$L_{diff} = \frac{P_m - P_a}{P_m - P_v} = e^{(-D/\beta Q)} \qquad \text{Equation 5.4}$$

Where D is a measure of conductance of the gill, referred to as 'diffusing capacity' (Piiper 1982), β is the solubility of oxygen in abalone haemolymph in the $Po_2$ range encountered at the gills and Q is mean haemolymph flow through the gill. In the abalone gill it is assumed that all resistance to diffusion occurs across the exchange surfaces of the lamellae, this being the case, D is equal to the diffusive conductance, $G_{diff}$. The interesting association between $L_{diff}$ and D is shown in figure 5.7. A 4-fold variation is seen in individual $G_{diff}$ values. At diffusing capacities greater than 0.2 µmol $O_2$.kg$^{-1}$.min$^{-1}$.Torr$^{-1}$, $L_{diff}$ remains at a remarkably low 0.3; as $G_{diff}$ declines below 0.2 µmol $O_2$.kg$^{-1}$.min$^{-1}$.Torr$^{-1}$, $L_{diff}$ is seen to rise exponentially to values approaching, and even (impossibly) exceeding 1 and shows considerable variability. A decline in $G_{diff}$ occurs as a result of reduced oxygen uptake

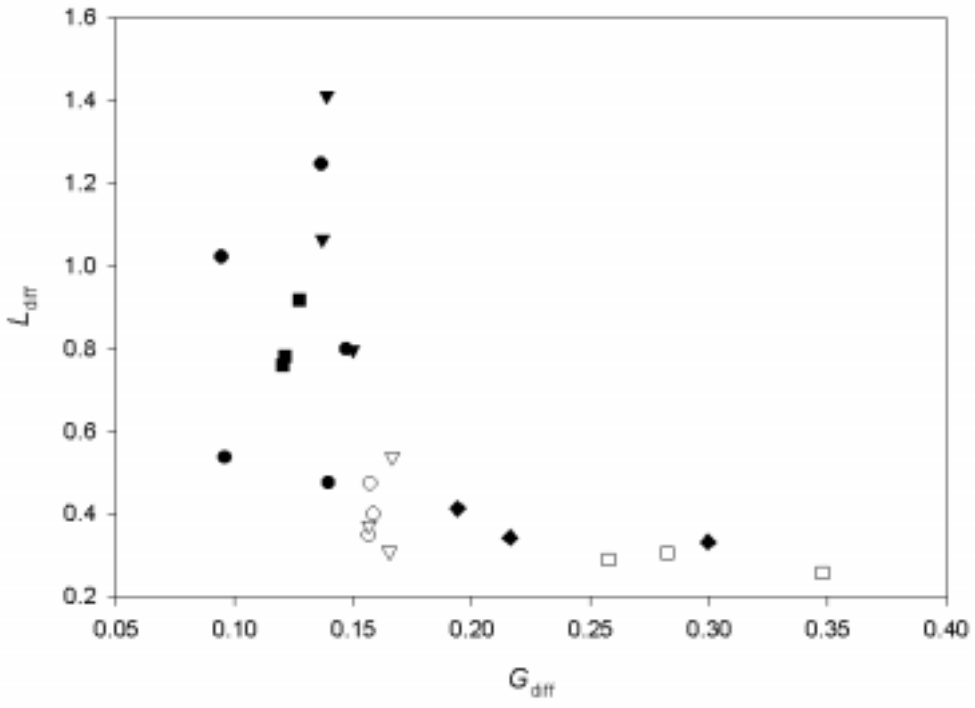


**Figure 5.7**: Relationship between the diffusion limitation index ($L_{diff}$) and diffusive conductance ($G_{diff}$) in the right gill of *Haliotis iris*. Replicate data from individual animals bear the same symbol.

or an increase in the mean $Po_2$ gradient between the haemolymph and the ventilatory water (equation 5.3). The corresponding increase in $L_{diff}$ implies that the latter mechanism is reducing $G_{diff}$. Low $G_{diff}$ may therefore be attributable to physical increases in the diffusive resistance of the exchange surface, perhaps due to mucus accumulation, causing an increased haemolymph-water $Po_2$ gradient. Above a $G_{diff}$ of 0.2 µmol $O_2$.$kg^{-1}$.$min^{-1}$.$Torr^{-1}$, $L_{diff}$ can attain an apparent asymptote of ~0.3, at which point diffusive capacitance is presumably influenced exclusively by increased convection or reduced overall $O_2$ consumption. If, as shown above, the ventilation/perfusion conductance ratio is well matched, Piiper and Scheid (1984) suggest that $L_{diff}$ must be less than 0.37 before a counter-current exchanger has inherent advantage over a co-current system. Interestingly, measured $L_{diff}$ in fish gills rarely, if ever, enters this region, while it can be attained in the resting abalone gill.

Very little data is available for diffusion limitation in other molluscs. Using mean $Po_2$ values published for the conch, *Busycon* (Mangum and Polites 1980), $L_{diff}$ was estimated to be 0.37 for the pectinibranch gill plus mantle gas exchanger. Piiper (1982) suggests that low $L_{diff}$, such as the values determined in *Busycon* and *H. iris*, implies greater functionality under hypoxia.

*$Po_2$ Overlap*

An alternative ratio, related to $L_{diff}$, was proposed by Piiper and Scheid (1984) to examine $Po_2$ overlap (*u*) in the pre-branchial and post-branchial fluids (table 5.2). The overlap ratio returns a value between 1 and –1, describing perfect and non-existent $O_2$ transfer, respectively. Values greater than zero imply a level of efficiency only attainable from a true counter-current exchanger. The calculated *u* for the abalone right gill was close to zero (table 5.2), indicative of an efficient system where exhalant water and efferent haemolymph are well equilibrated (figure 5.4).

# 5.5. Conclusions and future work

Data presented here show the right gill of *H. iris* functions as an efficient gas exchange organ and implies that the paired bipectinate gill system is well suited to meet the oxygen demand of the resting abalone. The capacity of the system to accommodate an increase in oxygen demand now remains to be determined. Neutral values for $L_{diff}$ and the ventilation/perfusion conductance ratio suggest that both ventilation and perfusion would have to be increased to effect an increase in $Mo_2$. Data presented in chapter 4 show that *H. iris* displays little ability to alter its endogenous ventilation rate. However $Mo_2$ in abalone can be increased considerably (e.g. Donovan and Carefoot 1997). The results presented here suggest that simply increasing the rate of gill perfusion will not bring about an increase in $Mo_2$. However, more refined systems may operate, the most obvious being the recruitment of additional lamellae. Resting fish perfuse approximately 60% of their lamellae at rest, the bias being towards the basal side, distal lamellae are recruited as $Mo_2$ increases (Randall and Daxboeck, 1984). Abalone may employ a similar system, utilising lamellae towards the anterior (distal) end of the gills to increase diffusive area. Alternatively, adjusting the relative contribution made by the left and right gill could bring about flexibility in gas exchange. This suggestion has become the focus of on-going work by the authors (see chapter 6).

On the basis of the findings presented there is no reason to suggest that inherent inefficiencies in the bipectinate design as a gas exchanger have driven evolutionary processes towards its abandonment in higher prosobranchs. The authors concur with the sentiments of Scheid (1982) who, having compared alveolar and parabronchial lungs to gills concluded that, while the systems theoretically have very different efficiencies they are likely to be similar under real situations, which are *therefore unlikely to drive the evolution of a particular organ design.*

# Chapter 6

# Oxygen uptake regulation by heterogeneous perfusion of the paired bipectinate gills of the abalone

## 6.1. Introduction

*Paired organs*

Over the course of evolutionary time, gastropod molluscs have tended to abandon the bilaterally-symmetrical body plan and paired organs characteristic of ancestral forms (e.g. Fretter and Graham 1994). Amongst the prosobranch gastropods the need to accommodate the visceral organs within a coiled shell has led to a characteristic reduction or loss of the ancestral right-side organs (e.g. Voltzow 1994). A small number of extant archaeogastropod families, however, have retained functional right-side organs, the most successful and accessible being the Haliotidae. Haliotids, or abalone, are not bilaterally symmetrical, the visceral organs being displaced to the left by the large right shell adductor muscle (Yonge 1947). Right and left kidneys have been retained but are morphologically and functionally disparate (Harrison 1962) and have lost any specific association to the right or left-side vasculature (see chapter 3). The right and left gills*, however, are morphologically similar (Crofts 1929, chapter 3 – this thesis), they are supplied from a common haemolymph space and drain into the corresponding left or right auricle of the heart. Thus the gills and associated vasculature apparently resemble the ancestral condition.

*Importance of the right gill in gas exchange*

McMahon and Wilkins (1983) state that "attainment of oxygen is the major modifying factor in the evolutionary design of, and major controlling factor in the operation of, respiratory systems". In agreement with this sentiment, the examination of the efficiency of acquisition of $O_2$ has formed the basis for the current studies of the abalone gills. In the previous chapter the gas exchange efficacy of the right gill of *Haliotis iris* was examined. The gill was found to be surprisingly efficient, with ventilation, perfusion and diffusion all well matched. However, the study focused specifically upon gas exchange in resting animals, raising two obvious lines of enquiry. Firstly, the

* The terms 'gill' and, more correctly, 'ctenidium' are used synonymously in this study.

relative contribution of the left gill needs to be established before the efficiency of the complete gas exchange organ can be reliably assessed. Secondly the capacity of the gill system to accommodate increased oxygen demand must be established. The current study addresses both issues by comparing flow and oxygen levels of the haemolymph leaving either gill with the abalone at rest and whilst recovering from severe hypoxic stress. A further requirement for the integrated description of oxygen uptake in *H. iris* is to consider the role of other putative gas exchangers; these investigations have been addressed elsewhere (chapter 4).

*Effects of Activity*

The objective of the present study was principally to quantify the relative contribution of the left and right gills of resting and stressed abalone. However, a number of serendipitous opportunities were presented to examine these parameters whilst the animal displayed its typical avoidance behaviours of either clamping to the substratum or raising and twisting its shell. The greater part of the abalone's tissue bulk is composed of powerful muscle blocks, notably the right shell adductor muscle and the foot (the foot alone represents 66.1% of flesh weight in *H. cracherodii*; Jorgensen et al. 1984). The capacity to maintain haemolymph circulation in conjunction with substantial contractions of these muscle blocks has long been a topic of interest (e.g. Bourne and Redmond 1977a, Russell and Evans 1989). Reciprocally, the abalone's ability to protect delicate vasculature from potentially damaging pressure surges caused by acute muscle contraction is perhaps of even greater importance.

*Metabolic responses to stress*

An animal's metabolic rate increases during periods of stress. The increased energy demand will be accommodated by an increase in aerobic metabolism up to the individual's aerobic threshold, beyond which some, or all, metabolic energy requirements must be met by anaerobic respiration. Abalone are facultative anaerobes, readily switching to particular anaerobic pathways that have formed the basis for many other studies (e.g. Wells and Baldwin 1995, Gäde 1988). In contrast, the present study has focused on the aerobic capacity of the abalone, in other words the amount of reserve present in the gas exchange system at rest that can be brought into play as $O_2$ demand increases. In related studies it has been determined that the gills are the site of almost all oxygen uptake in *H. iris* resting in normoxic seawater and that the fraction of $O_2$ taken up by the gills increases with increasing hypoxia (chapter 4 of this thesis). When searching for reserve capacity in the gas exchange systems of abalone, it therefore seems reasonable to focus on the gills.

As mentioned, abalone will readily operate beyond their aerobic threshold and thus incur an oxygen debt. Hence it is of considerable physiological relevance to also determine the extent to which the gas exchange system is up-regulated to accommodate the need to repay $O_2$ debt. Hence, in addition to an examination of gill performance under resting conditions and extreme stress (maximum demand), the interim recovery period has also been studied. The Blackfoot abalone, *Haliotis iris* Martyn 1784 was chosen as the experimental subject, to compliment previous studies

describing the efficiency of oxygen uptake at the right gill in this species (chapter 5). The perfusion rates and oxygen removal by the left and right gills were compared over a range of $O_2$ demands. A hypothesis was constructed on the basis of the conclusions of the previous chapter, stating that the contribution of either gill would be similar and that a modest reserve capacity to increase $O_2$ uptake might be seen as increased perfusion if some lamellae normally remained unperfused at rest.

# 6.2. Methods

*Collection and holding systems*

Adult *Haliotis iris* (250 – 615g, mean 367.8g) were collected between January and March 2002 from South Bay, Kaikoura (New Zealand) and held as described in chapter 5. Animals were held in the recirculating seawater facilities of the University of Canterbury for at least 2 months prior to experimentation during which time they received a diet of Adam & Amos™ AAFD pellets and *Gracilaria* spp. fragments fed *ad libitum*. Experiments were conducted between April and July 2002.

*Experimental design*

Haemolymph flow and net oxygen contribution of both gills was examined under 3 predefined conditions:

STRESSED – Describes the condition of the abalone immediately after immersion in the experimental system. The animal has just endured approximately 1h of hypoxia, desiccation and physical trauma associated with cannulation and Doppler probe positioning. This condition was arbitrarily deemed to prevail for 2h after cannulation and 1h after any subsequent handling.

RESTING – The animal has remained undisturbed for at least 24h, visual inspection shows the animal to be alert, with all tentacles extended ('Alert', using the definitions of Donovan and Carefoot 1998) and its tissues re-inflated, indicating haemolymph volume recovery (see chapter 2).

RECOVERING – Intermediate condition between the above. Typically within 12 - 24h of cannulation, abalone still appears clamped ('Quiescent' in the Donovan and Carefoot (1998) system), its cephalic and epipodal tentacles are withdrawn, the soft tissues are presumably still recovering lost fluid volume (chapter 2).

The experimental design stipulated that oxygen partial pressure ($Po_2$) should be determined in triplicate, paired samples of left and right post-branchial haemolymph for each of the above states. A simultaneous record of haemolymph flow from either vessel and heart rate were also to be taken during the period of haemolymph sampling (typically 2 – 3 min per vein). However, the logistical difficulties associated with the simultaneous maintenance of patent cannulae and reliable Doppler signals (measuring haemolymph flow), as well as the idiosyncratic nature of individual animals, invariably led to a compromise in the design.

On several occasions animals exhibited characteristic avoidance behaviour, either clamping to the chamber floor or raising and twisting the shell. Where possible the above parameters were also measured under these activity conditions.

*Animal preparation*

Abalone were starved for 24h prior to any handling, all manipulations took place in moist air at 4 - 6°C above an ice bath covered by seawater-soaked cloth. Initial preparation required the use of a high speed diamond grinding wheel fitted to a flexible-shaft Dremel™ drill to cut two openings in the shell. The first measured approximately 20x10mm and exposed the posterior section of the right efferent ctenidial vein (figure 6.1). A second, 40x10mm, opening was cut ventrally to the first, immediately above the thickened shell margin to expose the left mantle surface (figure 6.1). Two 1.5mm holes were drilled, one dorsal, and one ventral to the pericardial region. Impedance coupler leads (0.202mm insulated copper wire) were secured to the shell and their exposed ends sealed into the holes with cyanoacrylate glue (heart rate assessment using the impedance coupler is described below). The animals were given 2 – 7 days to recover in the holding system.

Once recovered, i.e. alert and feeding and showing no sign of tissue damage or haemorrhage, each abalone was cannulated as follows. A 20cm length of 0.6mm internal/ 0.8mm external diameter polyethylene tubing with a tapered end was threaded through the sleeve of a custom-built pulsed-Doppler assembly (see below and figures 5.2a - c). A 23gauge needle was used to puncture the right efferent ctenidial vein approximately 10mm anterior to the pericardium, the tapered cannula was inserted for a distance of 5mm retrograde to the haemolymph flow. The cannula was tested for patency and secured to the shell with cyanoacrylate glue. The Doppler crystal was manoeuvred onto the mantle surface immediately posterior to the cannula insertion point by using its leads. The leads were then secured to the shell by means of a friction mount, permitting subsequent minor adjustments in crystal position.

The left efferent ctenidial vein was located by carefully displacing the mantle roll dorsally, the vein could then be identified by 2 fine lines of lateral cartilage running antero-posteriorly along the left mantle, defining the vessel walls. Haemolymph sampling and Doppler signal reliability were improved by use of a u-shaped cannula which was prepared and mounted as described above. The cannulae were stoppered, the impedance and Doppler leads connected and the animal placed into an experimental chamber. Each chamber (described in detail in chapter 5 and figure 5.3) consisted of a 1.0 litre circular polycarbonate bowl that housed the animal on a removable surface. The chamber was constantly supplied with high quality, 15°C seawater from a recirculating reservoir.

*Heart rate*

Heart rate was determined with the use of an impedance coupler (Strathkelvin Instruments A100) connected to fine, insulated leads with bare ends contacting the epidermis either side of the pericardium. A clear signal was obtained as impedance varied due to tissue movement during the ventricular pulse. Impedance coupler output was digitally recorded using PowerLab™ 4/20

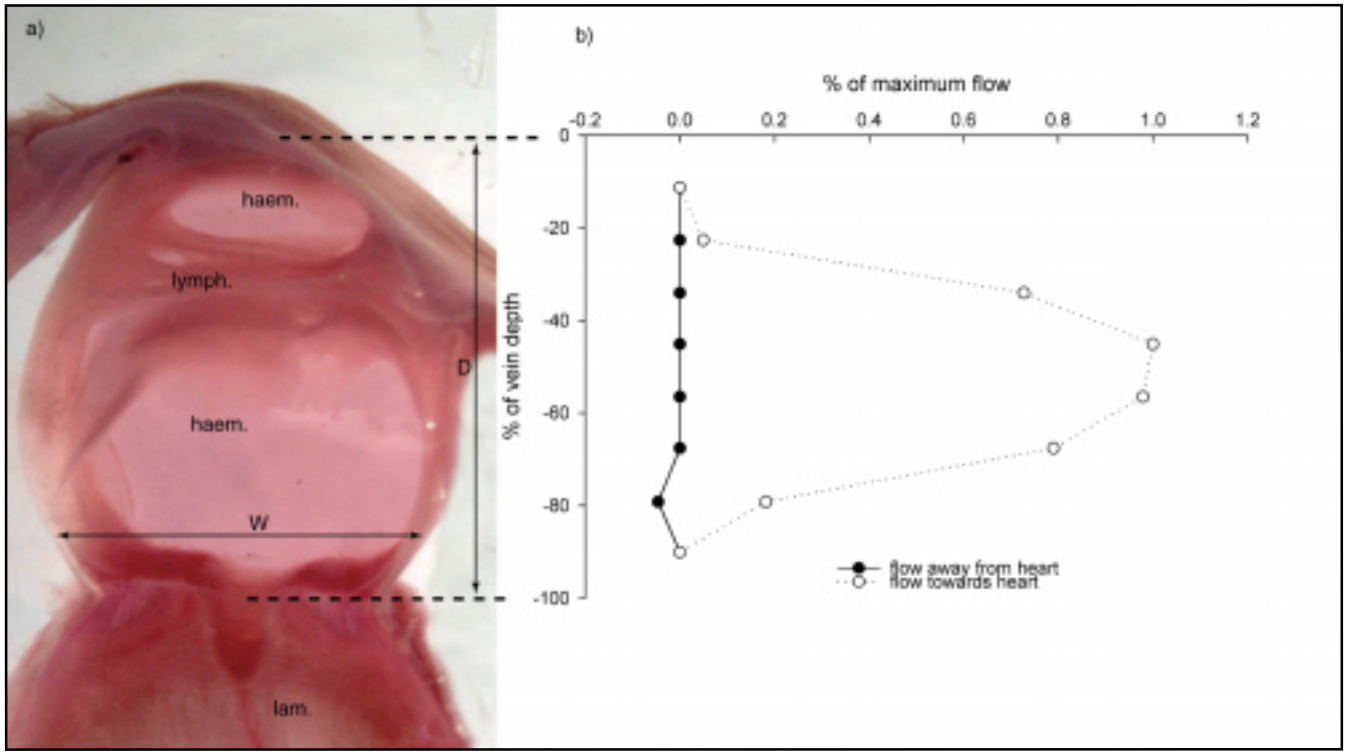


**Figure 6.1**: Position of shell windows cut in *Haliotis iris*. Dorsal window A allows access to the right efferent ctenidial vein, ventral window B to the left efferent ctenidial vein (chapter 6) and aorta (chapter 7). Window C is scored and left *in situ* over the heart to allow later exposure of the pericardium (chapter 7). Arrows indicate positions of two 1.5mm holes drilled to accommodate impedance coupler leads, seen here coiled around a cork for storage whilst the animal recovers in the holding system.

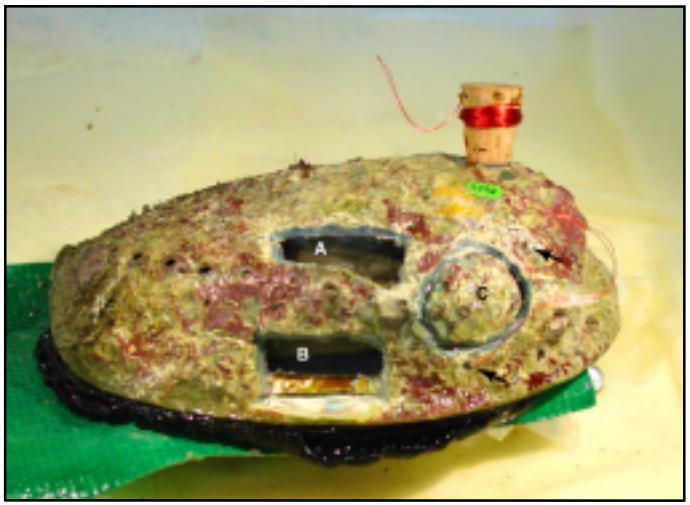


**Figure 6.2**: **a)** Image showing TS of right efferent ctenidial vein of *Haliotis iris*, hyper-inflated with amaranth-stained gelatin. Haemocoelic spaces (haem.) and 'lymphoid' tissue (lymph.) are marked, along with the depth (D) and width (W) dimensions. **b)** Velocity flow profile from a representative animal, showing a parabolic distribution. Point velocities are mean flow velocities expressed as a fraction of the peak measured velocity.

(ADInstruments) data acquisition hardware and Chart™ 4.1.2 (ADInstruments) software. The rate-meter function of Chart™ was used to determine mean heart rate by counting peaks during the desired period.

*Haemolymph flow measurement*

Haemolymph flow rate was determined by Doppler sonometry. A piezoelectric crystal transceiver transmits an acoustic 20 MHz signal and receives an echo of shifted frequency, the magnitude of which is determined by the direction and velocity of the reflecting surfaces. The pulsed-Doppler flowmeter was developed to measure blood flow in vertebrates where sufficient red blood cells circulate to reflect a clear signal (Anon. 1986, Levick 1991). Trial and error has shown that, with a little modification, the same device can reliably measure flow in abalone haemolymph provided crystal orientation and very close proximity to the vessel wall are maintained. It is assumed that large proteins in suspension, principally haemocyanin, reflect the ultrasound. A directional pulsed-Doppler flowmeter (Bioengineering 545C-4) translated the Doppler frequency shift into an audible signal and electrical output. Signals from the left and right efferent ctenidial probes were acquired simultaneously using the PowerLab equipment described above. Once a signal was acquired minor adjustments were made to the crystal position and focal range until a maximal signal was obtained.

The notoriously problematic task of calibrating the Doppler flow signal (e.g. Farrell and Jones 1992) was attempted in two ways. The first involved the creation of an *in situ* calibration curve for each crystal placement. At the end of the experiment the abalone was decapitated and the ventricle cut to create a low resistance path for the calibrating perfusate. A suspension of zeolite particles (<80µm, commercial barbecue deodorizer) in seawater was passed through the right efferent ctenidial cannula at a range of flows using a calibrated peristaltic pump, and the Doppler signal recorded. Chart™ software was subsequently used to integrate each calibration signal that was then standardised by time to produce a mean output in mV. Mean output at each flow rate was used to generate a calibration curve translating mV into mL.min$^{-1}$.

The second calibration technique adopted the approach usually used in humans (Levick 1991), where geometric assumptions are used to calculate velocity using the *Doppler equation* (equation 6.1, Anon. 1986).

$$V = \frac{F_d.C}{2F_o.\mathrm{Cos}A} \qquad \text{Equation 6.1}$$

Where $V$ is the mean velocity of blood (mm s$^{-1}$), $F_d$ the Doppler shift frequency (in this machine 0.5V º 1KHz shift), $C$ is the velocity of sound in blood (1,565,000 mm s$^{-1}$), $F_o$ the transmitter frequency (20,000 KHz) and $A$ the angle between beam and blood velocity vector, *assumed* to be 45º.

Vessel cross-sectional area was determined by a low-pressure injection of gelatin dissolved in seawater and coloured with amaranth. The tissues were fixed in 70% ethanol in seawater and the right efferent ctenidial vein dissected. A calibrated digital micrograph was taken of the transverse

section corresponding to the crystal position, the right efferent ctenidial vein perimeter was defined and its area calculated using image analysis software, Scion Image™ beta 4.0.2 (downloaded from: www.scioncorp.com). The product of vessel cross section and velocity gave an estimate of mean instantaneous flow. Both of the above calibration techniques were then repeated on the left efferent ctenidial vein.

Equation 6.1 was devised to describe mean flow velocity in a mammalian blood vessel of circular cross-section. It was assumed that blood flow was laminar with a parabolic profile and that the Doppler signal is acquired from the fastest, midstream flow which is therefore exactly twice the mean flow velocity (Anon. 1986, Vogel 1994). The assumption may be invalid in the efferent ctenidial veins of abalone due to the presence of a thick band of connective and 'lymphoid' tissue (Crofts 1929) transecting the lumen. The assumption of parabolic flow tested by plotting the Doppler signal strength against focal depth, which was increased in 50mV (= 0.5mm penetration) increments.

Mean haemolymph flow during a sample period (typically 2 – 5min) was determined by the use of Chart™ software to calculate mean integral Doppler signal (integral($V$/d$t$)) which was then processed using the 2 calibration techniques described above. Where known-flow calibration data were available, the technique provided consistent values that were not prone to the vagaries of geometric assumption. Hence, wherever possible, the *in situ* calibrating flow technique was used to determine absolute flow. On numerous occasions however, it was impossible to obtain a calibrating signal due to changes in crystal position or cannula blockage before calibration could be carried out, in these instances a geometric calibration was used.

Morphometric determination of vein cross-sectional area proved unreliable, as the vessels were prone to lateral compression during sectioning. A more stable dimension was the diameter measured across the lamellar drainage surface ('D', figure 6.2a) which was supported by the elaborate cartilage skeleton of the lamellae. The vessel was assumed to have a circular cross-section with this diameter and the flow calculated accordingly (area = $\pi(0.5D)^2$). To assess the validity of the geometric technique, predicted flows were compared to those determined by known-flow calibration in individuals where both were available. Geometric flow estimates were more variable and slightly lower (83.4 ±4.7% of known-flow) but considered acceptable in cases where no other calibration was available. Geometrically calibrated flows were accordingly corrected (multiply by 1/0.834) to provide the best estimate of flow.

It was critical to ascertain that the flow data were genuine and that an absent signal did not simply represent flow below the detection threshold of the Doppler flowmeter. The signal threshold of the device varied depending upon the specific crystal placement, however, it typically provided readable signals when calculated velocity exceeded 2 – 3mm.s$^{-1}$. Minimum measurable volumetric flow was subsequently dependent upon vessel diameter and therefore varied considerably between individuals. Typically individual pulses of 0.01 – 0.02mL could be detected (3 – 6% of stroke volume – see chapter 7). The Doppler flowmeter was equipped with an acoustic output that proved rather more sensitive than the recordable electrical signal; during 'no-flow' periods measured in the

left efferent ctenidial vein no audible signal was apparent, implying true cessation of flow. Although the left gill is somewhat longer than the right (Crofts 1929), the radii of the efferent veins were not significantly different ($t_{.025,19df} = 1.02$, $p = 0.32$), calculated cross-sections were 8.32 ±1.26mm$^2$ for the left and 6.58 ±0.70mm$^2$ for the right efferent vein (n = 20). It is, however, noted that the Hagen-Poiseuille equation shows that volume flow is proportional to the fourth power of vessel diameter, small differences in diameter therefore have a major impact on flow rate (Vogel 1994). Hence, whilst low signal cut-off may tend to underestimate low flows, the error should apply equally to both gills.

*Oxygen partial pressure measurement*

Haemolymph was sampled at the intervals described below to determine the partial pressure of oxygen leaving either gill. A Hamilton Gastight™ syringe was used to anaerobically sample 100µL of haemolymph by directly fitting the fixed needle into the cannula line. This initial sample was used to clear dead-space and 'prime' the oxygen electrode. A second 100µL were then withdrawn and injected into the electrode chamber, $P\mathrm{o}_2$ was recorded after a 2min stabilizing period. Whilst it was impossible to measure left and right efferent ctenidial $P\mathrm{o}_2$ simultaneously in this way, all samples were paired and taken within 5min of each other. The sampling order was randomised.

Seawater was sampled to determine $P\mathrm{o}_2$ in conjunction with paired left and right post-branchial haemolymph samples. Circulating water in the experimental container was taken to represent inhalant $P\mathrm{o}_2$, whilst branchial chamber water taken from immediately inside the dorsal shell holes was assumed to be exhalant (see chapter 5).

*Haemocyanin concentration*

During the course of each animal trial an additional pair of 100µL haemolymph samples were taken to determine their haemocyanin (Hc) content. The data served 3 functions, to confirm that no heterogeneity in [Hc] existed between the post-branchial sites, to allow haemolymph oxygen capacitance to be estimated and to ensure that samples were not contaminated with seawater indicating leakage.

Each haemolymph sample was centrifuged (9,000*g* for 3 min) to remove cells; 75µL of supernatant were then mixed with 900µL of aerated EDTA (pH 8.8 buffered: 10 mmol.L$^{-1}$ EDTA, 50 mmol.L$^{-1}$ glycine) in an optical cuvette (1mL, 1cm path length). Haemocyanin concentration was determined from absorbence at the oxyhaemocyanin peak of 346nm (after Nickerson and van Holde 1971). Haemocyanin copper was then calculated using the *H. iris* haemocyanin/copper millimolar extinction co-efficient, $E_{\mathrm{mM\ Cu,\ 1cm}} = 11.424$ (Behrens et al. 2002). Molar [Hc] was then determined by assuming 2 copper atoms are contained within each haemocyanin monomer.

*Net $O_2$ contribution by either gill*

Oxygen content of the post-branchial haemolymph was not determined. However, the haemolymph $P\mathrm{o}_2$ range encountered across the gills of *H. iris* in normoxic seawater keeps the haemocyanin

largely saturated (mean afferent ctenidial $Po_2$ = 37.2 ±3.6 Torr (chapter 5 of this thesis), physiological $P_{50}$ ranges from 3.9 –12.2 Torr (Behrens et al. 2002)). Consequently the haemolymph capacitance co-efficient was found to be approximately linear in the $Po_2$ range encountered across *H. iris* gills (chapter 5 of this thesis). It was therefore possible to estimate the total amount of $O_2$ transported from each gill in the haemolymph by use of the mean haemolymph capacitance co-efficient, 2.64 ±0.17 μmol.$L^{-1}$.$Torr^{-1}$ (see chapter 5). Total $O_2$ flux leaving either gill was calculated as the product of capacitance co-efficient, haemolymph $Po_2$ and haemolymph flow rate.

*Haemolymph Pressure*

On a small number of occasions simultaneous pressure records were also taken from the left and right efferent ctenidial veins. A pressure transducer (Peter von Berg DPT-3 disposable) was pre-calibrated against known manometric head ($cmH_2O$) then connected to a 2.1mmØ polyethylene tube. The pressure system was then filled with degassed, sterilized seawater and zeroed on the abalone chamber water surface. Tight concentric tubing was used to seal the pressure line into the right efferent ctenidial cannula. A few microlitres of saline were forced into the vein to establish patency before recording commenced. An identical system was connected to the left efferent cannula, the output from both transducers was recorded (via a PowerLab ML110 bridge amplifier), along with simultaneous Doppler flow and impedance signal, using the PowerLab.

Results were analysed using Statistica™ 6.0 software (StatSoft Inc., USA), generally using model I Anova with replicate samples nested within individual animal, followed by Fisher's least significant difference pairwaise comparison of means. Data are expressed as mean ± standard error of the mean.

# 6.3. Results

A total of 29 abalone yielded data in this experiment, records from 6 were subsequently discarded due to tissue damage, cannula leakage or because the animals became moribund during the course of the experiment. No animals died during the 2 – 4 days of sampling. In all of the statistical analyses performed, individual replications were nested within the corresponding treatment (i.e. state: resting, recovery or stress). All of the parameters examined showed significant inter-individual variability.

*Doppler calibration*

A transverse flow profile was constructed for the right efferent ctenidial vein of 12 individuals. In all cases a reasonable approximation of parabolic flow was observed (a representative individual is shown in figure 6.2b). There was no discernible back-flow at any point in the cardiac cycle (figure 6.2b).

*Haemolymph flow*

Total haemolymph flow through both gills increased significantly from 3.7 ±1.0 mL.$min^{-1}$ at rest to 9.2 ±1.3 mL.$min^{-1}$ under stress and declined significantly during subsequent recovery to 8.6 ±1.5

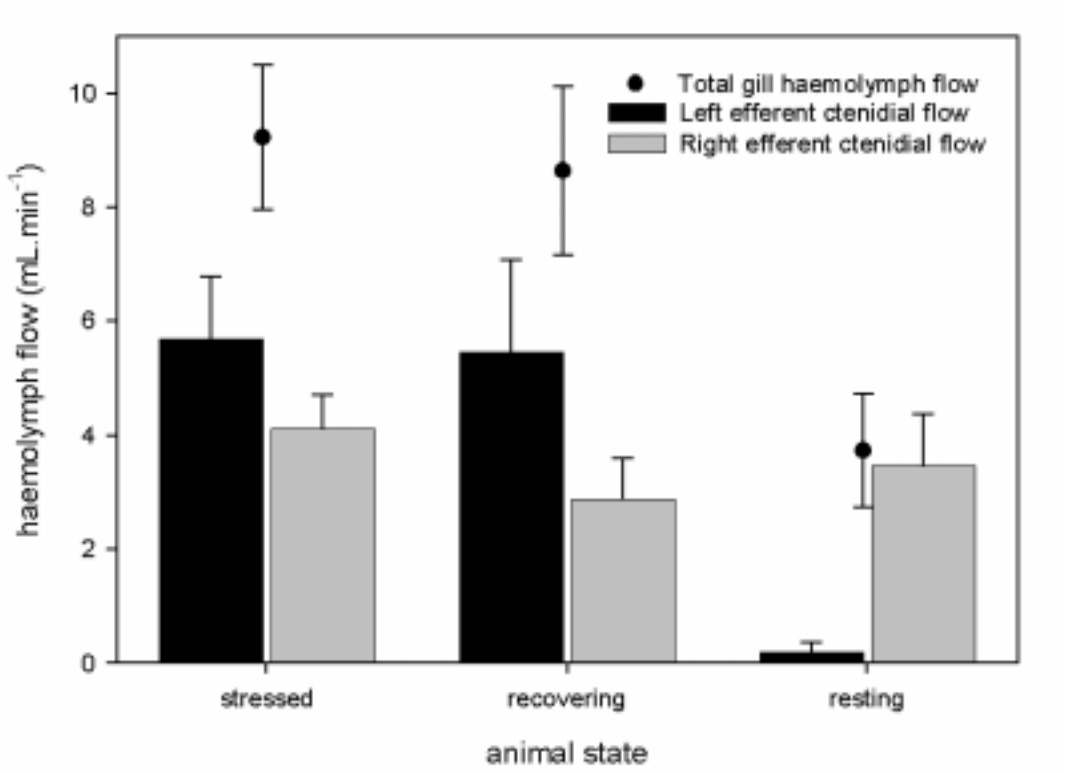


**Figure 6.3**: Absolute haemolymph flow rates leaving the left and right gills of stressed, recovering and resting *Haliotis iris*.

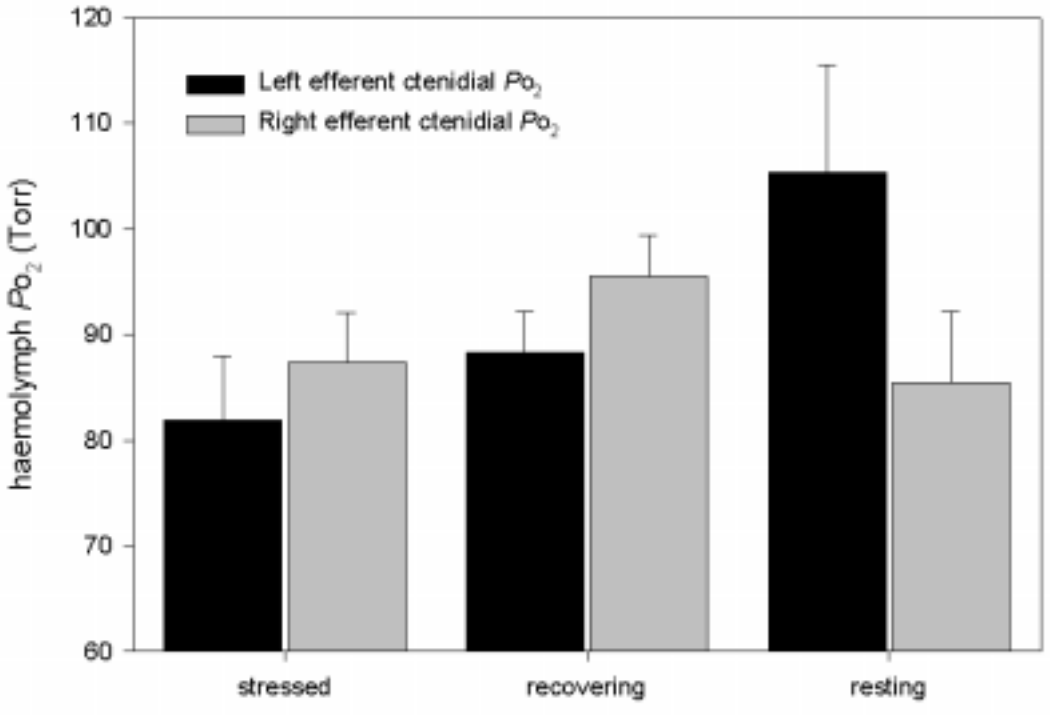


**Figure 6.4**: Mean $Po_2$ measured in the post-branchial haemolymph of the left and right gills of stressed, recovering and resting *Haliotis iris.*

mL.min$^{-1}$ ($F_{2,35}$ = 20.0, p < 0.001; figure 6.3). If total flow is standardised to biomass the 3 states remain significantly different ($F_{2,29}$ = 31.8, p < 0.001; Fisher LSD p<0.02 for all comparisons), 9.1 ±2.1 µL.g$^{-1}$.min$^{-1}$ flows at rest, 24.4 ± 3.6 µL.g$^{-1}$.min$^{-1}$ under stress and 25.8 ±5.7 µL.g$^{-1}$.min$^{-1}$ during recovery.

Mean absolute haemolymph flow leaving each gill in abalone that were resting, stressed or in an interim recovery phase, are shown in figure 6.3. There were marked left-right differences and effects of animal state. At rest the right gill conveyed virtually all of the branchial haemolymph, carrying 3.48 ±0.88mL.min$^{-1}$ compared to 0.20 ±0.16 mL.min$^{-1}$ by the left gill (n = 6). When the abalone was subjected to extreme stress, mean right gill haemolymph flow increased slightly (4.12 ±0.59 mL.min$^{-1}$, n = 15) and decreased again during subsequent recovery (2.89 ±0.71 mL.min$^{-1}$, n = 10). The difference was not significant (P > 0.22). In the left gill, perfusion increased approximately 30-fold during stress, conveying 5.68 ±1.10 mL.min$^{-1}$, rather more than the right gill. Bulk haemolymph flow through the left gill was generally maintained during the recovery period (5.46 ±1.61 mL.min$^{-1}$), but response varied between individuals.

The effect of animal state on right-left haemolymph flow difference, $\Delta Q_{R\text{-}L}$, was highly significant ($F_{2,35}$ = 15.77, p < 0.001). The substantial positive difference at rest (3.2 ±0.8 mL.min$^{-1}$) became negative when the left gill was preferentially perfused under stress (-1.6 ±1.2 mL.min$^{-1}$); $\Delta Q_{R\text{-}L}$ during recovery was somewhat greater (-2.8 ±2.0 mL.min$^{-1}$) but not significantly so (p = 0.18, Fisher LSD). If the relative perfusion of either gill is examined, the left gill is calculated to receive only 4.3 ±3.7% of total gill haemolymph at rest. Left and right gills appear to be perfused equally during stress or recovery, with the left gill receiving 49.9 ±4.1% and 52.5 ±11.4% respectively, contrary to the apparent disparity seen between unstandardised flows in figure 6.3.

*Haemolymph $Po_2$*

The partial pressure of oxygen in the blood leaving each gill showed a reciprocal pattern to flow (cf. figure 6.3 to 6.4). Right gill efferent $Po_2$ did not change between the resting and stressed states (86.8 ±4.4 Torr (n = 7) and 86.0 ±3.3 Torr (n = 11), respectively). Right efferent $Po_2$ increased slightly during recovery (95.5 ±3.8 Torr, n = 10) but, as with the corresponding decrease in flow rate, the change was non-significant (p > 0.08). During slow, resting perfusion, left efferent haemolymph $Po_2$ (114.2 ±3.5 Torr) remained significantly higher than the right (p < 0.001). The right-left $Po_2$ relationship reverses with the preferential left perfusion under conditions of stress or recovery, with left efferent $Po_2$ of 83.0 ±4.0 Torr and 85.2 ±3.2 Torr, respectively (figure 6.4). The right-left $Po_2$ difference ($\Delta Po_{2\ R\text{-}L}$) differed significantly between each condition ($F_{2,37}$ = 53.3, p < 0.001), changing in magnitude and sign from -27.4±3.0 Torr at rest to 3.1 ±2.8 Torr under stress and 9.0 ±3.4 during recovery.

*Net $O_2$ contribution by each gill*

The estimated total $O_2$ flux carried in the post-branchial haemolymph of each gill is summarised in figure 6.5. The pattern of net $O_2$ contribution made by either gill (figure 6.5) was seen to closely

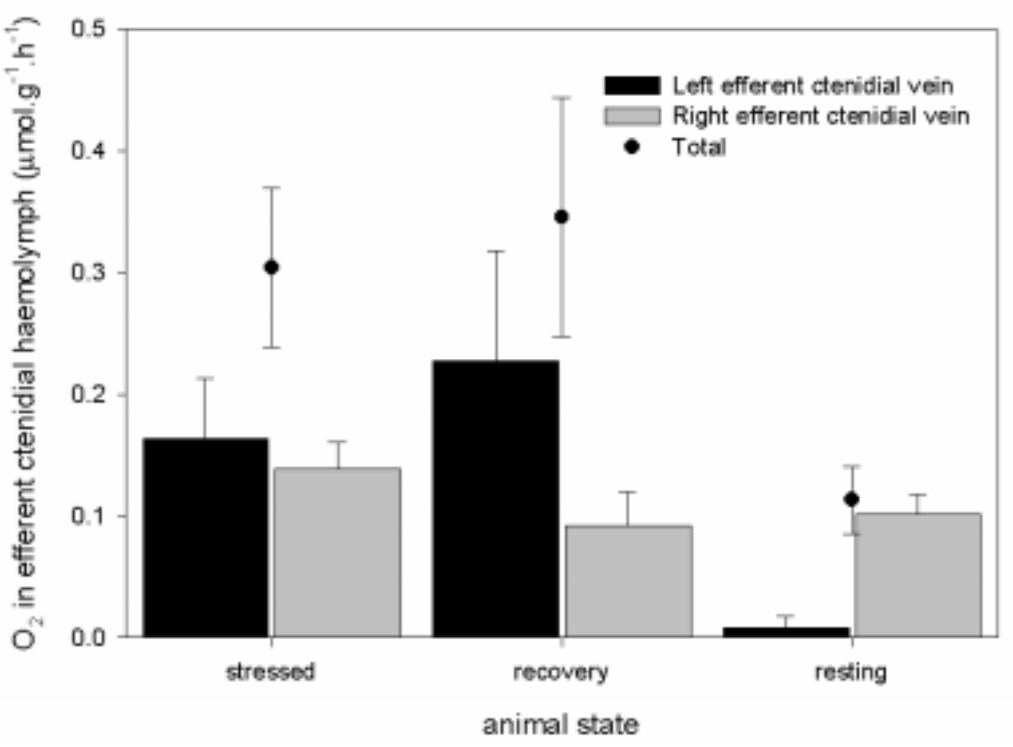


**Figure 6.5**: Estimated oxygen flux in post-branchial haemolymph leaving the left and right gill of *Haliotis iris* during conditions of stress, recovery and at rest.

resemble that of absolute haemolymph flow rate (figure 6.3 and above text). In other words, although high post-branchial haemolymph $Po_2$ were recorded in the left gill, the contribution to the animal was minimal due to limited convection (haemolymph flow).

*$O_2$ uptake from ventilatory water*

Inhalant seawater $Po_2$ was 148.7 ±0.9Torr. At rest, exhalant $Po_2$ was found to be 104.5 ±3.1Torr, exhalant $Po_2$ did not change significantly under stress (103.5 ±4.2Torr) or recovery (99.1 ±2.4Torr; $F_{2,37} = 0.8$, $p = 0.44$).

*Heart rate*

No significant decrease in heart rate was associated with the decrease in bilateral perfusion between stressed and resting animals (28.2 ±1.1 bpm and 28.5 ±0.9 bpm respectively). A small but significant increase in heart rate was observed during recovery (31.8 ±0.8 bpm; $F_{2,33} = 5.4$, $p = 0.009$).

*Cardiac cycling*

On numerous occasions the pulsed-Doppler signal was seen to cycle over a period of 7 – 11 heartbeats, apparent as a change in maximum haemolymph velocity and total haemolymph displaced through the vein during each pulse. The phenomenon was seen occasionally in either vein during recovery, but was consistently apparent in the left efferent ctenidial vein of resting abalone. The peak Doppler signal was seen to cycle from near-zero values to maximum displacement over 3 – 5 heartbeats before cycling down again (figure 6.6a).

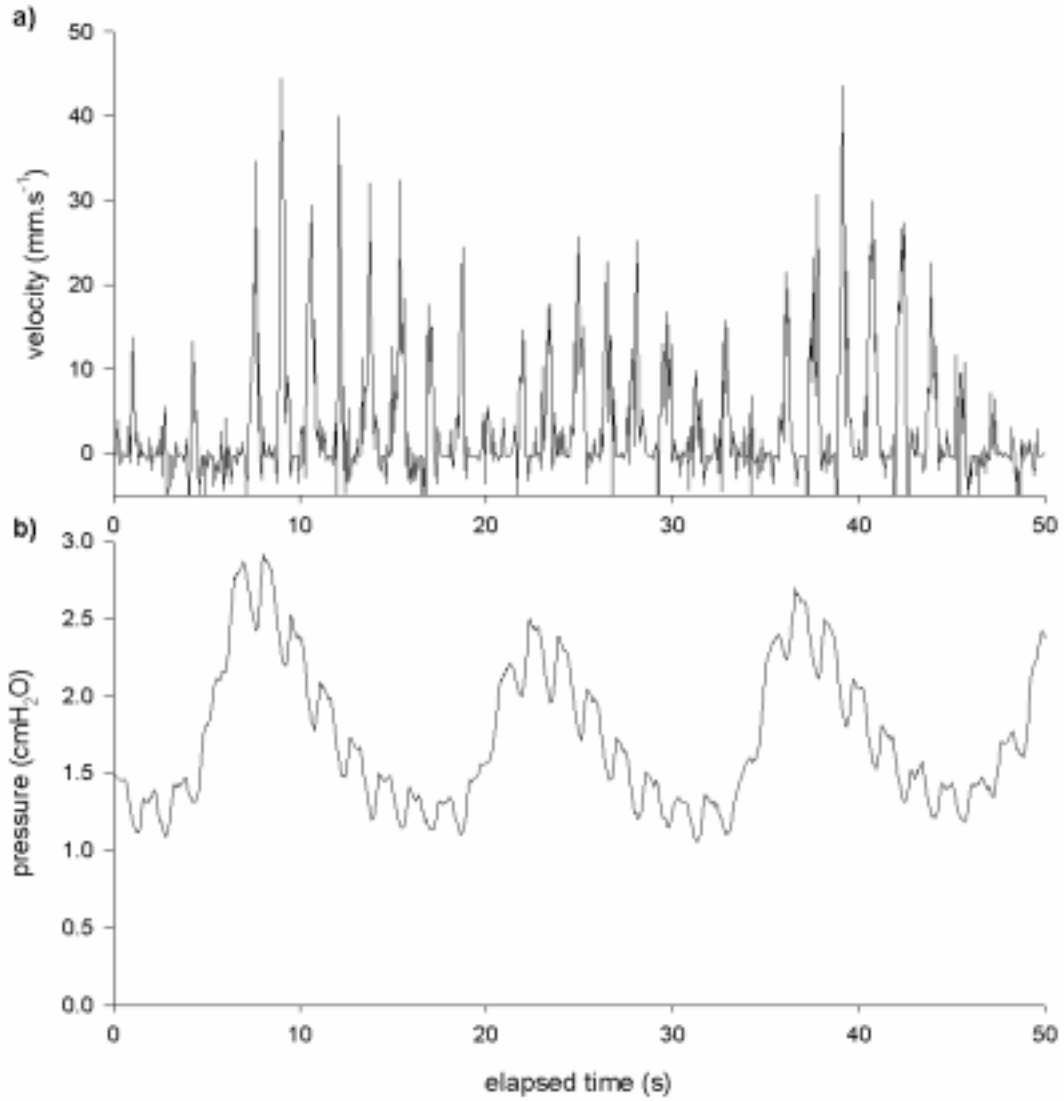


**Figure 6.6**: Reciprocal cycling of mean flow (**a**) and pressure (**b**) over approximately 10 heartbeats in the left efferent ctenidial vein of resting *Haliotis iris.*

*Pressure-flow relationship*

Reliable simultaneous records of pressure and flow from both post-branchial vessels were only obtained from two animals (partial data sets from 5 more. These data, however, proved instructive). Pressures (recorded during recovery) were low and pulsatile, mean values ranging from 4cm$H_2O$ down to ambient. Left efferent pressure was generally higher and its pulse appeared to lag behind the right slightly (figure 6.7b), but both signals were in perfect antiphase with their corresponding flow signal (figure 6.7a and b). In other words, the propagation of flow in both efferent ctenidial vessels is associated with a *fall* in pressure.

During the flow cycling described above, pressure oscillations were pronounced. The steady increase in left efferent ctenidial flow pulse was associated with a rapid *increase* in mean haemolymph pressure over 1 – 2 heartbeats. Mean pressure then followed an exponential decline lasting a further 5 – 8 beats (figure 6.7b). The magnitude of the pressure drop associated with flow appeared to increase slightly at elevated baseline pressure. A corresponding cycling of baseline pressure was

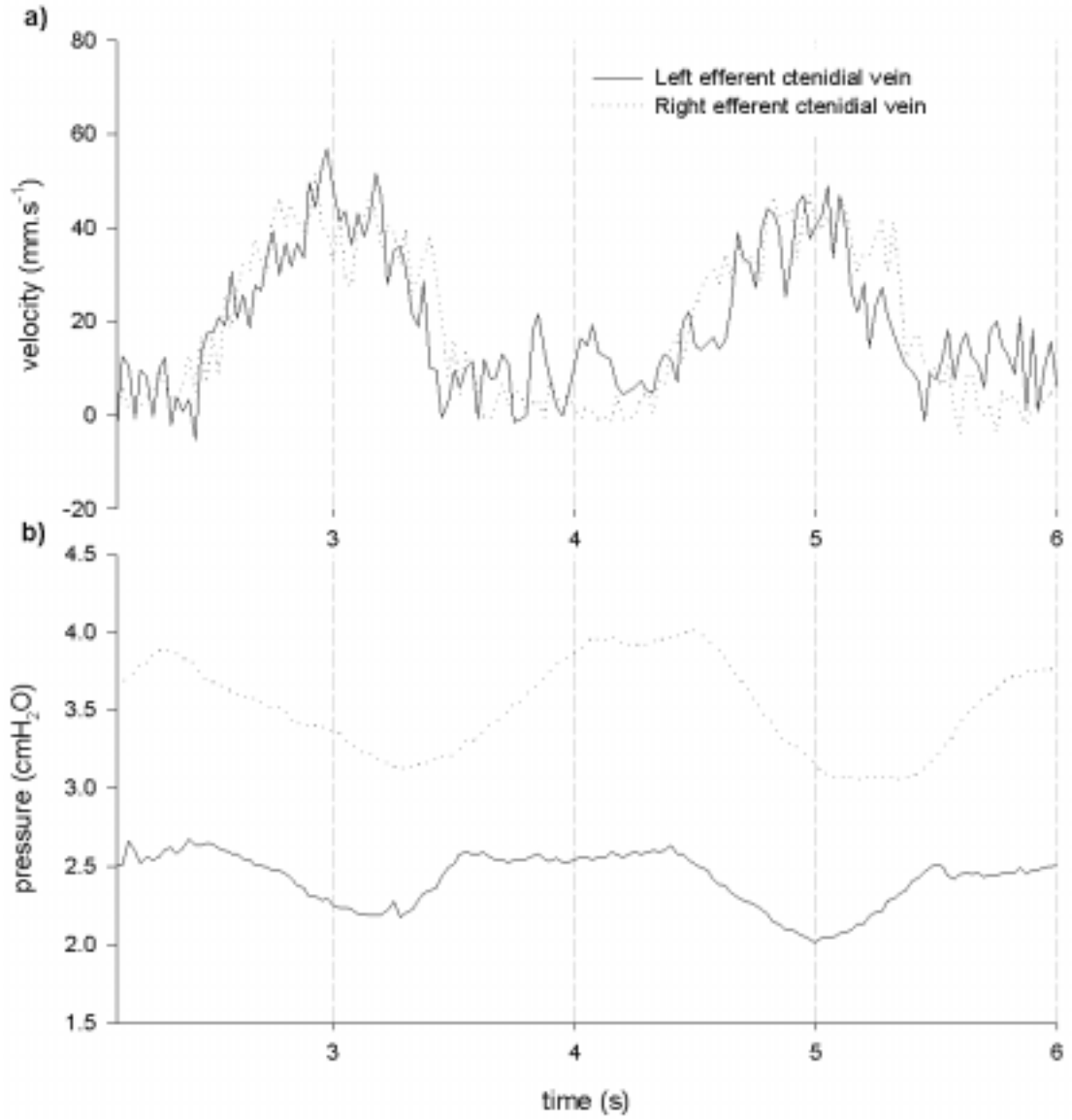


**Figure 6.7**: Pressure/flow relationships in the left and right efferent ctenidial veins of *Haliotis iris* recovering from stress. **a)** Doppler flow and **b)** pressure are shown over 2 cardiac cycles.

also seen in the right efferent ctenidial vein but the oscillations were more modest and the effect on flow indistinct.

*The effects of activity*

In 12 individuals spontaneous avoidance activity was displayed during a period of data recording, thereby allowing the effects of either clamping or shell twisting upon efferent ctenidial haemolymph flow and heart rate to be determined. Whilst the exact nature of the haemodynamic response was dependent upon individual and on the duration of activity, general patterns were apparent. At the onset of clamping (figure 6.8) or twisting (figure 6.9) heartbeat became erratic or showed complete arrest. During twisting (shaded regions of figure 6.9) the impedance signal was also disrupted by the large body movements, but efferent ctenidial flow clearly fell to zero in the left gill and became intermittent in the right gill. Normal impedance signal was rapidly re-acquired after cessation of twisting (<20s), haemolymph flow was usually detected in the right gill a few heartbeats before the

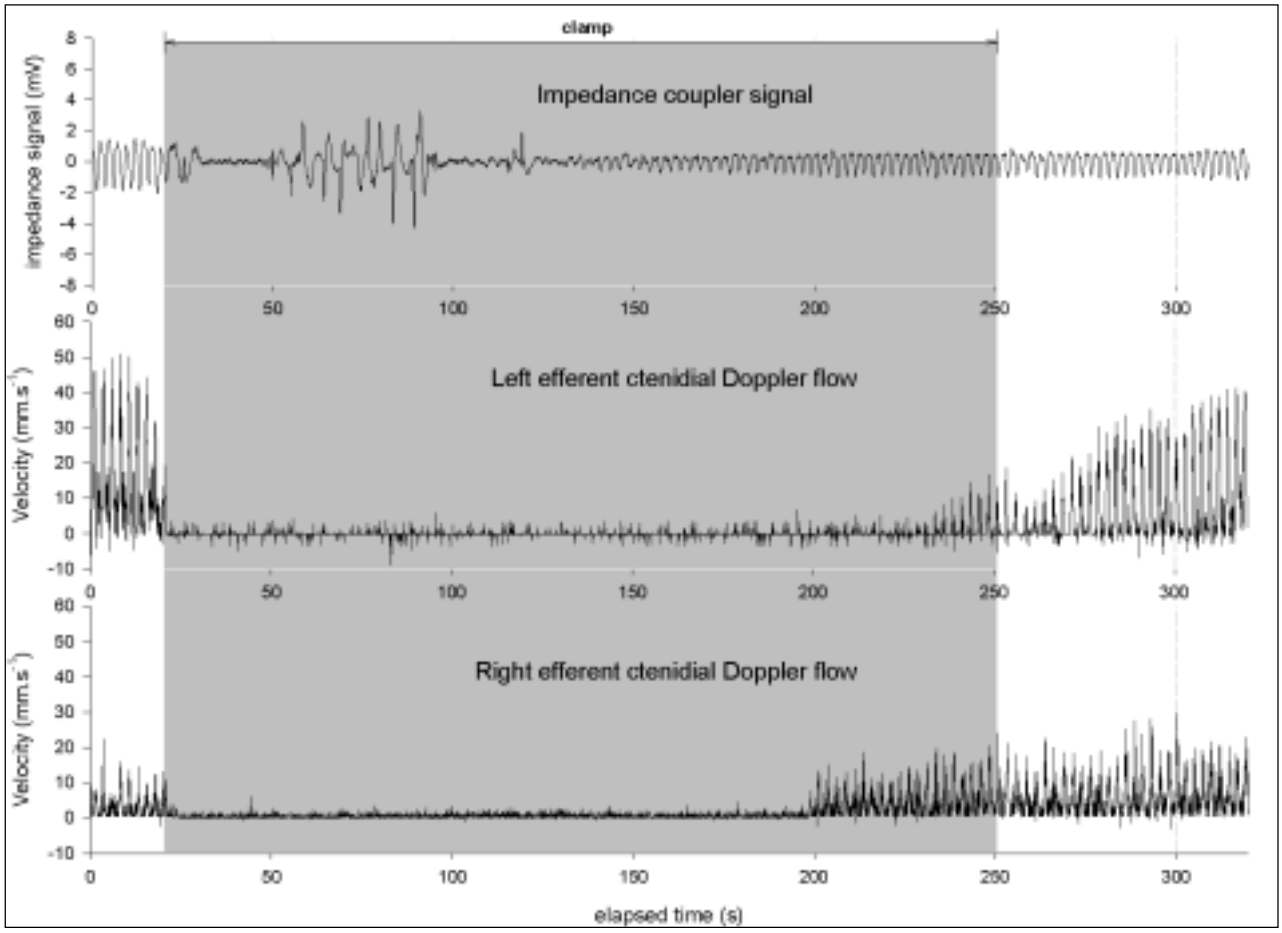


**Figure 6.8**: Effect of clamping on heart rate and post-branchial haemolymph flow in *Haliotis iris*. Shaded region represents sustained period of spontaneous clamp.

left; haemolymph flow then assumed a typical recovery pattern. If an animal clamped for more than about 60s a regular heartbeat resumed, proceeded by flow through the right and then the left gill. A recovery pattern ensued regardless of whether the animal released its clamp or not (figure 6.8).

*Haemocyanin concentration*

Mean haemocyanin levels of 0.054 ±0.004mmol.$L^{-1}$ were measured, with individual levels ranging from 0.027 – 0.092mmol.$L^{-1}$. No signs of water contamination were detected in any sample and no discernible difference was found between left and right efferent ctenidial haemolymph ($t_{.05,14}$ = -0.5).

# 6.4. Discussion

*Regulation of oxygen uptake and delivery*

If the gills of *Haliotis iris* are treated as a single functional unit, the response to stress is to increase biomass-specific gill perfusion rate by 280%, resulting in a corresponding increase in $O_2$ carried from the gills by haemolymph flow (0.10 ±0.02µmol.$g^{-1}$.$h^{-1}$ at rest, 0.28 ±0.07µmol.$g^{-1}$.$h^{-1}$ under

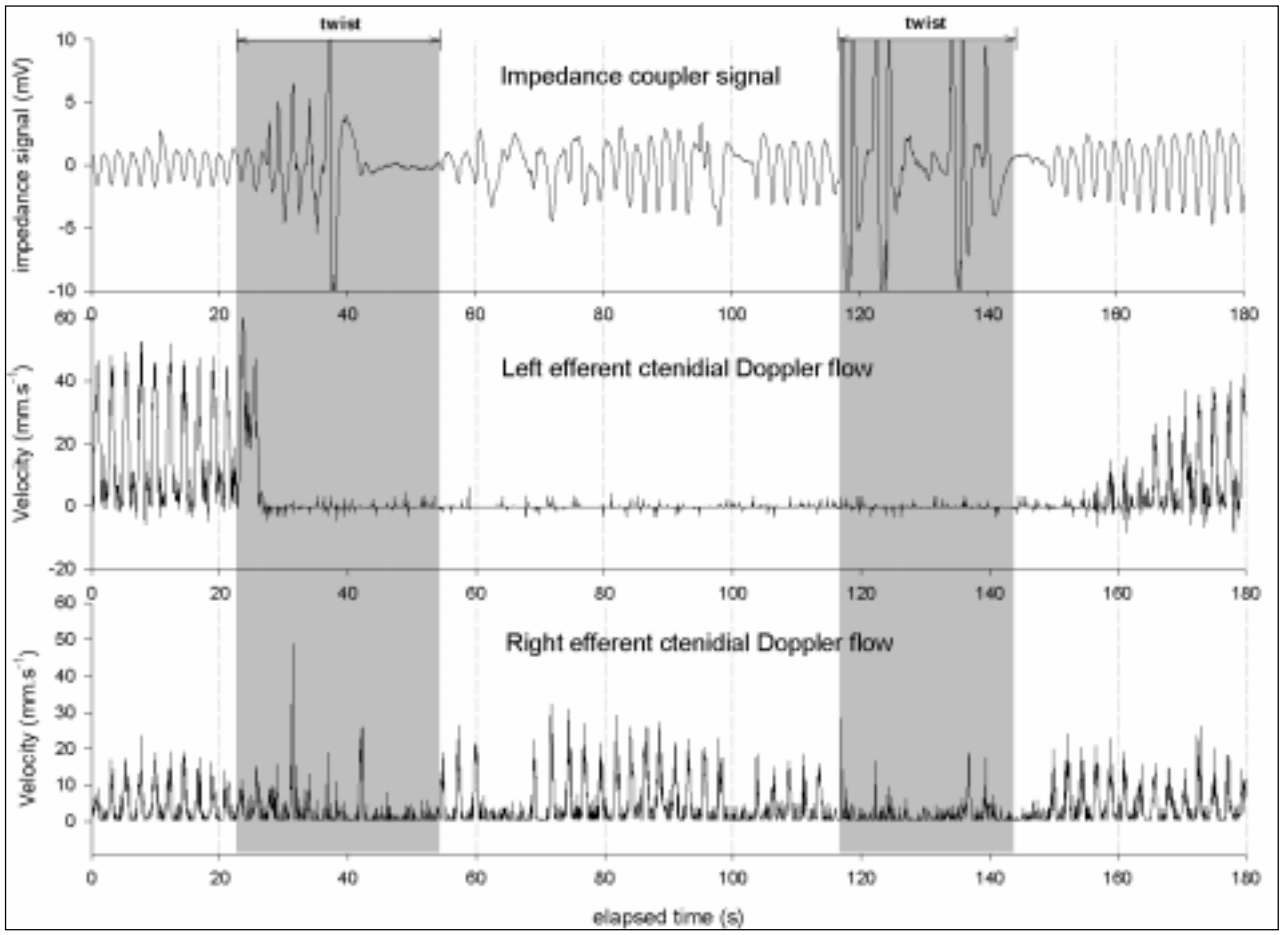


**Figure 6.9**: Effect of twisting on heart rate and post-branchial haemolymph flow in *Haliotis iris*. Shaded regions represent bouts of twisting activity.

stress). The flexibility in $O_2$ convection from the gills is consistent with the range of $Mo_2$ observed in other abalone species. For example, Donovan and Carefoot (1998) describe a 1.6-fold increase in $Mo_2$ when a previously quiescent *H. kamtschatkana* starts to locomote, whilst some individuals showed 2.5 – 3.5-fold increases at fast crawling speeds (Donovan and Carefoot 1997). Harris et al. (1998) found mean $Mo_2$ of *H. laevigata* could increase 1.88 times in response to elevated levels of environmental ammonia. The manipulations associated with cannulation, that resulted in the 'stressed' state involved extended emersion (~1h); in air the gills of abalone tend to collapse, supporting little or no gas exchange, i.e. the animal is subjected to environmental hypoxia (Baldwin et al. 1992). The mantle epidermis exposed by shell cutting was extremely sensitive to touch, hence the abalone responded to the frequent contact associated with cannulation and Doppler crystal placement by vigorous twisting of the right adductor muscle and extension of the foot. Such movements are highly dynamic for this animal and inevitably result in a state of functional hypoxia. Although care was taken to ensure no haemorrhage occurred during cannulation, it has previously been shown that abalone handled extensively lost an average of 10.1mL haemolymph.100g wet tissue$^{-1}$, approximately 20% of their haemolymph volume (chapter 2, part 2 – this thesis). The cost of volume recovery is therefore also implicit in the stress associated with handling. Once re-immersed, stressed abalone would therefore be expected to increase oxygen consumption ($Mo_2$) as part of their

stress response and to accommodate the need to repay oxygen debt, the increased $Mo_2$ is reflected in the observed increase in gill perfusion.

The 'recovery' condition is less well defined. The abalone appear to have recovered haemolymph volume (foot and epipodium extend beyond the shell margin) but are presumed to continue oxygen debt repayment. Mean total gill perfusion (figure 6.3) and estimated oxygen removal are reminiscent of the stressed condition, but are characterised by greater variability. It is suggested that oxygen uptake by the gills reaches maximal rates during stress and that these rates are sustained until oxygen debt is repaid. Increased variability is attributed to the loose definition of the recovery state.

*Heterogeneity in response between the L and R gill*

In resting abalone relative haemolymph flow through the left gill is extremely small, accounting for only 4.3% of total gill perfusion (figure 6.3). Furthermore, flow through the left gill may apparently cease for several heartbeats during a repeating 7 – 11 beat oscillation.

Critically, post-branchial haemolymph $Po_2$ showed a negative relationship to haemolymph flow. At rest, left efferent ctenidial $Po_2$ (105.3 ±10.2 Torr) was significantly higher than the right (85.5 ±6.8Torr, figure 6.4), having apparently attained equilibrium with the exhalant seawater (104.5 ±3.1Torr). The observation is consistent with a slowly perfused gas-exchange surface where ventilation has not been correspondingly down-regulated.

As oxygen demand increased during periods of stress or recovery, the functional heterogeneity between gills disappeared. Under stress the left gill received 50.4 ±4.2% of total gill perfusion, and the corresponding haemolymph $Po_2$ fell to 83.0 ±4.0Torr (figure 6.4), no longer significantly different from $Po_2$ of the right post-branchial haemolymph. Of an estimated total rate of $O_2$ convection from the gills of 0.304 ±0.065µmol.$g^{-1}$.$h^{-1}$ under stress, the left gill contributed 0.164 ±0.049µmol.$g^{-1}$.$h^{-1}$. A similar relationship between the gills prevailed during recovery but was, as mentioned above, characterised by increased variability.

*Heterogeneous function of respiratory organs in other animals*

In other animals, the study of heterogeneity between gas exchangers is usually restricted to sites that show clear morphological differences, often related to a bimodal, typically amphibian lifestyle.

Heterogeneity in the function of paired gas exchangers has, until now, been the exclusive province of the decapod crustaceans. The heterogeneity is derived from unilateral scaphognathite ventilation, observed in lobsters, shrimp, crayfish and crabs (McMahon and Wilkins 1983, Mangum 1983). In the crabs *Carcinus maenas* and *Ovalipes catharus* it has been shown that gill conductance varies enormously over the range of *in vivo* transmural pressures experienced (Taylor 1990). Positive transmural pressure, necessary for high conductance, is largely attributed to sub-ambient branchial chamber pressures caused by forward ('normal') ventilation by the scaphognathite (Taylor 1990). If a single scaphognathite spontaneously stops beating the conductance of the corresponding gill decreases presumably resulting in the preferential perfusion of the ventilating gill (Taylor 1990), an

effect that will be amplified by flow rectification due to valves in the efferent sinus (Taylor and Taylor 1986). During unilateral ventilation in the crab *Cancer magister*, mixed post-branchial haemolymph $Po_2$ was found to be lower than that leaving the ventilated gill only (McMahon and Wilkins 1983), indicating a ventilation/perfusion mismatch in the unventilated gill. In other words decapods experience unilateral apnea and probably a reduction in corresponding gill perfusion, however some haemolymph flow is maintained. In contrast, resting *H. iris* experience unilateral reduction in perfusion, almost to the point of cessation, but show no corresponding adjustment of ventilation (chapter 4).

It seems unlikely that non-perfusion of a gas exchanger module would prove a useful strategy for the higher taxa as cessation of blood flow through a complex vascular system carries the attendant risk of thrombosis. The mollusca lack clotting factors (Armstrong 1971, Taylor et al. 1994), and haemolymph generally has a low viscosity (~1.5 cps at a shear rate of 450 $s^{-1}$, Taylor 1993) increasing the perfusion strategies available.

Perhaps a closer functional analogue to the abalone gas exchanger would be the gills of fish. Whilst whole gills are not shut down in times of reduced $O_2$ demand in fish, the number of lamellae perfused typically falls to 60% of the total (Randall and Daxboeck 1984); as in abalone, the under-perfused lamellae are still ventilated. Similarly amphibians reliant upon cutaneous gas exchange may recruit additional surface capillaries during increased $O_2$ demand, in the absence of obvious augmentation to ventilation (Feder 1995).

*General ventilation/perfusion adjustments to increased oxygen demand*

With the exception of a relatively minor vascular route through the right mantle, all haemolymph returns to the abalone heart via either the left or right gill (Crofts 1929, chapter 4 – this thesis). Hence total gill flow provides a reasonable estimate of cardiac output. Total gill haemolymph flow increased from 9.1 $\mu L.g^{-1}.min^{-1}$ to 24.4 $\mu L.g^{-1}.min^{-1}$ under stress, with no associated increase in heart rate. It is therefore deduced that all cardiac compensation to increased oxygen demand occurs as adjustment to stroke volume, which increases 2.8 times from an estimated 0.37 ±0.15 mL.kg live $weight^{-1}$ to 0.99 ±0.21 $mL.kg^{-1}$ under stress (note that cardiac output and stroke volume are examined directly in the next chapter).

*Oxygen extraction efficiency during increased $O_2$ demand*

The ventilatory extraction efficiency measures the amount of oxygen removed from the ventilatory flow ($P_i - P_e$), expressed as a percentage of inhalant $Po_2$ ($P_i$). In the current study exhalant $Po_2$, and therefore extraction efficiency, did not change significantly between resting, stressed and recovery states (29.6 ±2.7% at rest, 33.0 ±3.3% under stress and 32.0 ±2.5% during recovery). Other studies (e.g. Donovan and Carefoot 1997, Harris et al. 1998) and the observed increase in $O_2$ removed from the gills by haemolymph convection, suggest that stressed or recovering abalone will consume more oxygen. If the relative contribution of the branchial chamber to whole animal $Mo_2$ requirement

does not change, ventilation rates must be elevated. As extraction efficiency remains constant, ventilation rate is expected to mirror the 2.8-fold increase in $O_2$ convection by the post-branchial haemolymph. However, direct measurements showed ventilation rates to be essentially fixed, when challenged with increasing levels of hypoxia and during subsequent recovery (chapter 4 of this thesis). Corresponding small, but significant changes in extraction efficiency were also seen when abalone were artificially ventilated at a variety of rates (chapter 4). The data imply that either the abalone's regulatory responses to progressive hypoxia and increased $O_2$ demand in normoxia are fundamentally different or that increased ventilation exploits a different exhalant route, in addition to the shell holes.

Fish also tend to maintain their extraction efficiency whilst elevating ventilation in response to increased $O_2$ demand (Scheid 1982, Randall and Daxboeck 1984). Amongst crustaceans of similar size to *H. iris*, the change in efficiency of $O_2$ extraction from ventilatory water is highly species dependant; extraction efficiency may either decrease as ventilation increases during exercise (*Callinectes*, lobsters, crayfish) or it may remain unchanged (*Carcinus*, *Cancer*; McMahon and Wilkins 1983). The extraction efficiencies of molluscs are discussed in chapter 5 of this thesis.

*Metabolic scope and expansibility*

Using the activity states defined by Jones and Randall (1978), 'standard metabolic rate' describes the true resting state, 'active metabolic rate' the state at which $M_{O_2}$ is at its maximum. It is suggested that the 'resting' and 'stressed' states defined here approximate these metabolic states and difference gives an indication of 'metabolic scope', the maximum sustainable aerobic metabolic rate (Jones and Randall 1978). As other body surfaces play a very minor role in oxygen uptake in abalone (chapter 4), all accommodation of increased $M_{O_2}$ is assumed to occur at the gills. It is therefore suggested that the $O_2$ demand flexibility of metabolic scope is met almost entirely by the left gill. If the oxygen requirements of the gill tissues remain constant, metabolic scope can be estimated from the increase in $O_2$ transported in the post-branchial haemolymph, i.e. approximately 0.191 μmol.g$^{-1}$.h$^{-1}$. A comparable strategy is adopted by bimodally breathing amphibians that tend to rely predominantly on cutaneous exchange at rest ('standard metabolism') and accommodate increased $O_2$ demand ('metabolic scope') using internal respiratory organs (Feder 1995).

*Pressure/flow relationship and the constant volume heart*

The concept of the constant volume molluscan heart was introduced by Ramsay (1952) and has subsequently gained general acceptance (e.g. Fretter and Graham 1994). The model requires all impetus for haemolymph flow to be derived from the musculature of the ventricle. Ventricular systole displaces haemolymph into the aortic trunk and during this displacement, pressure is correspondingly lowered in the pericardial fluid, expanding the thin-walled auricle(s). In other words, ventricular systole acts as a simultaneous reciprocating pump. The efferent ctenidial veins of *H. iris* drain directly into the corresponding auricles and therefore their pressures are directly influenced by the constant volume effect. Ventricular and auricular pressure are shown to be in

antiphase in *H. corrugata* and auricle and pericardial fluid to be in phase, observations that Bourne and Redmond (1977a) suggest confirm the functioning of the constant volume model in abalone. The effectiveness of auricular suction has been shown here by the highly pulsatile nature of haemolymph flow in both the right and left efferent ctenidial veins (in stressed/recovering animals), where compliance in the systemic and branchial circulation would otherwise completely damp any oscillation. Critically, confirmation of the constant volume hypothesis has lacked an *in vivo* demonstration of the antiphase relationship between pressure and flow. This relationship has been shown here (figure 6.7), where a fall in pressure is seen to drive flow in the efferent ctenidial veins (this discussion is expanded in the following chapter).

The oscillation in hydrostatic haemolymph pressure (mean circulatory filling pressure) over a 7 – 11 beat cycle was a highly repeatable observation. In contrast to the antiphase pressure-flow relationship seen in the efferent ctenidial veins during the cardiac cycle, greater volume flows are associated with the highest hydrostatic pressures (figure 6.6). Further elucidation of this phenomenon was not possible with the limited data available from the current study. Determination of the possible causes and implications of these oscillations for the systemic circulation therefore formed part of the objective of a more detailed haemodynamic investigation reported in chapter 7.

*Perfusion control*

The right gill of *H. iris* is preferentially perfused at rest, a bias that disappears as the animal's oxygen requirements increase. Clearly the relative resistance of the perfusion paths through the right and left gills are altered to bring about these observations. It appears that all the vessels associated with the gills are muscular and capable of lumen adjustment (see chapter 4). The contractility of molluscan vessels is well known, the vasoactivity in the vessels of *Aplysia*, for example, are particularly well described (Brownell and Ligman 1992). The vessels of the pinto abalone, *H. kamtschatkana*, have also been shown to react to the molluscan neuropeptide FMRF-amide (Krajniak and Bourne 1987) and to serotonin (5-HT; Krajniak and Bourne 1989). Varicose nerve fibres showing 5-HT immunoreactivity were found in the walls of all the haemolymph vessels of *H. ruber* examined by Russell and Evans (1989), including the afferent ctenidial veins. Both the left and right afferent and efferent veins of *H. iris* have been observed to locally occlude in response to severe irritation or damage (personal observation). However, the most highly developed muscular systems influencing the gills are longitudinal muscle blocks and associated cartilage located on either side of the efferent ctenidial vein at the level of the lamellar connections (figure 3.59a). Asymmetric contraction of these muscle blocks would distort the gill along its midline, occluding the median pores that drain haemolymph from the lamellae into the efferent ctenidial vein (figure 3.59b). The smaller lateral pores are unaffected by this action, hence the gill is not completely occluded; resistance, however, would be expected to increase considerably.

Alternatively resistance effects may be passive, as seen in the gills of crabs. In the crab gill a certain amount of perfusion pressure is required to inflate the lamellae, thereby lowering the vascular resistance and allowing effective perfusion (Taylor 1990). The fact that transient increases in

hydrostatic pressure of the haemolymph promoted flow in the left gill adds some weight to this suggestion. However, the left gill is larger than the right, the vessels are wider and it carries more parallel elements (lamellae) and therefore would be expected to have a lower resistance. If the perfusion effects were entirely passive, the left gill would be expected to receive preferential flow at rest. The occlusion of the median pores is therefore proposed as the principal control mechanism.

*Bloodflow and the left kidney*

The idea that haemolymph flow through the left gill can effectively cease whilst the heart continues to beat is, at first, somewhat puzzling if the efferent gill vessels are taken to be discrete and parallel. Ventricular systole causes passive distension of the auricles by transmission of negative pressure through the pericardial fluid. Equal force must therefore act on the two similar-sized auricles. As the modest flow through the left gill at rest is still highly pulsatile, it appears the left auricle still exerts an influence; reduced flow is therefore not caused by an increased resistance (occlusion) downstream of the gill. Reduced flow is therefore attributed to increased resistance in the gill itself, presenting the left auricle with 2 possibilities. The first is to only partially fill during each cardiac cycle, the second is to fill completely supplementing left efferent ctenidial haemolymph with another source. Anatomical investigations show the left kidney connects the right efferent ctenidial vein to the left auricle, with valves preventing backflow (Crofts 1929, chapter 4 of this thesis). Interestingly, a low pressure perfusion of casting resin into the right efferent ctenidial vein preferentially passes through the left kidney and fill the left auricle before the right. It therefore seems reasonable to suggest that the left auricle will inflate using supplemental haemolymph from the right efferent ctenidial vein if the left gill resistance is relatively high.

*Gill perfusion during activity*

Bourne and Redmond (1977a) note that the onset of activity in *H. corrugata* causes a transient hydrostatic pressure spike throughout the vascular system; as no net pressure gradient is developed, they predict that haemolymph flow will not be assisted by these muscular contractions. Direct flow recordings taken from the gills of *H. iris* during twisting and clamping corroborate this suggestion. In fact, rather than augmenting flow, the sudden avoidance reactions of *H. iris* can indirectly impede haemolymph circulation by causing cardiac arrest (figures 6.8 and 6.9). Cardiac arrest has also been observed in the pink abalone, *H. corrugata*, following cannulation (Bourne and Redmond 1977a). A similar phenomenon is seen during activity in the tarantula, *Eurypelma californicum*, where the prosoma flattens driving haemolymph pressure as high as 300 Torr to allow hydraulic extension of the legs; confronted with potentially damaging pressures the heart enters cardiac arrest until activity ceases and haemolymph pressure falls (Paul 1986). A similar reflex may operate in *H. iris* causing the heart to stop when confronted with even the modest pressure spikes associated with sudden movement. The aortic pressure traces recorded by Trueman and Brown (1985) also show evidence that cardiac arrest may ensue in *H. midae* following the onset of clamping (this topic is further developed in chapter 7). If the activity is sustained, normal heart rate is resumed followed by renewed flow through the right gill. The left gill typically remains unperfused until activity ceases, at which

point the animal technically enters a state of recovery and left gill haemolymph flow is correspondingly seen to rise, exceeding right gill perfusion rates (figure 6.8 and 6.9).

*Modeling gas exchange in functionally heterogeneous gills*

The previous chapter examined the extent to which $O_2$ diffusion across the lamellae of the right gill limited gas exchange; this was achieved by application of the diffusion limitation index, $L_{diff}$ (Piiper 1982, equation 6.2). An $L_{diff}$ value of 0 implies that diffusion offers no barrier to exchange, which is therefore limited exclusively by perfusion, an $L_{diff}$ of 1 would be entirely diffusion limited, with no exchange occurring regardless of perfusion rate.

$$L_{diff} = \frac{P_m - P_a}{P_m - P_v} \qquad \text{Equation 6.2}$$

Where $P_m$ is the mean $Po_2$ in the medium, $P_v$ and $P_a$ are the $Po_2$ of pre- and post-branchial haemolymph, respectively.

Scheid (1982) warns that the most common violation of the assumptions of respiratory models is the failure to account for regional heterogeneity, for $L_{diff}$ this refers in particular to heterogeneity between modules of the organ (Piiper 1982). Hence, having established the presence of functional heterogeneity between the gills of *H. iris*, it is of value to estimate $L_{diff}$ for both. Using equation 6.2, $P_m$ could be determined as the mean of inhalant and exhalant medium $Po_2$, but $P_v$, the $Po_2$ of the afferent ctenidial haemolymph, was not measured during the current experiment. Mean $P_v$ for resting abalone (37.3 ±3.6 Torr) determined in chapter 5 was therefore used. In a subset of the animals used in chapter 5 $P_v$ was also measured following handling or strenuous exercise, the mean of which was taken to be the best estimate available for $P_v$ in stressed animals and used to calculate $L_{diff}$ accordingly (stressed $P_v$ = 32.2 ±3.8 Torr, n = 12). The $L_{diff}$ of the right gill at rest was thus estimated to be 0.44 ±0.08, for the present series which is comparable to the previously measured value of 0.48 ±0.02 (chapter 5). Right gill $L_{diff}$ decreased slightly under stress to 0.40 ±0.06 as a result of the apparent increase in $P_a$ - $P_v$ difference. In the left gill, resting $L_{diff}$ was estimated to be 0.14 ±0.07, i.e. highly perfusion limited. Under stress the left gill $L_{diff}$ rose to 0.46 ±0.07, a value similar to that of the right gill and indicating that neither diffusion nor perfusion prevailed to limit exchange.

A useful model was described by Jones and Randall (1978), who used ventilatory dead-space to examine the mechanisms available for increasing $Mo_2$. Three forms of dead-space were described: 'diffusion dead-space' when the blood/water contact time is too short, 'distribution' when ventilation and perfusion conductances are mis-matched and 'anatomical' describes water taking a non-respiratory route. In fish ventilation is increased to accommodate increased $O_2$ demand, this increases the diffusion dead-space but is off-set by a recruitment of additional lamellae, reducing the anatomical and distribution dead-space (Jones and Randall 1978). In decapods McMahon and Wilkins (1983) suggest that all forms of dead-space are increased as ventilatory rates increase. In abalone, as in fish, the extraction efficiency of $O_2$ from ventilatory water does not change significantly with increased $Mo_2$, it is therefore suggested that a similar dynamic balance is achieved between diffusion and distribution dead-space.

# 6.5. Conclusions

A novel gas exchange strategy has been revealed in the abalone, *Haliotis iris*. The right gill is perfused at a fairly constant rate, regardless of demand. Right gill $M_{O_2}$ plus direct oxygen diffusion to peripheral tissues effectively supports the routine metabolism of the abalone. The left gill is chronically under-perfused in resting *H. iris*, to the extent that haemolymph flow may cease. During periods of increased oxygen demand perfusion rates in the left gill increase approximately 30-fold, matching the $O_2$ uptake of the right gill as a gas exchange organ. Oxygen uptake at the left gill therefore effectively supports the metabolic scope of the abalone. The hypothesis that the paired gills of abalone consistently perform a similar function is therefore rejected.

The recruitment of an entire gill appears to be an effective method to augment oxygen uptake. The response is coarse however, allowing little opportunity to fine tune gill perfusion to $O_2$ demand within the extremes observed.

A number of unusual mechanisms warrant further investigation. The physical mechanisms determining gill resistance should be examined, particularly in the left gill. Potential control factors (neuropeptides, direct pressure effects etc.) should also be elucidated. Haemolymph supply to the left kidney is intimately associated with the heterogenous perfusion of the gills, this relationship should be described fully in consideration of the roles of the kidney as an excretory organ and site of haemoconcentration. The capacity to temporarily shut-down a gill may have facilitated the evolutionary abandonment of the paired gill design. With the retention of only one gill, higher prosobranchs can not exploit the gas exchange regulation strategy described here. Comparative studies examining the strategies utilised by pectinibranch snails to regulate oxygen uptake would therefore be of considerable interest.

In the previous chapter a number of respiratory models, developed for use in describing vertebrate gas exchange function, were applied to the right gill of *H. iris*. The suggestion was made that these indices, scaled appropriately, could be extrapolated to represent the integral 2-gill gas exchanger. The results presented here suggest that this assumption may be valid in stressed or recovering *H. iris*, but should be re-assessed given the heterogeneity in gill function in the resting abalone.

# Chapter 7

# Heart function and the respiratory haemolymph circulation in the archaeogastropod mollusc *Haliotis iris* Martyn 1784

## 7.1. Introduction

The circulatory system of the abalone (Prosobranchia: Haliotidae) must overcome a number of specific, often conflicting challenges. The blood volume is very large, with haemolymph accounting for more than half of the flesh volume (chapter 2). However the heart is small, accounting for approximately 0.04% of wet body (NLCR unpublished data) weight and only pumping 3% of the total haemolymph volume per minute [*]. The heart of similar sized cephalopods represents 0.17% of body weight compared to 0.22% in fish, 0.6% in mammals (Wells 1992) and 0.1 – 0.3% in most other invertebrates (DeFur and Mangum 1979). The vascular beds of gastropods are considered to present a high resistance to haemolymph flow (Bourne and Redmond 1977a, Voltzow 1994). However the tissues must receive haemolymph to support both metabolic and hydraulic functions. Conversely, the delicate vasculature must also be protected from potentially damaging pressure surges caused by large muscular contractions.

Abalone show little reliance upon direct diffusion of $O_2$ to respiring tissue, nor do they tend to use secondary $O_2$ uptake sites (chapter 4 of this thesis). The gills must therefore be effectively perfused and oxygen transported to the target tissues. The fine channels of the abalone gills have been shown to offer considerable resistance to haemolymph flow, accounting for 40% of systemic pressure loss in *Haliotis corrugata* (Bourne and Redmond 1977a). However, the gills are positioned at the end of the vascular circuit, draining directly into the auricles. How, then, is a sufficiently large pressure gradient maintained to allow suitable haemolymph flow across the gills? A number of factors may assist venous return through the gills: in molluscs the volume within the pericardial chamber is believed to remain constant (e.g. Ramsay 1952, Voltzow 1994). The effect of ventricular systole therefore, in addition to propelling haemolymph into the aortic bulb, is to decrease pericardial

[*] Based on mean haemolymph volume of 37.7 mL.100g live weight$^{-1}$, determined in chapter 2, resting heart rate of 28.2 bpm and stroke volume of 0.37 mL.kg$^{-1}$ measured in chapter 6.

fluid pressure and thus increase the auricular transmural pressure difference. Pressure within the auricles [▫] therefore falls, drawing haemolymph from the post-branchial veins by suction.

The present study was devised to assess the major factors that determine and influence haemolymph supply to the gas exchange surfaces of an abalone. The New Zealand blackfoot abalone (locally 'paua'), *Haliotis iris* Martyn 1784, was chosen as an experimental subject. Recent morphological discoveries in this species suggest the vascular arrangement of the abalone may assist in supplying haemolymph to the afferent gill veins with minimal systemic pressure loss (chapter 3 of this thesis). Vascular routes have been found that bypass most of the main organ regions, potentially allowing haemolymph to flow from the aorta to the afferent gill vessels with minimal interference. Part of the capacious right renal sinus has been shown to contact the proximal (left) wall of the pericardial sac; the outlet of the sinus has also been found to possess a valve (chapter 3 of this thesis). It is therefore possible that pericardial movements may facilitate haemolymph flow from the right kidney sinuses into the gills, with the valve preventing back-flow. This hypothesis and the effectiveness of the system of bypasses in optimising pre-branchial haemolymph pressure have been examined in the current study.

*The pallial vasculature*

One possible route exists for haemolymph to return to the heart without passing through the gills, that being to cross the right-side mantle tissue. In the most comprehensive study to date to examine the right mantle vasculature, Crofts (1929) identified two major vessels associated with the region, the 'circular pallial vein' and the 'right pallial vein' [*]. A detailed comparison between Crofts' description of the pallial vessels of *H. tuberculata* and those of the current study for *H. iris* is made in chapter 3 and the discussion below. Both pallial vessels were described by Crofts as being efferent to the right mantle. However, neither Crofts (1929) nor the present investigations (chapter 3) revealed any other vascular routes associated with the right mantle, implying that in contrast to Crofts' interpretation, one of these pathways must be afferent.

The right mantle is of particular interest as it represents a possible site of gas exchange. The mantle has repeatedly evolved into a gas exchange surface in higher prosobranchs, ultimately allowing the snails to occupy amphibious and terrestrial niches. An increased reliance upon mantle gas exchange can also be seen within some archaeogastropod groups; for example the limpet superfamily Patellacea: The Acmaea have retained the left bipectinate gill and developed the pallial vasculature allowing the mantle to function as a gas exchanger during intertidal emersion (Kingston 1968). The Patelloida have abandoned bipectinate gills entirely and developed folds in the mantle surface to function as a secondary gill (Barnes 1986).

---

[▫] The 'diotocardian' archaeogastropods, including abalone, retain 2 auricles. The right auricle has been lost in higher prosobranchs.

[*] In accordance with more contemporary nomenclature, these vessels and referred to here as the 'circum-pallial vessel' and 'pallial vein'.

The abalone's right mantle may therefore represent a site of oxygen uptake or a non-respiratory pallial route for haemolymph to bypass the gill. In either case an elucidation of haemolymph supply to this region is of importance in the understanding of respiratory circulation in the abalone. In the present study pressure gradients were examined in the 2 potential venous return pathways (branchial and pallial) in order to determine the direction of flow and potential for gas exchange function.

To provide an indication of the circulatory capabilities of *H. iris* the standard parameters of cardiac output, stroke volume and power, as well as mean circulatory filling pressure and total peripheral resistance were examined. As previously described (chapter 6 of this thesis), the unavoidable stress associated with animal preparation was exploited as a method to induce maximum cardiac output. The abalone were subsequently allowed 24h to recover to establish an indication of the degree of compensation available in the cardio-vascular system.

*The effects of activity*

For the abalone, the extreme activities associated with avoidance, either clamping to the rock surface or raising and twisting the shell, present the vascular system with conflicting requirements. The increased energy demands of the active muscle fibres must be matched by an increase in convective oxygen delivery during or after the exercise, but the main vasculature must in turn be protected from potentially damaging haemolymph surges caused by contracting muscle blocks (e.g. Bourne and Redmond 1977a). The act of clamping has raised particular interest as this commonly utilised strategy requires all tissues to be confined within the shell, which imposes additional hydrostatic pressure, beyond the effects of muscular contraction alone. The clamp may be sustained for extended periods, requiring circulation to proceed in the main vasculature which must, in turn, be protected from haemolymph surges from the contracted pedal muscle. Valves have been discovered in different abalone species guarding the entrance to the pedal arteries (Bourne and Redmond 1977a) and the connection between the pedal sinus and cephalopedal venous sinus (Crofts 1929). Russell and Evans (1989) postulated that a pressure surge in the foot caused by clamping could cause both valves to shut, isolating the pedal vasculature, while circulation continued in the main system via a shunt between the arterial and venous head sinuses. The potential functioning of such a mechanism is considered by comparing pedal sinus pressure to pressure in the main vascular system during clamp, results are discussed in conjunction with detailed anatomical observations made in chapter 3. Similarly the acute effects of twisting upon vascular pressure were examined.

# 7.2. Methods

*Collection and storage of animals*

Adult *Haliotis iris* were collected from South Bay, Kaikoura, New Zealand during June and July 2002. The animals were transported and held at the University of Canterbury, as described in chapters 5 and 6. Medium-sized individuals (230 – 550g wet weight) that remained vigorous and healthy during 2 months of tank acclimation were selected for the experiments, which took place between September and November 2002.

*Cannulation procedures*

Two animal preparations were utilised, as described below. Both required that 4 chronically implanted cannulae should remain in position and patent for a number of days, while causing the least possible disturbance to the animal. To achieve this, the importance of a number of procedural steps should be emphasised; the selection of vigorous individuals was essential for subsequent recovery, as was the need to minimise the duration and thermal shock associated with any manipulation. The appropriate cannula design, placement and material (flexible PVC or stiffer polyethylene (PE), depending on site) were also essential to maximise retention and minimise damage.

*General Preparation*

A selected animal was weighed and then placed on a cooled tray, providing an environment of damp air at 4 - 6°C. A diamond cutting wheel attached to a Dremel™ flexible-shaft drill (20,000rpm) was used to cut an opening, 40 x 10mm, in the left-ventral region of the shell, immediately dorsal to the thickened shell margin (figure 6.1), exposing the ventral mantle roll. A second opening was cut immediately posterior to the line of shell holes, to expose the right efferent ctenidial vein as it approached the heart (figure 6.1). The region of shell immediately overlying the heart was also scored (a circle of approximately 15mm diameter) but left *in situ*. Two 1.5mm holes were drilled either side of the scored circle and fine copper wire, with the terminal insulation removed, was glued into each, to later serve as impedance electrodes (figure 6.1). Animals destined for *preparation 1* (see below) also had an opening scored around the 3 – 4 oldest shell holes (figure 5.1). Each abalone was allowed a minimum of 24h recovery in the holding system.

The selected abalone was subsequently checked for signs of tissue damage or haemorrhage and, if sound, returned to the cool tray for cannulation. The ventral mantle roll was displaced dorsally using a spatula to expose the anterior aorta at the line of insertion between the mantle and epipodium. A 23gauge needle was used to puncture the aorta and a 0.8mm (external diameter) PE cannula inserted orthograde to haemolymph flow (see figure 7.1 for cannula design detail). The cannula and associated Doppler leads (see below) were then adhered to the shell using cyanoacrylic glue. A 23gauge puncture was then used to insert a second PE cannula, retrograde to flow, into the right efferent ctenidial vein. Each animal was then randomly allocated to *preparation 1* or *2*, to receive a further 2 cannulae. As noted by Bourne and Redmond (1977a) and Jorgensen et al. (1984), no haemolymph leakage was associated with the newly inserted cannulae due to low systemic pressure and localised muscle contraction around the wound (Armstrong et al. 1971).

*Preparation 1: main respiratory circulation*

The presence of a low resistance route bypassing the right kidney and close contact between the pericardium and efferent renal veins have been implicated as factors that enhance delivery of haemolymph to the gills. The haemodynamic effects of these structures were investigated by monitoring pressure in the renal bypass vessel and in the basibranchial sinus supplying the afferent gill vessels. The renal bypass vessel was located by inverting the abalone and displacing the foot to

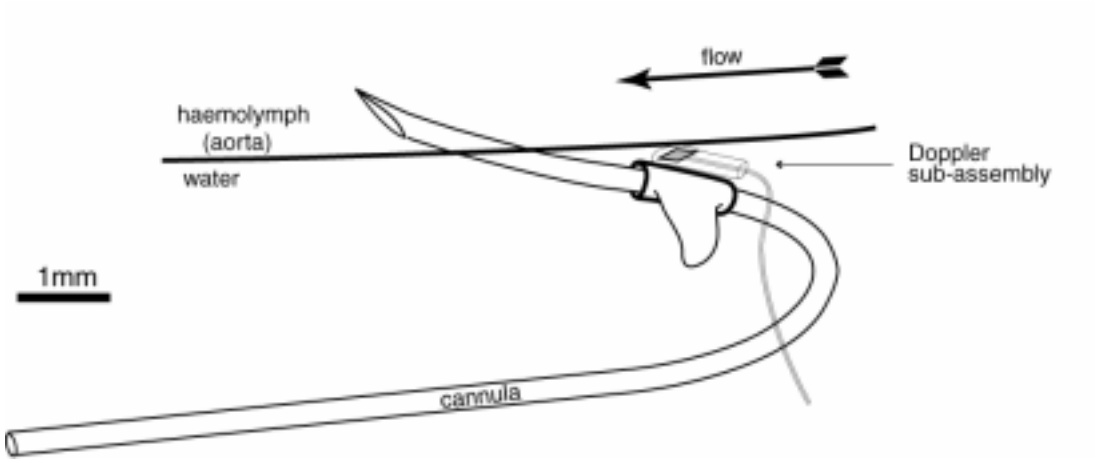


**Figure 7.1**: U-shaped 0.8mm (O.D.) polyethylene cannula fitted with a custom-built Doppler probe. The probe consists of a Doppler crystal sub-assembly attached to a 1mm (I.D.) polyethylene sleeve. When the cannula is inserted into the aorta of *Haliotis iris* the natural roll of the mantle tissue presses on a PVC vane attached to the sleeve, preventing the probe from rotating. Small movements of the Doppler leads allows fine tuning of crystal placement.

the right, revealing the mantle roll surrounding the branchial chamber. The anterior region of the mantle roll was then gently compressed, allowing the faint line of the bypass vessel to be discerned beneath the black epithelium as it ascends to join the intestinal sinus in the cephalic region (see figures 3.26 and 3.27). A 21gauge puncture was made and a flat-ended, 0.8mm diameter PVC cannula threaded approximately 10mm into the vessel, retrograde to flow. The cannula was secured to the shell margin, a bow in the tubing applying slight pressure to prevent removal by foot movement.

Initial uncertainty as to the exact location of the kidney bypass vessel prompted post-mortem corroboration of the cannula position. At the end of the experiment each abalone was rapidly killed by immersion in 90°C seawater and the body chilled. Using the recipe described in chapter 3, 20mL of corrosion casting compound were injected through the bypass vessel cannula. The animal was stored for 2h at 20°C to polymerise the cast then refrigerated overnight. The cast was then dissected from the body and the position of the cannula recorded. Of 6 animals examined in this way, the cannula was invariably found to be correctly located within the target vessel.

The basibranchial sinus was cannulated as described in chapter 5. Briefly: the shell window surrounding the exhalant holes was removed and a rubber dam placed between the gills to prevent their retraction during cannulation. A 23gauge needle was used to perforate the left afferent ctenidial vein (prominent, dorsally-presented vessel on the left gill) and a 0.6mm (O.D.) PVC cannula inserted for 40 – 50mm, coming to rest at the vessel's junction with the basibranchial sinus. All cannulae and leads were secured to the shell and the animal was placed into the experimental container (figure 5.3).

*Preparation 2: The pallial circulation*

Rather than returning to the heart via the gills, it is believed that haemolymph can flow via the right mantle, using the pallial veins (Crofts 1929). The nature of haemolymph flow across the right

mantle and its direction were established by monitoring pressure. Two vessels service the right mantle, the circum-pallial vessel (CPV) connecting to the oesophageal sinus on the left of the abalone, and the pallial vein, connecting the anterior and dorsal right mantle to the right efferent ctenidial vein immediately before it enters the heart. Both veins could be accessed for cannulation without the need for shell cutting.

The CPV was readily located on the left-hand side of the animal by inverting the abalone and displacing the foot and epipodium to the right. The CPV was seen as a relatively unpigmented antero-posterior line in the intensely melanised ventral surface of the left mantle (see figures 3.41a and b). A 23gauge needle was used to puncture the vein and a 0.8mm PVC cannula inserted approximately 20mm towards the posterior of the animal. The pallial vein was accessed by gently displacing the head ventrally (practically, this requires the animal to voluntarily 'bow', achieved by holding the abalone perpendicular to an attachment surface touching the posterior foot). The pallial vein was likewise seen as an unpigmented line within the mantle, following the contour of the adductor muscle. The region of vein directly above the head contains a nerve in its lumen and was therefore avoided. Hence the puncture was made to the right of the cephalic region, and the 0.8mm PVC cannula run 10mm towards the posterior. The cannulae were adhered to the shell margin and the animal placed in an experimental chamber (figure 5.3).

*Heart rate measurement*

As described in chapters 5 and 6, heart rate was determined independently of pressure and flow, by monitoring cyclic impedance changes in the cardiac region. An impedance coupler (Strathkelvin Instruments A100) was connected to the copper leads emerging from the holes drilled either side of the heart. The impedance signal was relayed to a PowerLab™ data acquisition system, where data recording and pulse rate determination were carried out using Chart™ 4.1.2 software (ADInstruments).

*Pressure measurement*

Pressure was recorded for each of the 4 cannulated vessels using Bell & Howell pressure transducers (type 4-327-0010). Two pressure recordings were made simultaneously and relayed to the data acquisition system via Gould universal bridge amplifiers. The transducers were attached to 2.1mmØ PE tubing filled with degassed, sterilized seawater, as an approximation of abalone saline. The pressure signal was calibrated with a known head of water and the abalone tank water surface used to establish a zero baseline. The baseline was checked between each measurement period. Pressure recordings were made by connecting the transducer tubing to the cannula via a tight-fitting lumen adapter, potential obstructions were then cleared by injection of a small volume (5 - 10µL) of the saline. All signal traces were subsequently recorded within 10min of line clearing as damping of the pressure pulse was often observed over longer periods, presumably due to haemocyte accumulation in the cannula.

*Flow measurement and calibration*

Cardiac output was estimated from haemolymph flow through the anterior aorta. Haemolymph flow was determined by acoustic pulsed-Doppler flow measurement, using a customised transceiver assembly mounted on the aortic cannula (figure 7.1). A directional pulsed-Doppler flowmeter (Bioengineering 545C-4) relayed electrical signals to the data acquisition system (see chapter 6 for details).

The raw Doppler signals were calibrated by use of *in situ* known-flow rates of a calibration liquid pumped through the aorta at the end of the experiment. The abalone was killed in 90°C seawater and the pericardium and ventricle opened to provide a low resistance path. A zeolite (commercial barbecue deodorizer) suspension (see chapter 6) was then pumped from a calibrated peristaltic pump, through the aortic cannula, flowing retrograde to normal haemolymph flow, exiting via the perforated ventricle. There was no visible indication of zeolite flow in the opposite direction, towards the head. Doppler signals were collected over a range of flows and a linear regression equation fitted to determine flow ($mL.min^{-1}$) from Doppler signal ($V$). The mean (integral($V$.dt/t)) of the pulsatile flow signals collected *in vivo* were then substituted into the regression equation to estimate flow.

*Experimental design*

Cardiovascular parameters were determined with the abalone in a 'stressed' condition. Using the definition stated in chapter 6, 'stressed' describes the condition of the abalone immediately after immersion in the experimental system. The animal has just endured approximately 1h of hypoxia, desiccation and physical trauma associated with cannulation and Doppler probe positioning. This condition was arbitrarily deemed to prevail for 2h after cannulation and 1h after any subsequent handling. Oxygen demand and cardiac output in stressed animals are apparently maximal (see chapter 6), the condition therefore represents the upper operating limit of the cardio-vascular system. All measurements were then repeated after the abalone had been left undisturbed for at least 24h.

Pressure measured in the right efferent ctenidial vein was considered to be representative of pre-cardiac haemolymph, while pressure and flow in the aorta were assumed to represent cardiac output. Simultaneous 2min records were therefore made of the right efferent ctenidial and aortic pressure, and of aortic flow. These records were used to determine cardiac output and stroke volume, stroke work and power, and total peripheral resistance. Paired pressure records were also taken from each of the vessel combinations shown in table 7.1. To avoid possible bias or phase lag associated with either of the pressure transducers their vessel allocation was randomised for each pair of recordings.

For each 2min pressure trace, Chart™ 4.1.2 software was used to determine mean pressure, $P$, by integrating the pulsatile signal (integral($P$.dt/t), e.g. after Levick 1991). Mean systolic maximum and diastolic minimum were also determined. During the first 2h of immersion in the experimental chamber triplicate pressure recordings were taken (in random order) from each of the vessel pairs

| Preparation | upstream vessel | downstream vessel |
|---|---|---|
| 1 & 2 | Aorta | R kidney bypass vessel |
| 1 | Aorta | L afferent ctenidial vein* |
| 1 | Aorta | R efferent ctenidial vein |
| 2 | Aorta | Circumpallial vein |
| 2 | Aorta | Pallial vein |
| 1 | R kidney bypass vessel | L afferent ctenidial vein* |
| 1 | L afferent ctenidial vein* | R efferent ctenidial vein |
| 2 | Circumpallial vein | Pallial vein |

(*Left afferent ctenidial vein = basibranchial sinus pressure)

**Table 7.1**: Paired pressure measurements taken to determine mean pressure gradients and phase relationships. All possible combinations were measured in triplicate in each animal under conditions of stress and subsequent recovery.

listed in table 7.1 to obtain pressure parameters under stress. The abalone was then left undisturbed for 24 – 36h and triplicate recordings taken again.

*Pressure phasing*

At the end of the experiment three representative *Preparation 1* animals and one *Preparation 2* animal were selected. Samples of the data record were extracted to graphically determine the phase relationship between the aortic pulse and flow and the pressure pulse of the 3 other cannulated vessels. Graphic records (SigmaPlot 2000 v.6.1, SPSS Inc.) were then superimposed and aligned using the aortic pulse as reference to provide an integrated image of pressure phasing within the individual.

*Cardiac power and stroke work*

Stroke work was estimated from equation 7.1 (after Farrell and Jones 1992).

$$W_s = V_s.(P_a - P_v) \qquad \text{Equation 7.1}$$

where stroke work, $W_s$ (in Joules), is the product of stroke volume, $V_s$ (in $m^3$), and driving pressure, the mean difference (in Pascals) between aortic ($P_a$) and central venous pressure ($P_v$). For comparative purposes stroke work is standardised by both animal wet weight and ventricle mass. In molluscs the ventricle actively lowers pressure in the veins approaching the heart (see discussion below), hence, rather than using central venous pressure, $P_v$ is taken to be right efferent ctenidial vein pressure immediately before the haemolymph enters the heart.

Myocardial power output is a valuable comparative tool as it provides an integrated measure of cardiac performance, encompassing both flow work and pressure work (Farrell and Jones 1992). Power output was determined according to equation 7.2 (after Vogel 1994).

$$M_p = Q.(P_a - P_v) \qquad \text{Equation 7.2}$$

Where myocardial power, $M_p$ (in Watts), is the product of cardiac output, (in $m^3.s^{-1}$) and the mean pressure gradient between the aorta and efferent ctenidial veins ($P_a - P_v$; in Pascals). In vertebrates $P_a$ is relatively high and venous pressures tend to approach ambient, hence $P_v$ is usually ignored (e.g. Farrell and Jones 1992); as the molluscan $P_a$ is low and the ventricle directly lowers pre-cardiac pressure, $P_v$ must be included to accurately determine power. Cardiac power is usually standardised by ventricle mass (Farrell and Jones 1992).

It was necessary to determine ventricle mass to standardise the above parameters. To this end the ventricle, identifiable as dense, pink, muscular tissue within the pericardium, was removed from the animal at the end of the experiment. Excess tissue associated with the rectum was carefully removed and the ventricle blotted and weighed.

*Peripheral resistance*

Vascular resistance was determined indirectly by application of Darcy's law (equation 7.3)

$$Q = C.\Delta P \qquad \text{Equation 7.3}$$

i.e. Haemolymph flow is determined by the product of hydraulic conductance, *C*, and the pressure gradient ($\Delta P$) across a given region. The equation can be re-arranged to calculate resistance (*R*), the reciprocal of conductance, from pressure gradient and flow (e.g. Guyton 1986, Levick 1991). In this way total peripheral resistance was calculated from equation 7.4. *R* was expressed in $cmH_2O.min.mL^{-1}$ *.

$$R = \frac{P_a - P_v}{Q} \qquad \text{Equation 7.4}$$

*Mean circulatory filling pressure*

At rest, abalone may exhibit brief periods of acardia. This occurred on a number of occasions during the current investigations resulting in an almost immediate plateau in haemolymph pressure to a common value throughout the system. The mean values of these plateau regions was determined and presented as an estimate of mean circulatory filling pressure in *H. iris*.

*Effects of activity*

Abalone that remained vigorous and responsive after all data had been collected were subsequently used to examine the pressure effects of avoidance activity. Paired pressure recordings, along with aortic flow and heart impedance signal, were recorded while the animal was induced to flinch (single downwards pump of the shell) or twist (raising and vigorous rotation of the shell) by tactile stimulation of the gill lamellae. The effects of clamping to the substratum were also examined by applying gentle torsion to the shell for 20 – 30s.

---

* To convert $cmH_2O.min.mL^{-1}$ into peripheral resistance units (PRU; i.e. $Torr.s.mL^{-1}$), multiply by 60×133.3. To convert PRU into $dyne.s.cm^{-5}$, multiply by 1333 (Guyton 1986).

The effects of clamping upon the pedal circulation were also examined, however this required a specific preparation in a separate sub-set of animals. In each case the abalone was inverted on a cool tray and the foot allowed to fully inflate and commence searching motions. The midline of the foot was identified by the inter-digitating pattern of the epidermis and an 18gauge needle inserted approximately 20mm posterior to the division of the anterior lobes. The needle was angled at 45°, towards the head, and inserted until haemolymph flowed freely, indicating the pedal sinus had been reached. A 0.8mmØ PVC cannula was threaded through the lumen of the needle, which was then carefully removed, leaving the cannula in place. As noted by Voltzow (1986), muscular resistance of the pedal sole alone was sufficient to maintain the cannula position.

The abalone was allowed to adhere to a plastic disc before being placed in the experimental chamber. The pedal sinus pressure was recorded in the stressed animal and during induced flinching and twisting and, most critically, sustained clamp. On one occasion, the aorta was also cannulated to allow the phase relationship between the pedal sinus and aortic pulse to be determined.

*Secondary effects of heartbeat*

Finally, the hypothesis that movements of the pericardium could assist in the propulsion of haemolymph from the renal sinus into the basibranchial sinus was examined. Using *preparation 1* animals, the amplitude of the pressure pulse was compared between the renal bypass vessel and the basibranchial sinus (respectively lying afferent and efferent to the region influenced by the pericardium). Towards the end of the experiment paired pressure readings from the renal bypass vessel and basibranchial sinus and from the aorta and right efferent ctenidial vein were taken to establish a baseline. The shell section overlying the pericardium was then removed, eliminating external resistance to any movement of the outer (i.e. left) surface of the pericardium. The animals were given 1 min to reposition following the disturbance and the haemolymph parameters subsequently monitored for 20min. More extended readings were not made as pericardial fluid volume was seen to increase, presumably influencing cardiac output.

*Statistical analyses*

All analyses were performed using Statistica™ 6.0 software (StatSoft Inc., USA). In general one-way nested analysis of variance was performed to examine the effects of the stressed versus recovering states on haemodynamics, while nesting individual variability within animal state.

# 7.3. Results

A total of 14 animals subjected to *preparation 1* yielded data, as did 10 *preparation 2* abalone and 7 in which the pedal sinus was cannulated. No accidental death occurred during the course of these experiments.

*Heart Rate*

The impedance coupler signal was invariably clear, requiring no repositioning of the impedance leads. The problems associated with the use of impedance leads in coiled shell gastropods (e.g. *Hemifusus*, Depledge and Phillips 1986), where the relative position of the heart to the shell changes during retraction are avoided in abalone. Depledge and Phillips (1986) noted auricular systole could be detected on the predominant ventricular signal of an impedance signal from the heart of *Hemifusus*. Similarly in *H. iris* an additional peak, presumably representing auricular movement, can occasionally be detected in the impedance signal that essentially reflects ventricle activity (e.g. figures 7.9 and 7.13).

The stressed heart rate of 24.99 ±0.81bpm increased by a small, but significant amount during subsequent recovery (25.99 ±0.94bpm, $F_{1,38} = 19.57$, $p < 0.001$).

*Cardiac output*

Mean cardiac output, estimated from aortic flow, was found to be 9.19 ±1.05mL.min$^{-1}$ in stressed abalone; this value showed no apparent change during subsequent recovery (9.03 ±1.31mL.min$^{-1}$). A similar lack of difference was seen between mean output under stressed and recovering conditions when standardised by abalone mass (25.17 ±2.68mL.kg wet weight$^{-1}$.min$^{-1}$ under stress, 25.99 ±4.03mL.kg$^{-1}$.min$^{-1}$ during recovery). However, when considering overall means the substantial differences in output between individuals masked the fact that a significant decrease occurred in output between the stressed and recovering states ($F_{1,243} = 11.16$, $p < 0.001$). A similar pattern was seen for stroke volume, which also decreased significantly during recovery ($F_{1,244} = 9.54$, $p = 0.002$), despite similar overall means (0.96 ±0.09mL.kg wet weight$^{-1}$ under stress, 0.93 ±0.13mL.kg$^{-1}$ during recovery).

*Haemolymph pressure*

Pressure gradients within the main vascular circuit supplying the gills (*preparation 1* animals) are shown in figure 7.2. Mean pressure was unaffected by the transition from stress to recovery states in the 4 vessels examined ($p > 0.08$). Mean resting pressure of 4.56 ±0.33cm$H_2O$ in the aorta fell to 3.50 ±0.07cm$H_2O$ in the renal bypass vessel. No significant pressure gradient was detected between the bypass vessel and the basibranchial sinus (3.30 ±0.22cm$H_2O$; $t_{0.05,15} = 0.36$, $p = 0.36$). The largest systemic pressure gradient occurred across the gills, where mean pressure fell below MCFP (see below) to 1.16 ±0.11cm$H_2O$ in the right efferent ctenidial vein. Pulse amplitude fell sharply from 2.23 ±0.20cm$H_2O$ in the aorta to 0.48 ±0.04cm$H_2O$ in the bypass vessel, showing no significant change as the haemolymph passed into the basibranchial sinus (0.49 ±1.16cm$H_2O$; $F_{1,13} = 0.15$, $p = 0.69$). Pulse amplitude increased to 0.72 ±0.04cm$H_2O$ on the efferent side of the gills.

In contrast to the main circulation, the pressure gradient within the pallial system was sensitive to stress (figure 7.3). During recovery, no significant gradient existed ($t_{0.025,16} = -0.44$, $p = 0.67$), with a mean pressure of 2.07 ±0.27cm$H_2O$ in the circum-pallial vessel (CPV) and 2.15 ±0.47cm$H_2O$ in the pallial vein. Under stress however, CPV pressure rose to 2.90 ±0.45cm$H_2O$, while in the

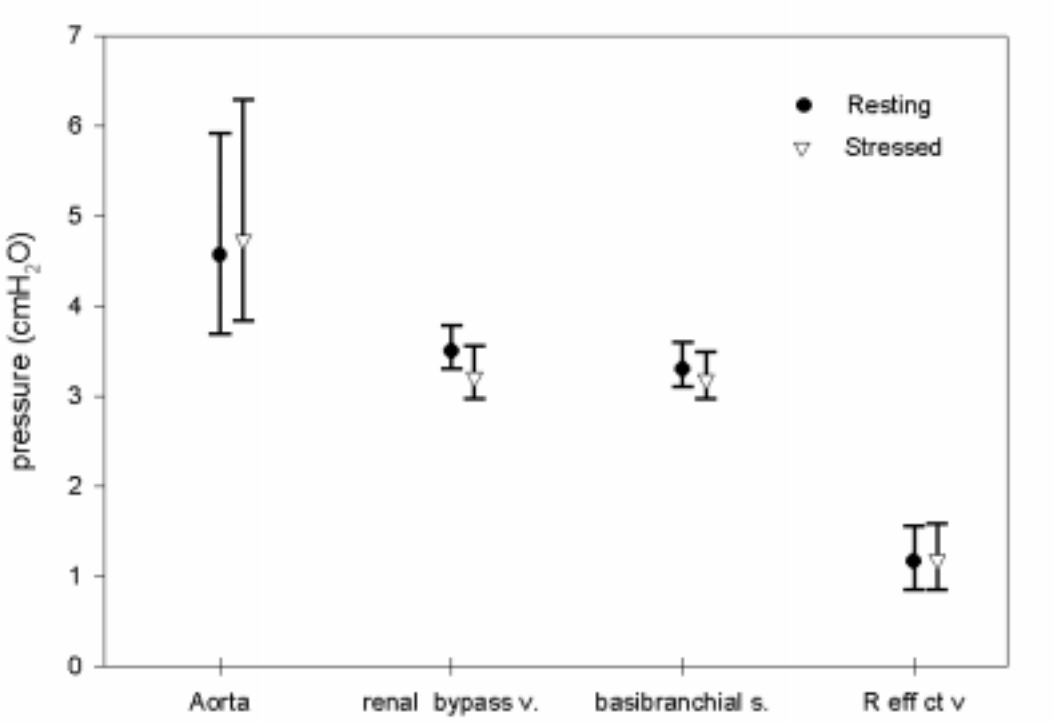


**Figure 7.2**: Pressure gradients in the main vascular circuit supplying the gills. Mean overall pressure, mean systolic maxima and diastolic minima are shown for animals at rest and during stress. Values were calculated from multiple paired pressure records of the anterior aorta, renal bypass vessel, basibranchial sinus and right efferent ctenidial vein taken from each of 14 individuals.

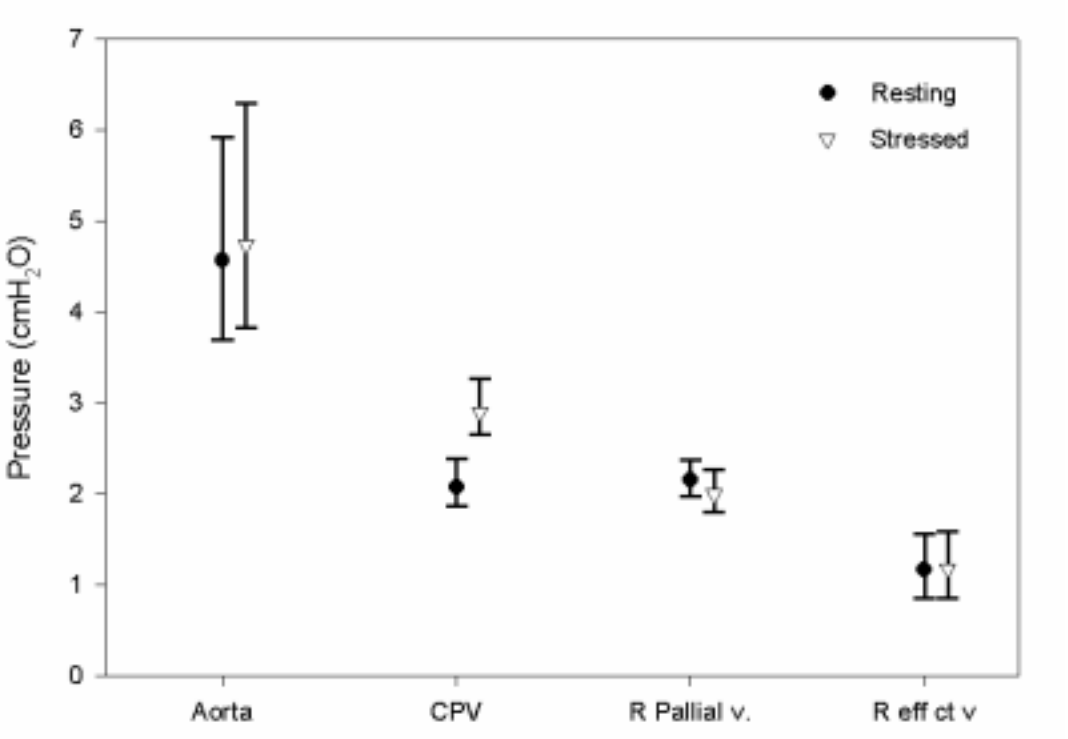


**Figure 7.3**: Pressure gradients in the pallial circuit supplying the right mantle. Mean overall pressure, mean systolic maxima and diastolic minima are shown for animals at rest and during stress. Values were calculated from multiple paired pressure records of the anterior aorta, circum-pallial vessel (CPV), right pallial vein and right efferent ctenidial vein taken from each of 10 individuals.

pallial vein pressure fell slightly to 2.00 ±0.39cm$H_2O$, resulting in a significant pressure gradient ($t_{0.025,24}$ = 2.28, p = 0.03).

*Mean circulatory filling pressure*

The resting abalone occasionally showed spontaneous acardia with almost immediate effects upon vascular pressure. In less than 500ms haemolymph pressure was found to plateau at 1.95 ±0.12cm$H_2O$ (n = 16) throughout the circulatory system, a value assumed to represent mean circulatory filling pressure.

*Peripheral resistance*

An estimated total peripheral resistance of 0.60 ±0.16cm$H_2O$.min.$mL^{-1}$ under stress rose to 0.66 ±0.18cm$H_2O$.min.$mL^{-1}$ during recovery, however the difference was found to be non-significant ($F_{1,26}$ = 0.32, p = 0.57).

*Pressure phasing*

To demonstrate consistency in phase relationships between individuals, graphic analyses of 3 representative *preparation 1* animals are shown here. The aortic pressure wave and corresponding haemolymph flow of each individual are shown in figures 7.4a, 7.5a and 7.6a. Aortic flow was seen to be highly pulsatile, velocity rising rapidly with increasing pressure to peak at 5 – 8mm.$s^{-1}$. Pressure subsequently fell rapidly to an incissura, identified by Bourne and Redmond (1977a) as a dichrotic notch, beyond which the rate of decline decreased until interupted by the rapid pressure increase associated with the next cardiac cycle. As the pressure began to fall, flow velocity also decreased rapidly, stopping completely at the dichrotic notch.

Simultaneous pressure recordings from the renal bypass vessel and the aorta are shown in figures 7.4b, 7.5b and 7.6b. While pressures in the bypass vessel are somewhat lower and the pulse clearly damped, there is no loss of synchronicity with the aorta. A similar conclusion can be drawn from the basibranchial sinus (figures 7.4c, 7.5c and 7.6c) where the pulse remains damped and in phase with the aorta. In contrast, haemolymph pressure on the efferent side of the gills, approaching the heart, is in perfect antiphase with aortic pressure. A distinctive feature of the right efferent ctenidial pressure wave was a transient spike occurring in synchrony with the aortic dichrotic notch (cf. Bourne and Redmond 1977a), this phenomenon is particularly clear in figures 7.4d and 7.5d.

By overlaying and aligning aortic pulse traces, the composite phase relationships in the selected individuals are revealed in figures 7.4e, 7.5e and 7.6e. The composite pressure waves reveal a slight lag between the bypass vessel and basibranchial sinus and emphasise the antiphase relationship in pressure pulse across the gills. A corresponding pressure pulse composite was also constructed for the pallial vasculature of a representative animal (figure 7.7). Pressure in the CPV shows a damped but perfect phase relationship to the aorta. Pressure in the pallial vein is only weakly pulsatile, but clearly in antiphase to the CPV and aorta, showing a close phase relationship to the right efferent ctenidial vein. Pressure in the pallial vein and right efferent ctenidial vein typically remained below mean circulatory filling pressure, with efferent ctenidial minima frequently becoming sub-ambient.

A representative pressure record from the single individual in which paired aortic and pedal sinus pressure were measured simultaneously is shown in figure 7.8. As with the renal bypass vessel and CPV, a pulse was clearly apparent in the pedal sinus, which was in phase with the aorta.

*Cardiac power and stroke work*

Stroke work, standardised by ventricle wet weight, was estimated to be 1.17 ±0.16mJ.g$^{-1}$ in stressed abalone; stroke work did not change significantly during subsequent recovery (1.15 ±0.19mJ.g$^{-1}$; $F_{1,26}$ = 0.014, p = 0.91). Cardiac power output also remained unchanged by the transition from a stressed (0.51 ±0.07mW.g ventricle$^{-1}$) to a recovering state (0.53 ±0.10mW.g$^{-1}$; $F_{1,26}$ = 0.45, p = 0.50; n = 14). When standardised by total wet weight, stroke work and power output were found to be 0.47 ±0.06mJ.kg$^{-1}$ and 0.21 ±0.03mW.kg$^{-1}$, respectively, under stress. During recovery mean stroke work was calculated to be 0.47 ±0.08mJ.kg$^{-1}$ and power to be 0.22 ±0.04mW.kg$^{-1}$.

*Effects of activity*

The abalone showed 3 distinct responses to acute disturbance, a flinch, in which the shell was pulled sharply towards the substratum and then released, a clamp, in which the shell was actively pulled against the substratum and a twist, where the shell was raised and rotated vigorously ±180º. Some variability was observed in the haemodynamic responses to these activities, a number of graphic examples are therefore given. Figure 7.9 shows the effects of several flinches followed by a twist upon aortic pressure and flow, impedance signal and renal bypass vessel pressure. In this individual, heart rate appears unaffected, but the body movements have apparently influenced the clarity of the impedance signal. The onset of activity was associated with a brief back-flow in the aorta and distinct pressure spikes of ~10cm$H_2O$ in the aorta and bypass vessel. Similar pressure spikes are also seen in the pedal sinus (figure 7.10). The effects of prolonged twisting (30s) upon aorta haemodynamics and right efferent ctenidial pressure are shown in figure 7.11. Aortic flow was seen to decrease during twisting, subsequently increasing in conjunction with increased haemolymph pressure in both vessels following the cessation of activity.

The act of clamping to the substratum resulted in 2 distinct vascular pressure responses in the main circulation. Either a small, transient pressure increase was seen, lasting ~10s after which normal pulse was resumed for the remainder of the clamp (figure 7.12), or a sustained elevation in pressure that only returned to normal when the clamp was released (figure 7.13). Heart rate was generally unaffected although cardiac output often fell during the clamp (represented by Doppler flow on figure 7.13). The pedal sinus, in contrast, showed pressure increases an order of magnitude higher than in the main circulation during clamp. Mean pressure rose from 4.97 ±0.58cm$H_2O$ to 16.62 ±1.63cm$H_2O$ (n = 7), remaining high and erratic until the clamp was released, when it abruptly returned to a baseline of 5.13 ±0.62cm$H_2O$ (figure 7.14).

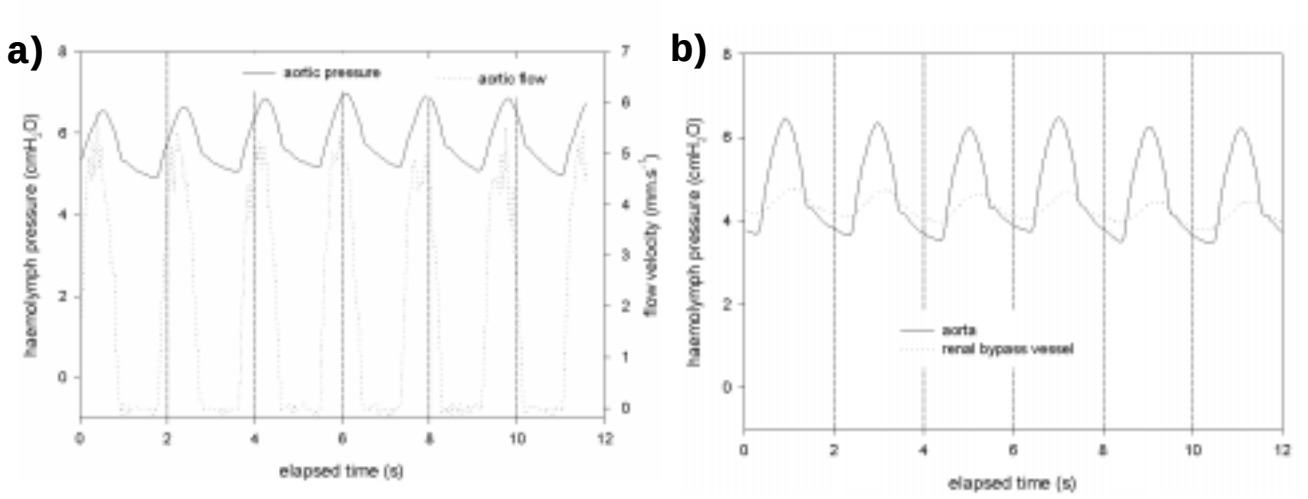


**Figure 7.4**: Pressure phase relationships in the main vascular circuit supplying the gills of abalone #M708. **a)** pressure-flow relationship in the aorta. Pressure phase relationship between the aorta and: **b)** the renal bypass vessel, **c)** the basibranchial sinus, **d)** the right efferent ctenidial vein. **e)** Composite pressure phase relationship for the main vascular circuit of M708.

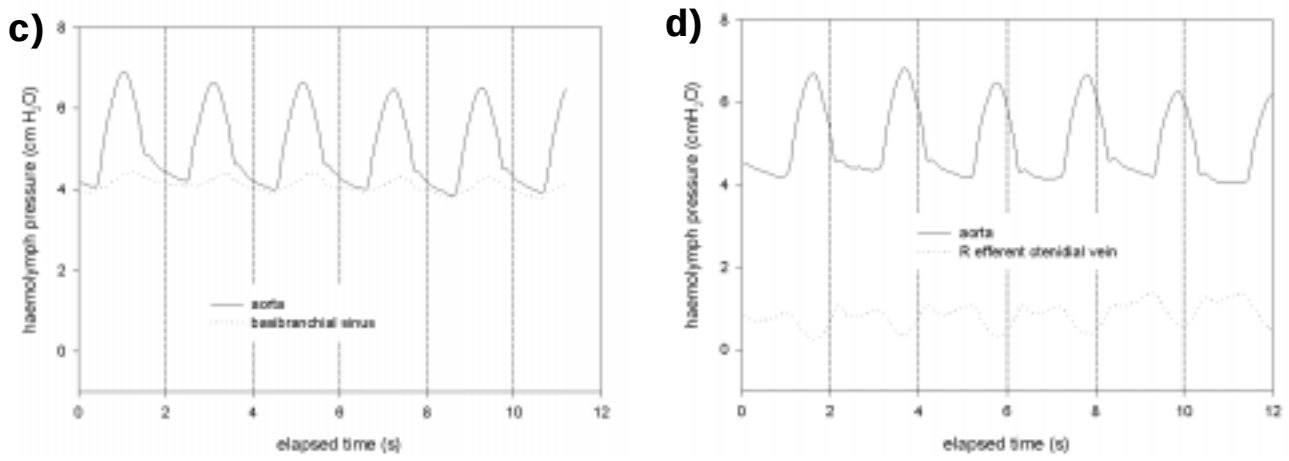


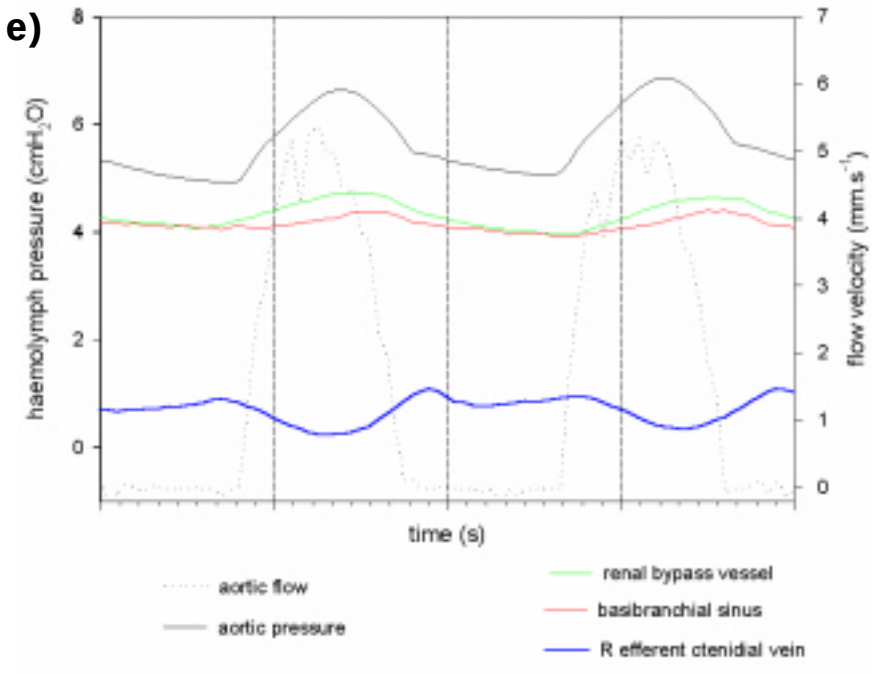

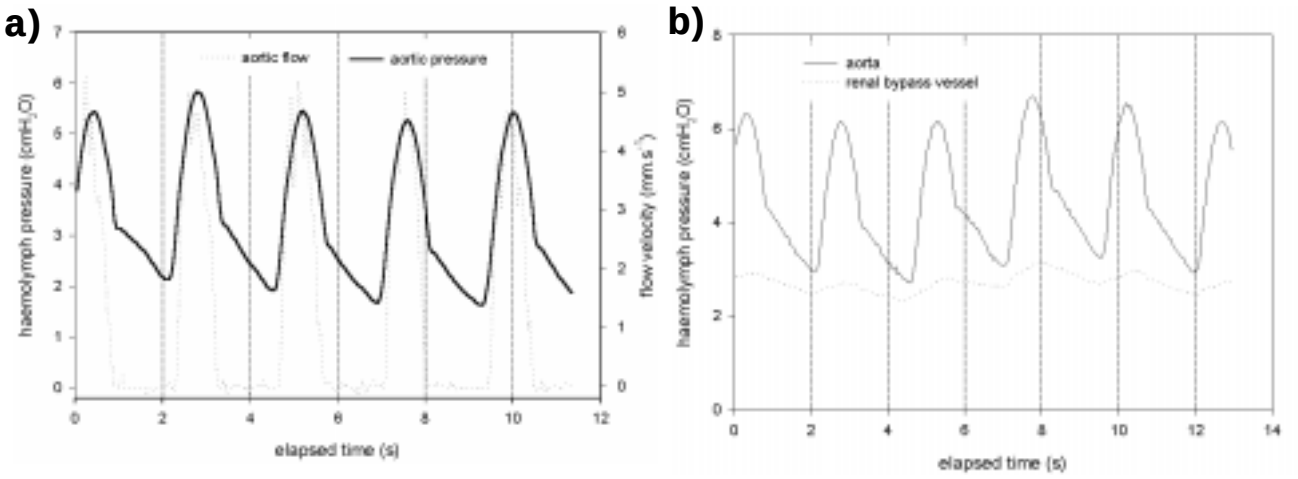


**Figure 7.5**: Pressure phase relationships in the main vascular circuit supplying the gills of abalone #M712. **a)** pressure-flow relationship in the aorta. Pressure phase relationship between the aorta and: **b)** the renal bypass vessel, **c)** the basibranchial sinus, **d)** the right efferent ctenidial vein. **e)** Composite pressure phase relationship for the main vascular circuit of M712.

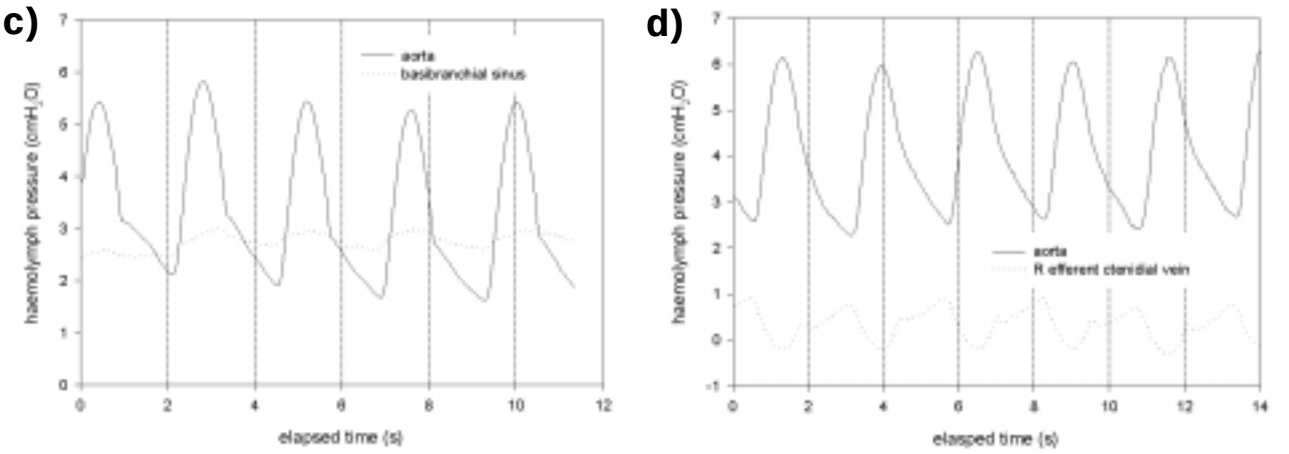


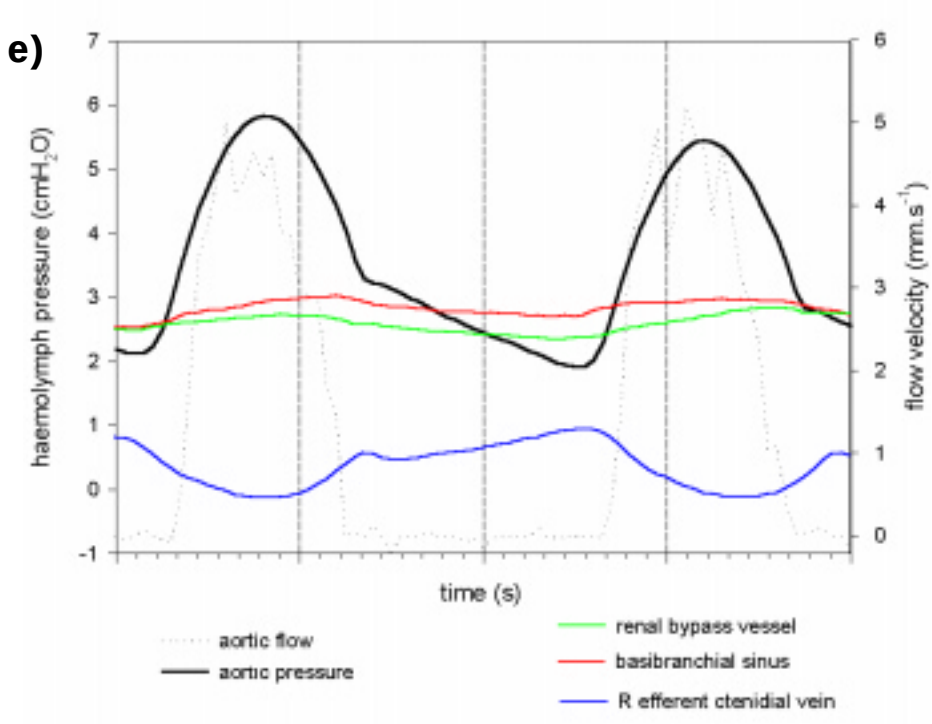

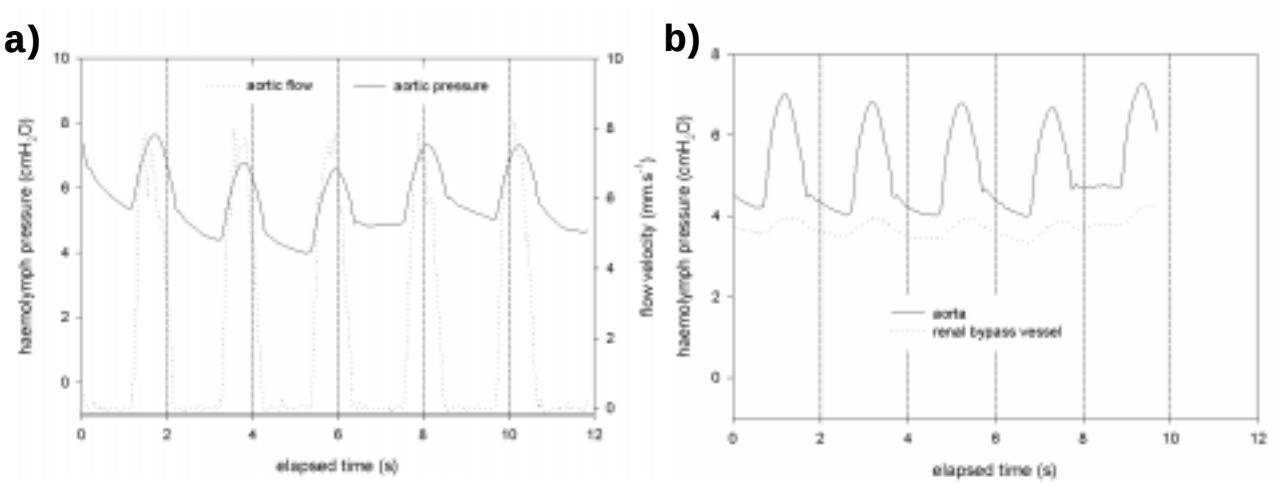


**Figure 7.6**: Pressure phase relationships in the main vascular circuit supplying the gills of abalone #M695. **a)** pressure-flow relationship in the aorta. Pressure phase relationship between the aorta and: **b)** the renal bypass vessel, **c)** the basibranchial sinus, **d)** the right efferent ctenidial vein. **e)** Composite pressure phase relationship for the main vascular circuit of M695.

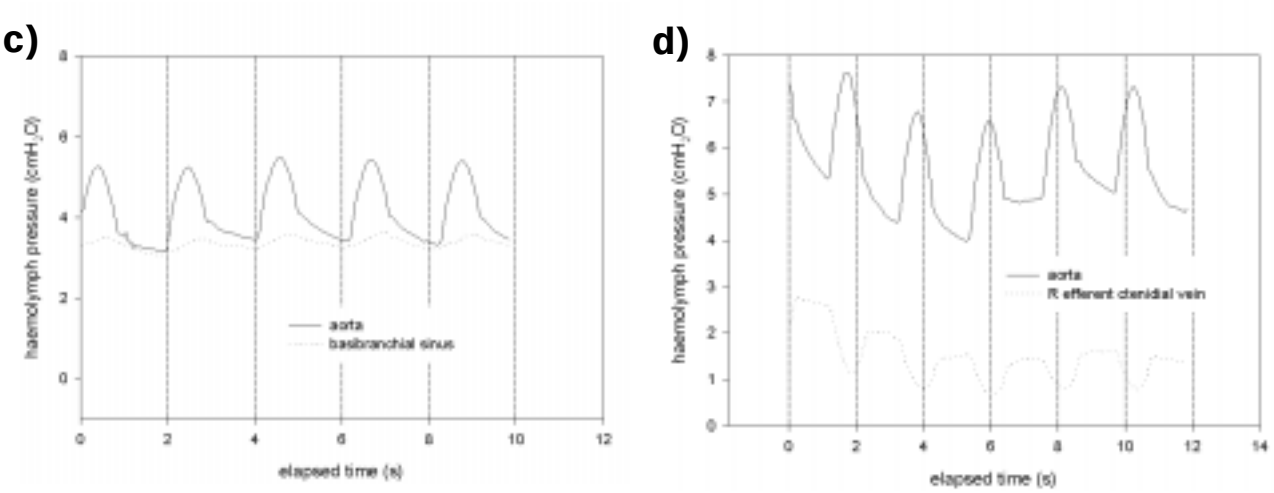


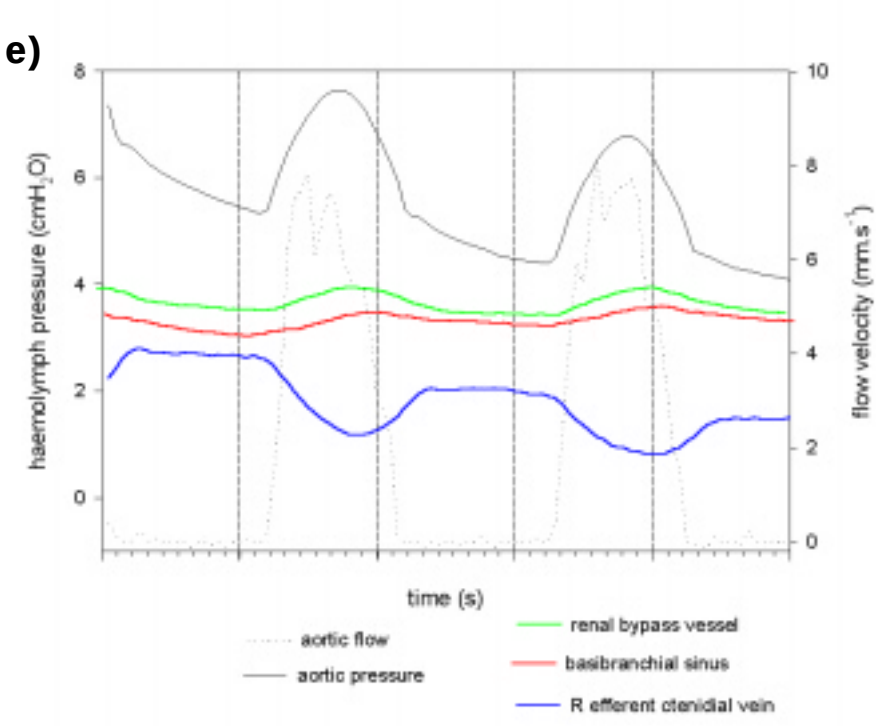

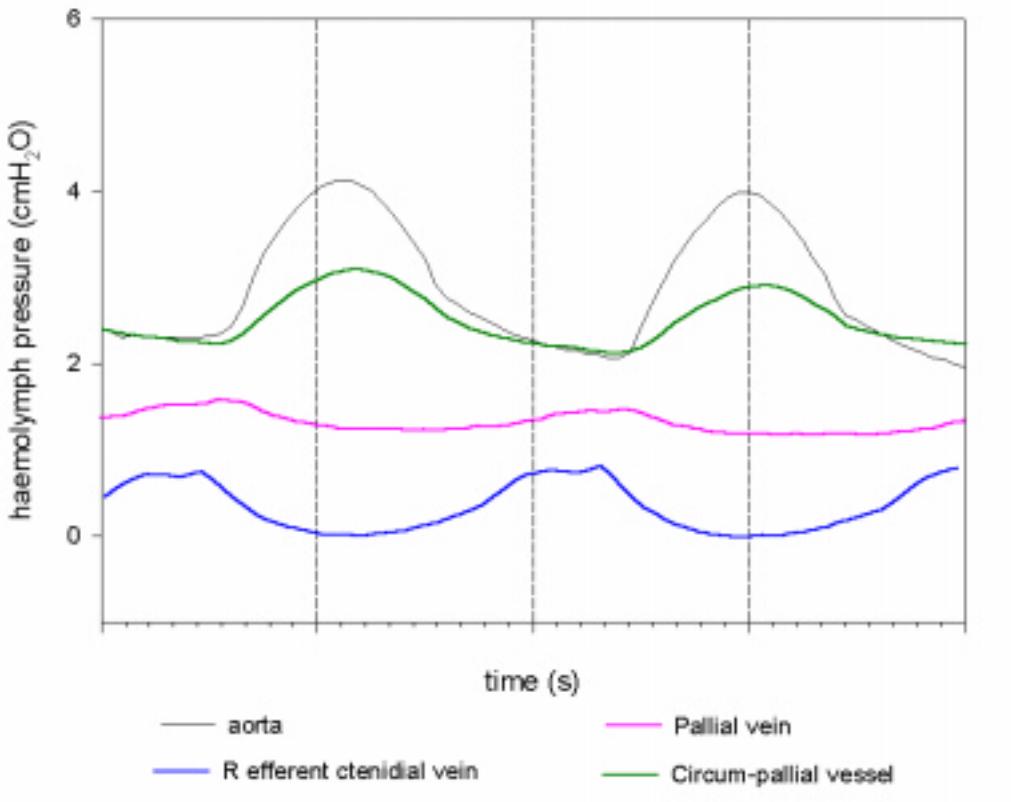


**Figure 7.7:** Composite pressure phase relationship for the pallial circulation of abalone #M712.

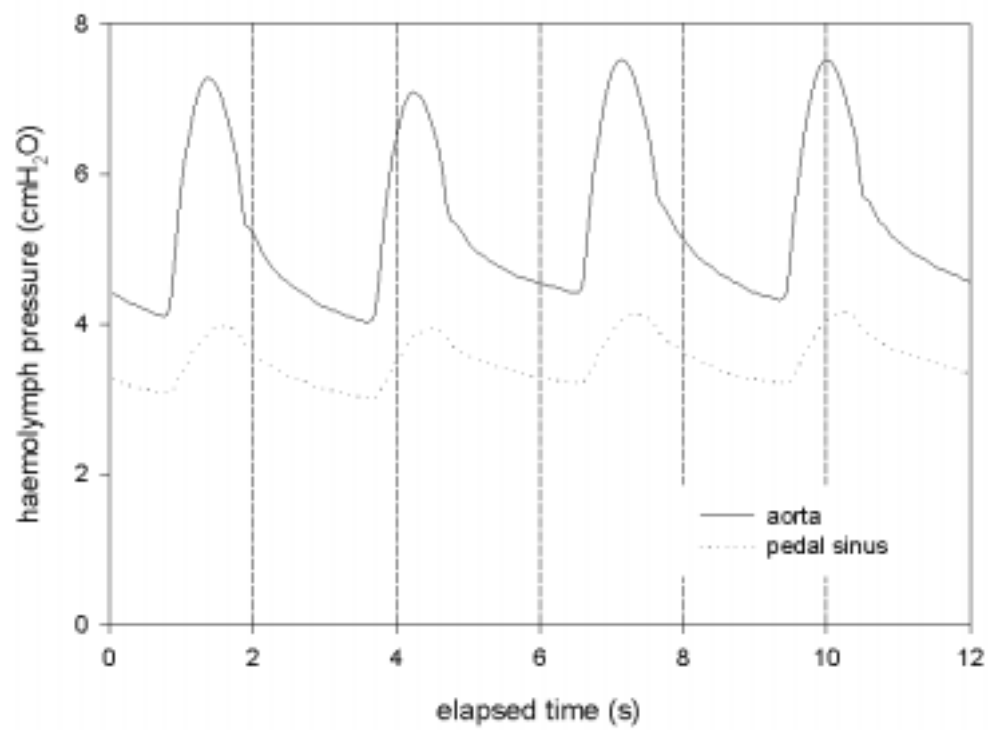


**Figure 7.8**: Pressure phase relationship between the aorta and the pedal sinus.

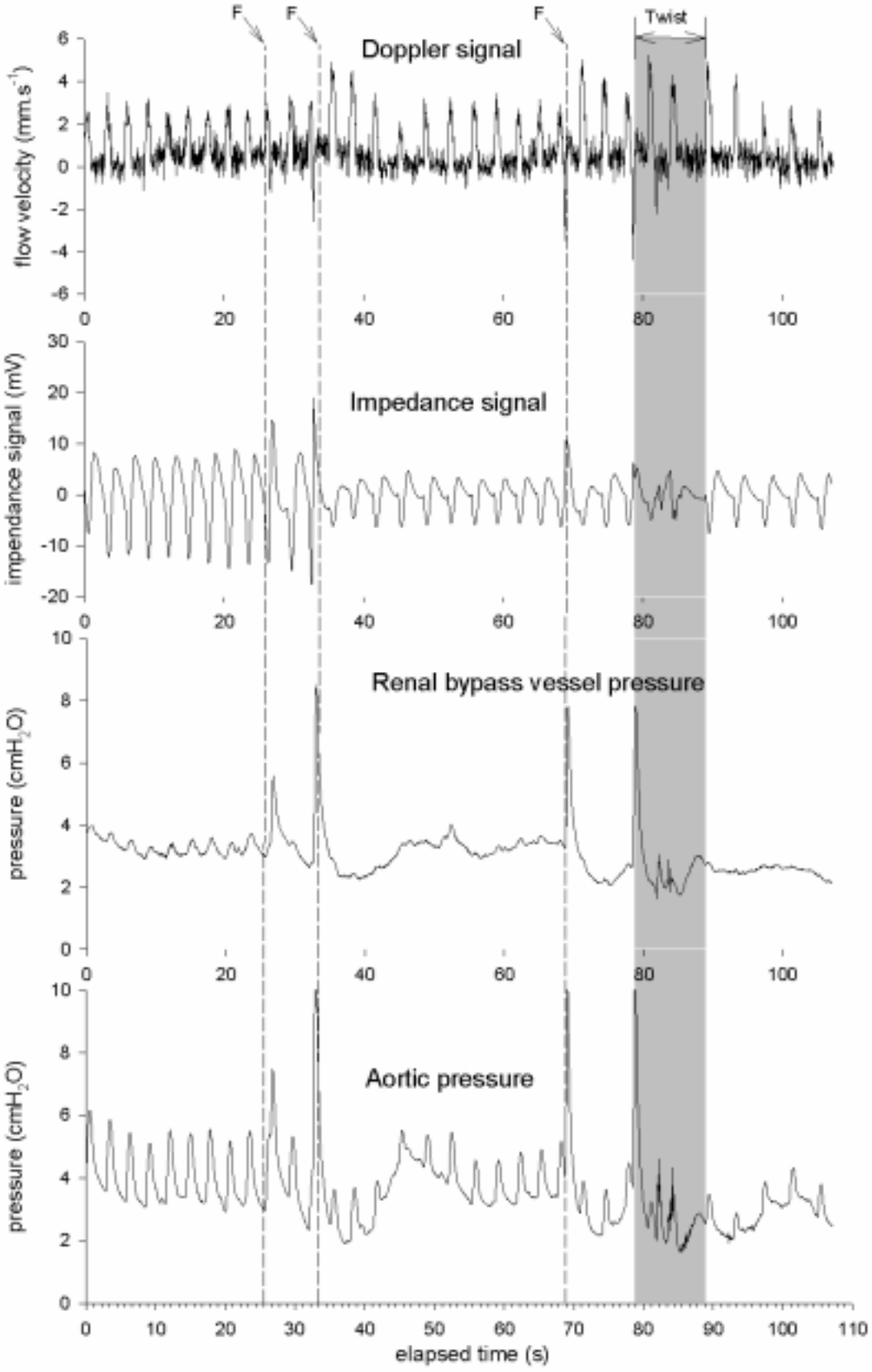


**Figure 7.9**: Haemodynamic effects of induced flinching and twisting upon the aorta and renal bypass vessel.

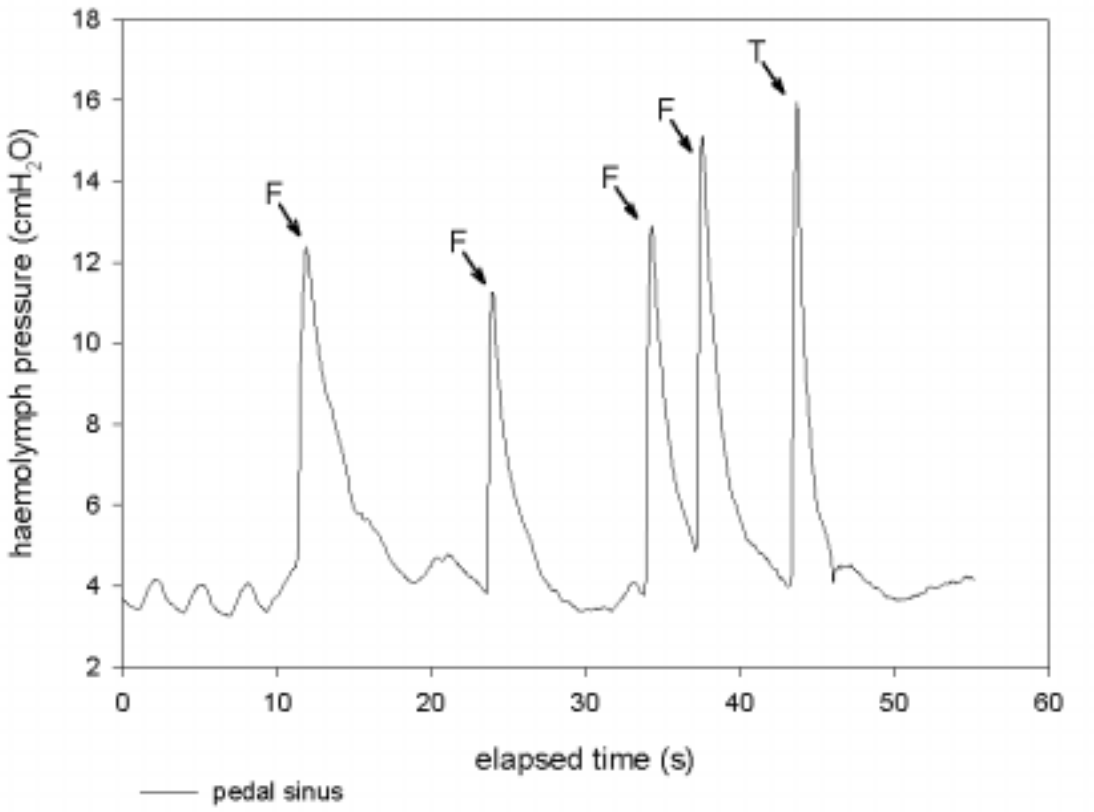


**Figure 7.10**: Effects of induced flinching and twisting upon haemolymph pressure in the pedal sinus.

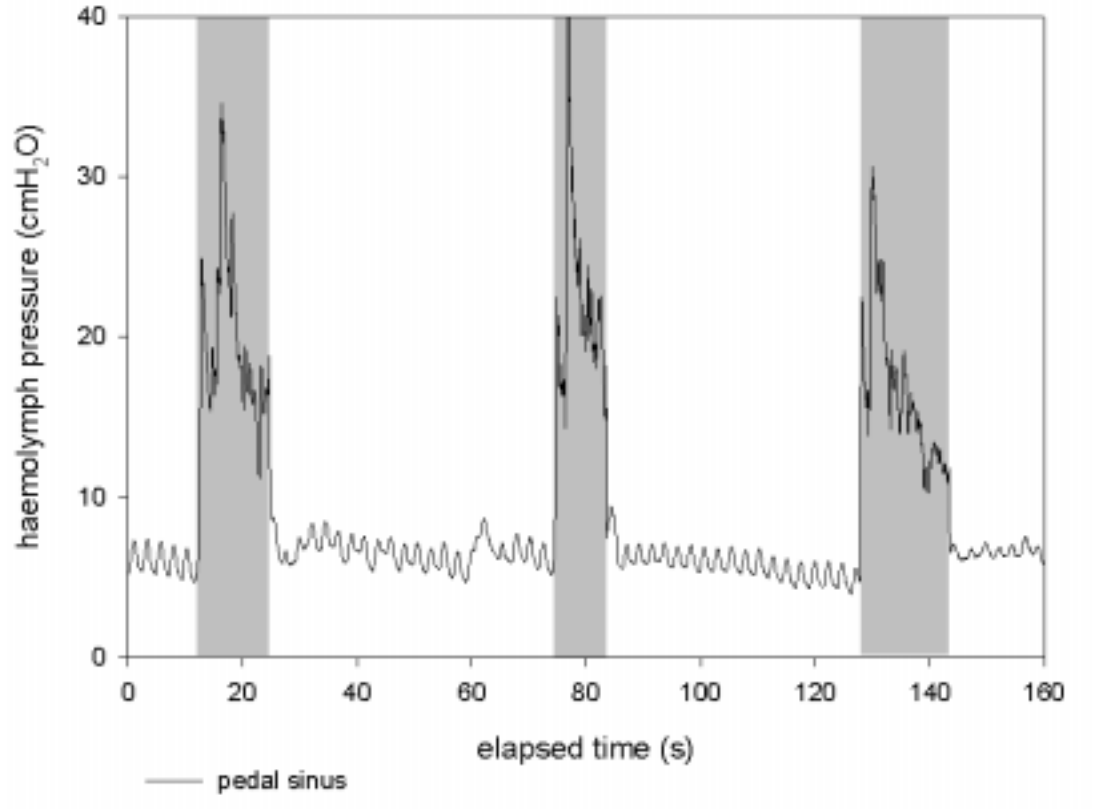


**Figure 7.14**: Pedal sinus pressure during 3 successive clamps.

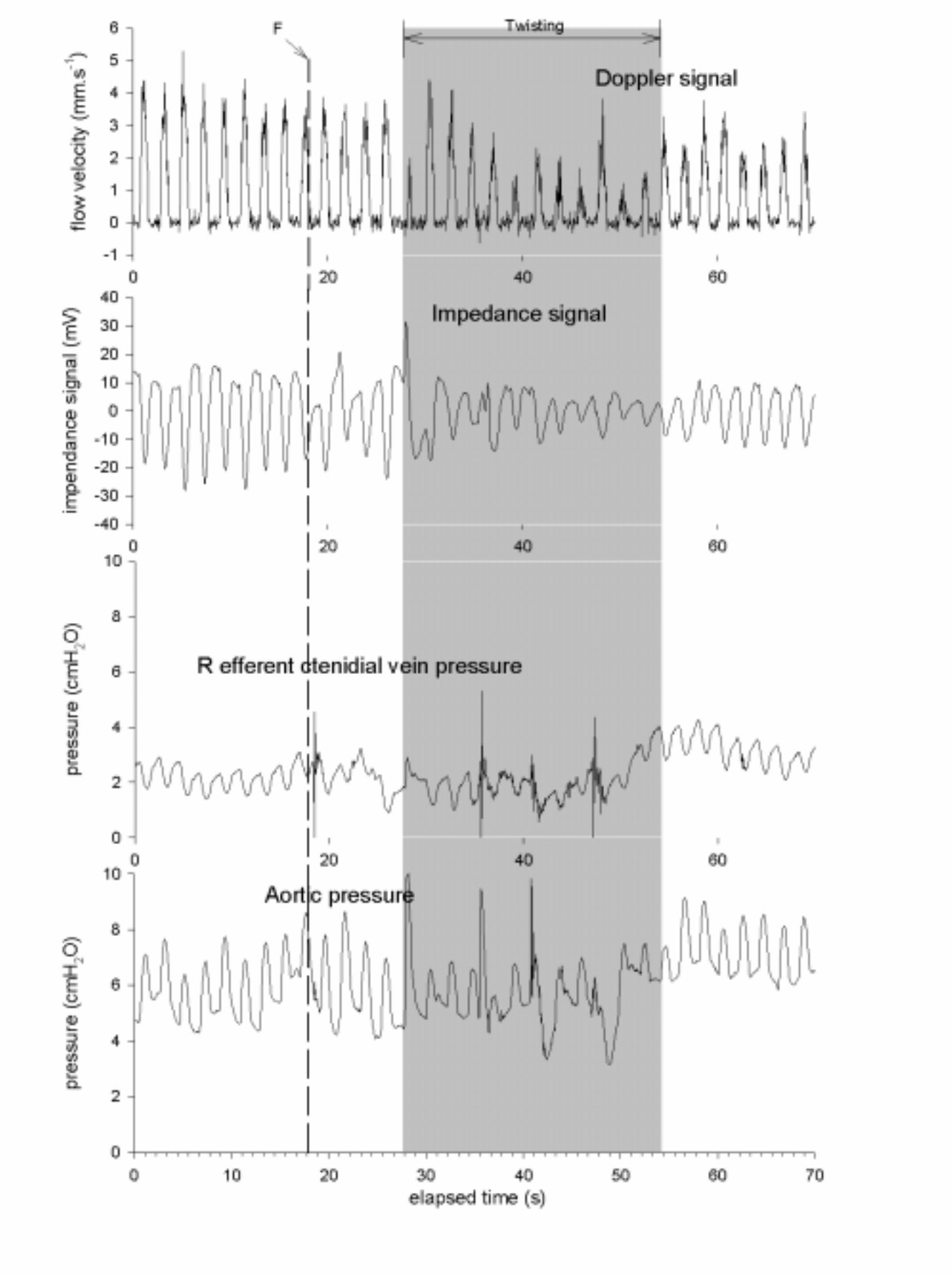


**Figure 7.11**: Aortic haemodynamics and right efferent ctenidial vein pressure during a flinch following by sustained twisting.

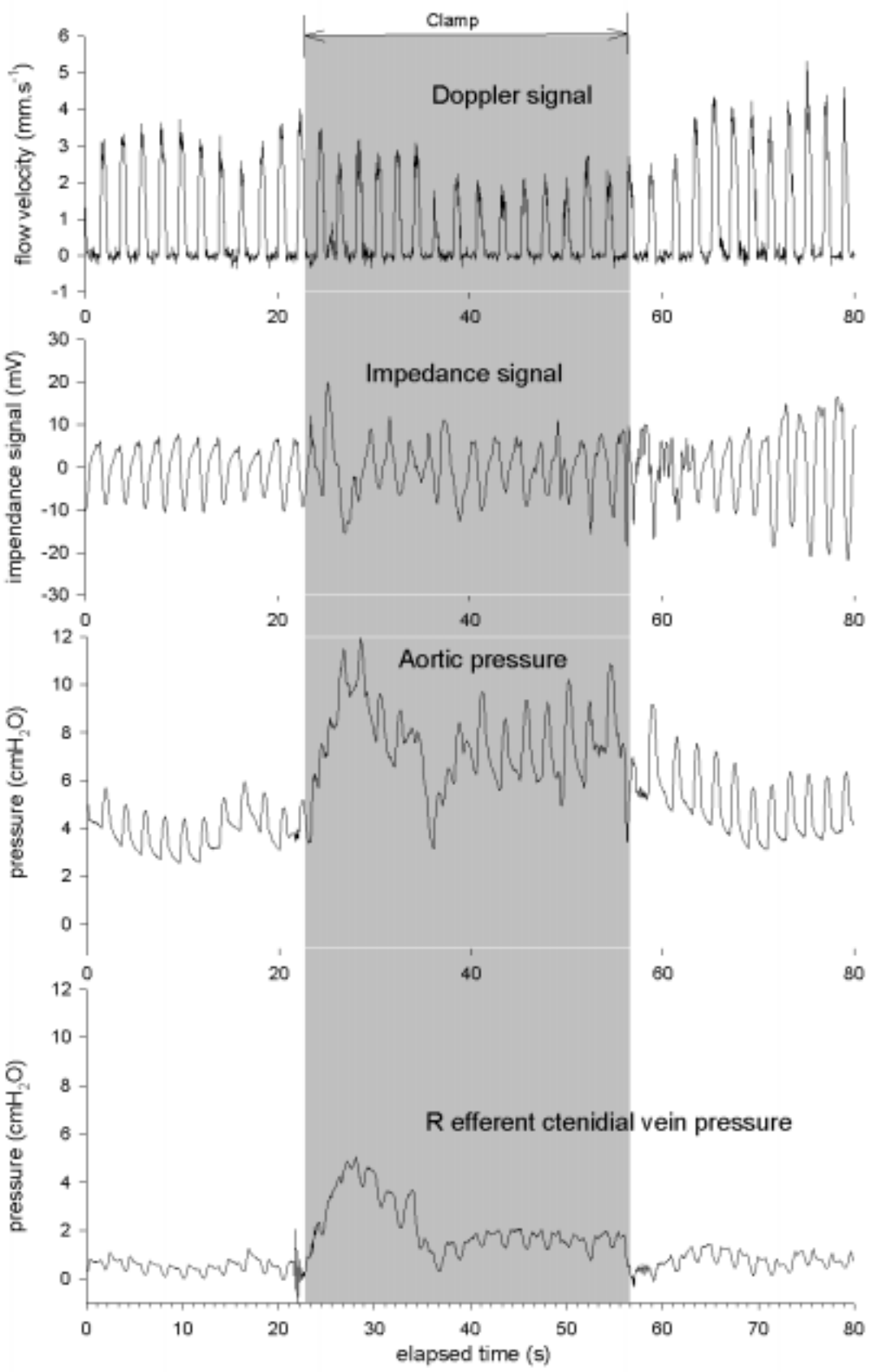


**Figure 7.12**: Aortic haemodynamics and right efferent ctenidial vein pressure during sustained clamping.

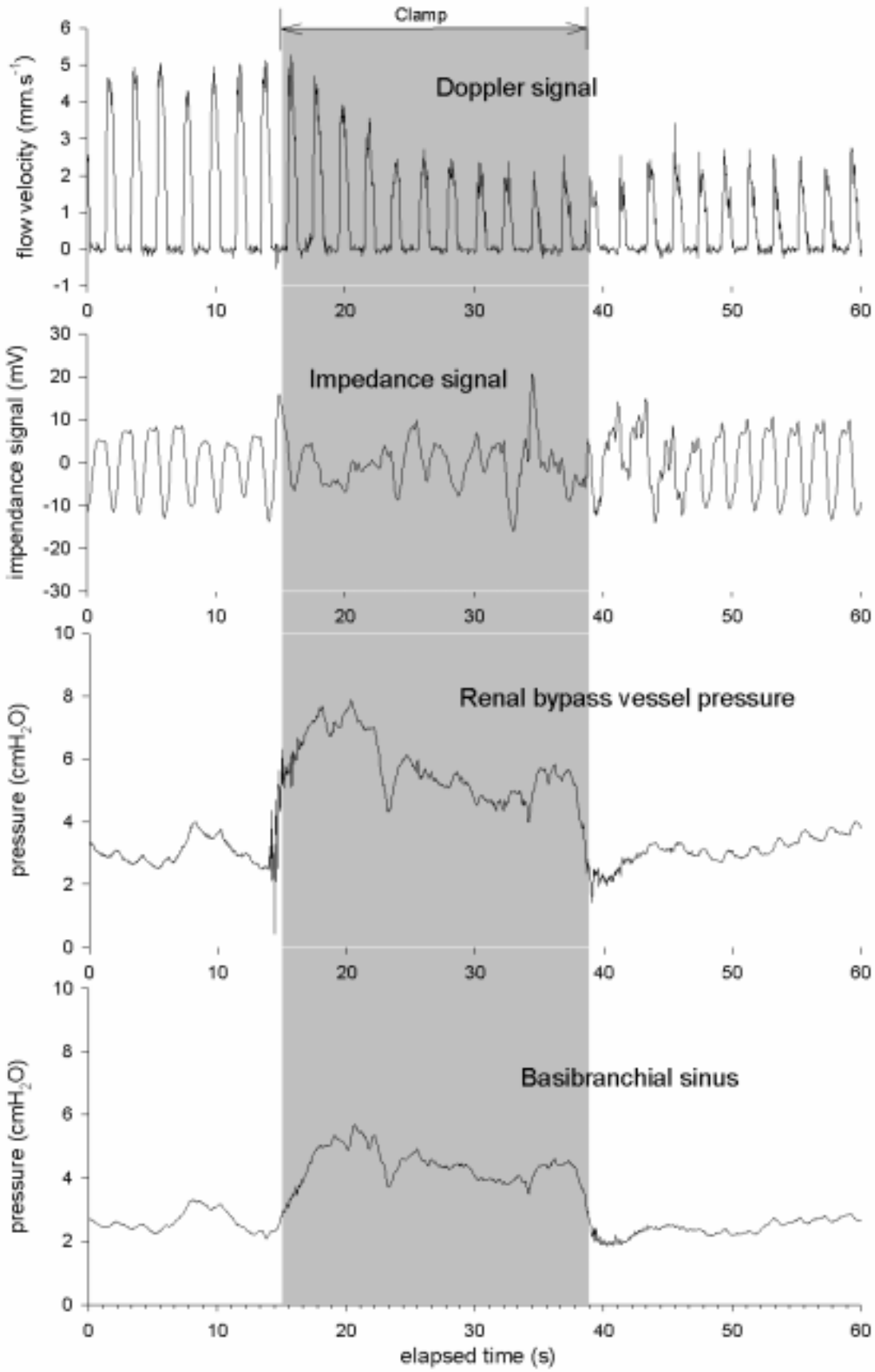


**Figure 7.13**: Renal bypass vessel and basibranchial sinus pressures and aortic flow during sustained clamping.

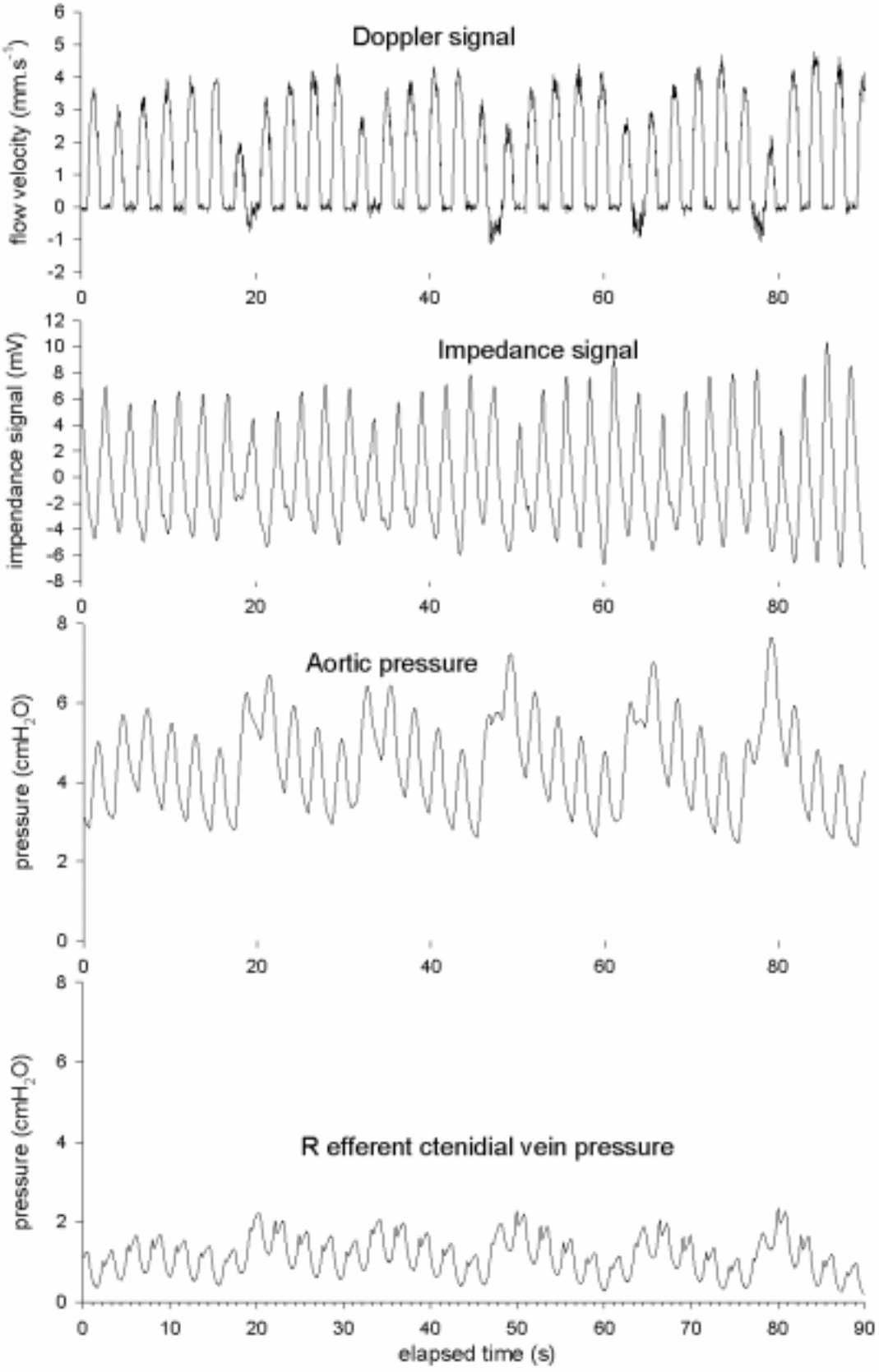


**Figure 7.15**: Haemodynamic oscillations seen in the aorta and right efferent ctenidial vein of abalone #M634 following recovery.

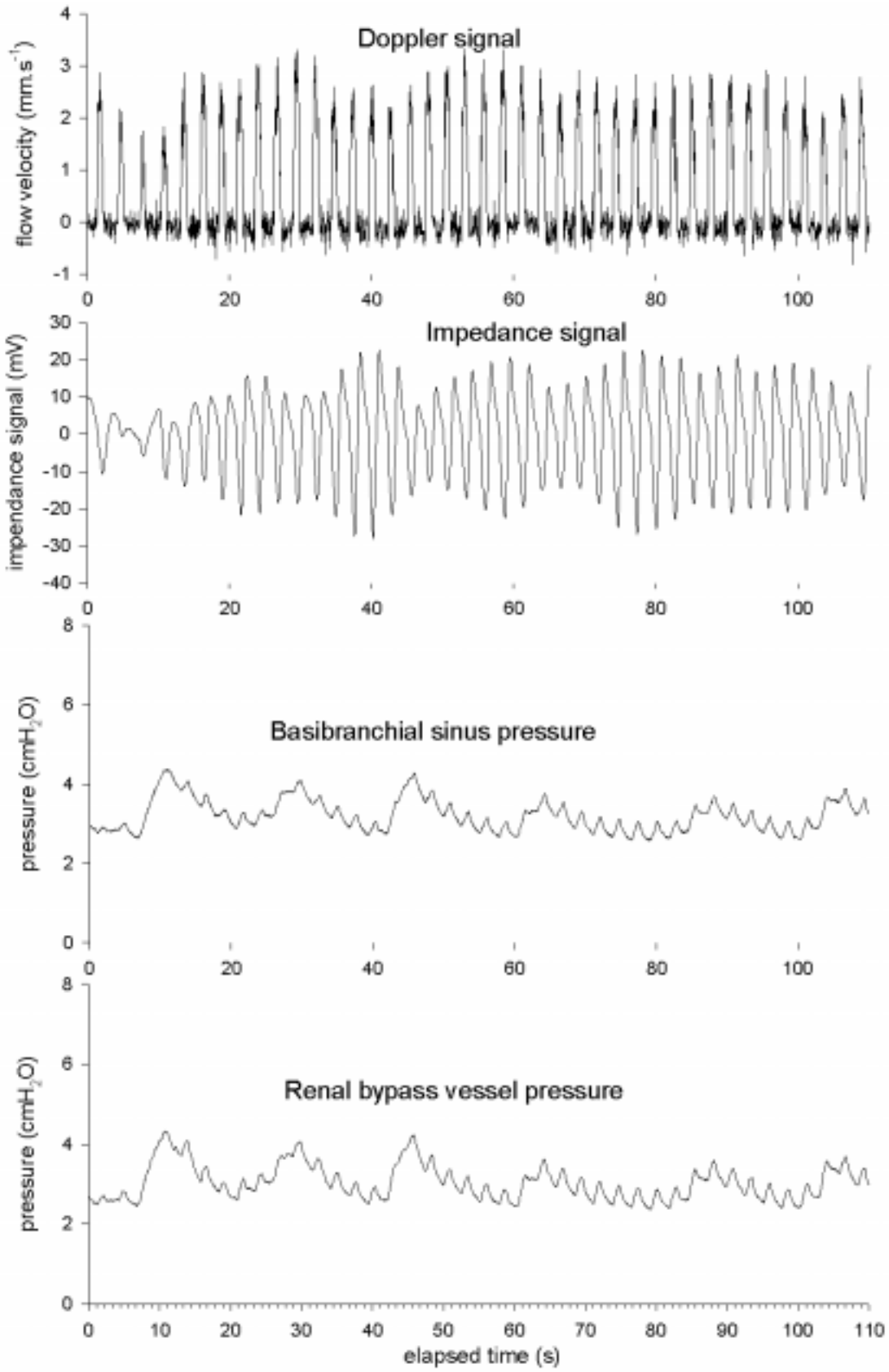


**Figure 7.16**: Rhythmic hydrostatic pressure oscillations seen in the basibranchial sinus and renal bypass vessel of abalone #M671 following recovery.

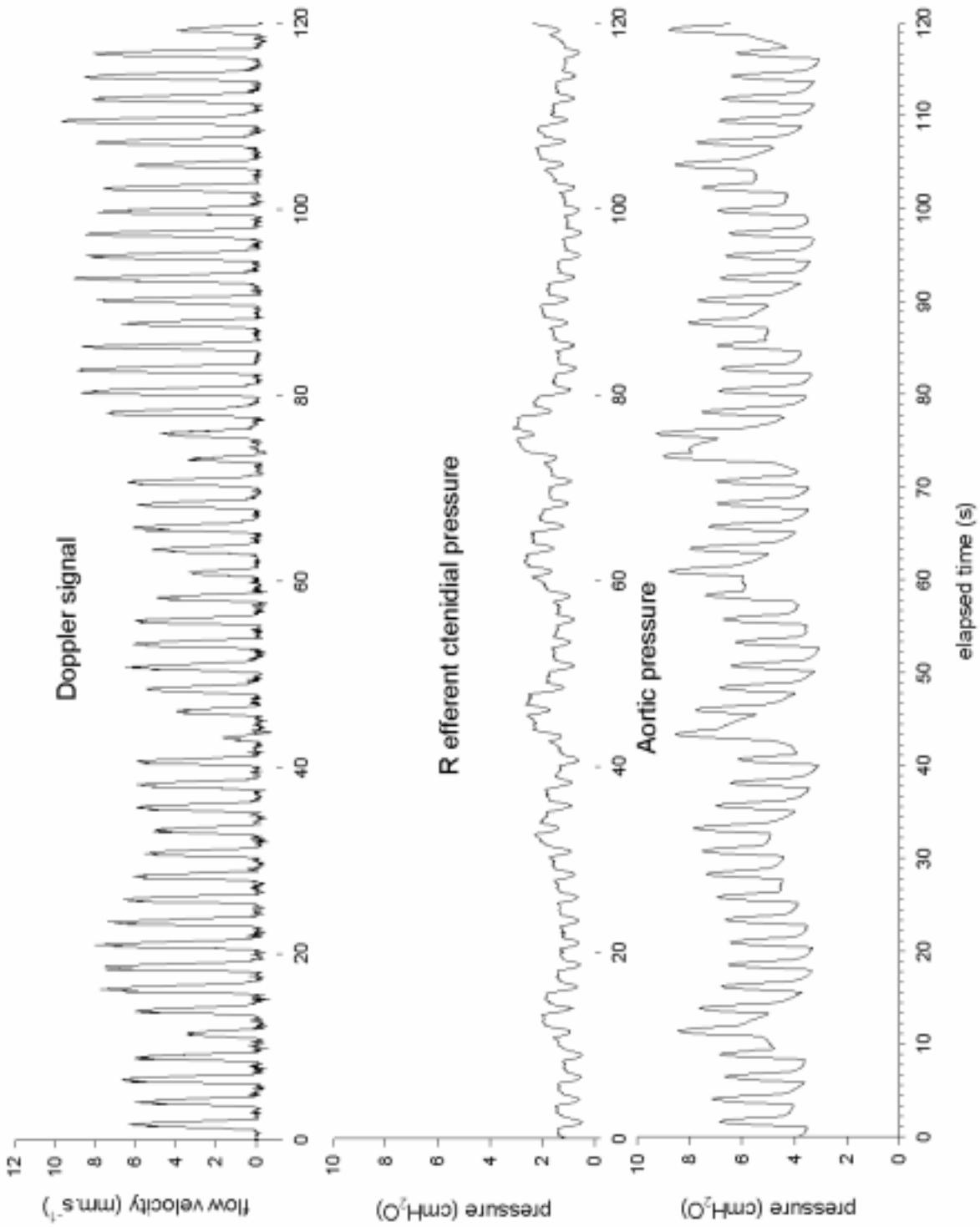


**Figure 7.17**: Haemodynamic oscillations seen in the aorta and right efferent ctenidial vein of abalone #M680 following recovery.

*Cardiac cycling*

A distinct recurring pattern was frequently seen in the haemodynamic parameters of recovering abalone. The cycling occurred with a rhythmicity of 5 – 8 heart beats, apparent as a rapid increase in hydrostatic haemolymph pressure, followed by a more gradual return to normal resting values (figures 7.15 – 7.17). Baseline hydrostatic pressure fluctuations were greatest in the aorta and were reflected in an oscillation in stroke volume (Doppler signals of figures 7.15 and 7.17). As baseline pressure increased, aortic flow (i.e. stroke volume) decreased, to the extent that minor diastolic back-flow was occasionally associated with peaks in baseline aortic pressure (Doppler signal of figure 7.15).

*Secondary effects of heart movement*

With the section of shell covering the pericardium removed, aortic flow and pressure fell to 80.6 ±11.3% and 85.2 ±5.7% of undisturbed values respectively. Mean pressure in the right efferent ctenidial vein was more variable, but found to be generally higher than undisturbed values (125.1 ±54.5%). As noted above, there was no apparent change in pressure wave magnitude, amplitude or phase between the renal bypass vessel and basibranchial sinus.

# 7.4. Discussion

### *7.4.1. Heart rate and cardiac output*

*Heart rate*

With the exception of spontaneous cardiac pause and disruption caused by disturbance to the animal, each individual abalone's heart rate remained constant. This observation is consistent with findings for other gastropods, where individual size and ambient temperature are the key determinants of heart rate (Fujino et al. 1984, Depledge and Phillips 1986, Russell and Evans 1989, Voltzow 1994). Mean heart rates recorded for *H. iris* during recovery from stress, 25.99 ±0.94bpm, resemble those of similar sized *H. rubra* (25bpm; Russell and Evans 1989) and *H. corrugata* (21bpm; Bourne and Redmond 1977a) and the large prosobranch *Hemifusus* (Depledge and Phillips 1986), measured at 15ºC. Adult *H. discus hannai* are smaller than the previously mentioned abalone species and correspondingly have a higher heart rate of 32bpm at 15ºC (Fujino et al. 1984). Resting decapod crustaceans of a corresponding size range typically exhibit a rather higher heart rate of 30 – 50bpm, however, as with *H. iris*, increased stress or activity have minimal effect on heart rate (McMahon and Wilkens 1983).

*In vitro* preparations have shown prosobranch hearts (including those of abalone) to exhibit dose-dependent chronotropic responses to the neurotransmitters FMRF-amide and serotonin (Smith and Hill 1986, Voltzow 1994, Matsumura et al. 1999). *In vivo* however, the heart rate of *H. iris* appears to show little response to either severe stress or acute disturbance, other than a transient period of acardia (discussed below).

*Cardiac output and Stroke volume*

In the present study, cardiac output was estimated from pulsed Doppler flow in the anterior aorta, close to its origin with the common aortic trunk. Inevitably cardiac output was therefore underestimated, as haemolymph leaving the ventricle via the median pallial artery and leaving the aortic trunck via the posterior aorta, remained unmeasured (see chapter 3. Posterior aorta = 'first visceral artery' described by Crofts 1929 and by Bourne and Redmond 1977a). An alternative measure of cardiac output was attempted in the previous chapter, where output was taken to equal the sum of haemolymph leaving the gills. The latter method, however, ignores haemolymph returning to the heart via the pallial system, and therefore also underestimates output. Intuitively it is suggested that either technique will represent approximately 90% of cardiac output. The aortic measurement technique is preferred as only a single site must be monitored and subsequent *in situ* calibration using known volumetric flow is more reliable due to the relatively non-compliant nature of the aorta compared to the efferent ctenidial veins.

Aortic monitoring presents one major disadvantage, however. As noted by Bourne and Redmond (1977a), abalone are particularly sensitive to cannulation of the aorta, reflected in the current study by the failure to attain a true 'resting' state even after 36h without disturbance. In contrast, in the study where only the left and right efferent ctenidial veins were cannulated (described in chapter 6), a resting state was established within 24h. The resting condition was characterised by fully inflated tissues, periodic acardia, preferential perfusion of the right gill and, critically, a baseline cardiac output (total gill flow) of 9.1 ±2.1 $mL.kg^{-1}.min^{-1}$. In the present study the abalone were still considered to be recovering after 24 – 36h as cardiac output remained high at 25.99 ±4.03$mL.kg^{-1}.min^{-1}$, corresponding to an output of 22.6 ±3.9$mL.kg^{-1}.min^{-1}$ measured in recovering abalone in the previous chapter. The unambiguous stressed condition ensuing after cannulation and handling resulted in maximal cardiac output of 23.3 ±2.9$mL.kg^{-1}.min^{-1}$ measured through the gills (chapter 6), corresponding closely to 25.17 ±2.68 $mL.kg^{-1}.min^{-1}$ measured through the aorta (current study).

Published values for cardiovascular parameters in other molluscs rarely consider the effects of the sampling procedures upon the animal's haemodynamic status. Given the difficulty in attaining a true resting state in *H. iris*, it is assumed that published values relate to animals that are either severely stressed or in the process of recovering from stress, unless stated otherwise.

Limited data are available for cardiac output in lower molluscs (i.e. non-cephalopods), as indirect assessment using the Fick principle (equation 7.5) are usually considered inappropriate, forcing researchers to rely on more challenging direct or morphometric determination. For example, Fick determination of cardiac output in the scallop overestimated values based on direct measurement by 300% (Thompson et al. 1980).

$$Q = \frac{Mo_2}{\Delta Co_2} \qquad \text{Equation 7.5}$$

i.e. Cardiac output, *Q*, is determined from total oxygen consumption ($Mo_2$) and the mean artero-venous oxygen content difference ($\Delta Co_2$). The equation assumes that all oxygen uptake occurs at the gills, and that there is no significant consumption by the gill epithelium (e.g. Jorgensen et al. 1984, Levick 1991); these assumptions are invalid in *H. iris* (see chapter 4) and presumably most other soft-bodied water breathers. For example, in fish the use of the Fick equation to determine cardiac ouput results in apparent errors of up to 40% (Farrell and Jones 1992).

The cardiac output values that have been determined in large prosobranchs of comparable size to adult *H. iris* vary by more than an order of magnitude. Bourne and Redmond (1977b) used an electromagnetic flow probe to determine output of 2.1 and 3.6 mL.min$^{-1}$ in two *H. corrugata* (5 – 9 mL.kg$^{-1}$.min$^{-1}$ if the abalone are assumed to weigh 400g). The authors point out, however, that the external aortic bypass required by their technique tended to severely compromise the animals. Jorgensen et al. (1984) used thermodilution and microsphere reference withdrawal to measure cardiac output, noting an inconsistent discrepancy of 15% between the techniques. Jorgensen et al. (1984) subsequently determined cardiac output in *H. cracherodii* to be 98 – 153mL.kg flesh weight$^{-1}$.min$^{-1}$, or approximately 60 – 90 mL.kg$^{-1}$.min$^{-1}$, if the shell is taken to represent 40% of total live weight. Jorgensen et al. (1984) determined mean stoke volume in *H. cracherodii* to be approximately 2.9 mL.kg$^{-1}$ and, citing similar values measured in the nautilus, suggest large stroke volumes and slow heart rates are a characteristic of less active molluscs. Voltzow (1994) points out that these values are considerably higher than those of mammals. Bourne and Redmond's (1977b) values are approximately 3 times lower, and Jorgensen et al.'s (1984) 3 times higher than the mean data presented here for *H. iris*.

Cardiac output values closer to those of *H. iris* have been measured in the large prosobranchs *Busycon* (25.9mL.kg$^{-1}$.min$^{-1}$; DeFur and Mangum 1979) and *Hemifusus* (~46mL.kg$^{-1}$.min$^{-1}$; Depledge and Phillips 1986). A mean output of 29 mL.kg$^{-1}$.min$^{-1}$ was measured in *Octopus vulgaris* of similar mass to *H. iris* (Wells and Smith 1987). In this case, however, the octopus were in a true resting state, the output is therefore comparable to 9.1 mL.kg$^{-1}$.min$^{-1}$ measured in *H. iris* in chapter 6. Bivalve molluscs tend to have rather lower cardiac outputs, e.g. 6.9mL.kg$^{-1}$.min$^{-1}$ in *Noetia ponderosa* and 12.6 mL.kg$^{-1}$.min$^{-1}$ in *Spisula solidissima* (DeFur and Mangum 1979). As an extreme example of the cardiac output possible within the confines of a molluscan body plan, Wells and Smith (1987) estimate the squid *Illex* to pump more than 400mL.kg$^{-1}$.min$^{-1}$ during rapid jetting.

In contrast to lower molluscs, decapod crustaceans of comparable mass to *H. iris* show a far higher cardiac output, typically 100 – 150 mL.kg$^{-1}$min$^{-1}$ (Mangum 1983, McMahon and Wilkens 1983). High cardiac output in crustaceans is attributed to total dependence upon haemolymph for $O_2$ transport from the gills, as impermeable chitin prevents the direct diffusion to tissues, as often exploited by molluscs (Mangum 1983). The oxygen carrying capacity of crustacean haemolymph is also low (typically 0.5 – 1.5 mmol.L$^{-1}$) but this is offset by a high cardiac frequency, made possible by sarcoplasmic reticulum enrichment in the myofibres (Mangum 1983). Wells (1992) standardised cardiac output to predict performance in a 400g animal, which corresponds to the mean weight of *H. iris* used in the current experiment; output in *Nautilus* was estimated to be 86mL.kg$^{-1}$.min$^{-1}$ and

in a mammal 222mL.kg$^{-1}$.min$^{-1}$. If scaling factors are ignored, allowing comparison to be made to vertebrates, cardiac output reported for *H. iris* falls within the range reported for elasmobranchs and temperate water teleosts (typically 20 – 45mL.kg$^{-1}$.min$^{-1}$; Farrell and Jones 1992). *H. iris* cardiac output is rather less than that of higher mammals, represented by the human male, 82mL.kg$^{-1}$.min$^{-1}$ (Guyton 1986). In a multispecies analysis, McMahon and Wilkens (1983) show a strong negative exponential relationship between cardiac output and blood oxygen capacity (figure 7.18). If *H. iris* haemolymph is taken to have a mean oxygen carrying capacity of 0.346 mmol.L$^{-1}$ (chapter 5 of this thesis) and a cardiac output of approximately 25 mL.kg$^{-1}$.min$^{-1}$, cardiac output appears to fall well below that predicted by the relationship shown in figure 7.18.

If 9.1mL.kg$^{-1}$.min$^{-1}$ is taken as representing true resting output in *H. iris* (measured in chapter 6) then extreme stress results in a 3-fold increase in cardiac output, resembling the change seen in trout taken from rest to maximal exercise (Jones and Randall 1978). This suggests that in abalone, as in fish, cardiac output is modulated by a highly labile stroke volume rather than by frequency (Jones and Randall 1978, Farrell and Jones 1992). Increased cardiac output presumably reflects increased oxygen demand by the tissues. The 3-fold increase in output by *H. iris* is accordingly similar to the 2.5 – 3.5-fold increase in $Mo_2$ measured in some *H. kamtschatkana* during the transition from rest to rapid locomotion (Donovan and Carefoot 1997; see chapter 6 of this thesis for an amplified discussion). A strikingly similar cardiac response pattern is also seen in *Octopus vulgaris*, which show a 2.3-fold increase in $Mo_2$ and cardiac output in response to stress or exercise, which remains unchanged during subsequent recovery until the oxygen debt is repaid (Wells and Smith 1987). As in *H. iris*, the octopus also maintains a constant heart rate, affecting changes by regulation of stroke volume (Wells and Smith 1987). Resting stroke volume in the octopus was measured to

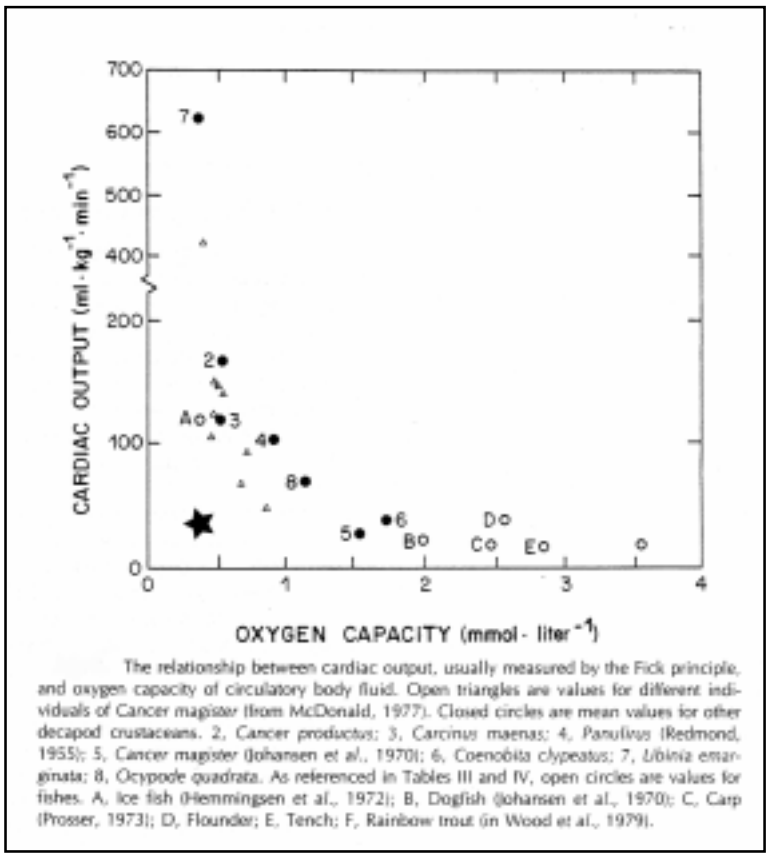


The relationship between cardiac output, usually measured by the Fick principle, and oxygen capacity of circulatory body fluid. Open triangles are values for different individuals of Cancer magister (from McDonald, 1977). Closed circles are mean values for other decapod crustaceans. 2, Cancer productus; 3, Carcinus maenas; 4, Panulirus (Redmond, 1955); 5, Cancer magister (Johansen et al., 1970); 6, Coenobita clypeatus; 7, Libinia emarginata; 8, Ocypode quadrata. As referenced in Tables III and IV, open circles are values for fishes. A, Ice fish (Hemmingsen et al., 1972); B, Dogfish (Johansen et al., 1970); C, Carp (Prosser, 1973); D, Flounder; E, Tench; F, Rainbow trout (in Wood et al., 1979).

**Figure 7.18**: Relationship between cardiac output and blood oxygen carrying capacity for a range of crustaceans and fish (extracted from McMahon and Wilkens 1983). Filled star indicates the position of *H. iris*.

be approximately 0.8 mL.kg$^{-1}$ (Wells and Smith 1987), with a corresponding mean of 0.37 mL.kg$^{-1}$ in *H. iris* (chapter 6 of this thesis). During stress and recovery these values rise to 1.8 mL.kg$^{-1}$ in the octopus and 0.93 – 0.96 mL.kg$^{-1}$ in the stressed or recovering *H. iris*. In contrast, in the bivalve mollusc *Placopecten magellanicus*, valve snapping exercise causes a 2 to 3-fold increase in heart rate, as well as a 2.4 to 4-fold increase in stroke volume, resulting in a 5-fold increase in cardiac output (Thompson et al. 1980).

*Circulation time*

Jones and Randall (1978) suggest that blood circulation time can be estimated if blood volume is divided by cardiac output. Using the mean haemolymph value of 55.4mL.100g flesh weight$^{-1}$ determined for resting *H. iris* (chapter 2 of this thesis) and a resting cardiac output of 9.1mL.kg$^{-1}$.min$^{-1}$ (chapter 6), circulation time is estimated to be 44min (shell of adult *H. iris* = 31.4% of body mass, unpublished data). Although a crude estimate, this value effectively corroborates the dogma that prosobranchs have a long circulatory time (Voltzow 1994). Handling stress causes mean *H. iris* haemolymph volume to fall to 44.0mL.100g$^{-1}$ (chapter 2). In the present study stress has been shown to elevate cardiac output to 25.2mL.kg$^{-1}$.min$^{-1}$. Estimated circulation time would therefore be reduced to 13min under stress, hinting at a possible adaptive advantage associated with temporarily reduced plasma volume. The haemolymph volume, however, is still large, inevitable resulting in circulation times considerably longer than the 1 – 5min estimated for salmonid fish which are, in turn, considered long compared to higher vertebrates (Jones and Randall 1978).

### *7.4.2. Stroke work and cardiac power*

The external, or stroke work of the ventricle is represented by the area under a pressure-volume loop graph. For practical purposes here, work has been determined as the product of stroke volume and driving pressure (equation 7.1), an estimation technique that tends to be within 20% of pressure-volume loop values (Farrell and Jones 1992). Stroke work in *H. iris* was not affected by the transition from the stressed to recovering state, remaining at 1.15 – 1.17 mJ.g ventricle$^{-1}$. Using the very high cardiac output and stroke volume data of Jorgensen et al. (1984), Bourne et al. (1990) calculated stroke work values for *H. cracherodii* of 0.032 – 0.042 mJ.g live weight$^{-1}$. When standardised to animal wet weight, mean stroke work in *H. iris* was found to be 0.00047 ±0.00008 mJ.g live weight$^{-1}$ under stress and 0.00047 ±0.00006 mJ.g$^{-1}$ during recovery, 2 orders of magnitude lower than the values of Jorgensen et al. (1984). Amongst other Mollusca, stroke work determinations have been limited to the high performance hearts of the cephalopods. In unrestrained octopus, stroke work was estimated to be 2.3 – 6.7mJ.g ventricle$^{-1}$, 3 – 10mJ.g$^{-1}$ in nautilus and 2.6mJ.g$^{-1}$ in the squid, *Loligo pealei* (Wells 1992). Stroke work in active fish fell into a similar range to that of cephalopods (2 – 3 mJ.g$^{-1}$; Farrell and Jones 1992). Compared to these performance hearts, it is perhaps unsurprising the stroke work in *H. iris* was found to be low.

Cardiac power is needed to overcome shear stress in the haemolymph vessels and resistance in the tissues (Vogel 1994). Cardiac power output in *H. iris* is more than an order of magnitude higher

than the values calculated for *H. cracherodii* (Bourne et al. 1990), as with stroke work, these low values are derived from the high cardiac output determined for this species (Jorgensen et al. 1984). The calculated mean power output by the abalone heart (0.641 and 0.655 mW.g ventricle$^{-1}$, 'stressed' and 'recovering', respectively) is somewhat lower than published values for most fish, which typically range from 0.9 – 1.8 mW.g$^{-1}$ in resting, temperate species, increasing 2 to 4-fold during stress or exercise (Farrell and Jones 1992). However, *H. iris* cardiac power is rather higher than peak performance measured in either the systemic (0.37mW.g$^{-1}$) or portal hearts (0.20mW.g$^{-1}$) of hagfish (Johnsson et al. 1996), more closely resembling work performed by the heart of eels (*Anguilla* spp.; Farrell and Jones 1992). Resting systemic heart power output in octopus of similar mass to *H. iris* (*Octopus vulgaris* and *Eledone cirrhosa*) was reported as 1.2 – 1.6mW.g$^{-1}$, increasing 4 - 7-fold during exercise stress (Wells and Smith 1987, Wells 1992). Similarly a small mammal representative of the size range (125g) is expected to have a resting cardiac power output of 36mW.g$^{-1}$, which increases 5-fold during exercise (Wells 1992). Resting cardiac power output could not be measured during the current experiments on *H. iris* but, given the similarity in response to the systemic heart of octopus, is assumed to be considerably lower than the stressed or recovering values.

Cardiac power is therefore considered to be low, compared to more active taxa. The low cardiac ATP demand associated with lower power output has been considered an advantage insofar as tolerance of hypoxia is likely to be increased (Farrell and Jones 1992), potentially of great importance to the abalone, where functional and local environmental hypoxia are routinely encountered (e.g. Gäde 1988, Baldwin et al. 1992). It should also be noted that the energy requirements of the main muscle blocks, the foot and adductor, are also low, even compared to other molluscs (Gäde 1988).

### *7.4.3. Pressure gradients, resistance and auxiliary pumps*

*Haemolymph pressure*

Under high aerobic demand (stress) the heart of *H. iris* maintained a mean pressure of 4.56cm$H_2O$ in the aorta and 1.16cm$H_2O$ in the pre-cardiac haemolymph of the right efferent ctenidial vein. Bourne and Redmond (1977a) also measured systemic pressures in pink abalone, *H. corrugata*, of similar size to *H. iris* under similar conditions (within a few minutes of cannulation) and recorded a mean aortic pressure of 7.4 cm$H_2O$ falling to 1.9 cm$H_2O$ in the efferent ctenidial vein. Similar pressures were also recorded in the ventricle of *H. rubra*, which were typically 8:4 cm$H_2O$ (systolic:diastolic; Russell and Evans 1989). The aortic pressures are typical of gastropods, e.g. *Hemifusus* systolic aortic pressure 6.4 – 10.6cm$H_2O$ (Depledge and Phillips 1986), *Aplysia* mean aortic pressure 4 – 7cm$H_2O$ (Brownell and Ligman 1992), *Patella vulgata* aorta 5:2 cm$H_2O$ (Voltzow 1994), *Littorina littorea* aorta 3.0:0.8 cm$H_2O$ (Andrews and Taylor 1988). Arterial pressure in *H. iris* is, however, low in comparison to other active animals of a similar size. Decapod crustacean aortic pressures, for example, range from 5 – 21cm$H_2O$ (diastolic), 8 – 47cm$H_2O$ (systolic; McMahon and Wilkens 1983). Aortic pressures in the closed vascular system of *Octopus vulgaris* ranged from 20cm$H_2O$ diastolic to 35cm$H_2O$ systolic (400g @20ºC Wells and Smith 1987). Mammalian mean aortic pressures are typically about 135cm$H_2O$, regardless of size (Wells 1992).

As the abalone in the current study did not return to a true resting state, systemic pressures could only be measured in stressed and recovering animals. As systemic pressure apparently increases with stroke volume in other prosobranchs (e.g. *Littorina*; Andrews and Taylor 1988), it is likely that resting pressures would be lower than those measured here. It seems likely that pressures measured in earlier studies of other abalone species also relate to recovering, rather than resting animals.

Bourne and Redmond (1977b) gave a detailed description of the mechanisms likely to cause each phase of the ventricular pressure pulse in *H. corrugata*. Applied to the aortic pressure pulse of *H. iris* (e.g. figures 7.4a and e, 7.5a and e, 7.6a and e): the pressure minimum represents the point where the aortic pocket valve is breached, allowing dynamic contraction of the ventricle, rapidly elevating aortic pressure and driving haemolymph flow. Pressure and flow subsequently decline as the ventricle empties; flow ceases as the pressure fall is interrupted by a dichrotic notch, representing the closing of the pocket valve (Bourne and Redmond 1977a, Andrews and Taylor 1988). The ventricle proceeds to fill and then begin isovolumetric contraction until pressure is once again sufficient to breach the valve. In the aorta however, pressure continues to slowly decline; this final phase differs between *H. iris* and *H. corrugata*. Bourne and Redmond (1977a) identify a distinct aortic bulb within the pericardium of *H. corrugata* that apparently helps maintain aortic flow after the pocket valve has closed (Bourne and Redmond 1977b). No aortic bulb was found in *H. iris* and flow is consequently seen to stop when the valve closes; it is suggested that the gradual subsequent decline in aortic pressure represents elastic recoil by the vessel walls.

Haemolymph from the aorta may either enter a number of arteries, particularly those supplying regions of the digestive or reproductive systems, or it may pass into the cephalic arterial sinus, from which anterior arteries arise (Crofts 1929). Venous return is initially collected in an extensive gastric sinus region surrounding the entire alimentary tract (see chapter 3). The renal bypass vessel originates from the gastric sinus in the region of the intestinal loop, to the right of the head (chapter 3). In the transition from aorta to bypass vessel, mean haemolymph pressure falls only slightly from 4.56 to 3.50cm$H_2O$ (figure 7.2), although pulse amplitude is damped (figures 7.4b, 7.5b and 7.6b). It is assumed that pressure is maintained as a result of low peripheral resistance in the lacuna beds and by direct arterial supply to the gastric sinuses (see chapter 3). The bypass vessel traverses the anterior right kidney region and drains into the renal sinus. The renal sinus, which also receives the efferent haemolymph of the right kidney, drains into the basibranchial sinus, via a short connecting vessel. This connecting vessel contains a large, collagenous valve of unknown function (see chapter 3). No net pressure gradient was found to exist between the bypass vessel, near it's origin in the head, and the basibranchial sinus. The absence of a significant pressure gradient implies that negligible resistance is encountered in the bypass vessel. The valve also appears to offer no discernible resistance.

How does haemolymph flow in the apparent absence of a pressure gradient? The Bernoulli Theory states that flow between 2 points occurs as a result of the fluid's mechanical energy, the product of pressure, potential and kinetic energy. It is therefore possible for haemolymph to flow in apparent defiance of Darcy's law, i.e. in the absence of a significant pressure gradient, if the fluid

has sufficient potential or kinetic energy (Levick 1991). Gravity is unlikely to have a net effect on the approximately planar circulation of abalone, imparting no potential energy. Kinetic energy gradients, however, are known to have important effects in facilitating flow through the great veins in humans, in particular assisting in auricular filling (Levick 1991) and may serve to fill the capacious renal and basibranchial sinuses. A small, but consistent phase shift in the weakly pulsatile pressure may also be important in permitting haemolymph flow (figure 7.4e, 7.5e and 7.6e). Phase relationship is certainly of paramount importance in permitting flow across the right mantle. In the recovering abalone, no significant difference was detected between the mean pressure in the CPV and the pallial vein. However the pressure pulse in these vessels were in antiphase, creating a maximal instantaneous pressure gradient, and thereby permitting flow, during ventricular systole.

The pressure drop across the right gill of *H. iris* represents the largest pressure decrease in the circuit. Mean resting pressure in the basibranchial sinus of 3.30cm$H_2O$ fell to 1.16cm$H_2O$ in the right efferent ctenidial vein (figure 7.2). The gills therefore appear to account for approximately 60% of the total pressure loss in the main circulation. Corresponding measurements made by Bourne and Redmond (1977a) revealed a similar situation in *H. corrugata*, where the gills, occupying only 4% of the body mass, were responsible for 40% of the systemic pressure drop. The gills are generally regarded as being a major component in vascular resistance in water breathers, requiring specific strategies to generate sufficient pressure gradients to allow perfusion to occur. In the pectininbranch gill of the mesogastropod *Littorina littorea*, however, a mean afferent ctenidial pressure of 0.6 cm$H_2O$ and an efferent ctenidial pressure of 0.4 cm$H_2O$ are maintained (Andrews and Taylor 1988). The small pressure gradient implies that reduced vascular resistance may accompany the evolutionary abandonment of the bipectinate gill design seen in abalone. In fish the high branchial vascular resistance (20 – 40% of total vascular resistance) is accommodated by supplying cardiac output directly to the gills then to the systemic circulation (Randall and Daxboeck 1984). The cost of such an arrangement is the need to strengthen lamellae to withstand large transmural pressure gradients (typically 20 – 40 Torr; Randall and Daxboeck 1984). Decapod crustaceans apparently benefit from assisted gill perfusion due to scaphognathite (gill baler) beating. The scaphognathites can generate negative branchial pressures during forward pumping (down to –4 Torr; McMahon and Wilkens 1983) which has been shown to expand the thin-walled lamellae and associated vessels, providing a transient decrease in resistance (Taylor 1990). Reciprocally, reverse pumping (up to +7 Torr) increases vascular resistance, impeding haemolymph flow through a gill (Taylor 1990).

A 1 – 2 Torr gradient is required for haemolymph to flow across crustacean gills, compared to approximately 8 Torr for a dogfish or 11 Torr for a trout (McMahon and Wilkens 1983). The relatively low requirement of crustacean gills is attributed to the low viscosity of haemolymph (McMahon and Wilkens 1983) and can readily be provided by pre-branchial pressures of 10 – 20 Torr (13 – 26cm$H_2O$). Abalone also have low haemolymph viscosity (Taylor 1993), but are unable to generate the pressures found in the crustacean circulation. It is therefore suggested that the mixed arterial and venous haemolymph gut sinuses and the low resistance renal bypass vessel exist, at least in part, as devices to maximise the pressure of haemolymph delivered to the gills.

*Auxiliary pumps*

Animals with venous gills (i.e. molluscs and crutaceans) and animals with large blood volumes have tended to evolve secondary pumps to assist in venous return and/or gill perfusion. Hagfish, for example, possess 5 hearts to assist in blood circulation through the capacious venous system and the perfusion of specific organs (Davison 1995). Venous suction by the constant volume heart of molluscs may also be considered an auxiliary pumping action facilitating venous return. The extensive musculature of molluscan vessels also provides the basis for other potential pumps. The most advanced developments are seen in the dibranchiate cephalopods, which use secondary hearts, beating synchronously with the systemic heart, assisting in perfusion of the gills (Wells and Smith 1987). Rhythmic contractions are also seen in octopus vessels, assisting in the perfusion of remote vasculature (Wells and Smith 1987). In *Aplysia* the gill itself contracts to assist in venous return; the pericardium is also contractile, potentially providing indirect assistance to the heart by clearing ultrafiltrate, thereby permitting a transient increase in cardiac filling (Brownell and Ligman 1992). No such mechanisms have, to date, been described in the abalone.

The effects of removal of the shell section overlying the heart proved inconclusive in identifying a possible secondary pumping action due to pericardial movement against the efferent renal vessels. This treatment did, however, produce a distinct reduction in the pressure gradient generated by the heart, lowering mean aortic pressure and raising efferent ctenidial pressure. A model proposed by van den Berg (1992) shows that pericardium rigidity should not influence the transmission of negative pressure through the pericardial fluid during ventricular systole. Removal of the shell overlying the heart of *Littorina* appeared to have no effect on systemic pressure, in agreement with the van den Berg model (Andrews and Taylor 1988). In the present study, however, external support of the pericardium of *H. iris* is shown to be essential for the effective functioning of the constant volume system. In the absence of shell support, the pericardium behaves as if its elastance * had increased, according to the van den Berg (1992) model, impeding the rate of ventricle emptying and thereby reducing stroke volume, cardiac output and, subsequently, pressure.

*Peripheral resistance*

Depledge and Phillips (1986) calculated total peripheral resistance for a range of molluscs, by using systolic aorta pressures and assuming venous return pressure to be ambient. These authors found exceptional variation amongst species, ranging from 62cm$H_2O$.$mL^{-1}$.$min^{-1}$ for *Littorina*, 50 for *Mytilus*, 5.3 for *Hemifusus*, 3.8 for *Haliotis corrugata* to 0.54cm$H_2O$.$mL^{-1}$.$min^{-1}$ for *Octopus*. Human total peripheral resistance is typically about 44cm$H_2O$.$mL^{-1}$.$min^{-1}$ and ranges from 16 to 310cm$H_2O$.$mL^{-1}$.$min^{-1}$ (Guyton 1986, Levick 1991). Mean peripheral resistance of *H. iris* (0.60 – 0.66 cm$H_2O$.$min$.$mL^{-1}$) therefore seems extremely low when compared to most organisms, even to *H. corrugata*, with values resembling those of *Octopus*. It should be noted that Depledge and Phillips (1986) used cardiac output measurements from Bourne and Redmond (1977b) in calculating the

* Elastance is a term coined by van den Berg (1992) to describe the physical properties of the pericardium (elasticity and compliance).

high peripheral resistance of *H. corrugata*, as discussed above, these values were obtained from physiologically compromised animals and are likely to represent an under-estimate of true output. Calculated resistance is therefore likely to be unrepresentatively high. The other comparisons listed must also be viewed with caution as no account is taken of scaling effect. Depledge and Phillips (1986) show the peripheral resistance of *Hemifusus* to fall by an order of magnitude with increase in shell length from 7.6 to 13.6cm, reflecting increased reliance on circulation and hence increased cardiac output. Hence the relatively small *Mytilus* and *Littorina*, with low cardiac output, possess high peripheral resistances. Humans, representing higher animals, rely on muscle-muscle antagonism, which has an inherently higher resistance than the muscle-hydrostat system of prosobranchs and bivalves (Wells and Smith 1987). Octopus also use muscle-muscle antagonism but circulation is assisted by secondary pumps, rendering *in vivo* resistance very difficult to assess accurately. It should be noted that while the muscle-hydrostat system imparts an apparent advantage by reducing vascular resistance, it is consequently more difficult to control regional perfusion (Brownell and Ligman 1992) and resistance is likely to increase during activity (Smith 1987, Wells and Smith 1987). Resistance of a muscle-muscle antagonist is expected to decrease during exercise (Jones and Randall 1978, Smith 1987). As suggested above, low resistance is a function of low haemolymph viscosity, and also reflects the large number of parallel channels found throughout the vasculature of *H. iris*.

### *7.4.5. Pressure phasing, flow and the constant volume heart*

*The constant volume heart*

Mechanisms to maximise pressure at the afferent side of the gills are discussed above. However abalone also increase the pressure gradient across the gills by actively lowering the pressure in the veins entering the heart. The phenomenon is attributed to the well-documented action of the constant volume molluscan heart. Ventricular systole, in addition to ejecting haemolymph into the aorta, also transmits negative pressure into the pericardial fluid (e.g. van den Berg 1992). Surrounded by incompressible pericardial fluid confined within the pericardium, the sub-ambient pressure acts on the most compliant surfaces available, the auricle walls (e.g. Bourne and Redmond 1977b). The ensuing pressure gradient results in auricular filling as a direct result of ventricular contraction (*vis-à-fronte*) rather than kinetic energy within the venous flow (*vis-à-tergo*). The net effect is seen in figures 7.2, 7.3, 7.4d, 7.5d and 7.6d, as right efferent ctenidial vein pressures are driven below the abalone's MCFP. The antiphase relationship between the ventricle and pericardial fluid pressure (e.g. in *H. rubra*; Russell and Evans 1989) or between the aorta and efferent ctenidial haemolymph (e.g. *H. corrugata*; Bourne and Redmond 1977a) is usually presented as evidence of a constant volume mechanism. Some caution is required, however, as the ventricle and pericardial fluid of *Littorina littorea* also show this relationship, but the total volume within the pericardium appears to fluctuate during the cardiac cycle (Andrews and Taylor 1988).

Apparent analogues to the *vis-à-fronte* filling of the constant volume molluscan heart are found throughout the animal kingdom. Systemic venous return in mammals (human model) also acquires

pulsatility in the thoracic region due to the effect of the right ventricle. Some similarity to the molluscan model is apparent insofar as peak flow in the vena cava is associated with a fall in pressure, during passive auricular and ventricular diastole (Levick 1991). The pressure gradients associated with venous return are, however, more than an order of magnitude less than those of the arterial system. Conversely the pressure decrease transmitted by the abalone auricles is of similar magnitude to the positive systolic pressure measured in the aorta.

In the mammalian heart ultimately about 25% of auricle filling is due to auricular diastole, the major factor being inertia in the venous return (Farrell and Jones 1992). More useful comparisons can be made to animals where the auricle is essentially passive, e.g. fish and crustacea. *Vis-à-fronte* filling is facilitated in elasmobranchs by a thick pericardium (Jones and Randall 1978), while performance teleosts possess a rigid musculoskeletal framework within the pericardium (Farrell and Jones 1992). Less active species rely exclusively on *vis-à-tergo* filling while, in active species, reliance upon *vis-à-tergo* increases with exercise (Farrell and Jones 1992). In fish, *vis-à-fronte* filling is considered advantageous insofar as it helps reduce the stressed volume of the capacious venous system, it apparently permits higher systolic pressure and allows more rapid auricle filling, driven by faster ventricular contraction rather than slower auricular diastole (Farrell and Jones 1992). The very small pressures that would exist in the abalone auricles in the absence of active aspiration from the ventricle would certainly result in extended filling times. Farrell and Jones (1992) suggest shortcomings of *vis-à-fronte* filling include the limitation to stroke volume imposed by a rigid pericardium and that sub-ambient pericardial pressure will tend to preferentially fill the sinus venosus rather than the atrium. The stroke volume of molluscs may also be limited by the pericardium, however no other passive structures, analogous to the sinus venosus occur with the pericardium, hence all negative pressure is transmitted to the auricles.

Higher crustaceans also utilise a variation on the constant volume heart, the pericardium (actually a haemocoelic space analogous to an auricle) is effectively rigid, the ventricle is suspended in its lumen by elastic alary ligaments. As the ventricle contracts, pressure in the pericardial haemolymph is lowered, thus increasing the pressure gradient available for venous return (McMahon and Wilkens 1983).

*Venous return and the constant volume heart*

The Frank-Starling law, applied to the vertebrate heart suggests that cardiac output is effectively determined by venous return (Guyton 1986). It is unclear to what extent the same mechanism may influence the constant volume molluscan heart. Farrell and Jones (1992) suggest that the thin and distensible nature of fish auricles apparently results in their highly sensitive output response to filling pressure. As mollusc auricles are even more compliant, the Starling effect may be particularly pronounced; however, in the present study, no significant changes in filling pressure were detected, preventing further elucidation of this suggestion. Anecdotal observations made while Doppler calibrating flows were passed through the aorta showed the ventricle of dead abalone would begin to beat at higher flows, implying that back-pressure from the aorta has a stimulating affect upon

ventricular contraction. Similar observations were made during forced perfusion of the mussel, *Mytilus edulis* (Famme 1981) and the isolated ventricle of *Littorina littorea* (Andrews and Taylor 1988). There is also some evidence that increased systemic pressure in crustaceans may increase heart rate (McMahon and Wilkens 1983).

*Mean Circulatory Filling Pressure*

MCFP is generally considered a valuable parameter as it represents a major factor determining the rate of venous return, and therefore cardiac output, in mammals; for example, MCFP increases 2-4-fold in humans in response to exercise (Guyton 1986). As MCFP was only measured during natural acardia at rest it is not possible to examine its relationship to cardiac output using the current data. However, it appears that transient increases in MCFP occur rhythmically in *H. iris* that have been allowed an extended recovery period (figures 7.15 – 7.17) and also during clamping (figures 7.12 and 7.13). These periods of increased MCFP appeared to cause a fall in cardiac output and stroke volume (discussed below). If the colloid osmotic pressure of *H. iris* haemolymph is assumed to be similar to that of the marine prosobranchs *Littorina* (1.45 $cmH_2O$; Andrews and Taylor 1988) and *Buccinum* (1.34 $cmH_2O$; Mangum and Johansen 1975 cited in Andrews and Taylor 1988) then it should be noted that the observed MCFP of 1.95 $cmH_2O$ is only just sufficient to resist the influx of water.

*Pressure phasing*

Despite the small size of the ventricle and large venous volume, haemolymph flow remains pulsatile throughout the vasculature of *H. iris*. Similar observations have been made in *H. corrugata* (Bourne and Redmond 1977a) and *H. rubra* (Russell and Evans 1989) and, distally, in the cephalopedal venous sinus of *H. midae* (Trueman and Brown 1985) and within the lacunar space of the pedal musculature of *H. kamtschatkana* (Voltzow 1986). Molluscan arteries are generally assumed to act as a single, highly extensible elastic chamber, in other words, a perfect Windkessel (Brownell and Ligman 1992). The Windkessel model states that kinetic energy is removed from the flowing blood during ventricular systole and subsequently passively discharged, allowing flow to proceed during systole (e.g. Shadwick et al. 1987). Cephalopods, notably octopus and nautilus, are now known to rely on a Windkessel to damp the pulse (Wells and Smith 1987) and elastic fibres, hinting at a Windkessel-type mechanism, have also been found in the arteries of *Littorina* (Andrews and Taylor 1988). In *H. iris*, however, aortic flow ceases as soon as the valve at the outlet of the ventricle closes, identified by the dichrotic notch during aortic pressure fall on figures 7.4a, 7.5a and 7.6a (after Bourne and Redmond 1977a). Clearly no Windkessel effect acts in the arterial system of *H. iris*. A similar relationship between pressure and flow is shown in the aorta of *H. corrugata* (Bourne and Redmond 1977b), however pressure dissipation following valve closure is more gradual than in *H. iris*, due to the action of the aortic bulb.

A critical feature of the circulation of *H. iris*, apparent from figures 7.4e, 7.5e, 7.6e and 7.7, is that pressure oscillations throughout the system remain in phase with the aorta until the gills or

right mantle are crossed, when the effect of *vis-à-fronte* suction reverses the phase relationship. The net result is that there is no phase lag between ventricular systole and flow generation at any point in the system. Flow is generated by the rapid increase in pressure in the aorta (*vis-à-tergo*, figures 7.4a & e, 7.5a & e, 7.6a & e) and by the corresponding fall in pressure in the efferent ctenidial veins (*vis-à-fronte*, figure 6.9). The effectiveness of the heart is therefore optimised, as peak influx pressure co-incides with a trough in efflux pressure across the major resistance elements of the gills and right mantle. Flow inertia is also maximised, as no lag occurs in *vis-à-tergo* flow before it is assisted by *vis-à-fronte* auricular suction.

Pressure pulse synchronicity within the arterial system is expected, as the heart drives the incompressible haemolymph at a low frequency (<1Hz) with a long wavelength relative to arterial length, resulting in an almost instantaneous transmission of pulse through the arterial tree (Brownell and Ligman 1992). For the phase relationship to be maintained throughout the venous system, however, is highly unusual. Even in *H. corrugata*, Bourne and Redmond (1977a) note that "Pressure waves in the epipodial artery and the afferent ctenidial vein essentially followed the aortic pressure wave by a phase angle that was dependent on the distance of these vessels from the aortic bulb". The apparent absence of major vascular shunts bypassing the right kidney and digestive gland in *H. corrugata*, the lack of an aortic bulb in *H. iris* and the differences in systemic pressure phasing suggest that fundamental differences exist between the haemodynamics of the 2 species. The strategy adopted by *H. iris* maximises the instantaneous pressure gradient across the gills, facilitating flow through these high resistance elements, but incurs 2 major disadvantages: Firstly, haemolymph flow to all other tissues is likely to be compromised. Secondly, flow to the systemic vasculature is energetically expensive if delivered in an undamped, pulsatile manner (Wells and Smith 1987).

### *7.4.6. Effects of activity, cardiac pause and hydrostatic pressure cycling*

*Cardiac pause*

Cardiac pause can be induced in *H. iris* by sudden disturbance, such as change in light intensity or at the onset of activity (e.g. figures 6.10 and 6.11). In *H. corrugata* extended cardiac pause (up to 9min.) was found to ensue from handling and cannulation stress (Bourne and Redmond 1977a). In a resting state, however, the abalone routinely show spontaneous pauses of 5 – 20s. Amongst other gastropods extended cardiac arrest was routinely observed in *Haliotis kamtschatkana*, the mesogastropods *Polinices lewisii* (Bourne et al. 1990) and *Littorina littorea* (Andrews and Taylor 1988), as well as in the nudibranch *Archidoris odhneri* (Bourne et al. 1990). Cardiac pause has also been documented in bivalves, which may close their valves and cease cardiac activity at low $Po_2$ but will occasionally gape widely and show a brief burst of cardiac activity (Booth and Mangum 1978). Booth and Mangum (1978) suggest these bursts may be associated with the need to clear accumulated $CO_2$ as shell material is dissolved to buffer falling pH. The cardiac pause in bivalves therefore represents a metabolic down-regulation in response to an unfavourable environment.

Observations of cardiac pause in crustaceans are perhaps more relevant to those seen in the abalone. Cardiac pauses, often lasting for several minutes, have frequently been described in resting decapod crustaceans, often associated with a synchronous cessation in scaphognathite beating (McMahon and Wilkens 1983). For example, spontaneous cardiac arrest is seen at rest in the crabs *Panopeus*, *Libinia* and *Calinectes*, typically lasting 30s – 1min (DeFur and Mangum 1979). The scaphognathite has a minimum effective frequency, hence intermittent beating is the only means of maintaining low ventilation rates (McDonald et al. 1980, McMahon and Wilkens 1983). A similar rationale could be used to explain cardiac pause in abalone. Heart rate is apparently inherent, with little modulation at a given temperature, hence haemolymph flow requirements below the minimum cardiac output require a periodic cessation of the heart. It is therefore suggested that the routine metabolism of *H. iris* in normoxic water requires less convective $O_2$ transport than the minimum continuous flow delivered by the heart, pauses are therefore incorporated to economise on cardiac energy expenditure. The process is, however, less efficient than the simultaneous acardia and apnea of decapods, as ciliary ventilation proceeds unnecessarily during these periods in abalone (see chapter 4).

*Effects of activity*

The effects of acute disturbance, rather than routine activity, have been examined here. As the disturbance response (twisting or clamping) begins, the abalone may enter a period of acardia, as discussed above, or show erratic bradycardia. Similar reactions have been noted in *H. corrugata* (Bourne and Redmond 1977a) and *Littorina*, where pulsatility also increased as heart rate decreased, perhaps reflecting increased peripheral resistance due to contracting muscles (Andrews and Taylor 1988). Erratic bradycardia at the onset of exercise is also observed in some fish, for example the rainbow trout and lingcod (Jones and Randall 1978). The onset of most avoidance activity in *H. iris* is usually marked by a flinch, where the shell is briefly pulled towards the substratum. In addition to bradycardia, flinching caused a transient pressure spike of about 10 $cmH_2O$ throughout the vascular system of *H. iris* (present study - figures 7.9 – 7.11) and *H. corrugata* (Bourne and Redmond 1977a) which Voltzow (1986) attributes to increased intramuscular pressure in the foot. If the avoidance activity of *H. iris* is sustained, normal heartbeat is resumed, but stoke volume is reduced (e.g. figures 7.11, 7.12 and 7.13). A similar phenomenon is observed in fish during anaerobic, burst exercise, where heart rate, stroke volume and aortic pressure are all reduced (Farrell and Jones 1992). Farrell and Jones (1992) suggest the response may serve to reduce systemic hypertension when skeletal muscle contraction obstructs peripheral flow. Given the low resistance of the main vascular routes in *H. iris*, this explanation seems inappropriate for the abalone. Instead it is proposed that erratic pressure surges disrupt the phasic relationship and flow inertia described above, reducing cardiac output.

Paradoxically, acute bursts of activity may directly assist in the movement of haemolymph. For muscular body movements to assist in venous return, they must impinge directly upon compressible veins or sinuses equipped with valves to direct the flow. Examples include the segmental

veins in the post-pelvic region of teleosts or the median fin sinuses of elasmobranchs (Jones and Randall 1978) or the prolific valves of the mammalian venous system, which are well known to facilitate venous return during exercise (e.g. Levick 1991). The only valve that might assist in this function in *H. iris* lies between the renal and basibranchial sinus, no evidence has, as yet, been presented to support the suggesting that this valve might rectify activity-induced flow. Correspondingly, no augmentation of flow was noted in either the aorta (figure 7.9, 7.11, 7.12 and 7.13) or the efferent ctenidial veins (figures 6.10 and 6.11) as a result of muscular exertion. In the absence of valves, major movements of the body and shell result in pressure spikes of equal magnitude throughout the main vasculature, thus, as observed by Bourne and Redmond (1977a) no net additional pressure gradient is created.

The definitive avoidance reaction of the abalone is the clamp. Clamping involves powerful contractions of the abalone's major muscle blocks, the foot and right shell adductor, and ultimately confinement within the shell. The clamp may also be actively maintained for extended periods. These facts have lead to speculation regarding the abalone's continued circulatory function during the clamp. As described in the introduction to the current study, valves appear to prevent surges of haemolymph flowing from the foot into the cephalopedal venous sinus (Crofts 1929) and cephalic arterial sinus (Bourne and Redmond 1977a); a shunt between these sinuses may then allow systemic circulation to proceed (Russell and Evans 1989). While morphological evidence for the existence of cephalopedal valves or a shunt between the sinuses in *H. iris* is equivocal, the physiological evidence is compelling. Pressure traces such as that shown in figure 7.14 clearly indicate that pedal sinus pressure rises to an order of magnitude higher than those measured elsewhere in the circulatory system during clamp. Pedal sinus pressure abruptly returns to its pulsatile baseline when the clamp is released. Following a brief disruption at the onset of the activity, aortic flow resumes, as does pressure pulse in the main circulation (figures 7.12 and 7.13). Hydrostatic baseline pressures remain slightly elevated during the clamp, reflecting analogous observations in other prosobranchs, including a transient pressure increase of approximately 5cm$H_2O$ in the cephalopedal venous sinus and ventricle of *H. midae*, lasting for 20 – 25s (Trueman and Brown 1985). A 1cm$H_2O$ increase in systemic pressure was observed in the snail *Hemifusus* during retraction within the shell (Depledge and Phillips 1986) and a spike of up to 12cm$H_2O$ in *Littorina* (Andrews and Taylor 1988). Clearly circulation continues in the main system during a clamp. As numerous shunts from the arterial system into the venous sinuses have been demonstrated (chapter 3), and only about 25% of cardiac output reaches the foot in the resting animal (Jorgensen et al. 1984), the need for a cephalic sinus shunt is somewhat academic. A physiological valve must retain haemolymph in the pedal sinus, resulting in the high, sustained pressures seen in figure 7.14. It has been suggested that a cephalopedal valve might protect the main circulation from damaging pressure surges leaving the foot (Bourne and Redmond 1977a). However, a more critical function may be to retain haemolymph in the foot to maintain hydrostatic muscle antagonism (Voltzow 1994), preserving pedal function, including adhesion and post-clamp locomotion. Abalone with deflated pedal musculature were observed to have reduced tenacity and severely compromised mobility, requiring extended periods (many minutes) for re-inflation (cf. extreme example of *Busycon*, which requires 15 – 20h to re-inflate its foot;

Mangum 1979). For the same reasons the pedal haemocoel may also become isolated during other activities, for example Voltzow (1986) recorded pedal intramuscular pressures up to 34cm$H_2O$ during twisting in *H. kamtschatkana*.

*Pressure cycling*

Rhythmic oscillations in baseline blood pressure and/or cardiac output, such as those regularly seen in the resting abalone (figures 6.8a and b) or following extended recovery (figures 7.15 – 7.17) are commonly observed in other animals. The most common source of such oscillation is from ventilatory movements. For example, in humans, inhalation reduces intra-thoracic pressure and increases abdominal pressure as the diaphragm contracts, with a resultant increase in flow in the vena cava. The effect is reversed during exhalation and compounded further by vagal bradycardia; this is known as sinus arrhythmia (Levick 1991). No tidal ventilatory movement was observed in the abalone, nor was any cycling of exhalant flow noted (see chapter 4). Octopus show 2 rhythms superimposed on the systemic pressure pulse, due to mantle ventilation and, possibly, efferent branchial vessel contractions (Wells and Smith 1987). As these 2 rhythms come in and out of phase, a cycling in the net pressure pulse is seen. However, as the cycling in octopus is reflected in the amplitude of the pulse, rather than the hydrostatic baseline, other mechanisms must account for the observations in *H. iris*. Hydrostatic pressure cycling was also observed in *Polinices lewisii* during the inflation of its pedal aquiferous system (Bourne et al. 1990). As the frequency of these oscillations was very slow (~0.2$min^{-1}$) and abalone lack an aquiferous space, it seems unlikely the oscillations observed in *H. iris* relate to active water uptake.

In the current study the abalone were quiescent, i.e. head and epipodium extended, with no significant locomotory activity. The largest oscillations were observed in the aorta, where maximal hydrostatic pressures were associated with reduced aortic flow and even slight back-flow (figure 7.15). Although the ventral cephalic region could not be directly observed, it seems likely that the oscillations reflect radula feeding movements. As the odotophore muscles retract the odontophore and radula, contained within the lumen of the cephalic arterial sinus and aorta, respectively (Crofts 1929), mass displacement in the arterial system increases vascular pressure and opposes aortic flow. While these movements appear detrimental in their disruption of aortic flow, the ensuing hydrostatic pressure increase causes haemolymph to flow across the otherwise poorly perfused left gill (see chapter 6). There may therefore by an adaptive association, exploiting passive pressure fluctuations to augment gas exchange during feeding. Reciprocally, it is also possible that haemolymph vessel wall tension is adjusted rhythmically. The cephalic arterial sinus has 5-HT reactive nerve fibres and may respond dynamically to the possible need to assist in radula movement by regional hydrostatic pressure fluctuations (Russell and Evans 1989). Rhythmic pressure oscillations were also noted in *H. corrugata*, but at a lower frequency of 1 – 2 $min^{-1}$ (Bourne and Redmond 1977a) compared to 3 – 4 $min^{-1}$ in *H. iris*. In both abalone species the apparent radula rasping frequencies are very low compared to those of patellid limpets (~60 $min^{-1}$; Boyden and Zeldis 1979). A formal corroboration of the association between radula movement and hydrostatic

pressure oscillation would therefore be of value. A broader study of the interactions between feeding and circulatory dynamics would also be of interest; in addition to the effects of radula movement and the need to support metabolic and transport processes in the gut, there may also be a coupling between cardiac movement and the ejection of faeces, as implicated in the mussel, *Perna viridis* (Nicholson 2003).

## 7.5. Conclusions

The vascular system of *Haliotis iris* is apparently poised towards the delivery of haemolymph to the gills. No phase shift is seen in haemolymph pressure between the aorta and the basibranchial sinus supplying the gills, while the post-branchial pressure pulse is in perfect antiphase, maximising the instantaneous pressure gradient across the gills. The current study appears to be the first to describe a systemic circulation that shows no phase shift in pressure, even showing clear differences in circulatory strategy to other members of the same genus. The haemolymph circulation of *H. iris* seems to favour the animal's sedentary habit, as hydrostatic pressure fluctuations associated with muscle activity reduce cardiac stroke volume.

# Chapter 8

# General Discussion

## 8.1. The integrated functioning of ventilation, gas exchange and haemolymph convection

The overall objective of the studies described in this thesis has been to provide an integrated description of the systems involved in the extraction of oxygen from the surrounding seawater and its delivery to the respiring tissues. These studies have specifically examined the mechanisms of ventilation, the efficacy of the gills in extracting oxygen and the role of secondary gas exchange surfaces. The role of the haemolymph in gas transport has been a major focus of the project, describing the anatomy of the vascular system in relation to gas exchange function, the volume and mixing of the haemolymph, convective $O_2$ removal from the gills, carrying capacity and delivery rates to the tissues. In this section these parameters, described in the previous 6 chapters, are integrated in descriptions of the physiological states of *Haliotis iris* that are routinely encountered in the laboratory. Values relate to adults typically of 250 – 350g live weight.

## 8.1.1. In the resting abalone

*How do we know an abalone is resting?* The question is not facetious. In fact the answer represents a principal objective of this work. Abalone are extremely aware of, and responsive to their environments, with serious implications for the interpretation of data. During the course of this work specific studies have been carried out into the effects of the obvious and major causes of stress associated with manipulation in the laboratory and during predator avoidance (see below). Under these circumstances the abalone is clearly not resting. 'Resting' is defined here as the unstressed condition, where stress represents "any strain or interference that disturbs the functioning of an organism" (Anon. 1974). Abalone react to seemingly minor stimuli, including small changes in temperature (e.g. Fujino et al. 1984) and light intensity, such as the passing shadow of a researcher (e.g. Trueman and Brown 1985); under such conditions the abalone is therefore not at rest. Ultimately there is no substitute for patience: extensive experience must be gained in abalone handling and cannulation before physiological parameters can be monitored without the animal reacting adversely to the process. A robust laboratory holding system is also essential, providing the animal with high quality seawater and obscuring external movement and direct light. The abalone must then be allowed sufficient time to recover from specific stress, usually a time-scale of days (see below).

Ultimately it did prove possible to establish a stable physiological baseline for abalone that had apparently experienced no recent disturbance; these parameters were therefore used to define the resting condition.

A resting adult *Haliotis iris* has a haemolymph volume of 55.4mL.100g tissue$^{-1}$, which is cleared at a rate of 10 – 15mL.100g$^{-1}$.d$^{-1}$, principally at the pericardial glands of Gröbben (e.g. Andrews 1985) of the heart auricles. The heart ventricle pumps the haemolymph at a rate of 9.1 mL.kg$^{-1}$.min$^{-1}$, as a result of a mean pulse rate of 28.5bpm and a stroke volume of approximately 320µL. Ventricular systole drives circulation by directly propelling haemolymph into the aorta and by an indirect *vis-à-fronte* suction of haemolymph into the passively inflating auricles. Haemolymph is rapidly driven around a low resistance loop in the main vasculature, whereby the anterior aorta directly and indirectly supplies a system of capacious sinuses surrounding the alimentary tract, bypassing the major muscle blocks in the process. Haemolymph from these gut sinuses can be directed into the digestive gland and right kidney, but may also bypass either, ultimately collecting in the basibranchial sinus and thence the afferent veins supplying the gills (ctenidia). Although the left gill is larger and potentially offers less resistance to flow, 95.7% of the haemolymph entering the basibranchial sinuses crosses the right gill. Haemolymph leaving the right gill drains directly into the right auricle and also crosses the left kidney to join haemolymph from the left gill in the left auricle.

Haemolymph mixing in the low resistance vascular loop, indicated by dilution of $^{14}$C-inulin, is relatively rapid (figure 2.1.1). A slower mixing phase is then seen, presumably representing marker perfusion into the organs that can be bypassed on the low resistance route (the foot and epipodium, digestive gland, right kidney, left gill and left kidney). A final mixing phase represents admixing into the distal lacunae, which appear to represent a very small fraction of the total haemocoel volume. A total of 10 – 12h are required before a marker is fully mixed in the system, determined by sampling haemolymph from the dense, poorly perfused tissue of the adductor muscle.

The resting abalone creates a constant water flow across its gill lamellae using dense bands of elongate lateral cilia. The cilia effectively drive the water counter-current to haemolymph flow to optimise gas exchange and create a unidirectional flow of 84 mL.kg$^{-1}$.min$^{-1}$ through the branchial chamber, entering above the head and exiting via the dorsal shell holes, as described by Voltzow (1983). As the abalone appears unable to regulate its ventilation (figure 4.14), 50% of the influent water is assumed to cross either gill. On the basis of this assumption, the conductance ratio of water to haemolymph flow across the preferentially perfused right gill is well matched (0.96, where 1 represents unity). In contrast, the water/haemolymph conductance ratio across the left gill must be chronically mis-matched to the low perfusion rates of this gill in resting *H. iris*. Extensive corrugation of the gas exchange surface of the right gill lamellae combine with high external surface area of individual cells and the proximity of the ventilatory cilia to minimise the diffusion barrier offered to oxygen. A calculated diffusion limitation index ($L_{diff}$) of 0.48 implies that diffusion and perfusion are well matched (0.5 represents equal perfusion and diffusion limitation), both would therefore have to be increased to augment oxygen uptake. The physiological indices imply that the right gill functions optimally under resting conditions.

Of all oxygen taken up by the resting abalone, the great majority is removed from the ventilatory flow irrigating the gills. A total of 13.9% of total $M_{O_2}$ is taken up by the epipodium and foot, presumably to support metabolism in local cells. Oxygen supply to the right mantle region also seems self-sufficient, as no net $O_2$ gradient was detected between the haemolymph entering and leaving this region.

Two specific cardiovascular phenomena are observed exclusively in resting abalone, and are therefore considered diagnostic of the resting state. These are spontaneous cardiac pause and the cyclic effects of feeding. As feeding is discussed below, only cardiac pause is mentioned here. The heart rate of *Haliotis iris* appears to be fixed for a given individual at a specific temperature. Control of output is achieved by adjusting stoke volume, a strategy that imposes a minimum operating rate, below which the ventricle cannot function. Analogous pauses in scaphognathite ventilation in crustaceans have been regarded as a strategy to save metabolic expenditure when requirements fall below the minimum constant delivery level (McMahon and Wilkens 1983). It is suggested that the same explanation can be applied to the cardiac pauses of *H. iris*.

## 8.1.2. The effects of stress

If a prime objective of this project was establish parameters of physiological performance definitive of the resting state, then the path towards this goal required a thorough understanding of factors that would result in a non-resting state, and of the nature of the abalone's response. In other words, this has to a great extent been a study of stress, its causes and effects. Stress was arbitrarily categorised as exogenous, relating to the unavoidable effects of experimental manipulation, and endogenous, which described the effects of the animal's own actions. Both forms of stress were constantly encountered and both were exploited experimentally. As endogenously-derived stress would be frequently encountered in the natural environment, the effects were of direct ecophysiological importance. During the course of the various experiments the abalone were induced to perform typical avoidance behaviours, notably flinching, clamping and twisting, and the ensuing effects examined. The exogenous stress effects associated with experimental manipulation were initially examined directly, during haemolymph volume and clearance trials, to provide an indication of the impact of such treatment and the time-course of recovery. In later experiments it became apparent that the severe stress associated with multiple cannulation could be used to elicit a maximal metabolic response, providing a valuable means of examining metabolic scope and system capabilities.

Observations made early in the project found that abalone that were weighed repeatedly at intervals of 10min for 1h lost up to 11% of their flesh weight. Subsequent investigation using the blood volume marker $^{14}$C-inulin revealed that most of this weight loss could be explained by a 18% loss in haemolymph volume. The sequence of events associated with weighing involved an initial flinch as the abalone perceived the approach of an object, a slight compression of the tissues as a plastic spatula was used to break the seal between foot and substratum, then about 0.5min of aerial exposure during draining and weighing. A systemic vascular pressure spike of approximately about 10 $cmH_2O$ was associated with a flinch which, together with compression from the spatula, may

have driven a transient ultrafiltration of haemolymph across the body surfaces. As handling was repeated the abalone eventually released mucus, also derived from haemolymph filtration, from the hypobranchial glands. These factors combine with mild desiccation during air exposure to cause severe hypovolaemic shock in animals subjected to the most innocuous of laboratory manipulations.

Considerably more stress was associated with the experiments designed to examine gill and heart function. During the final setup for these experiments 2 – 4 cannulae and 1 – 2 pulsed Doppler crystals were painstakingly positioned. These procedures involved continuous handling in cooled air for approximately an hour, during which time the repeated contact with the epidermis caused the animal to twist its foot violently. Hence, while little or no actual haemorrhage was associated with the preparation, the abalone began the experiments suffering from hypovolaemia due to handling and desiccation, environmental hypoxia due to compromised oxygen uptake in air and functional hypoxia as a result of continuous muscular exertion. Monitoring of Doppler signals revealed greatly elevated flow volumes and velocities, a situation that prevailed for many hours. The effect was most apparent in the gills. Haemolymph flowed at a rate of 4.12 $mL.min^{-1}$ through the right gill, compared with a mean resting value of 3.48 $mL.min^{-1}$. Most strikingly, the left gill received 5.68 $mL.min^{-1}$ under stress, 30 times higher than its resting perfusion rate (figure 6.3). Under extreme stress the left gill therefore donates about 54% of the total gill $O_2$ contribution to the haemolymph, compared to about 7% at rest (figure 6.5). As most haemolymph returns to the heart via the gills, the combined gill perfusion was used as a measure of cardiac output, which was seen to increase from 9.1 $mL.kg^{-1}.min^{-1}$ at rest to a maximal 24.4 $mL.kg^{-1}.min^{-1}$ under extreme stress. In a subsequent experiment cardiac output was measured by a calibrated Doppler signal recorded from the anterior aorta. The initial response to severe stress was again monitored and the resulting output, 25.2 $mL.kg^{-1}.min^{-1}$, found to agree closely with those determined from gill perfusion. Unfortunately the animals in this last experiment had been subjected to quadruple cannulation of 4 major vessels, the cumulative effect appeared to elicit a chronic stress response. Haemolymph volume appeared to be restored, but elevated cardiac output prevailed for several days until the experiment was halted due to cannula occlusion or loss of Doppler signal. The multiple cannulae were used to provide a portrait of pressure response across the vascular system; hence it proved impossible to provide this data for the resting state. However, no significant differences were observed between pressure parameters measured during stress and those measured during subsequent recovery. Hence, while the true resting state was not examined, it seems likely that pressure gradients and pulse phasing remain reasonably constant in the low resistance vasculature of *H. iris*.

Throughout the convoluted journey made by the haemolymph from the anterior aorta to the basibranchial sinus the mean pressure fell only slightly (from 4.56 to 3.30 cmH2O), reflecting the low resistance of the route. Pressure in the basibranchial sinus remained pulsatile and in perfect phase with the aortic pulse. As *vis-à-fronte* auricular filling actively lowered pressure in the efferent gill veins in phase with ventricular systole, the arrangement of the vascular system apparently served to maximise the pressure gradient, and therefore flow, across the gills during ventricular systole.

## 8.1.3. The effects of activity

Four types of activity were observed or deliberately induced during the course of vascular monitoring:

*Flinching* is the abalone's typical startle response. The cephalic and epipodal tentacles are rapidly withdrawn and the shell is pulled ventrally, compressing the soft tissues and causing a small pressure spike of approximately 10cm$H_2O$ throughout the vascular system. The adductor muscle contraction responsible for the shell movement is immediately released and resting systemic pressures are resumed, tentacles are slowly re-extended over ~1min. As the flinch lasts less than one cardiac cycle, the disruption of heart function can be minimal (e.g. figure 7.9 and 7.11), however the heart may stop as part of the startle response. This form of induced cardiac pause tends to be brief, lasting <5s, but is sufficient for systemic pressures to plateau at mean circulatory filling pressure (1.95cm$H_2O$). Cardiac output may subsequently remain elevated for 1 – 5min after a single pause. Isolated flinches caused no apparent stress and a resting status was immediately resumed. If the abalone is repeatedly induced to flinch cardiac output becomes chronically elevated, resembling the recovery condition described below. Repeated stimulation is also likely to induce a clamp.

*Clamping* is the standard avoidance strategy of *H. iris*. Major or repeated stimuli and, in particular, perceived contact with the shell will induce the epipodium, head and foot to retract and the right adductor to contract fully. The shell is pulled ventrally to form an occluding seal * with the substratum. Once contacted, opposition from the substratum allows the adductor to lift the central foot region, augmenting the tenacity of adhesion by creation of suction (e.g. Smith 1991). This dynamic position can be maintained for many hours (personal observation). The compression of soft tissue within the shell cavity results in a transient pressure increase of 2 – 3cm$H_2O$ within the main vasculature (figure 7.12 and 7.13). The greatest forces occur within the pedal musculature, where haemolymph is retained by a valve, or valve-like apparatus (figure 3.19; Crofts 1929, Bourne and Redmond 1977a). High mean haemolymph pressures of 16.6 cm$H_2O$, and peak pressures >30cm$H_2O$ (figure 7.14), were therefore sustained within the pedal sinus during a clamp. It is suggested that loss of pedal haemolymph to the main circulation would reduce foot volume, lowering adhesion tenacity and post-clamp locomotory ability as hydrostatic antagonism in the muscular-hydrostat system declines (Voltzow 1994). Pressure elevations associated with sustained clamping resulted in an 85% increase in haemolymph clearance and subsequent 21% loss of haemolymph volume. Haemocyanin was largely retained, and a corresponding haemoconcentration was therefore seen. However, whole haemolymph may also be vented from the posterior region of the branchial chamber at the onset of clamping. The ejection path resembles that of gametes during spawning, hence it is suggested that the haemolymph is released from the right kidney ureter. Loss of haemolymph volume seems to be indirectly adaptive, as it ultimately allows all soft tissues to be protected within the shell cavity, even if the resting tissue volume is greater than that of the shell cavity.

* The left margin of the shell of *H. iris* rises slightly, therefore the seal on a flat substratum is not technically a complete occlusion. As the shell holes cannot be plugged an environmental seal is not achievable, regardless of the quality of the seal to the substratum.

Cardiac activity is relatively undisturbed by the act of clamping. Stroke volume may decrease (figures 7.12 and 7.13) and the circulating haemolymph will bypass the foot, epipodium and adductor muscles. As the clamp is dynamic and the main muscle blocks are essentially unperfused it seems inevitable that the clamp causes a state of functional hypoxia. The animal correspondingly enters a post-clamp recovery period, as described below, with a duration proportional to the length of the clamp.

*Twisting* is the most extreme activity undertaken by *Haliotis iris*. The shell is raised and rotated vigorously from side to side in an attempt to dislodge particularly persistent predators, notably certain starfish. As natural bouts of twisting are both rare and brief (few seconds), the metabolic support of the activity is perhaps of less interest than the potential need to protect the delicate vascular regions from potentially damaging pressure surges. In fact the pressure surges caused by the extreme muscular movements are surprisingly small, resembling a sporadic flinch. Cardiac activity is essentially unaffected, except for a reduction in stroke volume during the brief spikes in aortic pressure (figures 7.9 and 7.11). Pedal sinus pressure also shows a simple spike response (figure 7.10), suggesting that pedal haemolymph flow is not impeded by valve action during this activity. At the cessation of twisting cardiac output is elevated to a 'recovery' response. As with clamping, however, the twist is usually associated with extended or severe disturbance, it is not therefore clear whether an ensuing stress response is due to the anaerobic impact of the burst activity or general agitation.

The function of the large valve guarding the entrance to the basibranchial sinus remains unclear. One possible function may be to isolate the gills and auricles from potentially damaging pressure surges during avoidance activity. Maximum spike pressures of 12cm$H_2O$ were recorded in the aorta and 8cm$H_2O$ in the renal bypass vessel, spikes could exceed 40cm$H_2O$ in the pedal sinus but were never higher than 6cm$H_2O$ in either the afferent or efferent ctenidial veins. A protective function for the valve is therefore not ruled out.

*Grazing*, while clearly an activity, is paradoxically used here to define the resting state. Two feeding activities are observed in adult *H. iris*. The more spectacular involves the animal rearing up and using its foot or shell margin to trap drifting macrophyte fragments. Such activity requires rapid water movement and the stimulus of particles within the water column (Allen et al. 2001). Grazing is a routine activity that involves everting the radula and rasping microflora from the substratum. An undisturbed abalone will spend most of its time grazing, while locomoting little if at all. The effects of muscular action moving the odontophore and radula can be detected throughout the vascular system. As the radula is retracted, hydrostatic baseline pressure rises rapidly in the aorta causing stroke volume to decline. Stroke volume gradually increases again as the radula is re-extended, allowing hydrostatic pressure to fall. A single radula rasp cycle lasts for 7 – 11 heartbeats (or 3 – 4 rasps $min^{-1}$). The cycling of baseline pressure is seen throughout the vascular system (figures 7.15 – 7.17), but seems to be of particular importance to perfusion of the gills. In the absence of grazing movements, virtually all haemolymph flow appears to pass through the right gill, with haemolymph flow from the left gill tending to fall below the detection threshold of a pulsed-Doppler flowmeter (i.e. <2 - 3mm.$s^{-1}$, probably zero). As hydrostatic pressure rises, pulsatile haemolymph flow is

detected leaving the left gill, cycling up to a maximum flow that coincides with highest baseline pressure, then cycling down below the detection threshold (figure 6.6). The effect clearly originates from a non-cardiac source as peak perfusion coincides with lowest cardiac output. The unusual perfusion pattern may be adaptive, augmenting oxygen uptake to supply the working red muscles of the odontophore.

It is proposed that the oscillating left gill perfusion pattern is diagnostic of the resting condition in *H. iris*. It is likely that the abalone can and does graze while moderately stressed (see 'recovery' below) but the increased stoke volume and preferential left gill perfusion occlude any influence upon haemolymph pressure or flow. The resting abalone may refrain from grazing for intervals lasting many hours, however grazing still occupies the greatest fraction of the day and allows confirmation that zero signal from the left gill haemolymph flow relates to a genuine phenomenon rather than instrument error.

*Recovery* is a term of convenience in the current project, arbitrarily describing the metabolic status of abalone that are neither suffering from severe stress nor resting. Note that the maximal cardiac output response due to severe stress was measured for 2h following removal of the stressor (i.e. after invasive manipulation), the animal was then left undisturbed for a further 10h before its condition could be described as 'recovering'. By definition, a recovery state ensued after any form of disturbance, the duration of recovery (minutes to days) was related to the duration, severity and frequency of the disturbance. Recovery was by far the prevalent condition observed in the laboratory. The definition is vague and the condition is labile, hence many parameters show considerable variability during recovery. Cardiac output is high (26.0 $mL.kg^{-1}.min^{-1}$ measured in the anterior aorta, 25.8 $mL.kg^{-1}.min^{-1}$ measured leaving the gills), these values were not significantly different from the maximal output measured under extreme stress. Accordingly the remaining cardiovascular parameters measured also resembled those of the highly stressed state. No difference was detected between the mean pressures measured throughout the main vasculature in highly stressed or recovering animals. Haemolymph flow and oxygen uptake at the gills also retained the left gill bias observed during extreme stress.

So what differentiates a highly stressed from a recovering abalone? Appearance. The stressors associated with the current project invariably caused severe haemolymph volume depletion (18% loss due to repeated handling, 21% from prolonged clamping). The abalone tissue volume becomes visibly reduced, fitting easily within the shell, the foot is noticeably shrunken and response to touch is minimal. When placed on a firm substratum the animal appears to be clamping, but the effect is passive and the abalone can easily be dislodged. In contrast the tissues of the recovering abalone appear fully inflated, the tentacles may be extended and the abalone may locomote or feed. In other words the recovering abalone looks like a resting abalone but its haemodynamic parameters resemble those of a highly stressed abalone. This observation is critical when interpreting the findings of metabolic or haemodynamic studies carried out on abalone, and probably most invertebrates. When interpreting published data it is suggested that, unless otherwise stated, an animal should be assumed to be in a state of recovery.

The time-course of recovery is of great interest to researchers and aquaculturists alike. A detailed study of the recovery period associated with different levels of stress would be valuable, as would a determination of the lethal level of stress exposure, beyond which an apparent recovery period ultimately results in death. As an indication of time-course, flesh weight is recovered within approximately 18h after the cessation of repeated handling (N. L. C. Ragg and H. H. Taylor, unpublished data); resting haemodynamic parameters are seen 24 – 48h after a single, traumatic stress (including 1h aerial exposure and multiple cannulation). Recovery can be greatly extended if the stress is reinforced by further disturbance. Recovery remained incomplete 4 – 6d after any cannulation of the aorta.

# 8.2. The role of haemocyanin

The primary function of circulating haemocyanin is to transport oxygen from the uptake site to within diffusing distance of the mitochondria (Mangum 1983). As the pigment is not cell-bound it also has other functions in the haemolymph, including pH buffering and acting as the principal effector of colloid osmotic pressure (Mangum 1983). In abalone, haemocyanin is considered to be the predominant, if not the only protein in the haemolymph (Ainslie 1980a). In this discussion the role of haemocyanin and its dynamics in *H. iris* are considered in the context of data published for other abalone species.

Of all oxygen taken up by the abalone in normoxia, approximately 87% is acquired from the water ventilating the branchial chamber. Epidermal tissues of the hypobranchial glands and the left mantle contact the ventilatory stream, however by far the greatest surface area and tissue mass belongs to the gills. It is therefore suspected that virtually all $O_2$ removed from the water is taken up by the gills, either supporting local metabolism or to be donated to the haemolymph. Branchial $M o_2$ and haemolymph oxygen uptake by both gills were not measured simultaneously, but can be compared if certain assumptions are made. Abalone that were artificially ventilated at 48 $mL.min^{-1}$ (chapter 5) appeared to be in a state of stress or recovery, demonstrated by a distinct increase in right gill haemolymph flow from the 'resting', unventilated state. If this is the case, both gills would be expected to take up similar quantities of oxygen into their haemolymph (chapter 6). During artificial ventilation the right gill takes up 39.8 ±7.5% of branchial $M o_2$ directly into the haemolymph, hence a total of approximately 80% of oxygen extracted from the ventilatory water (8.81 ±0.39 $\mu mol.kg^{-1}.min^{-1}$) is expected to enter the haemolymph. The observation corroborates the assumption that most of the abalone's $M o_2$ is taken up by the gills and implies that the gill tissues have a relatively low specific $O_2$ demand. Clearly oxygen supply to the respiring tissues of *H. iris* is highly dependent upon haemolymph convection.

If the haemolymph plasma is assumed to have the same $O_2$ capacitance as seawater (1.6218 $\mu mol.L^{-1}.Torr^{-1}$ at 15°C; Dejours 1981) the oxygen carrying capacity of the post-branchial haemolymph of resting *H. iris* (mean $P o_2$ of 77 Torr) is increased nearly 4-fold (from 0.125 to 0.346 $mmol.L^{-1}$) as a result of the presence of haemocyanin. However, at rest the haemolymph returns to the gills with a $P o_2$ of 37.2 Torr, having lost only 34.7% of its oxygen. The haemocyanin in the pre-

branchial haemolymph is still about 63% saturated, having contributed only 43.6% of the total oxygen released to the tissues. In other words, in the resting abalone more oxygen was delivered by simple solution in the plasma than bound to haemocyanin. This relationship was not examined directly under conditions of increased $O_2$ demand. However, it was noted that $Po_2$ concentrations across the right mantle, a parallel vascular route to the gills, the aorta and the right efferent ctenidial vein were unaffected by the level of stress (i.e. oxygen demand) affecting the animal. Hence it is suggested that the net $Po_2$ gradients in *H. iris* are reasonably independent of $O_2$ demand and that haemocyanin consequently plays a relatively minor role in $O_2$ delivery under normoxic conditions.

The contribution of haemocyanin in *H. iris* shows a marked contrast to the pigment's role in Australian abalone *H. rubra*, *H. laevigata* and *H. roei*, where haemocyanin supplies 86 – 97% of all oxygen reaching the tissues (Ainslie 1980a).

*Binding and effects of pH*

*Haliotis iris* haemocyanin has a very high affinity, demonstrated by a $P_{50}$ of 3 – 8 Torr at pH 7, depending on temperature (Wells et al. 1998, Behrens et al. 2002). At the pre-branchial $Po_2$ of 37.2 ±3.6 Torr measured in *H. iris* during the current investigations the pigment would be expected to be saturated. This is not the case. Mean haemocyanin saturation entering the gills was 63% saturated at an *in vivo* pH of 7.16. It seems likely that differences between the *in vivo* and *in vitro* environments account for the observed discrepancy. The haemocyanin of *H. tuberculata* occurs in 2 isoforms, HtH1 and HtH2, which usually occur as didecamers composed of twenty 400kDa subunits, each of which fold into eight 50kDa functional units reversibly binding one $O_2$ molecule to a binuclear copper site (summarised by Behrens et al. 2002). The localised environment can therefore affect binding characterisics directly, as described below, or influence the quarternary structures formed by the haemocyanin.

Most prosobranch haemocyanins exhibit a reverse Bohr effect at low pH (Voltzow 1994), which has been linked to oxygen retention during hypercapnia (Wells et al. 1998). The haemocyanin of *H. iris* has been shown to exhibit a particularly strong reverse Bohr effect between pH 6.57 and 8.25 (Wells et al. 1998), with φ values of +0.65 to +0.68 ($\varphi = \Delta \log P_{50}/\Delta pH$; Behrens et al. 2002). The 3 abalone species studied by Ainslie (1980b) also showed strong reverse Bohr shifts, particularly noticeable as a decline in $P_{50}$ as haemolymph $Pco_2$ was increased from 0 to 3 Torr. Ainslie (1980b) measured *in vivo* $Pco_2$ of 3.2 – 6.0 Torr in pre-branchial haemolymph, falling to 1.2 Torr in post-branchial haemolymph. The reverse Bohr therefore appears to be of fundamental importance to the oxygen loading of haemocyanin in normoxic *H. laevigata*, *H. rubra* and *H. roei*. Wells et al. (1998) measured mean pH values of 7.39 in the pedal sinus of resting *H. iris* and 6.51 following exercise and Baldwin et al. (1992) observed a pH fall in the foot tissue of *H. iris* from 7.32 to 6.64 as a result of 36h air exposure. These data imply a major *in vivo* role for the reverse Bohr in *H. iris*. During the current study, however, neutral pH values were recorded in the main circulation; these were relatively unaffected by activity and remained constant across the gills (7.16 ±0.01 pre-branchial, 7.17 ±0.01 post-branchial). It is therefore suggested that the influence of the reverse Bohr in *H. iris* is restricted to the localised unloading in the respiring tissues.

A reverse Root effect and reduced co-operativity have also been described at lowered pH in *H. iris* haemocyanin (Wells et al. 1998, Behrens et al. 2002). As with the reversed Bohr, these phenomena are also apparently associated with the retention of oxygen at lowered pH and have been associated with oxyregulation of hypoxia-acclimated *Buccinum undatum* (see Behrens et al. 2002). Behrens et al. (2002) also note that unshelled gastropoda tend to lack a pronounced reverse Bohr, implying the shift conveys an advantage during retraction/clamping within a shell. It may be that increased affinity prevents mass unloading of oxygen from the gills into the increasingly acidic/hypercapnic water trapped in the branchial chamber.

*Haemocyanin concentration*

During the course of experiments described in this thesis haemocyanin concentrations of 0.027 – 0.41 mmol.$L^{-1}$ were recorded (approximately 1.4 – 21.7 g.$L^{-1}$) by measuring oxyhaemocyanin absorbance at 346nm. The lower values, obtained during the experiment described in chapter 6, appear spurious however, apparently caused by extended freezing of samples at -18°C prior to measurement. Fresh haemolymph samples ranged from 0.15 – 0.41 mmol.$L^{-1}$ (7.9 – 21.7g.$L^{-1}$). i.e. approximately 3-fold variability was observed in resting, healthy *H. iris*. Wells et al. (1998) record somewhat lower concentrations in *H. iris* (3.43 ±0.87g.$L^{-1}$) and *H. australis* (4.22 ±1.34g.$L^{-1}$). Similar, but rather more varied haemocyanin concentrations have been reported in the Australian abalone *H. laevigata* (2.4 – 14.2g.$L^{-1}$), *H. rubra* (1.0 – 9.9g.$L^{-1}$) and *H. roei* (3.6 – 15.1g.$L^{-1}$; Ainslie 1980a) and in the Californian abalone *H. fulgens* (0.3 – 18.9g.$L^{-1}$), *H. corrugata* (0.02 – 15.3g.$L^{-1}$) and *H. cracherodii* (2.1 – 20.3g.$L^{-1}$; Pilson 1965).

Haemocyanin concentrations have been shown to increase during aestivation in *Helix* (Weisher 1965 cited in Ainslie 1980a) and in response to elevated summer temperatures in *Busycon* (Betzer and Pilson 1974 cited in Ainslie 1980a). The former is presumably a side-effect of dehydration, while the latter appears to be a reasonable adaptation to lowered environmental $Po_2$ associated with increased water temperatures. Pilson (1965) and Ainslie (1980a) were unable to find any corresponding correlates to the variations observed in abalone, although Ainslie (1980a) does note that concentration is highly seasonal. Two major sources of variation in haemocyanin concentration in *H. iris* were identified in the current studies. Both related to activity-induced increases in hydrostatic pressure resulting in loss of plasma volume from the haemolymph and, consequently, an elevation in haemocyanin concentration. Gentle handling at 10 - 30min intervals over 2h caused an 11.2% increase in haemocyanin concentration in *H. iris*, while 2h of clamping caused a 7% increase. It is suggested that hydrostatic changes associated with retraction and emergence must influence the plasma protein content of all shelled prosobranchs. A prosobranch may therefore experience transient haemoconcentration during retraction, analogous to clamping in *H. iris*, or subsequent haemodilution if whole haemolymph is vented during retraction, e.g. *Busycon* (Mangum 1979) and *Lymnaea* (Lever and Berkius 1965), and volume recovered by water influx on re-emergence.

The plasma loss caused by clamping may have adaptive value as an economical means of affecting a transient increase in haemocyanin concentration. Haemocyanin synthesis apparently

occurs in the rhogocytes (referred to as 'pore cells' by Skelding and Newell 1975 and 'lymphoid tissue' by Crofts 1929) found in the connective tissue of the mantle, digestive gland and foot (Albrecht et al. 2001). The process of producing these very large macromolecules is presumably energetically costly and slow to influence circulating concentration due to the large volume of the vascular system.

*Regional heterogeneity in haemocyanin concentration*

The conch Busycon shows extreme regional heterogeneity in its haemocyanin concentration due to its strategy of taking seawater directly into the pedal haemocoel to assist with inflation (Mangum 1979). No such heterogeneity was detected within the major vessels of *H. iris*, however a significantly reduced concentration was found in the haemolymph bathing the dorsal region of the right shell adductor muscle. The observation is equivocal, however, as the passive-pooling collection method used in the adductor may have allowed localised thrombosis to partially filter the protein from the collected haemolymph.

*Colloid osmotic pressure*

In addition to the metabolic cost of haemocyanin synthesis and, perhaps, the availability of copper, the influence of these molecules on colloid osmotic pressure is likely to influence the maximum circulating concentration. Although haemocyanin aggregation serves to lower its osmotic influence, it still results in a colloid osmotic pressure of 1.34 $cmH_2O$ in *Buccinum undatum* and 1.45 $cmH_2O$ in *Littorina* (Andrews and Taylor 1988). These colloid osmotic pressures approach the mean circulatory filling pressure of *H. iris* (1.95 $cmH_2O$). In crustaceans colloid osmotic pressures of 1.6 – 4.0 $cmH_2O$ have been measured, often exceeding hydrostatic pressure in the venous sinuses (Mangum 1983). Crustaceans, however, have relatively high arterial pressures and are protected by an impermeable chitinous exoskeleton. The molluscan cuticle is highly permeable to water and systemic pressures are low, hence colloid osmotic pressures higher than mean circulatory pressure would cause an influx of water and subsequent haemodilution.

*The role of haemocyanin in H. iris*

Wells et al. (1998) conclude that the function of haemocyanin in *H. iris* is biased towards storage, maintaining oxygen availability for aerobic tissues when supply becomes limited. The large haemolymph volume and tendency to retain more than half of the haemocyanin-bound oxygen measured in the current study corroborate this conclusion. However, morphological information presented here show a low resistance vascular circuit serves to rapidly convey haemolymph to the gills, bypassing the main organs and muscle blocks. Perfusion of these tissue beds must therefore be compromised to some extent and efferent haemolymph leaving the lacunar beds must mix with recently oxygenated haemolymph before returning to the gills. Hence haemolymph sampled from the main vasculature does not necessarily represent the haemolymph environment bathing the tissues. It is suggested that many of the tissues, particularly the muscles, may operate at very low $Po_2$, allowing localised unloading of haemocyanin oxygen. In this case a high affinity pigment prevents premature unloading, a feature which would be enhanced as $O_2$ demand increases and pH decreases.

# 8.3. Comparative vascular biology of abalone

The conservative external morphology shared by members of the family Haliotidae and the ancestral position of the group, compared to most extant prosobranchs, tends to lead to the assumption that the processes of evolutionary radiation have ceased to influence these 'living fossils'. A comparison of the vascular anatomy and haemodynamics of different abalone shows that this is not the case.

*Haliotis iris* lacks an aortic bulb, that has been identified and shown to effectively smooth the aortic pressure pulse in *H. rubra* (Russell and Evans 1989) and *H. corrugata* (Bourne 1975, Bourne and Redmond 1977a). Consequently ventricular pressure is transferred to the aorta of *H. iris* with little or no damping, causing flow to cease when the valve between the aortic trunk and ventricle closes. An extensive haemal sinus system surrounds the alimentary canal of *H. iris*, occupying an intermediate position between the arterial and venous systems. Despite the use of similar investigative techniques, no trace of this sinus system has been found in other abalone. The gut sinuses provided a low resistance path to the vessels bypassing the digestive gland and, conspicuously, the right kidney. With the exception of Perrier's (1889) description of *H. tuberculata* (later refuted by Crofts (1929)) no substantial route bypassing the right kidney has been identified in abalone. Virtually all of the haemolymph is therefore believed to pass through the right kidney during each circuit (e.g. Crofts 1929, Russell and Evans 1989). A study of pressure phasing in the circulatory system of *H. corrugata* made by Bourne and Redmond (1977a) corroborates the proposed vascular arrangement for this species (Bourne 1975), which closely resembles that described for *H. tuberculata* (Crofts 1929). In contrast the pressure phase relationships described in the current study show virtually no lag between the aorta and the pre-branchial vessels, which is consistent with the flow of haemolymph through a low resistance circuit provided by the gut sinuses and the renal bypass vessel. This arrangement is considered advantageous as is maximises the instantaneous pressure gradient across the gills, optimizing branchial flow at the cost of reduced perfusion of the other organs. Fundamental differences have also been described in the vascular connections of the left kidney of *H. tuberculata* (Crofts 1929), *H. rubra* (Russell and Evans 1989) and *H. iris* (present study, see figure 3.1).

Substantial morphological differences therefore exist between the vascular systems of different abalone species, resulting in fundamental differences in the physiological functioning of the haemolymph circulation. Brown and Murray (1992) note that genetic distances between gene loci in *Haliotis* are unusually large for a single genus. Lee and Vacquier (1995) used complementary cDNA sequences of *Haliotis* sperm lysin to establish 3 highly distinct groups within the genus; using their criteria *H. iris* was placed as the sole member of the subgenus *Paua*. It may be of relevance to note that the oldest fossil abalone to be found (*H. lomaensis*) has been assigned to the subgenus *Paua* (Lindberg 1992), perhaps implying that this group is more likely to represent the ancestral abalone. Clearly considerable radiation has occurred within the genus. The assumption that morphology and physiological function in abalone are representative of an ancestral condition in prosobranchs should therefore be treated with caution. Extrapolation of physiological data between abalone species should also be done with cautious objectivity.

## 8.4. Why has the abalone survived?… A summary and speculative discussion

The most obvious merits of being an abalone are tenacity and protection. The broad muscular foot provides a high tenacity adhesion to any hard substrate and the dense shell protects the soft tissues. Both adhesion tenacity and shell protection can be greatly enhanced by clamping, which is permitted by a transient loss of plasma, reducing the tissue volume of the abalone to the extent that it can be accommodated within the shell cavity. These factors have allowed the abalone to occupy a niche in high-energy rocky sublittoral areas. As such areas are characterised by rapidly flowing, highly oxygenated water there has been little need to refine the ancestral gas exchanger arrangement of 2 bipectinate gills irrigated by lateral cilia from a unidirectional ventilatory stream entering above the head and exiting from the dorsal shell holes. Adhesive tenacity and shell thickness increase with age, ultimately allowing the larger abalone species to enter a size refuge beyond the reach of most predators. Abalone subsequently remain fecund for many years (decades in the case of *H. iris* – personal observation) allowing reproductive effort to continue with low risk of mortality.

As discussed above, radiation within the abalone has subsequently allowed refinements to be made to specific ecological and geographical locations. In the case of *Haliotis iris* the current study has permitted some insights to be made in to the specific adaptations of this species' gas exchange and circulatory systems. Large sinuses surrounding the gut receive both venous and arterial haemolymph, and subsequently give rise to a major vessel that bypasses the right kidney, conveying haemolymph directly to the base of the gills. This arrangement forms a low resistance loop in the main circulation that allows haemolymph to pass from the aorta to the gills with minimum loss of pressure and no shift in the phase of the pressure pulse. The constant volume heart mechanism results in an active lowering of pressure in the post-branchial haemolymph that coincides with peak pre-branchial pressure. The instantaneous pressure gradient across the gills is therefore maximised during ventricular systole in *H. iris*, optimising respiratory flow across the high resistance gills.

The elaborate arrangement of muscle and skeletal, cartilage-like material associated with the efferent region of the gills allows complex movement of individual lamellae and the entire gill assembly. One such movement is a lateral displacement that appears to occlude the main drainage channels of the left gill (figure 3.59b). It is suggested that this strategy is employed when *H. iris* is at rest, reducing haemolymph flow in the left gill to almost zero while allowing the right gill to continue to function at optimal perfusion rates. If oxygen demand is increased, cardiac stroke volume can be elevated 2.8-fold and the left gill resistance lowered to receive similar haemolymph flow, and thereby contribute a similar amount of oxygen, to the right gill, resulting in a corresponding increase in oxygen uptake. If oxygen demand still exceeds supply, the aerobic tissues of *H. iris* are apparently supported by the large venous oxygen reserve resulting from a large haemolymph volume and high affinity haemocyanin that retains more than half of its bound oxygen in normoxic conditions. The working muscles of the foot and shell adductor receive less haemolymph than the other tissues and may become completely isolated during some activities, notably clamping. These tissues

consequently have a reasonable oxygen capacity which, combined with low ATP requirements, can allow extended tolerance to regional hypoxia (Gäde 1988, Wells et al. 1998).

## 8.5. Limitations to the abalone gas exchanger

An obvious limitation seen in abalone is the limited nature of the habitat in which they occur. Virtually all living abalone species are found exclusively on rocky substrata in shallow coastal areas where water movement is rapid. A number of theories have been proposed to explain this limitation in distribution. Classically the archaeogastropods, including abalone, were considered to be restricted to rocky substrata and clear water due to a predisposition to clogging of the bipectinate gills (Yonge 1947). More recently, however, it has been shown the bipectinate design conveys no specific disadvantage in turbid water compared to the pectinibranch gill of higher prosobranchs (Gilinsky 1984). Each bipectinate gill apparently forms a functional unit with a hypobranchial gland (Voltzow 1994) which traps smaller suspended particles in mucus that is ultimately sloughed off into the exhalant current (Fretter and Graham 1994). It therefore seems likely that high concentrations of fine suspended solids will incur a metabolic cost due to increased mucus production and, more seriously, may cause mucus blockage of the water channels of the gill lamellae. It would therefore be of value to determine the effects of sediment loading specifically in abalone. Abalone also avoid loose substrata as adhesion tenacity is lost and the cost of locomotion is raised due to increased locomotory mucus production (Werner et al. 1995).

A feature of the rocky benthos that is of greater relevance to the current study is the association, by definition, with rapidly moving water. *H. iris* can adequately ventilate its gills by ciliary action. However, even modest external water currents (from 0 to 4.6 $cm.s^{-1}$) result in significant increases in oxygen uptake, implying that externally-assisted ventilation has a beneficial effect. Head-on flow augments the natural rate of ventilation (Voltzow 1983, Tissot 1992). Ciliary pumping appears to proceed at a constant rate, regardless of the external conditions (figure 4.13); hence ventilatory costs are not reduced *per se*. However, increased ventilation reduces the volume fraction of oxygen that needs to be removed to sustain $M_{O_2}$, thus lowering the cost of oxygen extraction. It is also suggested that the rapid removal of exhalant water and any associated waste products is necessary to prevent re-inhalation, this is of particular importance if the animal is stressed and releasing mucus. The need to exploit externally-assisted ventilation seems to exert a selective pressure on the external shell morphology, which becomes pronouncedly sculpured, with raised tremata better able to exploit the Bernoulli principle to induce flow in abalone species from more sheltered areas (Tissot 1992). It is concluded that the abalone are dependent upon, and therefore limited by, external flow to assist in gas exchange.

The right gill of *H. iris* appears to operate optimally under resting, normoxic conditions, and shows little capacity to increase its oxygen uptake rate. Most accommodation of increased oxygen demand therefore occurs by recruitment of the left gill. The strategy is effective but coarse, as no intermediate response between resting perfusion and full deployment of both gills was apparent.

The increased perfusion rate required to recruit the left gill necessitates a 2.8-fold increase in stroke volume, which is sustained until the resting state is resumed. This all-or-nothing response is likely to represent an inefficient use of metabolic resources during intermediate levels of oxygen demand. Very low metabolic demand is accommodated more effectively by periodic cardiac pause, this method of down-regulation is imperfect, however, as ciliary ventilation continues.

The gas exchanger arrangement of paired bipectinate gills supplied by a unidirectional flow of seawater entering anteriorly and exiting through the shell holes seems to reach its operating limits in *H. iris*. Further improvements would therefore require a radical alteration of this arrangement, perhaps accounting for the progressive abandonment of the bipectinate gill system in higher prosobranchs. To further elucidate this suggestion, however, it would be necessary to carry out corresponding studies of respiratory function and haemodynamic flexibility in other prosobranch gas exchangers.

# 8.7. Future work

The integrated study of ventilation, diffusion and perfusion processes in the gas exchange system of *Haliotis iris* has allowed a reasonably comprehensive picture to be drawn of respiratory function in this abalone. The abalone gas exchanger arrangement is apparently ancestral in the Prosobranchia, although more recent refinements may also be present. These refinements may be species specific. A similar multi-disciplinary study of gas exchange in higher prosobranchs would be interesting in its own right, but, comparatively, may also allow a much needed insight into the pressures driving the extraordinary radiation in respiratory strategies seen within this group.

A number of important lines of investigation that would provide important insight into the physiological functioning of *Haliotis iris*, and to abalone in general, include:

*Stress and recovery.* The data presented in this thesis provide some indication of the cardio-vascular and respiratory implications of stress. Complimentary research that would be of value to researchers and commercial producers alike would involve an examination of the time course of recovery from specific levels of stress. It would also be of interest to determine the lethal levels of stress, beyond which the abalone will die, regardless of the recovery environment. The study would be based on the tendency of juvenile abalone to die long after (i.e. days/weeks) the source of stress has been removed (personal observation).

*Haemocyanin dynamics*. Considerable insight has been gained into the dynamics of haemocyanin in abalone with the determination of rhogocytes as the sites of synthesis (Albrecht et al. 2001), transient haemoconcentration due to behaviourally-induced increases in hydrostatic pressure and chronic haemoconcentration and storage in the left kidney (Behrens 1999). A large vascular space that appears to contain concentrated haemolymph extends anteriorly from the left kidney (figure 3.40) and may represent a spleen-like reservoir of haemocyanin. This possibility should be investigated along with a determination of the conditions that govern synthesis, storage or release of the pigment.

*Macro haemodynamics*. At the organism level the most pressing line of enquiry in *H. iris* relates to the functioning of the newly-discovered valve between the renal and basibranchial sinuses (figures 3.30 and 3.31). Occlusion of the valve may cause circulatory arrest and even partial obstruction is likely to have profound effects on the flow of haemolymph. The *in vivo* effects of the valve action should therefore be examined and the study expanded to establish whether this feature is present in other abalone species.

*Micro-haemodynamics*. At the tissue level, two fundamental lines of enquiry should be developed. The first is biochemical, relating to the need to describe the haemolymph micro-environment in the immediate vicinity of respiring tissues to further elucidate the unusual binding properties of abalone haemocyanin. The second is physical. The vascular system of *H. iris* provides the haemolymph with a number of low resistance shunts around the major tissues and muscle blocks. Clearly these regions are still effectively perfused, but the mechanisms allowing this are unclear. The true vascular resistance of the tissue lacunae should be established along with possible mechanisms of resistance control.

Any one of these studies is likely to lead to the researcher towards a greater understanding of the diverse, often unique solutions that have been devised to accommodate a fundamentally inefficient body plan… and hence to a greater appreciation of nature through the study of snails.

# Acknowledgements

Inevitably the principal acknowledgement must go to my supervisor, mentor and friend H. Harry Taylor. The customary thanks offered to a supervisor upon presentation of a thesis are woefully inadequate to describe my gratitude for Harry's extraordinary level of commitment to this project. This has been a long and exacting project, no part of which would have been possible without Harry's continuous support on every level. Special thanks are also due to Jan McKenzie, the jewel in the crown of Biological Sciences at Canterbury. Jan has provided technical support throughout this project and, more importantly, has been a light in the dark for myself and so many other students of biology. The electrical genius of Victor Menzel, responsible for some of the stranger and more successful devices used in the project, is also gratefully acknowledged. Major technical contributions were also made by Gavin Robinson, Franz Ditz and Nick Etheridge from the School of Biological Sciences and Ian Sheppard from the department of Civil Engineering. The diverse and entertaining co-inmates who have shared the confines of Harry's lab during the course of this project are Deepani Seneviratna, Jane Behrens, John Elias, Dagmar Hebel, David Just and Nadia Fawzi, all of whom have played their part in preserving my sanity and motivation.

Oh yes… and thanks to my wife Joanne, who brings the love, light and meaning to everything I do.

# References


Anon. 1974. The new Encyclopaedia Britannica: Micropaedia IX. Helen Hemingway Benton, London.

Anon. 1983. The Merck Index – An encyclopedia of chemicals, drugs and biologicals. M. Windholz, S. Bundavari, R. F. Blumetti, E. S. Otterbein (eds.). Merck & Co., Inc., USA.

Anon. 1986. 545C-4 Directional Pulsed Doppler Flowmeter. Technical Manual (revision 4). Bioengineering, University of Iowa.

Ainslie, R. (1977). The function of haemocyanin in the respiratory physiology of three species of South Australian abalone (Genus *Haliotis*). Unpublished Ph.D. Dissertation, University of Adelaide.

Ainslie, R. (1980a). Haemocyanin concentrations in field populations of three species of southern Australian abalone. Australian Journal of Marine and Freshwater Research, **31**, 627-633.

Ainslie, R. (1980b). The quantitative role of haemocyanin in the respiration of abalone. Journal of Experimental Zoology, **211**, 87-99.

Albrecht, U., Keller, H., Gebauer, W., & Markl, J. (2001). Rhogocytes (pore cells) as the site of hemocyanin biosynthesis in the marine gastropod *Haliotis tuberculata*. Cell and Tissue Research, **304**, 455-462.

Allen, V. J., Marsden, I. D., & Ragg, N. L. C. (2001). The use of stimulants as an aid to wean fishery caught blackfoot abalone (*Haliotis iris*) to artificial food. Journal of Shellfish Research, **20**(2), 647-651.

Andrews, E. B. (1981). Osmoregulation and excretion in prosobranch gastropods part 2: Structure in relation to function. Journal of Molluscan Studies, **47**, 248-289.

Andrews, E. B. (1985). Structure and function in the excretory system of archaeogastropods and their significance in the evolution of gastropods. Philosophical Transactions of the Royal Society of London: B, **310**, 383-406.

Andrews, E. B., & Taylor, P. M. (1988). Fine structure, mechanism of heart function and haemodynamics in the prosobranch mollusc *Littorina littorea* (L.). Journal of Comparative Physiology: B, **158**, 247-262.

Andrews, E. B., & Taylor, P. M. (1990). Reabsorption of organic solutes in some marine and freshwater prosobranch gastropods. Journal of Molluscan Studies, **56**, 147-162.

Armstrong, D. A., Armstrong, J. L., Krassner, S. M., & Pauley, G. B. (1971). Experimental wound repair in the Black abalone, *Haliotis cracherodii*. Journal of Invertebrate Pathology, **17**, 216-227.

Babiker, M. M., & Rankin, J. C. (1975). Rationale for the use of $^{51}$Cr EDTA for estimation of glomerular filtration rate in fish. Comparative Biochemistry and Physiology: A, **50**, 177-179.

Babiker, M. M., Rankin, J. C., & Eido, G. (1979). Renal clearance, tissue distribution and binding by plasma proteins of $^{51}$Cr EDTA in *Tilapia nilotica* (L.). Comparative Biochemistry and Physiology: A, **63**, 71-74.

Baldwin, J., Wells, R. M. G., Low, M., & Ryder, J. M. (1992). Tauropine and D-Lactate as metabolic stress indicators during transport and storage of live paua, (New Zealand abalone) (*Haliotis iris*). Journal of food science, **57**(2), 280-282.

Barkai, R., & Griffiths, C. L. (1987). Consumption, absorption efficiency, respiration and excretion in the South African abalone *Haliotis midae*. South African journal of marine science, **5**, 523-529.

Barnes, R. D. 1986. Invertebrate Zoology. 5th edition. Saunders College Publishing.

Barnes, R. S. K., Calow, P., Olive, P. J. W. & Golding, D. W. 1988. The invertabrates – a new synthesis. Blackwell Scientific Publications, Oxford.

Bayne, B. L. (1971). Ventilation, the heart beat and oxygen uptake by *Mytilus edulis* L. in declining oxygen tension. Comparative Biochemistry and Physiology: A, **40**, 1065-1085.

Behrens, J. W. (1999). Morphology and ultrastructure of the left kidney (papillary sac) in *Haliotis iris*: possible role in reabsorption and haemocyanin synthesis or storage. Blood and haemocyanin function in *Haliotis iris* : roles of the paillary sac and ionic effectors. Unpublished MSc Thesis, Aarhus University, Aarhus.

Behrens, J. W., Elias, J. P., Taylor, H. H., & Weber, R. E. (2002). The archaeogastropod mollusc *Haliotis iris*: tissue and blood metabolites and allosteric regulation of haemocyanin function. Journal of Experimental Biology, **205**, 253-263.

van den Berg, H. A. (1992). Model for mechanics of mollusc systemic heart. Comparative Biochemistry and Physiology: A, **101**(4), 835-844.

Berger, V. Y., Khlebovich, V. V., Kovaleva, N. M., & Natochin, Y. V. (1978). The changes of ionic composition and cell volume during adaptation of molluscs (*Littorina*) to lowered salinity. Comparative Biochemistry and Physiology: A, **60**, 447-452.

Beyenbach, K. W., & Kirschner, L. B. (1976). The unreliability of mammalian glomerular markers in teleostean renal studies. Journal of Experimental Biology, **64**, 369-378.

Biron, M., & Benfey, T. J. (1994). Cortisol, glucose and hematocrit changes during acute stress, cohort sampling, and the diel cycle in diploid and triploid brook trout (*Salvelinus fontinalis* Mitchill). Fish Physiology and Biochemistry, **13**(2), 153-160.

Bloomberg, S. (1981). An energy budget for the paua (*Haliotis iris* Martyn). Unpublished M.Sc Thesis, University of Canterbury, Christchurch.

Boone, W. R., & Schoffeniels, E. (1979). Hemocyanin synthesis during hypo-osmotic stress in the shore crab *Carcinus maenas* (L.). Comparative Biochemistry and Physiology: B, **63**, 207-214.

Booth, C. E., & Mangum, C. P. (1978). Oxygen uptake and transport in the lamellibranch mollusc *Modiolus demissus*. Physiological Zoology, **51**, 17-32.

Bourne, G. B., & Redmond, J. R. (1977a). Hemodynamics in the Pink abalone, *Haliotis corrugata* (Mollusca, Gastropoda). I: Pressure relations and pressure gradients in intact animals. Journal of Experimental Zoology, **200**, 9-16.

Bourne, G. B., & Redmond, J. R. (1977b). Hemodynamics in the Pink abalone, *Haliotis corrugata* (Mollusca, Gastropoda). II: Acute blood-flow measurements and their relationship to blood pressure. Journal of Experimental Zoology, **200**, 17-22.

Bourne, G. B., Redmond, J. R., & Jorgensen, D. D. (1990). Dynamics of the molluscan circulatory system: Open versus closed. Physiological Zoology, **63**(1), 140-166.

Boyden, C. R., & Zeldis, J. R. (1979). Preliminary observations using an attached microphonic sensor to study feeding behaviour of an intertidal limpet. Estuarine and Coastal Marine Science, **9**, 759-769.

Brown, A. C. (1964). Blood volumes, blood distribution and sea-water spaces in relation to expansion and retraction of the foot in *Bullia* (Gastropoda). Journal of Experimental Biology, **41**, 837-854.

Brown, L. D., & Murray, N. D. (1992). Genetic relationships within the genus *Haliotis*. In S. A. Shepherd, J. Tegner, & S. A. Guzman del Proo (Eds.), Abalone of the world: Biology, fisheries and culture (pp. 19-23). Oxford: Blackwell.

Brownell, P. H., & Ligman, S. H. (1992). Mechanisms of circulatory homeostasis and response in *Aplysia*. Experientia, **48**, 818-827.

Carefoot, T. H., Qian, P. Y., Taylor, B., West, T., & Osbourne, J. (1993). Effect of starvation on energy reserves and metabolism in the northern abalone *Haliotis kamtschatkana*. Aquaculture, **118**, 315-325.

Cech, J. J., Bartholow, S. D., Young, P. S., & Hopkins, T. E. (1996). Striped bass exercise and handling stress in freshwater: physiological responses to recovery environment. Transactions of the American Fisheries Society, **125**, 308-320.

Crofts, D. R. 1929. Haliotis. Liverpool Marine Biology Committee Memoirs on typical marine plants and animals, volume 29. J. Johnstone and R. F. Daniel (eds.). University Press of Liverpool.

Dale, B. (1974). Extusion, retraction and respiratory movements in *Helix pomatia* in relation to distribution and circulation of the blood. Journal of the Zoological Society of London, **173**, 427-439.

Dall, W. (1974). Indices of nutritional state in the Western Rock Lobster *Panulirus longipes* (Milne Edwards). I. Blood and tissue constituents and water content. Journal of Experimental Marine Biology and Ecology, **16**, 167-180.

Davidson, W., Axelsson, M., Forster, M., & Nilsson, S. (1995). Cardiovascular responses to acute handling stress in the Antarctic fish *Trematomus bernacchii* are not mediated by circulatory catecholamines. Fish Physiology and Biochemistry, **14**(3), 253-257.

Davison, W. (1995). What is the function of the hagfish portal heart? New Zealand Natural Sciences, **22**, 95-98.

deFur, P. L., & Mangum, C. P. (1979). The effects of environmental variables on the heart rates of invertebrates. Comparative Biochemistry and Physiology: A, **62**, 283-294.

Dejours, P. 1981. Principles of comparative respiratory physiology. 2nd edition. Elsevier/North-Holland Biomedical Press, Amsterdam.

Depledge, M. H., & Phillips, D. J. H. (1986). Circulation, respiration and fluid dymanics in the gastropod mollusc, *Hemifusus tuba* (Gmelin). Journal of Experimental Marine Biology and Ecology, **95**, 1-13.

De With, N. D. (1996). Oral water ingestion in the pulmonate freshwater snail, *Lymnaea stagnalis*. Journal of Comparative Physiology: B, **166**, 337-343.

Deyrup-Olsen, I., & Martin, A. W. (1980). Blood venting and surface exudation of fluid in terrestrial slugs. American Zoologist, **20**, 219.

Deyrup-Olsen, I., & Martin, A. W. (1982). Surface exudation in terrestrial slugs. Comparative Biochemistry and Physiology: C, **72**(1), 45-51.

Donovan, D., Baldwin, J., & Carefoot, T. (1999). The contribution of anaerobic energy to gastropod crawling and a re-estimation of minimum cost of transport in the abalone, *Haliotis kamtschatkana* (Jonas). Journal of Experimental Marine Biology and Ecology, **235**, 273-284.

Donovan, D. A., & Carefoot, T. H. (1997). Locomotion in the abalone *Haliotis kamtschatkana*: Pedal morphology and cost of transport. Journal of Experimental Biology, **200**, 1145-1153.

Donovan, D. A., & Carefoot, T. H. (1998). Effect of activity on energy allocation in the Northern Abalone, *Haliotis kamtschatkana*. Journal of Shellfish Research, **17**(3), 729-736.

Dunphy, B. J., & Wells, R. M. G. (2001). Endobiont infestation, shell strength and condition index in wild populations of New Zealand abalone, *Haliotis iris*. Marine and Freshwater Research, **52**, 781-786.

Edwards, S., Burke, C., Hindrum, S., & Johns, D. (2000). Recovery and growth effects of anaesthetic and mechanical removal on Greenlip (*Haliotis laevigata*) and Blacklip (*Haliotis rubra*) abalone. Journal of Shellfish Research, **19**(1), 510.

Edwards, S. J., Harris, J. O., Maguire, G. B., & Hindrum, S. M. (1997). Respirometry and energy balance of abalone under stress. In proceedings of the fourth annual abalone aquaculture workshop (pp. 39-42). Port Fairy.

Ellerton, H. D., & Lankovsky, T. (1983). Structure of the hemocyanin from the paua (abalone) *Haliotis iris*. In E. J. Wood (Ed.), Structure and function of invertebrate respiratory proteins. EMBO Workshop 1982, Leeds, UK (pp. 129-132). London: Harwood Academic.

Eno, N. C. (1994). The morphometrics of cephalopod gills. Journal of the Marine Biological Association U.K., **74**, 687-706.

Famme, P. (1981). Haemolymph circulation as a respiratory parameter in the mussel, *Mytilus edulis* L. Comparative Biochemistry and Physiology: A, **69**, 243-247.

Farrell, A. P., & Jones, D. R. (1992). The heart. In W. S. Hoar, D. J. Randall, & A. P. Farrell (Eds.), Fish Physiology (Vol. XII A, pp. 1-88). Academic Press, Inc.

Feder, M. E. (1995). The regulation of cutaneous gas exchange. In N. Heisler (Ed.), Advances in comparative and environmental physiology: 21. Mechanisms of systemic regulation: Respiration and circulation (pp. 3-23). Springer-Verlag.

Flecher, C. R. (1992). Stress and water balance in the plaice *Pleuronectes platessa*. Journal of Comparative Physiology: B, **162**, 513-519.

Fleming, A. E., Hone, P. W., & Higham, J. (1997). The effect of water velocity on consumption and growth of greenlip abalone in tanks. In proceedings of the fourth annual abalone aquaculture workshop (pp. 16-23). Port Fairy.

Forster, M. E., Davison, W., Satchell, G. H., & Taylor, H. H. (1989). The subcutaneous sinus of the hagfish, *Eptatretus cirrhatus* and its relation to the central circulating blood volume. Comparative Biochemistry and Physiology: A, **93**(3), 607-612.

Frescura, M., & Hodgson, A. N. (1992). The fine structure of the columellar muscle of some gastropod mollusks. The Veliger, **35**(4), 308-315.

Fretter, V., & Graham, A. (1994). The excretory and vascular systems. In British Prosobranch Molluscs - Their functional anatomy and ecology (Vol. 161). Dorchester: The Ray Society of London, Dorset Press.

Fujino, K., Yamamori, K., & Okumura, S. I. (1984). Heart rate responses of the Pacific abalone against water temperature changes. Bulletin of the Japanese Society of Scientific Fisheries, **50**(10), 1671-1675.

Gäde, G. (1988). Energy metabolism during anoxia and recovery in shell adductor and foot muscle of the gastropod mollusc *Haliotis lamellosa*: Formation of the novel anaerobic end product tauropine. Biological Bulletin, **175**, 122-131.

Gaty, G., & Wilson, J. H. (1986). Effect of body size, starvation, temperature and oxygen tension on the oxygen consumption of hatchery-reared ormers. Aquaculture, **56**, 229-237.

Gilinsky, N. L. (1984). Does archaeogastropod respiration fail in turbid water? Paleobiology, **10**(4), 459-468.

Greenaway, P. (1981). The fate of glomerular filtration markers injected into the haemolymph of the amphibious crab *Holthuisana transversa*. Journal of Experimental Biology, **91**, 339-347.

Guyton, A. C. (1986). Textbook of medical physiology (7th ed.). W. B. Saunders Company.

Harris, J. O., Maguire, G. B., Edwards, S. J., & Hindrum, S. M. (1998). effect of ammonia on growth rate and oxygen consumption of juvenile greenlip abalone, *Haliotis laevigata* Donovan. Aquaculture, **160**, 259-272.

Harris, J. O., Maguire, G. B., & Handlinger, J. H. (1998). Effects of chronic exposure of greenlip abalone, *Haliotis laevigata* Donovan, to high ammonia, nitrite and low dissolved oxygen concentrations on gill and kidney structure. Journal of Shellfish Research, **17**(3), 683-687.

Harris, R. R. (1976). Extracellular space changes in *Carcinus maenas* during adaptation to low environmental salinity. Journal of Physiology, **258**, 31-32.

Harris, R. R., & Andrews, M. B. (1982). Extracellular fluid volume changes in *Carcinus maenas* during acclimation to low and high environmental salinities. Journal of Experimental Biology, **99**, 161-173.

Harrison, F. M. (1962). Some excretory processes in the abalone, *Haliotis rufescens*. Journal of Experimental Biology, **39**, 179-192.

Hickman, C. P. (1972). determination of the extracellular fluid volume of a euryhaline flounder by kinetic and net retention methods using tritium-labeled inulin. Canadian Journal of Zoology, **50**, 1663-1671.

Hickman, C. S. 1988. Archaeogastropod evolution, phylogeny and systematics; a re-evaluation. Malacological Review – supplement 4: Prosobranch phylogeny. W. F. Ponder, D. J. Eenisse, J. H. Waterhouse (eds.).

Hodgson, A. N. (1981). The blood volume of *Scrobicularia plana*, an estimation of blood loss after siphonal wounding. Marine Behaviour and Physiology, **8**, 21-33.

Howes, N. H., & Wells, G. P. (1934). The water relations of snails and slugs. I. Weight rhythms in *Helix pomatia* L. Journal of Experimental Biology, **11**, 327-343.

Howes, N. H., & Wells, G. P. (1934). The water relations of snails and slugs. II. Weight rhythms in *Arion ater* L. and *Limax flavus* L. Journal of Experimental Biology, **11**, 344-351.

Hughes, G. M. 1982. An introduction to the study of gills. in: Gills. D .F. Houlihan, J. C. Rankin and T. J. Shuttleworth (eds.). Cambridge University Press, Cambridge.

Hughes, G. M. 1989. Morphometry of respiratory systems. in: Techniques in comparative respiratory physiology – An experimental approach. C. R. Bridges and P. J. Butler (eds.). Cambridge University Press, Cambridge.

Hughes, G. M., Knights, B., & Scammell, C. A. (1969). The distribution of $Po_2$ and hydrostatic pressure changes within the branchial chambers in relation to gill ventilation of the shore crab *Carcinus maenas*. Journal of Experimental Biology, **51**, 203-220.

Hughes, G. M., & Umezawa, S.-I. (1968). Oxygen consumption and gill water flow in the dogfish *Scyliorhinus canicula* L. Journal of Experimental Biology, **49**, 557-564.

Hughes, G. M., & Weibel, E. R. (1976). Morphometry of fish lungs. In G. M. Hughes (Ed.), Respiration of amphibious vertebrates (pp. 213-232). New York: Academic Press.

Jakob, G. S., & Wang, J.-K. (1994). The effect of manual handling on oyster growth in land-based cultivation. Journal of Shellfish Research, **13**(1), 183-186.

Johansen, K. 1982. Respiratory gas exchange of vertebrate gills. in: Gills. D .F. Houlihan, J. C. Rankin and T. J. Shuttleworth (eds.). Cambridge University Press, Cambridge.

Johnsson, M., Axelsson, M., Davison, W., Forster, M. E., & Nilsson, S. (1996). Effects of preload and afterliad on the performance of the *in situ* perfused portal heart of the New Zealand hagfish *Eptatretus cirrhatus*. Journal of Experimental Biology, **199**, 401-405.

Jones, D. R., & Randall, D. J. (1978). The respiratory and circulatory systems during exercise. In W. S. Hoar & D. J. Randall (Eds.), Fish Physiology. Locomotion (Vol. VII, pp. 425-501). : Academic Press.

Jones, H. D. 1983. Circulatory systems of gastropods and bivalves. Chapter 4 in: The Mollusca, Volume 5: Physiology, part 2. K. M. Wilbur (ed.). Academic Press, New York.

Jones, H. D., & Kamel, E. G. (1984). The effect of *Cryptocotyle lingua* infection on the blood volume of *Littorina littorea*. Comparative Biochemistry and Physiology: A, **79**(3), 493-494.

Jones, H. D., & Trueman, E. R. (1970). Locomotion of the limpet, *Patella vulgata* L. Journal of Experimental Biology, **52**, 201-216.

Jones, T. O., Bourne, N. F., Bower, S. M., & Iwama, G. K. (1993). Effect of repeated sampling on haemolymph pH, PO2 and haemocyte activity in the Pacific oyster, *Crassostrea gigas* (Thunberg). Journal of Experimental Marine Biology and Ecology, **167**, 1-10.

Jorgensen, D. D., Ware, S. K., & Redmond, J. R. (1984). Cardiac output and tissue blood flow in the abalone, *Haliotis cracherodii* (Mollusca, Gastropoda). Journal of Experimental Zoology, **231**, 309-324.

Kingston, R. S. (1968). Anatomical and oxygen electrode studies of respiratory surfaces and respiration in *Acmaea*. The Veliger, **11**(Supplement), 73-78.

Krajniak, K. G., & Bourne, G. B. (1988). Aortic and venous blood pressures in the intact Pinto abalone, *Haliotis kamtschatkana*. Comparative Biochemistry and Physiology: A, **89**(3), 405-407.

Lee, Y.-H., & Vacquier, V. D. (1995). Evolution and systematics in Haliotidae (Mollusca: Gastropoda): inferences from DNA sequeces of sperm lysin. Marine Biology, **124**, 267-278.

Lever, J., & Berkius, R. (1965). On the presence of an external hemal pore in *Lymnaea stagnalis* L. Experientia, **21**, 395-396.

Levick, J. R. (1991). Haemodynamics: pressure, flow and resistance. In An introduction to cardiovascular biology. London: Butterworths.

Lindberg, D. R. (1992). Evolution, distribution and systematics of Haliotidae. In S. A. Shepherd, M. J. Tegner, & S. A. Guzman del Proo (Eds.), Abalone of the world: Biology, fisheries and culture (pp. 3-17). Oxford: Blackwell.

Lindberg, D. R. and Ponder, W. F. 1996. An evolutionary tree for the Mollusca: Branches or roots? Chapter 5 in: Origin and evolutionary radiation of the Mollusca. J. D. Taylor (ed.). Oxford University Press.

Linsley, R. M. (1978). Shell form and the evolution of gastropods. American Scientist, 66, 432-441.

Little, C. (1967). Ionic regulation in the Queen conch, *Strombus gigas* (Gastropoda, Prosobranchia). Journal of Experimental Biology, **46**, 459-474.

Little, C. (1981). Osmoregulation in prosobranch gastropods. Part I: Physiology and biochemistry. Journal of Molluscan Studies, **47**, 221-247.

Maina, J. N. 1988. The gas exchangers: Structure, function and ecolution of the respiratory processes. Springer-Verlag, Berlin.

Malvin, G. M., & Hlastala, M. P. (1989). Effects of environmental O2 on blood flow and diffusing capacity in amphibian skin. Respiratory Physiology, **76**, 229-242.

Mangum, C. P. (1979). A note on blood and water mixing in large marine gastropods. Comparative Biochemistry and Physiology: A, **63**, 389-391.

Mangum, C. P. (1982). The functions of gills in several groups of invertebrate animals. In D. F. Houligan, J. C. Rankin, & T. J. Shuttleworth (Eds.), Gills (Society for Experimental Biology seminar series ed., Vol. 16, pp. 77-97). Cambridge: Cambridge University Press.

Mangum, C. P. (1983). Oxygen transport in the blood. In L. H. Mantel (Ed.), The biology of Crustacea volume 5: Internal anatomy and physiological regulation. New York: Academic Press.

Mangum, C. P., & Polites, G. (1980). Oxygen uptake and transport in the prosobranch mollusc *Busycon canaliculatum*. I. Gas exchange and the response to hypoxia. Biological Bulletin, **158**, 77-90.

Martin, A. W., & Deyrup-Olsen, I. (1982). Blood venting through the pneumostome in terrestrial slugs. Comparative Biochemistry and Physiology: C, **72**(1), 53-58.

Martin, A. W., Harrison, F. M., Huston, M. J., & Stewart, D. M. (1958). The blood volume of some representative molluscs. Journal of Experimental Biology, **35**, 260-279.

Massabuau, J.-C., Burtin, B., & Wheatly, M. (1991). How is $O_2$ consumption maintained independent of ambient oxygen in mussel *Anodonta cygnea*? Respiratory Physiology, **83**, 103-114.

Matanock, H. L., & Welsford, I. G. (1995). Contact rehydration in the terrestrial slug *Limax maximus* L. in the field. Canadian Journal of Zoology, **73**, 607-609.

Matsumura, S., Kurokawa, M., Kuwasawa, K., Hill, R. B., & Ohsuga, K. (1999). Serotonergic control of the heart and pericardium in the chiton *Acanthopleura japonica*. Comparative Biochemistry and Physiology: A, **124**, 561-567.

McBride, S. C., Rotem, E., Ben-Ezra, D., & Shpigel, M. (2001). Seasonal energetics of *Haliotis fulgens* (Philippi) and *Haliotis tuberculata* (L.). Journal of Shellfish Research, **20**(2), 659-665.

McDonald, D. G., Wood, C. M., & McMahon, B. R. (1980). Ventilation and oxygen consumption in the Dungeness crab, *Cancer magister*. Journal of Experimental Zoology, **213**, 123-136.

McMahon, B. R. (1986). Oxygen binding by hemocyanin: compensation during activity and environmental change. In B. Linzen (Ed.), Invertebrate oxygen carriers (pp. 299-320). Berlin: Springer-Verlag.

McMahon, B. R., & Wilkens, J. L. (1983). Ventilation, perfusion, and oxygen uptake. In D. E. Bliss (Series Ed.) & L. H. Mantel (Ed.), The biology of crustacea: 5. Internal anatomy and physiological regulation (pp. 289-373). Academic Press.

Murdock, G. R., & Vogel, S. (1978). Hydrodynamic induction of water flow through a keyhole limpet (Gastropoda, Fissurellidae). Comparative Biochemistry and Physiology: A, **61**, 227-231.

Mykles, D. L. (1980). The mechanism of fluid absorption at ecdysis in the American lobster, *Homarus americanus*. Journal of Experimental Biology, **84**, 89-101.

Nicholson, S. (2003). Cardiac and branchial phsiology associated with copper accumulation and detoxication in the mytilid mussel *Perna viridis*. Journal of Experimental Marine Biology and Ecology, **295**, 157-171.

Nickerson, K. W., & Van Holde, K. E. (1971). A comparison of molluscan and arthropod hemocyanin - I. Circular dichroism and absorption spectra. Comparative Biochemistry and Physiology: B, **39**, 855-872.

Norfolk, J. R. W. (1978). Internal volume and pressure redulation in *Carcinus maenas*. Journal of Experimental Biology, **74**, 123-132.

Nuwayhid, M. A., Spencer Davies, P., & Elder, H. Y. (1978). Gill structure in the common limpet *Patella vulgata*. Journal of the Marine Biological Association U.K., **58**, 817-823.

O'Dor, R. K., & Wells, M. J. (1984). Circulation time, blood reserves and extracellular space in a cephalopod. Journal of Experimental Biology, **113**, 461-464.

Olaechea, R. P., Ushio, H., Watabe, S., Takada, K., & Hatae, K. (1993). Toughness and collagen content of abalone muscles. Bioscience, Biotechnelogy and Biochemistry, **57**(1), 6-11.

Pankhurst, N. W., & Sharples, D. F. (1992). Effects of capture and confinement on plasma cortsol concentrations in the Snapper, *Pagrus auratus*. Australian Journal of Marine and Freshwater Research, **43**, 345-356.

Paterson, B. D., & Spanoghe, P. T. (1997). Stress indices in marine decapod crustaceans, with particular reference to the grading of western rock lobsters *Panulirus cygnus* during commercial handling. Marine and Freshwater Research, **48**, 829-834.

Paul, R. (1986). Gas exchange and gas transport in the tarantula *Eurypelma californicum* - an overview. In B. Linzen (Ed.), Invertebrate oxygen carriers (pp. 321-326). Berlin: Springer-Verlag.

Peck, L. S., Culley, M. B., & Helm, M. M. (1987). A laboratory energy budget for the ormer *Haliotis tuberculata* L. Journal of Experimental Marine Biology and Ecology, **106**, 103-123.

Perrier, R. (1890). Recherches sur l'anatomie et l'histologie du rein des gastéropodes prosobranches. Annales des Sciences Naturelles: Zoologie et Paléontologie, **IX**, 61-313.

Piiper, J. (1982). A model for evaluating diffusion limitation in gas-exchange organs of vertebrates. In C. R. Taylor, K. Johansen, & L. Bolis (Eds.), A companion to animal physiology (pp. 49-64). Cambridge University Press.

Piiper, J., & Scheid, P. (1984). Model analysis of gas transfer in fish gills. In W. S. Hoar & D. J. Randall (Eds.), Fish physiology (Vol. XA, pp. 229-262). Academic Press Inc.

Pilson, M. E. Q. (1965). Variation of hemocyanin concentration in the blood of four species of *Haliotis*. Biological Bulletin, **128**, 459-472.

Poore, G. C. B. (1972). Ecology of New Zealand abalones, *Haliotis* species (Mollusca: Gastropoda). 1. Feeding. New Zealand Journal of Marine and Freshwater Research, **6**, 11-22.

Potts, W. T. W. (1954). the rate of urine production of *Anodonta cygnea*. Journal of Experimental Biology, **31**, 614-618.

Powell, A. W. B. 1979. New Zealand mollusca: marine, land and freshwater snails. Collins, Auckland.

Purchon, R. D. 1977. The biology of the mollusca – second edition. Pergamon Press, Oxford.

Ragg, N. L. C., Taylor, H. H., Behrens, J. W. 2000. Stress and weight loss associated with handling in the blackfoot abalone, *Haliotis iris*. Journal of Shellfish Research **19**(1): 528-529.

Ramsay, J. A. R. 1952. Physiological approach to the lower animals. Cambridge University Press, Cambridge.

Randall, D. J., & Daxboeck, C. (1984). Oxygen and carbon dioxide transfer across fish gills. In W. S. Hoar & D. J. Randall (Eds.), Fish physiology (Vol. XA, pp. 263-314). Academic Press Inc.

Russell, C. W., & Evans, B. K. (1989). Cardiovascular anatomy and physiology of the Black-lip abalone, *Haliotis ruber*. Journal of Experimental Zoology, **252**, 105-117.

Ryder, J. M., Wells, R. M. G., & Baldwin, J. (1994). Tauropine and D-lactate as indicators of recovery of live paua (New Zealand abalone) (*Haliotis iris*) from handling stress, and of postmortem quality. Food Australia, **46**, 523-526.

Scheid, P. (1982). A model for comparing gas-exchange systems in vertebrates. In C. R. Taylor, K. Johansen, & L. Bolis (Eds.), A companion to animal physiology (pp. 3-16). : Cambridge University Press.

Schipp, R., & Hevert, F. (1981). Ultrafiltration in the branchial heart appendage of dibranchiate cephalopods: a comparative ultrastructural and physiological study. Journal of Experimental Biology, **92**, 23-35.

Senozan, N. M., & Briggs, M. (1989). Hemocyanin levels in the giant keyhole limpet *Megathura crenulata*, from the coast of California. Comparative Biochemistry and Physiology: A, **94**(2), 195-199.

Shadwick, R. E., Gosline, J. M., & Milsom, W. K. (1987). Arterial haemodynamics in the ceophalopod mollusc, *Octopus dofleini*. Journal of Experimental Biology, **130**, 87-106.

Shilling, F. M., Hoegh-Guldberg, O., & Manahan, D. T. (1996). Sources of energy for increased metabolic demand during metamorphosis of the abalone *Haliotis rufescens* (Mollusca). Biological Bulletin, **191**, 402-412.

Simkiss, K., & Wilbur, K. M. (1977). The molluscan epidermis and its secretions. Symposia of the Zoological Society of London, **39**, 35-76.

Skelding, J. M., & Newell, P. F. (1975). On the functions of pore cells in the connective tissue of terrestrial pulmonate molluscs. Cell and Tissue Research, **156**, 381-390.

Smith, A. M. (1991). The role of suction in the adhesion of limpets. Journal of Experimental Biology, **161**, 151-169.

Smith, P. J. S. (1987). Cardiac output in the Mollusca: Scope and regulation. Experientia, **43**, 956-965.

Smith, P. J. S., & Hill, R. B. (1986). Cardiac performance in response to loading pressures and perfusion with 5-hydroxytryptamine in the isolated heart of *Busycon canaliculatum* (Gastropoda, Prosobranchia). Journal of Experimental Biology, **123**, 243-253.

Spencer, B. E., Edwards, D. B., & Millican, P. F. (1992). Growing hatchery-reared Pacific oysters (*Crassostrea gigas* Thunberg) to marketable size in trays - observations on coasted small-scale culture methods and rough-handling trials. Aquaculture, **106**, 261-274.

Taylor, A. C., & Brand, A. R. (1975). A comparative study of the respiratory responses of the bivalves *Arctica islandica* (L.) and *Mytilus edulis* (L.) to declining oxygen tension. Proceedings of the Royal Society, London: B, **190**, 443-456.

Taylor, A. C., & Brand, A. R. (1975). Effects of hypoxia and body size on the oxygen consumption of the bivalve *Arctica islandica* (L.). Journal of Experimental Marine Biology and Ecology, **19**, 187-196.

Taylor, H. H. (1990). Pressure-flow charateristics of crab gills: Implications for regulation of hemolymph pressure. Physiological Zoology, **63**(1), 72-89.

Taylor, H. H., & Greenaway, P. (1994). The partitioning of water and solutes during evaporative water loss in three terrestrial crabs. Physiological Zoology, **67**(3), 539-565.

Taylor, H. H., & Taylor, E. W. (1986). Observations of valve-like structures and evidence for recification of flow within the gill lamellae of the crab *Carcinus maenas* (Crustacea, Decapoda). Zoomorphology, **106**, 1-11.

Taylor, H. H., & Taylor, E. W. (1991). The dorsoventral muscles of *Carcinus maenas*: Evidence for hydrostatic pressure control in a crab. Physiological Zoology, **64**(4), 1110-1129.

Taylor, H. H., & Taylor, E. W. (1992). Gills and lungs: The exchange of gases and ions. In Microscopic Anatomy of Invertebrates (Vol. 10: Decapod Crustacea, pp. 203-293). : Wiley-Liss, Inc.

Taylor, J. E. (1993). Responses to wounding resulting in haemorrhage in the Black Footed paua: *Haliotis iris* Gmelin (Mollusca, Gastropoda). Unpublished MSc Thesis, University of Canterbury (Christchurch; New Zealand).

Taylor, J. E., Schiel, D. R. T., & Taylor, H. H. (1994). The first cut is the deepest: Wounding and healing in Black-foot paua (*Haliotis iris*). Seafood New Zealand, **2**, 47-48.

Taylor, P. M., & Andrews, E. B. (1988). Osmoregulation in the intertidal gastropod *Littorina littorea*. Journal of Experimental Marine Biology and Ecology, **122**, 35-46.

Telford, M. (1983). An experimental analysis of lunule function in the sand dollar *Mellita quinquiesperforata*. Marine Biology, **76**, 125-134.

Telford, M., & Mooi, R. (1987, April 16). The art of standing still. New Scientist, 30-35.

Thompson, R. J., Bayne, C. J., Moore, M. N., & Carefoot, T. H. (1978). Haemolymph volume, changes in the biochemical composition of the blood, and cytological responses of the digestive cells in *Mytilus californianus* Conrad, induced by nutritional, thermal and exposure stress. Journal of Comparative Physiology, **127**, 287-298.

Thompson, R. J., Livingstone, D. R., & de Zwaan, A. (1980). Physiological and biochemical aspects of the valve snap and valve closure responses in the giant scallop *Placopecten magellanicus*. Journal of Comparative Physiology, **137**, 97-104.

Tissot, B. N. (1992). Water movement and the ecology and evolution of the Haliotidae. In S. A. Shepherd, M. J. Tegner, & S. A. Guzman del Proo (Eds.), Abalone of the world: Biology, fisheries and culture (pp. 34-45). Oxford: Blackwells.

Trueman, E. R., & Brown, A. C. (1985). The mechanism of shell elevation in *Haliotis* (Mollusca: Gastropoda) and a consideration of the evolution of the hydrostatic skeleton in Mollusca. Journal of the Zoological Society of London: A, **205**, 585-594.

Turgeon, D. D., Quinn, J. F., Bogan, A. E., Coan, E. V., Hochberg, F. G., Lyons, W. G., Mikkelsen, P. M., Neves, R. J., Roper, F. E., Rosenberg, G., Roth, B., Scheltema, A., Thompson, F. G., Vecchione, M. & Williams, J. D. (1998). Common and scientific names of aquatic invertebrates from the United States and Canada: Mollusks. 2nd edition. American Fisheries Society Special Publication 26. American Malacological Union, Bethesda, Maryland.

Ultsch, G. R., & Gros, G. (1979). Mucus as a diffusion barrier to oxygen: Possible role in $O_2$ uptake at low pH in carp (*Cyprinus carpio*) gills. Comparative Biochemistry and Physiology: A, **62**, 689-689.

Vogel, S. 1994. Life in moving fluids: The physical biology of flow. 2nd edition. Princeton University Press, Princeton, New Jersey.

Vogel, S., & LaBarbera, M. (1978). Simple flow tanks for research and teaching. BioScience, **28**, 638-643.

Voltzow, J. (1983). Flow though and around the abalone *Haliotis kamtschatkana*. The Veliger, **26**(1), 18-21.

Voltzow, J. (1986). Changes in pedal intramuscular pressure corresponding to behaviour and locomotion in the marine gastropods *Busycon contrarium* and *Haliotis kamtschatkana*. Canadian Journal of Zoology, **64**, 2288-2293.

Voltzow, J. (1994). Gastropoda: Prosobranchia. In F. W. Harrison (Series Ed.) & F. W. Harrison & A. J. Kohn (Eds.), Microscopic anatomy of invertebrates. Mollusca I (Vol. 5, pp. 111-252). New York: Wiley-Liss.

Wagner, P. J. 1996. Patterns of morphologic diversification during the initial radiation of the "Archaeogastropoda". Chapter 13 in: Origin and evolutionary radiation of the Mollusca. J. D. Taylor (ed.). Oxford University Press.

Warburton, K. (1976). Shell form, behaviour, and tolerance to water movement in the limpet *Patina pellucida* (L.) (Gastropoda: Prosobranchia). Journal of Experimental Marine Biology and Ecology, **23**, 307-325.

Wasson, J. G. (1984). A study of facultative anaerobiosis in the abalone *Haliotis cracherodii*. Unpublished MSc Thesis, California State Polytechnic University (Pomona).

Wells, M. J. (1992). The cephalopod heart: The evolution of a high-performance invertebrate pump. Experientia, **48**, 800-808.

Wells, M. J., & Smith, P. J. S. (1987). The performance of the octopus circulatory system: a triumph of engineering over design. Experientia, **43**, 487-499.

Wells, M. J., & Wells, J. (1985). Ventilation and oxygen uptake by *Nautilus*. Journal of Experimental Biology, **118**, 297-312.

Wells, M. J., & Wells, J. (1993). Fluid uptake and the maintenance of blood volume in *Octopus*. Journal of Experimental Biology, **175**, 211-218.

Wells, R. M. G. 1980. Invertebrate respiration. The Institute of Biology's Studies in Biology No.127. Edward Arnold Publishers Ltd., London.

Wells, R. M. G., & Baldwin, J. (1995). A comparison of metabolic stress during air exposure in two species of New Zealand abalone, *Haliotis iris* and *Haliotis australis*: implications for the handling and shipping of live animals. Aquaculture, **134**, 361-370.

Wells, R. M. G., Baldwin, J., Speed, S. R., & Weber, R. E. (1998). Haemocyanin function in the New Zealand abalones *Haliotis iris* and *Haliotis australis*: relationships between oxygen-binding properties, muscle metabolism and habitat. Marine and Freshwater Research, **49**, 143-149.

Werner, I., Flothmann, S., & Burnell, G. (1995). Behaviour studies on the mobility of two species of abalone (*Haliotis tuberculata* and *Haliotis discus hannai*) on sand: Implications for redeeding programmes. Marine and Freshwater Research, **46**, 681-687.

Willson, L. L., & Burnett, L. E. (2000). Whole animal and gill tissue oxygen uptake in the Eastern oyster, *Crassostrea virginica*: Effects of hypoxia, hypercapnia, air exposure and infection with the protozoan parasite *Perkinsus marinus*. Journal of Experimental Marine Biology and Ecology, **246**, 223-240.

Yonge, C. M. (1947). The pallial organs in the aspidobranch gastropoda and their evolution throughout the mollusca. Philosophical Transactions of the Royal Society of London: B, **232**, 443-519.